Dissertation zur Erlangung des Doktorgrades
der Fakultät für Chemie und Pharmazie
der Ludwig-Maximilians-Universität München

The Photopharmacology of Actin and Cytoskeletal Regulators

and

De novo Design of SARS-CoV-2 Main Protease Inhibitors

Nynke Anna Vepřek
aus
München, Deutschland

2021

Erklärung:

Diese Dissertation wurde im Sinne von § 7 der Promotionsordnung vom 28. November 2011 von Herrn Prof. Dr. Dirk Trauner betreut.

Eidesstattliche Versicherung:

Diese Dissertation wurde eigenständig und ohne unerlaubte Hilfe erarbeitet.

München, den 10. August, 2021

_____

(Nynke Anna Vepřek)

Dissertation eingereicht am: 11. August 2021

1. Gutachter: Prof. Dr. Dirk Trauner

2. Gutachter: Prof. Dr. Stefan Zahler

Mündliche Prüfung am: 21. September 2021

"*Hinfallen, aufstehen, Krönchen richten, weitermachen!*"

(unknown)

To my Family

Parts of this work have been accepted for publication:

C. Fischer, N. A. Vepřek,[#] Z. Peitsinis,[#] K.-P. Rühmann, C. Yang, J. N. Spradlin, D. Dovala, D. K. Nomura, Y. Zhang,* D. Trauner* **De novo Design of SARS-CoV-2 Main Protease Inhibitors**, *Synlett*, **2021**, *Accepted*.

Parts of this work have been presented at scientific conferences:

N. A. Vepřek,[#] F. Küllmer,[#] M. V. Nasufovic, M. Borowiak, O. Thorn-Seshold, H.-D. Arndt*, D. Trauner* **Optical Control of Actin Dynamics with Small Molecule Photoswitches** 7th Annual The *BRAIN* Initiative *Investigators Meeting*. Virtual Symposium, June 2021.

N. A. Vepřek,[#] F. Küllmer,[#] M. V. Nasufovic, M. Borowiak, O. Thorn-Seshold, H.-D. Arndt*, D. Trauner* **Optical Control of F-Actin Dynamics with Red-Shifted Optojasp** *New York Academy of Sciences, Chemical Biology Discussion Group Year-End Symposium,* Virtual Symposium, May 2021.

N. A. Vepřek, L. Gao, M. Maier, Dirk Trauner* **Toward the Optical Control of the Actin Cytoskeleton** *Gordon Research Seminar and Conference "Artificial Switches and Motors"*, Holderness, MA, USA, June 2019.

Parts of this work are currently prepared for publication:

N. A. Vepřek,[#] F. Küllmer,[#] M. V. Nasufovic, M. Borowiak, O. Thorn-Seshold, H.-D. Arndt*, D. Trauner* **Optical Control of F-Actin Dynamics with Red-Shifted Optojasp** *Manuscript in Preparation.*

A. C. Impastato,[#] A. Shemet,[#] N. A. Vepřek, G. Saper, H. Hess, and D. Trauner* **Optical Control of Mitosis with a Photoswitchable Eg5 Inhibitor** *Manuscript in Preparation.*

N. A. Vepřek, R. Bao, S. Folkerts, L. Laprell, T. Oertner, D. Trauner Optical Control of Actin with Photoswitchable Latrunculin *Manuscript in Preparation.*

Publications, which are not part of this thesis:

D. Trauner, N. Hartrampf, T. Seki, A. Baumann, P. Watson, A. Hoffmann-Röder, M. Tsuji, N. Vepřek, B. Hetzler, **Optical Control of Cytokine Production Using Photoswitchable Galactosylceramides**, *Chem. Eur. J.* **2019**, *26*, 4476 –4479.

[#] authors contributed equally

Abstract

Chapter 1: The Photopharmacology of Actin and Cytoskeletal Regulators

Actin is one of the most abundant proteins in eukaryotic cells and partakes in many essential cellular processes like cellular organization, proliferation, migration and signaling.

The main focus of this thesis is the optical control of actin dynamics by photoswitchable versions of the small-molecule actin modulators latrunculin and jasplakinolide.

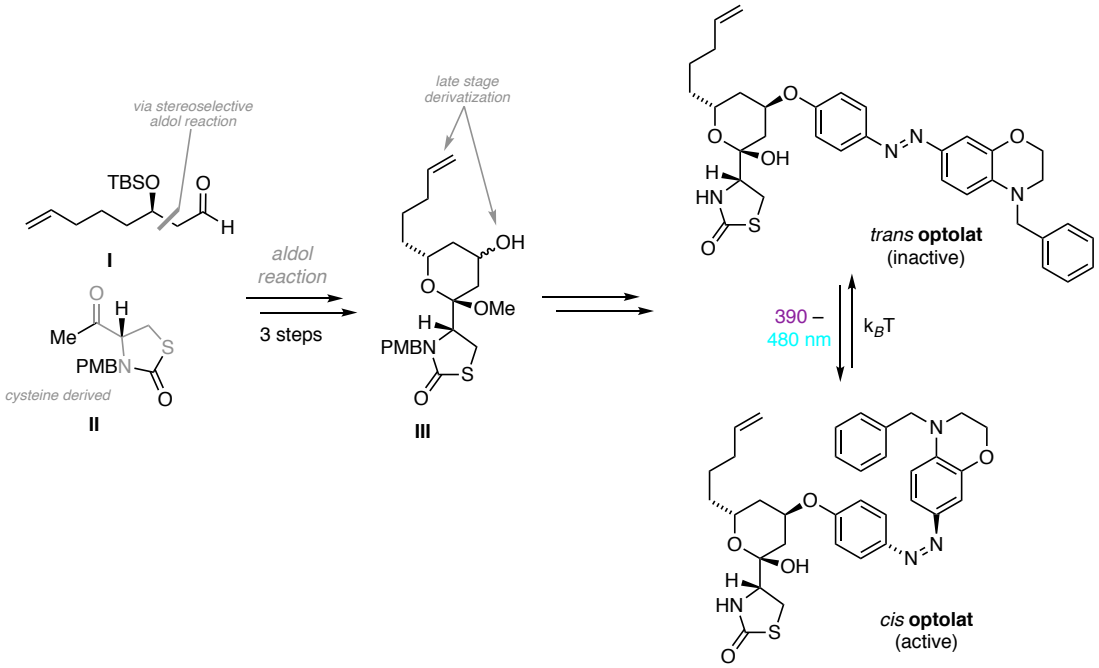

We optimized an efficient and scalable synthetic route towards advanced intermediates **III** of latrunculin natural product. These intermediates were further derivatized to explore a variety of functional substitutions around the northern half of the molecule.

The light-dependent effects of photoswitchable latrunculin (**optolat**) in human cancer cell line proliferation and on the dynamic function of microglia were demonstrated. Simultaneously, we developed a computational platform to aid the further optimization of optolatrunculin and truncated latrunculin analogs.

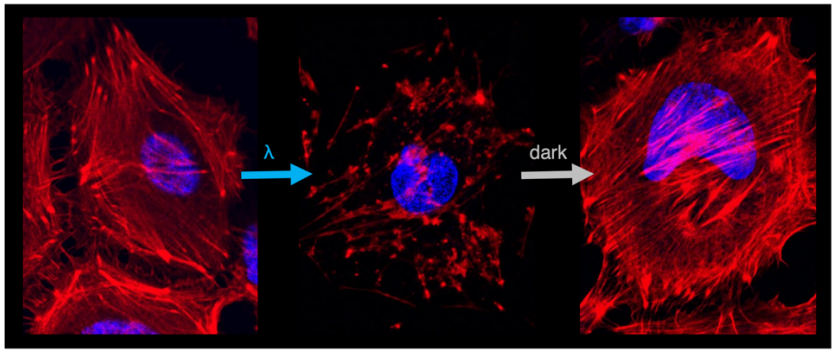

We developed a new generation of photoswitchable jasplakinolide analogs (optojasp) with improved photophysical and biological properties was developed. This tool can reversibly, locally, and temporally disrupt leading edge actin dynamics. We also demonstrate a light dependent reduction in wound healing without perturbing cell viability.

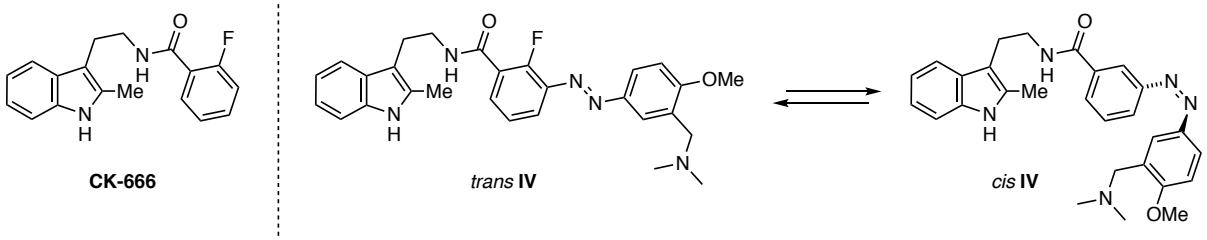

The regulation of actin dynamics in cortical networks depends on the nucleating properties of actin related protein 2/3 (Arp2/3). We synthesized a series of optimized photoswitchable analogs (e.g. **IV**) based on the Arp2/3 inhibitor CK-666. Initial experiments indicate that Arp2/3 dependent inhibition of actin branching can be achieved in the presence of a new photoswitchable CK-666.

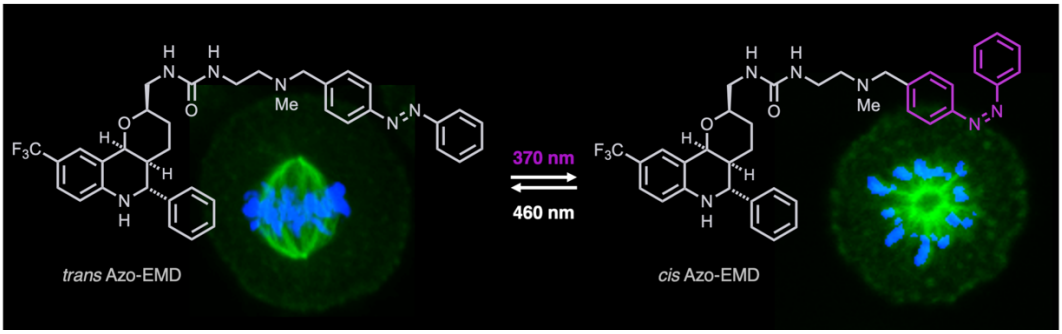

Kinesin Eg5 is important to bipolar spindle formation during mitosis. In a collaborative effort photoswitchable Kinesin Eg5 inhibitors were developed and investigated in cellular and biochemical assays. We show that under irradiated conditions, **Azo-EMD** caused monopolar spindle formation while the bipolar spindle was observed in the dark.

Chapter 2: De novo Design of SARS-CoV-2 Main Protease Inhibitors

In early 2020, a novel coronavirus, that was later termed SARS-CoV-2 caused a condition known as COVID-19. To date, 2.8 billion infections have been reported and about 4.3 million people have succumbed to COVID-19.[a]

The dire worldwide situation prompted academic and industrial scientists to develop vaccines and small molecule drugs against SARS-CoV-2.

The Main Protease (M^{Pro}) is highly conserved amongst corona viruses and its cleavage site does not exist in human proteases. For this reason, it poses an ideal target for clinical drug development.

Computational screening and molecular modelling on the recently published M^{Pro} crystal structures furnished structural lead pharmacophores that where synthesized and evaluated in biochemical assays. Based on a concise and diversifiable chemical approach, a series of micromolar pyridone small molecule inhibitors of SARS-CoV-2 M^{Pro} was developed.

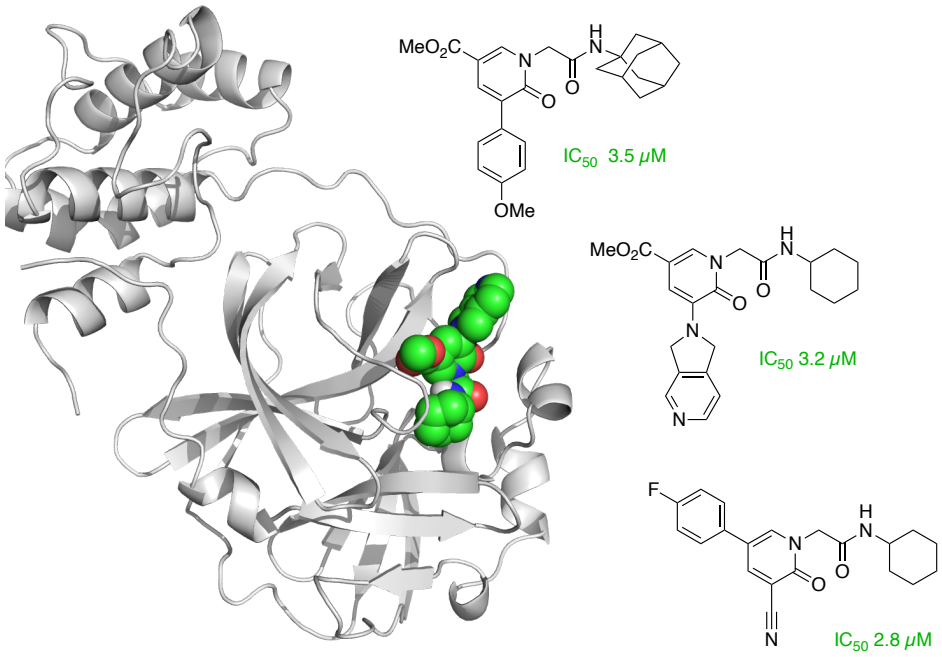

[a] https://covid19.who.int/ (08-07-2021)

Chapter 3: Towards the Photopharmacological Control of DREADD Receptors

Designer receptors exclusively activated by designer drugs (DREADDs) are a means to selectively target specific G-protein coupled receptors by drug administration in live, freely moving animals. The spatial and temporal control of DREADDs limited. Clozapine is an FDA approved drug that is used as a last resort treatment for schizophrenic disorders and can activate DREADDs. We have designed and synthesized clozapine based photoswitches for the optical control of DREADDs that are currently being investigated in brain slices expressing designer receptors.

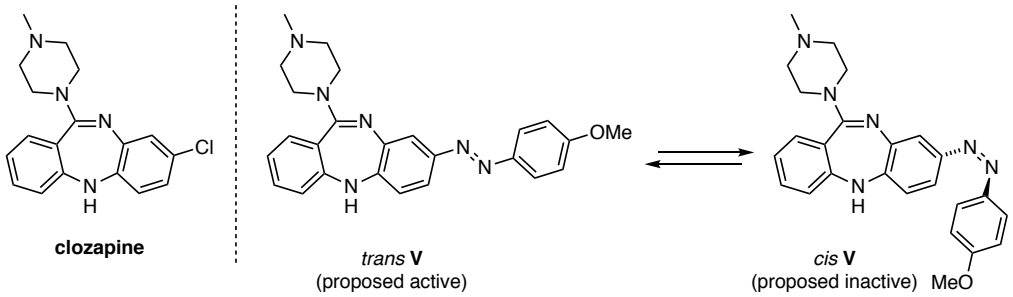

Acknowledgements

First and foremost, I would like to express my gratitude towards Prof. Dr. Dirk Trauner for giving me the opportunity to pursue my Ph.D. work under his guidance. I would like to thank him for his inspiring enthusiasm and contagious curiosity. I am grateful for the trust he put in my capabilities to independently explore new fields of research and thereby allowing me to expand my scientific horizons. I am also thankful for the unique experience of moving to New York City.

I would like to thank Prof. Dr. Stefan Zahler for kindly agreeing to be the second reviewer of this thesis. I thank Prof. Dr. Konstantin Karaghiosoff, Prof. Dr. Paramjit Arora, Prof. Dr. Daniel Merk and Prof. Dr. Susanne Koch for agreeing to serve on my examination committee.

This work benefited greatly from a variety of collaborations with different research laboratories and within the Trauner group.
I would like to thank Dr. Enrique J. Garcia, Jie-Ning (Emily) Yang and Prof. Liza Pon (Columbia University) for investigating optolatrunculin in *Saccheromyces Cerevisiae*. I would also like to thank Dr. Laura Laprell and Prof. Dr. Thomas Oertner (Center for Molecular Neurobiology Hamburg) for exploring optolatrunulin in microglia. I am grateful to Dr. Ruiyang Bao for joining and continuing this project. I would further like to acknowledge Madeleine Cooper and Prof. Dr. Bradley Zuchero (Stanford University), Pedro Guedes Diaz and Prof. Dr. Thomas Misgeld (Technical University of Munich) as well as Prof. Masato Sawada and Prof. Kazunobu Sawamoto (Nagoya University) for ongoing collaborations that have not yet been reported in this thesis.
The development of second generation optojasps greatly benefited from experimental advice for cell culture experiments from Dr. Malgorzara Borowiak and the synthesis of these compounds by Dr. Florian Küllmer, Dr. Veselin Nasufovic and Prof. Dr. Hans-Dieter Arndt (Friedrich-Schiller University of Jena).
I would like to thank Dr. Alan P. Tabatabai and Prof. Michael Murrell (Yale University), as well as Dr. Majdouline Abou-Ghali and Prof. Dr. Julie Plastino (Université Sorbonne) for initial studies on Arp2/3 modulating photoswitches.
I would like to thank Anna C. Impastato, Dr. Andrej Shemet, Dr. Gadiel Saper and Prof. Dr. Henry Hess (Columbia University) for a fruitful collaboration on the photoswitchable Kinesin Eg5 inhibitors.
For a sense of normality during the worst days of the pandemic, I would like to thank Dr. Christian Fischer and Zisis Peitsinis as well as Klaus-Peter Rühmann for a combined effort towards SARS-CoV-2 MPro inhibitors. It was fun to be in the lab and making a positive impact during lockdown. I would like to thank our collaborators, Chao Yang and Prof. Yingkai Zhang (NYU) as well as Jessica N. Spradlin and Prof. Daniel K. Nomura (University of California, Berkeley).
I would like to thank Sander Folkerts who joined me on the latrunculin project during his master's thesis and who despite the challenges of a pandemic kept his excitement and contributed important work to

this thesis. I would also like to acknowledge Arthur B. Faulstroh for synthetic assistance during his bachelor's studies.
I would like to acknowledge the German Academic Scholarship Foundation (Studienstiftung des deutschen Volkes) for 42 months of invaluable ideational and financial support.

I would like to express my gratitude towards the technical and administrative staff of LMU Munich. Most notably, Heike Traub, Aleksandra Sarman-Grilc, Dr. Martin Sumser and Carrie Louis, and Luis de la Osa de la Rosa who greatly facilitated my start in the Trauner group.
I would like to thank the technical and administrative staff at New York University, especially Dr. Chin Lin; Ronald McLurkin, and Dr. Yoel Tang for running the Shared Instrument Facility and Irene Kiriazi, Cherilyn Ramsay, Aneleen Dizon, as well as Dr. Danielle Nalband for invaluable help in administrative matters. I addition, I am grateful to the Center for Neural Science imaging core, the Langone Microscopy Laboratory and Prof. Daniella Bucella for granting me access to microscopes. I would like to thank Claudia Farb, Michael Cammer and Dr. Franziska Auer for tips in imaging and image analysis.

I would like to thank all current and former members of the Trauner group for their contribution to a collegial, productive and motivating environment. I would like to especially thank my Master's thesis advisor Dr. Giulio Volpin as well as Dr. Nina Hartrampf and Dr. Julius Reyes for important mentorship and guidance during the beginning of my graduate studies.
I would like to thank Belinda Hetzler and Anna C. Impastato for proof reading parts of this thesis and for their huge support over the past years. I am grateful to Dr. Martin Reynders for invaluable motivation and support.

I am grateful to *the pod*, Hannah, Julie and Nicole for a wonderful friendship and for providing that sparkle during the darkest times of the pandemic in New York City.
I would like to thank The Choral Society at Grace Church and their music director John Maclay for giving me a musical home in New York City.
I am deeply grateful to some very special people who have accompanied me for many years. Especially Eva, Anna, Oleg, Kira, Charlotte and last but not least Raphael are proof that good friendship prevails long distance.

I would like to express my deepest gratitude to my parents Stan and Maritza, for their endless love, support, advice, and encouragement that has allowed me to pursue all my dreams and manage and overcome all obstacles. I am grateful to my sister Libuše, as well as my brothers Miro and Ratko and all other members of our Vepřek-Heijman-Delaporte-Kräutler family for their love and support. Thank you for always believing in me.

Table of Contents

Chapter 1 The Photopharmacology of Actin and Cytoskeletal Regulators

1 Introduction

Actin is the most abundant protein in eukaryotic cells and is essential to many processes in the cell. As a structural protein, an intact actin network is essential to maintain cell shape and build interactions with other cells and tissues. Actin is involved the transport of cargo across the cell, organelle organization and contractile force generation, for example during cytokinesis. Equally important are actin turnover dynamics that drive cell migration in response to chemical and mechanical cues. In the nucleus, actin has been found to be important in transcriptional regulation and shuffling of various proteins and factors between the nucleus and cytosol.[1–3]

This thesis focuses on the development of different tools for the control of actin dynamics with light. The introduction aims at giving an overview over actin function, its regulation and how small molecules can mimic and influence the cell's actin network. Finally it is described how small molecules can be applied to target the actin network for pharmaceutical purposes, or for its investigation in cellular settings.

1.1 Actin Structure and Function

1.1.1 Basic Actin Structure and Function

Actin is highly conserved among species and bacteria have actin-related cytoskeletal structures.[1] In mammals six isoforms of actin are encoded in different genes. Four of these isoforms are primarily expressed in cardiac (α), skeletal (α), and smooth muscle (α, γ) tissues, while two other isoforms, β- and γ- cytosolic actin, are ubiquitously expressed. Although distinct in their biological function, their primary sequences only differ by a few amino acids that are mostly located at the N-terminus of the peptide. This results in small structural differences mainly on the outside of the polymerized actin filament (F-actin) and alters the interactions of actin isoforms with actin binding and regulating proteins.[4]

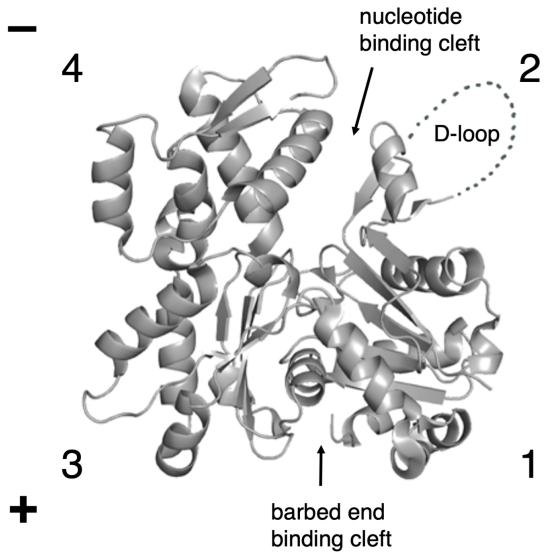

Figure 1: Crystal structure of G-actin; the subdomains and binding sites are indicated (pdb: 3hbt).

The actin protein folds into a monomeric globular structure (G-actin) with four subdomains (Figure 1). The barbed end binding cleft lies between subdomains 1 and 3 and the nucleotide binding cleft, which binds ADP or AT, is between subdomains 2 and 4. Subdomain 2 contains the DNase I binding loop (D-loop), a highly flexible amino acid sequence. The front surface of the G-actin monomer is hereafter referred to as the face, in which the D-loop is in the right upper quadrant (Figure 1). The face is solvent-exposed in F-actin and can interact with actin binding proteins (ABPs) and small molecules. Consequently, the back of the monomer is referred to as the face in which subdomain 4 is in the right upper quadrant. The monomers and filaments are hereafter oriented such that the minus (pointed end) is up (or to the right) and the plus (barbed end) is down (or to the left).[1]

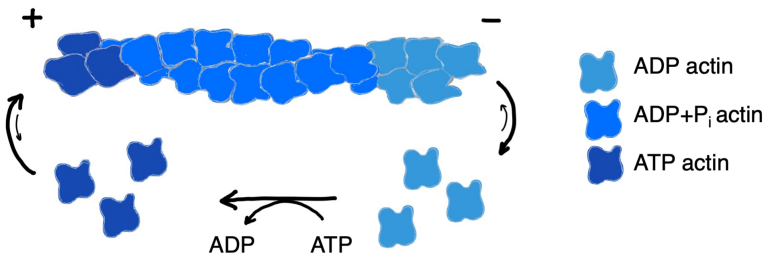

Figure 2: Actin polymerization and depolymerization mechanism (treadmilling).[b]

Actin monomers form spontaneous nucleates and polymerize under ATP hydrolysis to helical filaments (F-actin) in which the three following monomers (0, +1, +2) interact with each other (Figure 2). F-actin is a single left-handed helix (appears as slow right-handed helix) that

[b] Drawn by the author of this thesis based on the references cited.

repeats after approximately 6 turns and 13 monomers. ATP-bound monomers undergo a flattening when incorporated into the filament and subsequently, ATP hydrolyzes and P_i dissociates.[5–7] The nucleotide bound state entails structural consequences for the filament. Especially the D-loop, which lies right next to the nucleotide binding site is affected by ATP hydrolysis and P_i dissociation. The D-loop forms different conformational states that influence the stability of F-actin. The phosphate bound conformation is referred to as *open* conformation and forms stabilizing protomer interactions between the D-loop of monomer 0 and the barbed end binding cleft of subunit +2. Upon phosphate hydrolysis, the D-loop adopts the *closed* conformation which results in a weakening of the protomer interactions and ultimately depolymerization.[8–10] In the absence of actin regulating factors, actin polymerization and breakdown is solely concentration dependent and the steady state is referred to as *treadmilling*. Filament elongation is preferred on the plus (barbed) end, arguably because ATP-F-actin structurally resembles to G-actin. ADP-F-actin is destabilized and favors minus (pointed)-end depolymerization. Actin filaments are short lived, and monomers are recycled upon filament breakdown.[9,11]

While actin treadmilling can be simplistically demonstrated *in vitro*, actin turnover is highly regulated in cells. The distinct functions of actin, as well as their subcellular activation are determined by the different isoforms and a large variety of actin binding proteins (ABP) and regulating factors. ABPs have common binding motifs that bind to distinct regions of G-actin, the actin subunit, or the filament.[1,12]

1.1.2 Regulation of Actin Dynamics

In cells, actin dynamics are precisely controlled by numerous signaling pathways that regulate the activity of specific ABPs. Actin binding proteins generally occur in families of different isoforms that can be specific to individual species (e.g. human, budding yeast). In the following chapter, ABPs are described as representatives of their families by their structural characteristics and how they bind and influence actin homeostasis. Actin binding proteins that bind to similar binding sites on actin share partial homology.[12]

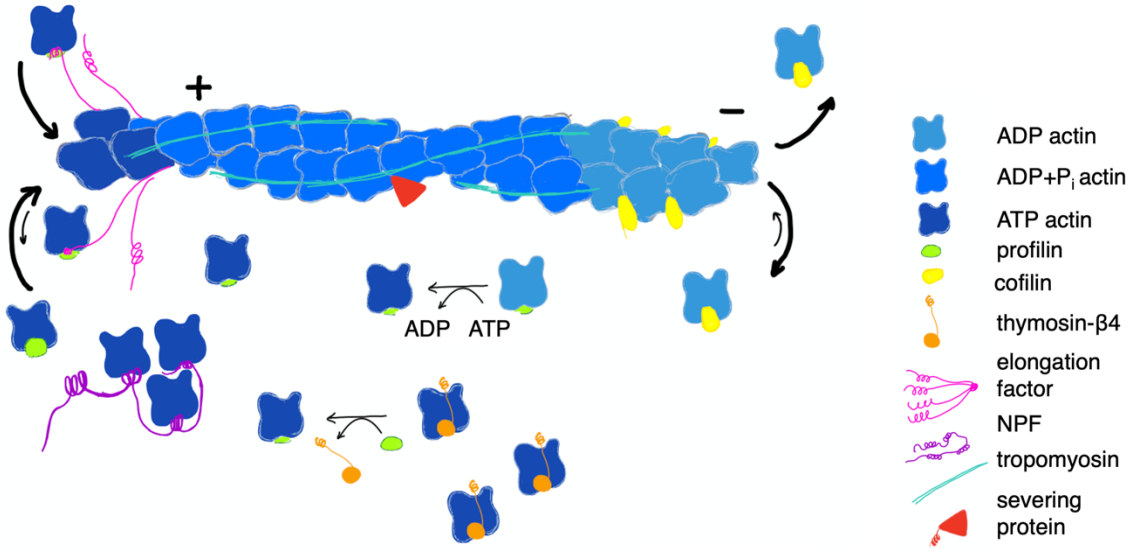

Figure 3: Actin turnover in cells is assisted by multiple ABPs.[c]

Cells maintain a large pool of mostly sequestered G-actin monomers that are bound by two functionally different actin sequestering proteins, thymosin-β4 and profilin. Thymosin-β4 consists of two subunits that are connected by a linker motif. The N-terminal motif has similarities to the WH2 binding motif and binds to the front of the barbed end binding cleft of G-actin while the C-terminal helix binds above subunits 2 and 4. Thymosin-β4 blocks both, pointed and barbed end monomer binding. Consequently, thymosin-β4 bound G-actin is polymerization incompetent and can be described as an actin buffer that competes with profilin for G-actin binding.[13] Profilin has a higher binding affinity and binds to the back of the target binding site of G-actin. Profilin catalyzes nucleotide exchange to ATP and can further bind poly proline rich domains. These domains are often found near WH2 binding domains in actin elongation factors like Ena/VASP. This colocalization of profilin and elongation factors allows for barbed end filament elongation by recruitment of profilin-actin.[14]

[c] Schematic representation drawn by the author of this thesis on the basis of the literature cited.

The first step in actin polymerization is the formation of stable G-actin di- and trimers and called nucleation. Nucleation needs to take place with local and temporal precision. It is thermodynamically costly and it is inhibited by G-actin sequestration in cells. Therefore, nucleation is mediated by a variety of nucleation promoting factors (NPF) in cells.[15,16]
Three classes of nucleation factors have been described: the actin related protein 2/3 (Arp2/3) complex, tandem monomer binding (TMB)[d] proteins and the formin family of proteins. The Arp2/3 complex is mainly relevant in the formation of branched networks while formins and TMBs mainly form unbranched actin structures.[17] The formation of higher actin structures will be discussed later. First, the general regulation of actin turnover will be discussed.

Actin nucleating proteins of the TMB and formin families contain similar binding motifs. The formin homology domain 2 (FH2) can occur in tandem repeats and binds G-actin in the barbed-end binding cleft. TMB and formin nucleation factors bring several G-actin monomers together to form an F-actin like nucleus that is then further elongated under the regulation of elongation factors. Formins form homodimers around the barbed end of the filament and recruit new profilin-G-actin monomers to the plus end by simultaneously binding profilin-ATP-actin in the barbed end binding cleft.[12,15,17–19]

F-actin filaments are stabilized by hydrophobic and electrostatic interactions (salt bridges) between the subunits of two strands. In addition the hydrophobic patch of the D-loop interacts with the target binding site of the protomer. This has also been described as the lock-and-key interaction between two neighboring subunits.[20] Changes to the D-loop geometry, e.g. caused by ATP hydrolysis and P_i dissociation, have been ascribed to the varying stability and flexibility throughout the filament lifetime.[10,20–22]

Actin filaments are decorated by various tropomyosin isoforms. Tropomyosin consists of two α-helices that form a coiled coil structure. The C and N termini of tropomyosin proteins can bind together, forming a polymer that assembles from the minus to the plus end along actin filaments.[20,23,24] These structures are important for the regulation of actin networks. Different tropomyosin isoforms regulate muscle contraction, filament stability and ABP binding.[25–27] Tropomyosin isoforms regulate specific physiological functions and are therefore implicated in the development of different diseases and cancer.[27]

[d] Tandem monomer binding proteins e.g.: Spire, Cordon-bleu, leiomodin.

Capping proteins regulate the amount of filaments that elongate by blocking the barbed end for monomer binding. The most important member of this class of ABP in non-muscle cells is actin capping protein (CP; homolog: CapZ). Members of the Ca^{2+} dependent gelsolin family[e] take over important functions as actin capping and severing proteins as well.[19,28,29]

Actin capping protein (CP) is a heterodimer and consists of an α- and β-subunit that are closely "intertwined". It binds to the two barbed end actin subunits with very high affinity and competes with filament elongation factors like formin for binding. The intracellular concentration of capping protein is so high, that if all capping protein was active, all barbed ends of actin filaments would be capped.[19] Actin capping protein activity is highly regulated by sequestration, like for example by blockage of the actin binding domain and by allosteric inhibition. Allosteric inhibition is mostly achieved by membrane-associated proteins that bear capping protein interacting motifs and can bind to actin-bound actin capping protein to induce uncapping due to loss of affinity in the barbed end binding region. Capping proteins are involved in the dynamic formation of filopodia, (long lived) actin cables and stress fibers. They also keep actin filaments in dendritic networks short, thereby favoring branching.[28]

Cell locomotion is proportional to actin turnover rates. Filament turnover can be increased by filament severing, which causes faster depolymerization.[30] An important class of severing proteins is the family of gelsolin ABPs. Gelsolins are activated by high Ca^{2+} concentrations. Ca^{2+} binding induces a conformational change exposing the actin binding domain that allows gelsolin to bind to F-actin inducing a twist in the bound actin subunit. The resulting subunit conformation resembles the G-actin conformation and consequently D-loop binding from the neighboring subunit is disfavored, leading to filament breakage. Gelsolins initially remain on the resulting barbed filament end. Gelsolin can, apart from filament elongation and severing, also nucleate G-actin leading to increased filament assembly. The severing and nucleating functionalities of gelsolin can be distinguished by phosphoinositides (PIP2) with high PIP2 concentrations favoring nucleation. In resting cells, Ca^{2+} concentrations are low while PIP2 concentrations are high, resulting in slow actin dynamics. In activated cells, such as motile cells, elevated Ca^{2+} concentrations induce severing activity, accelerating filament turnover.[19,31–33]

The members of the ADF/Cofilin protein family[f] generally lead to the breakdown of actin filaments and recycling of actin monomers by pointed end depolymerization or severing.

[e] in mammalian cells insluding: gelsolin, adseverin, villin, advillin, supervillin, flightless I homolog and CapG, fragmin.

[f] > 30 members identified, 13-19 kDa proteins. Actin binding domains highly conserved. Most important member cofilin 1.

Cofilins bind to ADP-actin filaments at the filament pointed ends and induce conformational changes in the actin subunits that lead to a loss of the longitudinal D-loop and barbed end binding interaction within the filament. ADF/cofilin severing occurs at the border between F-actin strand that is decorated by cooperative cofilin binding and the free filament.[34,35]

Depolymerized ADP-G-actin is quickly bound by available profilin, which catalyzes nucleoside exchange and forms the polymerization competent profilin-ATP-G-actin complex, that can reenter the treadmilling dynamics of actin filaments.[14]

1.1.3 Posttranslational Modifications of Actin

Like for many proteins, the posttranslational modification of actin is important for the cell to maintain actin homeostasis and function. The full scope of posttranslational modifications of actin isoforms remain poorly understood. Common posttranslational modifications include N-terminal acetylation, arginylation, the cross-linking of monomers, phosphorylation, ubiquitination, and various redox-modifications.[36]

Molecule Interacting with CasL proteins (MICAL) are a family of multidomain flavoprotein monooxygenase/ hydrolase enzymes that are induced by cellular signaling.[37,38] MICAL enzymes are conserved across species. MICAL selectively binds to F-actin and NADPH dependently oxidizes methionines M44 and M47 that are in the flexible and hydrophobic D-loop of subdomain 2. The resulting sulfoxide leads to a polarization and stiffening of the residue, destabilizing the longitudinal D-loop- barbed end interaction of protomers ultimately destabilizing F-actin. MICAL oxidation of F-actin is linked to catastrophic disassembly and branching of actin networks Furthermore, M44 and M47 oxidation render ADP-Pi actin susceptible to cofilin severing, further augmenting filament breakdown. M44 and M47 oxidized actin monomers are polymerization incompetent.[38–40] In cytokinesis, MICAL1 is recruited to the ESCRT machinery[g] at the abscission site to trigger the complete local actin clearance.[41]

Ubiquitination is a means of the cell to regulate and distinguish different protein functions and the polyubiquitination of proteins is a means to induce protein degradation. The ubiquitination of actin has been linked to three ubiquitin ligases, MuRF1, UbcH5 and Trim 32 and leads to a decrease in actin levels. Ubiquitin mediated actin degradation has been linked to muscle

[g] Endosomal sorting complexes required for transport (ESCRT); important among others for cellular abscission at the end of cytokinesis.

remodeling and atrophy. Polyubiquitinylation and degradation further controls the posttranscriptional modification of actin.[36,42]

1.1.4 Higher Ordered Structures of Actin and Regulatory Roles

Cells organize actin in different linear and branched networks. Actin network organization is based on the interplay and codependence of different actin nucleating factors and determines the function of actin substructures.[43,44]

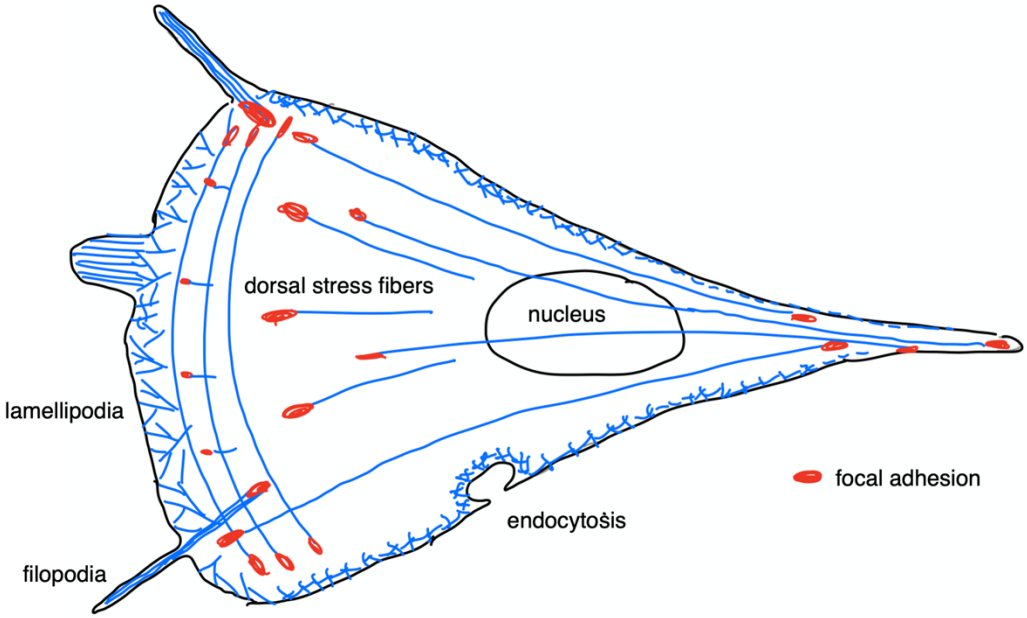

Figure 4: Higher stuctured actin networks in the cell.[h]

Cells depend on fast filament turnover in dendritic actin networks like lamellipodia for force generation and moving the cell membrane forward. These dendritic networks depend on a closely regulated interplay of Arp2/3, nucleation promoting factors (NPF) for nucleation and branching, capping protein for maintaining a dense meshwork of short actin filaments by barbed end capping, and cofilin, as well as profilin for filament turnover.[17,45–47]

[h] Simplified representation, based on the references cited.

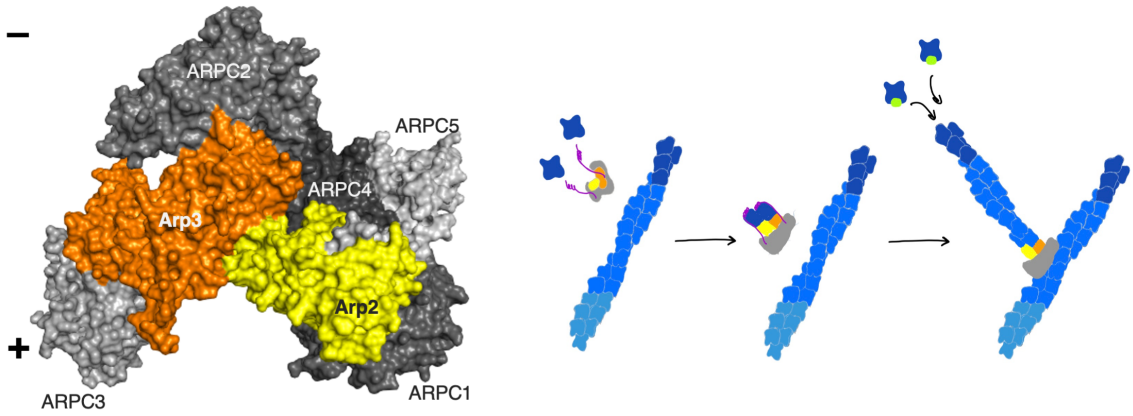

Figure 5: X-ray structure of the Arp 2/3 complex (pdb: 1k8k) and simplified schematic representation of its function.[i]

Arp2/3 is a seven multiprotein complex consisting of actin related proteins 2 and 3 and the subunits ArpC1-5 (figure 5, left).[48] The Arp2/3 complex is recruited to an existing F-actin filament by NPF proteins like the WASP family. WASP dimerization greatly enhances F-actin binding and together with ATP hydrolysis, a conformational change is induced that brings Arp2 and Apr3 subunits close together. This activated Arp2/3 complex mimics an F-actin structure, which is then elongated. Arp2/3 remains bound to the pointed end of the filament and upon ageing of the mother filament it is recycled and can induce branching at another filament (Figure 5, right).[49–53]

The different NPFs involved in Arp2/3 activation are induced by various signaling cascades and determine the localization of branched actin networks. Arp2/3 dependent networks are important in the propulsion of endosomes and pathogens and take over important roles in endocytosis.[51]

Linear, nonbranched actin structures are induced by the formin family of nucleating proteins and tandem monomer binding proteins (TMBs). They are heterogenous in their structure and function and can have uniform or mixed polarity. Actin bundles of uniform polarity have two main functions, they act as non-contractile tethers (dorsal stress fibers) or, as filopodia, push the cell membrane forward and function as a sensing system for the cell. Filopodia are formed in the dendritic actin network and extend toward the leading edge of the cell. The formation of filopodia is mediated by assembly of several formins, which induce filament formation into the same direction. Formins stay bound to the pointed end of F-actin while VASP stabilizes the

[i] The scheme was drawn by the author of this thesis on the basis of the literature cited in the text.

filament and promotes elongation. The individual filaments in unipolar bundles in filopodia stretch the whole length of the filopodium. Actin bundles of nonuniform polarity are a substrate for myosin II and therefore play important roles in contractile processes of the cell, like cytokinesis and mitochondrial fission. A third type of network are isotropic networks. Formins and Arp2/3 have been linked to these non-force generating networks that take over structure stabilizing function and likely play a role in the nucleus where actin is involved in the regulation of transcription. Isotropic actin networks have been found at the cell cortex and in membrane blebs. The formation and exact mechanism of function of isotropic networks has not been fully understood.[17,18,43]

Actin networks also work in coordination with motor proteins. The most well-known and studied systems are interactions of actin and myosin II. In muscles, actin and myosin II work together to build contractile forces that allow for muscle contraction. Nonmuscle myosin II-actin interactions take over important functions in cell contractions, such as force generation for cell migration or ring contraction in cytokinesis.[54–56]

1.2 Small Molecule Modulators

The regulation of actin dynamics in the cell is tightly controlled by actin binding proteins. Complementary to ABPs, small molecule toxins can take over the same roles in the sequestration, capping, severing and stabilization of actin.[57–59] Small molecule actin modulators have traditionally been classified as actin destabilizing or stabilizing compounds.[60] While these two categories simplify the mechanism of action and binding mode, they describe the overall observed effect of small molecule toxins on actin networks. However, this is a very rough classification. Many small molecule actin binders and ABPs have been found to have multiple mechanisms of action that can be linked to their actin binding motif. Many of these molecules are marine macrolides, but some have also been isolated from fungi, bacteria and algae. Notably, these natural products occur in large families with only very minor structural differences. Some structures can also be found across different species.[60,61]

During polymerization, the actin subunit exchanges ADP for ATP and undergoes a significant conformational change.[1] Binding of small molecules in this site blocks the nucleotide exchange and inhibits the necessary conformational twist. Therefore, small molecules binding in this site sequester actin monomers.[62] The effects caused by molecules that bind to the barbed end binding site are more complicated. Molecules can bind from the front or back of the actin

subunit. The back is buried in F-actin while the front is accessible to small-molecule protein interactions. For this reason, small molecules that bind to the back of the barbed end can sequester monomers and hinder filament elongation by capping, analogously to profilin and CP. Binding from the front side of the barbed end however, especially when in combination with extending interactions into the barbed end cleft competes with the lateral stabilizing interactions between two protomers and leads to the destabilization and severing of filaments. Destabilization of filaments can also be achieved by facilitating the dissociation of P_i by stabilization of the closed D-loop conformation. Severing small molecules can remain at the barbed end and cap this site from elongation. On the other hand, preformation of actin nucleotides, by binding multiple barbed ends simultaneously, or binding between several subunits can induce filament formation.[1,60,61]

During filament stabilization by small molecules, often the transversal monomers interact more strongly, either due to induced conformational changes, or by direct binding of a small molecule to up to three subunits. Essentially, these small molecules can act as oligomerizers, holding the subunits together. Furthermore, is binding of F-actin often accompanied by a blockage of conformational changes in the D-loop that are required for P_i dissociation. This leads to a delay in ageing of the filament and inhibits depolymerization. The timed binding of ABPs is depending on conformational changes that take place during a filament lifetime.[1,60,61,63]

In the next section, different actin targeting toxins are discussed and their binding sites and mechanisms highlighted. Many toxins are members of very large families of natural products with varying potency. In this case, one representative of the family is described, and some further prominent members are mentioned in footnotes.

1.2.1 Small Molecule Actin Destabilizers

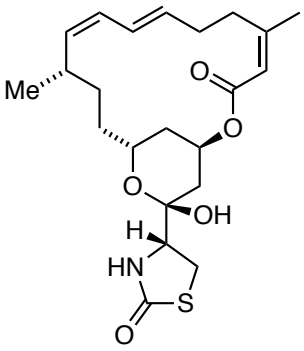

latrunculin A

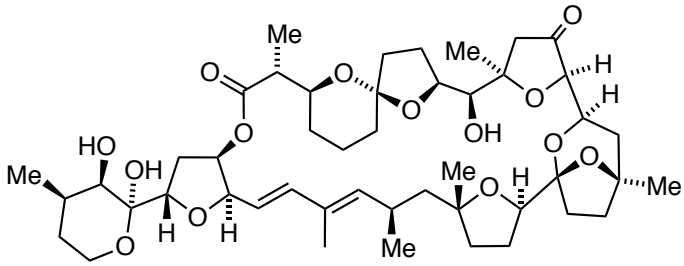

pectenotoxin-2

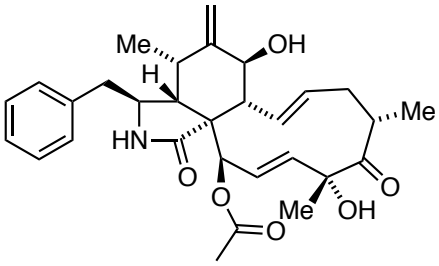

cytochalasin D

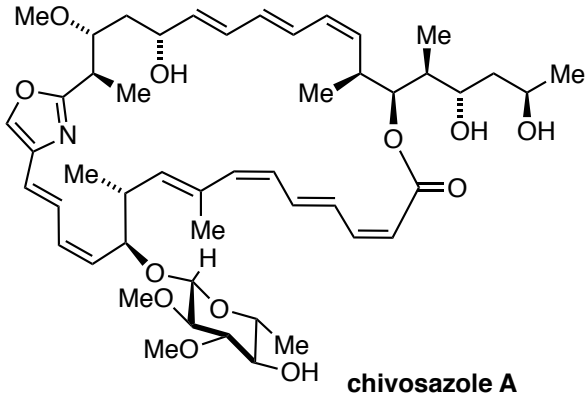

chivosazole A

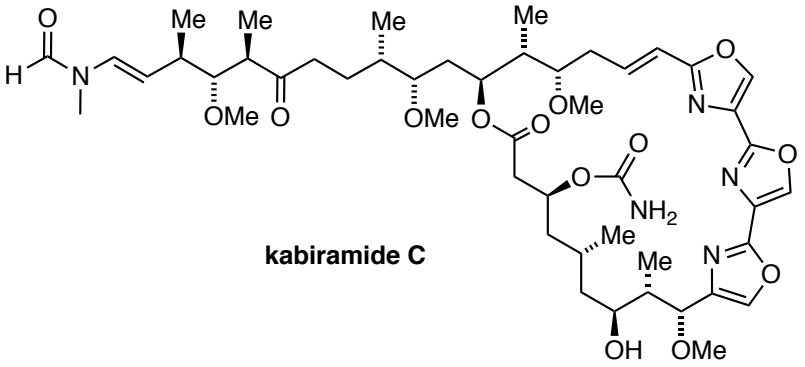

kabiramide C

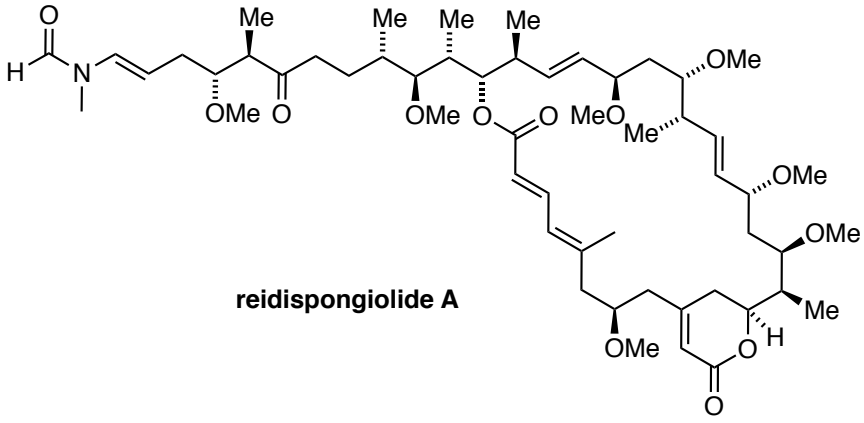

reidispongiolide A

Figure 6: Actin destabilizing small molecules (part 1).

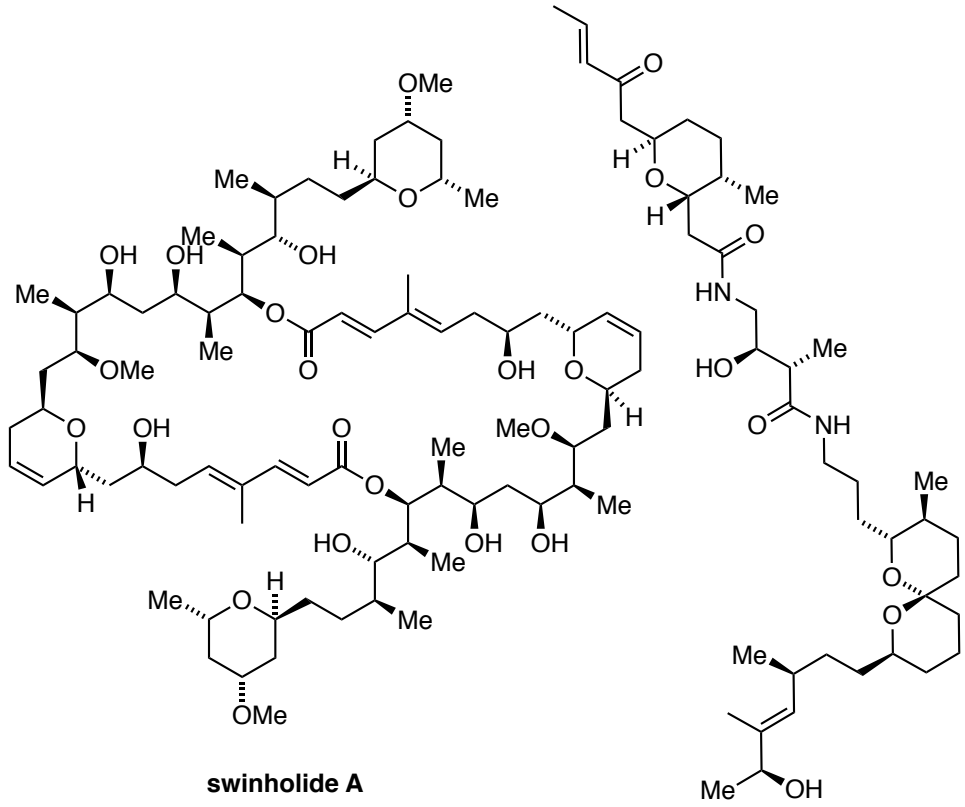

Figure 6: Actin destabilizing small molecules (part 2).

Actin destabilizers act similarly to destabilizing and sequestering ABPs. The nucleotide binding site is blocked by the actin sequestering natural products of the latrunculin family.[60]

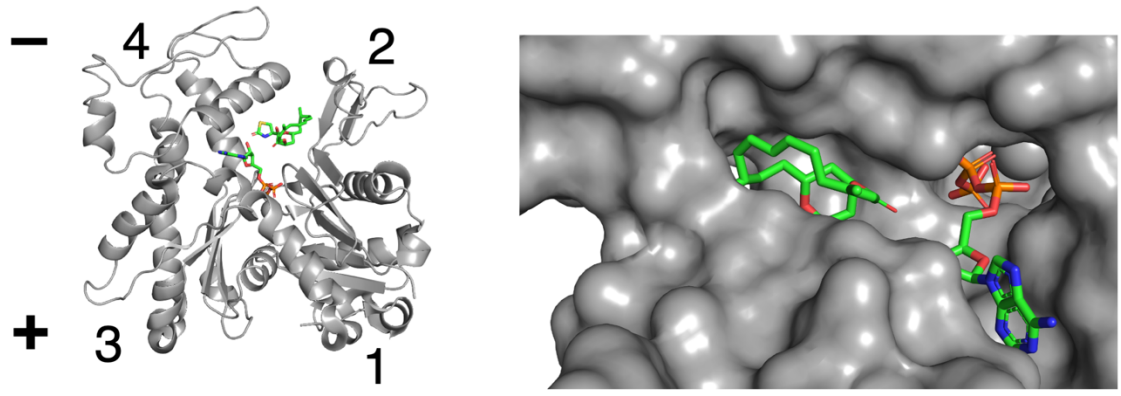

Figure 7: Binding of latrunculin A to G-actin (pdb: 1ijj).

Latrunculins A and B were first isolated from *Latrunculia Magnifica* in 1980[64] and described to lead to a breakdown of actin networks in cells[65,66]. They have since been also found in other marine sponges.[67–70] Latrunculins preferentially bind to ATP-G-actin adjacent the nucleotide binding site. The thiazolidinone and pyran moieties reach deep into the pocket and form multiple hydrogen bonds with the protein, while the macrocycle is solvent exposed and mainly undergoes hydrophobic interactions (fig. 6). Latrunculin A contains a 16 membered macrolactone with two hydrophobic conjugated double bonds, while the 14-membered macrocycle in latrunculin B is smaller. While latrunculin binding does not induce major conformational changes in G-actin, the main mechanism of action for latrunculin lies in the sequestration of actin monomers by inhibiting conformational changes that are essential for nucleation and filament elongation.[62] However, it was found that latrunculin A also binds to ADP-P_i-actin and ADP-actin, albeit with much lower affinity than ATP-actin monomers. These rare filament binding events are expected mainly at high latrunculin concentrations and can lead to filament severing. Severing by latrunculin A differs mechanistically from severing proteins, as latrunculin A promotes P_i dissociation on both uncapped filament ends ('aging') leading to increased depolymerization rates that are comparable to ADP-actin.[71]

The barbed end binding site (+ end) lies on the opposite site of the actin monomer, between subunits 1 and 3, and is bound by various macrocyclic toxins. Binding can occur from the front side, which is exposed in the filament, or the back side, which is located at the inside of the filament. Consequently, binding from the back of the barbed end can only occur in monomers or at the filament barbed end, causing either sequestration or capping. The front of the barbed end binding cleft can be accessed in F-actin, causing destabilization that can result in severing. The target binding cleft (+ end) is targeted by the cytochalasin and pectenotoxin natural product families.[60]

The cytochalasins are a large family of fungal metabolites that bear a hydrogenated isoindolone system that is fused to a macrocyclic carbocycle. Depending on the amino acid incorporation, as well as the polyketide moiety, over a hundred members can be categorized into different sub families.[72] Cytochalasin D is among the most widely used members of the natural product family, with respect to actin binding because of its high affinity for actin and because it was among the first described members of the family.[66,73]

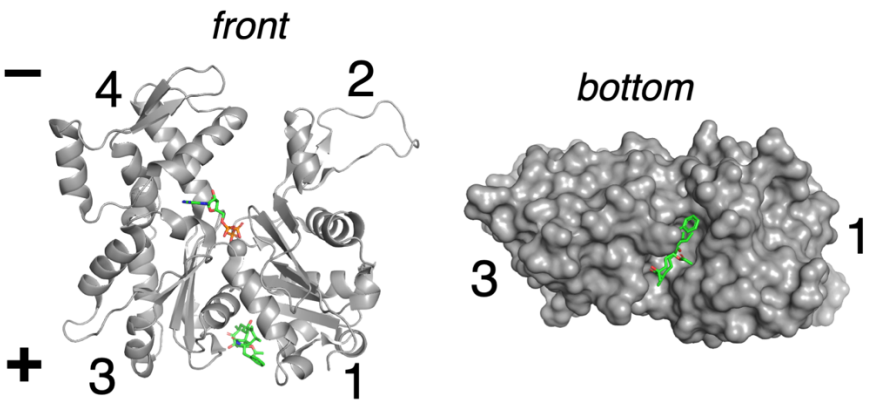

Figure 8: Cyrstal structure of Cytochalasin D bound to Ca^{2+}ATP-G-actin (pdb: 3eks).

Cytochalasin D mainly binds to the barbed end of F-actin where it has capping function. The molecule is fully inserted into the back half of the barbed end pocket with the macrocycle facing towards the back of actin (Figure 8). The reduced isoindolone core of cytochalasin builds extensive hydrogen bonds with actin while the macrocycle is mainly involved in van der Waals interactions. Binding of cytochalasin D induces a conformational change in the monomer that promotes nucleation by D-loop interactions with other G-actin molecules. This explains why polymerization rates have been observed to initially increase upon treatment, before being reduced due to the capping function of cytochalasin D.[74]

A crystal structure of pectenotoxin-2 binding to the back side of the barbed end binding cleft between subdomains 1 and 3 of G-actin (Figure 9). The macrocycle binds to a shallow groove with primarily hydrophobic interactions, while the tetrahydropyran side chain reaches into the barbed end binding pocket and builds hydrogen bonds with actin that are in part bridged by water molecules. Pectenotoxin-2 binds to the back face of the barbed end binding site between subdomains 1 and 3 and depolymerizes actin by sequestering monomers and capping the barbed end binding site of F-actin.[75]

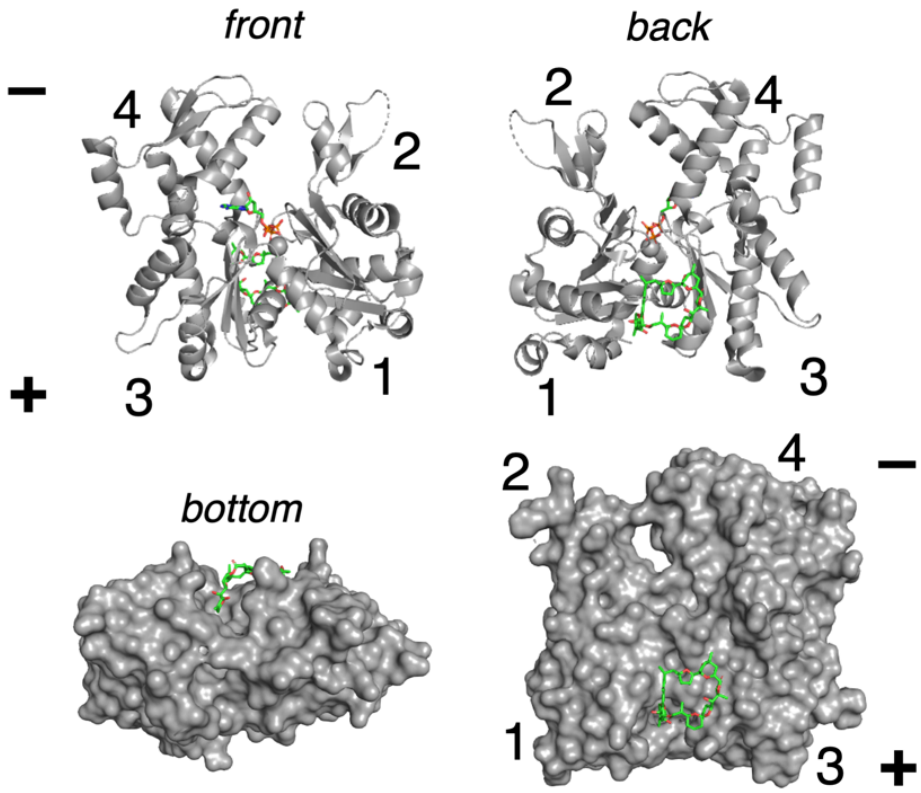

Figure 9: X-ray structure of the Ca^{2+}ATP-G-actin-pectenotoxin 2 complex (pdb: 2q0r).

The barbed end binding cleft is important for filament capping interactions of actin with small molecule toxins. The previously discussed pectenotoxins and cytochalasins target the barbed end binding cleft from the back of the subunit. In the filament, the back of the barbed end binding cleft is occluded and can therefore not be targeted. The hydrophobic region to the front of the barbed end binding cleft is however located to the outside of the filament.[1] Macrocyclic marine toxins like the trisoxazole family and related natural products, as well as bistramide A, can target the binding site between two lateral protomers in F-actin and cause severing.[60]

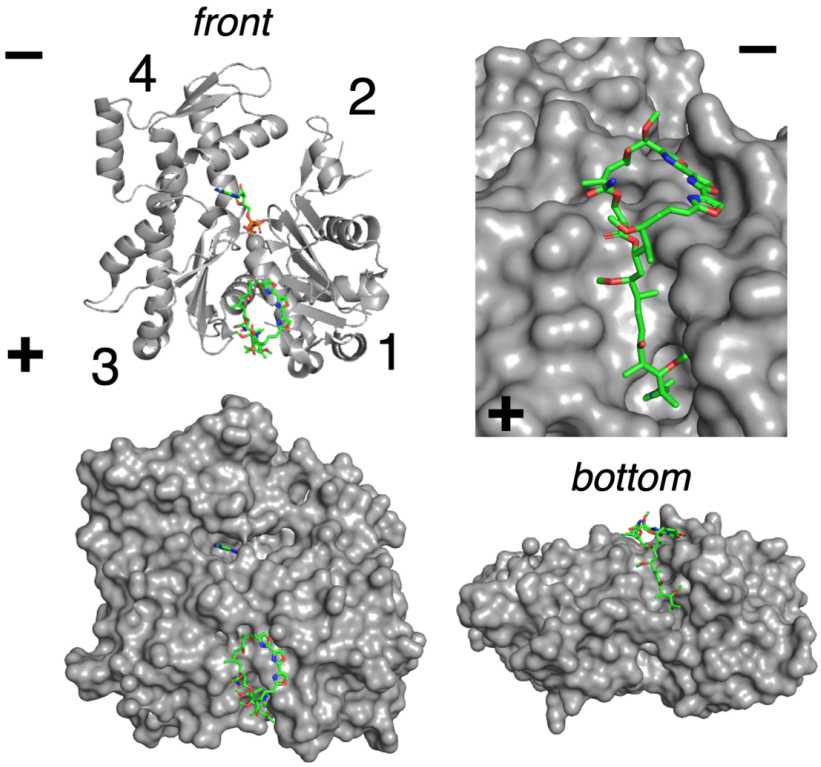

Figure 10: Xray of kabiramide C bound to actin (pdb: 1qz5).

Trisoxazole natural products such as kabiramide C[j], as well as reidispongiolide A[k] and their relatives contain a large hydrophobic macrocycle and a long side chain that terminates in an *N*-methyl vinylformamide.[76–80] Kabiramide C binds at the same binding site as actin capping protein and gelsolin and mimics the function of these ABPs in their capping and severing function, as well as blocking nucleotide exchange (Figure 10). It was demonstrated that kabiramide C binds in a two-step sequence: first, a fast hydrophobic binding of the macrocycle on the front of the barbed end cleft which is exposed in F-actin is established. In a second step, the side-chain of the natural product is inserted into the barbed end cleft between subdomains 1 and 3. This is the protein site in which protomers are stabilized by lateral interactions between the D-loop and barbed end cleft of two adjacent subdomains. The competition of kabiramide C with this interaction leads to a filament severing. Kabiramide C remains bound to the + end of the severed filament.[57,58] The interaction of the side chain of kabiramide C with actin has been compared to the WH2 binding domain in actin severing proteins.[57,58]

[j] Further members of the natural product family include e.g.: mycalolide A, jaspisamide A, halichondramide, halishigamide A, mycalolide B, ulapualides A and B.

[k] Related natural products e.g.: sphinxolide natural products, tolytoxin, scytophycin C, aplyronine A, misakinolide A, rhizoporin.

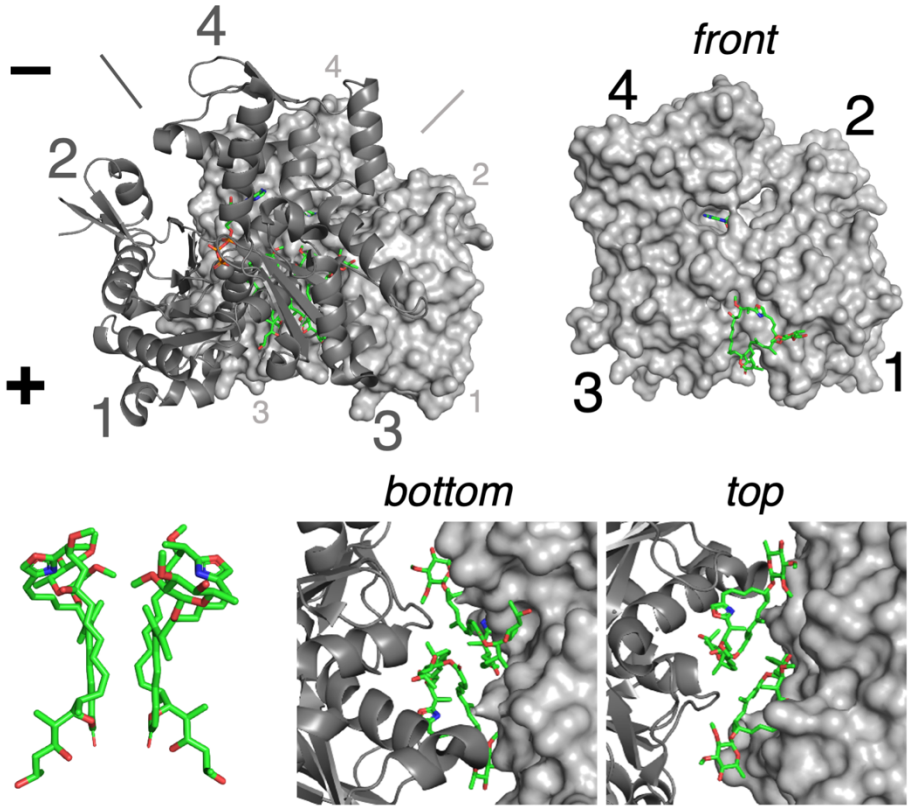

Figure 11: Crystal structure of chivosazole A bound G-actin and dimerization of the complex. (pdb: 6qri).

The chivosazoles are a distinct class of actin targeting macrolides from the myxobacterium *Sorangium cellulosum.*[81] Chivosazole F is the aglycan while chivosazole A is a glycoside of 6-deoxyglucose. The chivosazoles destabilize actin and induce depolymerization of actin filaments.[81–83] Chivosazole A binds to the front of the barbed end of the actin subunit and inserts its side chain into the front of the cleft between subdomains 1 and 3 (Figure 11). While this is a binding region that is occupied by various other actin targeting macrolides, the binding of chivosazole is distinct because it only competes in with the lateral actin protomer interaction slightly and induces an allosteric conformational change that leads to the destabilization of F-actin.[84] Chivosazole sequesters monomers, inhibits their nucleation and disfavors polymerization of actin. Interestingly, size-exclusion chromatography showed dimerization of actin - Chivosazole A complexes. This was confirmed by X-ray analysis that shows that this dimerization results from interactions between two chivosazole molecules (Figure 11).[84]

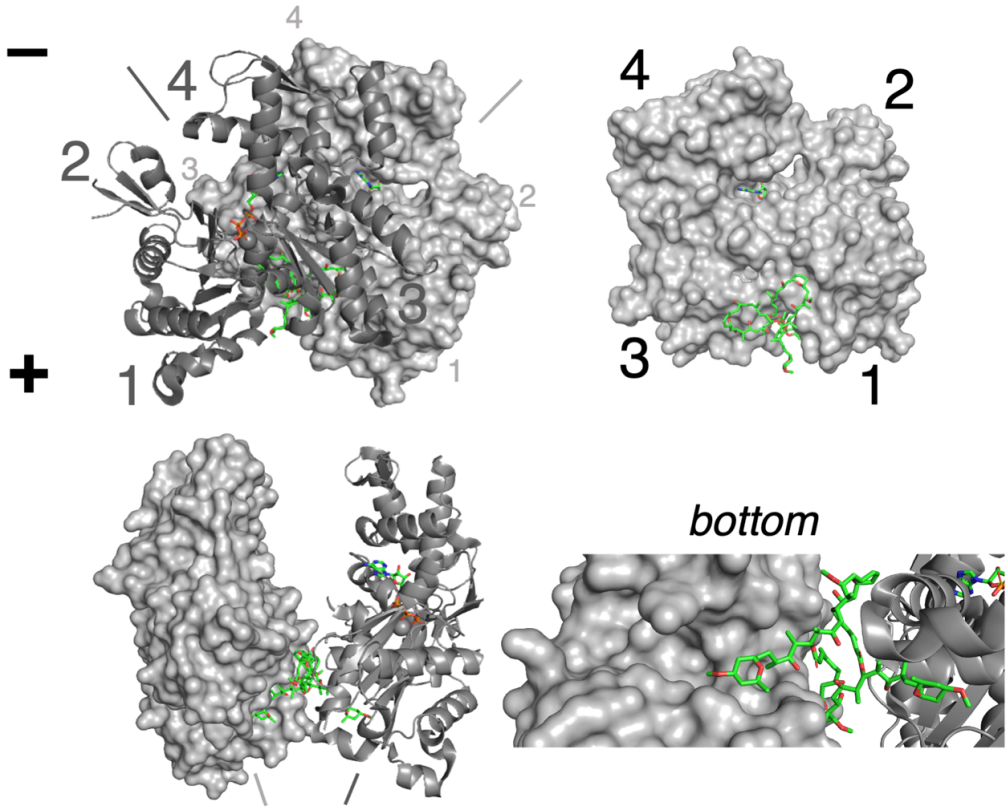

Figure 12: Crystal Structure of Swinholide A (pdb: 1yxq).

Swinholide A[I] severs actin filaments similar to the trisoxazole natural products by destabilization of the lateral actin stabilization in the barbed end binding cleft. Swinholide A is a dimeric macrolide and can bind two actin monomers simultaneously (Figure 12). Therefore it sequesters actin dimers, in addition to filament severing.[85,86] The actin monomers face each other with the front side of the monomer and both monomers are twisted and tilted with respect to each other (see the axes relative to each other indicated in figure 12). The side chain of swinholide A is inserted into the first half of the barbed end cleft from the front side and the actin subunits do not show any interactions with each other. This dimer has thus no physiological activity.[59]

[I] Closely related: Bistheonellide A

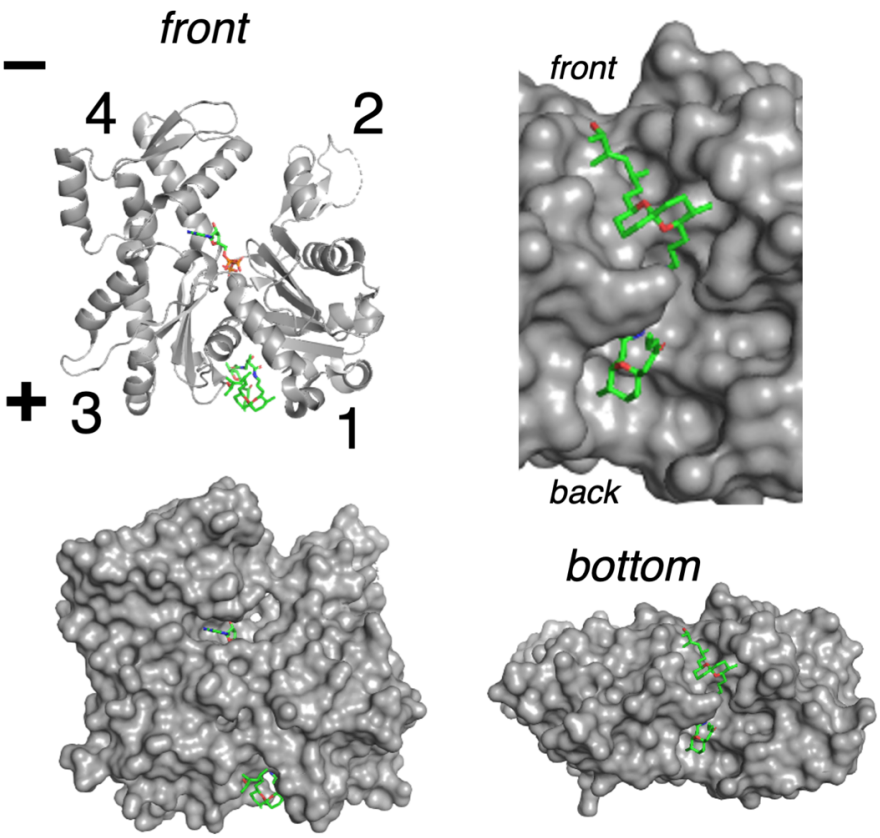

Figure 13: Crystal structure of bistramide A (pdb: 2fxu).

Bistramide A is a marine toxin and binds to actin by inserting into the barbed end binding cleft.[87] Bistramide A spans the whole length of the cleft between subdomains 1 and 3 and thereby severs and sequesters actin filaments (Figure 13).[88,89] The sequestration of G-actin is further amplified by the formation of a covalent bond between bistramide A and G-actin *via* a Michael addition of Cys374 to the terminal enone. It was also argued that this covalent bond formation is responsible for the increased toxicity of bistramide A compared to other marine toxins.[87,90] Bistramide A and its synthetic analogues have been investigated as potential anticancer agents.[89]

1.2.2 Small Molecule Actin Stabilizers

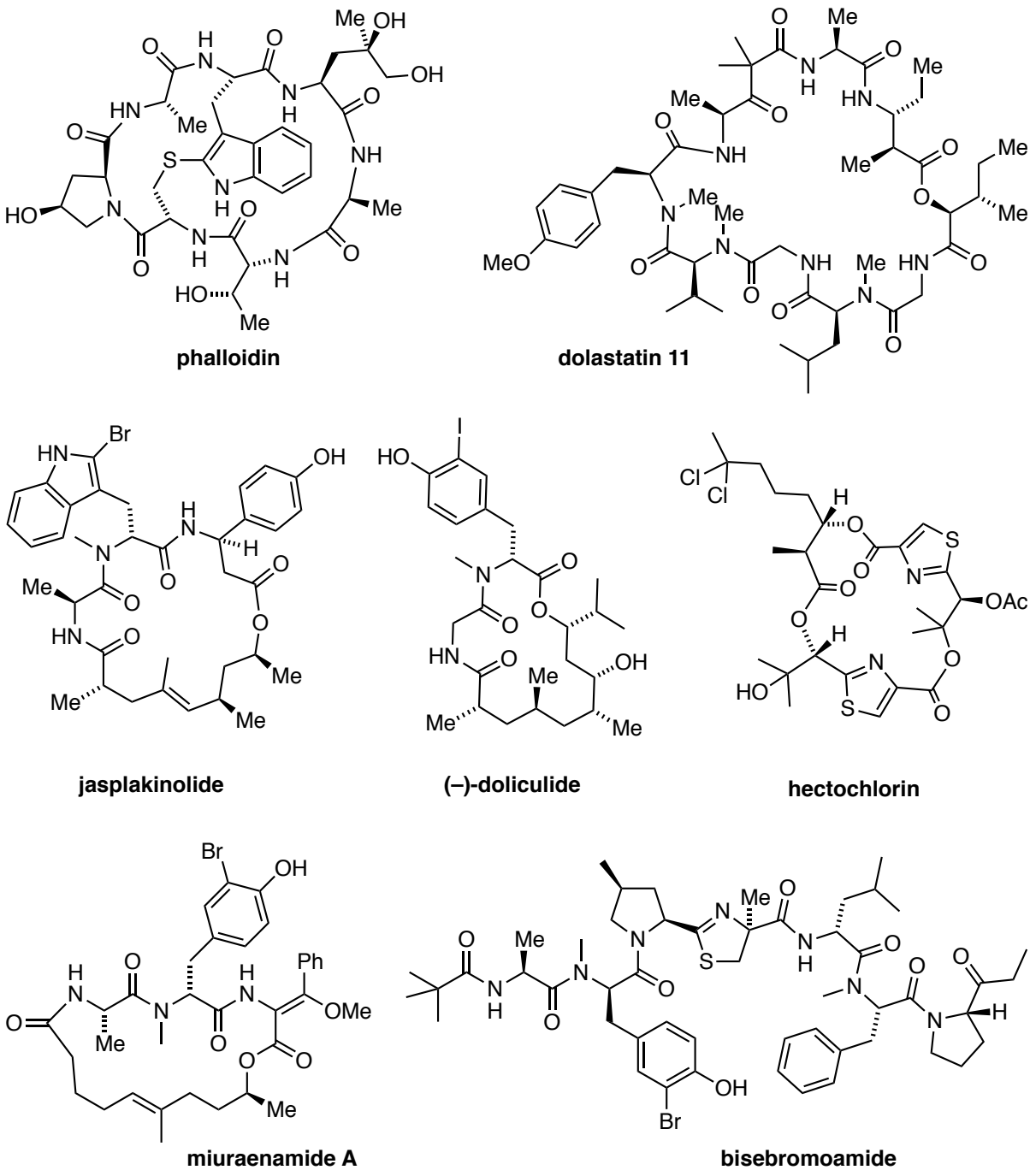

Figure 14: Actin filament stabilizers.

While actin destabilization through sequestration, capping and severing is caused by binding to the nucleotide or barbed end binding sites, F-actin can be stabilized by small molecules that bind at the transversal intersection of three actin subunits (Figure 14).[60] The established contacts between the molecule and F-actin influence conformational changes of the D-loop

that are important to filament ageing, thereby delaying this process.[91] Stabilization of actin filaments in networks with fast turnover primarily leads to the inhibition of depolymerization and over extended periods of time, to hyperpolarization of actin networks. The binding of small molecule stabilizers can also induce polymerization by preforming nucleates.[92]

Many small molecule families are known to stabilize actin filaments with distinct binding modes. In this chapter, the most important actin stabilizing natural products families and their binding sites will be described.

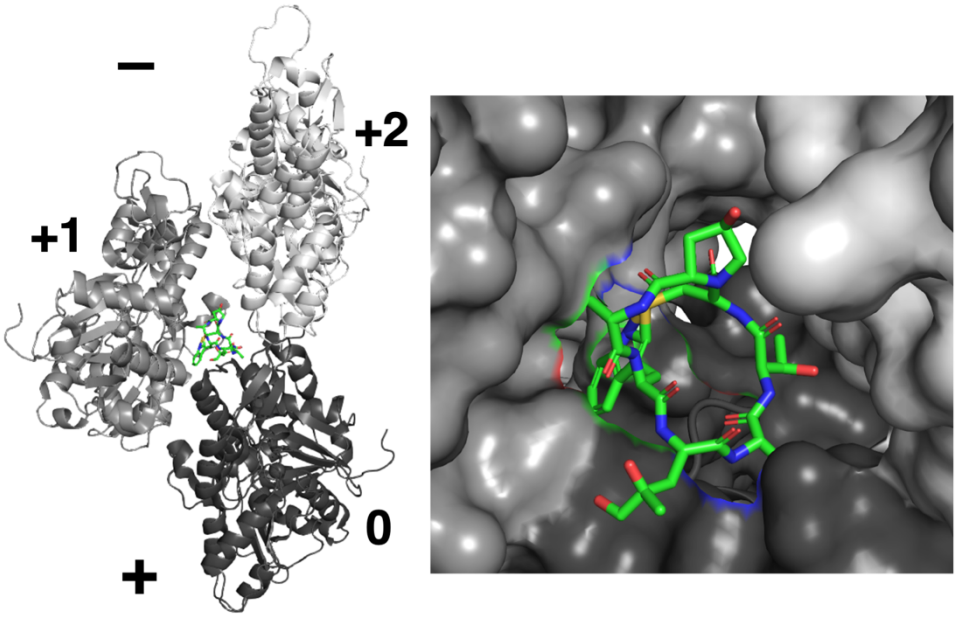

Figure 15: Crystal structure of Phalloidin bound F-actin (pdb: 6c1d).

Phalloidin[m] is a bicyclic heptapeptide and the first known actin stabilizer. It was first isolated from *Amanita phalloides* (death cap mushroom) in 1938.[93,94] The toxicity of the death cap mushroom is not attributed to phalloidin itself due to its poor membrane permeability, but rather to the closely related and permeable amatoxins.[94–96] Phalloidin is a non covalent F-actin stabilizer and binds at the intersection of three F-actin subunits, inducing actin polymerization by nucleation and filament stabilization (Figure 15). The main hydrophobic and hydrogen bonding interaction between phalloidin and F-actin are between two transversal subunits (0, +1) and minor hydrophobic interactions are detected to the third subunit (+2).[97] Phalloidin binding delays the release of phosphate, which is an essential step towards the destabilization of F-actin in regular turnover. Phalloidin can bind to both, open and closed D-loop conformations and binding does not significantly alter the overall filament conformation, but rather inhibits conformational changes that would induce destabilization of F-actin.[21,91,92]

[m] Closely related: phallotoxins, amanatoxins, virotoxins.

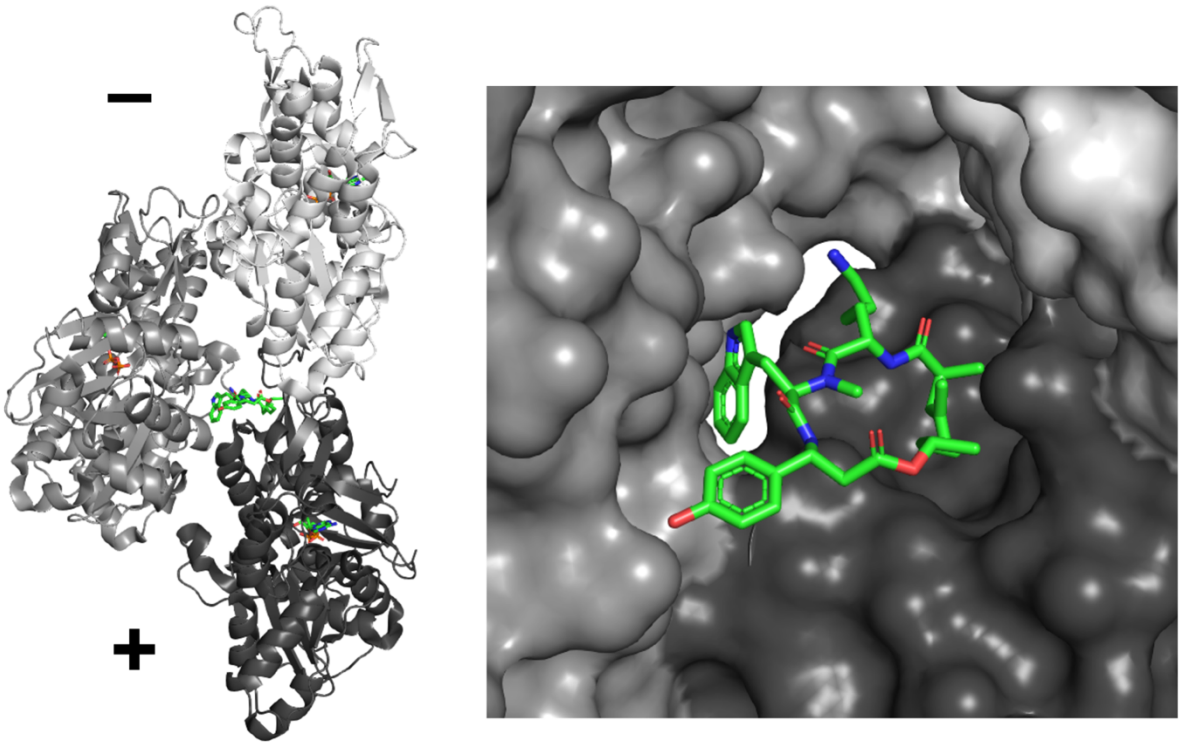

Figure 16: X-ray structure of jasplakinolide bound to F-actin (pdb: 5ood).

The marine depsipeptide jasplakinolide (also called jaspamide)[n] is a 19 membered macrocycle of amino acid and terpenoid origin and it was first isolated from the marine sponge *Jaspis johnstoni*.[98,99] It binds to the same binding site as phalloidin and has overall very similar effects on actin (Figure 16). Both toxins delay aging of F-actin (and P_i release), however, jasplakinolide has been reported to bind actin more efficiently than phalloidin.[92,100] It has been demonstrated, that jasplakinolide can also bind to the open and closed D-loop conformations but in contrast to phalloidin, jasplakinolide binding was found to increase the affinity of F-actin to P_i, suggesting a different functional mechanism for jasplakinolide than for phalloidin. The elucidation of the exact mechanisms of action for phalloidin and jasplakinolide and how their binding affects actin-ABP interactions are a field of active investigation.[92]

Jasplakinolide and the closely related Chondramaides have been subject to extensive structure-activity relationship studies[101,102] and full synthetic approaches[103–109]. These studies have led to a deepened understanding of functional and structural properties of the natural product and were further the basis for the development of jasplakinolide derived tools for live-cell imaging[110,111] and the optical control of F-actin[112].

[n] Closely related structures: seragamide A, chondramide, geodiamolide, neosiphoniamolide.

(–)-Doliculide is a marine 16 membered macrocyclic depsipeptide[113] that shows hyperpolarization effects on actin that are comparable to jasplakinolide. The binding site of (–)-doliculide was determined by competition experiments in which fluorescent phalloidin was replaced by (–)-doliculide binding.[114,115] No X-ray or cryoEM structure of (–)-doliculide binding to actin has been published to date[o].

The miuraenamides are cyclic depsipeptides that are structurally and functionally closely related to jasplakinolide and chondramide natural products.[116–118] Miuraenamide A effects filament stabilization by stabilization of early stage oligomers that are formed during nucleation, as well as delaying filament depolymerization. The binding site of miuraenamides was predicted to be different, albeit very close, to the phalloidin binding site and either influence phalloidin binding directly or through allosteric effects.[63] Miuraenamide A induces a conformational change that leads to an increase in interactions between the D-loop and barbed end of protomers. This stabilization was shown to selectively interfere with cofilin binding. Jasplakinolide did not show this effect.[63]

While the linear polypeptides dolostatin 10 and 15 target tubulin[119,119], the 30 membered macrocycle dolostatin 11 selectively targets actin. Competition assays with fluorescent phalloidin revealed that dolostatin 11 does not bind to the phalloidin binding site of F-actin despite inducing actin polymerization similar to jasplakinolide.[114]

Bisebromoamide[120] is a linear polypeptide that targets F-actin and leads to filament disruption and aggregation. Bisebromoamide is known to target several signaling pathways that play a role in cancer angiogenesis and tumor formation and progression. Its exact mechanism of action remains to be further elucidated.[118,121]

Hectochlorin is a cyclic lipopeptide closely related to dolabellin and lyngbyabellins.[122] Hectochlorin showed strong antiproliferative activity at similar concentrations as jasplakinolide. It was shown that hectochlorin targets actin and induces actin assembly. The mechanism is however distinct from jasplakinolide mediated filament assembly as overall thicker filament bundles are observed rather than a higher number of filaments, which is observed with other stabilizing natural products. Furthermore, hectochlorin was found to not bind to the phalloidin binding cleft.[123]

[o] June 2021.

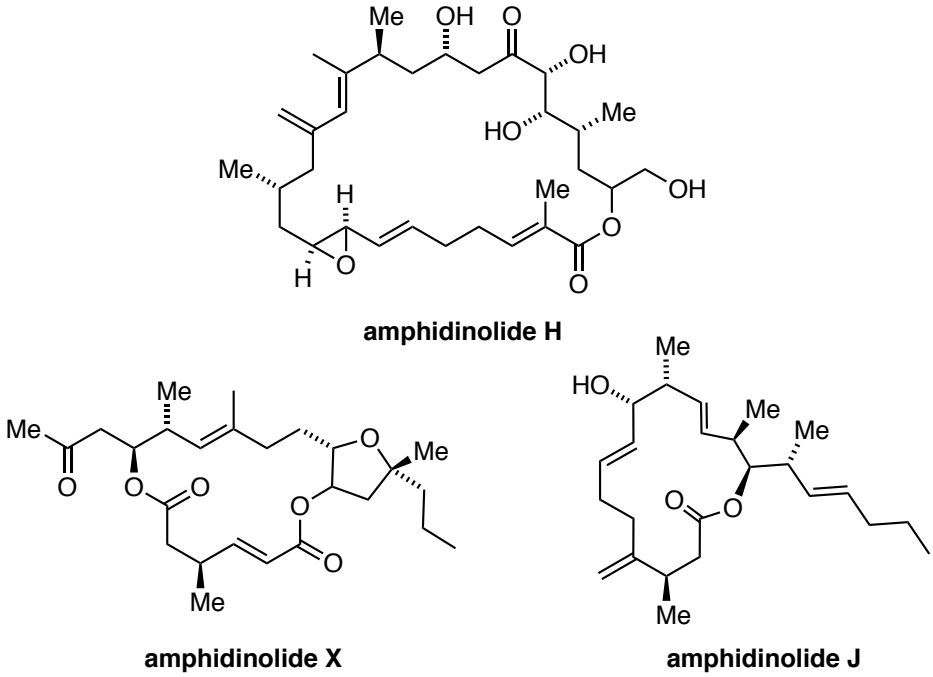

Figure 17: Amphidinolide natural products.

The amphidinolide natural products are macrolides from the dinoflagellate *Amphidinium* and have received attention for their diverse structural and biological properties. Especially amphidinolides H, X and J have been found to be potent modulators of the actin cytoskeleton (Figure 17).[124]

Amphidinolide H is a 27 membered macrolide covalently binds to actin and stabilizes its filaments. Amphidinolide H binds actin at subdomain 4. It is expected that the covalent binding of Amphidinolide H by Tyr200 on actin is filament specific because the binding loop is exposed through conformational changes during actin polymerization.[125] Amphidinolides X and J are structurally related to amphidinolide H but smaller in size and do not possess a functional group that can engage in covalent bond formation. Amphidinolides X and J were found to destabilize actin networks and their predicted binding site on the barbed end of actin, is similar to cytochalasin. These predictions were made based on *in silico* simulations and phenotype analysis on fixed cells. [126]

1.2.3 Synthetic Small Molecule Modulators of Actin Binding Proteins

The interplay of numerous actin binding proteins and their partly overlapping functions has motivated efforts for the identification of small molecule inhibitors of specific isoforms of ABPs to elucidate on how they regulate actin. Some small molecule inhibitors were identified from screening of chemical libraries against a specific ABP isoform *in vitro*. In some cases, polypharmacology limited the applicability of de-novo inhibitors *in vivo* and complicated the interpretation of experimental results. Notable examples are discussed.

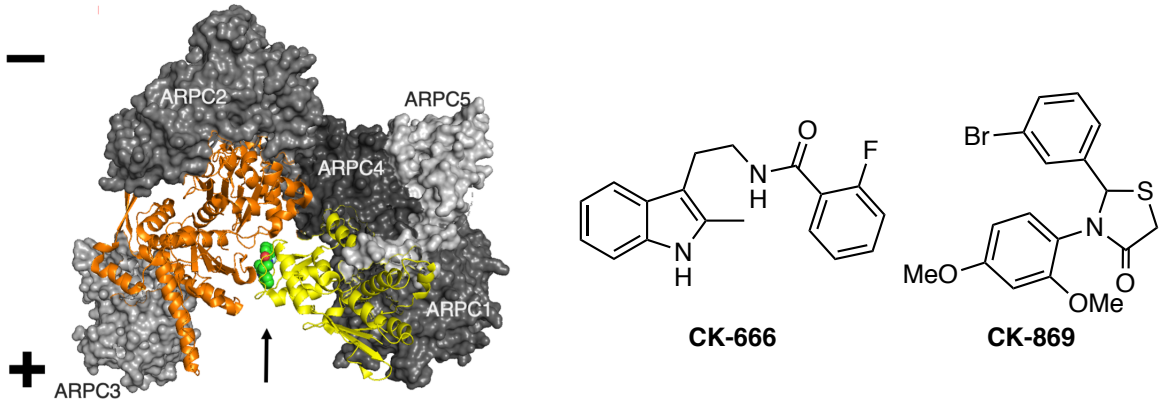

Figure 18: Arp2/3 inhibitors derived from small molecule library screen and x-ray structure of CK-666 bound to the Arp2/3 complex: orange Arp3, yellow Arp2, greys: ARPC1-5, minus indicates pointed end of a branch when Arp2/3 induced on the mother filament, plus indicates the direction of filament elongation if a Arp2/3 branch is formed (pdb:3ukr).

The Arp2/3 complex is an important regulator of cell migration. In order to more closely study Arp2/3 dependent processes like cancer cell migration and the actin comet tail driven motility of *Listeria monocytogens*, small molecule inhibitors of Arp2/3 were developed from an initial library screen.[127] CK-666 binds at the interface of Arp2 and Arp3 and forms close interactions with both subunits (Figure 18).[128] CK-869 is structurally distinct from CK-666 and binds to an allosteric site of Arp3 (pdb: 3uku, not shown). While CK-666 is active across species, CK-869 is an inhibitor of bovine and human Arp2/3.[127] Both small molecule inhibitors disturb the dynamic changes in the Arp2/3 complex that lead to filament branching. CK666 functions by blocking the conformational change that is necessary to induce nucleation and filament branching while CK869 allosterically destabilizes the Arp2 and Arp3 dimer interactions.[129] So far, off-target effects have only been reported for CK869.[130,131]

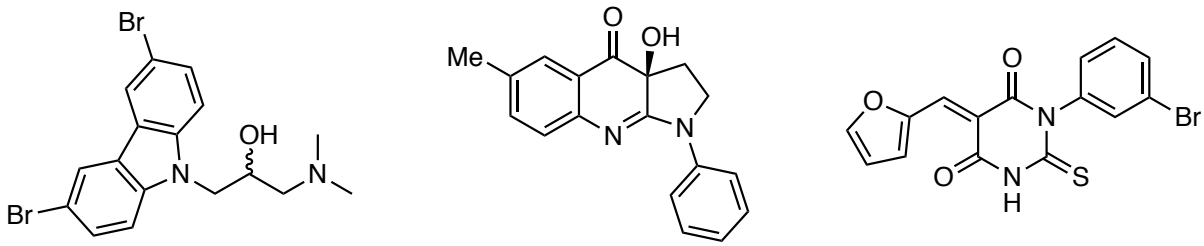

(±)-wiskostatin **(–)-blebbistatin** **SMIFH2**

Figure 19: Actin regulator targeting small molecules wiskostatin, blebbistatin and SMIFH2.

WASP is a nucleation promoting factor that activates the Arp2/3 complex. The small molecule wiskostatin was identified as a selective inhibitor of neural Wiskott-Aldrich Syndrome Protein (N-WASP) by library screen and evaluation *in vitro*.[132] Wiskostatin is sometimes used in cellular studies, however those studies require careful control experiments because it was shown that wiskostatin can lead to strong adverse effects that are ascribed to dose-dependent ATP reduction.[133,134]

Actin-myosin II interactions drive contractile processes that are essential in muscle contraction, cell migration and cytokinesis.[135] Myosin II can be inhibited by (–)-blebbistatin, which was originally identified as a highly selective inhibitor of skeletal and nonmuscle myosin II from a high-throughput screen.[136,137] (–)-Blebbistatin binds myosin II allosterically and blocks nucleotide exchange.[138–141] Interestingly, (–)-Blebbistatin is photoreactive and has an absorption maximum at 430 nm. The photochemical decomposition products themselves are not cytotoxic because the hydroxy group that builds essential hydrogen bonds with the protein is photochemically cleaved and furnishes the cytotoxic hydroxy radical. It therefore has to be used cautiously in live-cell imaging applications.[140,142,143] Blebbistatin is considered as a photosensitizer for photodynamic therapy applications.[143–145]

Formin is an actin nucleator that remains attached to the barbed end of a filament and catalyzes elongation (Chapter 1.1.2). Formins can form filament bundles and are important for filopodia formation. SMIFH2 is a small molecule inhibitor that targets the FH2 domain in formins. It was identified by library screen and inhibits formin dependent processes across species.[146] SMIFH2 has been used in a broad range of biological investigations to elucidate formin dependent processes.[147] Synthetic studies towards isoform specific formin inhibitors are underway and benefit from the synthetic accessibility of SMIFH2 analogs.[148] The small molecule formin inhibitor has been found to cause downregulation of p53 activity and inhibition of myosins, especially upon prolonged incubation times and high concentrations. This requires a cautious application of SMIFH2 as a selective formin inhibitor, calls for extensive control

studies and careful interpretation of experimental findings.[147,149] Further optimization of the inhibitor's specificity towards formins and its isoforms is needed to make SMIFH2 a reliable tool for cell biology.[146,148]

Other actin binding and regulating proteins have been targeted by small molecule modulators. Other examples were mainly aimed at identifying means to elucidate and target functions that are important in cancer growth and progression. They are discussed in the next chapter.

1.3 Actin as a Therapeutic Target

The cytoskeleton has been a target in anti-cancer therapy for decades. Tubulin targeting small molecules, such as colchicine, taxol, vinblastine, and their derivatives have found broad application as chemotherapeutic agents. Their high success in limiting the growth of and reducing the size of carcinogenic tissue is based on the disruption of mitosis and induction of apoptosis. Microtubule targeting anti-cancer agents are unfortunately accompanied by severe side effects as well as the development of resistance that demands for the development of improved novel strategies in the fight against cancer.[150–152]

Actin is involved in many different signaling cascades and plays crucial roles in all eukaryotic cells. Malignant cells present with a change in morphology, cell proliferation and migration compared to healthy cells. For the involvement of Actin in all of these processes, actin and its regulatory functions have been investigated as a pharmacological target.[153–156]

Overall, the anti-cancer effects of actin binding small molecules have been attributed to the unspecific disruption of actin homeostasis. This includes healthy tissues that depend on functioning actin dynamics. The broad targeting of actin by jasplakinolide, latrunculin or dolostatin 12 has been accompanied by strong adverse effects and cardio toxicity in mammals.[157,158] Actin has not been established as a primary target in clinical applications because of these liabilities. It is unclear whether the severe adverse effects are a result of general actin disturbance, or if they are linked to the regiospecific binding of the structures.[114] The high general toxicity of unselectively impairing the actin cytoskeleton and in addition the limited availability of actin targeting drugs from natural sources suggest that alternative strategies that specifically target distinct actin functionalities would be beneficial.[159–161] To this end, different strategies have been investigated that use low concentrations of actin binders in cotreatment with other drugs, develop analogs of natural products that are synthetically accessible and the indirect targeting of specific actin subfunctions through actin binding

proteins. An example for the symbiotic application of actin binders is the suppression of actin-dependent repair mechanisms of doxorubicin-induced DNA damage by sub-toxic concentrations of actin binders. In this study, latrunculin B was used to enhance doxorubicin treatment *in vivo*, without showing the previously reported adverse effects.[162]

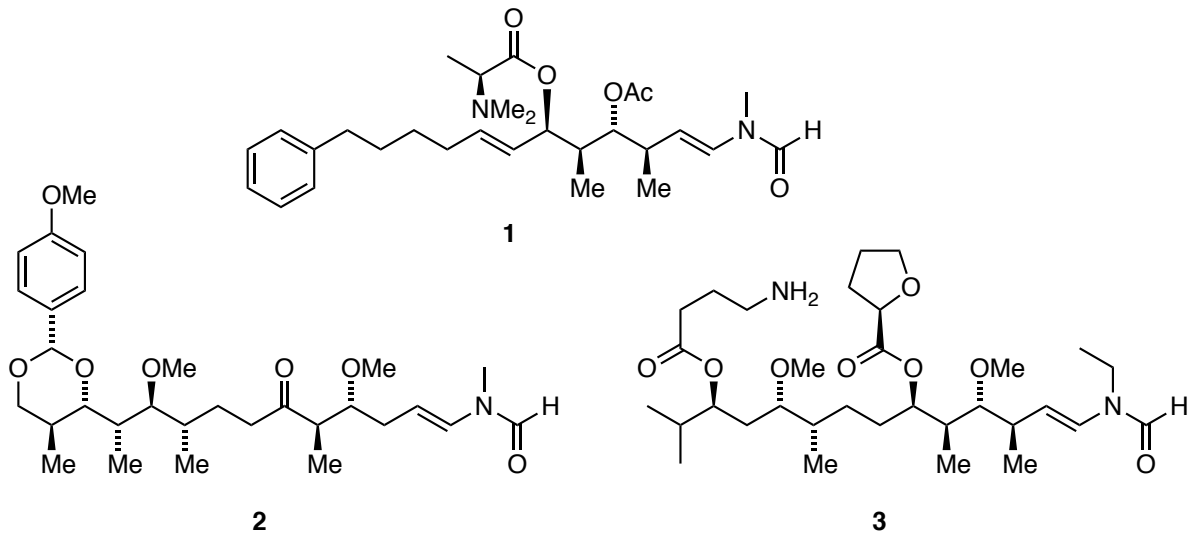

Figure 20: Synthetic analogs of the kabiramide C and related natural products.

The binding mechanism of actin severin macrolides like kabiramide C, reisospongiolide A, aplyronine A and mycalolide B indicates that their tail alone can destabilize actin filaments. Actin disruption was achieved with synthetically accessible analogs **1**-**3** of the natural product tail (Figure 20). The active molecules are comparable in size to the tail moiety of the natural products. Shorter fragments were less effective at disturbing protomer interactions. Notably, the bioactivity of the underlying natural products was unmet by synthetic analogs, as they are lacking the macrocyclic structure that is important for initial protein binding.[159,163,164]

A different strategy involves the selective direct targeting of ABPs. The development of small molecule inhibitors of formins and myosin II was not explored for therapeutics and was therefore discussed in the previous chapter. Other ABPs like tropomyosins, CapZβ as well as cofilin and profilin inhibitors were investigated as potential anticancer targets and will be discussed next.

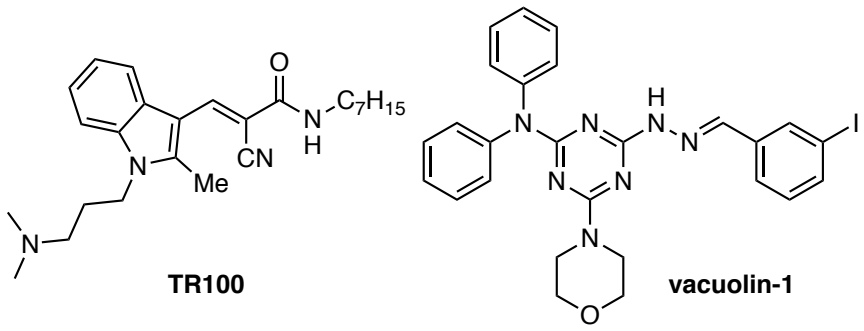

Figure 21: Chemical structures of TR100 and vacuolin-1.

Under the regulation of complex pathways, tropomyosins divide actin into networks of distinct functions.[27,160,165,166] In cancer, the tropomyosin profile is generally shifted towards lower molecular weight (LMW) isoforms. TR100 (Figure 21) is a selective inhibitor of LMW tropomyosin Tm5NM1/2 (=Tpm3.1)[167] and showed strong dose-dependent antitumor activity by the destabilization of F-actin in melanoma and glioblastoma mouse models. Tm5NM1/2 expression levels were reduced while cardiac and liver health remained unaffected.[168] The detailed mechanistic function of TR100 is still under investigation.[169]

Vacuolin-1 is an effective inhibitor of autophagy and endosomal trafficking.[170–173] It efficiently reduces cancer migration and invasion via integrin pathways by binding to actin capping protein CapZβ, which is important in the early to late endosome transition. This example highlights the involvement of ABPs in different interconnected pathways. The detailed mechanistic function of CapZβ in this process remains to be elucidated.[174]

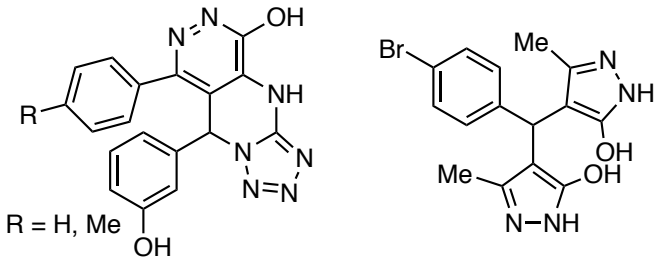

4 **5**

Profilin serves as a means of the cell to regulate actin polymerization through cellular signaling.[175] Recently, the first class of inhibitors (**4**,**5**) of the protein-protein interaction of profilin and actin have been described.[176] Profilin-1 was found to be overexpressed in clear-cell renal cell carcinoma (ccRCC) and associated with the cancer's aggressiveness and poor patient outcomes. Inhibitors derived from **4** reduced ccRCC progression and invasion in

subcutaneous tumors in mice.[177] Irregular angiogenesis is an underlying factor of proliferative diabetic retinopathy and related diseases. **5** showed promise in taming profilin overexpression in angiogenesis-dependent retinal diseases.[178] It should be mentioned that although profilin and cofilin misregulation is linked to aggressive cancer progression, both ABPs are involved in and regulated by many signalling pathways and their complex roles and functions.[179] Attempts to target cofilin have been reported but are still very early in development.[180,180,181] Thus although initial results are promising they require further thorough investigation.

Apart from the mentioned strategies, a promising approach could be the use of locally confined actin or ABP binding drugs, for example by local release or activation. Nanoparticle encapsulation methods or photopharmacological approaches where an actin targeting drug is selectively activated or released in a confined area would be promising approaches. An advantage of photopharmacology would be the possibility of photochemical deactivation outside the target region.[182–184]

1.4 Tools for Actin

While therapeutic targeting of actin has been considered unfeasible due to high general toxicity, many tools for the investigation of actin structure and function have been developed. These approaches are often based on natural products and derivatives thereof. Complementory to small molecules, other methods are based on actin binding proteins (ABPs) and include genetic and optogenetic engineering.[185,186]

1.4.1 Visualization of Actin

A general and common method to visualize proteins are protein-specific antibodies that stem from a species (primary antibody) that can then be selectively bound by fluorophore conjugates of species-selective antibodies (secondary antibody).[187] In some cases, direct immunofluorescence, in which an antibody is coupled to a fluorophore is a convenient choice due to a simplified work flow. With indirect staining methods, secondary antibodies can increase the fluorescence signal and therefore the sensitivity of the sample. Non-selective antibody binding in the staining sample, however can lead to increased background. Immunofluorescence allows for a flexible combination of fluorophores and antibodies in the same sample.

A widely distributed and highly convenient tool for the staining of F-actin in cells and tissue are phalloidin fluorophore conjugates that bind F-actin with high selectivity (Figure 22).[188–190]

Phalloidin is not sufficiently cell permeable. For its fluorophore conjugates to be an effective tool, cells must be permeabilized (e.g. in fixed samples) or the fluorophore conjugate must be microinjected into living cells.[191,192] Jasplakinolide and Chondramide derived fluorophore conjugates overcome the necessity of permeabilization because the underlying natural products are membrane permeable.[111] Especially SiR-actin, which allows for super-resolution imaging of F-actin in live-cells (Figure 22).[110,193,194] It is important to consider SiR-actin dosing when imaging live-cells to maintain endogenous actin dynamics and avoid adverse effects. Interestingly, phalloidin and jasplakinolide fluorophore conjugates stabilize different conformations of the D-loop and hence have a preference for slightly different actin states. While phalloidin binding induces a closed D-loop structure, jasplakinolide binding results in the open conformation. Hence phalloidin staining is biased for ADP-actin and jasplakinolide for ADP-Pi respectively.[91]

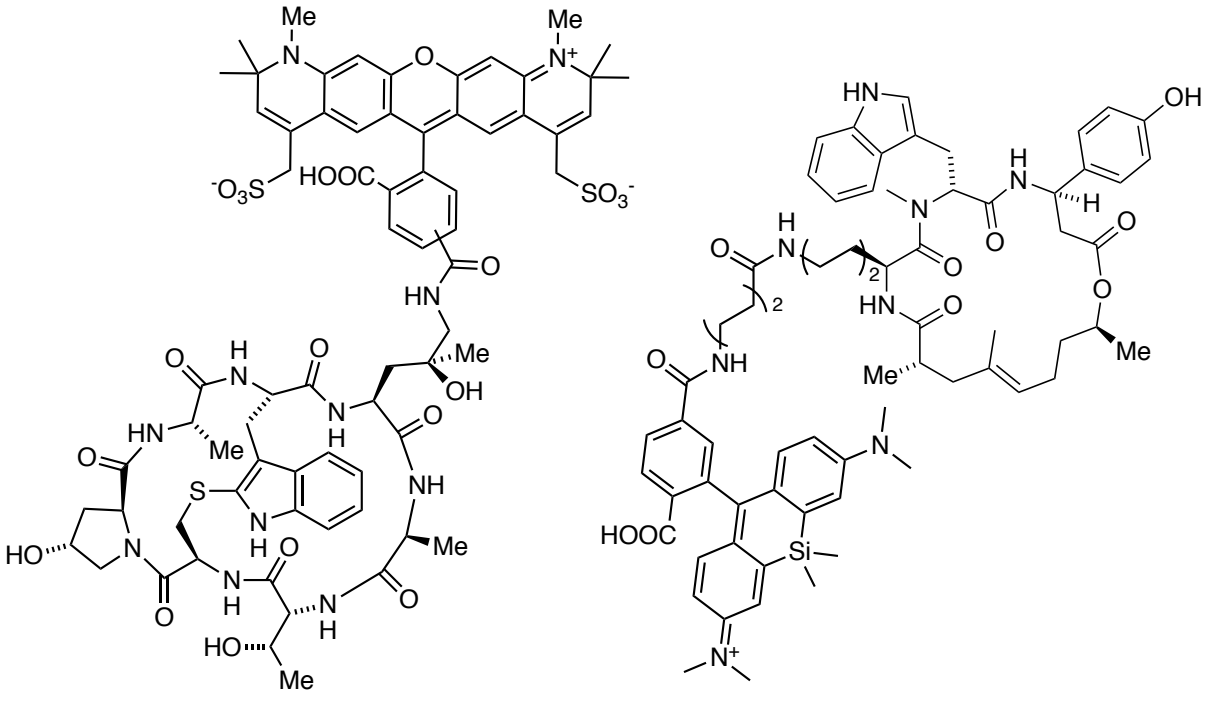

AlexaFluor 594 Phalloidin **SiR-actin**

Figure 22: Natural product fluorophore conjugates for the visualization of actin filaments in cells.[195]

The stable expression of fluorescently labelled proteins such as LifeAct, F-tractin, utropin-derived UTrCH or GTP-actin in cells is possible for experiments requiring long term visualization. These tools are based on proteins that are important to the regulation of actin dynamics. Therefore a bias towards particular F-actin actin structures exist which will be

represented more prominently than others. This can lead to misinterpretation of the observed effects. Additionally, the fluorophore size must be considered. For example, in the case of GFP-actin the large size of GFP relative to actin is known to lead to an irregular incorporation of GFP-actin in actin structures. Furthermore. the careful control of the expression levels of modified proteins is essential to maintain unaltered actin dynamics of the actin network.[192,196,197]

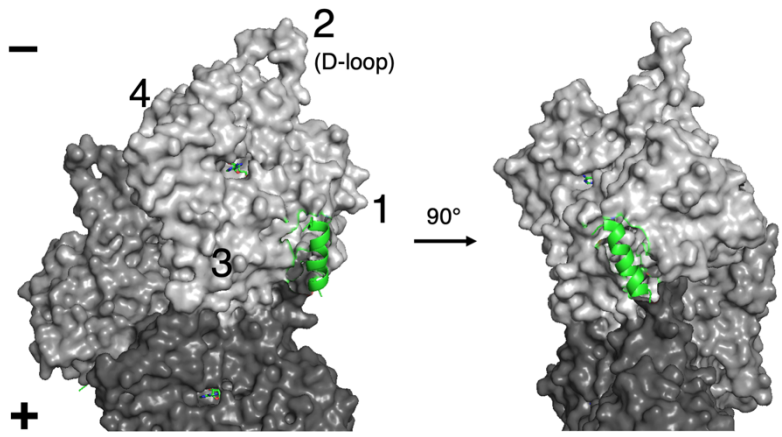

Figure 23: Cryo-EM structure of LifeAct bound to F-actin.

LifeAct is a 17 amino acid polypeptide that was derived from actin binding protein 140, which is conserved in *Saccharomyces cerevisiae* and its close relatives. Tagged to fluorescent protein, LifeAct can be used in low concentrations or controlled expression levels respectively to visualize F-actin across organisms, in plants, fungi and human cell lines.[196,198] Its relatively small molecular structure makes it easily accessible and it can be used to make fusion structures with peptides or chemically active compounds to investigate actin networks.[198] LifeAct binds to G-actin as well as F-actin. However, its binding affinity to the filament is higher as more hydrophobic interactions between LifeAct and F-actin can be established. LifeAct binds ADP-actin (closed D-loop) with a 3-4 fold preference over ADP-Pi actin. The recent elucidation of the LifeAct actin structure by cryo EM allows for further optimization of the tool (Figure 23).[91]

While a variety of complementary methods for the labelling of F-actin exist, the labelling of G-actin is more difficult as an ideal fluorescent tag should not interefere with the regulation of the native protein. As mentioned above, the expression of fluorescent G-actin alternates the functional incorporation of GFP- actin into certain networks. Additionally, the well established

G-actin binding domains are important in the control of actin polymerization (see chapter 1.1.2). DNase I regulates actin networks by binding to the flexible loop in subdomain 2.[199,200] Fluorescent conjugates of DNase I have been used for the visualization of G-actin levels in cells.[201,202]

1.4.2 Photopharmacology of Actin

The wide interest in controlling actin dynamics in live-cells has not been overlooked by photopharmacology. Briefly, photopharmacology describes the equipment of a bioactive small molecule or protein with a photosensitive chemical cage or switch (e.g. an azobenzene, diazocine, diarylethene, hemothioindigo) that can be used to change the binding affinity of the molecule to a protein of interest. For photocaged probes, the unmodified native pharmacophore is obtained by photochemical cleavage in the area where the light is focused. The initially high local concentration of the released compound decreases by diffusion. An alternative approach is the incorporation of an azobenzene into the structure of the pharmacophore (azologization), or the extension of the small molecule with an azobenzene photoswitch (azoextension).[203] Azobenzene photoswitches undergo isomerization from their thermodynamically preferred linear, planar *trans* to the bend *cis* isomer. This isomerization entails a change in shape and electrostatic properties of the ligand and can cause a change in binding affinity to the protein.[204] The *cis* isomer is thermodynamically labile and undergoes thermal relaxation back into the *trans* state. The thermal half-life of the *cis*-azobenzene is temperature dependent and further changes with substitution pattern. Thermal half-lives typically range from seconds to days. The UV-Vis absorption of the unsubstituted *trans* isobenzene is in the UV spectrum but absorption properties can be engineered and azobenzene photoswitches with absorption up to IR-wavelengths have been reported.[205,206] The activation of azobenzene photoswitches is fully reversible, either by irradiation with a second wavelength or thermal relaxation and can be repeated over many cycles.[183,203,207–209]

Both types of photopharmacology have recently been applied to actin binding small molecules. Recently, a preprint was published, in which Cytochalasin D was caged with Nvoc-Cl cage on the secondary hydroxy group that binds deep inside the barbed end binding cleft of actin (Figure 24).[210] The steric hindrance caused by masking this hydroxy group renders cytochalasin D inactive. Upon irradiation with 360 or 405 nm light, cytochalasin D is liberated and can hence forth bind to actin. The irradiation can be applied globally or within a specified

area of irradiation and leads to the disassembly of actin networks in the irradiated cell or close to the irradiation area outside of the cell. Upon diffusion of cytochalasin D, the actin network in the cell was reestablished.

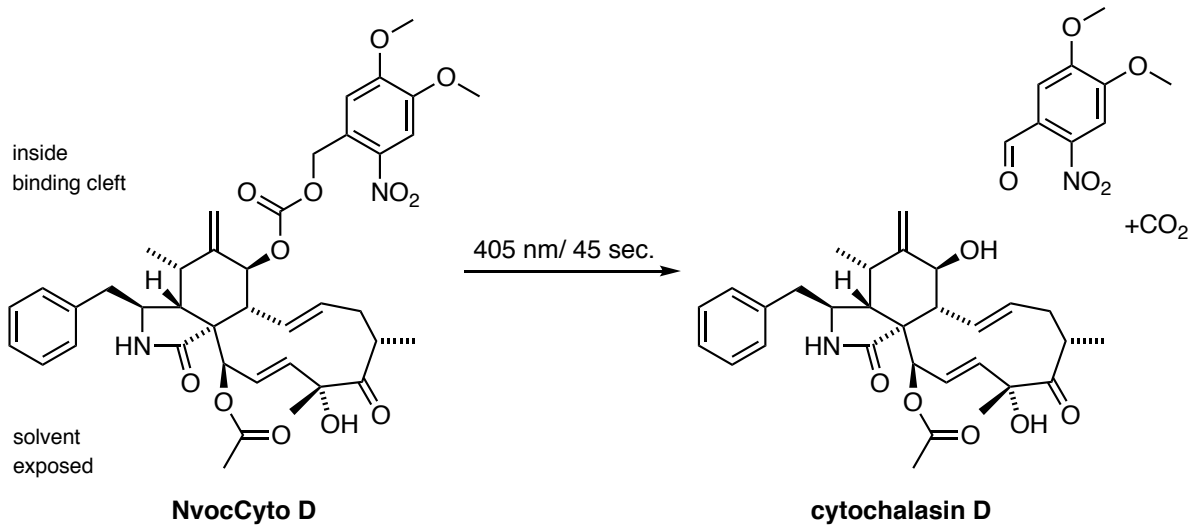

Figure 24: Structure and photolytic activation of NvocCytoD.

However, high concentrations (50 µM) of **NvocCytoD**, as well as extended irradiation times were required to observe this effect. This is likely a result of the relatively inefficient uncaging process and the dilution of the active compound due to diffusion. For cellular applications, photocage design must be carefully balanced between sufficient stability under (reduced) ambient light and physiological conditions on one hand and sufficiently high reactivity to allows for an effective photouncaging reaction. Another potential downside of photocages is the generation of potentially toxic byproducts.

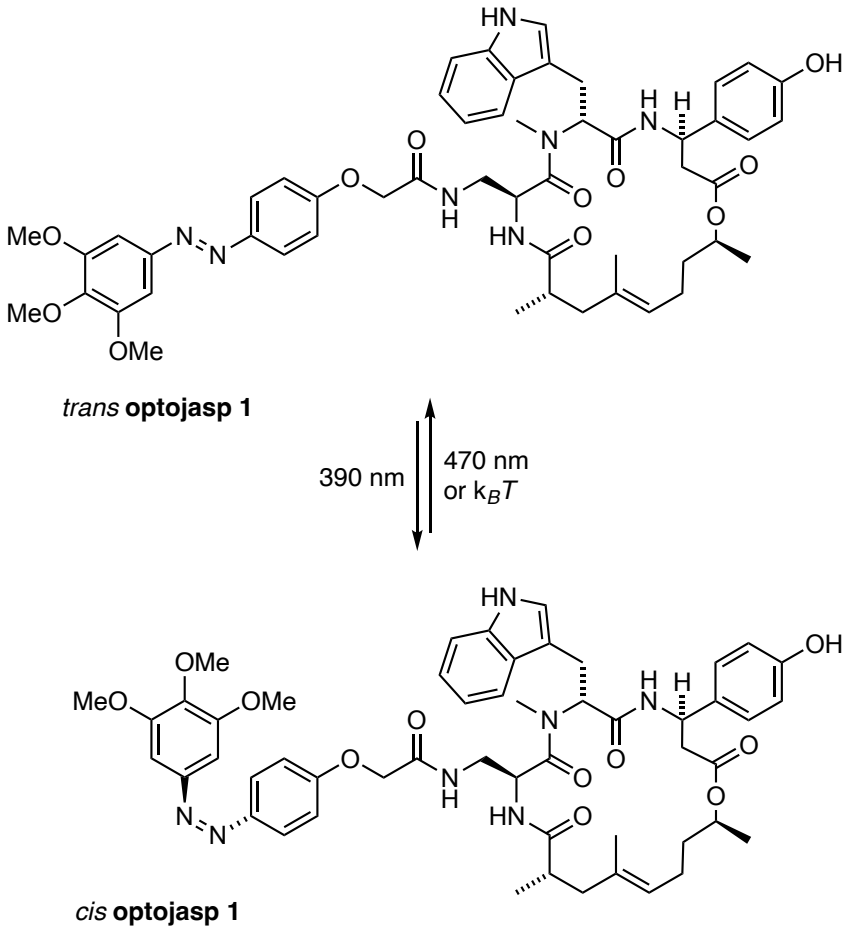

Figure 25: structure of *cis* and *trans* optojasp 1.

Photocontrol of actin dynamics and actin dependent processes by means of actin stabilization has been demonstrated. The design of optojasps was inspired SiR-actin and related fluorophore conjugates of jasplakinolide. It was shown that optojasps selectively lead to the aggregation of actin under activation conditions and the probe could be used for light dependent reduction of cell migration, disruption of cytokinesis, and the actin dependent regulation of actin mediated shuttling of myocardin related transcription factor between the nucleus and cytosol.[112] Despite the general reversibility of optojasp-induced actin aggregation in fixed cells, no functional reversibility was demonstrated. Furthermore, does the use of UV-light for activation of **optojasp 1** pose some limitations to its general applicability in certain cells and tissues due to their higher photosensitivity and limited tissue penetration depth.

2 Latrunculin

2.1 Project Outline and Aim of the Project

The interest in developing photoswitchable tools for the actin cytoskeleton has been long standing in the Trauner group. After the successful development of the photostatins[211], which inhibit tubulin polymerization light dependently, it was the goal to develop photoswitchable latrunculin derivatives that work in a similar logic on actin.

Latrunculin natural products and their derivatives have received attention from the synthetic community for a long time. Initial total synthetic approaches by Smith and White employed a Wittig olefination strategy to install the *Z*-olefin and macrocyclic ring closure was achieved under Mitsunobu conditions.[212–215] Fürstner focused his work around a ring closing alkyne metathesis followed by Lindlar reduction and Watson explored olefin metathesis to install the macrocycle in latrunculin B.[216–218] Fürstner further explored a variety of fully synthetic structures for their bioactivity.[219,220] The El Sayed and Hamann groups explored the natural product diversification of latrunculins A and B.[221–223] Further, Lampe *et al.* explored broad structure activity relationships of in part highly truncated latrunculin analogs.[224]
Our efforts towards the optical control of G-actin sequestration as well as exploring truncated latrunculin analogs is based on these studies. We aim at improving the efficiency and synthetic access to latrunculin structures.

Briefly, this project was addressed by Martin S. Maier during the beginning of his PhD studies and Li Gao during his Master's thesis.[225] Dr. Malgorzata Borowiak and Luis Osa de la Rosa then performed biological evaluation experiments, however no initial structures were found to be active or achieve the optical control of actin.
Computational studies were conducted with Sander Folkerts, who joined the Trauner group as a Master student from February – August 2020. While the author of this dissertation only gives an overview over this study, extended computational details can be found in his Master's thesis.[226]
In November 2020, Dr. Ruiyang Bao joined the project to focus primarily on further optimizing the synthetic strategy and synthesizing further derivatives of latrunculin photoswitches as well as truncated synthetic analogs. Any structures that were provided by him are indicated in footnotes.

The aim of this project is the development of a photoswitchable Latrunculin analog for the optical control of actin dynamics by light-dependent G-actin sequestration. Further we aimed at improving the synthetic access to bioactive truncated latrunculin derivatives that may help overcome the limited natural supply of latrunculins A and B from natural sources.

2.2 Results and Discussion Optolatrunculin and Latrunulogs

2.2.1 Synthesis and General Biological Assessment

The synthesis of latrunculin analogs and latrunculin-based photoswitches was based on known synthetic approaches towards the latrunculin family of natural products and analogs.[216–220] We decided to use a divergent approach that would allow for the late-stage incorporation of azobenzene photoswitches on advanced intermediates. We further focus on the smaller latrunculin B core and omitted the methyl stereocenter in position 8 of the macrocycle for simplified synthetic access.[220] In addition, truncated and open chain analogs were explored that would render the synthesis less laborious.

As was described previously, latrunculins can be accessed by merging thiazolidinone **8** with aldehydes of type **7** *via* aldol reaction.[212,213,217,218] Acid-mediated cyclization would yield two diastereomers which can both be further used to install a variety of fragments on the upper eastern site of the molecule and allow access to macrocyclic, as well as open-chain latrunculin analogs (Scheme 1).

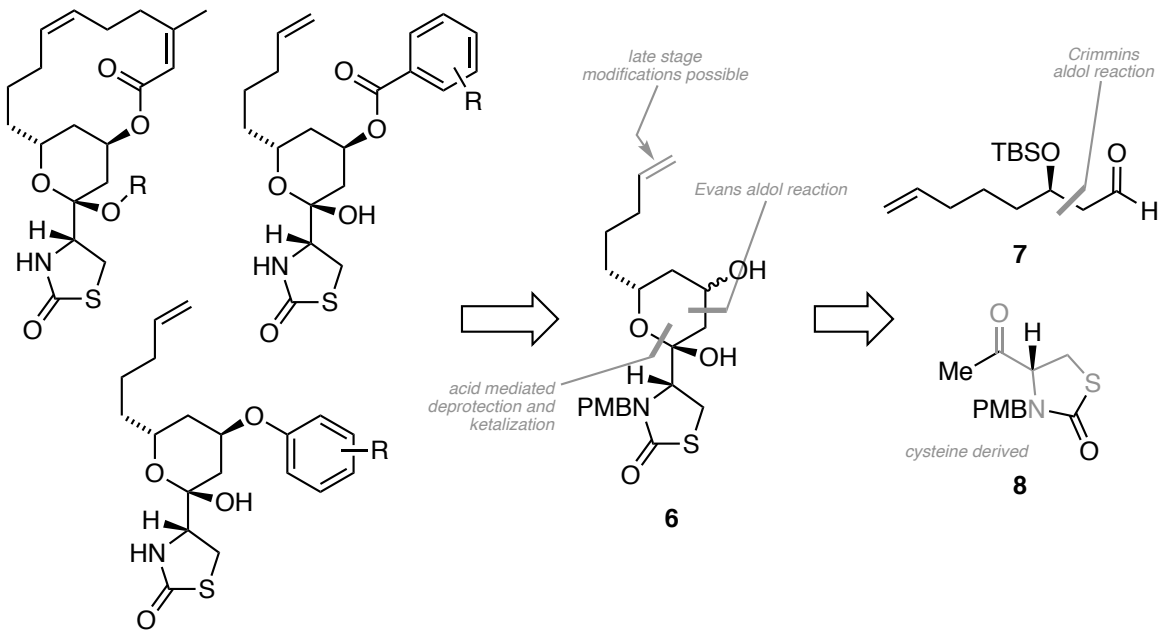

Scheme 1: General synthetic approach to different latrunculin derivatives R= H, Aryl.

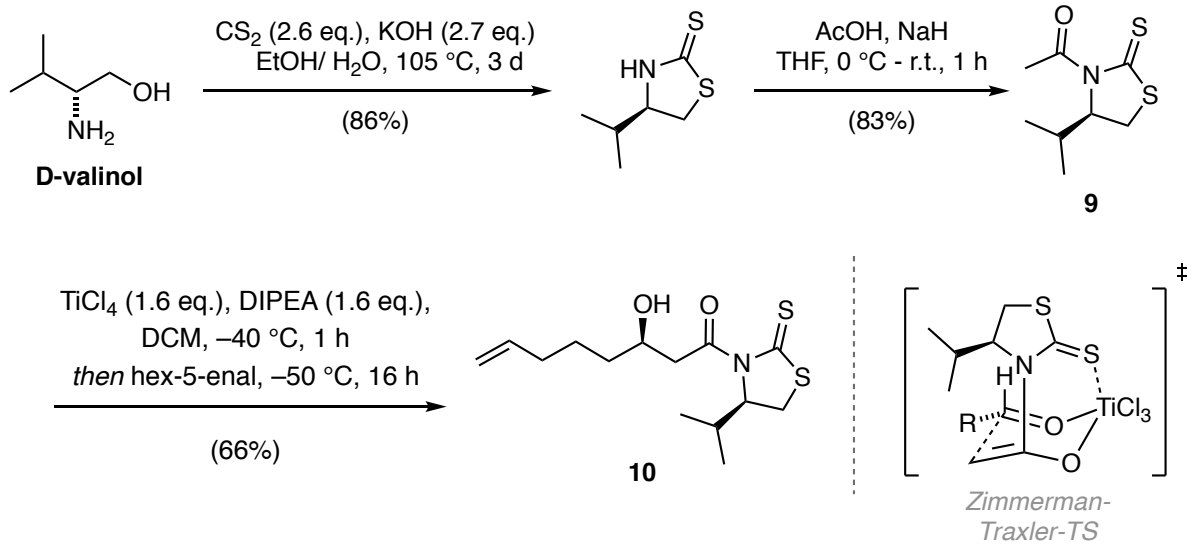

Scheme 2: Crimmins-Evans Aldol reaction and closed Zimmerman-Traxler transition state.

The synthesis of chiral aldehyde **7** commenced with an asymmetric Crimmins aldol reaction using Nagao's auxiliary (**9**) *via* a closed Zimmerman-Traxler transition state (Scheme 2).[227–229] The yield reported herein is for a gram-scale transformation. At smaller scales, even higher yields were achieved, and it is expected that yields would improve upon further optimization. Hex-5-enal was obtained by oxidation of commercial hex-5-enol under Swern conditions. The secondary alcohol was silyl protected, followed by auxiliary cleavage. It had been observed previously that the direct reduction of the thioxothiazolidine in one step was not efficient for **11**[225], therefore, a two-step procedure *via* methyl ester **12** was used (Scheme 3).[228]

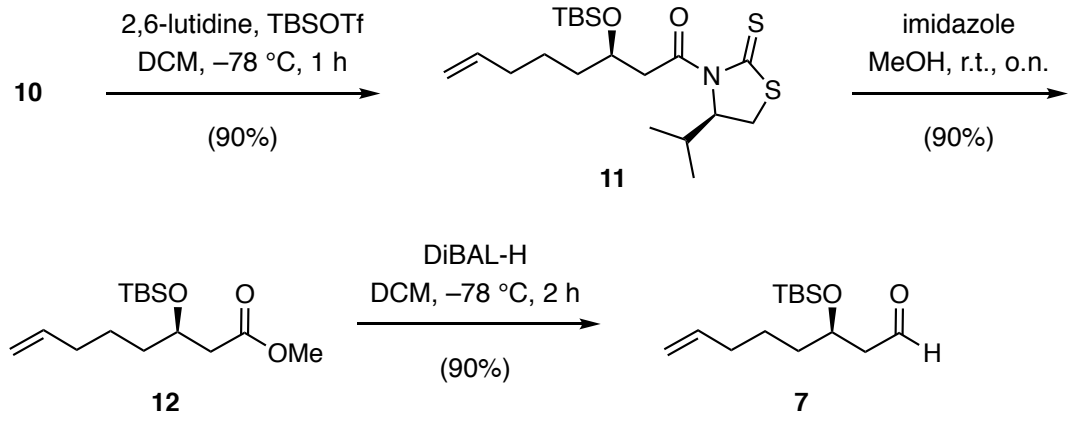

Scheme 3: Silyl-protection of secondary alcohol followed by auxiliary cleavage.

Overall, (*R*)-**7** as synthesized efficiently and every transformation in this sequence was performed on (multi)gram scale and in high yields. Thiazolidinone building block **8** was

obtained efficiently in multi gram scale transformations starting from L-cysteine ethyl ester (Scheme 4).[215,220,230]

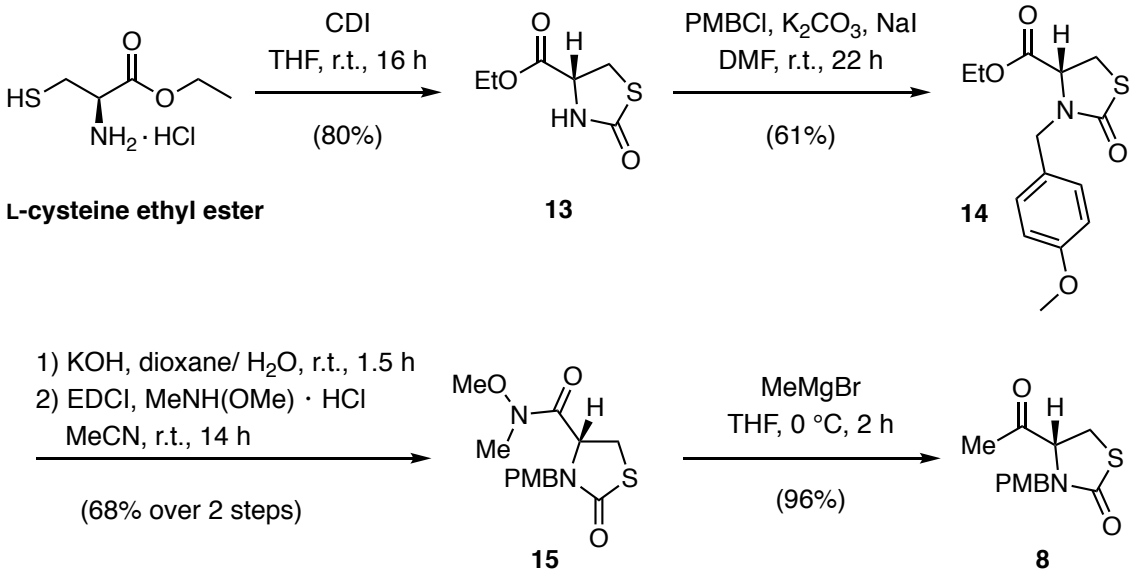

Scheme 4: Synthesis of thiazolidinone building block **8**.

The subsequent aldol reaction of thiazolidinone **8** and chiral aldehyde **7** was achieved using aldol conditions. Initial efforts relied on the use of excess aldehyde and careful temperature control, which yielded aldol product **16** in excellent yields and with slight diastereomeric preference (Scheme 5). The reaction was further optimized using *N*-methyl pyrrolidinone and sub equimolar aldehyde **7**, rendering the transformation more economical.[p] The two diastereomers that resulted from this aldol reaction were isolated as a mixture (*d.r.*: 1:1.3) and acid mediated silyl deprotection induced hemiketal formation furnishing tetrahydropyran structures (*S*)-**17** and (*R*)-**17** with slight diastereomeric preference of (*S*)-**17**. The diastereoselective preference can be attributed to an oxonium intermediate **18**. (*S*)-**17** is thermodynamically favored over (*R*)-**17**. *Fürstner* et al. explained this with a 1,3-diaxial strain (**19**) that disfavors (*R*)-**17** thermodynamically (Scheme 4).[220] The stereoselectivity of the ketal stereocenter is governed by an anomeric effect between the ring oxygen and the hydroxy group of the hemi ketal.

[p] This optimization was performed by Dr. Ruiyang Bao.

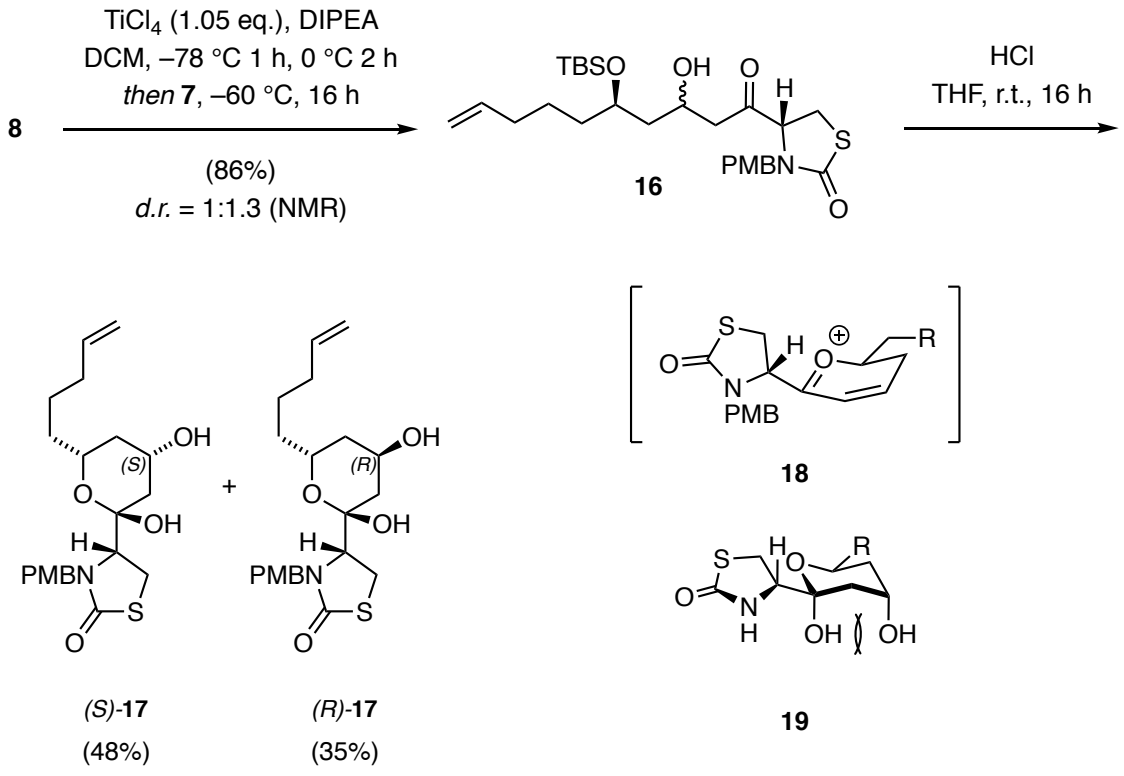

Scheme 5: Merging of the chiral aldehyde **7** and thiazolidinone building **8** blocks and ketal formation.

16 could be converted to methyl ketals (*R*/*S*)**-20** in one step using PPTS and methanol as reported previously.[225] However, we found that the diastereomers (*R*)**-20** and (*S*)**-20** were copolar on silica and therefore difficult to separate. Hemiketals (*R*/*S*)**-17** were however easily be separated by column chromatography. (*R*)**-17** appears less polar, likely due an intramolecular hydrogen bond that lessens the polarity of this diastereomer compared to (*S*)**-17**. Thus (*R*)**-17** and (*S*)**-17** were readily separated after cyclization and individually protected in the next step. We obtained both diastereomers in hundreds of milligrams to grams scales (Scheme 6). The stereochemistry of (*S*)**-20** could be confirmed by a NOESY correlation between the protons on positions 3 and 5 of the tetrahydropyran ring. This correlation was absent in (*R*)**-20.**

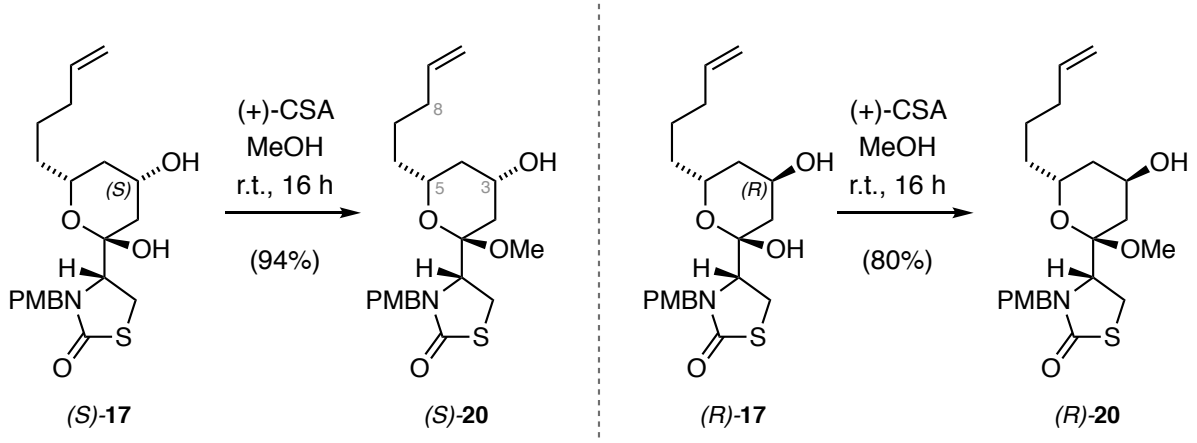

Scheme 6: Protection of the acetals (*R*/*S*)-**17**.

The two diastereomeric structures (*S*)**-20** and (*R*)**-20** formed the basis for further derivatizations. First, analogs of latrunculin B lacking the 8-methyl group were explored.

For the Synthesis of latrunculins A and B, as well as derivatives thereof, Fürstner *et al.* relied on an alkyne metathesis followed by Lindlar semi-reduction to establish the macrolactone.[216] Watson reported the use of Grubbs 2nd Generation catalyst to achieve the same goal.[218]

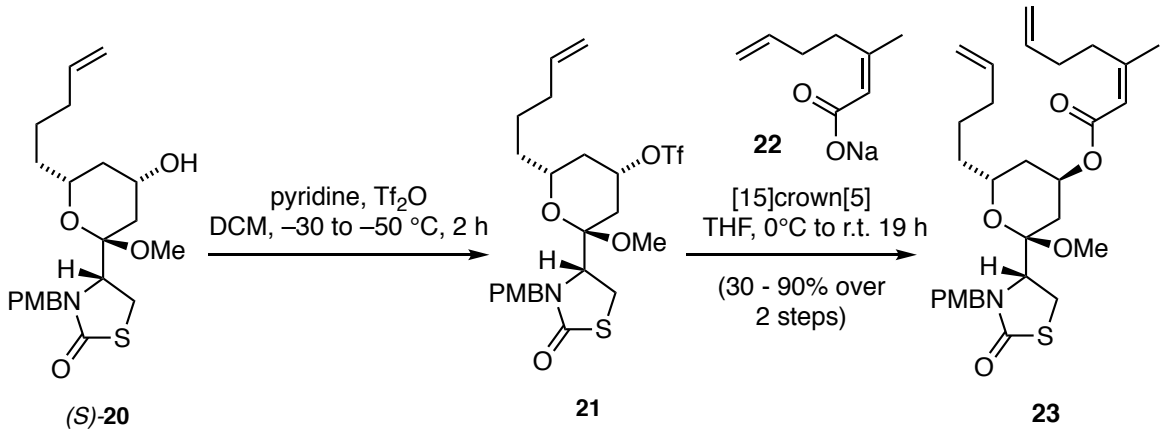

Scheme 7: Preparation of the ring closing metathesis precursor **23**.

Triene **23** was obtained after triflation of (*S*)-**20** and substitution with the sodium salt of dienoic acid **22** using S_N2 conditions (Scheme 7).[216,218] The yields of this transformation were variable and likely dependent on the stability of triflate intermediate **21**.

We set out to explore the ring closing metathesis initially using Grubbs 2nd generation catalyst. The reaction proceeded with a preference of (*E*) over (*Z*) product (*E*:*Z* = 6:4) in good yields

(Scheme 8). Watson reported a (*E*):(*Z*) ratio of approximately 8:2 for the 8-methyl analog to this substrate.[218] This difference in diastereomeric ratios likely stems from an increased steric effect from the additional stereocenter in their study. When we employed the (*Z*)-selective adamantly-Grubbs catalyst[231,232], (*Z*)-**24** was selectively obtained but the reaction did not go to completion.

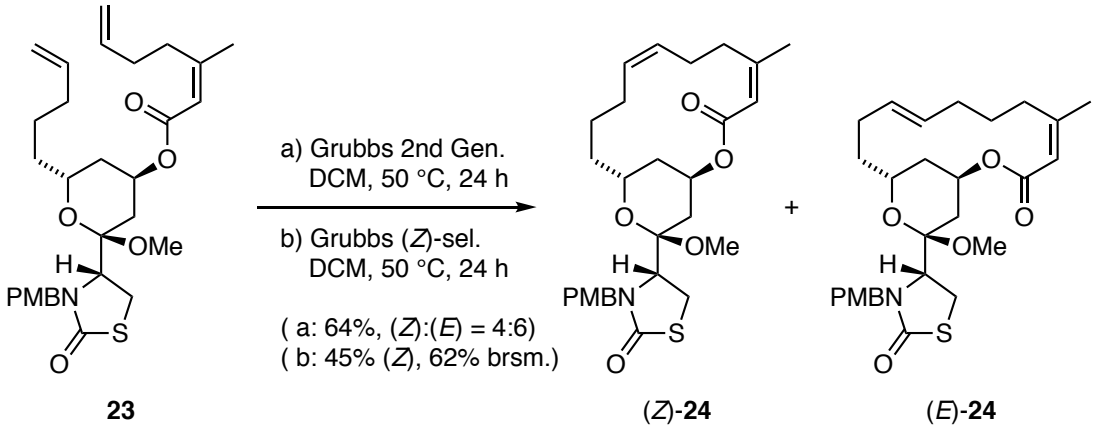

23 (*Z*)-**24** (*E*)-**24**

Scheme 8: Ring closing metathesis of **23** gave 14-membered macrolactones **24**.

Increasing catalyst loadings or subsequently adding the catalyst over time did not improve the yield indicating that the low conversion is not attributed solely to catalyst decomposition. It has been described that the *p*-methoxybenzyl protecting group can lead to a conformation of the diene with both olefins distant to each other that leads to low conversion rates. Better conversion was reported by changing the thiazolidinone nitrogen protecting group to Teoc.[216] However, attempts to changing the protecting group early in the synthesis were incompatible with the synthetic approach.[q]

We decided to use the (*E*):(*Z*)-mixture to explore first azolatrunculin derivatives. This series of azolatrunuclin derivatives was inspired by reports of phenethyl ketal derivative of latrunculin A that were reported to show superior activity than latrunculin A against actin polymerization and cell proliferation.[222] We rationalized that even though latrunculin B is less active than latrunculin A, a light dependent effect could still be sufficient for the photocontrol of actin.

[q] Explored by the author of this thesis and Dr. R. Bao.

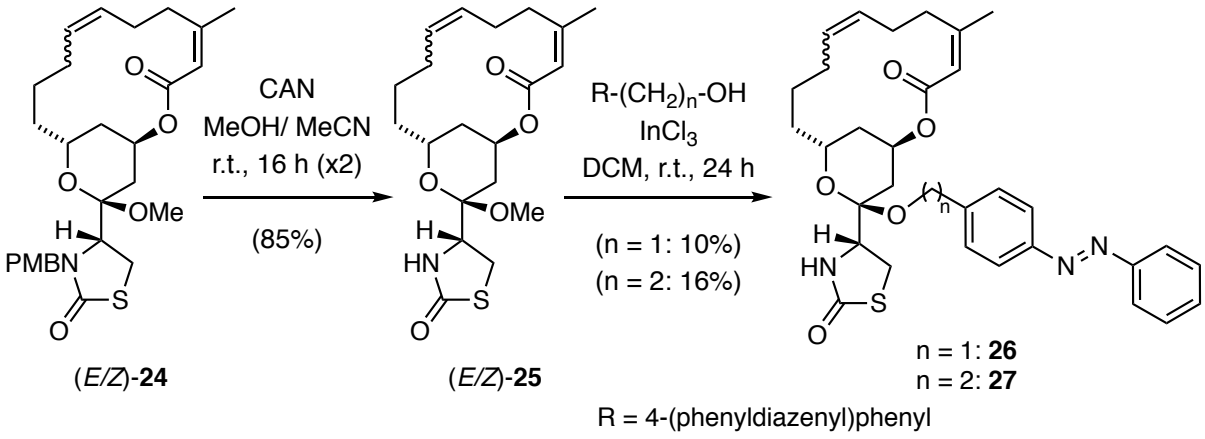

Scheme 9: Synthesis of azolatrunculin analogs **26** and **27**.

The thiazolidinone was deprotected oxidatively using cerium(IV) ammonium nitrate (CAN) in methanol to avoid partial methyl ketal cleavage. Acetonitrile was added to enhance solubility. The reaction stalled after 14 h and when left for longer, the formation of various side products was observed by TLC. The yield was optimized by resubmission of the starting material to identical reaction conditions. The yield reported was obtained after one resubmission as combination of both reactions. We introduced the azobenzene photoswitch by lewis acid mediated transketalization[233] using the respective azobenzene methanol and ethanol derivatives and obtained **26** and **27** in sufficient yields for further preliminary evaluation (Scheme 9).

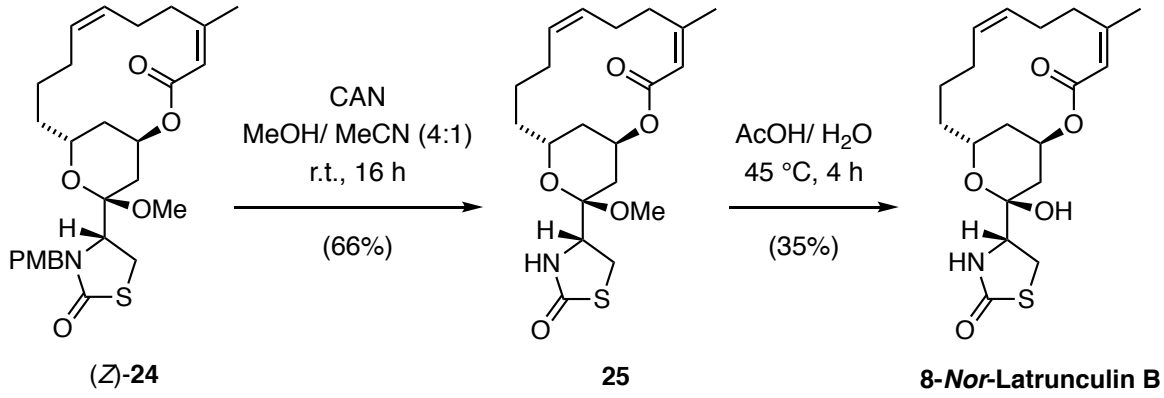

Scheme 10: Deprotection sequence leading to 8-*Nor*-Latrunculin B.

While this work was underway, we further explored the preparation of the pure (*Z*)-isomer of 8-*Nor*-Latrunculin B. The (*Z*)-selective ring closing metathesis proceeded in moderate yields but sufficient amounts of (*Z*)-**24** could be obtained (Scheme 8). A two-step deprotection

sequence gave 8-*Nor*-latrunculin B which served as a control compound for the following biological studies.

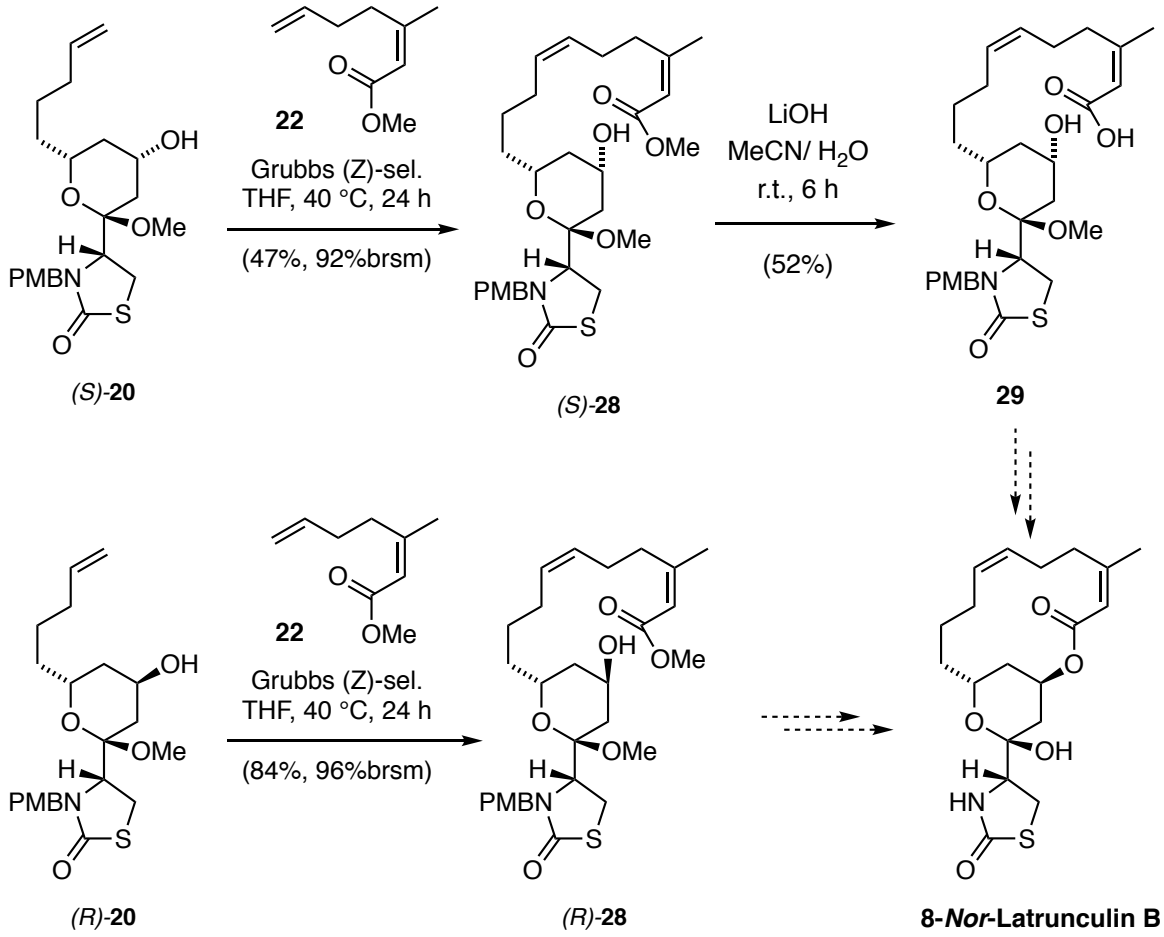

Scheme 11: Cross metathesis strategy explored toward 8-*Nor*-Latrunculin B.

We further explored whether 8-*Nor*-Latrunculin B could be accessed *via* a cross-metathesis strategy to circumvent the conformationally difficult ring-closing metathesis. Indeed, cross metathesis with methyl dienoic ester **22** gave products that stand in analogy with Wittig product intermediates in the total syntheses by Smith and White.[212–215] Both reported the final macrocyclic ring closure under Mitsunobu conditions. In the case of the (*R*)-isomer, esterification conditions could instead be applied. This explorative sequence shows a promising alternative route towards latrunculin natural products and their analogs.

Photoswitchable Latrunculin – Ketal Derivatives

The photophysical properties of **26** and **27** are typical for alkyl-substituted azobenzenes: isomerization from the thermodynamically preferred *trans* into *cis* isomer is achieved with 365 nm light whereas the isomerization can be reversed with 460 nm light. The thermal conversion of *cis* to *trans* is slow, thus pre-irradiation of **26** and **27** before the addition to experiments that are limited to a few hours is possible.

(*E*/*Z*)-8-*Nor*-Latrunculin B served as control and both photoswitchable latrunculogs **26** and **27** were investigated in *Saccheromyces Cerevisiae* by imaging Retrograde Actin Cable Flow (RACF).[r] RACF is an essential process in the proliferation of budding yeast to ensure that the daughter cell inherits good organelles from the mother cell.[234,235] The formation of actin cables is highly dynamic and can be readily suppressed in the presence of latrunculin A or B.

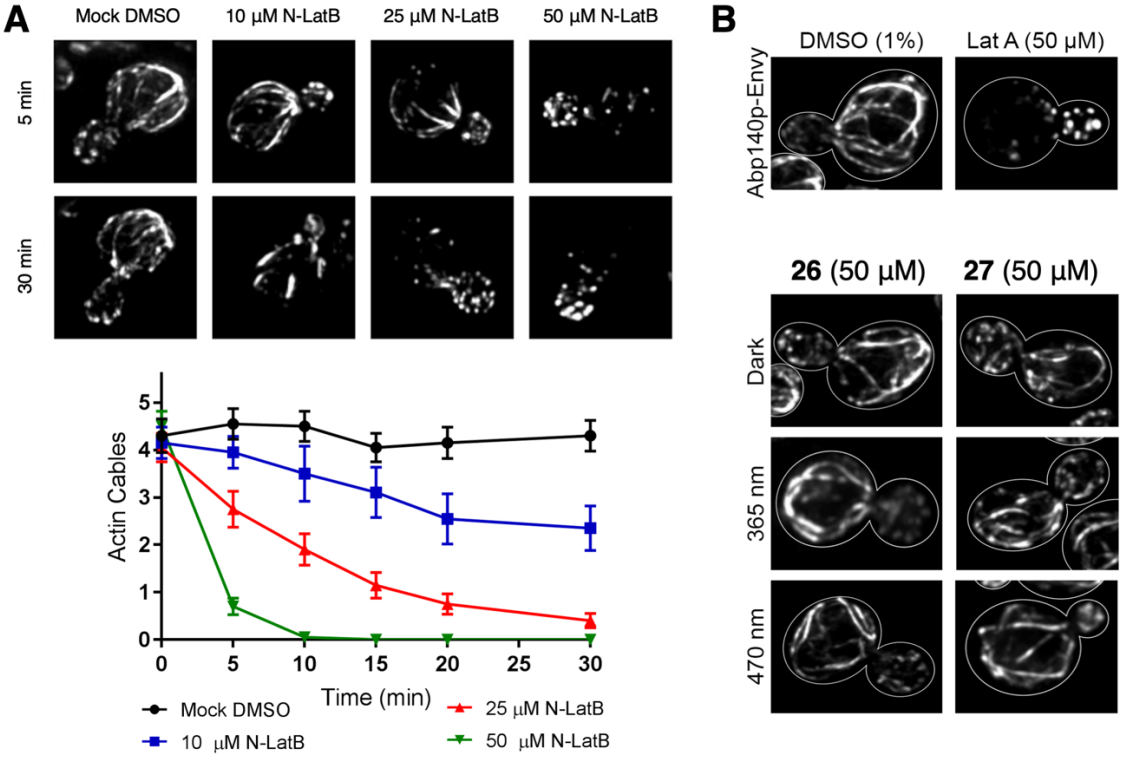

Figure 26: RACF assay on *Saccheromyces Cerevisiae* with (E/Z)-8-*Nor*-Latrunculin B as a control and Azolatrunculin derivatives $AzoLat1$ and $AzoLat2$.

(*E*/*Z*)-8-*Nor*-Latrunculin B was obtained after hydrolysis of methyl ketal (*E*/*Z*)-**25** in analogy to the pure (*Z*)-isomer and used as a positive control to confirm the bioactivity of our synthetic latrunculin analogs. RACF was monitored by light microscopy over 30 minutes at increasing

[r] *S. Cerevisiae* experiments were done by Dr. E. Garcia in the lab of Prof. Liza Pon at Columbia University, Department of Pathology and Cell biology, New York, USA.

concentrations. While the DMSO control showed bright actin cables in mother cell and bud, already at 10 µM (*E*/*Z*)-8-*Nor*-Latrunculin B, a decrease in actin cables was observed. The effect was much stronger at higher concentrations and accompanied with an increased number of actin patches in the bud (Figure 26A). Actin patches are branched actin networks that are mainly localized in the bud and are essential to functional cell polarization during budding.[236]

26 and **27** were pre-irradiated with 365 nm and 470 nm light and added to a final concentration of 50 µM to the cells. Unfortunately, actin cables appeared unchanged under both conditions indicating that both compounds were inactive in budding yeast (Figure 26B).

Actin targeting small molecules show different potencies across species. To investigate, whether the observed inactivity of **26** and **27** was species dependent, we performed cell proliferation assays on HeLa[s] cells. **26** was completely inactive at concentrations up to 50 µM and **27** showed slight antiproliferative activity at 100 µM with no light dependence. Higher concentrations than 100 µM would be unfeasible to our biology experiments and require large compound quantities. Therefore higher concentrations were not investigated.

Going forward, we decided to investigate whether the newly synthesized structures were still biologically active and whether a light-dependent difference in activity could be observed using a standard cell proliferation assay. 3-(4,5-Dimethylthiazol-2-yl)-2,5-diphenyltetrazolium bromide (MTT) is a yellow tetrazonium dye, that is cell permeable and can be reduced by NAD(P)H dependent cellular oxidoreductase enzymes to form the purple formazan dye. The relative concentration of formazan dye correlates with relative cell viability and can be determined by colorimetric readout.[237,238]

Photoswitchable Latrunuclin – Open Chain Derivatives

Our divergent synthetic approach, that allowed us to have gram quantities of (*S*)- and (*R*)-**20** in hand quickly allowed us to change our strategy towards photoswitchable latrunculin derivatives.

We decided to investigate, whether an open macrocyclic structure that is equipped with a photoswitch would be able to light-dependently induce cytotoxicity. Initially, Li Gao in his Master's thesis investigated truncated azolatrunculin structures that bared shortened or fully saturated side aliphatic substituents on the eastern half of the open macrocycle.[225] He could show that methyl derivatives like **30** remained completely inactive in cell proliferation assays. A pentyl side chain in structures like **31** showed cytotoxicity in HeLa cells. However, it was

[s] Human cervical carcinoma.

reported that the compounds suffered from low solubility, as crystals were observed at the bottom of the assay plates.[225] When compounds crystallize out or precipitate during an assay, decreased cellular viability is commonly observed. Further, strongly truncated analogs of latrunculin have been reported as antimalarials and it was reported that although the antimalarial effect was strong, toxicity towards mammalian actin was comparatively low.[239,240]

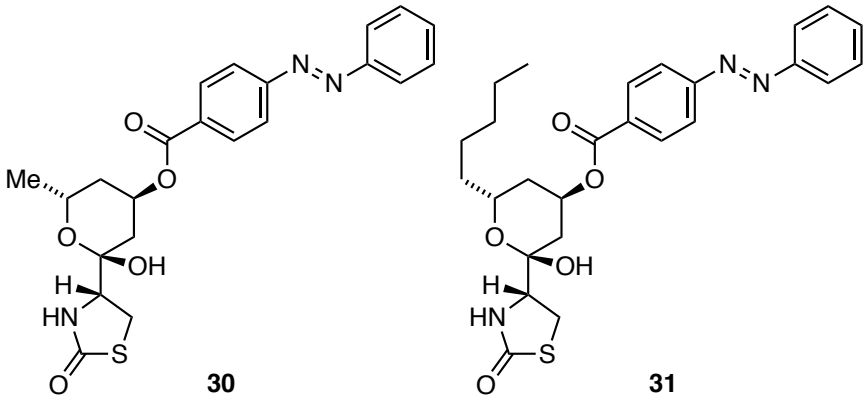

Figure 27: Structures investigated by Li Gao.

We concluded that future derivatives required a higher degree of unsaturation on the northeastern fragment.

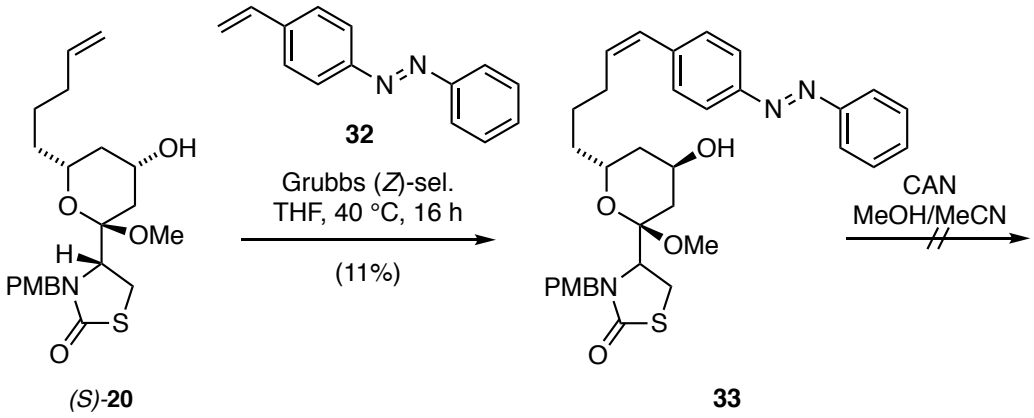

Scheme 12: Installation of an azobenzene via cross metathesis.

We attempted to install an azobenzene on the northeastern olefin of (*S*)-**20** using (*Z*)-selective metathesis and styrene azobenzene **32** (Scheme 12). Unfortunately, due to low yields, likely because of poor solubility of the styryl azobenzene under the reaction conditions, and challenges in the subsequent oxidative deprotection, this strategy was not further pursued.

We next revisited the azoextension at the northeastern site of (*S*)-**20**. X-ray structure analysis had indicated the favorable hydrogen bond interactions of the ester motif in latrunculins A and B.[62] This motivated us to append a series of azobenzene and diazocine moieties *via* an ester bond using Mitsunobu conditions (Scheme 13).

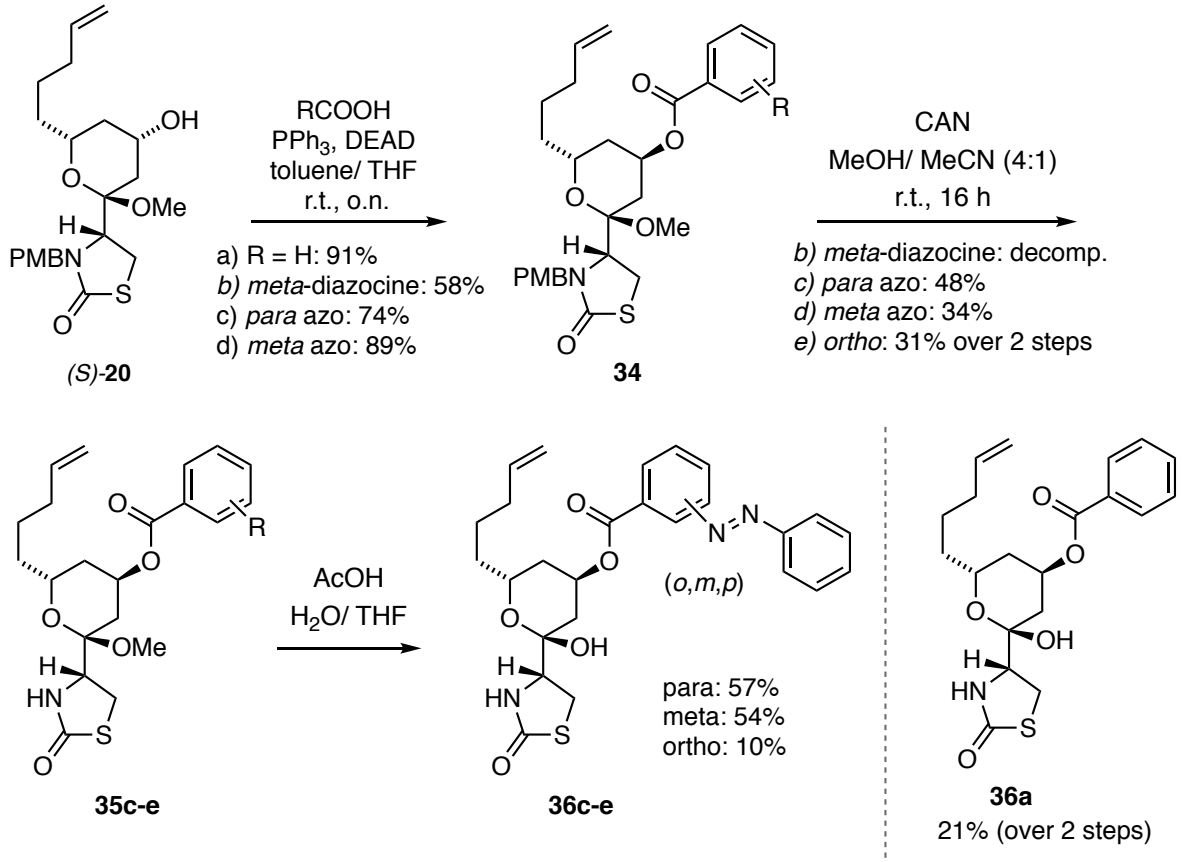

Scheme 13: Preparation of ester-bridged azolatrunculins **36c-e** *via* Mitsunobu conditions.

We observed that oxidative PMB cleavage was not tolerated by electron rich photoswitches, such as diazocine **38**[t], resulting in low yields and decomposition. Therefore, we decided to perform this transformation before the installation of the photoswitch going forward (Scheme 14).

[t] Kindly provided by Martin S. Maier.

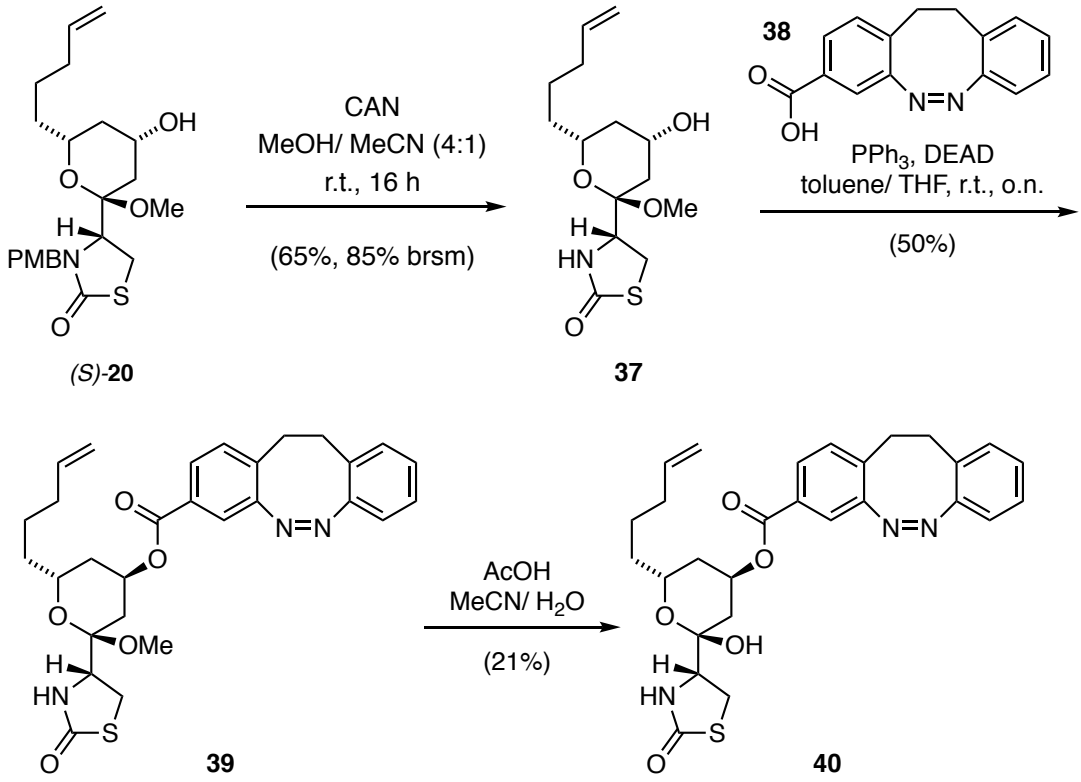

Scheme 14: Reversed approach to the azolatrunuclin series.

During the acid mediated ketal deprotection, side products were observed that indicated elimination of the carboxylate photoswitches. Mechanistically, deprotonation can occur on 2-position of the oxonium ion intermediate, allowing for conjugated elimination of the carboxylate. This is in analogy to the acid sensitivity of latrunculins reported previously.[241]

Overall, ester derivatives could be obtained and were subsequently investigated using cell proliferation assays (Table 1). Hemiketal structures all remained bioactive, with a slight increase of EC_{50} value compared to 8-*Nor*-Latrunculin B. Methyl ketals showed reduced to no potency, especially in combination with large azobenzenes. This may result in altered cellular uptake. A light-dependence of the antiproliferative effect of ester-bridged azolatrunculins was not observed.

Table 1: Antiproliferative activity of ester-appended photolatrunculins.

compound	EC_{50} (light)	EC_{50} (dark)	note
36a	NA	29.1	active
35c	20.5	18.4	no difference, ca. 50% inhibition
36c	21.0	21.5	no difference
35d	24.1	25.8	no difference, ca. 50% inhibition
36d	21.5	>25	no difference
36e	32.7	36.8	no difference
39	–	–	not active
40	20.4	28.7	no difference
8-*Nor*-latrunuclin B	NA	14.0	slow slope
latrunculin B	NA	1.6 µM	slow slope

Based on our findings, we concluded that the latrunculin pharmacophore in ester-bridged structures was still able to bind to the nucleotide binding site of G-actin. The slight decrease in bioactivity may be a result of the loss of hydrophobic interactions of the macrolactone, in the binding pocket, but also in primary protein interactions, as mentioned above for the relative activity difference of Latrunculin A and B. Comparable toxicities for light and dark were thought to result from insufficient change in steric clash with the protein, even for derivatives with proposed higher steric demand. This may be due to the open solvent exposed site above the pharmacophore binding cleft. We later confirmed this hypothesis with computational studies on the binding ability of latrunculin derivatives to G-actin (Chapter 1-2.4).

As a consequence of the possible elimination of ester-bridged azobenzenes, and in order to bring the photoswitchable motive closer to the pharmacophore, we next explored ether-bridged derivatives. Due to the previously observed reduced activity of protected ketals, we henceforth only investigated the hemiketal products.

Overall, *p*-azobenzene phenols were conveniently synthesized using diazonium coupling conditions (see experimental) and subsequently appended onto latrunculin core structure **37** using Mitsunobu conditions (Scheme 15). We also added a diazocine photoswitch to the latrunculin core[u]. Unfortunately, only very small light-dependent differences were observed in cell proliferation assays (Table 2). The difference found for **42** could not be exploited to observe light-dependent changes in actin morphology using immunofluorescence on fixed cells.

[u] The diazocine photoswitch was kindly provided by Martin S. Maier.

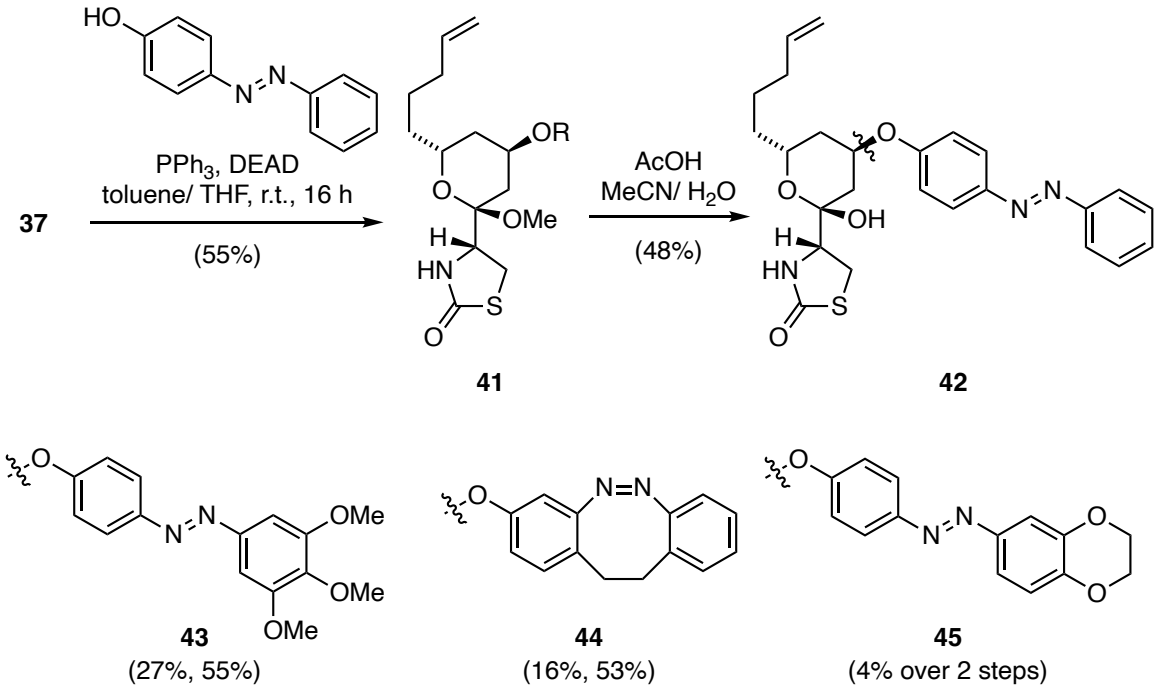

Scheme 15: Synthesis of ether bridged photoswitchable latrunculin analogs.

Table 2: Antiproliferative activity of ether bridged photoswitchable latrunculins.

compound	EC_{50}(light)	EC_{50} (dark)	note
42	17.4	32.3	small difference
43	25.8	30.5	no difference
44	29.4	37.9	no difference
45	47.2	38.7	no difference

So far, the photoswitches applied were well tolerated by the nucleotide binding site in both isomers with the dioxine switch showing the lowest affinity. Going forward, we decided to vastly increase steric demand of the photoswitch. We decided to try if *N*-benzyl oxazine derivative **48** would introduce sufficient steric clash in one isomer and allow efficient actin binding in the other to allow for light-dependent sequesteration of G-actin.

Photoswitch **47** was synthesized in 4 steps and good overall yield and subsequently appended onto the latrunculin pharmacophore using the Mitsunobu conditions as previously discussed (Scheme 16). Overall, the conversion of the Mitsunobu reaction was good but the product could not easily be separated from H_2DEAD. The following deprotection on the product mixture was low yielding. It is expected that the overall yield over two steps may be improved if the Mitsunobu reaction product is fully purified before ketal hydrolysis.

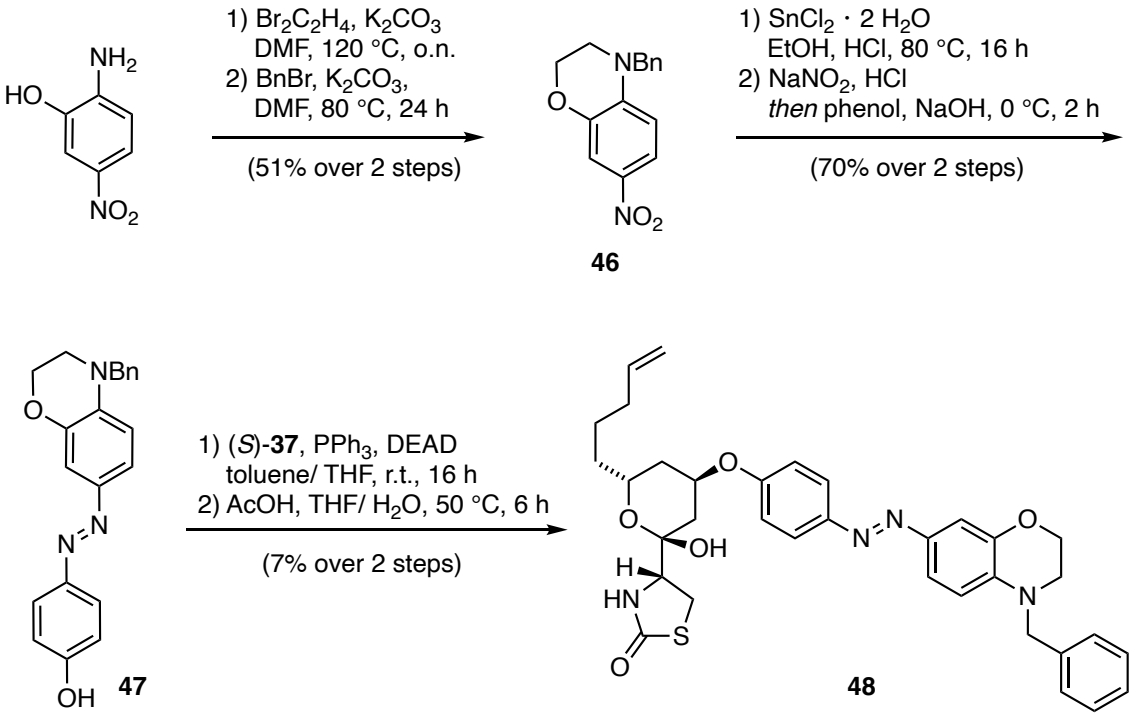

Scheme 16: Synthesis of *N*-benzyl oxazine azobenzene photoswitch **47** and optolatrunculin **48**.

48 was termed **optolat** and investigated in cell proliferation assays on HeLa cells where it showed strong light-dependent activity. While *trans* **48** remained mostly inactive in the dark, activation with 410, 440 and 477 nm resulted in strongly dose dependent cytotoxicity with EC_{50} values of 5.9, 4.1 and 8.6 µM respectively (Figure 18). Optolat (**48**) shows an absorption maximum at 440 nm and isosbestic points between the *cis* and *trans* isomers are 374 and 505 nm. Isomerization from *trans* to *cis* is observed with all wavelengths between these two intersections (Figure 28).

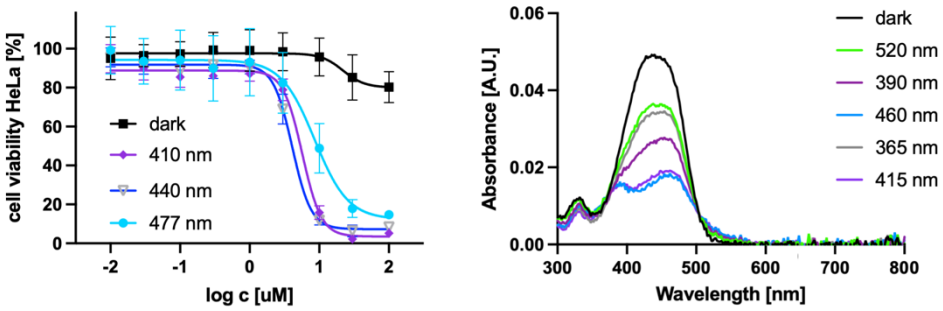

Figure 28: Antiproliferative Effect on HeLa cells and UV-Vis absorption of $**XX**$.

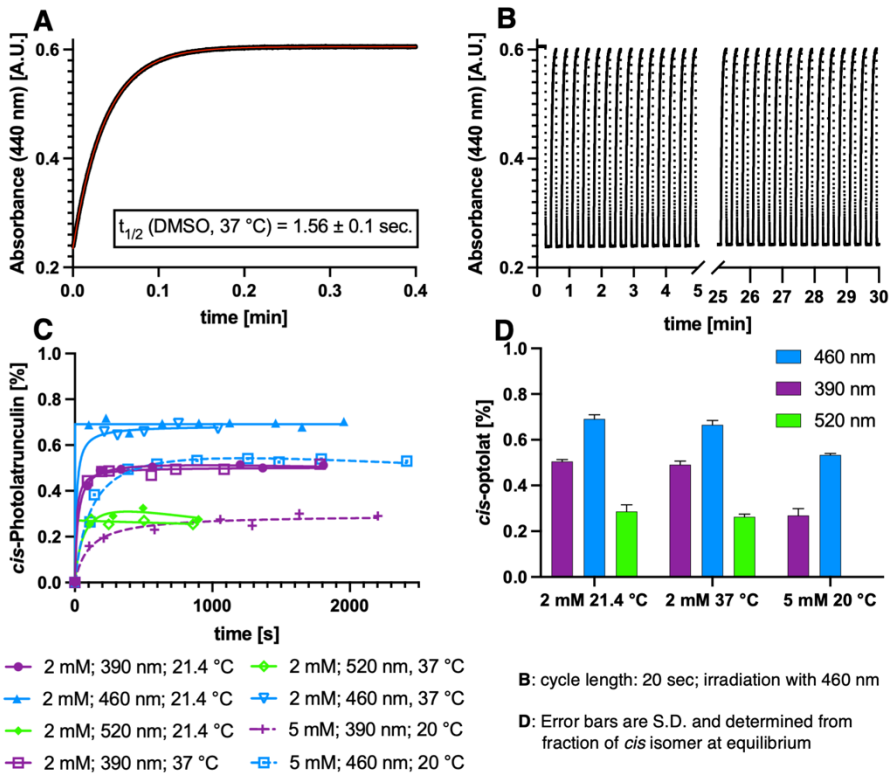

Figure 29: Photophysical properties and *cis*:*trans* ratios determined by NMR for **48**.

The thermal half-life of *cis* **48** is 1.56 ± 0.1 s in DMSO and the photoswitch is thus fast relaxing. Due to the fast thermal relaxation of the photoswitch, photoisomeric ratios of *cis* and *trans* had to be determined by NMR studies with *in-situ* irradiation. NMR spectra were obtained by standard proton NMR with 16 scans under continuous irradiation using prizmatix Ultra-High-Power Collimated LEDs. Light delivery was achieved by insertion of an optical fiber with a stripped and sanded 7 cm end into the compound solution using a coaxial insert. The number of scans was chosen as a trade-off between signal to noise ratio and the fast kinetics of the system. This setup could be further optimized for future more in-depth investigation of the system.

The fraction of *cis* isomer reached was not significantly influenced by the, for thermodynamic considerations, small temperature change from 20 °C to 37 °C. A concentration increase of 2.5 fold (2 mM to 5 mM) however, had a strong influence on the equilibrium state yielding 69% and 53% for 460 nm irradiation and 51% and 27% for 390 nm respectively (Figure 29).The fast kinetics at 2 mM concentration suggest that the concentration is low enough to not be subject to a concentration dependent decrease in light intensity according to Lambert-Beer's law.

Biological investigations were conducted at a maximum concentration of 100 µM. Given the concentration dependence of photoisomerization, it could be argued that lower concentration may lead to an even higher *cis*:*trans* ratio. The fast kinetics observed at 2 mM concentration however, *i.e.* that the *cis*:*trans* ratio is reached essentially immediately (within the time constraints of the setup), led us to conclude that the maximum *cis:trans* ratio of 69:31 that can be achieved with 460 nm is observed in this measurement. It should be noted that the absolute effective concentration of *cis* isomer in an experimental setup will always be dependent on the intensity of the LEDs used and the irradiation protocol. The illumination conditions must be individually adjusted to fit the experimental conditions and are typically a general trade-off between maximum irradiation intensity and phototoxicity. Optolat **48** does not show significant residual activity in the dark and therefore allows for the administration of high concentrations of inactive probe, that can then be (locally) activated to the desired final concentration using color dosing by means of favorable wavelengths or pulse protocols.

2.2.2 Biological Evaluation of Optolatrunculin

Having established optolat **48** as our lead structure towards the light dependent sequestration of actin, we investigated the light-dependent effects in fixed cells using fluorescent labelling in HeLa cells.

When cells were treated for 24 h with optolat **48**, a strong morphological change was observed under activated (light) conditions, while cells appeared unaltered in the dark.

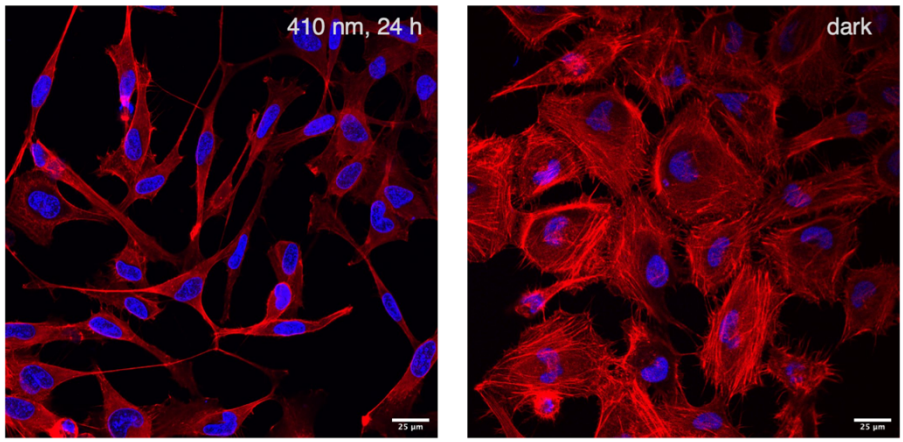

Figure 30: Fluorescence staining on fixed HeLa cells after 24 h treatment with optolatrunculin **48** (20 µM) under light irradiation (410 nm, 25 ms/ 0.5 s) or in the dark; scale bar = 25 µm; Nucleus stained with Hoechst (blue), Actin stained with Phalloidin-AF594. Confocal Fluorescence Microscopy, 63x objective.

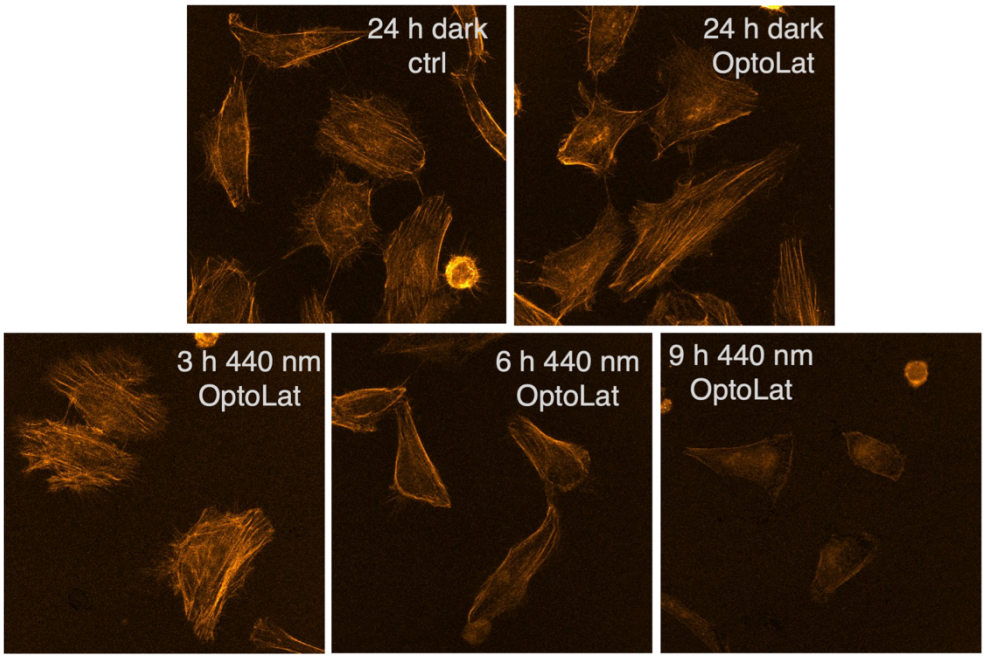

Figure 31: Fluorescent imaging of fixed HeLa cells upon treatment with optolatrunculin **48** in the dark or under irradiation with 440 nm light. F-actin was stained using Phalloidin-AF594. Images are Max projection of z-stack.

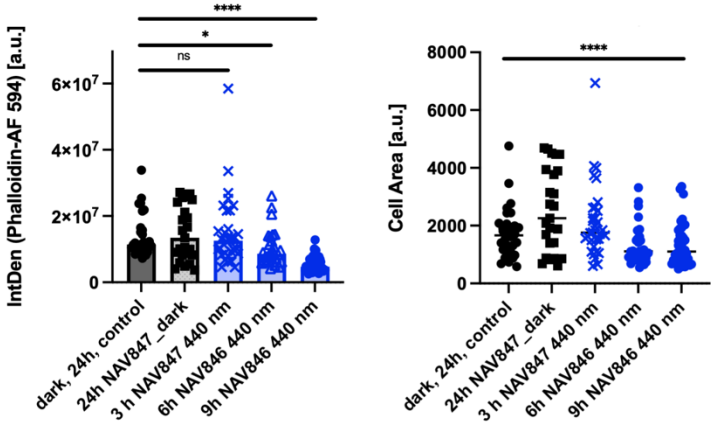

Figure 32: Quantification of Fluorescence and Cell Size upon treatment with Optolat. Quantification from Max-projection of z-stack. Statistics: Kruskal-Wallis test, **** $p < 0.0001$, * $p < 0.01$, ns = not significant.

The observed effects do not precisely compare to the effects of Latrunculin A. This may in part be because latrunculin A is typically applied in high concentration with respect to its EC_{50} values and leads to a rapid collapse of actin networks. We observed, that the effects of low doses of latrunculins A and B compared better to the observed effect with optolat. We concluded that higher concentrations of optolat would be needed and investigated this in a dose-escalation experiment. Unfortunately, we did not observe strong changes in actin

structure with increasing concentrations of optolat under activated (irradiated) conditions, even after pre-incubation of cells with the probe in the dark and overnight to ensure cellular uptake. Overall, we concluded that further engineering of the photoswitch may allow for better uptake and solubility. Further developments hereto are currently underway.

To further test the effects of optolatrunculin, we started investigating its effect on different cell lines. We observed that different cell lines have different sensitivities to latrunculins A and B. In comparison to HeLa cells, latrunculin B showed increased activity in U2-OS[v] (1.6 µM) and MDA-MB-231[w] (EC_{50} = 1.3 µM) while MCF7[x] and HEK-293T[y] cells showed lower sensitivity. We found that azolatrunculins (*p*-Ph), dioxine and optolat **48** showed this effect as well. The photoswitches showed slightly lower EC_{50} values in U2-OS cells (Table 3). This indicates, that in order to exploit a large light-dependence of optolat activity, a more latrunculin sensitive cell line needs to be identified. Especially cells that show fast actin turnover would be a system of choice.

Table 3: Comparison of antiproliferative activity of latrunculins optolat in different cell lines

cell line	compound	dark	light (25 ms/ 0.5 s)	comment
U2OS	latrunculin B	1.7 µM	–	slow slope
HeLa	latrunculin B	1.6 µM	–	slow slope
U2OS	latrunculin A	0.16 µM	0.2 µM	steep dose-response
U2OS	optolat **48**	>9.93 (>60%)	3.1 µM (440 nm)	steep dose-response
HeLa	optolat **48**	>80%	5.7 µM (410 nm)	steep dose-response
HeLa	optolat **48**	>80%	4.1 µM (440 nm)	steep dose-response
HeLa	optolat **48**	>80%	8.6 µM (477 nm)	steep dose-response

>XX% indicates remaining viable cells

While the investigations on mammalian cancer cell lines were underway in our laboratory, we collaborated with Dr. Laura Laprell and Prof. Dr. Thomas Oertner to investigate the effect of optolat **48** on microglia. Microglia are highly branched cells in the mammalian brain that in their resting state continuously scan the brain parenchyma for signs of injury or inflammation. They function as the primary immune cell in the brain and continuously remove pathogens and damaged cells through phagocytosis and secrete signaling molecules the help elevate and regulate the immune response.[242–244] The scanning function of microglia is based on the continuous extension and retraction of filopodia like protrusions, while their gross structure remains constant.[245] It has been shown, that the fast protrusion dynamics in microglia depend

[v] Human bone osteosarcoma epithelial cells
[w] Human triple negative breast cancer cells
[x] Human breast cancer cells
[y] Human embryonic kidney cells

on actin dynamics and that these dynamics can be inhibited with actin-modulating drugs while microglia ramification is dependent on microtubule networks.[246,247] Organotypic hippocampal slice cultures were treated with optolatrunculin overnight and imaged the following day. It was observed that under irradiation of optolatrunculin with 475 nm pulsed light (1 Hz), microglia surveillance decreased with extended irradiation, and upon removal of the light, the surveillance index recovered. The ramification index, that describes the overall gross structure of the cell, remained constant.[248]

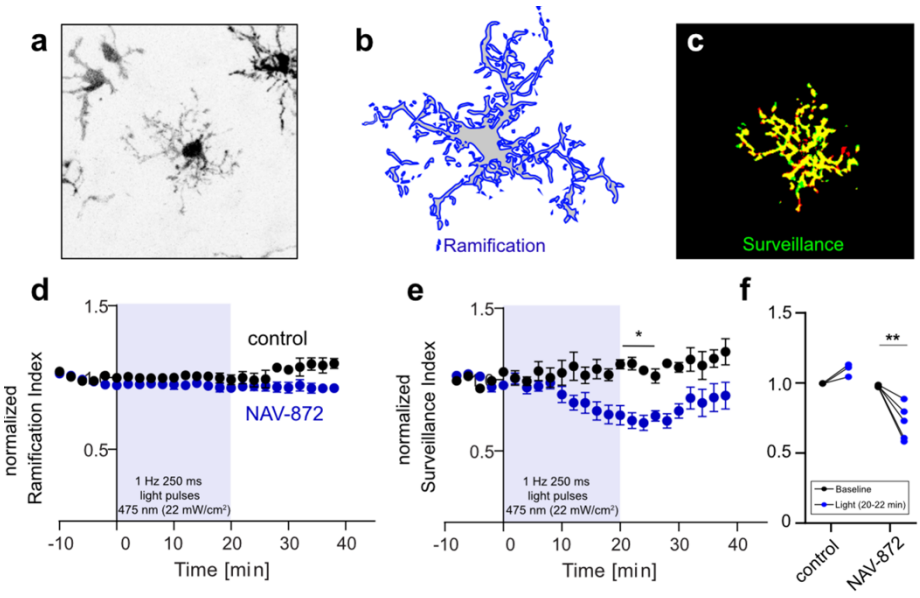

Figure 33: NAV-872 is optolat **48.** A) microglia cell, b) ramification of a microglia cell: represents the surface c) microglia surveillance – fine structures that scan the gross area of microglia using actin networks. D) quantification of photoactivation of **48** versus dark on ramification e/f) quantification of effect of **48** on the surveillance of microglia. Two photon microscopy in brain slices; Statistical analysis: two way ANOVA with Bonferroni post-hoc test.

This experiment clearly demonstrates the light-dependent activity of optolat **48** on the actin network of highly dynamic microglia surveillance. Furthermore, it demonstrates that optolat was incorporated into the tissue and remained in the cells even when under perfusion for a few hours (three microglia cells were imaged per brain slice).

2.2.3 Synthetic truncated latrunculin analogs and further studies.

Latrunculin is very unique in its actin binding mechanism. Its origin from rare marine species strongly limits its availability and the biosynthesis of latrunculin natural products in other organisms has not yet been achieved. The fact that our first truncated latrunculin analogs (latrunculogs) showed almost no activity, that truncated antimalarial latrunculin derivatives have been shown to not affect mammalian cells significantly[240] and the lack of SAR studies on highly truncated, non-macrocyclic latrunculin analogs motivated us to study truncated latrunculin analogs and their bioactivity.

Based on our optimized synthetic route, we were able to accumulate significant amounts of intermediates **20** (Chapter 1-2.2.1) from which we further explored different structure activity relationships (Figure 34 and Table 4).

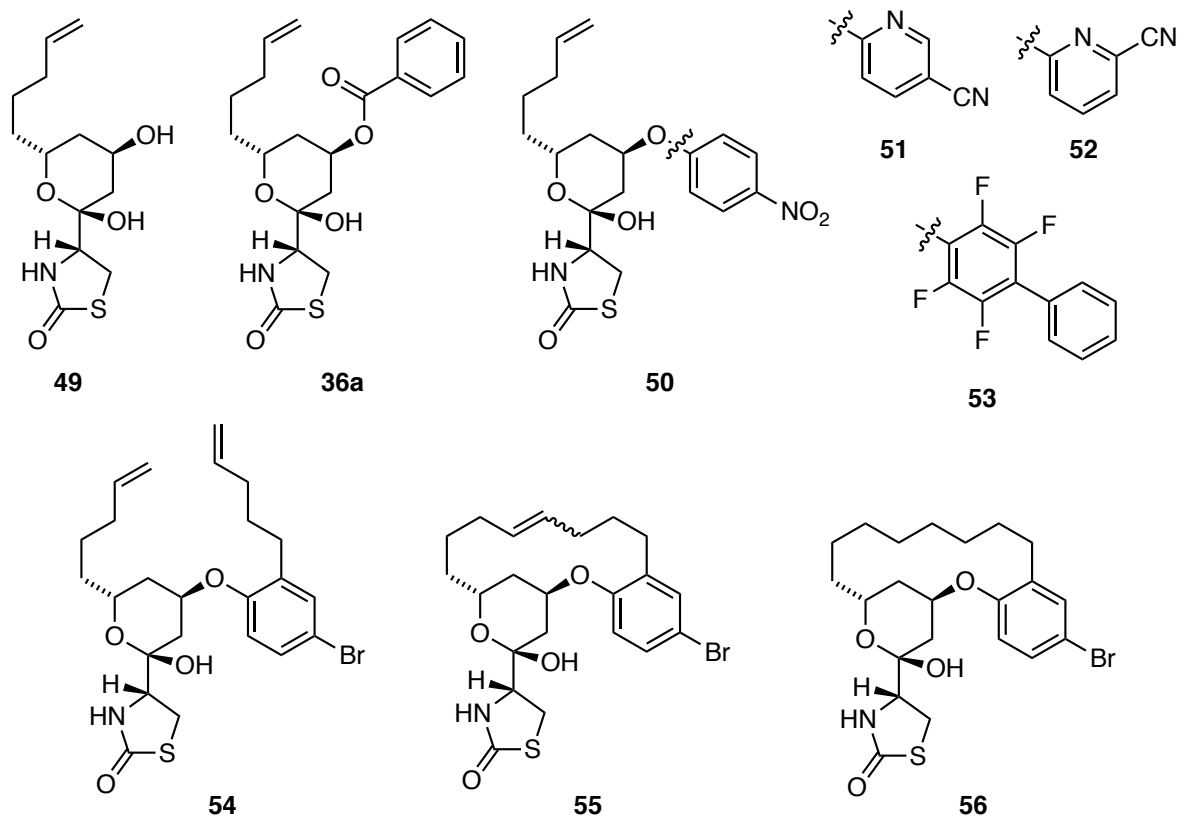

Figure 34: Latrunculog structures investigated.

Secondary alcohol **49** showed no bioactivity. It would be expected that such a structure would in principle be able to bind into the latrunculin binding pocket. It is likely, that the loss of hydrophobicity reduces protein – ligand interactions rendering the molecule inactive. The

installation of phenylester in **36a** restored the bioactivity of latrunculin. Phenylether substituted latrunculogs[z], especially **50, 52, 53** showed improved bioactivity.

Table 4: Antiproliferative activity of Latrunculogs.

structure	EC_{50}	note
49	–	not active
36a	29.1	active
50	13.1	active
51	23.6	active
52	11.2	active
53	12.1	active
54	>30	low solubility
55	>30	low solubility
56	>30	low solubility

Interestingly, bromides **54-56** showed only low activity. Since we have demonstrated that phenyl ether latrunculogs showed good bioactivity, we concluded that possibly, the bromine substituent is disadvantageous to bioactivity. It had been introduced into the structure as a handle for further diversification. This work is currently underway.

In correlation with our computational studies (chapter 1-2.4), we are currently also investigating alterations on the northwestern side chain moiety to probe whether an additional hydrogen bond with Glu207 that was identified in computational work can indeed be exploited.

[z] These latrunculogs were synthesized by Dr. Ruiyang Bao.

2.4 Results and Discussion Computational Studies

The broad variety of structure activity investigations on the latrunculin family of natural products has also furnished a variety of *in silico* investigations of the nucleotide binding site of G-actin and potential latrunculin derivatives.[220,223,249]

The goal of this study was to develop a reliable computational workflow for the prediction of relative binding energies of different latrunculin analogs. To this end, we used the computation platform Maestro (Schrödinger).

2.4.1 Initial Considerations

First, we analyzed all published crystal structures with latrunuclin A and B and decided to use the two crystal structures with the highest resolution for either Latrunculin A or B, 3SJH[250] and 2Q0U[75] respectively. Since both natural products have significant differences in bioactivity, we concluded that possible latrunculin analogs had to be investigated taking some flexibility of the binding pocket into account.

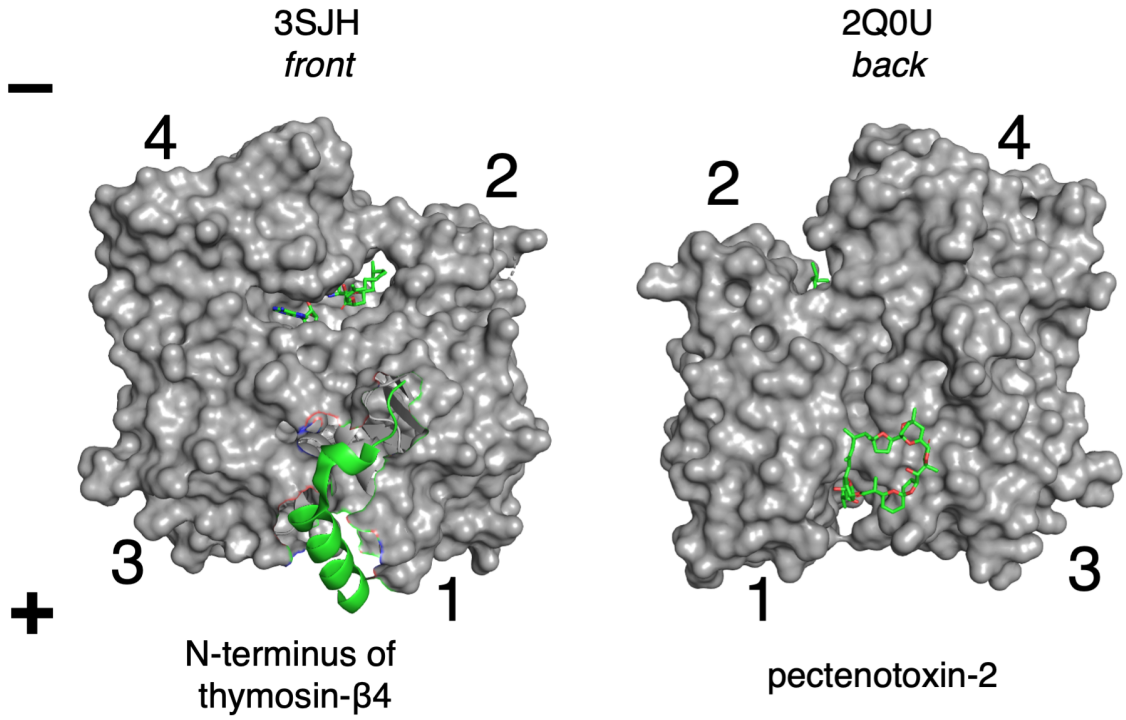

Figure 35: crystal structures used for computational studies.

It should be noted that crystal structure 3SJH contains the N-terminal domain of actin sequestering protein thymosin-β4 bound between subdomains 1 and 3 on the front of the barbed end binding cleft, whereas 2Q0U is G-actin bound to pectenotoxin-2, which binds

analogously to profilin to the back of the barbed end binding cleft.[1] Both crystal structures thus represent important protein conformations in the actin pool. The nature of G-actin however, especially whether the nucleotide binding cleft is accessible, could influence the binding affinity to the small molecule inhibitor and therefore alter the relationship between *in silico* predictions and actual cellular activity.

In the first step towards developing our computational platform, all ligands, ions, and water molecules were removed from the crystal structure. This was important to avoid blockage of possible protein binding sites by ligands that freely diffuse in the structure. We observed that when the ATP binding cleft was unoccupied, large ligand residues would occupy this site in the predicted binding pose. Since about 80% of cellular actin however is bound do ATP[251], we reasoned that in order to represent a realistic scenario, the ATP pocket had to be occupied for our *in-silico* studies.

Macrocyclic structures have many degrees of freedom and can thus adopt many conformations. Compared to very rigid, three dimensionally confined structures with little conformational freedom, a conformational search has to be much wider for flexible structures. Conformational search is computationally expensive. For this reason, we made use of the HPC prince computing cluster and were able to screen up to 10.000 conformations quickly. We tested whether this approach was superior to using a standard conformational search before docking that would identify the 10 energetically most favored conformers. Indeed, re-docking latrunculins A and B into both crystal structures resulted in much better scores when the HPC based conformational search was used (Table 5).

Table 5: comparison of basic conformational search and HPC-based conformational search

	3SJH (Lat XA)		**2Q0U (Lat XB)**	
	HPC based	basic	HPC based	basic
latrunculin A	–9.1	–3.3	–8.4	–7.5
latrunculin B	–8.0	–3.6	–8.6	–3.7

First, we docked the structure activity relationships reported by *Fürstner*.[219] They had described the bioactivity of different latrunculin analogs qualitatively. Strongly active (indicated as +++), medium (±) and inactive (–) compounds could be categorized into three groups. With our computer-based screening, docking scores were in comparable ranges for active and inactive compounds, however derivatives with medium activity were difficult to assess (Figure 36). This may in part be because our prediction cannot assess solubility or cellular uptake, but solely focuses on ligand binding on the isolated protein. The comparable scores for latrunculins A and B, which in the cells show large differences in activity, gave docking

scores in comparable ranges. This is likely because for a ligand to be active, not solely the goodness of fit into the protein pocket, but also early interactions with the protein, solubility and membrane permeability are essential. Structures with large nitrogen and hemiacetal substituents were not suited for this model, because the protein was generally considered rigid. Such structures would require advanced induced fit calculations that are very costly and go beyond the scope of our work.

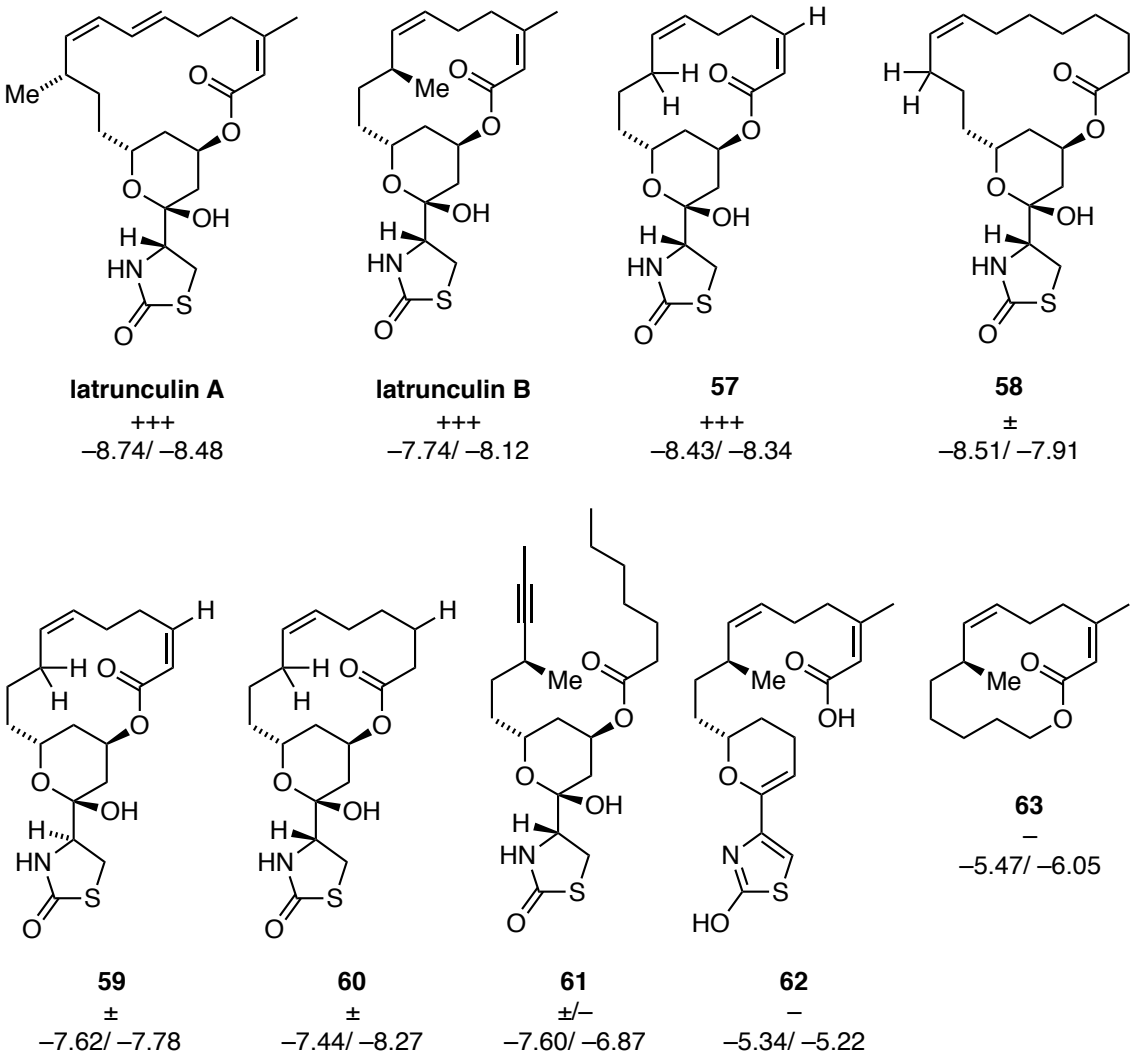

Figure 36: Docking scores (HPC based method) for structures reported by Fürstner *et al.*: left value was docked into 3SJH and the right value into the 2Q0U-based system.

We designed and docked structures of two different kinds. Firstly, structures with an open macrocycle were investigated for their simpler synthetic accessibility. We focused on photoswitches with different substitution patterns and compared docking scores for *cis* and *trans* isomers. Further, we investigated whether modifications of the western macrocycle

fragment could potentially increase ligand activity. For macrocyclic structures, we looked at varying macrocycle sizes and substitution patterns for the azobenzene.

2.4.2 Non-Macrocyclic Photoswitches

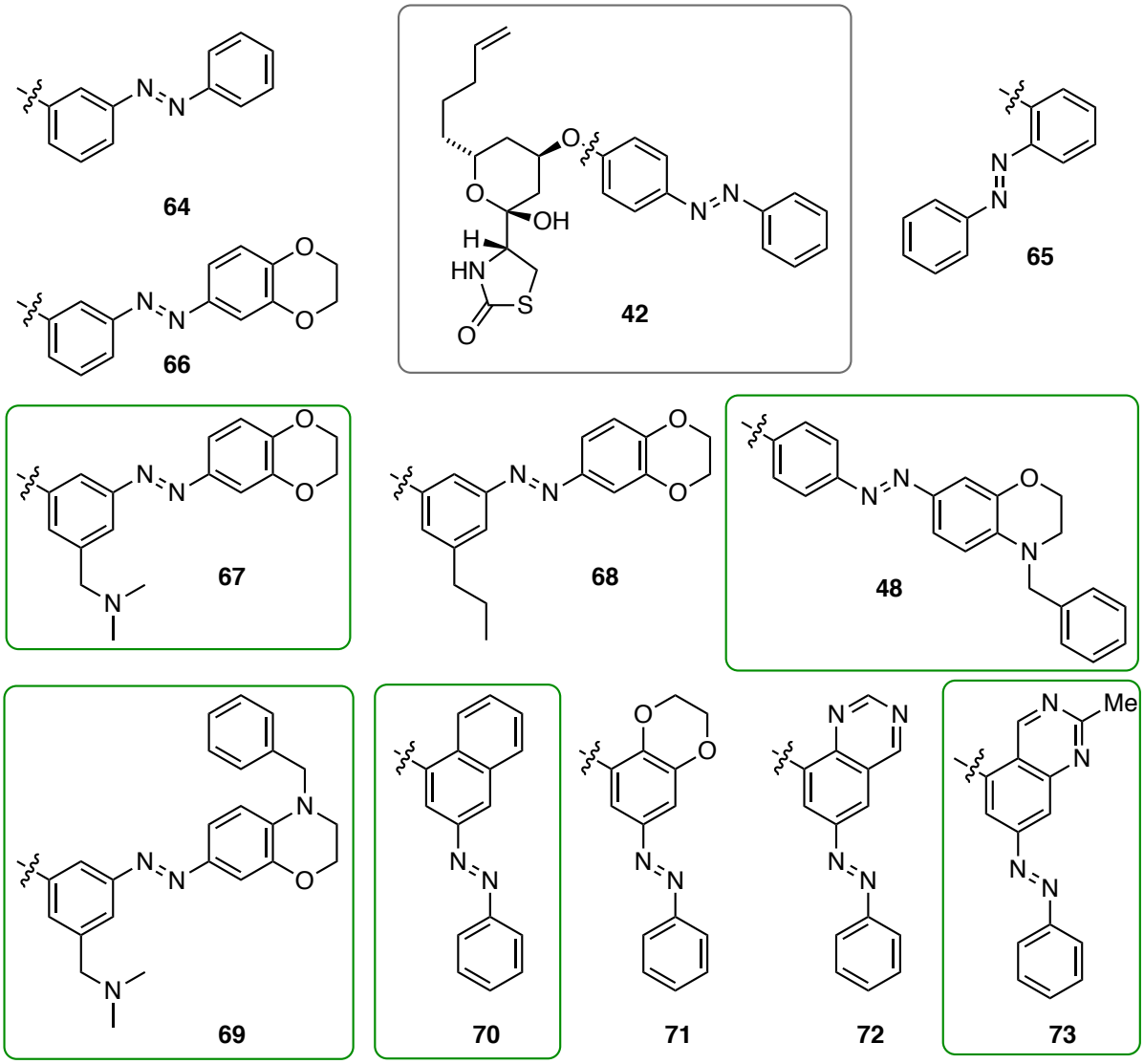

Figure 37: Structures of docked (hypothetical: **64-73**) non macrocyclic azolatrunculin analogs.

Table 6: Docking scores for *cis* and *trans* non-macrocyclic photolatrunculins in both crystal structures and difference in docking value.

	cis		***trans***		**Δ (*trans–cis*)**	
	3SJH	**2Q0U**	**3SJH**	**2Q0U**	**3SJH**	**2Q0U**
42	–7.36	–6.54	–6.96	–6.13	0.40	0.41
64	–7.42	–6.83	–7.18	–6.34	0.24	0.49
65	–7.17	–6.17	–7.12	–6.38	0.05	–0.21
66	–7.32	–7.02	–6.59	–6.39	0.73	0.63

67	–8.33	–6.32	–6.64	–5.82	**1.70**	0.49
68	–7.52	–6.71	–7.04	–6.27	0.48	0.44
optolat **48**	–7.99	–7.30	–7.38	–5.37	0.61	**1.93**
69	–8.02	–7.63	–5.87	–6.43	**2.15**	**1.21**
70	–7.36	–6.53	–5.59	–4.67	**2.77**	**1.86**
71	–6.85	–4.75	–6.75	–4.75	0.10	0.00
72	–7.03	–6.28	–7.13	–5.16	-0.10	**1.13**
73	–7.11	–6.69	–5.41	–4.91	**1.97**	**1.78**

In non-macrocyclic structures, both upper arms of the latrunculin analogs have great conformational freedom to adapt the conformation that causes least steric clash with the protein. As a consequence, azobenzene switches with *ortho*, *meta*, *para* substitution had comparable binding scores for *cis* and *trans* isomers (Figure 37, Table 6). Optolat (**48**) bearing a *para*-*N*-benzyloxazin photoswitch gave binding scores of a large difference of about 1.9 docked into crystal structure 2Q0U. Interestingly, the difference in binding scores was around 0.6 in 3SJH. Azolatrunculins **67** and **68** bearing a dimethyl amino methyl substituent on the first aryl ring of the photoswitch showed a larger score difference in 3SJH than in 2Q0U. Quinoline derivative **70** shows very promising binding score differences. While *cis* is predicted to bind G-actin, no sensical binding pose could be generated for the *trans* isomer. Quinazoline derivatives like **72** did show only slight differences in binding poses whereas 2-methyl quinazoline derivative **73** is predicted to bind preferentially in as the *cis* isomer. Overall the derivatives with quinoline derived azobenzene photoswitches show lower docking scores than previous structures, especially in 2Q0U, indicating their predicted lower binding affinity.

The open-chain azolatrunculins shown demonstrate the importance to investigate several crystal structures of high quality, since predicted selectivity of *cis* or *trans* occurs in both considered systems. It remains to be determined if the results can be regarded interchangeably as a prediction for actin binding ability or whether one crystal structure gives more realistic predictions.

A comparison of experimentally determined cellular bioactivity and predicted activity can be found at the end of this chapter.

2.4.3 Macrocyclic Photoswitches

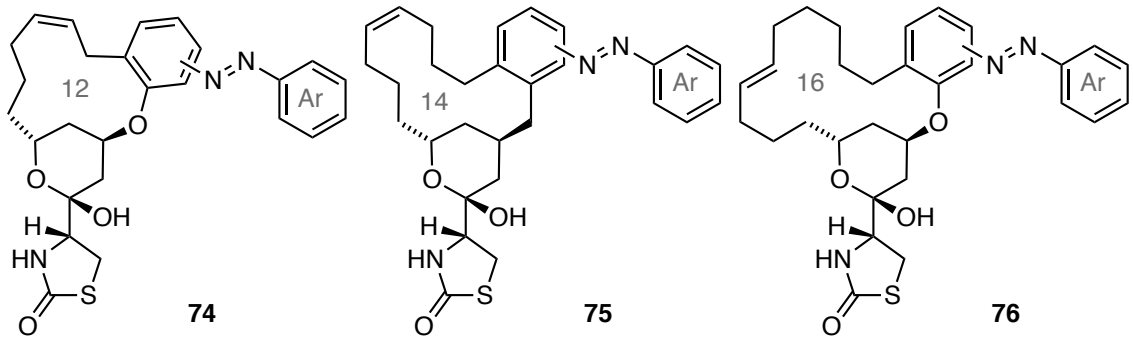

Figure 38: Series of hypothetical macrocyclic latrunculin structures investigated.

The macrocycle decreases the rotational freedom of both upper arms of the latrunculin derivatives and locks the bound azobenzene photoswitch into a conformation with much more rigidity. As a consequence, a steric clash that is caused by the one isomer cannot simply be evaded by rotation and results in reduced binding affinity. Oftentimes, we found that even though a good docking score was reported, the docking pose was non sensical because the latrunculin pharmacophore was not bound in the binding pocket in the correct conformation. This was especially the case for *o*,*o*'-substituted 14- and 16-membered macrocycles. The substitution caused too much steric clash that the *trans* azobenzenes could not be docked into the latrunculin binding site, or at least only under strong conformational alteration which is expected to strongly attenuate binding affinity. In a 12-membered macrocycle, which leaves more room for the photoswitch, ortho substitution resulted in strong differences between the docking scores of *cis* and *trans*. While meta substitution on the 16-membered macrocycle allowed for docking of the *cis* isomer, the *trans* isomer did not fit. This trend continues for 12- and 14-membered macrocycles.[aa]

[aa] For more details see Ref. 216.

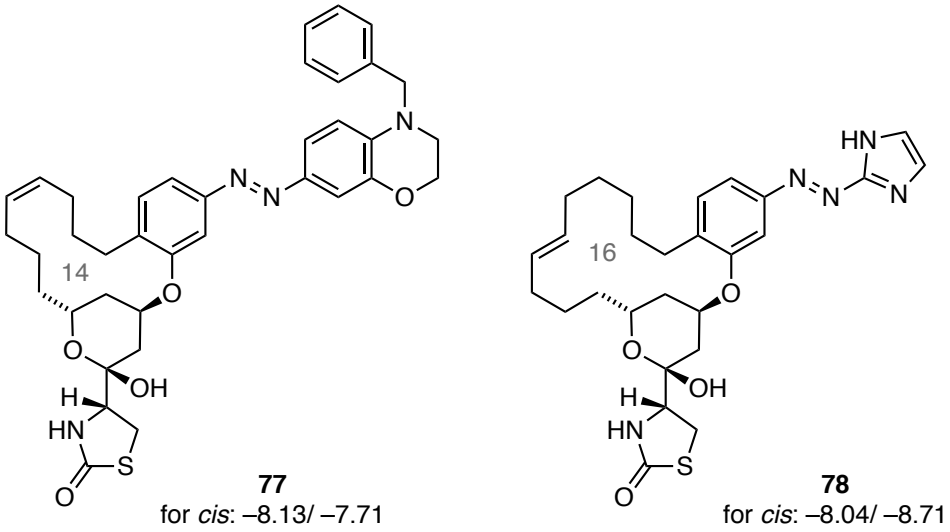

77
for *cis*: –8.13/ –7.71

78
for *cis*: –8.04/ –8.71

Figure 39: Hypothetical macrocyclic photolatrunculin derivatives with diversification on the distal arene that indicated no efficient binding of the *trans* isomer but gave high docking scores for the *cis* isomer. Docking scores for *cis* isomer in 3SJH/ 2Q0U.

We further substituted the distal arene of the photoswitch with either large, bulky substituents like *N*-benzyl oxazine derivative **77** or heteroarenes as in **78** (Figure 39). In both cases, *trans* isomers did not efficiently bind the binding pocket of latrunculin, whereas the *cis* isomers bound with high docking scores. *Para*-substitution of the azobenzene with respect to the ether bridge overall gave no differences in binding affinity for G-actin, because the azobenzene photoswitch reaches far outside the latrunculin binding pocket and steric clash cannot be generated upon isomerization.

Overall it can be concluded, that the size of the macrocycle can be varied according to synthetic feasibility and the model predicts that especially *meta*-substitution with respect to the ether bridge would lead to strong affinity differences between *cis* and *trans*.

2.4.4 Towards Improved Non-Macrocyclic Structures

In a next step, we investigated whether alteration of the northwestern side chain of the open chain latrunculin derivatives would yield better predicted binding scores and therefore promising structural patterns for latrunculog development.

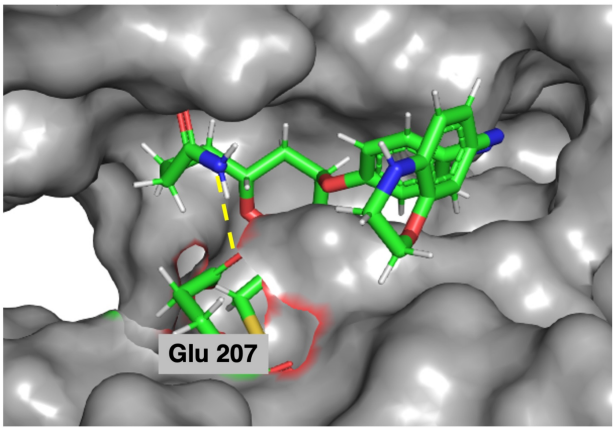

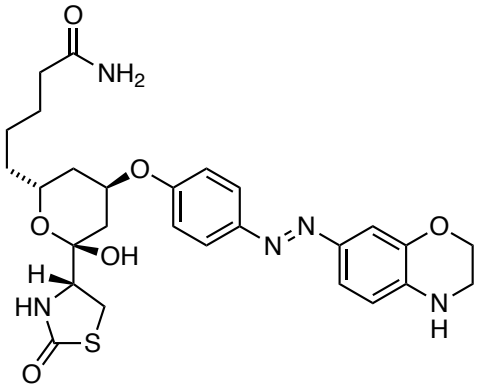

79

Figure 40: Identification of a possibly advantageous hydrogen bond between the northwestern side chain of hypothetical latrunculin analog *trans* **79** and G-actin (indicated in yellow, dashed) (pdb: 2q0u).

We discovered that a hydrogen bond donor on this residue could potentially build hydrogen bonding interactions with Glu207 of G-actin (Figure 40). Such an additional strong interaction between the ligand and protein would be expected to increase the potency of a fully synthetic latrunculin analog significantly. Studies investigating this experimentally are currently underway.

2.4.4 Comparison of *In Silico* Studies with Cell Proliferation Assays

Overall, a preliminary comparison shows that the theoretical studies match our experimental results. Ester bridged non-macrocyclic photoswitchable latrunculins bound G-actin with comparable affinity as latrunculin B and switching of the photoswitch was ineffective for the binding affinity, because the photoswitch reached too far out of the binding pocket. When connected *via* an ether bridge, even azobenzenes that are generally considered sterically more demanding, did not lead to different affinities depending on their isomerization state.

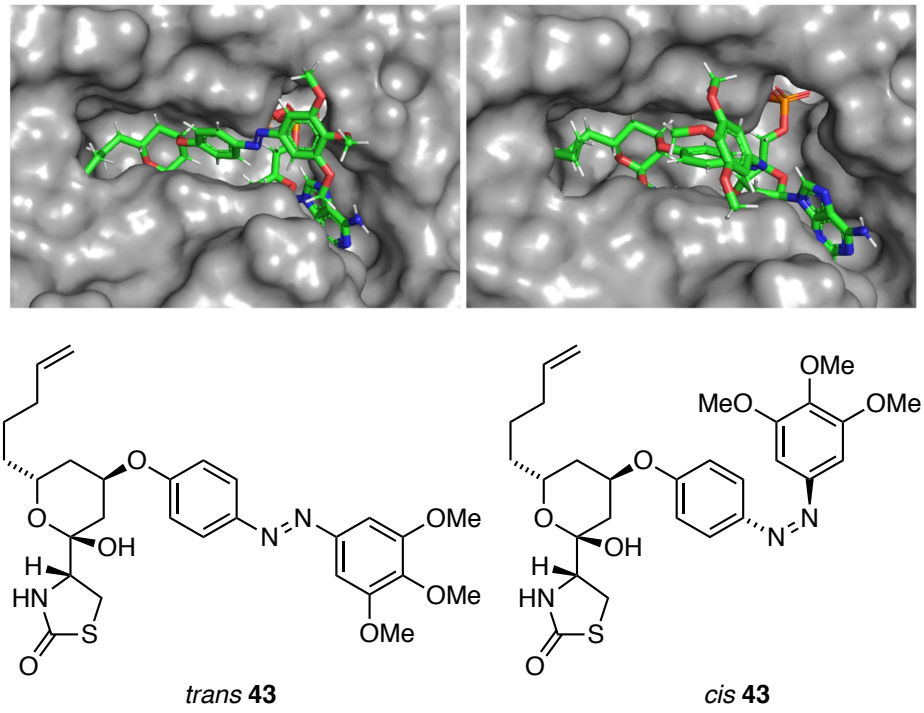

Figure 41: Docked structures of *cis*- and *trans*-**43** alongside ATP into crystal structure 3SJH.

This is nicely observed in figure 41, where *cis para*-trimethoxy azobenzene does not cause steric clashes with G-actin (Figure 41). The *trans* isomer would just reach out into the solvent space. When considering the same docking pose, it can be expected that *ortho*- and *meta*-substitution would result in a similar toleration of the photoswitch.

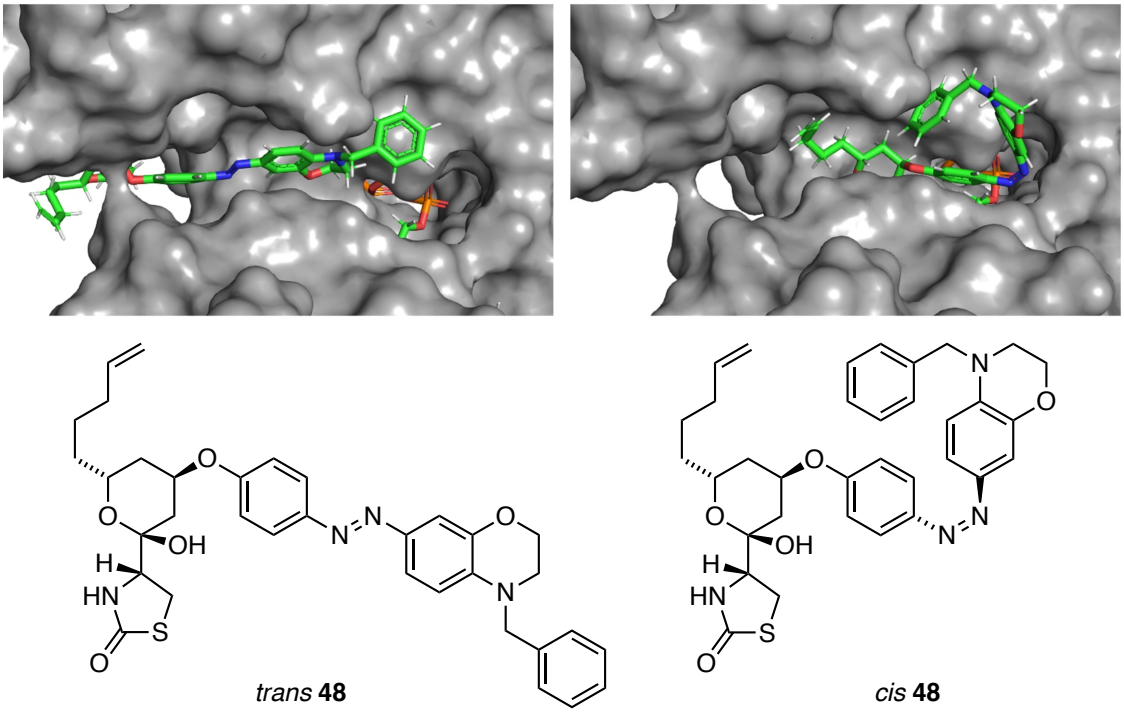

Figure 42: predicted binding poses of *trans* (left) and *cis* **48** (right) alongside ATP (pdb:2q0u).

We were pleased to find, that the very bulky azolatrunculin **48** that was predicted to have a strongly light dependent binding affinity to latrunculin also showed this effect in our biological investigations. **48** was able to bind G-actin only in the *cis* isomer in the crystal structure 2Q0U, whereas the pose for *trans* was unreasonable (Figure 42). In 3SJH, two relatively good poses could be generated, however the *trans* diazine bond appears to be rotated. Clearly, in this case, 2Q0U derived prediction matches the biological results.

An initial induced fit calculation gave that 3SJH would favor *trans* binding, while 2Q0U preferentially binds the *cis* isomer. The experimental result in cells is again matched by the 2Q0U-derived system. 2Q0U is the crystal structure of G-actin bound with pectenotoxin-2, which binds analogously to profilin and has comparable biological effects on actin. 2Q0U thus represents the polymerization competent profilin-ATP-actin and not the sequestered thymosin-β4-ATP-actin complex,[1] which would explain the better matching predictions with the 2Q0U derived crystal structure towards actual biological results.

2.5 Summary and Outlook

The results described in this work clearly highlight the promise of latrunculin derived structures to target actin. The efficient and scalable synthesis allows for access of gram quantities of important advanced intermediates that can then be diversified in a few steps to provide target molecules.

Optolat **48** shows clear light-dependent effects on the actin morphology of human cancer cells and was successfully applied in the light-dependent control of dynamic processes in microglia. In ongoing studies, we address the current limitations of cell permeability and aim at improving the pharmacological effects by structural modifications of the photoswitch and latrunculin core. Further investigations in *Saccharomyces Cerevisiae* and on primary cell lines and neural cell cultures are underway and a broader group of human cancer cells will be screened for increased sensitivity towards optolatrunculin. Live-cell imaging in presence of optolatrunculin will be conducted to explore the capabilities of optolatrunculin to alter actin dynamics by locally sequestering G-actin in highly motile cells. To this end, we initially plan on employing the m-Cherry LifeAct expressing MDA-MB-231 cells, that we have used in our studies towards a second generation optojasp (chapter 1-3).

In-silico studies indicate, that a further increase in potency of readily accessible synthetic latrunculogs is possible. The synthesis of such structures is currently underway.

3 Jasplakinolide

3.1 Project Outline

Following the first generation optojasps that were developed by Dr. Malgorzata Borowiak and Dr. Florian Küllmer in a broad collaboration, we sought to further optimize this tool in terms of binding affinity and biological applicability.

The synthesis of optojasps was conducted in the labs of Prof. H.-D. Arndt at the Friedrich Schiller University of Jena by Dr. F. Küllmer and Dr. V. Nasufović. They also determined the optimum switching wavelength for preliminary biological investigation. Cell Proliferation Assays and subsequent migration assays and imaging were performed by the author of this thesis herself.

The Discussion below is part of a manuscript that is currently prepared for publication.

The first generation optojasp showed that structural and functional properties of actin could be altered light-dependently by means of a light-activatable jasplakinolide derivative. Its activation was most efficiently achieved with 390 nm light and the activated *cis* isomer (EC_{50}(HeLa) = 1.5 µM) underwent slow thermal relaxation ($t_{1/2}$ = 36 h). The *cis* to *trans* isomerization was photochemically achieved at wavelengths above 470 nm.[252]

In our follow-up study we aimed at developing a second generation optojasp, that would in an ideal case be completely inactive in the dark state and show F-actin binding affinity that is comparable to jasplakinolide in the activated isomer. Further, we envisioned that longer activation wavelengths would allow for the application of optojasps in a broad range of cells and tissues that are known to be more sensitive to violet light. Paired with a more efficient thermal deactivation (shorter thermal half-life of the activated isomer), new optojasps would provide a superior tool for the investigation of dynamic actin-dependent effects in a variety of cells and tissues.

3.2 Results and Discussion

3.2.1 Evaluation of Structure Activity Relationship of Optolat Derivatives

The new photoswitchable jasplakinolide analogs were synthesized by solid-phase peptide synthesis, followed by closure of the macrocycle and extension with azobenzene photoswitches as described previously.[102,108,112] The new structures varied in linker length and substitution patterns of the photoswitch. Further, the polyketide moiety was modified and the ester of the cyclodepsipeptide was replaced by *N*-hydrogen and *N*-methyl amides (Figure 43).

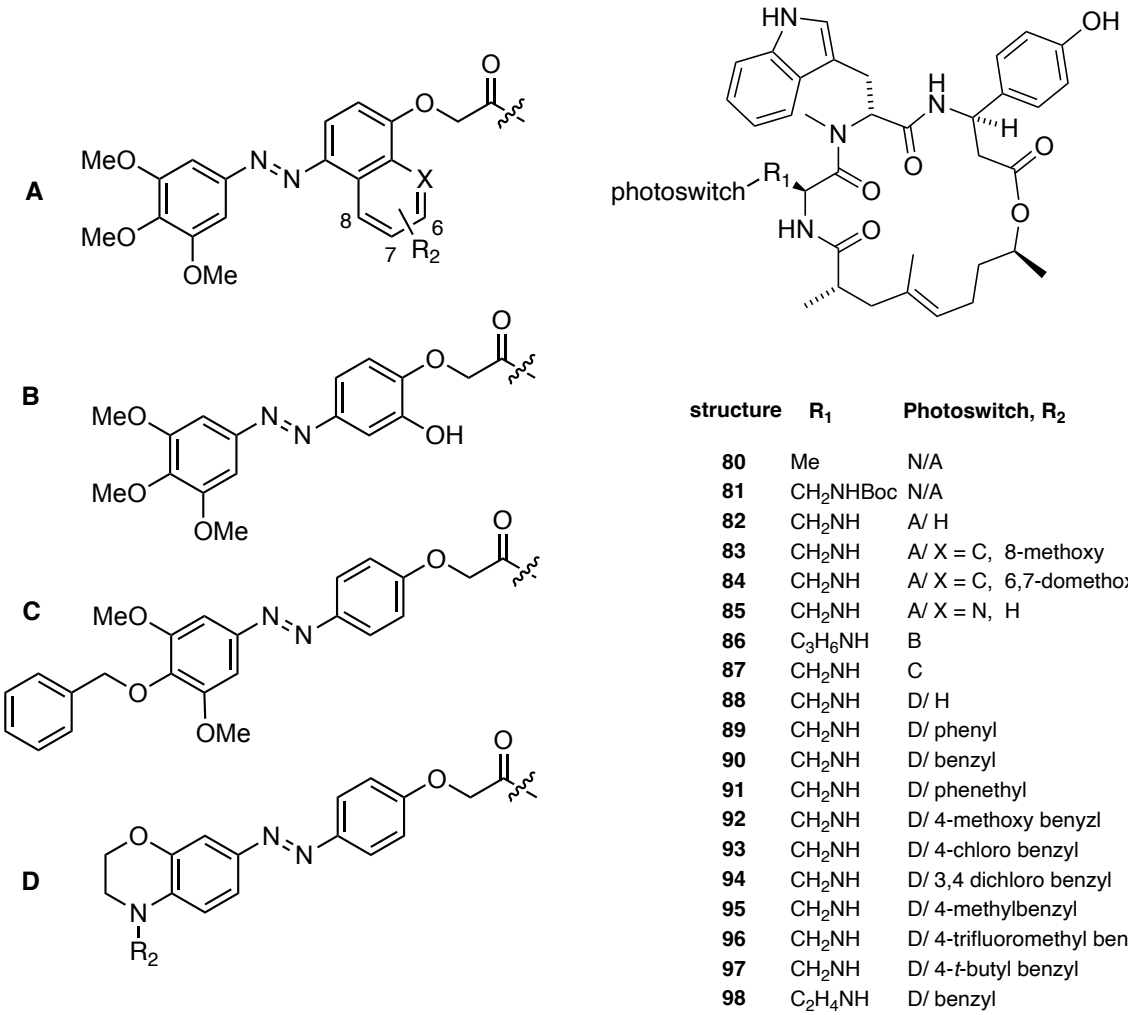

structure	R_1	Photoswitch, R_2
80	Me	N/A
81	CH_2NHBoc	N/A
82	CH_2NH	A/ H
83	CH_2NH	A/ X = C, 8-methoxy
84	CH_2NH	A/ X = C, 6,7-domethoxy
85	CH_2NH	A/ X = N, H
86	C_3H_6NH	B
87	CH_2NH	C
88	CH_2NH	D/ H
89	CH_2NH	D/ phenyl
90	CH_2NH	D/ benzyl
91	CH_2NH	D/ phenethyl
92	CH_2NH	D/ 4-methoxy benyzl
93	CH_2NH	D/ 4-chloro benzyl
94	CH_2NH	D/ 3,4 dichloro benzyl
95	CH_2NH	D/ 4-methylbenzyl
96	CH_2NH	D/ 4-trifluoromethyl benzyl
97	CH_2NH	D/ 4-*t*-butyl benzyl
98	C_2H_4NH	D/ benzyl

Figure 43: Optojasps with different photoswitches and linker lengths.

The first series focused on the variation of different photoswitches that were installed with varying linker lengths (Figure 43). Interestingly, optojasps with naphthyl-photoswitch (**82**) and analogs thereof (**83**-**85**) were completely inactive (Table 7). An additional hydroxy group *ortho* to the diazine bond (**86**) that was thought to have the potential to increase steric demand did not increase potency. Oxazine **88** showed strong antiproliferative activity with potencies in a similar range as jasplakinolide, however the activity was not light-depedent. The installation of

a benzyl group on the oxazine nitrogen (**90**) lead to strong antiproliferative activity under activated conditions. In the dark, **90** was fully inactive. Interestingly, phenethyl derivative **91** was inactive in both isomers.

Table 7: Antiproliferative activity of optojasp derivatives with different photoswitches and linker lengths. slow = 75 ms/ 15 s, fast = 25 ms/ 0.5 s. + > 50% antiproliferative, – inactive.

#	λ [nm] / protocol	EC_{50} [μM] light	EC_{50} [μM] dark	activity	Δ light/ dark
80	N/A	0.07	0.07	+	N/A
81	N/A	1.01	1.37	+	N/A
82	390 nm/ slow	-	-	–	-
83	370 nm/ slow	1.07	1.19	<50%	-
84	390 nm/ slow	-	-	–	-
85	390 nm/ slow	2.21	2.75	<50%	-
86	390 nm/ slow	0.43	0.53	<50%	-
87	390 nm/ slow	-	-	–	-
88	410 nm/ fast	0.37	0.54	+	-
90	410 nm/ fast	0.74	-	+	++
91	410 nm/ fast	-	-	–	-

Based on the very selective antiproliferative activity of optojasp **90**, and the inactivity of **91** we investigated various substitution patterns on the oxazine to explore the binding site. Further, *para* substitution on the benzyl group with methyl-, trifluoromethyl- or the 3,4-dichloro-derivatives were well tolerated. *tert*-Butyl substitution led to complete inactivity of optojasps and *para*-methoxy or chloro substitution only led to partial antiproliferative activity (Figure 43, Table 8).

Table 8: Antiproliferative activity of optojasp with different *N*-aryl substituents.

#	λ [nm] / protocol	EC_{50} [μM] light	EC_{50} [μM] dark	activity	Δ light/ dark
89	410 nm/ fast	0.45	-	+	++
92	410 nm/ fast	0.80	-	<50%	-
93	410 nm/ fast	1.07	-	<50%	-
94	410 nm/ fast	0.59	-	+	++
95	410 nm/ fast	0.99	-	+	++
96	410 nm/ fast	0.57	-	+	++
97	410 nm/ fast	-	-	–	-
98	410 nm/ fast	0.18	4.94	+	+

In the next series the ester of the cyclodepsipeptide was replaced by *N*-hydrogen or *N*-methyl amides (Figure 44). These derivatives showed no antiproliferative activity in both, irradiated and dark conditions (Table 9). This was surprising, because the amide analog **99** was found

to have comparable activity in *in vitro* actin polymerization as jasplakinolide.[bb] The reason for this strong activity difference between *in vitro* and cellular activity may be based on different cell permeabilities of the compounds. It is known that seemingly small structural differences as found between amatoxin and phalloidin can completely alter membrane permeability, rendering compounds less or fully inactive in cell-based investigations.[96]

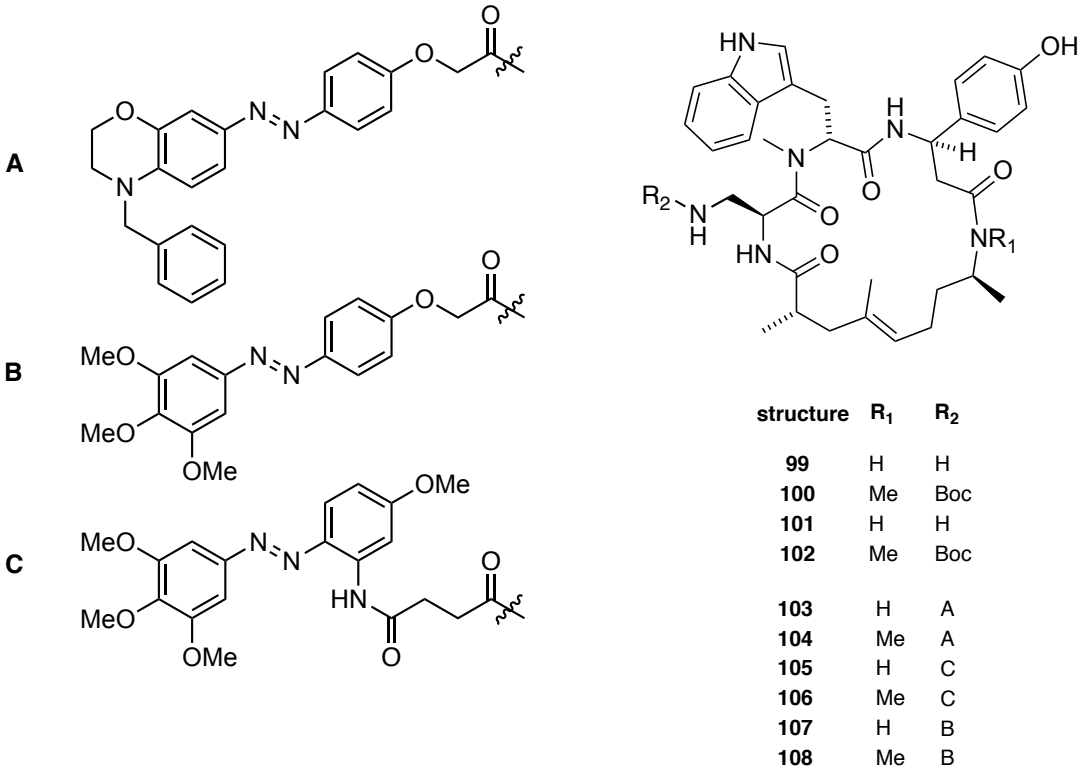

structure	R_1	R_2
99	H	H
100	Me	Boc
101	H	H
102	Me	Boc
103	H	A
104	Me	A
105	H	C
106	Me	C
107	H	B
108	Me	B

Figure 44: Amide series of jasplakinolide derivatives.

[bb] The *in-vitro* actin polymerization assay was performed by Dr. F. Küllmer and Dr. V. Nasufović.

Table 9: Amide derivatives of optojasp

#	λ [nm] / protocol	EC_{50} [μM] light	EC_{50} [μM] dark	activity	Δ light/ dark
99	N/A	-	-	–	N/A
100	N/A	-	-	–	N/A
101	N/A	-	-	–	N/A
102	N/A	-	-	–	N/A
103	410 nm/ fast	-	-	–	-
104	410 nm/ fast	-	-	–	-
105	390 nm/ slow	2.29	3.18	<50%	-
106	390 nm/ slow	-	-	–	-
107	370 nm/ slow	-	-	–	-
108	370 nm/ slow	-	-	–	-
103	410 nm/ fast	-	-	–	-
104	410 nm/ fast	-	-	–	-

We were interested in the influence of the alkyl sidechain substitution and geometry of the previously investigated "optojasp 8"[112,253] on antiproliferative activity (Figure 45). Interestingly, while the removal of the methyl group next to the ester increased antiproliferative activity of the photoswitch compared to the previous communication, albeit without light-dependence, introduction of an additional methyl group and the variation of the olefin substitution pattern was not tolerated (Table 10).

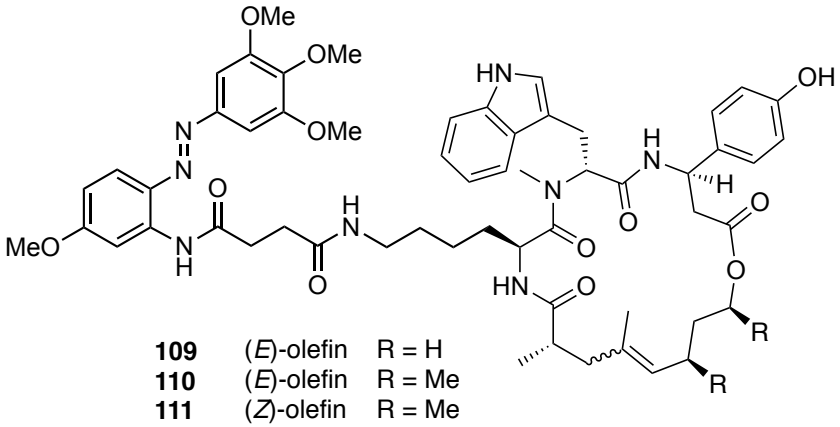

109 (*E*)-olefin R = H
110 (*E*)-olefin R = Me
111 (*Z*)-olefin R = Me

Figure 45: Analogs of "optojasp 8" with different alkyl substitution patterns and olefin geometry.

Table 10: Antiproliferative activity of optojasp derivatives with altered alkyl moiety and olefin geometry.

#	λ [nm] / protocol	EC_{50} [μM] light	EC_{50} [μM] dark	activity	Δ light/ dark
109	380 nm/ slow	0.19	0.19	+	-
110	390 nm/ slow	-	-	–	-
111	390 nm/ slow	-	-	–	-

3.2.1 Photophysical Properties of optojasp 90

Optojasp **90** stood out among the new series for its superior light vs. dark selectivity and the general advantages on biological systems, when longer wavelengths could be used to achieve activation of optojasp. Additionally, the fast thermal relaxation which essentially allowed full deactivation of optojasp as soon as irradiation was stopped, was promising. To confirm our assumption, that optojasp **90** can be efficiently activated with a broad range of wavelengths, we reevaluated antiproliferative activity at different wavelengths between 410 and 565 nm (Figure 46).

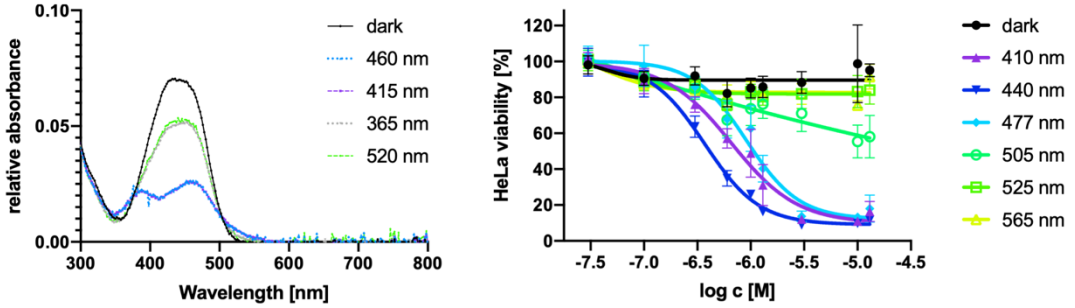

Figure 46: UV-Vis spectrum of optojasp **90** (left) and wavelength dependent cell proliferation assay in HeLa cells (right).

From the UV-Vis spectrum (Figure 46, left) it is apparent, that any wavelength between the two isosbestic points (375 and 504 nm) would lead to at least partial activation of optojasp. Indeed, strong antiproliferative activity was observed at 410 nm (EC_{50} = 0.66 µM), 440 nm (EC_{50} = 0.37 µM) and 477 nm (EC_{50} = 0.91 µM). 440 nm is clearly the preferred activation wavelength for **90**.

3.3.1 Biological evaluation of optojasp 90

Following our initial biological evaluation through cell proliferation assays and having established the advantageous photophysical properties of **90**, we proceeded to establish its function in a variety of biological settings. In addition to visualization with immunofluorescence in fixed cells, we monitored the activity of **90** using live-cell imaging. Further, we investigated the effect of our lead compound on cellular migration in wound healing assays.

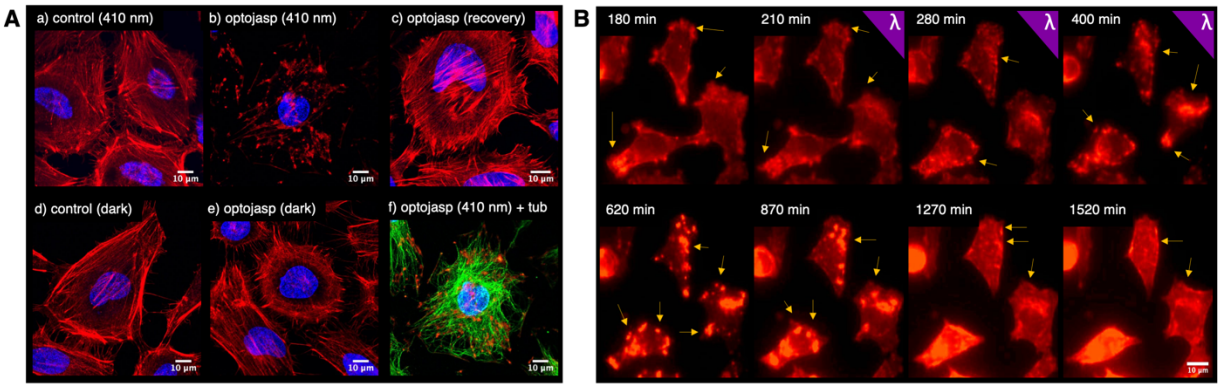

Figure 47: Light-dependent effect of optojasp **90** on human cancer cells under global irradiation. **A**) HeLa cells were treated with optojasp **90**, 3 uM or control (cosolvent) and exposed to either dark (5 h), 410 nm pulsed irradiation (5 h, 25 ms/ 0.5 s) conditions or first irradiation (5 h) followed by dark (16 h). Upon treatment, cells were fixed, permeabilized and stained; nucleus: blue, actin: red, tubulin: green. (40 x, confocal microscope). **B**) live-cell imaging of MDA-MB-231 mCherry LifeAct treated with optojasp **90** first in the dark (0-180 min), then under pulsed irradiation with 395 nm (25 ms/ 0.5 s) (181 – 420 min) followed by dark. (40x, widefield microscope).

Figure 47A shows the effect of **90** on HeLa cells using immunofluorescence on fixed cells. In the activated (irradiated) form, **90** induced aggregation of actin in a concentration dependent manner (Fig. 47Ab; other concentrations not shown). The tubulin network remained unaffected under these conditions (Fig. 47Af). Treatment with **90** in the inactive (dark-adapted) form resulted in no change in actin phenotype (Fig. 47Ae). Notably, the aggregates formed under irradiation gradually disappeared once the light was turned off, which results in the thermal deactivation of the filament stabilizer (16 h dark after 5 h 410 nm; Fig 47Ac). The reversibility of jasplakinolide induced F-actin aggregation upon washout has been described before.[254] Our first generation of optojasp, which do not thermally relax quickly, required irradiation with a second wavelength to favor the inactive form. Therefore, full reversibility was difficult to demonstrate.[112]

The full reversibility of **90** could be demonstrated using live-cell imaging. For this we used MDA-MB-231 cells stably expressing mCherry LifeAct[cc], which is commonly employed to visualize F-actin.[198] Notably, the onset of aggregation was delayed following light administration. However, within 30 minutes of irradiation, lamellipodium protrusions were reduced, followed by retraction (Fig. 47B, t = 210 min). Subsequently, aggregate formation was observed (t = 280, 400 min). After the light was turned off, these aggregates first continued to grow in size and fused to form larger structures (t = 620 min). Subsequently, they migrated

[cc] The cell line was kindly provided by Prof. A. Akhmanova, Utrecht University, The Netherlands.

inwards and began to disassemble (*t* = 870 min). Approximately 20 h after irradiation stopped, the aggregates appeared to be largely dissolved (t = 1270, 1520 min). Under control conditions, i.e. in the absence of compound, the cell motility and protrusion dynamics remained unaffected during irradiation (Fig. 48).

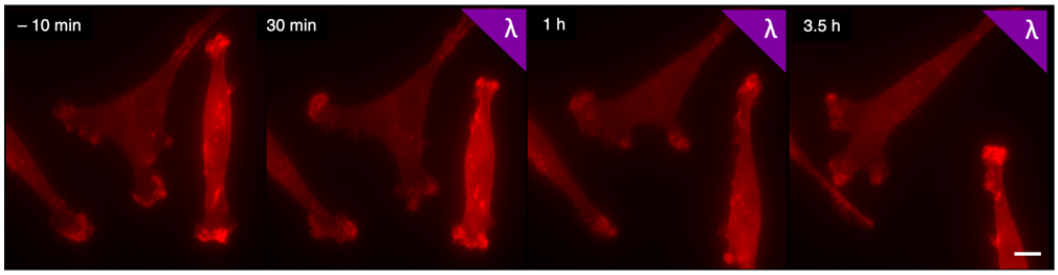

Figure 48: Live-cell imaging of MDA-MB-231 mCherry LifeAct cells under control conditions: cells were incubated with cosolvent only, imaged 3 h in the dark, then 4 h under light: λ = 395 nm, 25 ms/ 0.5 s. Scale bar = 10 µm.

Our observations are in agreement with reports that describe that the initial effect of jasplakinolide is the inhibition of actin turnover and retrograde flow in lamellipodia.[47,255] Filament polymerization and depolymerization in lamellipodia are essential for efficient treadmilling and filament turnover takes place within seconds to minutes.[47,256] General stabilization of F-actin and hence inhibition of depolymerization leads to attenuated (leading edge) lamellipodium protrusion dynamics. Further, jasplakinolide has been reported to induce nucleation, which leads to a fast depletion of sequestered G-actin and also prevents filament elongation by monomer sequersteration.[100] Jasplakinolide treatment leads to the formation of F-actin punctae, i.e. amorphous aggregates that coalesce into large aggresomes and inclusion bodies that resemble Hirano bodies.[257,258] Hirano bodies are actin-inclusion bodies that have been linked to the development and progression of neurodegenerative diseases.[259] The cellular formation of these aggregates has been reported to be highly cell type dependent and to be linked to polymerization competent G-actin concentrations. In cells with strongly pronounced actin cables and stress fibers, significant aggregate formation is observed only after the G-actin concentration has been augmented by remodeling of stress fibers.[100] Myosin II is involved in the formation of these aggresomes.[260]

The delayed observation of aggregate formation with respect to light administration can be explained by a sudden drop in the concentration of G-actin capable of polymerization upon optojasp binding. Before filament elongation and aggregation can occur a reorganization of the actin network is required. The prolonged growth and coalescence of actin aggregates after deactivation of optojasp **90** (light off), as well as retrograde flow is linked to myosin II dynamics.

Since myosin II is not affected by jasplakinolide (and hence optojasp), such a delay is expected.[47,257] Deaggregation depends on chaperones, microtubules, proteasomes and autophagy,[254] which explains the observed slow disassembly of actin aggregates.

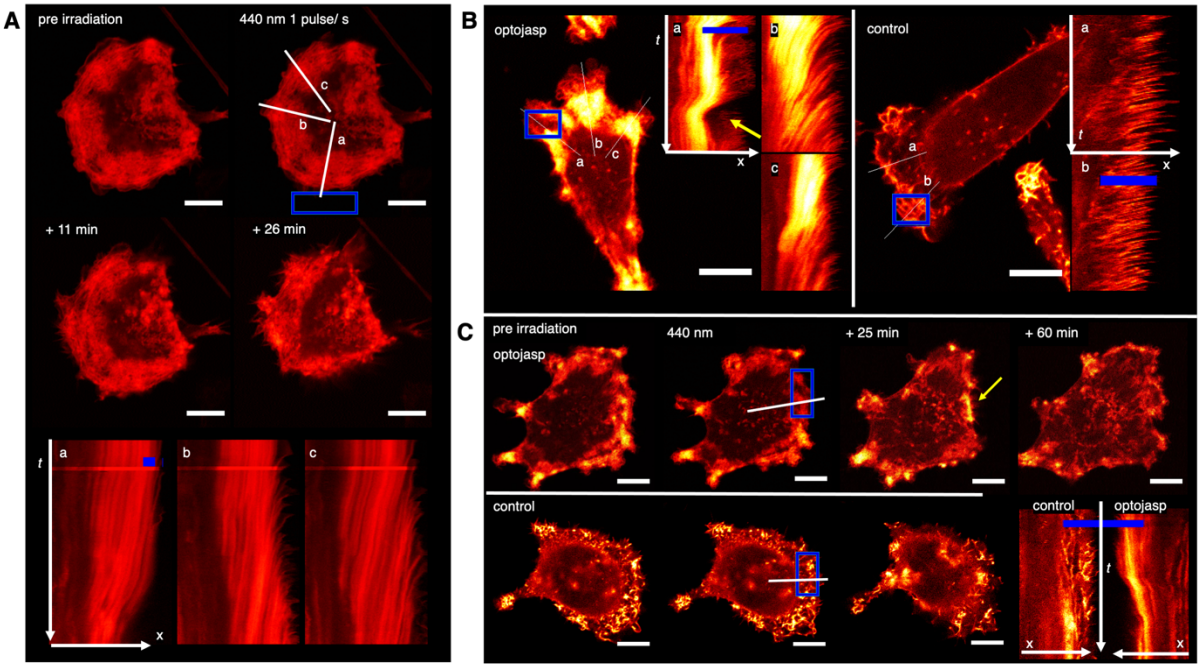

Figure 49: Live-cell Imaging under local activation of optojasp **90**: **A**) A small region (ROI, blue) outside of the MDA-MB-231 mCherry LifaAct cell was irradiated with 440 nm pulses (1 min, ca. 1 pulse/s) lines and a/b/c indicate axes represented in kymographs. **B**) in the presence of optojasp, MDA-MB-231 mCherry LifeAct cells react strongly to ROI with 440 nm light pulses (1 puls/ sec.): control: no change in actin dynamics. **C**) MDA-MB-231 mCherry LifeAct cells with irradiation in the lamellipodium. Top row in presence of optojasp, bottom row control (cosolvent). Bottom right direct comparison of kymographs of treated and untreated cell; scale bar: 10 µm; C-E: confocal microscope, 63x objective. mCherry LifeAct signal: gradient from red (lower intensity) to yellow (high intensity), intensities between images/ cells are not comparable (LifeAct expression different between cells).

The advantage of photoswitchable jasplakinolide is the possibility of dosing the drug with high local and spatial precision. As such, we next set out to achieve local activation of optojasp **90** by irradiation of a small region outside of the cell. We observed that this mode of activation led to strongly localized responses (Fig. 49A). Initially, actin turnover slowed down in the lamellipodium protrusions proximal to the region of irradiation (ROI). Several minutes after light administration, this was followed by retraction of this cellular region, while protrusion dynamics remained unaltered or even accelerated in areas of the cell that were not in close proximity of the ROI. This effect can be best illustrated using a kymograph, which show time dependent changes along a specified axis (Fig. 49Aa-c). As shown in Fig 49Ab, an increase in actin protrusion dynamics can be observed in the lamellipodium region distant to the ROI.

On the other hand, in the lamellipodium region close to the ROI, actin dynamics initially slowed upon irradiation before the lamellipodium was retracted (Fig. 49Aa).
Our results demonstrate that the active *cis* form of **90** can be locally generated within a specified area outside of the cell and then diffuse through the cell membrane to reach the actin networks inside the cell. Notably, the decline of the effective concentration of *cis*-**90** through dilution is overlayed by the thermal inactivation of the photoswitch.

Next, we envisaged that activation inside the cell would be possible as well. We selected an area within a lamellipodium that was irradiated with the same light regime as previously applied. Again, protrusion dynamics first slowed down before the lamellipodium was retracted. Aggregates were dissolved over time and the lamellipodium forefront reestablished (Figure 49B/C). As observed before, actin dynamics in regions that were more distant from the activation area, and therefore not in immediate contact with *cis*-optojasp **90**, did not show this effect. While retraction and reversion are processes that are often observed in migrating cells, this process is fast in unirradiated areas that were not affected by optojasp or in control cells. These dynamics appeared to be much slower when induced by *cis*-optojasp **90** (see above).

It has been reported that the speed with which cells respond to jasplakinolide itself, can vary strongly between differently polarized cells and different cell types.[100,255] In polarized cells, the actin networks are organized such that fast filament turnover can be ensured to drive directional membrane extension.[2] In nonpolarized cells, the barbed ends of actin filaments are capped and filament turnover is much slower.[261] It is therefore not surprising, that the effects of *cis*-optojasp **90** take place on different time scales depending on the actin network organization of a particular cell.

Collectively, our experiments demonstrate that optojasp **90** can be activated with equal efficiency outside and inside of the cell and that the photophysical properties of optojasp **90** are not greatly affected by the presence of an intracellular milieu.

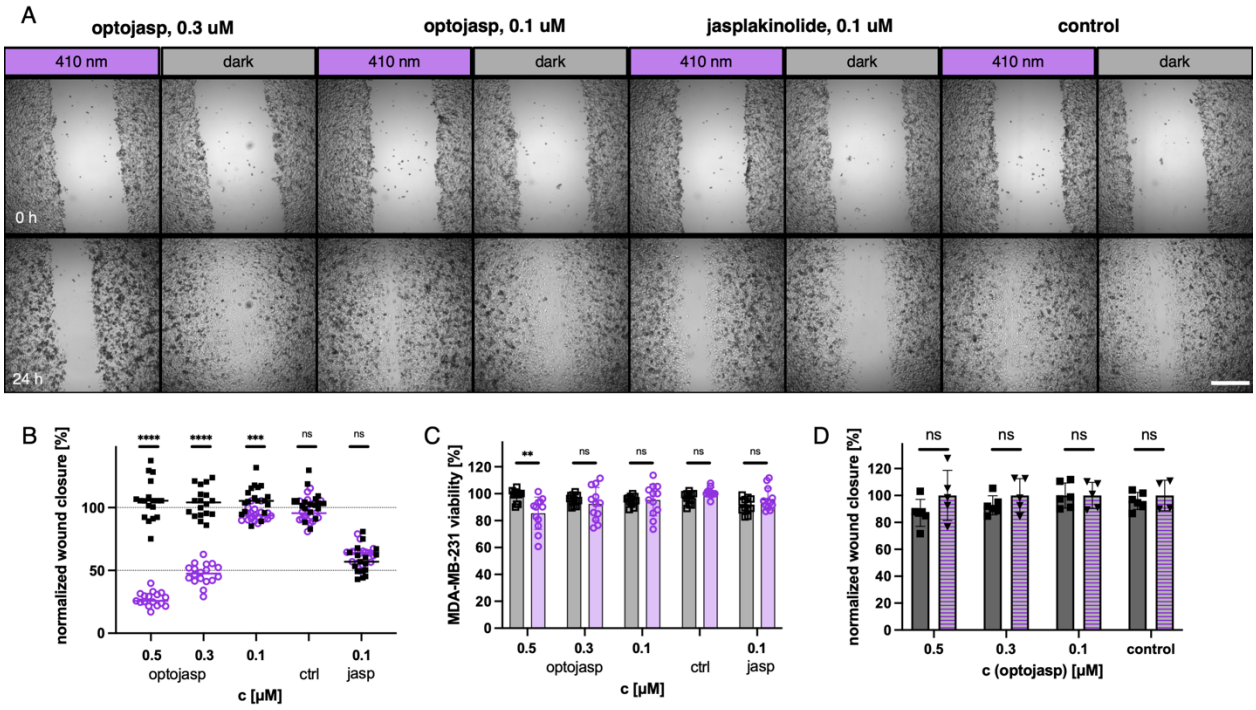

Figure 50: Wound healing assay on MDA-MB-231 cells. **A**) representative images of wound closure before treatment (t = 0 h, top row) and after treatment (t = 24 h, bottom row) under dark or pulsed irradiation (410 nm, 25 ms/ 1 s) conditions for selected concentrations and control. (2.5x, widefield microscope), scale bar = 500 µm. **B**) normalized wound closure from three independent experiments n = 17-18, round: light, squares: dark; line indicates median. **C**) MDA-MB-231 viability (PrestoBlue) after 48 h treatment with optojasp or jasplakinolide light/dark. **D**) comparison of wound closure between rescue (2 h 410 nm (25 ms/ 1 s), then dark) and dark. squares: dark, triangle: rescue; Statistics: $p \leq 0.00001$ ****, $p \leq 0.0001$ ***,$p \leq 0.001$ **, ns = not significant; Multiple Mann-Whitney test for comparison between light/dark.

Next, we monitored the effect of optojasp **90** on the migratory behavior of invasive human breast cancer cell line MDA-MB-231 in wound healing assays. To ensure that cytotoxicity did not interfere with migration, we chose low concentrations of optojasp. Under control conditions, full wound closure occurred between 24 and 48 h. Therefore, quantification of the effects of optojasp **90** was based on relative wound closure after 24 h. While wound closure in the presence of inactive *trans* **90** (i.e. in the dark) was comparable to the control, activation of optojasp with light resulted in a strongly concentration dependent reduction of wound closure (Fig. 50B). Cell viability after 48 h of treatment indicated only low cytotoxicity of *cis* optojasp **90** at 0.5 µM and lower concentrations appeared not to be cytotoxic at all.

We then investigated, whether cell migration could be recovered following thermal relaxation after 2 h of pulsed light activation. Indeed, the degree of wound closure in these rescue experiments was comparable to the extend observed in the dark (Fig. 50D). While reports about an increase in migration of cells treated with very low doses of jasplakinolide exist, we have not observed this effect in our study.

3.3 Summary and Outlook

We have introduced a new generation of optojasps that has superior qualities in terms of wavelength, thermal relaxation, and reversibility. Our chemical probe complements (opto-) genetic tools that have been developed to control the actin cytoskeleton.[185,186,262] While it forgoes the power of genetic targeting of individual cell types, it does not require the over expression of a factor that could disturb the biological nature of the cell. However, we have demonstrated that the local activation is possible in cell culture, which should translate into the local activation in tissues.

Photouncaging of protected native ligands, as well as microinjection offer great ways to locally administer drugs to a system. Photocaging always requires a balance between the stability of the probe to allow for benchtop handling, while the cleavage has to occur under non cytotoxic conditions. Oftentimes, high concentrations of the probe, shorter wavelengths and high light intensities are required to achieve effective concentrations, as the photochemical cleavage reaction is not very efficient. Furthermore, side products are formed that can potentially interfere with cellular dynamics. Once released or injected, the drug is deactivated by dilution and can hence also target areas, albeit in reduced concentration, that are outside of the field of investigation. **90** has the advantage, that in addition to dilution, thermal deactivation strongly decreases the action radius, making dosing more precise. This is especially important when studying actin dynamics, as even very low concentrations of actin binders have been found to induce cellular responses.

In comparison to our first generation optojasps, **90** shows superior qualities. The very efficient activation at 480 nm and partial activation at 520 nm, allows for the use of optojasp **90** in cells and biological systems that are more sensitive to UV- and blue light. The low thermal stability of *cis* **90**, combined with the possibility of applying high concentrations of the inactive isomer, allows for the local activation of high concentrations of *cis* **90** in a confined area of interest.

Depending on the biological questions under investigation optojasp **90** would be a useful tool. Especially its local activation in sub-cellular regions, or right outside the cell membrane in a confined area, combined with the full auto deactivation of the probe may offer unique possibilities for the investigation of processes that are either dependent on actin turnover, like exo- and endocytosis, or that cause actin network reorganization induced by a signaling cascade, like for example ion channel responses, or receptor signaling.

Currently, optojasp **90** is being applied in different laboratories for its locally constrained and reversible actin binding properties.

4 Arp2/3 Complex

4.1 Project Outline

The Actin related protein 2/3 (Arp2/3) complex is an actin nucleator that is essential to the formation of skeletal actin networks (see chapter 1.1.1.3). Branched actin networks form lamellipodia that drive cell movement. Pathogens like *Listeria monocytogens* use the host cytoskeleton to drive pathogen motility and invasion through Arp2/3 mediated actin nucleation.[263] Furthermore, cell motility and invasion are characteristics that have been ascribed to the invasiveness and metastasis of different cancer cell lines and are therefore an active field of investigation. As discussed in chapter 1.1, the Arp2/3 complex can be inhibited by small molecule inhibitors CK-666 and CK-636 and their analogs (Figure 51).

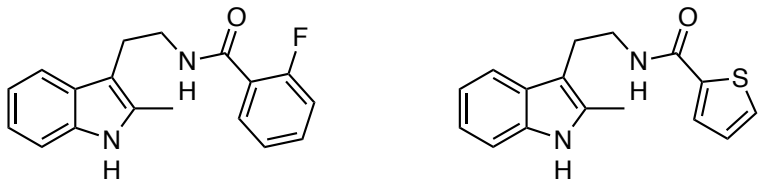

Figure 51: Structures of CK-666 and CK-636.

In previous work by Dr. Chenbin (Friedrich) Lu and Dr. Nils Winter in the Trauner group, a series of photoswitchable CK-666 analogs (Figure 52) were developed and evaluated *in vitro*.

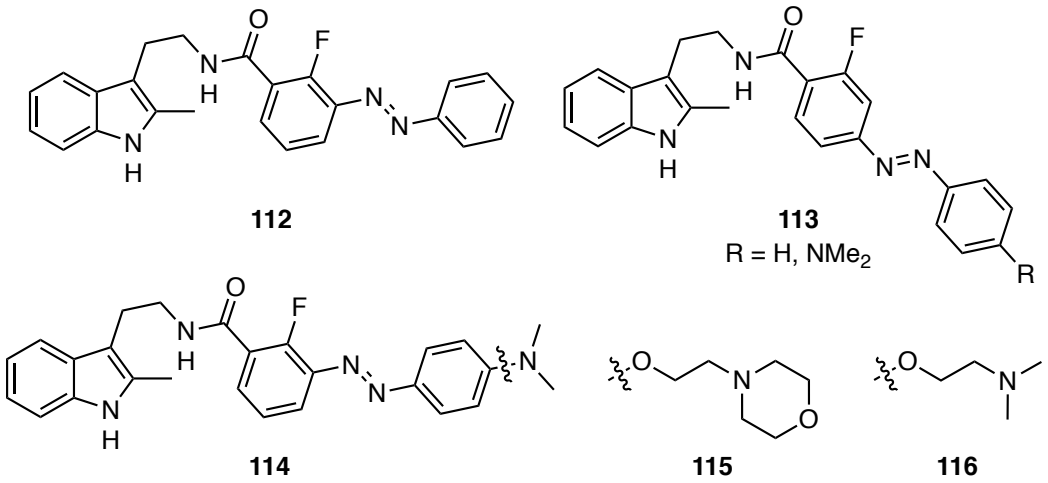

Figure 52: Previously synthesized investigated azo-CK-666 derivatives that provided a basis for this work. R = H, NMe_2

The assay was conducted by M. Abou-Ghali (lab of J. Plastino, Institute Curie Recherche de Paris, France) is a model system that is based on listeria motility. Briefly, WASP coated beads are treated with Arp2/3, VASP, profilin and capping protein. Upon addition of pyrene actin, polymerization occurs that results in comet tail formation and bead movement. This process is observed using microscopy (Figure 53).[264] It was found, that an extension of the fluorophenyl ring of CK-666 in 3 position was generally tolerated and phenyl-, as well as dimethylaniline derivatives were successful at inhibiting Arp2/3 dependent actin polymerization in the dark. Azo extension in 4 position did not result in Arp2/3 inhibition, as did thiophene analogs. **112** did not show Arp2/3 inhibition after illumination with 365 nm. Fluorophore labelled actin was sensitive to extended UV-irradiation that was required for full photoconversion of the azobenzene due to its high concentrations. Therefore, the deactivation of **112** had to be performed before addition to the assay. The fast-relaxing aniline derivative could not be assessed in its *cis* configuration using this setup, because continued pulsed light irradiation would be needed. Another limitation in the initial investigation was the reported limited solubility of these compounds under the physiological conditions. In an attempt to circumvent this, more soluble substituents were introduced in derivatives **115** and **116**. Unfortunately, both analogs did not show Arp2/3 inhibition analogously to **112**.

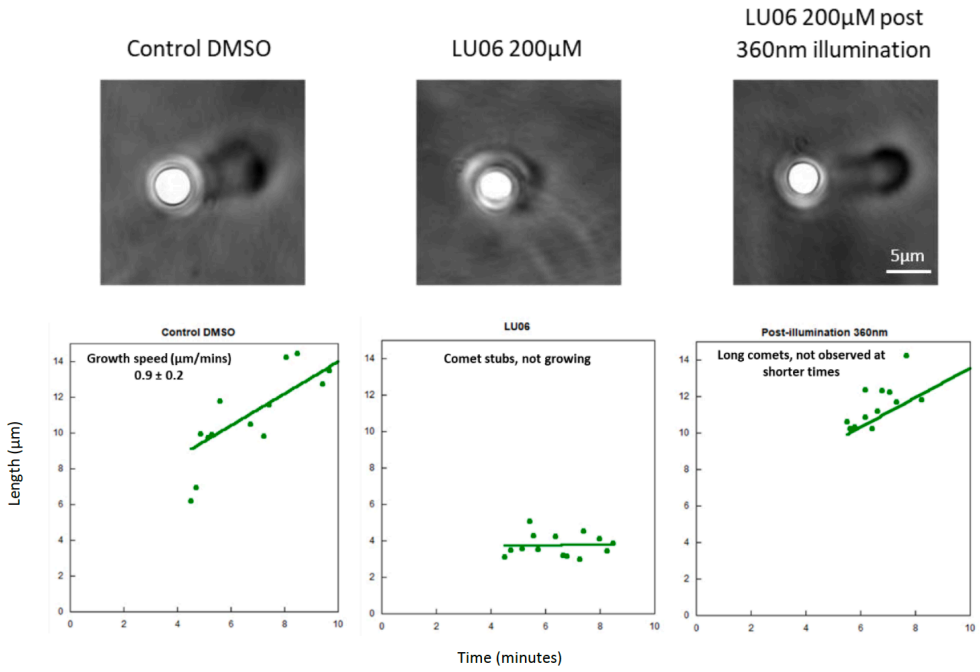

Figure 53: Initial effects of LU06 (**112**) on a bead-based actin comet assay.[264]

Motivated by the initially very promising light dependent activity of **112**, we decided to readdress this project and develop new CK-666 analogs suited for use in *in vitro* and cell-based assays.

4.2 Results and Discussion

New photoswitchable derivatives of Arp2/3 inhibitor CK666 were synthesized following a general synthetic route. Commercial nitrobenzene 117 was reduced to the aniline which was subsequently oxidized to the nitrosobenzene using oxone. The nitrosobenzene then underwent azo coupling under Baeyer–Mills conditions yielding the azobenzene photoswitches in good yields. In the next step, the methyl ester was hydrolyzed under basic conditions and submitted to a peptide coupling with 2-methyl tryptamine. Diazocine derivative **121** was obtained from a peptide coupling with the carboxylic acid[dd] **120**.

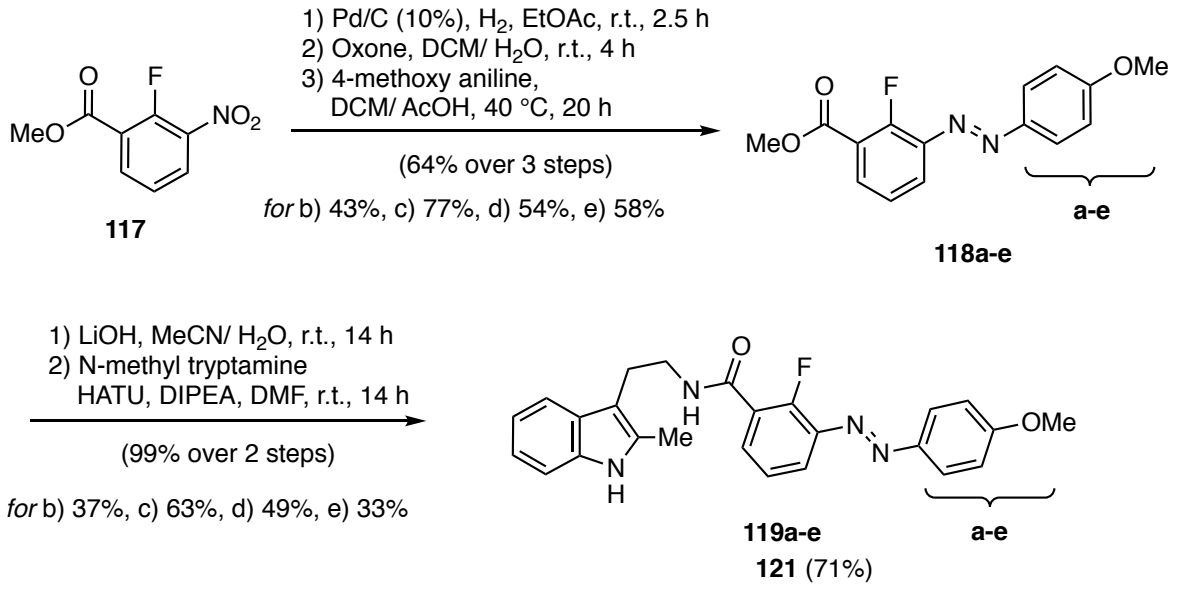

Scheme 17 Synthesis of photoswitchable CK-666 analogs.

[dd] Kindly provided by Martin S. Maier.

CK-666 analogs **119a-c and 121** were stable photoswitches that could be switched between the *cis* and *trans* isomers multiple times without noticeable photo fatigue. Methoxy substituted derivatives **119a** and **119b** showed a slight bathochromic shift of the π-π* transition where maximal *trans -> cis* isomerization was obtained with 390 nm compared to unsubstituted azobenzene **112** reported previously. Although switching was reversible, reverse isomerization was only partially possible due to the overlap of n-π* absorption of both isomers that did not allow for efficient *cis -> trans* conversion. Amines **119c,d** showed most efficient cis *-> trans* isomerization under 370 nm irradiation and the reverse isomerization was near quantitative at 430 nm. The thermal dark relaxation in the dark of the excited cis state was remarkably slow. This could be attributed to the possible formation of an intramolecular hydrogen bond between the carbonyl group of the peptide bond and the ammonium substituent on the distal phenyl ring of the azobenzene that would stabilize the *cis*-isomer. Diazocines have been shown to reverse the logic of azobenzene photoswitches in photopharmacology because their thermodynamically preferred isomer is the bent *cis* form. They typically undergo thermal relaxation more readily than their diphenyl diazine counterparts.[265,266] Diazocine derivative **121** was efficiently isomerized with 400 nm light and this process was reversed using 480 nm. The thermal half-life of the activated *trans* state was strongly reduced compared to the azobenzene photoswitches.

Table 11: Photophysical properties of photoswitchable CK-666 analogs.

azo-CK666	$[\lambda]_{max}$ / (ibp[ee])	$[\lambda]_{switch}$	$t_{1/2}$ (DMSO)
119a	358 nm (418 nm)	380 nm	20 h
119b	367 nm (–)	390 nm	18.5 h
119c	328 nm (390 nm)	370 nm	55.5 h
119d	324 nm (380 nm)	360 nm	>207 h
119e	365 nm (424 nm)	390 nm	25 h
121	400 nm (430 nm)	390 nm	2 h

The new series of compounds was investigated in a different *in vitro* assay for Arp2/3 dependent nucleation in collaboration with Dr. A. Tabatabai in the lab of Prof. M. Murrell (Yale University, New Haven, USA).

[ee] ibp: iosbestic point between pi-pi* and n-pi* absorption bands of *cis* and *trans* isomers

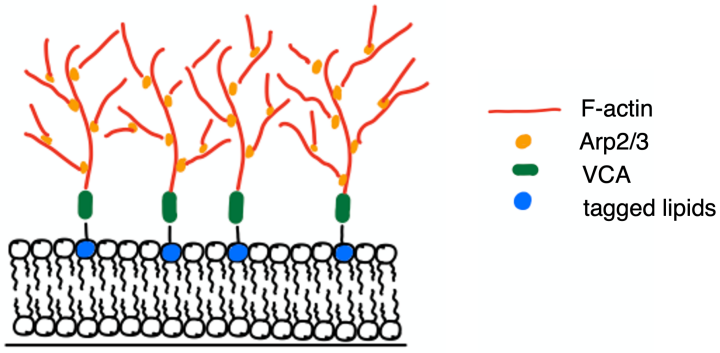

Figure 54: Schematic description of the assay used.[ff]

In this assay actin polymerization can be observed and quantified under the influence of various polymerization regulating factors and their inhibitors. Briefly, a lipid bilayer that was established on top of a glass coverslip and contained VCA tagged lipids. VCA is a protein domain of WASP, which is responsible for the activation of Arp2/3. Under control conditions, Arp2/3 dependent nucleation results in the formation of dense networks that grow in star shapes from filaments originating at VCA nuclei. The process is observed at one fixed plane by confocal fluorescent microscopy (Figure 54).[267] This assay setup bears the potential to locally induce photoisomerization of azo-CK-666 in a confined area and activate a sub-population of Arp2/3.

Our initial evaluation of compounds **119a-c, 121** confirmed that the introduction of solubility enhancing groups enabled the use of highly concentration of azo-CK-666 derivatives better. **119c** delayed the formation of branched actin nuclei in the abovementioned assay light dependently. This suggests, that *trans* **119c** inhibits Arp2/3 function. Figure 55A shows images taken at comparable time points of the assay relative to t_0 treated with *trans* **119c** and *cis* **119c** after pre-irradiation with 365 nm. A quantification of relative fluorescence intensity (Figure 55B) shows that actin polymerization is strongly suppressed in presence of CK-666 and *trans* **119c**, while the slope under treatment with inactive *cis* **119c** is comparable to the negative control.

[ff] Drawn based on the reference cited and personal communications with Dr. A. Tabatabai

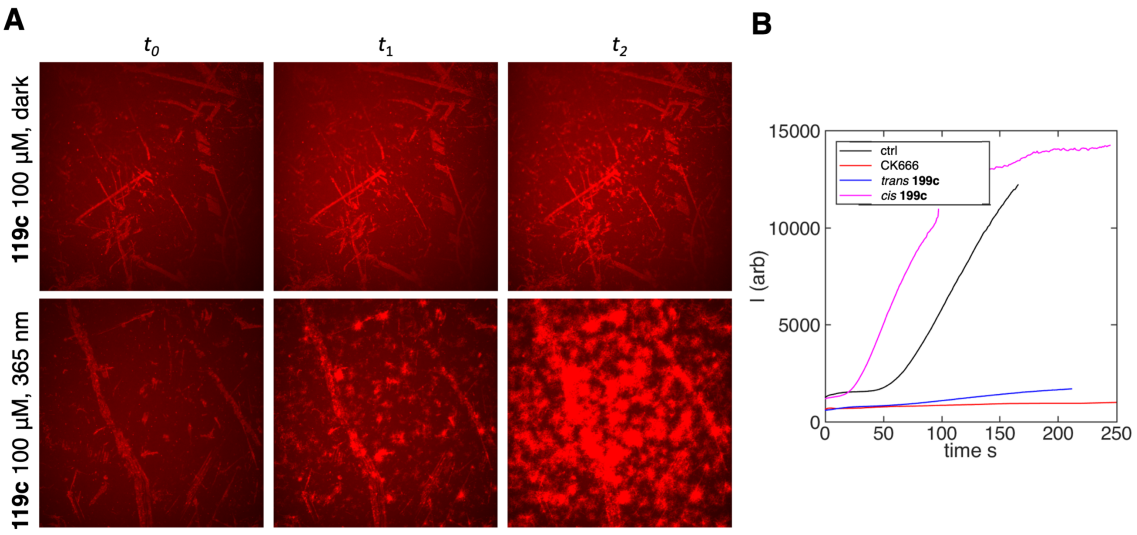

Figure 55: Light dependent reduction of Arp2/3 mediated nucleation *in vitro* in the presence of **119c**.

Ultimately, our goal was to be able to inhibit Arp2/3 dependent actin branching followed by deactivation of the photoswitchable inhibitor using local irradiation with the light sources typically available on microscope setups. The pre-irradiation of **119c** with 365 nm is practically feasible, but *in vitro* irradiation with the 405 nm excitation source in the microscope would not be efficient. The n-π* absorption of the *cis* isomer dominates over the n-π* absorption of the *trans* isomer, resulting in neglectable *trans* -> *cis* isomerization (Figure 56).

In order to improve the photophysical properties and to allow for efficient photoconversion at 405 nm, **119e** was synthesized following the route described before. We rationalized that a *para* methoxy group would result in a bathochromic shift of the UV-Vis absorption spectrum, while the tertiary methylamine should help improve solubility. Indeed, *trans* -> *cis* isomerization was efficient at 380 nm and the reverse process was achieved with 440 nm light. Thermal reversion was comparable to the methoxy derivatives discussed above (Figure 56).

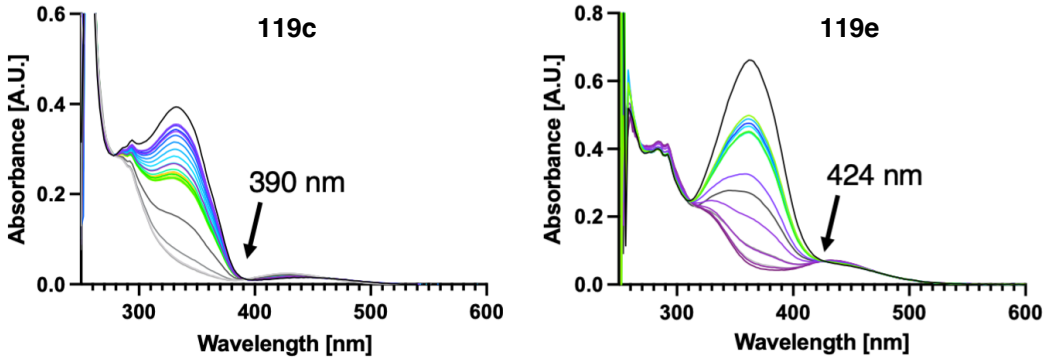

Figure 56: UV-Vis spectra of **119c** (left) and **119e** (right).

4.1 Summary and Outlook

In conclusion, our preliminary investigation of new photoswitchable CK-666 derivatives is very promising. Going further, our initial experiments require more thorough investigation and analysis to confirm that azo-CK-666 derivatives impair the function of Arp2/3. The evaluation of tertiary amines **119d,e** *in vitro* remain. Further will the azo-CK-666 switches be investigated in cell proliferation and wound healing assays as described previously (Chapter 1, 3).

5 Kinesin Eg5 Inhibitor

5.1 Project Outline

The aim of this project was to establish the optical control of kinesin Eg5, which is essential to the formation of bipolar spindles during mitosis.

A variety of photoswitchable analogs of kinesin Eg5 inhibitors monastrol, EMD-534085 and Ispinesib were synthesized and evaluated by Anna C. Impastato and Dr. Andrej Shemet. Anna Impastato further conducted cell cycle analysis for the light-dependent mitotic arrest and Dr. Gadiel Saper (Prof. H. Hess Lab at Columbia University, New York, USA) conducted gliding assays.

The author of this thesis contributed to the project by establishing cell cycle synchronization procedure using a double thymidine block and demonstrated the light-dependent formation of the monoastral phenotype that is characteristic for Eg5-inhibition using confocal fluorescence microscopy on fixed cells.

The manuscript to this publication has been submitted for review and was included in this thesis with permission of all co-authors.

5.2 Manuscript in Preparation

Optical Control of Mitosis with a Photoswitchable Eg5 Inhibitor

Anna C. Impastato,[a#] Andrej Shemet, [a#] Nynke A. Vepřek,[a,b] Gadiel Saper,[c] Henry Hess,[c] and Dirk Trauner [a*]

Dedicated to Prof. Samuel J. Danishefsky on the occasion of his 85th Birthday

[a] Anna C. Impastato, Andrej Shemet, Nynke A. Vepřek, Dirk Trauner
Department of Chemistry, New York University
New York, 10003, USA
E-mail: dirktrauner@nyu.edu
[b] Nynke A. Vepřek,
Department of Chemistry, Ludwig-Maximilians University of Munich
81377 Munich, Germany
[c] Gadiel Saper, Henry Hess
Department of Biomedical Engineering, Columbia University
New York, 10025, USA
E-mail: hhess@columbia.edu
# These authors contributed equally to this work.

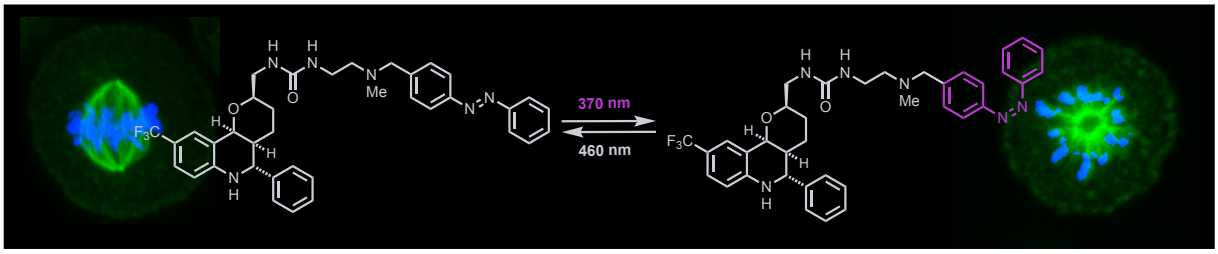

The photo-control of the mitotic kinesin, Eg5, is achieved using an azobenzene containing analog of EMD-534085.

Abstract: *Eg5 is a kinesin motor protein that is responsible for bipolar spindle formation and plays a crucial role during mitosis. Loss of Eg5 function leads to the formation of monopolar spindles, followed by mitotic arrest, and subsequent cell death. Several cell-permeable small molecules have been reported to inhibit Eg5 and some have been evaluated as anticancer agents. We now describe the design, synthesis, and biological evaluation of photoswitchable variants with five different pharmacophores. Our lead compound* ***AzoEMD*** *is a cell permeable azobenzene that inhibits Eg5 more potently in its light-induced cis form. This activity decreased movement in microtubule gliding assays, promoted formation of monopolar spindles, and led to mitotic arrest in a light dependent way.*

Mitosis followed by cytokinesis is a process in which a replicated set of chromosomes is evenly distributed and a single cell is divided into two daughter cells. Hundreds of proteins are involved in this highly complex but tightly controlled event[268], including, amongst other mitotic kinesins, the kinesin spindle protein (KSP, KIF11, or Eg5)[269]. Eg5 is a motor protein that is primarily responsible for generating the forces necessary to organize spindles and separate the centrosomes[270]. Structurally, Eg5 is a homotetramer, which crosslinks and slides apart antiparallel microtubules. Mechanistically, it moves along the microtubules by repetition of an ATP hydrolysis-driven cycle of attachment, sliding, and dissociation[271]. Eg5 specific inhibitors cause cell cycle arrest and apoptotic cell death with a characteristic monopolar spindle phenotype, thus underscoring the importance of this protein during mitosis[272] (Fig. 1A).

Due to their key roles in cell proliferation, mitotic kinesins have emerged as targets in cancer therapy.[273] Their inhibition results in mitotic arrest without directly affecting microtubule dynamics. As such, Eg5 inhibitors provide an alternative mode of inhibition to taxanes and vinca alkaloids[150], which also affect microtubules in non-dividing cells causing serious side effects. In the past decades, several small molecules that target Eg5, such as monastrol[272], S-trityl-L-cysteine[274], ispinesib[275], and filanesib[276], have been investigated as potential cancer therapeutics[277] (Fig. 1B). These allosteric Eg5 inhibitors bind to a hydrophobic pocket and prevent ADP release by forming a ternary complex with the protein and ADP[278–280]. To date, at least nine Eg5 inhibitors have progressed through Phase I/II clinical trials but most have failed due to low efficacy and the rapid emergence of inactivating mutations[277,281–287].

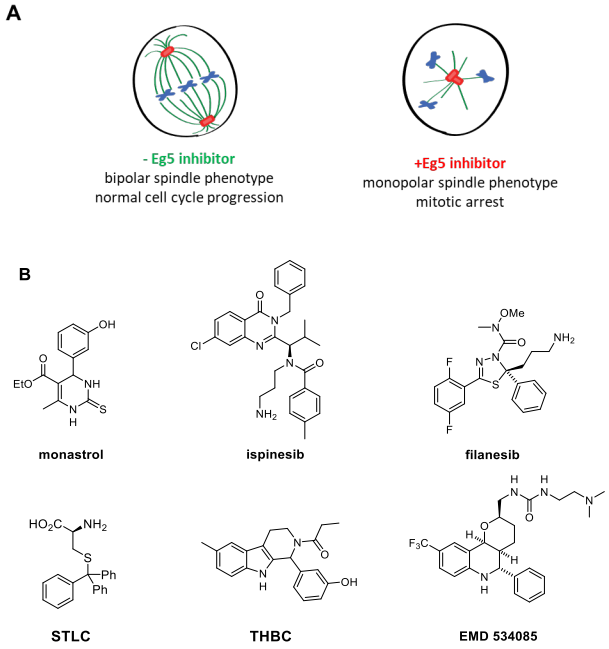

Figure 1. A) Eg5 is involved in the formation of the bipolar spindle during mitosis. When its function is inhibited monopolar spindle formation is observed, which is followed by subsequent mitotic arrest. B) Structural diversity of allosteric Eg5 inhibitors.

Photopharmacology is an attempt to control biological activity with synthetic light-responsive molecules[288,289]. It has been successfully applied to shaping tubulin and actin dynamics with photoswitchable versions of combretastatin A[211], paclitaxel, and jasplakinolide[252], respectively. However, this approach has rarely been attempted with motor proteins. The Tamaoki group introduced photoswitchable inhibitors of the mitotic kinesin CENP-E based on the small molecule GSK923295[290]. Recently, Maruta and colleagues introduced photoswitchable inhibitors that enabled reversible control of Eg5 *in vitro*.[24–28] However, they did not demonstrate activity in cells, possibly due to insufficient cell permeability and solubility of their compounds. We now report the design, synthesis, and systematic evaluation of photoswitchable Eg5 kinesin inhibitors that can permeate membranes and function in cells. We based our approach on five different Eg5 pharmacophores: ispinesib[275], S-trityl-L-cysteine (STLC)[274], monastrol[272], tetrahydro-b-carbolines[291], and EMD-534085[292]. This resulted in the photoswitchable molecules **1a-c**, derived from monastrol, **2a-c**, derived from ispinesib, **3**, modelled after STLC, **4a,b** derived from a class of b-carboline inhibitors, and **5a-c**, derived from EMD-534085. Amongst these, **5c**, also termed **Azo-EMD** emerged as the most successful. As such, it underwent full characterization in photophysical, biochemical, and cellular assays.

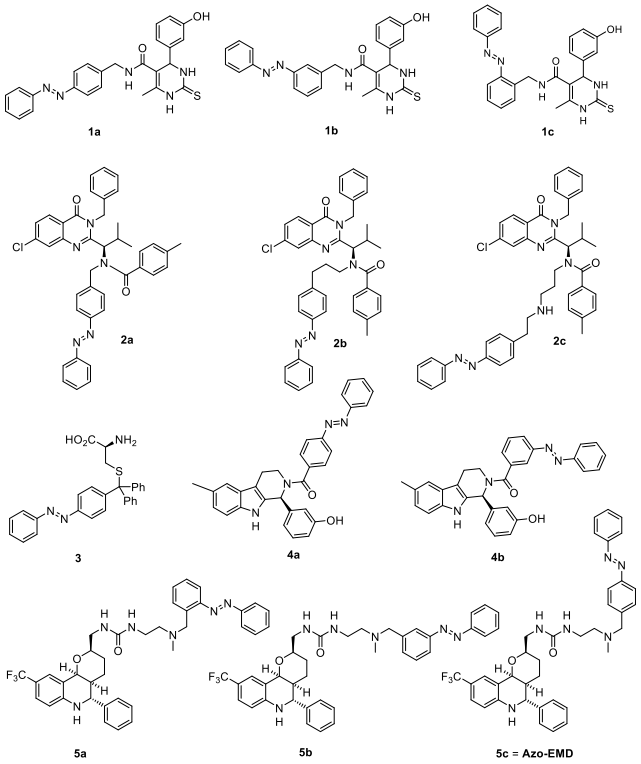

Figure 2. Photoswitchable inhibitors of Eg5 synthesized and tested in this study based on the pharmacophores monastrol, ispinesib, STLC, and EMD-534085.

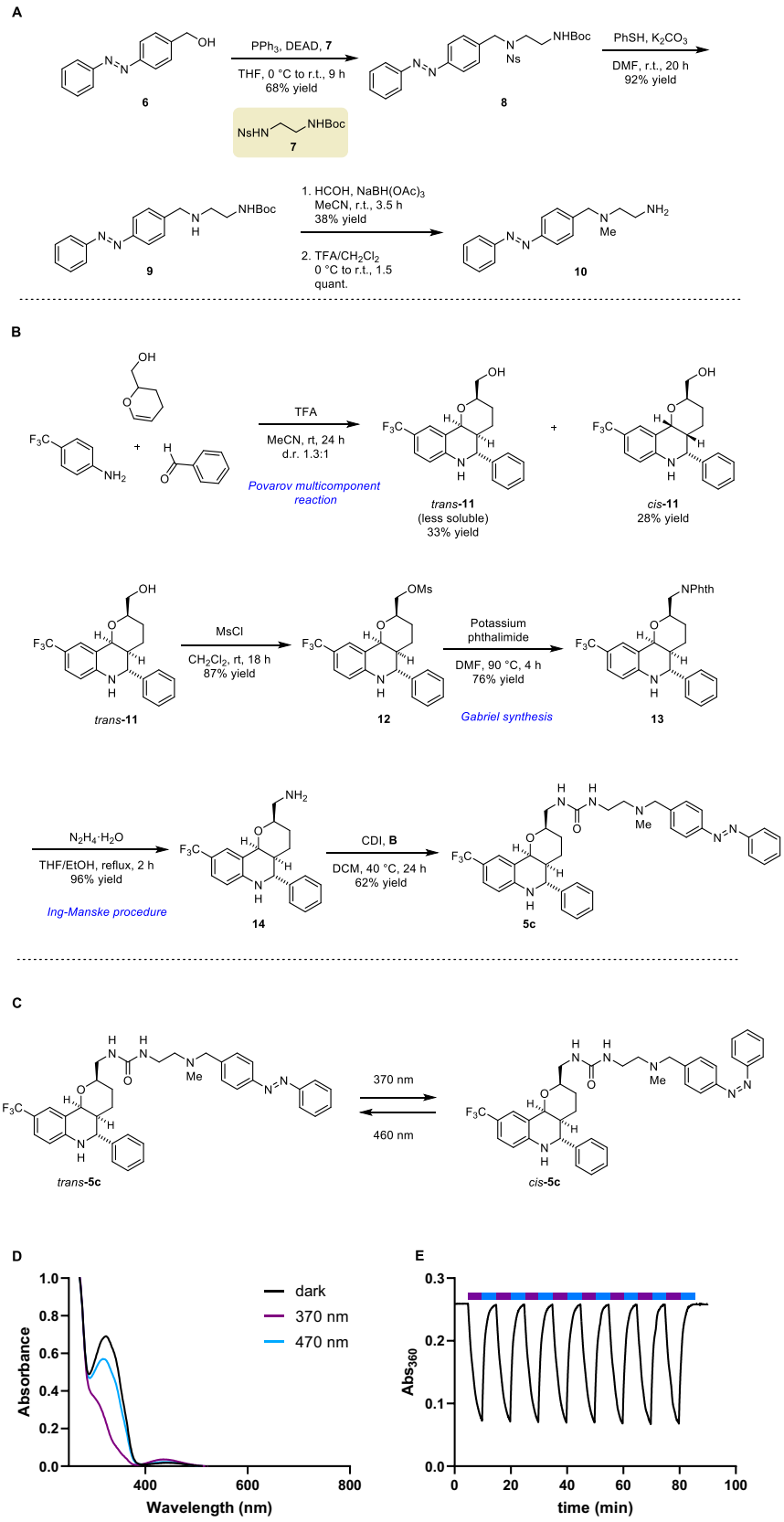

Scheme 1. A) Synthesis of the photoswitchable side chain **B**. B) Synthesis of Azo-EMD. C) Light-dependent reversible isomerization of Azo-EMD. D) Absorption spectra of photoswitchable EMD-534085 in the dark-adapted state and at 370 and 460 nm. E) Reversible isomerization of Azo-EMD over multiple switching cycles.

The design of photoswitchable compounds was based on structure-activity data available for various Eg5 inhibitors and the analysis of X-ray structures of monastrol (pdb 1X88), ispinesib (pdb 4AP0), and EMD-534085 (pdb 3L9H) bound to Eg5. These inhibitors bind to the same allosteric site, which is about 10 Å away from the ATP binding pocket in a region formed by helix α2/loop L5 and helix α3. The accommodation ofstructurally different compounds in the same binding pocket implies that Eg5 exhibits some degree of flexibility to allow for conformational changes upon binding of ligand. Keeping this in mind, we opted for an azo-extension[288] approach, where an azobenzene is appended to a vector that projects toward solvent and can accommodate the photoswitch. This led us to synthesize and evaluate azobenzene derivatives **1-5** (Fig. 2).

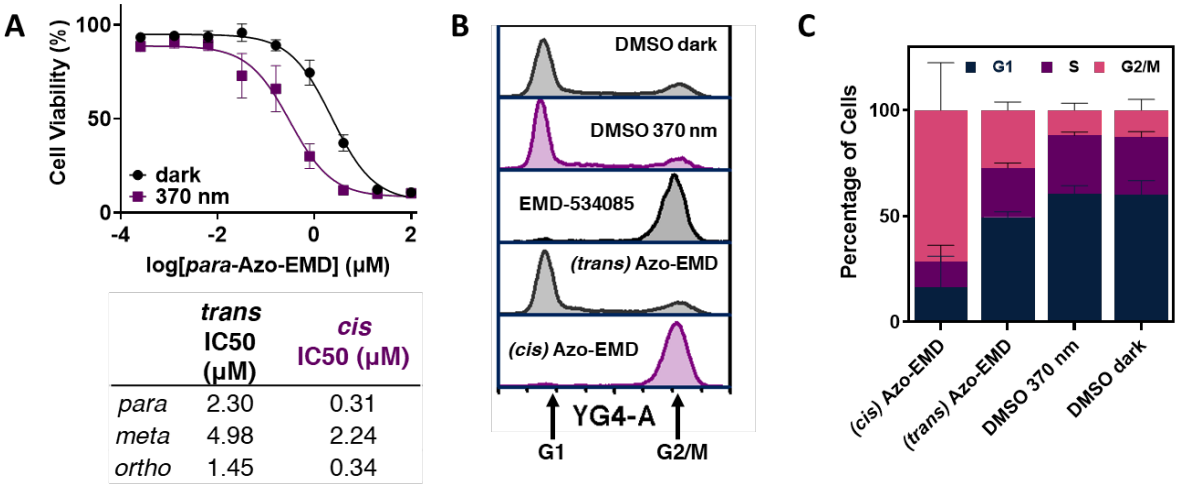

	trans IC50 (μM)	*cis* IC50 (μM)
para	2.30	0.31
meta	4.98	2.24
ortho	1.45	0.34

Figure 3. A) Cell viability assay: HeLa cells were treated with increasing concentrations of compound under dark or pulsed irradiation conditions for 48h and cell viability was assessed using MTT assays. n=3, N=3; B, C) Cell cycle distribution of HeLa cells treated with Azo-EMD (3 μM), EMD 532085 (0.1 μM), or DMSO under dark or pulsed irradiation for 48h. Cells were fixed in EtOH, stained with propidium iodide and analyzed by flow cytometry. N=3. Data shown are mean values ± SD.

The syntheses of compounds **1a-c**, **2a-c**, **3**, and **4a,b** is described in the Supporting Information. The racemic synthesis[293] of our lead compound **Azo-EMD** commenced with a Povarov multi-component reaction[294] (Scheme 1B). It provided access to the tetrahydroquinoline core containing three stereocenters in a single step starting from commercially available materials. The relative configuration was confirmed by X-ray crystallography (see Supporting Information.) Following a few steps to convert the alcohol to the amine, the azobenzene photoswitch functionality was introduced using a CDI mediated

urea coupling. In addition to the *para* substituted derivative **Azo-EMD** (**5c**) we also synthesized *ortho* and *meta* substituted variants by coupling the common building block **12** with CDI and the corresponding azobenzyl amine (Scheme 1A). All analogs show photophysical properties of classic azobenzene photoswitches[295]. For instance, **Azo-EMD** can reversibly switch from the trans→cis conformation with alternating 365/465 nm light and is bi-stable, showing slow thermal relaxation from the *cis*-state at 37 °C (Fig. 1D and Supporting Information). As expected, the switching could be repeated over several cycles without fatigue (Fig. 1E).

Since Eg5-inhibition ultimately results in cell death[296], we first screened our photoswitchable compounds in cell viability assays (Fig. 3A, Supporting Information). HeLa cells were treated for 48h with each photoswitch under dark or pulsed-light conditions. Monastrol derivates **1a-c** were inactive or showed no light dependency. The usefulness of these compounds was also limited by their poor solubility. Ispinesib derivates **2a-b** were marginally better. Consistent with the reported structure activity relationships of ispinesib analogs[297], the alkyl amine proved to be critical for Eg5 inhibition. Accordingly, **2c,** which maintains the alkyl amine proved to be a good inhibitor, however **2c** did not show light dependency. S-trityl cysteine derivate **3** was inactive. THBC derivates **4a,b** were active inhibitors but not in a light-dependent way.

EMD-534085 derivates, **5a-c**, on the other hand, were active and showed lighted dependency in the cell viability assays**. Azo-EMD** provided the largest difference in potency between cis/trans (IC_{50}: trans = 2.3 μM; cis = 0.31 μM). While the ortho-substituted azobenzene provided similar results to the *para* derivative, the *meta* version was the least active. For these reasons, we carried the *para* substituted compound (**5c**) forward through further biological investigations.

Cell cycle analysis by DNA content showed that treatment with ***cis* AzoEMD** (370 nm pulsed irradiation, 3 μM) induced a strong shift towards the G2/M phases (Figure 3 B,C). In comparison, cells treated with trans **AzoEMD** in the dark (3 μM) did not show a shift in cell cycle populations compared with co-solvent treated cells. In agreement with the cell viability assays, the cell cycle analysis therefore shows that **AzoEMD** is *cis*-active. This effect is dose-dependent, and the largest light/dark difference is seen at 3 μM (see Supporting Information). The shift in cell cycle population towards G2/M is consistent with the observed effects of Eg5 inhibitors, such as EMD-534085 (Figure B,C), monastrol[272], and filanesib[276].

The function of Eg5 motor activity can be observed using microtubule gliding assays where the Eg5 motor domain is attached to a glass slide and propels fluorescent stabilized microtubules across the surface[298]. In the presence of 1 μM **Azo-EMD** irradiated with 460 nm

light (*trans* **Azo-EMD**) microtubule movement is not affected, while 1 μM **Azo-EMD** activated with 370 nm light (*cis* **Azo-EMD**) significantly reduced the fraction of moving microtubules ($p<10^{-5}$; Figure 4, Supplemental Videos 1-2). As expected, 1 μM EMD-534085 inhibits microtubule movement. In this assay, when Eg5 is treated with active inhibitors (*cis* **Azo-EMD** or EMD-534085) we observed that the number of microtubules on the surface is reduced. This result suggests that *cis* **Azo-EMD** inhibits the binding between microtubules and Eg5 and that there is less active Eg5. These observations are consistent with the modes of inhibition of other allosteric Eg5 inhibitors, including ispinesib, which alters how Eg5 binds to the microtubules and prevents its movement.[275]

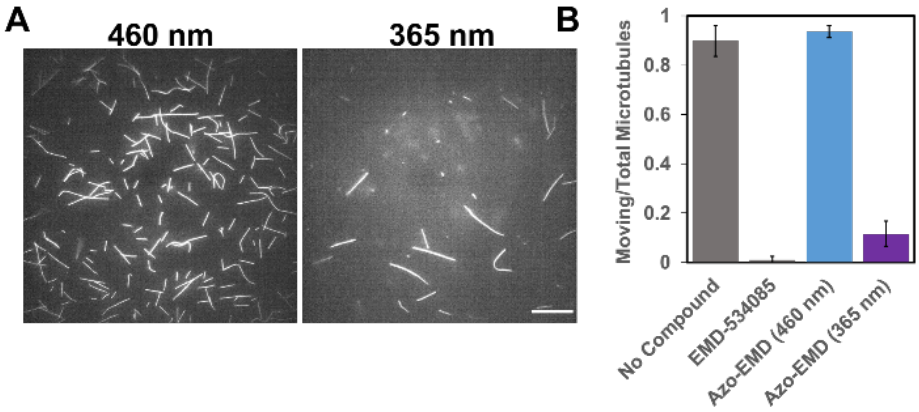

Figure 4. Azo-EMD only inhibits Eg5 kinesin after 365 nm illumination. A) Fluorescence microscopy images of kinesin propelled microtubules with Azo-EMD after 465 nm (left, supplementary video 1) or 365 nm (right, supplementary video 2) illumination. Scale bar 20 μm. The ratio of the number of microtubules in the field of view for measurements with Azo-EMD after illumination with 365 nm to measurements after illumination with 465 nm is 0.29 ± 0.17 (average ± standard error). B) The ratio of stuck to moving microtubules for assays performed with no compound, EMD-534085, Azo-EMD after illumination with 465 nm and Azo-EMD after illumination with 365 nm. Error bars represent the standard error.

Finally, we evaluated our photoswitches in fluorescence imaging assays to confirm that the observed effects on cell viability and the cell cycle are due to Eg5 inhibition (Figure 5). Eg5 inhibition is characterized by collapse of the bipolar mitotic spindle into a monopolar spindle phenotype (monoastral)[299]. In the presence of **Azo-EMD** (1 μM) and in the absence of irradiation, most cells show the normal bipolar spindle phenotype, which is observed as the linear arrangement of the stained chromosomes. By contrast, upon pulse-irradiation with 370 nm light, most dividing cells show the monoastral phenotype, corresponding to Eg5 inhibition, where the chromatin is arranged radially. HeLa cells treated with EMD-534085 (1 μM) exhibit the characteristic monopolar spindle both in the dark and under pulsed 370 nm irradiation.

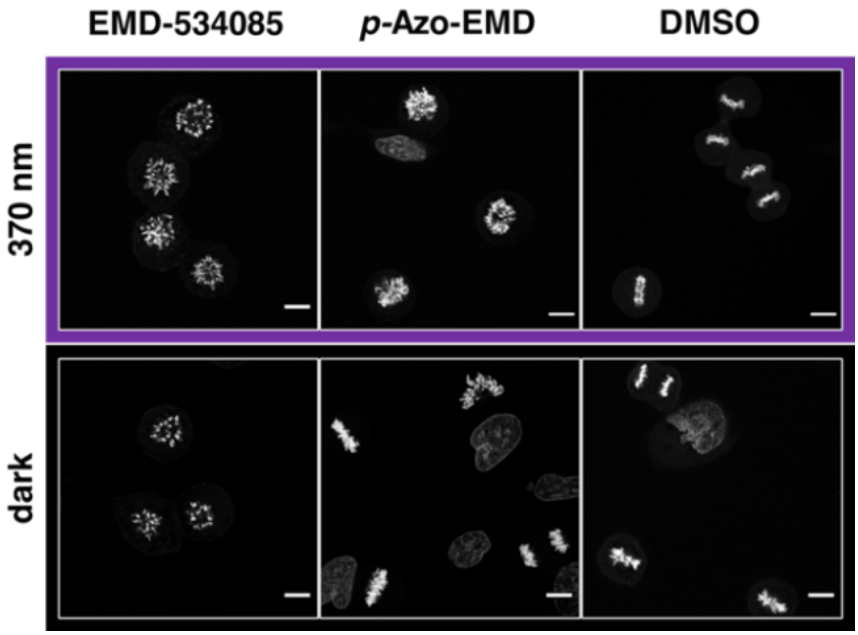

Figure 5. Synchronized HeLa cells were treated with EMD-534085 (1 μM), Azo-EMD (1 μM) or DMSO under dark or pulsed irradiation followed by fixation, permeabilization and staining. Scale bar 10 μm. **Middle:** Azo-EMD shows mostly regular mitotic phenotype under dark conditions and upon activation (370 nm) the star-like DNA phenotype that is a consequence of monopolar spindle formation is observed. **Left/Right**: +/– control.

In summary, we have described the design, synthesis, and biological evaluation of a photoswitchable cell permeable Eg5 inhibitor, termed **AzoEMD.** At an appropriate concentration **AzoEMD** is inactive in the dark, is activated by irradiation with UV-A light, and has enabled the optical control of Eg5-dependent biology. The optical control of kinesin function can also be achieved using optogenetics. For instance, a photosensitive kinesin-3 was developed that could be activated through homodimerization upon blue light irradiation[300,301]. An optogenetic approach to kinetochore function in mitosis has also been described.[302] To the best of our knowledge, however, the optogenetic control of Eg5 itself has

not been achieved. Compared with optogenetic approaches, small molecules have the advantage that they are easy to use and they do not require genetic manipulations that can lead to unphysiological situations. A photoswitchable Eg5 inhibitor with cellular activity could provide a useful tool for studying the role of the kinisin with high spatial and temporal precision. Additionally, localized and reversible control of Eg5 at different phases of the cell cycle may serve to probe the directional forces involved in centrosome separation. Since the photostationary states of photoswitches are a function of the wavelength used, the concentration of the active form can be changed *in situ* (colordosing)[211]. Light-activatable Eg5 inhibitors, such as **AzoEMD**, could also be interesting candidates for precision cancer chemotherapeutics that can avoid systemic toxicity and reduce the risk of resistance mutations, which have hampered the clinical development of Eg5 inhibitors[287].

Acknowledgements

A.C.I. is supported by the NYU MacCracken Fellowship. A.S. thanks the Swiss National Science Foundation (SNSF) for a postdoctoral fellowship (P2EZP_181623). N.A.V. thanks the German Academic Scholarship Foundation (Studienstiftung) for a PhD Fellowship. G.S. and H.H. are supported by NSF grant 1807514. This research was supported by the National Institute of General Medical Sciences of the National Institutes of Health under award number R01GM126228 (to D.T.). We are grateful to Dr. Michelle C. Neary (Hunter College, New York) for X-ray crystallographic analysis of **trans-11**.

Keywords: photopharmacology • Eg5 kinesin • Povarov multicomponent reaction • cytoskeleton • mitosis • azobenzene

References for Chapter 1

(1) Dominguez, R.; Holmes, K. C. Actin Structure and Function. *Ann. Rev. Biophys.* **2011**, *40* (1), 169–186. https://doi.org/10.1146/annurev-biophys-042910-155359.

(2) Pollard, T. D.; Borisy, G. G. Cellular Motility Driven by Assembly and Disassembly of Actin Filaments. *Cell* **2003**, *112* (4), 453–465. https://doi.org/10.1016/S0092-8674(03)00120-X.

(3) Kristó, I.; Bajusz, I.; Bajusz, C.; Borkúti, P.; Vilmos, P. Actin, Actin-Binding Proteins, and Actin-Related Proteins in the Nucleus. *Histochem Cell Biol* **2016**, *145* (4), 373–388. https://doi.org/10.1007/s00418-015-1400-9.

(4) Perrin, B. J.; Ervasti, J. M. The Actin Gene Family: Function Follows Isoform. *Cytoskeleton* **2010**, *67* (10), 630–634. https://doi.org/10.1002/cm.20475.

(5) Fujii, T.; Iwane, A. H.; Yanagida, T.; Namba, K. Direct Visualization of Secondary Structures of F-Actin by Electron Cryomicroscopy. *Nature* **2010**, *467* (7316), 724–728. https://doi.org/10.1038/nature09372.

(6) Holmes, K. C.; Angert, I.; Jon Kull, F.; Jahn, W.; Schröder, R. R. Electron Cryo-Microscopy Shows How Strong Binding of Myosin to Actin Releases Nucleotide. *Nature* **2003**, *425* (6956), 423–427. https://doi.org/10.1038/nature02005.

(7) Oda, T.; Iwasa, M.; Aihara, T.; Maéda, Y.; Narita, A. The Nature of the Globular- to Fibrous-Actin Transition. *Nature* **2009**, *457* (7228), 441–445. https://doi.org/10.1038/nature07685.

(8) Merino, F.; Pospich, S.; Funk, J.; Wagner, T.; Küllmer, F.; Arndt, H.-D.; Bieling, P.; Raunser, S. Structural Transitions of F-Actin upon ATP Hydrolysis at near-Atomic Resolution Revealed by Cryo-EM. *Nat. Struct. Mol. Biol.* **2018**, *25* (6), 528–537. https://doi.org/10.1038/s41594-018-0074-0.

(9) Chou, S. Z.; Pollard, T. D. Mechanism of Actin Polymerization Revealed by Cryo-EM Structures of Actin Filaments with Three Different Bound Nucleotides. *Proc. Natl. Acad. Sci.* **2019**, *116* (10), 4265–4274. https://doi.org/10.1073/pnas.1807028115.

(10) Oztug Durer, Z. A.; Diraviyam, K.; Sept, D.; Kudryashov, D. S.; Reisler, E. F-Actin Structure Destabilization and DNase I Binding Loop Fluctuations. *J. Mol. Biol.* **2010**, *395* (3), 544–557. https://doi.org/10.1016/j.jmb.2009.11.001.

(11) Dominguez, R. Nucleotide-Dependent Conformational Changes in the Actin Filament: Subtler than Expected. *Proc. Natl. Acad. Sci.* **2019**, *116* (10), 3959–3961. https://doi.org/10.1073/pnas.1900799116.

(12) Dominguez, R. Actin-Binding Proteins – a Unifying Hypothesis. *Trends Biochem. Sci.* **2004**, *29* (11), 572–578. https://doi.org/10.1016/j.tibs.2004.09.004.

(13) Xue, B.; Leyrat, C.; Grimes, J. M.; Robinson, R. C. Structural Basis of Thymosin- 4/Profilin Exchange Leading to Actin Filament Polymerization. *Proc. Natl. Acad. Sci.* **2014**, *111* (43), E4596–E4605. https://doi.org/10.1073/pnas.1412271111.

(14) Ferron, F.; Rebowski, G.; Lee, S. H.; Dominguez, R. Structural Basis for the Recruitment of Profilin–Actin Complexes during Filament Elongation by Ena/VASP. *The EMBO Journal* **2007**, *26* (21), 4597–4606. https://doi.org/10.1038/sj.emboj.7601874.

(15) Dominguez, R. Actin Filament Nucleation and Elongation Factors – Structure–Function Relationships. *Crit. Rev. Biochem. Mol. Biol.* **2009**, *44*, 351–366.

(16) Firat-Karalar, E. N.; Welch, M. D. New Mechanisms and Functions of Actin Nucleation. *Curr. Opin. Cell Biol.* **2011**, *23* (1), 4–13. https://doi.org/10.1016/j.ceb.2010.10.007.

(17) Skau, C. T.; Waterman, C. M. Specification of Architecture and Function of Actin Structures by Actin Nucleation Factors. *Annu. Rev. Biophys.* **2015**, *44* (1), 285–310. https://doi.org/10.1146/annurev-biophys-060414-034308.

(18) Pollard, T. D. Regulation of Actin Filament Assembly by Arp2/3 Complex and Formins. *Annu. Rev. Biophys. Biomol. Strct.* **2007**, *36* (1), 451–477. https://doi.org/10.1146/annurev.biophys.35.040405.101936.

(19) Shekhar, S.; Pernier, J.; Carlier, M.-F. Regulators of Actin Filament Barbed Ends at a Glance. *J. Cell Sci.* **2016**, jcs.179994. https://doi.org/10.1242/jcs.179994.

(20) von der Ecken, J.; Müller, M.; Lehman, W.; Manstein, D. J.; Penczek, P. A.; Raunser, S. Structure of the F-Actin-Tropomyosin Complex. *Nature* **2015**, *519* (7541), 114-117. http://dx.doi.org.proxy.library.nyu.edu/10.1038/nature14033.

(21) Das, S.; Ge, P.; Oztug Durer, Z. A.; Grintsevich, E. E.; Zhou, Z. H.; Reisler, E. D-Loop Dynamics and Near-Atomic-Resolution Cryo-EM Structure of Phalloidin-Bound F-Actin. *Structure* **2020**, *28* (5), 586-593.e3. https://doi.org/10.1016/j.str.2020.04.004.
(22) Gruszczynska-Biegala, J.; Stefan, A.; Kasprzak, A. A.; Dobryszycki, P.; Khaitlina, S.; Strzelecka-Gołaszewska, H. Myopathy-Sensitive G-Actin Segment 227-235 Is Involved in Salt-Induced Stabilization of Contacts within the Actin Filament. *Int. J. Mol. Sci.* **2021**, *22* (5), 2327. https://doi.org/10.3390/ijms22052327.
(23) McLachlan, A. D.; Stewart, M. Tropomyosin Coiled-Coil Interactions: Evidence for an Unstaggered Structure. *J. Mol. Biol.* **1975**, *98* (2), 293–304. https://doi.org/10.1016/S0022-2836(75)80119-7.
(24) Bugyi, B.; Didry, D.; Carlier, M.-F. How Tropomyosin Regulates Lamellipodial Actin-based Motility: A Combined Biochemical and Reconstituted Motility Approach. *The EMBO Journal* **2010**, *29*, 14-26. https://doi.org/10.1038/emboj.2009.316.
(25) Brown, J. H.; Zhou, Z.; Reshetnikova, L.; Robinson, H.; Yammani, R. D.; Tobacman, L. S.; Cohen, C. Structure of the Mid-Region of Tropomyosin: Bending and Binding Sites for Actin. *Proc. Natl. Acad. Sci.* **2005**, *102* (52), 18878–18883. https://doi.org/10.1073/pnas.0509269102.
(26) Manstein, D. J.; Meiring, J. C. M.; Hardeman, E. C.; Gunning, P. W. Actin–Tropomyosin Distribution in Non-Muscle Cells. *J. Muscle. Res. Cell. Motil.* **2020**, *41* (1), 11–22. https://doi.org/10.1007/s10974-019-09514-0.
(27) Gunning, P. W.; Hardeman, E. C.; Lappalainen, P.; Mulvihill, D. P. Tropomyosin – Master Regulator of Actin Filament Function in the Cytoskeleton. *J. Cell Sci.* **2015**, *128* (16), 2965-2974. https://doi.org/10.1242/jcs.172502.
(28) Edwards, M.; Zwolak, A.; Schafer, D. A.; Sept, D.; Dominguez, R.; Cooper, J. A. Capping Protein Regulators Fine-Tune Actin Assembly Dynamics. *Nat. Rev. Mol. Cell Biol.* **2014**, *15* (10), 677–689. https://doi.org/10.1038/nrm3869.
(29) Weeds, A.; Maciver, S. F-Actin Capping Proteins. *Curr. Opin. Cell Biol.* **1993**, *5* (1), 63–69. https://doi.org/10.1016/S0955-0674(05)80009-2.
(30) McGrath, J. L.; Osborn, E. A.; Tardy, Y. S.; Dewey, C. F.; Hartwig, J. H. Regulation of the Actin Cycle in Vivo by Actin Filament Severing. *Proc. Natl. Acad. Sci.* **2000**, *97* (12), 6532–6537. https://doi.org/10.1073/pnas.100023397.
(31) Matsudaira, P. Pieces in the Actin-Severing Protein Puzzle. *Cell* **1988**, *54* (2), 139–140. https://doi.org/10.1016/0092-8674(88)90542-9.
(32) Burtnick, L. D.; Koepf, E. K.; Grimes, J.; Jones, E. Y.; Stuart, D. I.; McLaughlin, P. J.; Robinson, R. C. The Crystal Structure of Plasma Gelsolin: Implications for Actin Severing, Capping, and Nucleation. *Cell* **1997**, *90* (4), 661–670. https://doi.org/10.1016/S0092-8674(00)80527-9.
(33) Sun, H. Q.; Yamamoto, M.; Mejillano, M.; Yin, H. L.; ‡. Gelsolin, a Multifunctional Actin Regulatory Protein. *J. Biol. Chem.* **1999**, *274* (47), 33179–33182. https://doi.org/10.1074/jbc.274.47.33179.
(34) Huehn, A. R.; Bibeau, J. P.; Schramm, A. C.; Cao, W.; De La Cruz, E. M.; Sindelar, C. V. Structures of Cofilin-Induced Structural Changes Reveal Local and Asymmetric Perturbations of Actin Filaments. *Proc. Natl. Acad. Sci.* **2020**, *117* (3), 1478–1484. https://doi.org/10.1073/pnas.1915987117.
(35) Bamburg, J. R. Proteins of the ADF/Cofilin Family: Essential Regulators of Actin Dynamics. *Annu. Rev. Cell Dev. Biol.* **1999**, *15* (1), 185–230. https://doi.org/10.1146/annurev.cellbio.15.1.185.
(36) Terman, J. R.; Kashina, A. Post-Translational Modification and Regulation of Actin. *Curr. Opin. Cell Biol.* **2013**, *25* (1), 30–38. https://doi.org/10.1016/j.ceb.2012.10.009.
(37) Hung, R.-J.; Yazdani, U.; Yoon, J.; Wu, H.; Yang, T.; Gupta, N.; Huang, Z.; van Berkel, W. J. H.; Terman, J. R. Mical Links Semaphorins to F-Actin Disassembly. *Nature* **2010**, *463* (7282), 823–827. https://doi.org/10.1038/nature08724.
(38) Hung, R.-J.; Pak, C. W.; Terman, J. R. Direct Redox Regulation of F-Actin Assembly and Disassembly by Mical. *Science* **2011**, *334* (6063), 1710–1713. https://doi.org/10.1126/science.1211956.
(39) Grintsevich, E. E.; Ge, P.; Sawaya, M. R.; Yesilyurt, H. G.; Terman, J. R.; Zhou, Z. H.; Reisler, E. Catastrophic Disassembly of Actin Filaments via Mical-Mediated Oxidation. *Nat. Commun.* **2017**, *8* (1), 2183. https://doi.org/10.1038/s41467-017-02357-8.
(40) Grintsevich, E. E.; Yesilyurt, H. G.; Rich, S. K.; Hung, R.-J.; Terman, J. R.; Reisler, E. F-Actin Dismantling through a Redox-Driven Synergy between Mical and Cofilin. *Nat Cell Biol* **2016**, *18* (8), 876–885. https://doi.org/10.1038/ncb3390.

(41) Frémont, S.; Hammich, H.; Bai, J.; Wioland, H.; Klinkert, K.; Rocancourt, M.; Kikuti, C.; Stroebel, D.; Romet-Lemonne, G.; Pylypenko, O.; Houdusse, A.; Echard, A. Oxidation of F-Actin Controls the Terminal Steps of Cytokinesis. *Nat. Commun.* **2017**, *8* (1), 14528. https://doi.org/10.1038/ncomms14528.
(42) Polge, C.; Heng, A.-E.; Jarzaguet, M.; Ventadour, S.; Claustre, A.; Combaret, L.; Béchet, D.; Matondo, M.; Uttenweiler-Joseph, S.; Monsarrat, B.; Attaix, D.; Taillandier, D. Muscle Actin Is Polyubiquitinylated in Vitro and in Vivo and Targeted for Breakdown by the E3 Ligase MuRF1. *The FASEB Journal* **2011**, *25* (11), 3790–3802. https://doi.org/10.1096/fj.11-180968.
(43) Siton-Mendelson, O.; Bernheim-Groswasser, A. Functional Actin Networks under Construction: The Cooperative Action of Actin Nucleation and Elongation Factors. *Trends Biochem. Sci.* **2017**, *42*, 414–430. http://dx.doi.org/10.1016/j.tibs.2017.03.002.
(44) Kadzik, R. S.; Homa, K. E.; Kovar, D. R. F-Actin Cytoskeleton Network Self-Organization Through Competition and Cooperation. *Annu. Rev. Cell Dev. Biol.* **2020**, *36*, 35–60. https://doi.org/10.1146/annurev-cellbio-032320- 094706.
(45) Schaks, M.; Giannone, G.; Rottner, K. Actin Dynamics in Cell Migration. *Essays Biochem.* **2019**, *63* (5), 483–495. https://doi.org/10.1042/EBC20190015.
(46) Le Clainche, C.; Carlier, M.-F. Regulation of Actin Assembly Associated With Protrusion and Adhesion in Cell Migration. *Physiol. Rev.* **2008**, *88* (2), 489–513. https://doi.org/10.1152/physrev.00021.2007.
(47) Ponti, A. Two Distinct Actin Networks Drive the Protrusion of Migrating Cells. *Science* **2004**, *305* (5691), 1782–1786. https://doi.org/10.1126/science.1100533.
(48) Robinson, R. C.; Turbedsky, K.; Kaiser, D. A.; Marchand, J.-B.; Higgs, H. N.; Choe, S.; Pollard, T. D. Crystal Structure of Arp2/3 Complex. *Science* **2001**, *294*, 7.
(49) Rodal, A. A.; Sokolova, O.; Robins, D. B.; Daugherty, K. M.; Hippenmeyer, S.; Riezman, H.; Grigorieff, N.; Goode, B. L. Conformational Changes in the Arp2/3 Complex Leading to Actin Nucleation. *Nat. Struct. Mol. Biol.* **2005**, *12* (1), 26–31. https://doi.org/10.1038/nsmb870.
(50) Goley, E. D.; Rodenbusch, S. E.; Martin, A. C.; Welch, M. D. Critical Conformational Changes in the Arp2/3 Complex Are Induced by Nucleotide and Nucleation Promoting Factor. *Mol. Cell* **2004**, *16* (2), 269–279. https://doi.org/10.1016/j.molcel.2004.09.018.
(51) Goley, E. D.; Welch, M. D. The ARP2/3 Complex: An Actin Nucleator Comes of Age. *Nat. Rev. Mol. Cell Biol.* **2006**, *7* (10), 713–726. https://doi.org/10.1038/nrm2026.
(52) Padrick, S. B.; Doolittle, L. K.; Brautigam, C. A.; King, D. S.; Rosen, M. K. Arp2/3 Complex Is Bound and Activated by Two WASP Proteins. *Proc. Natl. Acad. Sci.* **2011**, *108* (33), E472–E479. https://doi.org/10.1073/pnas.1100236108.
(53) Rottner, K.; Hänisch, J.; Campellone, K. G. WASH, WHAMM and JMY: Regulation of Arp2/3 Complex and Beyond. *Trends Cell Biol.* **2010**, *20* (11), 650–661. https://doi.org/10.1016/j.tcb.2010.08.014.
(54) Lee, G.; Leech, G.; Rust, M. J.; Das, M.; McGorty, R. J.; Ross, J. L.; Robertson-Anderson, R. M. Myosin-Driven Actin-Microtubule Networks Exhibit Self-Organized Contractile Dynamics. *Sci. Adv.* **2021**, *7* (6), eabe4334. https://doi.org/10.1126/sciadv.abe4334.
(55) Burgess, D. R. Cytokinesis: New Roles for Myosin. *Curr. Biol.* **2005**, *15* (8), R310–R311. https://doi.org/10.1016/j.cub.2005.04.008.
(56) Vicente-Manzanares, M.; Ma, X.; Adelstein, R. S.; Horwitz, A. R. Non-Muscle Myosin II Takes Centre Stage in Cell Adhesion and Migration. *Nat. Rev. Mol. Cell Biol.* **2009**, *10* (11), 778–790. https://doi.org/10.1038/nrm2786.
(57) Klenchin, V. A.; Allingham, J. S.; King, R.; Tanaka, J.; Marriott, G.; Rayment, I. Trisoxazole Macrolide Toxins Mimic the Binding of Actin-Capping Proteins to Actin. *Nat. Struct. Mol. Biol.* **2003**, *10* (12), 1058–1063. https://doi.org/10.1038/nsb1006.
(58) Tanaka, J.; Yan, Y.; Choi, J.; Bai, J.; Klenchin, V. A.; Rayment, I.; Marriott, G. Biomolecular Mimicry in the Actin Cytoskeleton: Mechanisms Underlying the Cytotoxicity of Kabiramide C and Related Macrolides. *Proc. Natl. Acad. Sci.* **2003**, 13851–16856.
(59) Klenchin, V. A.; King, R.; Tanaka, J.; Marriott, G.; Rayment, I. Structural Basis of Swinholide A Binding to Actin. *Chem. Biol.* **2005**, *12* (3), 287–291. https://doi.org/10.1016/j.chembiol.2005.02.011.
(60) Allingham, J. S.; Klenchin, V. A.; Rayment, I. Actin-Targeting Natural Products: Structures, Properties and Mechanisms of Action. *Cell. Mol. Life Sci.* **2006**, *63* (18), 2119–2134. https://doi.org/10.1007/s00018-006-6157-9.

(61) Fenteany, G.; Zhu, S. Small-Molecule Inhibitors of Actin Dynamics and Cell Motility. *Curr. Top. Med. Chem.* **2003**, *3* (6), 593–616. https://doi.org/10.2174/1568026033452348.
(62) Morton, W. M.; Ayscough, K. R.; McLaughlin, P. J. Latrunculin Alters the Actin-Monomer Subunit Interface to Prevent Polymerization. *Nat. Cell Biol.* **2000**, *2* (6), 376–378. https://doi.org/10.1038/35014075.
(63) Wang, S.; Crevenna, A. H.; Ugur, I.; Marion, A.; Antes, I.; Kazmaier, U.; Hoyer, M.; Lamb, D. C.; Gegenfurtner, F.; Kliesmete, Z.; Ziegenhain, C.; Enard, W.; Vollmar, A.; Zahler, S. Actin Stabilizing Compounds Show Specific Biological Effects Due to Their Binding Mode. *Sci. Rep.* **2019**, *9* (1), 9731. https://doi.org/10.1038/s41598-019-46282-w.
(64) Kashman, Y.; A Groweiss; Shmueli, U. Latrunculin, A New 2-Thiazolidinone Macrolide from the Marina Sponhe Latrunculia Magnifica. *Tet. Lett.* **1980**, *21*, 3629–3632. https://doi.org/10.1016/0040-4039(80)80255-3.
(65) Spector, I.; Shochet, N.; Kashman, Y.; Groweiss, A. Latrunculins: Novel Marine Toxins That Disrupt Microfilament Organization in Cultured Cells. *Science* **1983**, *219* (4584), 493–495. https://doi.org/10.1126/science.6681676.
(66) Spector, I.; Shochet, N. R.; Blasberger, D.; Kashman, Y. Latrunculins—Novel Marine Macrolides That Disrupt Microfilament Organization and Affect Cell Growth: I. Comparison with Cytochalasin D. *Cell Motil. Cytoskelet.* **1989**, *13* (3), 127–144. https://doi.org/10.1002/cm.970130302.
(67) Vilozny, B.; Amagata, T.; Mooberry, S. L.; Crews, P. A New Dimension to the Biosynthetic Products Isolated from the Sponge *Negombata Magnifica*. *J. Nat. Prod.* **2004**, *67* (6), 1055–1057. https://doi.org/10.1021/np0340753.
(68) Gulavita, N. K.; Gunasekera, S. P.; Pomponi, S. A. Isolation of Latrunculin A, 6,7-Epoxylatrunculin A, Fijianolide A, and Euryfuran from a New Genus of the Family Thorectidae. *J. Nat. Prod.* **1992**, *55* (4), 506–508. https://doi.org/10.1021/np50082a019.
(69) Tanaka, J.; Higa, T.; Bernardinelli, G.; Jefford, C. W. New Cytotoxic Macrolides from the Sponge *Fasciospongia Rimosa*. *Chem. Lett.* **1996**, *25* (4), 255–256. https://doi.org/10.1246/cl.1996.255.
(70) Pika, J.; John Faulkner, D. Unusual Chlorinated Homo-Diterpenes from the South African Nudibranch Chromodoris Hamiltoni. *Tetrahedron* **1995**, *51* (30), 8189–8198. https://doi.org/10.1016/0040-4020(95)00440-J.
(71) Fujiwara, I.; Zweifel, M. E.; Courtemanche, N.; Pollard, T. D. Latrunculin A Accelerates Actin Filament Depolymerization in Addition to Sequestering Actin Monomers. *Curr. Biol.* **2018**, *28* (19), 3183-3192.e2. https://doi.org/10.1016/j.cub.2018.07.082.
(72) Scherlach, K.; Boettger, D.; Remme, N.; Hertweck, C. The Chemistry and Biology of Cytochalasans. *Nat. Prod. Rep.* **2010**, *27* (6), 869–886. https://doi.org/10.1039/B903913A.
(73) Aldridge, D. C.; Armstrong, J. J.; Speake, R. N.; Turner, W. B. The Cytochalasins, a New Class of Biologically Active Mould Metabolites. *Chem. Commun.* **1967**, No. 1, 26–27. https://doi.org/10.1039/C19670000026.
(74) Nair, U. B.; Joel, P. B.; Wan, Q.; Lowey, S.; Rould, M. A.; Trybus, K. M. Crystal Structures of Monomeric Actin Bound to Cytochalasin D. *J. Mol. Biol.* **2008**, *384* (4), 848–864. https://doi.org/10.1016/j.jmb.2008.09.082.
(75) Allingham, J. S.; Miles, C. O.; Rayment, I. A Structural Basis for Regulation of Actin Polymerization by Pectenotoxins. *J. Mol. Biol.* **2007**, *371* (4), 959–970. https://doi.org/10.1016/j.jmb.2007.05.056.
(76) Hori, M.; Saito, S.; Shin, Y. Z.; Ozaki, H.; Fusetani, N.; Karaki, H. Mycalolide-B, a Novel and Specific Inhibitor of Actomyosin ATPase Isolated from Marine Sponge. *FEBS Letters* **1993**, *322* (2), 151–154. https://doi.org/10.1016/0014-5793(93)81557-G.
(77) Saito, S.; Watanabe, S.; Ozaki, H; Fusetani, N.; Karaki, H. Mycalolide B, a Novel Actin Depolymerizing Agent. *J. Biol. Chem.* **1994**, *269* (47) 29710-29714. https://doi.org/10.1016/S0021-9258(18)43938-5
(78) Roesener, J. A.; Scheuer, P. J. Ulapualide A and B, Extraordinary Antitumor Macrolides from Nudibranch Eggmasses. *J. Am. Chem. Soc.* **1986**, *108* (4), 846–847. https://doi.org/10.1021/ja00264a052.
(79) Guella, G.; Mancini, I.; Chiasera, G.; Pietra, F. Sphinxolide, a 26-Membered Antitumoral Macrolide Isolated from an Unidentified Pacific Nudibranch. *Helv. Chim. Acta* **1989**, *72* (2), 237–246. https://doi.org/10.1002/hlca.19890720207.

(80) Ishibashi, M.; Moore, R. E.; Patterson, G. M. L.; Xu, C.; Clardy, J. Scytophycins, Cytotoxic and Antimycotic Agents from the Cyanophyte Scytonema Pseudohofmanni. *J. Org. Chem.* **1986**, *51* (26), 5300–5306. https://doi.org/10.1021/jo00376a047.
(81) Irschik, H.; Jansen, R.; Gerth, K.; Höfle, G.; Reichenbach, H. Chivosazol A, a New Inhibitor of Eukaryotic Organisms Isolated from Myxobacteria. *J. Antibiot.* **1995**, *48* (9), 962–966. https://doi.org/10.7164/antibiotics.48.962.
(82) Diestel, R.; Irschik, H.; Jansen, R.; Khalil, M. W.; Reichenbach, H.; Sasse, F. Chivosazoles A and F, Cytostatic Macrolides from Myxobacteria, Interfere with Actin. *ChemBioChem* **2009**, *10* (18), 2900–2903. https://doi.org/10.1002/cbic.200900562.
(83) Filipuzzi, I.; Thomas, J. R.; Pries, V.; Estoppey, D.; Salcius, M.; Studer, C.; Schirle, M.; Hoepfner, D. Direct Interaction of Chivosazole F with Actin Elicits Cell Responses Similar to Latrunculin A but Distinct from Chondramide. *ACS Chem. Biol.* **2017**, *12* (9), 2264–2269. https://doi.org/10.1021/acschembio.7b00385.
(84) Wang, S.; Gegenfurtner, F. A.; Crevenna, A. H.; Ziegenhain, C.; Kliesmete, Z.; Enard, W.; Müller, R.; Vollmar, A. M.; Schneider, S.; Zahler, S. Chivosazole A Modulates Protein–Protein Interactions of Actin. *J. Nat. Prod.* **2019**, *82* (7), 1961–1970. https://doi.org/10.1021/acs.jnatprod.9b00335.
(85) Bubb, M. R.; Spector, I. Swinholide A Is a Microfilament Disrupting Marine Toxin That Stabilizes Actin Dimers and Severs Actin Filaments. *J. Biol. Chem.* **1995**, *270* (8), 3463-3466. https://doi.org/10.1074/jbc.270.8.3463
(86) Saito, S.; Watabe, S.; Ozaki, H.; Kobayashi, M.; Suzuki, T.; Kobayashi, H.; Fusetani, N.; Karaki, H. Actin-Depolymerizing Effect of Dimeric Macrolides, Bistheonellide A and Swinholide A. *J. Biochem.* **1998**, *123* (4), 571-578. https://doi.org/10.1093/oxfordjournals.jbchem.a021975
(87) Bistramide A, a New Toxin from the Urochordata Lissoclinum Bistratum Sluiter: Isolation and Preliminary Characterization. *Toxicon* **1988**, *26* (12), 1129–1136. https://doi.org/10.1016/0041-0101(88)90297-8.
(88) Rizvi, S. A.; Tereshko, V.; Kossiakoff, A. A.; Kozmin, S. A. Structure of Bistramide A–Actin Complex at a 1.35 Å Resolution. *J. Am. Chem. Soc.* **2006**, *128* (12), 3882–3883. https://doi.org/10.1021/ja058319c.
(89) Statsuk, A. V.; Bai, R.; Baryza, J. L.; Verma, V. A.; Hamel, E.; Wender, P. A.; Kozmin, S. A. Actin Is the Primary Cellular Receptor of Bistramide A. *Nat. Chem. Biol.* **2005**, *1* (7), 383-388. https://doi.org/10.1038/nchembio748
(90) Rizvi, S. A.; Courson, D. S.; Keller, V. A.; Rock, R. S.; Kozmin, S. A. The Dual Mode of Action of Bistramide A Entails Severing of Filamentous Actin and Covalent Protein Modification. *Proc. Natl. Acad. Sci.* **2008**, *105* (11), 4088-4092. https://doi.org/10.1073/pnas.0710727105
(91) Kumari, A.; Kesarwani, S.; Javoor, M. G.; Vinothkumar, K. R.; Sirajuddin, M. Structural Insights into Actin Filament Recognition by Commonly Used Cellular Actin Markers. *The EMBO Journal* **2020**, *39* (14), e104006. https://doi.org/10.15252/embj.2019104006.
(92) Pospich, S.; Merino, F.; Raunser, S. Structural Effects and Functional Implications of Phalloidin and Jasplakinolide Binding to Actin Filaments. *Structure* **2020**, *28* (4), 437-449.e5. https://doi.org/10.1016/j.str.2020.01.014.
(93) Lynen, F.; Wieland, U. Über die Giftstoffe des Knollenblätterpilzes. IV. *J. Liebigs Ann. Chem.* **1938**, *533* (1), 93-117. https://doi.org/10.1002/jlac.19385330105.
(94) Wieland, T. The Toxic Peptides from Amanita Mushrooms. *Int. J. Pept. Prot. Res.* **1983**, *22* (3), 257–276. https://doi.org/10.1111/j.1399-3011.1983.tb02093.x.
(95) Vetter, J. Toxins of Amanita Phalloides. *Toxicon* **1998**, *36* (1), 13–24. https://doi.org/10.1016/S0041-0101(97)00074-3.
(96) Karlson-Stiber, C.; Persson, H. Cytotoxic Fungi—an Overview. *Toxicon* **2003**, *42* (4), 339–349. https://doi.org/10.1016/S0041-0101(03)00238-1.
(97) Mentes, A.; Huehn, A.; Liu, X.; Zwolak, A.; Dominguez, R.; Shuman, H.; Ostap, E. M.; Sindelar, C. V. High-Resolution Cryo-EM Structures of Actin-Bound Myosin States Reveal the Mechanism of Myosin Force Sensing. *Proc. Natl. Acad. Sci.* **2018**, *115* (6), 1292–1297. https://doi.org/10.1073/pnas.1718316115.
(98) Zabriskie, T. Mark.; Klocke, J. A.; Ireland, C. M.; Marcus, A. H.; Molinski, T. F.; Faulkner, D. John.; Xu, Changfu.; Clardy, Jon. Jaspamide, a Modified Peptide from a Jaspis Sponge, with Insecticidal and Antifungal Activity. *J. Am. Chem. Soc.* **1986**, *108* (11), 3123–3124. https://doi.org/10.1021/ja00271a062.

(99) Crews, P.; Manes, L. V.; Boehler, M. Jasplakinolide, a Cyclodepsipeptide from the Marine Sponge *Jaspis Sp. Tet. Lett.* **1986**, *27* (25), 2797–2800. https://doi.org/10.1016/S0040-4039(00)84645-6.

(100) Spector, I.; Bubb, M. R.; Beyer, B. B.; Fosen, K. M. Effects of Jasplakinolide on the Kinetics of Actin Polymerization: an Explanation for Certain in vivo Observations *J. Biol. Chem.* **2000**, *275* (7), 5163–5170. https://doi.org/10.1074/jbc.275.7.5163.

(101) Robinson, S. J.; Morinaka, B. I.; Amagata, T.; Tenney, K.; Bray, W. M.; Gassner, N. C.; Lokey, R. S.; Crews, P. New Structures and Bioactivity Properties of Jasplakinolide (Jaspamide) Analogues from Marine Sponges. *J. Med. Chem.* **2010**, *53* (4), 1651–1661. https://doi.org/10.1021/jm9013554.

(102) Tannert, R.; Milroy, L.-G.; Ellinger, B.; Hu, T.-S.; Arndt, H.-D.; Waldmann, H. Synthesis and Structure–Activity Correlation of Natural-Product Inspired Cyclodepsipeptides Stabilizing F-Actin. *J. Am. Chem. Soc.* **2010**, *132* (9), 3063–3077. https://doi.org/10.1021/ja9095126.

(103) Total Syntheses of Jaspamide (Jasplakinolide) and Geodiamolide A and B - 1. Stereoselective Synthesis of (2S,4E,6R,8S)-8-Hydroxy-2,4,6-Trimethyl-4-Nonenoicic Acid1. *Tet. Lett.* **1988**, *29* (11), 1269–1270. https://doi.org/10.1016/S0040-4039(00)80273-7.

(104) Xu, Y.-Y. Advances in the Total Synthesis of Cyclodepsipeptide ( )-Jasplakinolide (Jaspamide) and Its Analogs. *Curr. Org. Synth.* **2013**, *10* (1), 67–89. https://doi.org/10.2174/1570179411310010004.

(105) Chu, K. S.; Negrete, G. R.; Konopelski, J. P. Asymmetric Total Synthesis of (+)-Jasplakinolide. *J. Org. Chem.* **1991**, *56* (17), 5196–5202. https://doi.org/10.1021/jo00017a037.

(106) Grieco, P. A.; Hon, Y. Son.; Perez-Medrano, Arturo. Convergent, Enantiospecific Total Synthesis of the Novel Cyclodepsipeptide (+)-Jasplakinolide (Jaspamide). *J. Am. Chem. Soc.* **1988**, *110* (5), 1630–1631. https://doi.org/10.1021/ja00213a050.

(107) Ghosh, A. K.; Moon, D. K. Enantioselective Total Synthesis of (+)-Jasplakinolide. *Org. Lett.* **2007**, *9* (12), 2425–2427. https://doi.org/10.1021/ol070855h.

(108) Tannert, R.; Hu, T.-S.; Arndt, H.-D.; Waldmann, H. Solid-Phase Based Total Synthesis of Jasplakinolide by Ring-Closing Metathesis. *Chem. Commun.* **2009**, No. 12, 1493–1495. https://doi.org/10.1039/B900342H.

(109) Hirai, Y. Studies on the Novel Cyclodepsipeptides. A Total Synthesis of (+)-Jasplakinolide (Jaspamide). *Heterocycles* **1994**, *39* (2), 603–612. https://doi.org/10.3987/COM-94-S(B)52.

(110) Lukinavičius, G.; Umezawa, K.; Olivier, N.; Honigmann, A.; Yang, G.; Plass, T.; Mueller, V.; Reymond, L.; Corrêa Jr, I. R.; Luo, Z.-G.; Schultz, C.; Lemke, E. A.; Heppenstall, P.; Eggeling, C.; Manley, S.; Johnsson, K. A Near-Infrared Fluorophore for Live-Cell Super-Resolution Microscopy of Cellular Proteins. *Nat. Chem.* **2013**, *5* (2), 132–139. https://doi.org/10.1038/nchem.1546.

(111) Milroy, L.-G.; Rizzo, S.; Calderon, A.; Ellinger, B.; Erdmann, S.; Mondry, J.; Verveer, P.; Bastiaens, P.; Waldmann, H.; Dehmelt, L.; Arndt, H.-D. Selective Chemical Imaging of Static Actin in Live Cells. *J. Am. Chem. Soc.* **2012**, *134* (20), 8480–8486. https://doi.org/10.1021/ja211708z.

(112) Borowiak, M.; Küllmer, F.; Gegenfurtner, F.; Peil, S.; Nasufovic, V.; Zahler, S.; Thorn-Seshold, O.; Trauner, D.; Arndt, H.-D. Optical Manipulation of F-Actin with Photoswitchable Small Molecules. *J. Am. Chem. Soc.* **2020**, *142* (20), 9240–9249. https://doi.org/10.1021/jacs.9b12898.

(113) Ishiwata, H.; Nemoto, T.; Ojika, M.; Yamada, K. Isolation and Stereostructure of Doliculide, a Cytotoxic Cyclodepsipeptide from the Japanese Sea Hare Dolabella Auricularia. *J. Org. Chem.* **1994**, *59* (17), 4710–4711. https://doi.org/10.1021/jo00096a002.

(114) Bai, R.; Verdier-Pinard, P.; Gangwar, S.; Stessman, C. C.; McClure, K. J.; Sausville, E. A.; Pettit, G. R.; Bates, R. B.; Hamel, E. Dolastatin 11, a Marine Depsipeptide, Arrests Cells at Cytokinesis and Induces Hyperpolymerization of Purified Actin. *Mol. Pharmacol.* **2001**, *59* (3), 462–469. https://doi.org/10.1124/mol.59.3.462.

(115) Foerster, F.; Braig, S.; Chen, T.; Altmann, K.-H.; Vollmar, A. M. Pharmacological Characterization of Actin-Binding (–)-Doliculide. *Bioorg. Med. Chem.* **2014**, *22* (18), 5117–5122. https://doi.org/10.1016/j.bmc.2014.03.003.

(116) Iizuka, T.; Fudou, R.; Jojima, Y.; Ogawa, S.; Yamanaka, S.; Inukai, Y.; Ojika, M. Miuraenamides A and B, Novel Antimicrobial Cyclic Depsipeptides from a New Slightly Halophilic Myxobacterium: Taxonomy, Production, and Biological Properties. *J. Antibiot.* **2006**, *59* (7), 385–391. https://doi.org/10.1038/ja.2006.55.

(117) Ojika, M.; Inukai, Y.; Kito, Y.; Hirata, M.; Iizuka, T.; Fudou, R. Miuraenamides: Antimicrobial Cyclic Depsipeptides Isolated from a Rare and Slightly Halophilic Myxobacterium. *Chem. Asian J.* **2008**, *3* (1), 126–133. https://doi.org/10.1002/asia.200700233.
(118) Sumiya, E.; Shimogawa, H.; Sasaki, H.; Tsutsumi, M.; Yoshita, K.; Ojika, M.; Suenaga, K.; Uesugi, M. Cell-Morphology Profiling of a Natural Product Library Identifies Bisebromoamide and Miuraenamide A as Actin Filament Stabilizers. *ACS Chem. Biol.* **2011**, *6* (5), 425–431. https://doi.org/10.1021/cb1003459.
(119) Bai, R. L.; Pettit, G. R.; Hamel, E. Binding of Dolastatin 10 to Tubulin at a Distinct Site for Peptide Antimitotic Agents near the Exchangeable Nucleotide and Vinca Alkaloid Sites. *J. Biol. Chem.* **1990**, *265* (28), 17141–17149. https://doi.org/10.1016/S0021-9258(17)44880-0.
(120) Teruya, T.; Sasaki, H.; Fukazawa, H.; Suenaga, K. Bisebromoamide, a Potent Cytotoxic Peptide from the Marine Cyanobacterium *Lyngbya* Sp.: Isolation, Stereostructure, and Biological Activity. *Org. Lett.* **2009**, *11* (21), 5062–5065. https://doi.org/10.1021/ol9020546.
(121) Suzuki, K.; Mizuno, R.; Suenaga, K.; Teruya, T.; Tanaka, N.; Kosaka, T.; Oya, M. Bisebromoamide, an Extract from Lyngbya Species, Induces Apoptosis through ERK and MTOR Inhibitions in Renal Cancer Cells. *Cancer Medicine* **2013**, *2* (1), 32–39. https://doi.org/10.1002/cam4.53.
(122) Suntornchashwej, S.; Chaichit, N.; Isobe, M.; Suwanborirux, K. Hectochlorin and Morpholine Derivatives from the Thai Sea Hare, Bursatella Leachii. *J. Nat. Prod.* **2005**, *68* (6), 951–955. https://doi.org/10.1021/np0500124.
(123) Marquez, B. L.; Watts, K. S.; Yokochi, A.; Roberts, M. A.; Verdier-Pinard, P.; Jimenez, J. I.; Hamel, E.; Scheuer, P. J.; Gerwick, W. H. Structure and Absolute Stereochemistry of Hectochlorin, a Potent Stimulator of Actin Assembly. *J. Nat. Prod.* **2002**, *65* (6), 866–871. https://doi.org/10.1021/np0106283.
(124) Kobayashi, J. Amphidinolides and Its Related Macrolides from Marine Dinoflagellates. *J. Antibiot.* **2008**, *61* (5), 271–284. https://doi.org/10.1038/ja.2008.39.
(125) Usui, T.; Kazami, S.; Dohmae, N.; Mashimo, Y.; Kondo, H.; Tsuda, M.; Terasaki, A. G.; Ohashi, K.; Kobayashi, J.; Osada, H. Amphidinolide H, a Potent Cytotoxic Macrolide, Covalently Binds on Actin Subdomain 4 and Stabilizes Actin Filament. *Chem. Biol.* **2004**, 1269–1277.
(126) Trigili, C.; Pera, B.; Barbazanges, M.; Cossy, J.; Meyer, C.; Pineda, O.; Rodríguez-Escrich, C.; Urpí, F.; Vilarrasa, J.; Díaz, J. F.; Barasoain, I. Mechanism of Action of the Cytotoxic Macrolides Amphidinolide X and J. *ChemBioChem* **2011**, *12* (7), 1027–1030. https://doi.org/10.1002/cbic.201100042.
(127) Nolen, B. J.; Tomasevic, N.; Russell, A.; Pierce, D. W.; Jia, Z.; McCormick, C. D.; Hartman, J.; Sakowicz, R.; Pollard, T. D. Characterization of Two Classes of Small Molecule Inhibitors of Arp2/3 Complex. *Nature* **2009**, *460* (7258), 1031–1034. https://doi.org/10.1038/nature08231.
(128) Baggett, A. W.; Cournia, Z.; Han, M. S.; Patargias, G.; Glass, A. C.; Liu, S.-Y.; Nolen, B. J. Structural Characterization and Computer-Aided Optimization of a Small-Molecule Inhibitor of the Arp2/3 Complex, a Key Regulator of the Actin Cytoskeleton. *ChemMedChem* **2012**, *7* (7), 1286–1294. https://doi.org/10.1002/cmdc.201200104.
(129) Hetrick, B.; Han, M. S.; Helgeson, L. A.; Nolen, B. J. Small Molecules CK-666 and CK-869 Inhibit Actin-Related Protein 2/3 Complex by Blocking an Activating Conformational Change. *Chem. Biol.* **2013**, *20* (5), 701–712. https://doi.org/10.1016/j.chembiol.2013.03.019.
(130) Rotty, J. D.; Wu, C.; Bear, J. E. New Insights into the Regulation and Cellular Functions of the Arp2/3 Complex. *Nat. Rev. Mol. Cell Biol.* **2013**, *14* (1), 7–12. https://doi.org/10.1038/nrm3492.
(131) Beghein, E.; Devriese, D.; Van Hoey, E.; Gettemans, J. Cortactin and Fascin-1 Regulate Extracellular Vesicle Release by Controlling Endosomal Trafficking or Invadopodia Formation and Function. *Sci. Rep.* **2018**, *8* (1), 15606. https://doi.org/10.1038/s41598-018-33868-z.
(132) Peterson, J. R.; Bickford, L. C.; Morgan, D.; Kim, A. S.; Ouerfelli, O.; Kirschner, M. W.; Rosen, M. K. Chemical Inhibition of N-WASP by Stabilization of a Native Autoinhibited Conformation. *Nat. Struct. Mol. Biol.* **2004**, *11* (8), 747–755. https://doi.org/10.1038/nsmb796.
(133) Guerriero, C. J.; Weisz, O. A. N-WASP Inhibitor Wiskostatin Nonselectively Perturbs Membrane Transport by Decreasing Cellular ATP Levels. *Am. J. Physiol. Cell Physiol.* **2007**, *292* (4), C1562–C1566. https://doi.org/10.1152/ajpcell.00426.2006.
(134) Bompard, G.; Rabeharivelo, G.; Morin, N. Inhibition of Cytokinesis by Wiskostatin Does Not Rely on N-WASP/Arp2/3 Complex Pathway. *BMC Cell Biol.* **2008**, *9* (1), 42. https://doi.org/10.1186/1471-2121-9-42.

(135) Müller, M.; Diensthuber, R. P.; Chizhov, I.; Claus, P.; Heissler, S. M.; Preller, M.; Taft, M. H.; Manstein, D. J. Distinct Functional Interactions between Actin Isoforms and Nonsarcomeric Myosins. *PloS one* **2013**, *8* (7), e70636. https://doi.org/10.1371/journal.pone.0070636.
(136) Straight, A. F.; Cheung, A.; Limouze, J.; Chen, I.; Westwood, N. J.; Sellers, J. R.; Mitchison, T. J. Dissecting Temporal and Spatial Control of Cytokinesis with a Myosin II Inhibitor. *Science* **2003**, *299* (5613), 1743–1747. https://doi.org/10.1126/science.1081412.
(137) Limouze, J.; Straight, A. F.; Mitchison, T.; Sellers, J. R. Specificity of Blebbistatin, an Inhibitor of Myosin II. *J. Muscle Res. Cell Motil.* **2004**, *25* (4–5), 337–341. https://doi.org/10.1007/s10974-004-6060-7.
(138) Kovács, M.; Tóth, J.; Hetényi, C.; Málnási-Csizmadia, A.; Sellers, J. R. Mechanism of Blebbistatin Inhibition of Myosin II. *J. Biol. Chem.* **2004**, *279* (34), 35557–35563. https://doi.org/10.1074/jbc.M405319200.
(139) Ramamurthy, B.; Yengo, C. M.; Straight, A. F.; Mitchison, T. J.; Sweeney, H. L. Kinetic Mechanism of Blebbistatin Inhibition of Nonmuscle Myosin IIB. *Biochemistry* **2004**, *43* (46), 14832–14839. https://doi.org/10.1021/bi0490284.
(140) Allingham, J. S.; Smith, R.; Rayment, I. The Structural Basis of Blebbistatin Inhibition and Specificity for Myosin II. *Nat. Struct. Mol. Biol.* **2005**, *12* (4), 378–379. https://doi.org/10.1038/nsmb908.
(141) Ewert, W.; Franz, P.; Tsiavaliaris, G.; Preller, M. Structural and Computational Insights into a Blebbistatin-Bound Myosin•ADP Complex with Characteristics of an ADP-Release Conformation along the Two-Step Myosin Power Stoke. *Int. J. Mol. Sci.* **2020**, *21* (19), 7417. https://doi.org/10.3390/ijms21197417.
(142) Kolega, J. Phototoxicity and Photoinactivation of Blebbistatin in UV and Visible Light. *Biochem. Biophys. Res. Commun.* **2004**, *320* (3), 1020–1025. https://doi.org/10.1016/j.bbrc.2004.06.045.
(143) Li, M.-D.; Wong, N.-K.; Xiao, J.; Zhu, R.; Wu, L.; Dai, S.-Y.; Chen, F.; Huang, G.; Xu, L.; Bai, X.; Geraskina, M. R.; Winter, A. H.; Chen, X.; Liu, Y.; Fang, W.; Yang, D.; Phillips, D. L. Dynamics of Oxygen-Independent Photocleavage of Blebbistatin as a One-Photon Blue or Two-Photon Near-Infrared Light-Gated Hydroxyl Radical Photocage. *J. Am. Chem. Soc.* **2018**, *140* (46), 15957–15968. https://doi.org/10.1021/jacs.8b10235.
(144) Rauscher, A. Á.; Gyimesi, M.; Kovács, M.; Málnási-Csizmadia, A. Targeting Myosin by Blebbistatin Derivatives: Optimization and Pharmacological Potential. *Trends Biochem. Sci.* **2018**, *43* (9), 700–713. https://doi.org/10.1016/j.tibs.2018.06.006.
(145) Gyimesi, M.; Rauscher, A. Á.; Suthar, S. K.; Hamow, K. Á.; Oravecz, K.; Lőrincz, I.; Borhegyi, Z.; Déri, M. T.; Kiss, Á. F.; Monostory, K.; Szabó, P. T.; Nag, S.; Tomasic, I.; Krans, J.; Tierney, P. J.; Kovács, M.; Kornya, L.; Málnási-Csizmadia, A. Improved Inhibitory and Absorption, Distribution, Metabolism, Excretion, and Toxicology (ADMET) Properties of Blebbistatin Derivatives Indicate That Blebbistatin Scaffold Is Ideal for Drug Development Targeting Myosin-2. *J. Pharmacol. Exp. Ther.* **2021**, *376* (3), 358–373. https://doi.org/10.1124/jpet.120.000167.
(146) Rizvi, S. A.; Neidt, E. M.; Cui, J.; Feiger, Z.; Skau, C. T.; Gardel, M. L.; Kozmin, S. A.; Kovar, D. R. Identification and Characterization of a Small Molecule Inhibitor of Formin-Mediated Actin Assembly. *Chem. Biol.* **2009**, *16* (11), 1158–1168. https://doi.org/10.1016/j.chembiol.2009.10.006.
(147) Isogai, T.; van der Kammen, R.; Innocenti, M. SMIFH2 Has Effects on Formins and P53 That Perturb the Cell Cytoskeleton. *Sci. Rep.* **2015**, *5* (1), 9802. https://doi.org/10.1038/srep09802.
(148) Landis, M.; Orman, M.; Vadakkan, J.; Liu, S.; Rojas, C. M.; Vizcarra, C. L. Structure-Activity Relationship Studies of Formin Inhibitor SMIFH2 *Journal Abstracts of Papers, 259th ACS National Meeting & Exposition*, Philadelphia, PA, United States, March 22-26, 2020.
(149) Nishimura, Y.; Shi, S.; Zhang, F.; Liu, R.; Takagi, Y.; Bershadsky, A. D.; Viasnoff, V.; Sellers, J. R. The Formin Inhibitor SMIFH2 Inhibits Members of the Myosin Superfamily. *J. Cell Sci.* **2021**, *134* (8), jcs253708. https://doi.org/10.1242/jcs.253708.
(150) Jordan, M. A.; Wilson, L. Microtubules as a Target for Anticancer Drugs. *Nat. Rev. Cancer* **2004**, *4* (4), 253–265. https://doi.org/10.1038/nrc1317.
(151) Čermák, V.; Dostál, V.; Jelínek, M.; Libusová, L.; Kovář, J.; Rösel, D.; Brábek, J. Microtubule-Targeting Agents and Their Impact on Cancer Treatment. *Eur. J. Cell Biol.* **2020**, *99* (4), 151075. https://doi.org/10.1016/j.ejcb.2020.151075.

(152) Tangutur, A. D.; Kumar, D.; Krishna, K. V.; Kantevari, S. Microtubule Targeting Agents as Cancer Chemotherapeutics: An Overview of Molecular Hybrids as Stabilizing and Destabilizing Agents. *Curr. Top. Med. Chem.* **2017**, *17* (22), 2523–2537. 10.2174/1568026617666170104145640
(153) Izdebska, M.; Zielińska, W.; Grzanka, D.; Gagat, M. The Role of Actin Dynamics and Actin-Binding Proteins Expression in Epithelial-to-Mesenchymal Transition and Its Association with Cancer Progression and Evaluation of Possible Therapeutic Targets. *BioMed Res. Int.* **2018**, *2018*, e4578373. https://doi.org/10.1155/2018/4578373.
(154) Hall, A. The Cytoskeleton and Cancer. *Cancer Metastasis Rev.* **2009**, *28* (1–2), 5–14. https://doi.org/10.1007/s10555-008-9166-3.
(155) Yamaguchi, H.; Condeelis, J. Regulation of the Actin Cytoskeleton in Cancer Cell Migration and Invasion. *Biochim. Biophys. Acta Mol. Cell Res.* **2007**, *1773* (5), 642–652. https://doi.org/10.1016/j.bbamcr.2006.07.001.
(156) Foerster, F.; Braig, S.; Moser, C.; Kubisch, R.; Busse, J.; Wagner, E.; Schmoeckel, E.; Mayr, D.; Schmitt, S.; Huettel, S.; Zischka, H.; Mueller, R.; Vollmar, A. M. Targeting the Actin Cytoskeleton: Selective Antitumor Action via Trapping PKCε. *Cell Death Dis.* **2014**, *5* (8), e1398–e1398. https://doi.org/10.1038/cddis.2014.363.
(157) Schindler-Horvat, J. E.; Fairchild, D. G.; Hassler, C.; Tomaszewski, J. E.; Donohue, S. J.; Tyson, C. A. Toxicity of Jasplakinolide (NSC 613009) in Rats and Dogs. In *Proc. Am. Assoc. Cancer Res.* **1998**, *39*, A4063.
(158) Sierra-Paredes, G.; Oreiro-García, T.; Núñez-Rodriguez, A.; Vázquez-López, A.; Sierra-Marcuño, G. Seizures Induced by in Vivo Latrunculin A and Jasplakinolide Microperfusion in the Rat Hippocampus. *J. Mol. Neurosci.* **2006**, *28* (2), 151–160. https://doi.org/10.1385/JMN:28:2:151.
(159) Pereira, J. H.; Petchprayoon, C.; Hoepker, A. C.; Moriarty, N. W.; Fink, S. J.; Cecere, G.; Paterson, I.; Adams, P. D.; Marriott, G. Structural and Biochemical Studies of Actin in Complex with Synthetic Macrolide Tail Analogues. *ChemMedChem* **2014**, *9* (10), 2286–2293. https://doi.org/10.1002/cmdc.201402150.
(160) Stehn, J.; Schevzov, G.; O'Neill, G.; Gunning, P. Specialisation of the Tropomyosin Composition of Actin Filaments Provides New Potential Targets for Chemotherapy. *Curr. Cancer Drug Targets* **2006**, *6* (3), 245–256. https://doi.org/10.2174/156800906776842948.
(161) Bonello, T. T.; Stehn, J. R.; Gunning, P. W. New Approaches to Targeting the Actin Cytoskeleton for Chemotherapy. *Future Med. Chem.* **2009**, *1* (7), 1311–1331. https://doi.org/10.4155/fmc.09.99.
(162) Pfitzer, L.; Moser, C.; Gegenfurtner, F.; Arner, A.; Foerster, F.; Atzberger, C.; Zisis, T.; Kubisch-Dohmen, R.; Busse, J.; Smith, R.; Timinszky, G.; Kalinina, O. V.; Müller, R.; Wagner, E.; Vollmar, A. M.; Zahler, S. Targeting Actin Inhibits Repair of Doxorubicin-Induced DNA Damage: A Novel Therapeutic Approach for Combination Therapy. *Cell Death Dis.* **2019**, *10* (4), 1–14. https://doi.org/10.1038/s41419-019-1546-9.
(163) Ohno, O.; Morita, M.; Kitamura, K.; Teruya, T.; Yoneda, K.; Kita, M.; Kigoshi, H.; Suenaga, K. Apoptosis-Inducing Activity of the Actin-Depolymerizing Agent Aplyronine A and Its Side-Chain Derivatives. *Bioorg. Med. Chem. Lett.* **2013**, *23* (5), 1467–1471. https://doi.org/10.1016/j.bmcl.2012.12.052.
(164) Pipaliya, B. V.; Trofimova, D. N.; Grange, R. L.; Aeluri, M.; Deng, X.; Shah, K.; Craig, A. W.; Allingham, J. S.; Evans, P. A. Truncated Actin-Targeting Macrolide Derivative Blocks Cancer Cell Motility and Invasion of Extracellular Matrix. *J. Am. Chem. Soc.* **2021**, *143* (18), 6847–6854. https://doi.org/10.1021/jacs.0c12404.
(165) Janco, M.; Bonello, T. T.; Byun, A.; Coster, A. C. F.; Lebhar, H.; Dedova, I.; Gunning, P. W.; Böcking, T. The Impact of Tropomyosins on Actin Filament Assembly Is Isoform Specific. *BioArchitecture* **2016**, *6* (4), 61–75. https://doi.org/10.1080/19490992.2016.1201619.
(166) Gateva, G.; Kremneva, E.; Reindl, T.; Kotila, T.; Kogan, K.; Gressin, L.; Gunning, P. W.; Manstein, D. J.; Michelot, A.; Lappalainen, P. Tropomyosin Isoforms Specify Functionally Distinct Actin Filament Populations In Vitro. *Curr. Biol.* **2017**, *27* (5), 705–713. https://doi.org/10.1016/j.cub.2017.01.018.
(167) Geeves, M. A.; Hitchcock-DeGregori, S. E.; Gunning, P. W. A Systematic Nomenclature for Mammalian Tropomyosin Isoforms. *J. Muscle Res. Cell Motil.* **2015**, *36* (2), 147–153. https://doi.org/10.1007/s10974-014-9389-6.
(168) Stehn, J. R.; Haass, N. K.; Bonello, T.; Desouza, M.; Kottyan, G.; Treutlein, H.; Zeng, J.; Nascimento, P. R. B. B.; Sequeira, V. B.; Butler, T. L.; Allanson, M.; Fath, T.; Hill, T. A.; McCluskey, A.; Schevzov, G.; Palmer, S. J.; Hardeman, E. C.; Winlaw, D.; Reeve, V. E.; Dixon,

I.; Weninger, W.; Cripe, T. P.; Gunning, P. W. A Novel Class of Anticancer Compounds Targets the Actin Cytoskeleton in Tumor Cells. *Cancer Res.* **2013**, *73* (16), 5169–5182. https://doi.org/10.1158/0008-5472.CAN-12-4501.

(169) Bonello, T. T.; Janco, M.; Hook, J.; Byun, A.; Appaduray, M.; Dedova, I.; Hitchcock-DeGregori, S.; Hardeman, E. C.; Stehn, J. R.; Böcking, T.; Gunning, P. W. A Small Molecule Inhibitor of Tropomyosin Dissociates Actin Binding from Tropomyosin-Directed Regulation of Actin Dynamics. *Sci. Rep.* **2016**, *6* (1), 19816. https://doi.org/10.1038/srep19816.

(170) The Small Chemical Vacuolin-1 Inhibits Ca2+-Dependent Lysosomal Exocytosis but Not Cell Resealing. *EMBO reports* **2004**, *5* (9), 883–888. https://doi.org/10.1038/sj.embor.7400243.

(171) Lu, Y.; Dong, S.; Hao, B.; Li, C.; Zhu, K.; Guo, W.; Wang, Q.; Cheung, K.-H.; Wong, C. W.; Wu, W.-T.; Markus, H.; Yue, J. Vacuolin-1 Potently and Reversibly Inhibits Autophagosome-Lysosome Fusion by Activating RAB5A. *Autophagy* **2014**, *10* (11), 1895–1905. https://doi.org/10.4161/auto.32200.

(172) Shaik, G. M.; Dráberová, L.; Heneberg, P.; Dráber, P. Vacuolin-1-Modulated Exocytosis and Cell Resealing in Mast Cells. *Cell. Signal.* **2009**, *21* (8), 1337–1345. https://doi.org/10.1016/j.cellsig.2009.04.001.

(173) Huynh, C.; Andrews, N. W. The Small Chemical Vacuolin-1 Alters the Morphology of Lysosomes without Inhibiting Ca2+-Regulated Exocytosis. *EMBO Rep.* **2005**, *6* (9), 843–847. https://doi.org/10.1038/sj.embor.7400495.

(174) Ye, Z.; Wang, D.; Lu, Y.; He, Y.; Yu, J.; Wei, W.; Chen, C.; Wang, R.; Zhang, L.; Zhang, L.; Le, M. T. N.; Cho, W. C.; Yang, M.; Zhang, H.; Yue, J. Vacuolin-1 Inhibits Endosomal Trafficking and Metastasis via CapZβ. *Oncogene* **2021**, *40* (10), 1775–1791. https://doi.org/10.1038/s41388-021-01662-3.

(175) Pimm, M. L.; Hotaling, J.; Henty-Ridilla, J. L. Profilin Choreographs Actin and Microtubules in Cells and Cancer *Int. Rev. Cell Mol. Biol.*; **2020**; *355*, 155–204. https://doi.org/10.1016/bs.ircmb.2020.05.005.

(176) Gau, D.; Lewis, T.; McDermott, L.; Wipf, P.; Koes, D.; Roy, P. Structure-Based Virtual Screening Identifies a Small-Molecule Inhibitor of the Profilin 1–Actin Interaction. *J. Biol. Chem.* **2018**, *293* (7), 2606–2616. https://doi.org/10.1074/jbc.M117.809137.

(177) Allen, A.; Gau, D.; Francoeur, P.; Sturm, J.; Wang, Y.; Martin, R.; Maranchie, J.; Duensing, A.; Kaczorowski, A.; Duensing, S.; Wu, L.; Lotze, M. T.; Koes, D.; Storkus, W. J.; Roy, P. Actin-Binding Protein Profilin1 Promotes Aggressiveness of Clear-Cell Renal Cell Carcinoma Cells. *J. Biol. Chem.* **2020**, *295* (46), 15636–15649. https://doi.org/10.1074/jbc.RA120.013963.

(178) Gau, D.; Vignaud, L.; Allen, A.; Guo, Z.; Sahel, J.; Boone, D.; Koes, D.; Guillonneau, X.; Roy, P. Disruption of Profilin1 Function Suppresses Developmental and Pathological Retinal Neovascularization. *J. Biol. Chem.* **2020**, *295* (28), 9618–9629. https://doi.org/10.1074/jbc.RA120.012613.

(179) Coumans, J. V. F.; Davey, R. J.; Moens, P. D. J. Cofilin and Profilin: Partners in Cancer Aggressiveness. *Biophys. Rev.* **2018**, *10* (5), 1323–1335. https://doi.org/10.1007/s12551-018-0445-0.

(180) Alaqel, S.; Tillekeratne, V.; Shah, Z. A. Development of a Cofilin Inhibitor for the Treatment of Hemorrhagic Brain Injury-Induced Neuroinflammation. US 2020/0369603 A1.

(181) Huang, X.; Sun, D.; Pan, Q.; Wen, W.; Chen, Y.; Xin, X.; Huang, M.; Ding, J.; Geng, M. JG6, a Novel Marine-Derived Oligosaccharide, Suppresses Breast Cancer Metastasis via Binding to Cofilin. *Oncotarget* **2014**, *5* (11), 3568–3578. https://doi.org/10.18632/oncotarget.1959.

(182) Chander, N.; Morstein, J.; Bolten, J. S.; Shemet, A.; Cullis, P. R.; Trauner, D.; Witzigmann, D. Optimized Photoactivatable Lipid Nanoparticles Enable Red Light Triggered Drug Release. *Small* **2021**, *17* (21), 2008198. https://doi.org/10.1002/smll.202008198.

(183) Lerch, M. M.; Hansen, M. J.; van Dam, G. M.; Szymanski, W.; Feringa, B. L. Emerging Targets in Photopharmacology. *Angew. Chem. Int. Ed.* **2016**, *55* (37), 10978–10999. https://doi.org/10.1002/anie.201601931.

(184) Mitchell, M. J.; Billingsley, M. M.; Haley, R. M.; Wechsler, M. E.; Peppas, N. A.; Langer, R. Engineering Precision Nanoparticles for Drug Delivery. *Nat. Rev. Drug Discov.* **2021**, *20* (2), 101–124. https://doi.org/10.1038/s41573-020-0090-8.

(185) Harterink, M.; da Silva, M. E.; Will, L.; Turan, J.; Ibrahim, A.; Lang, A. E.; van Battum, E. Y.; Pasterkamp, R. J.; Kapitein, L. C.; Kudryashov, D.; Barres, B. A.; Hoogenraad, C. C.; Zuchero, J. B. DeActs: Genetically Encoded Tools for Perturbing the Actin Cytoskeleton in Single Cells. *Nat. Methods* **2017**, *14* (5), 479–482. https://doi.org/10.1038/nmeth.4257.

(186) Stone, O. J.; Pankow, N.; Liu, B.; Sharma, V. P.; Eddy, R. J.; Wang, H.; Putz, A. T.; Teets, F. D.; Kuhlman, B.; Condeelis, J. S.; Hahn, K. M. Optogenetic Control of Cofilin and ATAT in Living Cells Using Z-Lock. *Nat. Chem. Biol.* **2019**, *15* (12), 1183–1190. https://doi.org/10.1038/s41589-019-0405-4.

(187) Lazarides, E.; Weber, K. Actin Antibody: The Specific Visualization of Actin Filaments in Non-Muscle Cells. *Proc. Natl. Acad. Sci.* **1974**, *71* (6), 2268–2272. https://doi.org/10.1073/pnas.71.6.2268.

(188) Wulf, E.; Deboben, A.; Bautz, F. A.; Faulstich, H.; Wieland, T. Fluorescent Phallotoxin, a Tool for the Visualization of Cellular Actin. *Proc. Natl. Acad. Sci.* **1979**, *76* (9), 4498–4502. https://doi.org/10.1073/pnas.76.9.4498.

(189) Faulstich, H.; Trischmann, H.; Mayer, D. Preparation of Tetramethylrhodaminyl-Phalloidin and Uptake of the Toxin into Short-Term Cultured Hepatocytes by Endocytosis. *Exp. Cell Res.* **1983**, *144* (1), 73–82. https://doi.org/10.1016/0014-4827(83)90443-3.

(190) Wieland, T.; Miura, T.; Seeliger, A. Analogs of Phalloidin. *Int. J. Pept. Prot. Res.* **1983**, *21* (1), 3–10. https://doi.org/10.1111/j.1399-3011.1983.tb03071.x.

(191) Adams, A. E. M.; Pringle, J. R. [51] Staining of Actin with Fluorochrome-Conjugated Phalloidin. *Meth. Enzymol.* **1991**, *194*, 729–731. https://doi.org/10.1016/0076-6879(91)94054-G.

(192) Burkel, B. M.; Dassow, G. von; Bement, W. M. Versatile Fluorescent Probes for Actin Filaments Based on the Actin-Binding Domain of Utrophin. *Cell Motil.* **2007**, *64* (11), 822–832. https://doi.org/10.1002/cm.20226.

(193) Lukinavičius, G.; Reymond, L.; D'Este, E.; Masharina, A.; Göttfert, F.; Ta, H.; Güther, A.; Fournier, M.; Rizzo, S.; Waldmann, H.; Blaukopf, C.; Sommer, C.; Gerlich, D. W.; Arndt, H.-D.; Hell, S. W.; Johnsson, K. Fluorogenic Probes for Live-Cell Imaging of the Cytoskeleton. *Nat. Methods* **2014**, *11* (7), 731–733. https://doi.org/10.1038/nmeth.2972.

(194) Gerasimaitė, R.; Seikowski, J.; Schimpfhauser, J.; Kostiuk, G.; Gilat, T.; D'Este, E.; Schnorrenberg, S.; Lukinavičius, G. Efflux Pump Insensitive Rhodamine–Jasplakinolide Conjugates for G- and F-Actin Imaging in Living Cells. *Org. Biomol. Chem.* **2020**, *18* (15), 2929–2937. https://doi.org/10.1039/D0OB00369G.

(195) *Alexa Fluor™ 594 Phalloidin*. https://www.thermofisher.com/order/catalog/product/A12381 (accessed 2021-07-06).

(196) Melak, M.; Plessner, M.; Grosse, R. Actin Visualization at a Glance. *J. Cell Sci.* **2017**, *130* (3), 525–530. https://doi.org/10.1242/jcs.189068.

(197) Belin, B. J.; Goins, L. M.; Mullins, R. D. Comparative Analysis of Tools for Live Cell Imaging of Actin Network Architecture. *BioArchitecture* **2014**, *4* (6), 189–202. https://doi.org/10.1080/19490992.2014.1047714.

(198) Riedl, J.; Crevenna, A. H.; Kessenbrock, K.; Yu, J. H.; Neukirchen, D.; Bista, M.; Bradke, F.; Jenne, D.; Holak, T. A.; Werb, Z.; Sixt, M.; Wedlich-Soldner, R. Lifeact: A Versatile Marker to Visualize F-Actin. *Nat. Methods* **2008**, *5* (7), 605–607. https://doi.org/10.1038/nmeth.1220.

(199) Chhabra, D.; Bao, S.; Remedios, C. G. D. The Distribution of Cofilin and DNase I in Vivo. *Cell Res.* **2002**, *12* (3–4), 207–214. https://doi.org/10.1038/sj.cr.7290126.

(200) Kabsch, W.; Mannherz, H. G.; Suck, D.; Pai, E. F.; Holmes, K. C. Atomic Structure of the Actin: DNase I Complex. *Nature* **1990**, *347* (6288), 37–44. https://doi.org/10.1038/347037a0.

(201) Cramer, L. P.; Briggs, L. J.; Dawe, H. R. Use of fluorescently labelled deoxyribonuclease I to spatially measure G-actin levels in migrating and non-migrating cells. *Cell Motil.* **2002**, *51* (1), 27–38. https://doi.org/10.1002/cm.10013.

(202) Haugland, R. P.; You, W.; Paragas, V. B.; Wells, K. S.; DuBose, D. A. Simultaneous Visualization of G- and F-Actin in Endothelial Cells. *J. Histochem. Cytochem.* **1994**, *42* (3), 345–350. https://doi.org/10.1177/42.3.8308251.

(203) Broichhagen, J.; Frank, J. A.; Trauner, D. A Roadmap to Success in Photopharmacology. *Acc. Chem. Res.* **2015**, *48* (7), 1947–1960. https://doi.org/10.1021/acs.accounts.5b00129.

(204) Klaja, O.; Frank, J. A.; Trauner, D.; Bondar, A.-N. Potential Energy Function for a Photo-Switchable Lipid Molecule. *J. Comput. Chem.* **2020**, *41* (27), 2336–2351. https://doi.org/10.1002/jcc.26387.

(205) Dong, M.; Babalhavaeji, A.; Samanta, S.; Beharry, A. A.; Woolley, G. A. Red-Shifting Azobenzene Photoswitches for in Vivo Use. *Acc. Chem. Res.* **2015**, *48* (10), 2662–2670. https://doi.org/10.1021/acs.accounts.5b00270.

(206) Yang, Y.; Hughes, R. P.; Aprahamian, I. Near-Infrared Light Activated Azo-BF2 Switches. *J. Am. Chem. Soc.* **2014**, *136* (38), 13190–13193. https://doi.org/10.1021/ja508125n.

(207) Velema, W. A.; Szymanski, W.; Feringa, B. L. Photopharmacology: Beyond Proof of Principle. *J. Am. Chem. Soc.* **2014**, *136* (6), 2178–2191. https://doi.org/10.1021/ja413063e.
(208) Hüll, K.; Morstein, J.; Trauner, D. In Vivo Photopharmacology. *Chem. Rev.* **2018**, *118* (21), 10710–10747. https://doi.org/10.1021/acs.chemrev.8b00037.
(209) Welleman, I. M.; Hoorens, M. W. H.; Feringa, B. L.; Boersma, H. H.; Szymański, W. Photoresponsive Molecular Tools for Emerging Applications of Light in Medicine. *Chem. Sci.* **2020**, *11* (43), 11672–11691. https://doi.org/10.1039/D0SC04187D.
(210) Nair, R. V.; Zhao, S.; Terriac, E.; Lautenschläger, F.; Hetmanski, J. H. R.; Caswell, P. T.; del Campo, A. *Possibilities and Limitations of Photoactivatable Cytochalasin D for the Spatiotemporal Regulation of Actin Dynamics*; *ChemRxiv* **2020**. https://doi.org/10.26434/chemrxiv.12609545.v1.
(211) Borowiak, M.; Nahaboo, W.; Reynders, M.; Nekolla, K.; Jalinot, P.; Hasserodt, J.; Rehberg, M.; Delattre, M.; Zahler, S.; Vollmar, A.; Trauner, D.; Thorn-Seshold, O. Photoswitchable Inhibitors of Microtubule Dynamics Optically Control Mitosis and Cell Death. *Cell* **2015**, *162* (2), 403–411. https://doi.org/10.1016/j.cell.2015.06.049.
(212) White, J. D.; Kawasaki, M. Total Synthesis of (+)-Latrunculin A, an Ichthyotoxic Metabolite of the Sponge Latrunculia Magnifica and Its C-15 Epimer. *J. Org. Chem.* **1992**, *57* (20), 5292–5300. https://doi.org/10.1021/jo00046a008.
(213) White, J. D.; Kawasaki, M. Total Synthesis of (+)-Latrunculin A. *J. Am. Chem. Soc.* **1990**, *112* (12), 4991–4993. https://doi.org/10.1021/ja00168a071.
(214) Smith, A. B.; Noda, I.; Remiszewski, S. W.; Liverton, N. J.; Zibuck, R. Total Synthesis of (+)-Latrunculin A. *J. Org. Chem.* **1990**, *55* (13), 3977–3979. https://doi.org/10.1021/jo00300a006.
(215) Smith, A. B.; Leahy, J. W.; Noda, I.; Remiszewski, S. W.; Liverton, N. J.; Zibuck, R. Total Synthesis of the Latrunculins. *J. Am. Chem. Soc.* **1992**, *114* (8), 2995–3007. https://doi.org/10.1021/ja00034a036.
(216) Fürstner, A.; Turet, L. Concise and Practical Synthesis of Latrunculin A by Ring-Closing Enyne-Yne Metathesis. *Angew. Chem. Int. Ed.* **2005**, *44* (22), 3462–3466. https://doi.org/10.1002/anie.200500390.
(217) Fürstner, A.; De Souza, D.; Turet, L.; Fenster, M. D. B.; Parra-Rapado, L.; Wirtz, C.; Mynott, R.; Lehmann, C. W. Total Syntheses of the Actin-Binding Macrolides Latrunculin A, B, C, M, S and 16-Epi-Latrunculin B. *Chem. Eur. J.* **2007**, *13* (1), 115–134. https://doi.org/10.1002/chem.200601135.
(218) She, J.; Lampe, J. W.; Polianski, A. B.; Watson, P. S. Examination of the Olefin–Olefin Ring Closing Metathesis to Prepare Latrunculin B. *Tet. Lett.* **2009**, *50* (3), 298–301. https://doi.org/10.1016/j.tetlet.2008.10.144.
(219) Fürstner, A.; Kirk, D.; Fenster, M. D. B.; Aïssa, C.; De Souza, D.; Müller, O. Diverted Total Synthesis: Preparation of a Focused Library of Latrunculin Analogues and Evaluation of Their Actin-Binding Properties. *Proc. Natl. Acad. Sci.* **2005**, *102* (23), 8103–8108. https://doi.org/10.1073/pnas.0501441102.
(220) Fürstner, A.; Kirk, D.; Fenster, M. D. B.; Aïssa, C.; De Souza, D.; Nevado, C.; Tuttle, T.; Thiel, W.; Müller, O. Latrunculin Analogues with Improved Biological Profiles by "Diverted Total Synthesis": Preparation, Evaluation, and Computational Analysis. *Chem. Eur. J.* **2007**, *13* (1), 135–149. https://doi.org/10.1002/chem.200601136.
(221) El Sayed, K. A.; Youssef, D. T. A.; Marchetti, D. Bioactive Natural and Semisynthetic Latrunculins. *J. Nat. Prod.* **2006**, *69* (2), 219–223. https://doi.org/10.1021/np050372r.
(222) Khanfar, M. A.; Youssef, D. T. A.; El Sayed, K. A. Semisynthetic Latrunculin Derivatives as Inhibitors of Metastatic Breast Cancer: Biological Evaluations, Preliminary Structure–Activity Relationship and Molecular Modeling Studies. *ChemMedChem* **2010**, *5* (2), 274–285. https://doi.org/10.1002/cmdc.200900430.
(223) Kudrimoti, S.; Ahmed, S. A.; Daga, P. R.; Wahba, A. E.; Khalifa, S. I.; Doerksen, R. J.; Hamann, M. T. Semisynthetic Latrunculin B Analogs: Studies of Actin Docking Support a Proposed Mechanism for Latrunculin Bioactivity. *Bioorg. Med. Chem.* **9**, *17* (21), 7517–7522. https://doi.org/10.1016/j.bmc.2009.09.012.
(224) Watson, P. S. Cytoskeletal Active Compounds, Composition and Use. US 2006/0217427 A1.
(225) Gao, L. Studies towards a Light Dependant Actin Inhibitor Based on the Marine Toxine Family of Latrunculin. Master Thesis, Ludwig Maximilians Universität, München, 2016.
(226) Folkerts, S. Computational Prediction of Photo-Switchable Latrunculin Analogs to Target G-Actin. Masters Thesis, Rheinisch-Westfälische Technische Hochschule Aachen, 2020.

(227) Symkenberg, G.; Kalesse, M. Structure Elucidation and Total Synthesis of Kulkenon. *Angew. Chem. Int. Ed.* **2014**, *53* (7), 1795–1798. https://doi.org/10.1002/anie.201309386.
(228) Crimmins, M. T.; Chaudhary, K. Titanium Enolates of Thiazolidinethione Chiral Auxiliaries: Versatile Tools for Asymmetric Aldol Additions. *Org. Lett.* **2000**, *2* (6), 775–777. https://doi.org/10.1021/ol9913901.
(229) Crimmins, M. T.; King, B. W.; Tabet, E. A. Asymmetric Aldol Additions with Titanium Enolates of Acyloxazolidinethiones: Dependence of Selectivity on Amine Base and Lewis Acid Stoichiometry. *J. Am. Chem. Soc.* **1997**, *119* (33), 7883–7884. https://doi.org/10.1021/ja9716721.
(230) Aeluri, M.; Dasari, B.; Arya, P. Divergent Approach to Building a Latrunculin Family Derived Hybrid Macrocyclic Toolbox. *Org. Lett.* **2015**, *17* (3), 472–475. https://doi.org/10.1021/ol503465p.
(231) Herbert, M. B.; Grubbs, R. H. Z-Selective Cross Metathesis with Ruthenium Catalysts: Synthetic Applications and Mechanistic Implications. *Angew. Chem. Int. Ed.* **2015**, *54* (17), 5018–5024. https://doi.org/10.1002/anie.201411588.
(232) Keitz, B. K.; Endo, K.; Patel, P. R.; Herbert, M. B.; Grubbs, R. H. Improved Ruthenium Catalysts for Z-Selective Olefin Metathesis. *J. Am. Chem. Soc.* **2012**, *134* (1), 693–699. https://doi.org/10.1021/ja210225e.
(233) Aitken, H. R. M.; Furkert, D. P.; Hubert, J. G.; Wood, J. M.; Brimble, M. A. Enantioselective Access to Benzannulated Spiroketals Using a Chiral Sulfoxide Auxiliary. *Org. Biomol. Chem.* **2013**, *11* (31), 5147–5155. https://doi.org/10.1039/C3OB41065J.
(234) Fehrenbacher, K. L.; Yang, H.-C.; Gay, A. C.; Huckaba, T. M.; Pon, L. A. Live Cell Imaging of Mitochondrial Movement along Actin Cables in Budding Yeast. *Curr. Biol.* **2004**, *14* (22), 1996–2004. https://doi.org/10.1016/j.cub.2004.11.004.
(235) Higuchi, R.; Vevea, J. D.; Swayne, T. C.; Chojnowski, R.; Hill, V.; Boldogh, I. R.; Pon, L. A. Actin Dynamics Affect Mitochondrial Quality Control and Aging in Budding Yeast. *Curr. Biol.* **2013**, *23* (23), 2417–2422. https://doi.org/10.1016/j.cub.2013.10.022.
(236) Higuchi-Sanabria, R.; Swayne, T. C.; Boldogh, I. R.; Pon, L. A. Imaging of the Actin Cytoskeleton and Mitochondria in Fixed Budding Yeast Cells. In *Cytoskeleton Methods and Protocols*; Gavin, R. H., Ed.; Springer New York: New York, NY, 2016; Vol. 1365, pp 63–81. https://doi.org/10.1007/978-1-4939-3124-8_3.
(237) Mosmann, T. Rapid Colorimetric Assay for Cellular Growth and Survival: Application to Proliferation and Cytotoxicity Assays. *J. Immunol. Meth.* **1983**, *65* (1), 55–63. https://doi.org/10.1016/0022-1759(83)90303-4.
(238) Berridge, M. V.; Herst, P. M.; Tan, A. S. Tetrazolium Dyes as Tools in Cell Biology: New Insights into Their Cellular Reduction. In *Biotechnol. Annu. Rev.* **2005**, *11*, 127–152. https://doi.org/10.1016/S1387-2656(05)11004-7.
(239) Johnson, S.; Rahmani, R.; Drew, D. R.; Williams, M. J.; Wilkinson, M.; Tan, Y. H.; Huang, J. X.; Tonkin, C. J.; Beeson, J. G.; Baum, J.; Smith, B. J.; Baell, J. B. Truncated Latrunculins as Actin Inhibitors Targeting *Plasmodium Falciparum* Motility and Host Cell Invasion. *J. Med. Chem.* **2016**, *59* (24), 10994–11005. https://doi.org/10.1021/acs.jmedchem.6b01109.
(240) Varghese, S.; Rahmani, R.; Drew, D. R.; Beeson, J. G.; Baum, J.; Smith, B. J.; Baell, J. B. Structure-Activity Studies of Truncated Latrunculin Analogues with Antimalarial Activity. *ChemMedChem* **2020**, cmdc.202000399. https://doi.org/10.1002/cmdc.202000399.
(241) Blasberger, D.; Carmely, S.; Kashman, Y.; Cojocaru, M.; Spector, I.; Shochet, N. R. On the Chemistry of Latrunculins A and B. *Liebigs Ann. Chem.* **1989**, *1989* (12), 1171–1188. https://doi.org/10.1002/jlac.198919890289.
(242) *Microglial Function in the Healthy Brain*, The Green Lab. https://faculty.sites.uci.edu/kimgreen/bio/microglia-in-the-healthy-brain/ (accessed 2021-08-05).
(243) *Microglia, the brain's trash collector cells, may play larger role in brain health, may reveal clues to disease treatments*. National Institute on Aging. http://www.nia.nih.gov/news/microglia-brains-trash-collector-cells-may-play-larger-role-brain-health-may-reveal-clues (accessed 2021-08-05).
(244) Colonna, M.; Butovsky, O. Microglia Function in the Central Nervous System During Health and Neurodegeneration. *Annu. Rev. Immunol.* **2017**, *35* (1), 441–468. https://doi.org/10.1146/annurev-immunol-051116-052358.

(245) Nimmerjahn, A.; Kirchhoff, F.; Helmchen, F. Resting Microglial Cells Are Highly Dynamic Surveillants of Brain Parenchyma in Vivo. *Science* **2005**, *308* (5726), 1314-1318. https://doi.org/10.1126/science.1110647

(246) Nolte, C.; Moller, T.; Walter, T.; Kettenmann, H. Complement 5a Controls Motility of Murine Microglial Cells in Vitro via Activation of an Inhibitory G-Protein and the Rearrangement of the Actin Cytoskeleton. *Neuroscience* **1996**, *73* (4), 1091–1107. https://doi.org/10.1016/0306-4522(96)00106-6.

(247) Bernier, L.-P.; Bohlen, C. J.; York, E. M.; Choi, H. B.; Kamyabi, A.; Dissing-Olesen, L.; Hefendehl, J. K.; Collins, H. Y.; Stevens, B.; Barres, B. A.; MacVicar, B. A. Nanoscale Surveillance of the Brain by Microglia via CAMP-Regulated Filopodia. *Cell Rep.* **2019**, *27* (10), 2895-2908.e4. https://doi.org/10.1016/j.celrep.2019.05.010.

(248) Laprell, L.; Schulze, C.; Brehme, M.-L.; Oertner, T. G. The Role of Microglia Membrane Potential in Chemotaxis. *J. Neuroinflammation* **2021**, *18* (1), 21. https://doi.org/10.1186/s12974-020-02048-0.

(249) Helal, M. A.; Khalifa, S.; Ahmed, S. Differential Binding of Latrunculins to G-Actin: A Molecular Dynamics Study. *J. Chem. Inf. Model* **2013**, *53* (9), 2369–2375. https://doi.org/10.1021/ci400317j.

(250) How a Single Residue in Individual β-Thymosin/WH2 Domains Controls Their Functions in Actin Assembly. *The EMBO Journal* **2012**, *31* (4), 1000–1013. https://doi.org/10.1038/emboj.2011.461.

(251) Rosenblatt, J.; Peluso, P.; Mitchison, T. J. The Bulk of Unpolymerized Actin in Xenopus Egg Extracts Is ATP-Bound. *Mol. Biol. Cell* **1995**, *6* (2), 227–236. https://doi.org/10.1091/mbc.6.2.227.

(252) Borowiak, M.; Küllmer, F.; Gegenfurtner, F.; Peil, S.; Nasufovic, V.; Zahler, S.; Thorn-Seshold, O.; Trauner, D.; Arndt, H.-D. Optical Manipulation of F-Actin with Photoswitchable Small Molecules. *J. Am. Chem. Soc.* **2020**, *142* (20), 9240–9249. https://doi.org/10.1021/jacs.9b12898.

(253) Pospich, S.; Küllmer, F.; Nasufović, V.; Funk, J.; Belyy, A.; Bieling, P.; Arndt, H.-D.; Raunser, S. Cryo-EM Resolves Molecular Recognition Of An Optojasp Photoswitch Bound To Actin Filaments In Both Switch States. *Angew. Chem. Int. Ed.* **2021**, *60* (16), 8678–8682. https://doi.org/10.1002/anie.202013193.

(254) Lázaro-Diéguez, F.; Knecht, E.; Egea, G. Clearance of a Hirano Body-like F-Actin Aggresome Generated by Jasplakinolide. *Autophagy* **2008**, *4* (5), 717–720. https://doi.org/10.4161/auto.6345.

(255) Cramer, L. P. Role of Actin-Filament Disassembly in Lamellipodium Protrusion in Motile Cells Revealed Using the Drug Jasplakinolide. *Curr. Biol.* **1999**, *9* (19), 1095–1105. https://doi.org/10.1016/S0960-9822(99)80478-3.

(256) Zigmond, S. H. Recent Quantitative Studies of Actin Filament Turnover during Cell Locomotion. *Cell Motil.* **1993**, *25* (4), 309–316. https://doi.org/10.1002/cm.970250402.

(257) Lázaro-Diéguez, F.; Aguado, C.; Mato, E.; Sánchez-Ruíz, Y.; Esteban, I.; Alberch, J.; Knecht, E.; Egea, G. Dynamics of an F-Actin Aggresome Generated by the Actin-Stabilizing Toxin Jasplakinolide. *J. Cell Sci.* **2008**, *121* (9), 1415–1425. https://doi.org/10.1242/jcs.017665.

(258) Lee, E.; Shelden, E. A.; Knecht, D. A. Formation of F-Actin Aggregates in Cells Treated with Actin Stabilizing Drugs. *Cell Motil.* **1998**, *39* (2), 122–133. https://doi.org/10.1002/(SICI)1097-0169(1998)39:2<122::AID-CM3>3.0.CO;2-8.

(259) Hirano, A. Hirano Bodies and Related Neuronal Inclusions. *Neuropathol. Appl. Neurobiol.* **1994**, *20* (1), 3–11. https://doi.org/10.1111/j.1365-2990.1994.tb00951.x.

(260) Soares e Silva, M.; Depken, M.; Stuhrmann, B.; Korsten, M.; MacKintosh, F. C.; Koenderink, G. H. Active Multistage Coarsening of Actin Networks Driven by Myosin Motors. *Proc. Natl. Acad. Sci.* **2011**, *108* (23), 9408–9413. https://doi.org/10.1073/pnas.1016616108.

(261) Pantaloni, D. Mechanism of Actin-Based Motility. *Science* **2001**, *292* (5521), 1502–1506. https://doi.org/10.1126/science.1059975.

(262) Leung, D. W.; Otomo, C.; Chory, J.; Rosen, M. K. Genetically Encoded Photoswitching of Actin Assembly through the Cdc42-WASP-Arp2/3 Complex Pathway. *Proc. Natl. Acad. Sci.* **2008**, *105* (35), 12797–12802. https://doi.org/10.1073/pnas.0801232105.

(263) Tilney, L. G.; Portnoy, D. A. Actin Filaments and the Growth, Movement, and Spread of the Intracellular Bacterial Parasite, Listeria Monocytogenes. *J. Cell Biol.* **1989**, *109* (4), 1597–1608. https://doi.org/10.1083/jcb.109.4.1597.

(264) Abou-Ghali, M. Actin Network Architecture and Dynamics Studied in Vitro and in Vivo. These de doctorat de Biologie, Sorbonne Université, Paris, 2019.
(265) Trads, J. B.; Hüll, K.; Matsuura, B. S.; Laprell, L.; Fehrentz, T.; Görldt, N.; Kozek, K. A.; Weaver, C. D.; Klöcker, N.; Barber, D. M.; Trauner, D. Sign Inversion in Photopharmacology: Incorporation of Cyclic Azobenzenes in Photoswitchable Potassium Channel Blockers and Openers. *Angew. Chem. Int. Ed.* **2019**, *58* (43), 15421–15428. https://doi.org/10.1002/anie.201905790.
(266) Maier, M. S.; Hüll, K.; Reynders, M.; Matsuura, B. S.; Leippe, P.; Ko, T.; Schäffer, L.; Trauner, D. Oxidative Approach Enables Efficient Access to Cyclic Azobenzenes. *J. Am. Chem. Soc.* **2019**, *141* (43), 17295–17304. https://doi.org/10.1021/jacs.9b08794.
(267) Yadav, V.; Banerjee, D. S.; Tabatabai, A. P.; Kovar, D. R.; Kim, T.; Banerjee, S.; Murrell, M. P. Filament Nucleation Tunes Mechanical Memory in Active Polymer Networks. *Adv. Funct. Mat.* **2019**, *29* (49), 1905243. https://doi.org/10.1002/adfm.201905243.
(268) O'Connor, C. Cell Division: Stages of Mitosis. *Nature Education* **2008**, *1* (1), 188.
(269) Wordeman, L. How Kinesin Motor Proteins Drive Mitotic Spindle Function: Lessons from Molecular Assays. *Semin. Cell Dev. Biol.* **2010**, *21* (3), 260–268. https://doi.org/10.1016/j.semcdb.2010.01.018.
(270) Mann, B. J.; Wadsworth, P. Kinesin-5 Regulation and Function in Mitosis. *Trends Cell Biol.* **2019**, *29* (1), 66–79. https://doi.org/10.1016/j.tcb.2018.08.004.
(271) Valentine, M. T.; Gilbert, S. P. To Step or Not to Step? How Biochemistry and Mechanics Influence Processivity in Kinesin and Eg5. *Curr. Opin. Cell Biol* **2007**, *19* (1), 75–81. https://doi.org/10.1016/j.ceb.2006.12.011.
(272) Mayer, T. U.; Kapoor, T. M.; Haggarty, S. J.; King, R. W.; Schreiber, S. L.; Mitchison, T. J. Small Molecule Inhibitor of Mitotic Spindle Bipolarity Identified in a Phenotype-Based Screen. *Science* **1999**, *286* (5441), 971–974. https://doi.org/10.1126/science.286.5441.971.
(273) Rath, O.; Kozielski, F. Kinesins and Cancer. *Nat. Rev. Cancer* **2012**, *12* (8), 527–539. https://doi.org/10.1038/nrc3310.
(274) DeBonis, S.; Skoufias, D. A.; Indorato, R.-L.; Liger, F.; Marquet, B.; Laggner, C.; Joseph, B.; Kozielski, F. Structure–Activity Relationship of S-Trityl-l-Cysteine Analogues as Inhibitors of the Human Mitotic Kinesin Eg5. *J. Med. Chem.* **2008**, *51* (5), 1115–1125. https://doi.org/10.1021/jm070606z.
(275) Lad, L.; Luo, L.; Carson, J. D.; Wood, K. W.; Hartman, J. J.; Copeland, R. A.; Sakowicz, R. Mechanism of Inhibition of Human KSP by Ispinesib. *Biochemistry* **2008**, *47* (11), 3576–3585. https://doi.org/10.1021/bi702061g.
(276) Carter, B. Z.; Mak, D. H.; Woessner, R.; Gross, S.; Schober, W. D.; Estrov, Z.; Kantarjian, H.; Andreeff, M. Inhibition of KSP by ARRY-520 Induces Cell Cycle Block and Cell Death via the Mitochondrial Pathway in AML Cells. *Leukemia* **2009**, *23* (10), 1755–1762. https://doi.org/10.1038/leu.2009.101.
(277) Garcia-Saez, I.; Skoufias, D. A. Eg5 Targeting Agents: From New Anti-Mitotic Based Inhibitor Discovery to Cancer Therapy and Resistance. *Biochem. Pharmacol.* **2021**, *184*, 114364. https://doi.org/10.1016/j.bcp.2020.114364.
(278) Nagarajan, S.; Sakkiah, S. Exploring a Potential Allosteric Inhibition Mechanism in the Motor Domain of Human Eg-5. *J. Biomol. Struct. Dyn.* **2019**, *37* (9), 2394–2403. https://doi.org/10.1080/07391102.2018.1486229.
(279) Behnke-Parks, W. M.; Vendome, J.; Honig, B.; Maliga, Z.; Moores, C.; Rosenfeld, S. S. Loop L5 Acts as a Conformational Latch in the Mitotic Kinesin Eg5*. *J. Biol. Chem.* **2011**, *286* (7), 5242–5253. https://doi.org/10.1074/jbc.M110.192930.
(280) Kaan, H. Y. K.; Major, J.; Tkocz, K.; Kozielski, F.; Rosenfeld, S. S. "Snapshots" of Ispinesib-Induced Conformational Changes in the Mitotic Kinesin Eg5. *J. Biol. Chem.* **2013**, *288* (25), 18588–18598. https://doi.org/10.1074/jbc.M113.462648.
(281) O'Connor, O. A.; Gerecitano, J.; Deventer, H. V.; Hainsworth, J.; Zullo, K. M.; Saikali, K.; Seroogy, J.; Wolff, A.; Escandón, R. The Addition of Granulocyte-Colony Stimulating Factor Shifts the Dose Limiting Toxicity and Markedly Increases the Maximum Tolerated Dose and Activity of the Kinesin Spindle Protein Inhibitor SB-743921 in Patients with Relapsed or Refractory Lymphoma: Results of an International, Multicenter Phase I/II Study. *Leuk. Lymphoma* **2015**, *56* (9), 2585–2591. https://doi.org/10.3109/10428194.2015.1004167.
(282) Hollebecque, A.; Deutsch, E.; Massard, C.; Gomez-Roca, C.; Bahleda, R.; Ribrag, V.; Bourgier, C.; Lazar, V.; Lacroix, L.; Gazzah, A.; Varga, A.; de Baere, T.; Beier, F.; Kroesser, S.; Trang,

K.; Zenke, F. T.; Klevesath, M.; Soria, J.-C. A Phase I, Dose-Escalation Study of the Eg5-Inhibitor EMD 534085 in Patients with Advanced Solid Tumors or Lymphoma. *Invest. New Drugs* **2013**, *31* (6), 1530–1538. https://doi.org/10.1007/s10637-013-0026-9.

(283) Khoury, H. J.; Garcia-Manero, G.; Borthakur, G.; Kadia, T.; Foudray, M. C.; Arellano, M.; Langston, A.; Bethelmie-Bryan, B.; Rush, S.; Litwiler, K.; Karan, S.; Simmons, H.; Marcus, A. I.; Ptaszynski, M.; Kantarjian, H. A Phase 1 Dose-Escalation Study of ARRY-520, a Kinesin Spindle Protein Inhibitor, in Patients with Advanced Myeloid Leukemias. *Cancer* **2012**, *118* (14), 3556–3564. https://doi.org/10.1002/cncr.26664.

(284) Wakui, H.; Yamamoto, N.; Kitazono, S.; Mizugaki, H.; Nakamichi, S.; Fujiwara, Y.; Nokihara, H.; Yamada, Y.; Suzuki, K.; Kanda, H.; Akinaga, S.; Tamura, T. A Phase 1 and Dose-Finding Study of LY2523355 (Litronesib), an Eg5 Inhibitor, in Japanese Patients with Advanced Solid Tumors. *Cancer Chemother. Pharmacol.* **2014**, *74* (1), 15–23. https://doi.org/10.1007/s00280-014-2467-z.

(285) Jones, R.; Vuky, J.; Elliott, T.; Mead, G.; Arranz, J. A.; Chester, J.; Chowdhury, S.; Dudek, A. Z.; Müller-Mattheis, V.; Grimm, M.-O.; Gschwend, J. E.; Wülfing, C.; Albers, P.; Li, J.; Osmukhina, A.; Skolnik, J.; Hudes, G. Phase II Study to Assess the Efficacy, Safety and Tolerability of the Mitotic Spindle Kinesin Inhibitor AZD4877 in Patients with Recurrent Advanced Urothelial Cancer. *Invest. New Drugs* **2013**, *31* (4), 1001–1007. https://doi.org/10.1007/s10637-013-9926-y.

(286) Kantarjian, H. M.; Padmanabhan, S.; Stock, W.; Tallman, M. S.; Curt, G. A.; Li, J.; Osmukhina, A.; Wu, K.; Huszar, D.; Borthukar, G.; Faderl, S.; Garcia-Manero, G.; Kadia, T.; Sankhala, K.; Odenike, O.; Altman, J. K.; Minden, M. Phase I/II Multicenter Study to Assess the Safety, Tolerability, Pharmacokinetics and Pharmacodynamics of AZD4877 in Patients with Refractory Acute Myeloid Leukemia. *Invest. New Drugs* **2012**, *30* (3), 1107–1115. https://doi.org/10.1007/s10637-011-9660-2.

(287) Indorato, R.-L.; Talapatra, S. K.; Lin, F.; Haider, S.; Mackay, S. P.; Kozielski, F.; Skoufias, D. A. Is the Fate of Clinical Candidate Arry-520 Already Sealed? Predicting Resistance in Eg5–Inhibitor Complexes. *Mol. Cancer Ther.* **2019**, *18* (12), 2394–2406. https://doi.org/10.1158/1535-7163.MCT-19-0154.

(288) Broichhagen, J.; Frank, J. A.; Trauner, D. A Roadmap to Success in Photopharmacology. *Acc. Chem. Res.* **2015**, *48* (7), 1947–1960. https://doi.org/10.1021/acs.accounts.5b00129.

(289) Hüll, K.; Morstein, J.; Trauner, D. In Vivo Photopharmacology. *Chem. Rev.* **2018**, *118* (21), 10710–10747. https://doi.org/10.1021/acs.chemrev.8b00037.

(290) Mafy, N. N.; Matsuo, K.; Hiruma, S.; Uehara, R.; Tamaoki, N. Photoswitchable CENP-E Inhibitor Enabling the Dynamic Control of Chromosome Movement and Mitotic Progression. *J. Am. Chem. Soc.* **2020**, *142* (4), 1763–1767. https://doi.org/10.1021/jacs.9b12782.

(291) Barsanti, P. A.; Wang, W.; Ni, Z.-J.; Duhl, D.; Brammeier, N.; Martin, E.; Bussiere, D.; Walter, A. O. The Discovery of Tetrahydro-β-Carbolines as Inhibitors of the Kinesin Eg5. *Bioorg. Med. Chem. Lett.* **2010**, *20* (1), 157–160. https://doi.org/10.1016/j.bmcl.2009.11.012.

(292) Schiemann, K.; Finsinger, D.; Zenke, F.; Amendt, C.; Knöchel, T.; Bruge, D.; Buchstaller, H.-P.; Emde, U.; Stähle, W.; Anzali, S. The Discovery and Optimization of Hexahydro-2H-Pyrano[3,2-c]Quinolines (HHPQs) as Potent and Selective Inhibitors of the Mitotic Kinesin-5. *Bioorg. Med. Chem. Lett.* **2010**, *20* (5), 1491–1495. https://doi.org/10.1016/j.bmcl.2010.01.110.

(293) Schiemann, K.; Emde, U.; Schlueter, T.; Saal, C.; Maiwald, M. Polymorphic Forms and Process US 8,198.452 B2.

(294) Povarov, L. S. A β-Unsaturated Ethers and their Analogues in Reactions of Diene Synthesis *Russ. Chem. Rev.* **1967**, *36* (9), 656–670. https://doi.org/10.1070/RC1967v036n09ABEH001680.

(295) Sadovski, O.; Beharry, A. A.; Zhang, F.; Woolley, G. A. Spectral Tuning of Azobenzene Photoswitches for Biological Applications. *Angew. Chem. Int. Ed.* **2009**, *48* (8), 1484–1486. https://doi.org/10.1002/anie.200805013.

(296) Marcus, A. I.; Peters, U.; Thomas, S. L.; Garrett, S.; Zelnak, A.; Kapoor, T. M.; Giannakakou, P. Mitotic Kinesin Inhibitors Induce Mitotic Arrest and Cell Death in Taxol-Resistant and -Sensitive Cancer Cells. *J. Biol. Chem.* **2005**, *280* (12), 11569–11577. https://doi.org/10.1074/jbc.M413471200.

(297) Good, J. A. D.; Berretta, G.; Anthony, N. G.; Mackay, S. P. The Discovery and Development of Eg5 Inhibitors for the Clinic. In *Kinesins and Cancer*; Kozielski, F., Frank, Ed.; Springer Netherlands: Dordrecht, 2015; pp 27–52. https://doi.org/10.1007/978-94-017-9732-0_2.

(298) Howard, J.; Hunt, A. J.; Baek, S. Chapter 10 Assay of Microtubule Movement Driven by Single Kinesin Molecules. In *Methods in Cell Biology*; Scholey, J. M., Ed.; Motility Assays for Motor Proteins; Academic Press, 1993; Vol. 39, pp 137–147. https://doi.org/10.1016/S0091-679X(08)60167-3.

(299) Mayer, T. U.; Kapoor, T. M.; Haggarty, S. J.; King, R. W.; Schreiber, S. L.; Mitchison, T. J. Small Molecule Inhibitor of Mitotic Spindle Bipolarity Identified in a Phenotype-Based Screen. *Science* **1999**, *286* (5441), 971–974. https://doi.org/10.1126/science.286.5441.971.

(300) van Bergeijk, P.; Adrian, M.; Hoogenraad, C. C.; Kapitein, L. C. Optogenetic Control of Organelle Transport and Positioning. *Nature* **2015**, *518* (7537), 111–114. https://doi.org/10.1038/nature14128.

(301) Nijenhuis, W.; van Grinsven, M. M. P.; Kapitein, L. C. An Optimized Toolbox for the Optogenetic Control of Intracellular Transport. *J. Cell Biol.* **2020**, *219* (4), e201907149. https://doi.org/10.1083/jcb.201907149.

(302) Zhang, H.; Aonbangkhen, C.; Tarasovetc, E. V.; Ballister, E. R.; Chenoweth, D. M.; Lampson, M. A. Optogenetic Control of Kinetochore Function. *Nat. Chem. Biol.* **2017**, *13* (10), 1096–1101. https://doi.org/10.1038/nchembio.2456.

Chapter 2 De novo Design of SARS-CoV-2 Main Protease Inhibitors

1 Project Outline

In March 2020, New York City was severely hit by the SARS-CoV-2 pandemic. The rapid increase in hospitalizations resulted in a shutdown of all nonessential work in New York City under the Executive Order of the Governor of New York, *New York Pause.* As a result, New York University also suspended all nonessential research. Aside from providing local hospitals with hand sanitizer and sterile mask fit-testing solutions, the Trauner group became involved in a collaborative effort for the *de novo* design of inhibitors of the SARS-CoV-2 main protease (M^{Pro}), based on an initial computational screen.

The initial synthetic plan and collaboration with the Prof. Dr. Yingkai Zhang (NYU, computational studies) and Prof. Dr. Daniel Nomura (Berkeley, biochemical evaluation) groups was led by Dr. Christian Fischer. The author of this thesis was together with Zisis Peitsinis involved in the abovementioned work and synthesized initial target molecules but also identified and further developed many substituted pyridone derivatives that were shown to have micromolar activity against M^{Pro}. Klaus-Peter Rühmann worked on peptide structures. Chao Yang (Zhang lab, NYU) did the calculations and Jessica N. Spradlin (Nomura Lab, Berkeley) conducted biochemical assays.

The manuscript for this publication was accepted in Synlett (Wiley) in July, 2021 and is included in this thesis with permission of the co-authors.

2 Accepted Manuscript

De novo Design of SARS-CoV-2 Main Protease Inhibitors

Christian Fischer,[a] Nynke A. Vepřek,[‡,a,b] Zisis Peitsinis,[‡,a] Klaus-Peter Rühmann,[a] Chao Yang,[a] Jessica N. Spradlin,[c] Dustin Dovala,[d] Daniel K. Nomura,[c] Yingkai Zhang,[*a] Dirk Trauner[*a]

[a] Department of Chemistry, New York University, 100 Washington Sq East, New York, NY, 10003, United States.

[b] Department of Chemistry, Ludwig-Maximilian University Munich, Butenandtstrasse 5-13, 81377 München, Germany.

[c] Innovative Genomics Institute, University of California, Berkeley, Berkeley, CA, 94720, United States.

[d] Novartis Institutes for BioMedical Research, Emeryville, CA, 94608, United States.

* indicates the main/corresponding author. ‡ indicates equal contributions.

yz22@nyu.edu; dirktrauner@nyu.edu

Abstract

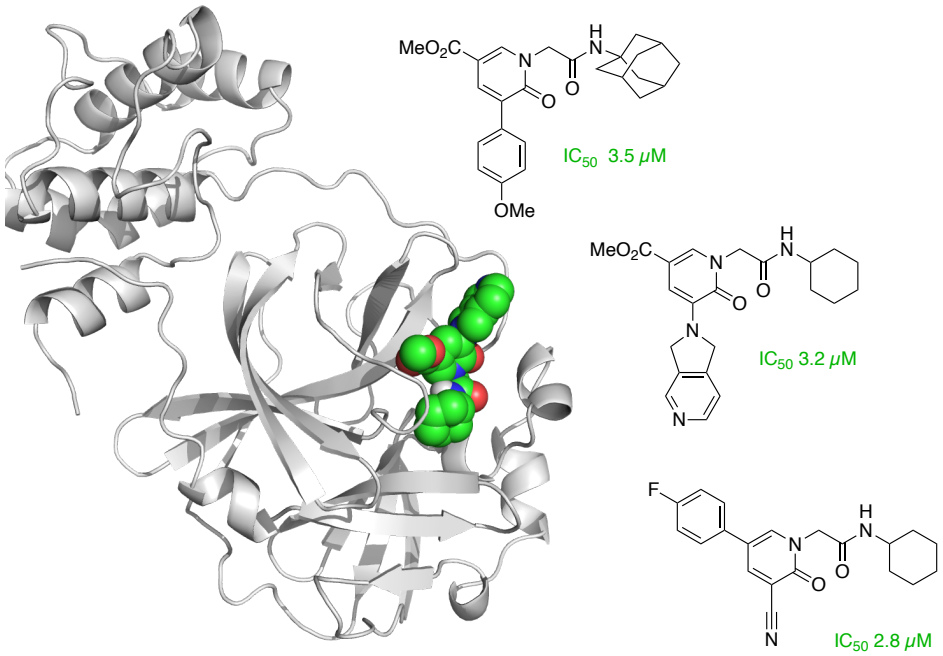

The COVID-19 pandemic prompted many scientists to investigate remedies against SARS-CoV-2 and related viruses that are likely to appear in the future. As the main protease of the virus, MPro, is highly conserved among coronaviruses, it has emerged as a prime target for developing inhibitors. Using a combination of virtual screening and molecular modeling, we identified small molecules that were easily accessible and could be quickly diversified. Biochemical assays confirmed a class of pyridones as low micromolar non-covalent inhibitors of the viral main protease.

Key words: Viral Main Protease, Small-Molecule Inhibitor, SARS-CoV-2, Coronavirus, Molecular Modeling

Introduction:

Small molecules continue to play a crucial role in the fight against viral diseases. Examples for their success include medications for HIV and HCV, which have been made manageable or can be cured by inhibitors of proteases and RNA polymerases.[1] This will likely be the case for the current COVID-19 pandemic as well. Although vaccines based on chemically modified mRNA packaged in lipid nanoparticles have proven to be highly effective, their future usefulness may be impeded by rapid mutations in the viral envelope.[2] In addition, vaccines are less effective in the immunocompromised and are not embraced by a substantial portion of the population for a variety of reasons. Therefore, the development of easily applicable and stable small molecules that fight SARS-CoV-2 and related coronaviruses remains a priority.[3]

Amongst the limited set of viral target proteins, the SARS-CoV-2 main protease (MPro, also called 3CLPro) stands out. This enzyme, a cysteine protease, cleaves its substrate after a glutamine residue, which appears to be unknown for human cysteine proteases that could be responsible for off-target effects.[4] Over the course of the COVID-19 pandemic, the amino acid sequence of MPro has remained remarkably conserved,[5] although it has not been challenged yet by drugs on a large scale. Numerous X-ray structures of MPro with covalent and non-covalent inhibitors and small molecule fragments bound are available to aid computational designs.[6] In addition, SARS-CoV-2 MPro is highly homologous to corresponding proteases of other coronaviruses and enteroviruses and likely to be related to proteases of harmful viruses that will emerge in the future.[7]

As such, efforts to develop MPro inhibitors have been launched on a large scale. To date, they have mostly been centered on covalent inhibitors derived from peptides that correspond to the natural cleavage site of the MPro substrate.[8] Given the rapid advance of this approach, which had been pursued for coronaviruses well before the emergence of SARS-CoV-2, we decided to take an alternative one: the de novo design of molecules through virtual screening and further refinement of the best candidates with molecular docking. This was always done with an eye on synthetic accessibility and the ability to quickly diversify successful candidates. As an additional distinguishing criterium, we decided to work on molecules that bind non-covalently, at least in the first phase of our program. We now disclose series of small molecules that fulfill criteria for "druggability" and can be assembled in a few synthetic steps. Our most successful ones inhibit MPro at single digit micromolar concentrations in biochemical assays.

Results and Discussions:

Identification of a Small-Molecule lead scaffold

The ASINEX PPI non-macrocyclic screening library consists of 11870 fragments and compounds that were computationally docked into the catalytic site of the crystal structure of the SARS-CoV-2 main protease (PDB: 6LU7 and 6Y84; details can be found in the Supporting Information).[9] This provided a virtual spectrum of docking score vs ligand efficiency (Figure 1a, blue) in which some of initial virtual hits were manually evaluated and optimized in terms of ligand efficiency, synthetic accessibility, and docking score (Figure 1a, red). Based on these parameters, we selected three distinct types of molecules, represented by compounds 1-3 for synthesis and biological testing (Figure 1b).

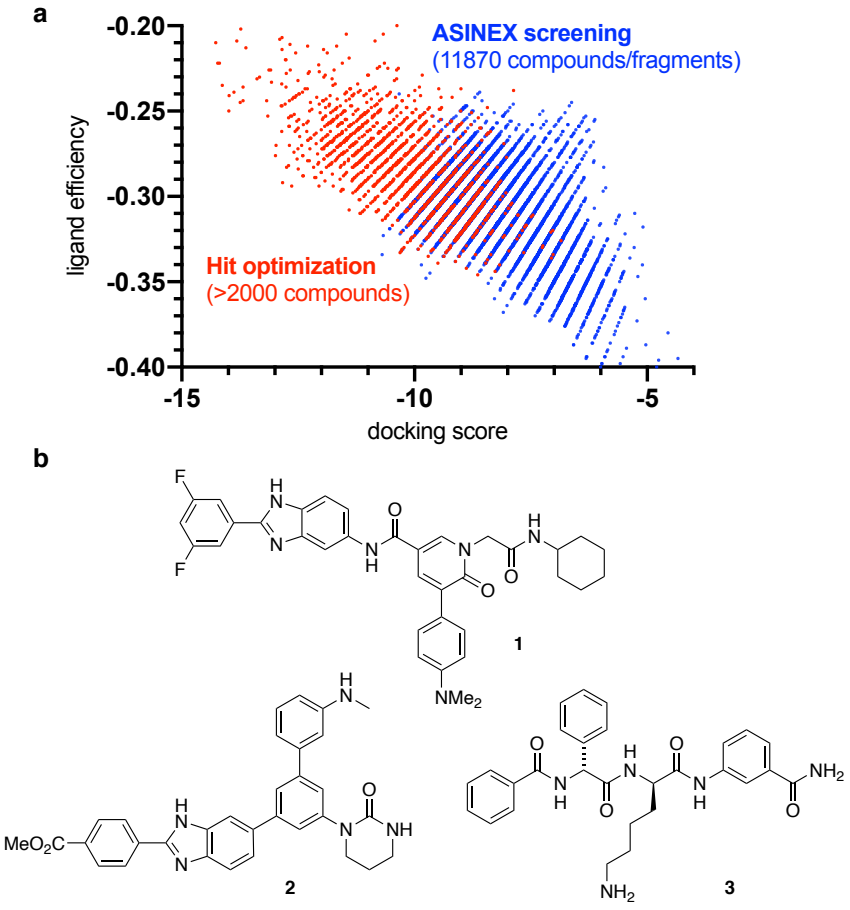

Figure 1. **a)** Computational lead identification (red) by optimizing initial hits in the ASINEX screening (blue). **b)** Representative target compounds 1-3 with excellent docking scores.

N-Alkyl-3-arylpyridone 5-carboxamides of type **1** were recognized as an easily accessible scaffold as well as *m*-teraryl linked cyclic ureas of type **2**. In addition to these, short D-Phg-D-Lys peptides of type **3** were identified as potential inhibitors that should remain proteolytically

stable and capable to disrupt the natural function of the protease. Methyl 6-hydroxynicotinate (**4**) is selectively *N*-alkylated with chloroacetamide **5a** using K_2CO_3 (Scheme 1a). Bromination and Suzuki cross-coupling allow access to the arylated pyridone methyl ester **6a**, which is subsequently hydrolyzed. The resulting carboxylic acid is coupled using HATU to the benzimidazole amine **7** to form *N* alkyl-3-arylpyridone 5-carboxamide **1**. The cyclic urea **2** was synthesized in similar efficiency (Scheme 1b). The initial isocyanate addition to 3,5-dibromoaniline (**8**) was followed by the cyclization of the urea moiety using NaH. Two sequential Suzuki cross-coupling reactions on the dibromide **9** with aryl boronic acid pinacol esters **10** and **11** rendered the desired *m*-teraryl linked urea **2**. The short D-Phg- D-Lys peptide **3** was manually assembled starting from Fmoc- D-Lys(Boc)-OH **12** by a tailored sequence of EDCI/HOBt-based couplings and protecting group removals (Scheme 1c).

With our first target molecules in hand, we proceeded to test them in enzymatic activity assays that monitor the formation of fluorescent cleavage products (see Supporting Information).[10] Despite their excellent docking scores, pyridone **1**, the cyclic urea **2**, and the D-peptide **3** failed to inhibit the viral main protease even at high concentrations. Gratifyingly, however, some synthetic intermediates that were also tested showed activities that were worth following up upon. For instance, the Boc-protected intermediate **16** inhibited MPro with an IC_{50} of 121 µM. The truncated pyridone methyl ester intermediate **6a** showed more substantial inhibition (IC_{50} = 19 µM). Replacing the benzimidazole amide of **1** with a methyl ester not only reduces the molecular weight but also the lipophilicity (clogP lowered from ~4.4 to ~3.5). Therefore, this pyridone scaffold was identified as a promising lead for further optimization and our subsequent investigations focused on this class of compounds.

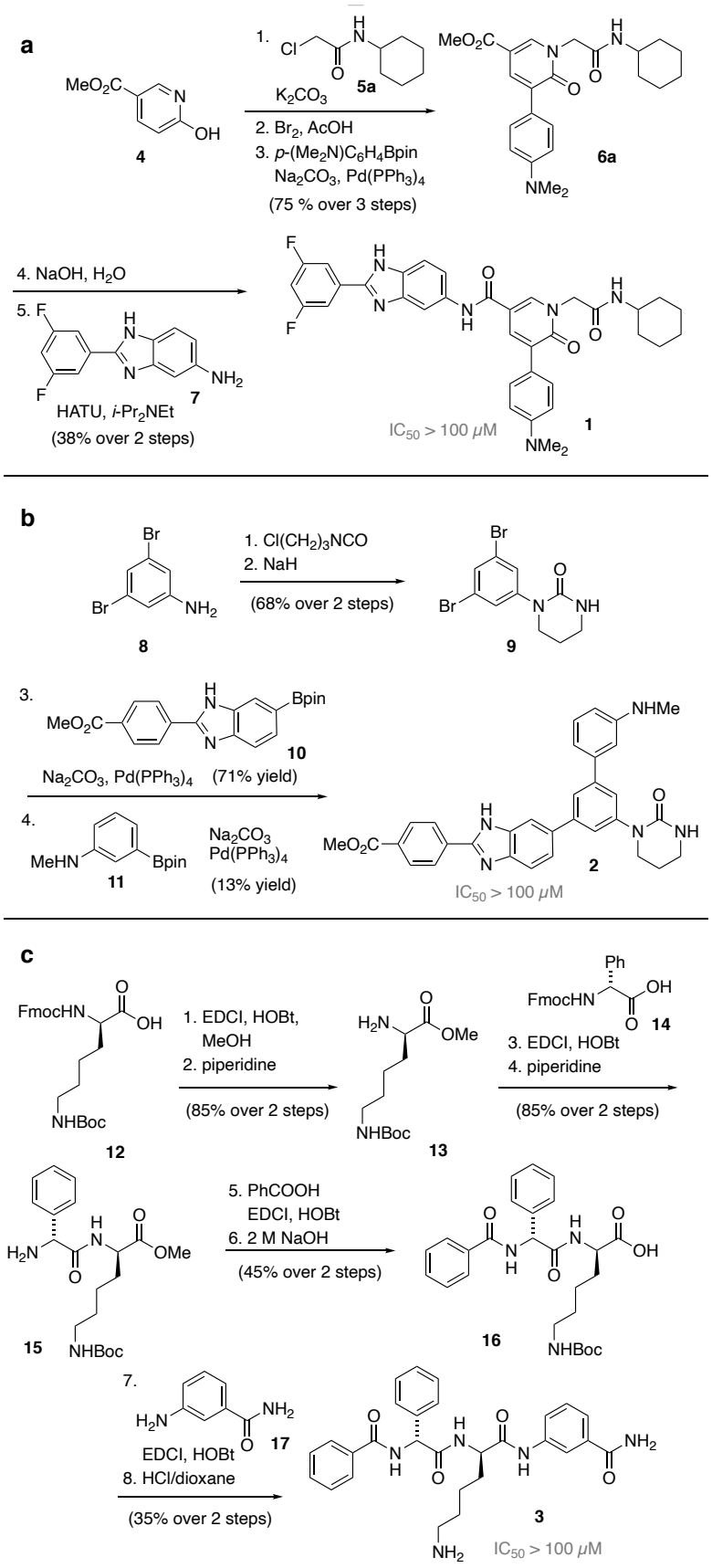

Scheme 1. Assembly of initially identified compounds 1-3.

SAR Investigations

The succinct synthesis of pyridone methyl ester **6a**, outlined in Scheme 1, was generally applicable to various other derivatives but also allowed a broad range of cross-coupling reactions (see Supporting Information for details). Initial structure-activity relationship (SAR) investigations showed that a substituent next to the pyridine carbonyl was critical. For instance, unsubstituted pyridone **4'** did not show any activity. Also the activities of the unsubstituted phenyl **6b** and the more lipophilic fluoro aryls **6c-e** were negligibly low. While the CF_3 derivative **6f** and the acetamide **6g** showed improved IC_{50} values, the sulfonamide **6h** remained inactive. In the absence of an X-ray structure, systematic synthesis and biological evaluation was required to improve our understanding of how the pyridone series interacts with the binding site. We anticipate that a favorable interaction (e.g. hydrogen bonding) very close to the 4-position of the aryl substituent is required to further lower the IC_{50}. Therefore, the 4-pyridyl **6i** and **6j** was synthesized, showing increased activity at 14 and 12 µM, respectively. Also, 4-anisole **6k** as well as methoxy-pyrimidine **6l** supported this hypothesis with an increase in activity, whereas the corresponding aryloxy ether **6m** is likely missing such a key interaction. Possibly due the orientation of the sulfur lone pairs the thiomorpholine **6n** is less optimal. The more extended morpholine **6o**, the sulfone analog **6p** and the piperidine-4-carbonitrile **6q** seem to be missing this favorable interaction as well. A stark increase in inhibition of the main protease was found with dihydropyrrolopyridine **6r** having an IC_{50} of 3.2 µM. To probe the length of the substituent further, we examined ethynylpyridine **6s** in comparison to ethynylbenzene **6t**. Both had diminishing effects on the potency. Hence a more favorable interaction could be imagined with a smaller functional group. Whereas the alkyne **6u** was ineffective, the nitrile **6v** was inhibiting the main protease with an IC_{50} of 3.3 µM. In addition to the improved potency, the nitrile **6v** had also a favorable calculated logP of 1.1 and a polar surface area of 101 Å, which promise good cell permeation.

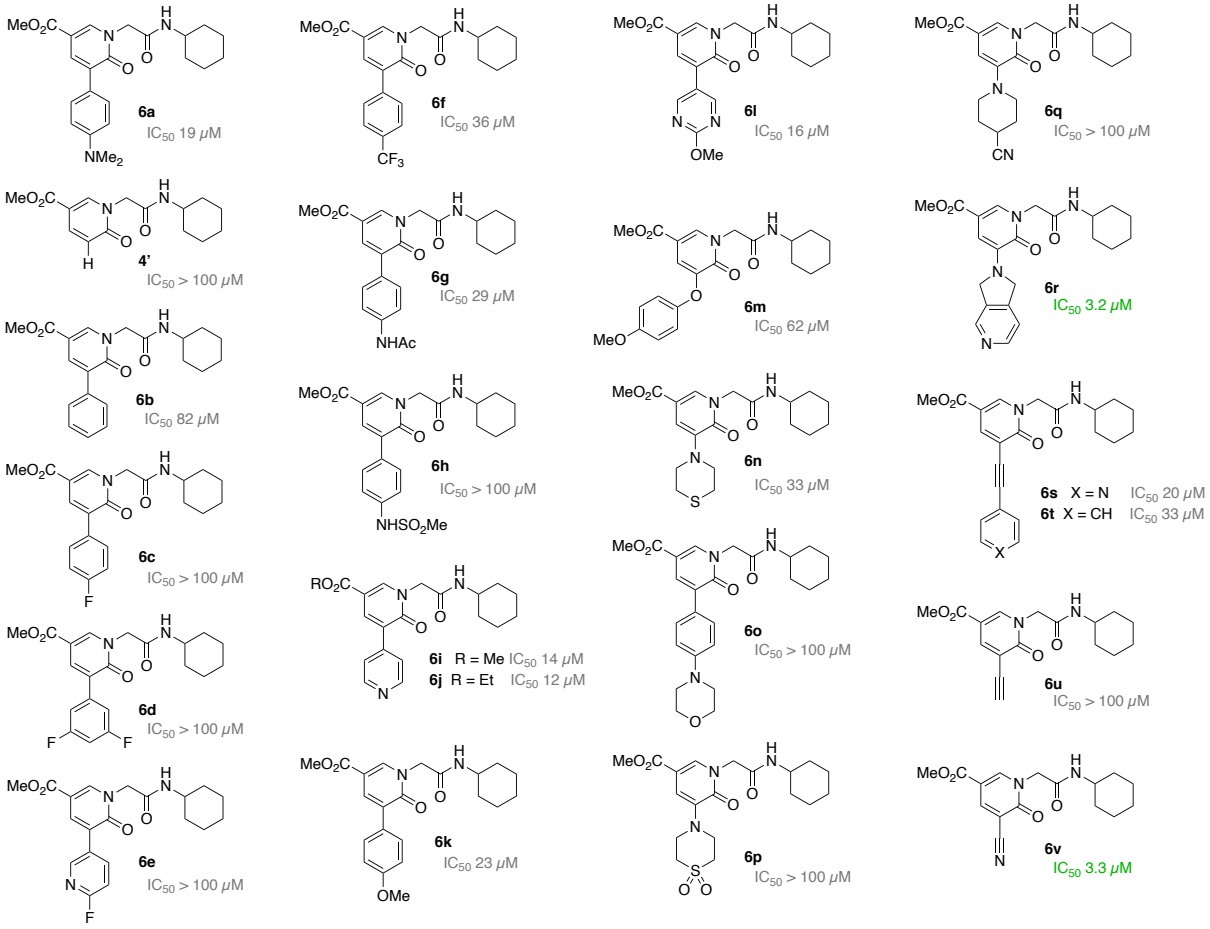

Figure 2. Synthesized pyridone esters **4'**, **6a-v** to inhibit the SARS-CoV-2 main protease and investigate the structure-activity relationship of the scaffold.

During our SAR investigations, we realized that some of the pyridones, such as the acetylated derivative **6g** showed strong fluorescence (λ_{abs} 318 nm; λ_{em} 420 nm in aq. PBS with 1% DMSO). This reaffirmed our selection of a bathochromically shifted rhodamine based fluorescent probe for the enzymatic assays that did not interfere with our inhibitors (see Supporting Information for details).

To further improve the activity of the pyridone scaffold we decided to explore variations in the acetamide side chain. Unfortunately, Suzuki cross-coupling reactions on the free 4-bromo-6-hydroxynicotinate core were met with limited success.

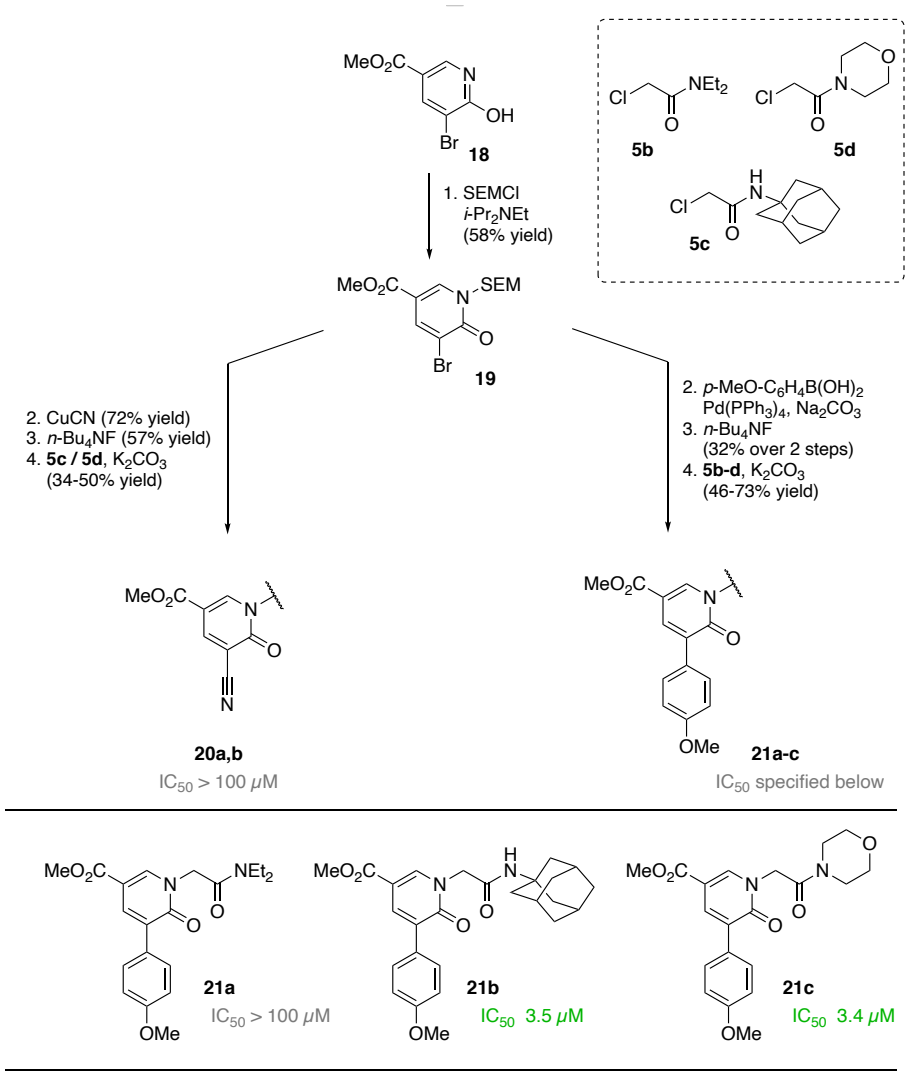

Scheme 2. Derivatizing the pyridone side chain of the nitrile and anisole analog.

Based on reports by Gademann and co-workers the hydroxypyridine **18** was protected first using SEM-Cl (Scheme 2).[11] This enabled derivatization like the nitrile substitution and Suzuki cross-coupling reaction. As anisole is a neutral, fairly stable moiety and showed an IC_{50} of 23 µM in derivative **6k**, it was chosen together with the more active nitrile for further exploration. After deprotection of the SEM group, the acetamides were installed under the previously introduced conditions. For the nitrile, both the morpholine amide **20a** and the adamantanyl amide **20b** did not show any inhibition in the enzyme assay. Interestingly, for the anisole, a *N,N*-diethylamide **21a** lost the activity completely. However, the adamantyl amide **21b** and the morpholino amide **21c** showed a nearly tenfold lower IC_{50} of 3.5 µM and 3.4 µM, respectively. Our concern of the pyridone methyl ester hydrolysis as a serious liability grew when we observed a significantly increased IC_{50} of the corresponding carboxylic acid of the anisole derivative **22a**. The installation of dimethyl amides, morpholino amides and phenyl amides

were examined for both 4-anisole and nitrile derivatives **22a-c** and **23a,b** (Scheme 3a). Disappointingly, all derivatives showed a complete loss of activity. In search of another functional group we decided to explore the installation of an aryl moiety instead. *N*-Alkylation of 5-bromopyridin-2-ol (**25**) using chloroacetamide **5a** allowed the installation of the fluorophenyl via Suzuki cross-coupling (Scheme 3b). Installation of a nitrile at the 3-position leads to **28,** a significantly more active SARS-CoV-2 main protease inhibitor at an IC_{50} of 2.8 µM. This is our strongest inhibitor to date and is in stark contrast to the activity of compound **27**, which lacks the nitrile ($IC_{50} \approx 77$ µM).

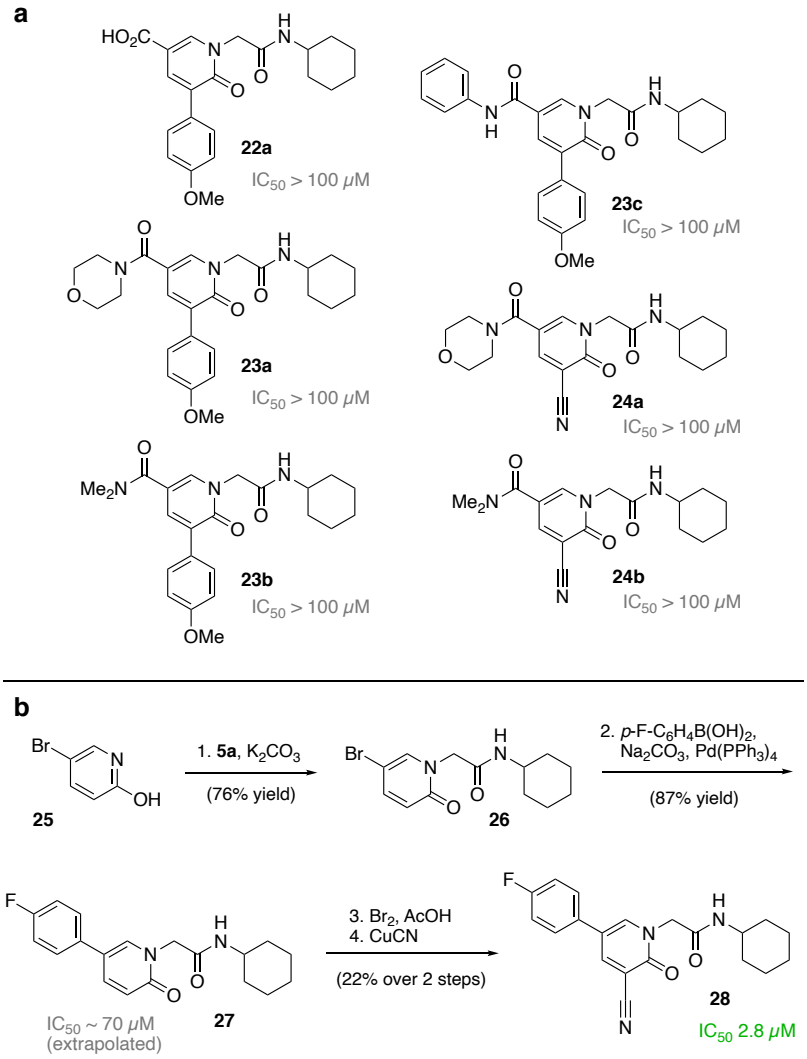

Scheme 3. **a)** As the carboxylic acid **22a** loses significant activity, amides **23a-c** and **24a/b** have been synthesized. **b)** Outline of the synthesis route to the highly active SARS-CoV-2 M^{Pro} inhibitor **28**.

In sum, we have introduced small molecules that could potentially be developed into antivirals against SARS-CoV-2. Using a combination of virtual screening, molecular docking, and luck, we quickly were able to identify low micromolar inhibitors of the viral main protease M^{Pro}. Their

further development will require X-ray crystallographic studies, which will provide insights into the binding site and pose of our inhibitors and can also serve to calibrate our docking results. Attempts in this direction are well underway and results will be reported in due course.

Funding Information

D.T. and his group are thankful for the COVID-19 Catalyst Grant by NYU. Y.Z. would like to acknowledge the support by the National Institutes of Health grant R35 GM127040. C.F. thanks the Swiss National Science Foundation (SNSF) for a postdoctoral fellowship (178569). N.A.V. thanks the German Academic Scholarship Foundation (Studienstiftung des Deutschen Volkes) for a PhD Fellowship. Z.P. and K.P.R. are supported by the NYU MacCracken Fellowship.

References and Notes Chapter 2

(1) (a) De Clercq, E.; Li, G. *Clin. Microbiol. Rev.* **2016**, *29*, 695–747. (b) de Leuw, P.; Stephan, C. *Expert Opin. Pharmacother.* **2018**, *19*, 577–587. (c) Flexner, C. *N. Engl. J. Med.* **1998**, *338*, 1281–1293.

(2) (a) Harvey, W. T.; Carabelli, A. M.; Jackson, B.; Gupta, R. K.; Thomson, E. C.; Harrison, E. M.; Ludden, C.; Reeve, R.; Rambaut, A.; COVID-19 Genomics UK Consortium, Peacock, S. J.; Robertson, D. L. *Nat. Rev. Microbiol.* **2021**, *19*, 409–424. (b) Krammer, F. *Nature* **2020**, *586*, 516–527.

(3) (a) Press Release of the United States Department of Health and Human Services: **June 17, 2021**, "*Biden Administration to Invest $3 Billion from American Rescue Plan as Part of COVID-19 Antiviral Development Strategy"*, accessed June 25, 2021. (b) Tummino, T. A.; Rezelj, V. V.; Fischer, B.; Fischer, A.; O'Meara, M. J.; Monel, B.; Vallet, T.; White, K. M.; Zhang, Z.; Alon, A.; et al. *Science* **2021**, *doi: 10.1126/science.abi4708*. (c) Cannalire, R.; Cerchia, C.; Beccari, A. R.; Di Leva, F. S.; Summa, V. *J. Med. Chem.* **2020**, *doi: 10.1021/acs.jmedchem.0c01140.*

(4) (a) Zhang, L.; Lin, D.; Sun, X.; Curth, U.; Drosten, C.; Sauerhering, L.; Becker, S.; Rox, K.; Hilgenfeld, R. *Science* **2020**, *368*, 409–412; see also Ref. 9a. (b) Yang, H.; Yang, J. *RSC Med. Chem.* **2021**, doi: 10.1039/D1MD00066G. (c) Ullrich, S.; Nitsche, C. *Bioorg. Med. Chem. Lett.* **2020**, *30*, 127377.

(5) (a) Zhu, G.; Zhu, C.; Zhu, Y.; Sun, F. *Curr. Res. Microb. Sci.* **2020**, *1*, 53–61. (b) Hilgenfeld, R. *FEBS J.* **2014**, 4085–4096. (c) Mengist, H. M.; Dilnessa, T.; Jin, T. *Front. Chem.* **2021**, doi: 10.3389/fchem.2021.622898.

(6) (a) Kneller, D.; Philips, G.; O'Neill, H. M.; Jedrzejczak, R.; Stols, L.; Langan, P.; Joachimiak, A.; Coates, L.; Kovalevsky, A. *Nat. Comm.* **2020**, *11*, 3202. (b) Lockbaum, G. J.; Reyes, A. C.; Lee, M. J.; Tilvawala, R.; Nalivaika, E. A.; Ali, A.; Yilmaz, N. K.; Thompson, P. R.; Schiffer, Celia A. Viruses 2021, 13, 174. (c) Douangamath, A.; Fearon, D.; Gehrtz, P.; Krojer, T.; Lukacik, P.; Owen, C. D.; Resnick, E.; Strain-Damerell, C.; et al. *Nat. Commun.* **2020**, *11*, 5047. (d) Crystal structure for the SARS-Cov-1 main protease: Yang, H.; Yang, M.; Ding, Y.; Liu, Y.; Lou, Z.; Zhou, Z.; Sun, L.; Mo, L.; Ye, S.; Pang, H.; Gao, G. F.; Anand, K.; Bartlam, M.; Hilgenfeld, R.; Rao, Z. *Proc. Natl. Acad. Sci. U.S.A.* **2003**, *100*, 13190–13195. As well as Ref. 4a and 9a.

(7) (a) Stoermer M. *ChemRxiv*. **2020,** doi: 10.26434/chemrxiv.11637294.v3. (b) Zhang, L.; Lin, D.; Kusov, Y.; Nian, Y.; Ma, Q.; Wang, J.; von Brunn, A.; Leyssen, P.; Lanko, K.; Neyts, J.; de Wilde, A.; Snijder, E. J.; Liu, H.; Hilgenfeld, R. *J. Med. Chem.* **2020**, *63*, 4562–4578.

(8) (a) Pillaiyar, T.; Manickam, M.; Namasivayam, V.; Hayashi, Y.; Jung, S.-H. *J. Med. Chem.* **2016**, *59*, 6595–6628. (b) non-covalent □-lactam inhibitors: Malla, T. R.; Tumber, A.; John, T.; Brewitz, L.; Strain-Damerell, C.; Owen, C. D.; Lukacik, P.; Chan, H. T. H.; Maheswaran, P.; Salah, E.; Duarte, F.; Yang, H.; Rao, Z.; Walsh, M. A.; Schofield, C. J. *Chem. Commun.* **2021**, *57*, 1430–1433.

(9) (a) Jin, Z.; Du, X.; Xu, Y.; Deng, Y.; Liu, M.; Zhao, Y.; Zhang, B.; Li, X.; Zhang, L.; Peng, C.; et al. *Nature* **2020**, *582*, 289–293.

(10) Biering, S. B.; Van Dis, E.; Wehri, E.; Yamashiro, L. H.; Nguyenla, X.; Dugast-Darzacq, C.; Graham, T. G. W.; Stroumza, J. R.; Golovkine, G. R.; Roberts, A. W.; Fines, D. M.; Spradlin, J. N.; Ward, C. C.; Bajaj, T.;
Dovala, D.; Schulze-Gamen, U.; Bajaj, R.; Fox, D. M.; Ott, M.; Murthy, N.; Nomura, D. K.; Schaletzky, J.; Stanley, S. A. *ACS Infect. Dis.* **2021**, doi: 10.1021/acsinfecdis.1c00017.

(11) (a) Jessen, H. J.; Schumacher, A.; Shaw, T.; Pfaltz, A.; Gademann, K. *Angew. Chem. Int. Ed.* **2011**, *50*, 4222–4226; (b) Breugst, M.; Mayr, H. *J. Amer. Chem. Soc.* **2010**, *132*, 15380–15389.

Chapter 3 Towards the Photopharmacological Control of DREADD Receptors

1. Project Outline

Designer receptors exclusively activated by designer drugs (DREADD) are artificial, engineered G-protein coupled receptors (GPCRs) that are designed to be activated solely by a "designer ligand". Such a ligand does not bind with high affinity to native receptors and does thus not cause adverse effects in wild-type systems. The first reported DREADD was obtained by two point mutations in human M_3 muscarinic acetylcholine receptor (hM_3) and the authors claimed the selective silencing of the **d**esigner hM3**D**q receptor using clozapine-*N*-oxide (CNO) while the wild-type receptor remained unaffected. Further, the hM3Dq was unresponsive to its native ligand, acetylcholine (Figure 1). CNO was inert against native receptors. Subsequently, the authors expanded this technology to a series of allegedly CNO-responsive DREADDs to control human M_1, M_2, M_4 and M_5 muscarinic receptors.[1]

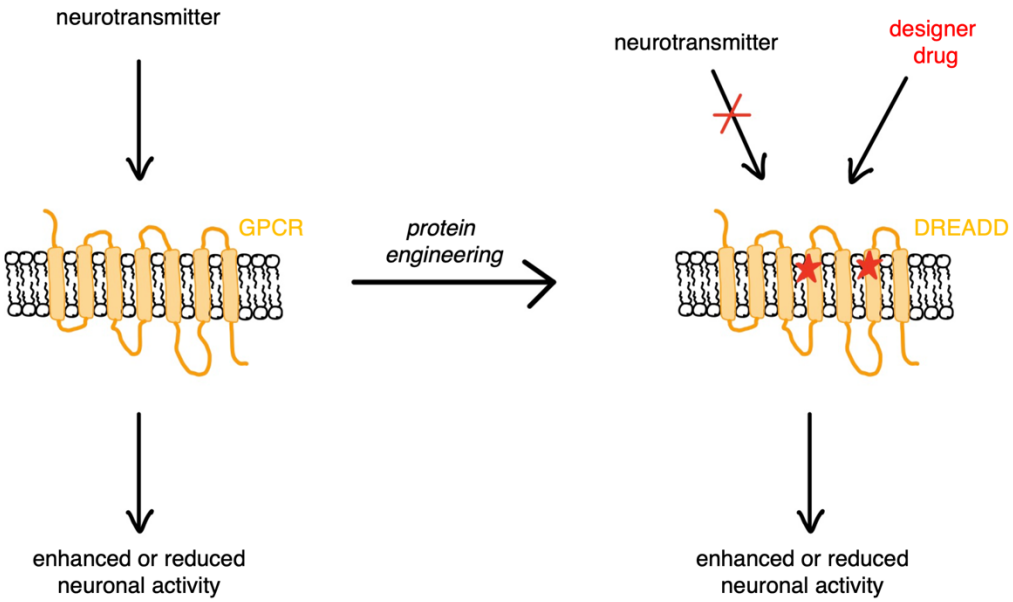

Figure 1: Concept of DREADDs.[gg]

The selective investigation of specific GPCR functions by their genetic manipulation is often met with limitations due to strong adverse effects and loss of activity and/or specificity of these proteins.[1] Animal models (and cell lines) can be readily obtained by viral transformation of the

[gg] drawing inspired by Dr. Justin English https://benchling.com/pub/dreadds (10-10-2017).

wild-type. For this reason, DREADDs have become a much appreciated tool for the *in vivo* study of GPCRs in freely moving animals.[2,3]

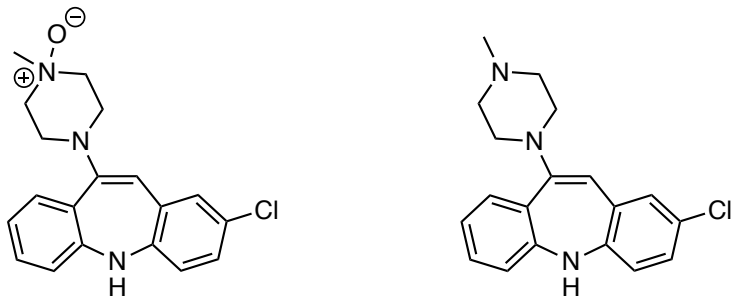

CNO **clozapine**

Figure 2: Chemical structures of CNO and clozapine.

Despite the wide-spread application of this "designer" system, the mechanism of action of CNO was only elucidated ten years after the initial implementation of DREADDs. *N*-oxides are metabolic intermediates of trisubstituted amines and it was known that CNO is reversibly metabolized to clozapine in mammals (Figure 2).[4–7] Gomez *et al.* conducted a focused study on the effects of CNO and clozapine itself on DREADD expressing HEK-293 cells and later hM4Di expressing rodents. They found that CNO was itself inactive on DREADDS and that the receptors are actually highly sensitive to clozapine.[8] It was demonstrated that CNO-related activity in the brains of rodents was due to the metabolism of CNO to blood brain barrier permeable clozapine, especially under systemic CNO administration. This also matched the often observed delayed onset of response with respect to CNO administration as well as the increased clozapine concentrations in cerebrospinal fluid that reach their maximum about 2-3 hours after CNO administration.[8,9] It was suggested that a selective and careful dosing of the FDA approved drug clozapine or derivatives thereof like perlapine or the free secondary amine would be superior actuators for DREADDs.[10,11] For the known and broadly investigated adverse effects of clozapine however, close control studies are necessary.[8,10]

Photopharmacology is a means to add spatial and temporal control to the activity of a biological ligand and it has been widely applied to GPCRs.[12,13] We envisioned that the limitations that stem from the polypharmacology of clozapine, as well as the limited spatial and temporal precision of DREADD activation by wash in of clozapine could be met by photopharmacology. Further could this system be expanded by tethering the photoswitch to specific neighboring cells which would allow for the investigation of cellular interactions with high spatial and temporal accuracy.[14]

2. Design of Photoswitchable Clozapine Derivatives

Clozapine is an FDA approved drug with known polypharmacology. For this reason its structure-activity relationships (SAR) have been thoroughly studied.[15–18] Calculations by Neil Patel and Prof. Dr. Seva Katrich (The Broad Institute at USC) indicated that the replacement of the aryl chlorine substitution of CNO with a photoswitch, that can then be further linked to a tether, would allow for efficient binding of the ligand in the *trans* form while the *cis* isomer would clash with the protein, resulting in lower binding affinity (Figure 3).

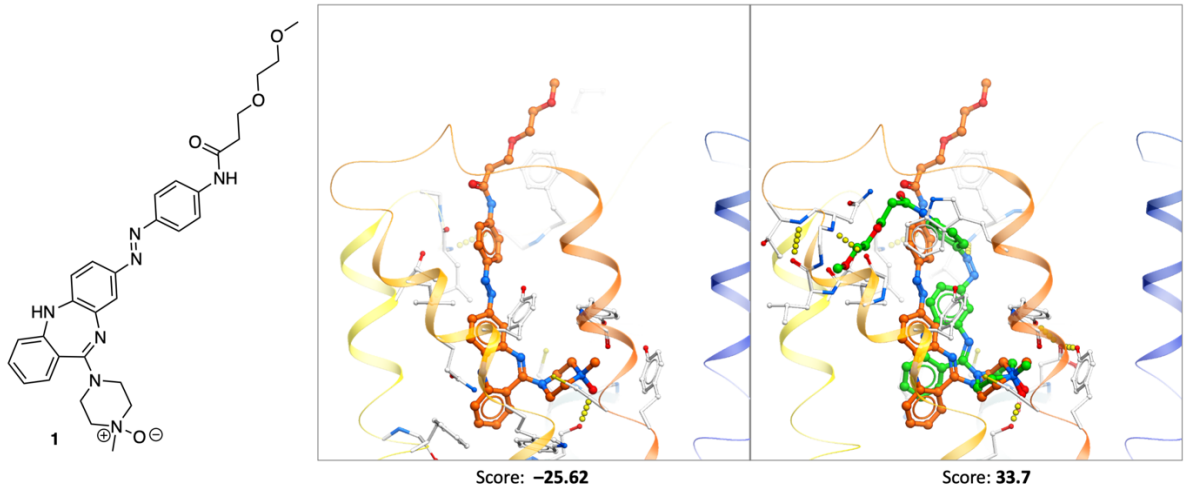

Figure 3: In silico prediction of the binding of hypotethical photoswitchable clozapine derivative **1** to a DREADD receptor; orange: *cis*, green structure: *trans*.

Motivated by these results, we decided to synthesize a small set of photoswitchable clozapine derivatives. For simplified synthetic access and since it had been shown that clozapine is the real ligand for DREADDs, we decided to omit the *N*-oxide in our target structures.

3. Synthesis of Photoswitchable Clozapine Derivatives

Clozapine was readily synthesized in gram quantities following known procedures (Scheme 1).[15–18]

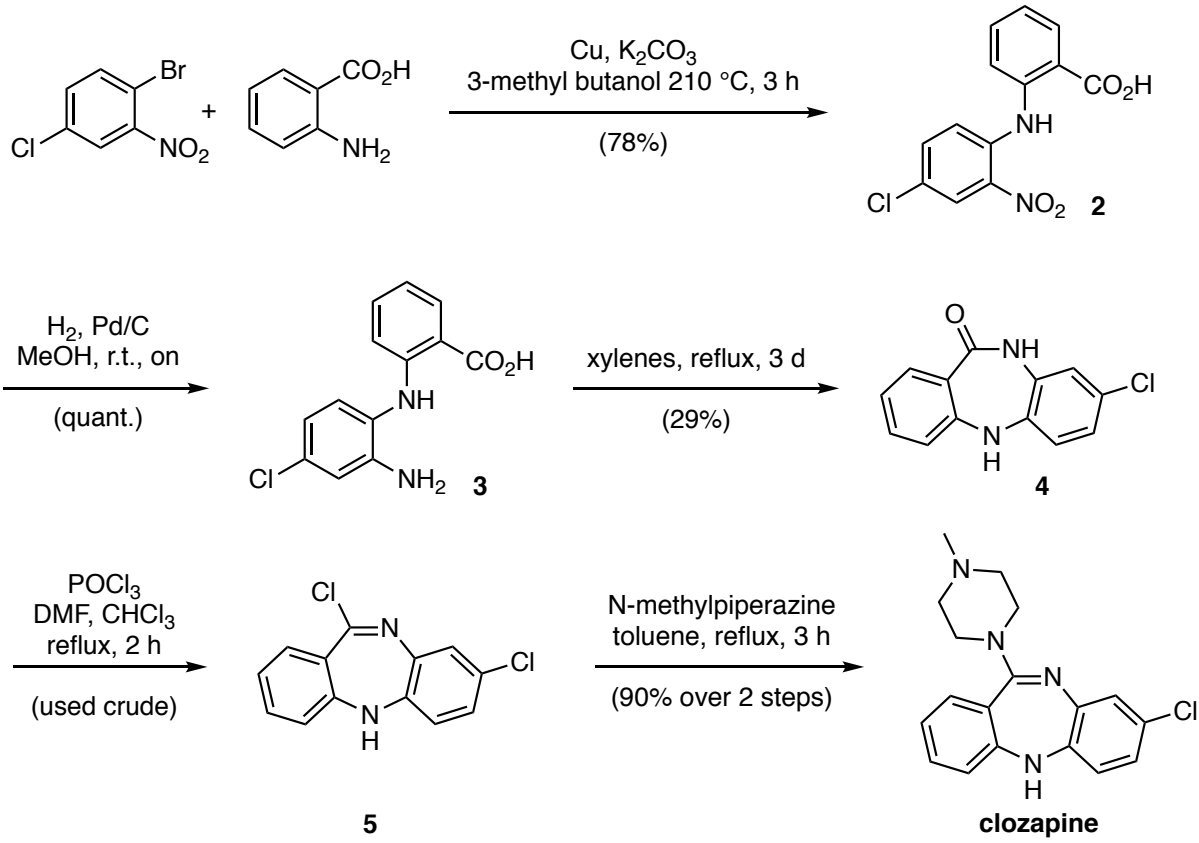

Scheme 1: Synthesis of clozapine.

In our first attempt, we followed a procedure using π-cinnamoyl palladium (II) chloride dimer to install the azobenzene (Scheme 2).[19] While sufficient amounts of the desired **6** could be obtained, substantial amounts of the hydrazine were observed. Briefly, the oxidation of the hydrazine byproduct using $FeCl_3$, MnO_2 or air was explored but unsuccessful.

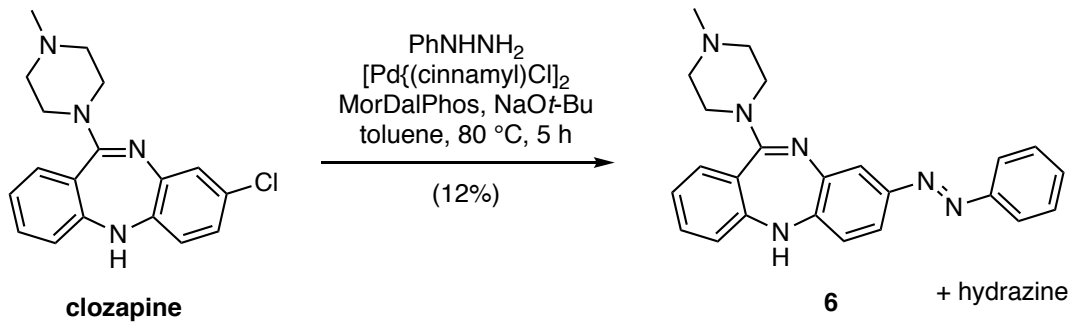

Scheme 2: Cross coupling of aryl chloride with phenyl hydrazine.

To access further photoswitchable clozapine derivatives with a handle for further diversification, we decided to apply a Buchwald-Hartwig amination of the aryl chloride using *N*-Boc-*N*-aryl hydrazine derivatives that could quickly be accessed from the respective aryl iodides and *N*-Boc-hydrazine (see experimental data).[20,21] The diary aniline in clozapine was Boc-protected to facilitate the transformation. The clean conversion of the cross coupling that could easily be monitored by LCMS and difficulties in separating the product from the starting material as well as hydrazine byproduct by simple column chromatography prompted us to isolate the product mixture. The subsequent deprotection was performed after silica-filtration to remove the catalyst. *N*-Boc-hydrazines could efficiently be oxidized *via* deprotonation and copper-(I) mediated E1cB mechanism.[22] The following Boc-deprotection was achieved thermally (Scheme 3).

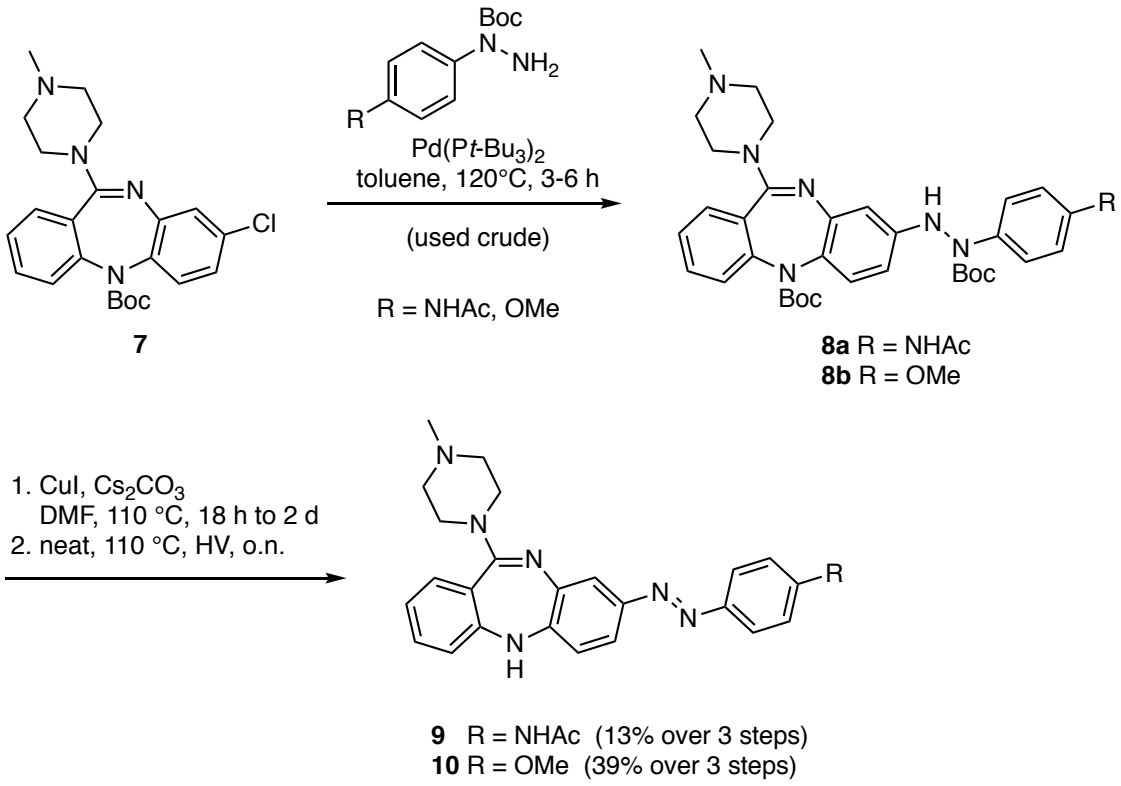

Scheme 3: Buchwald-Hartwig amination with *N*-aryl-*N*-Boc-hydrazines followed by oxidation and thermal decarboxylation.

The broad absorption spectrum of the clozapine photoswitches is a result of the highly conjugated heteroaromatic π-system. The UV-spectra show that enrichment of the predicted inactive *cis* isomer is possible with wavelengths up to 504 nm (isosbestic point), which has advantages in improved tissue penetration and lower phototoxicity compared to UV-light, especially upon prolonged exposure. Enrichment of the *trans* isomer can be achieved

thermally, or by irradiation with wavelengths above 504, below 320 nm, or by combination of irradiation and thermal relaxation.

4. Conclusion and Outlook

Overall, three photoswitchable clozapine analogs (**7, 9, 10**) were synthesized *via* an efficient 4-step procedure from clozapine. The photophysical properties were determined (details see experimental data) and the compounds were given to our collaborators at the Siegelbaum lab (Columbia University, New York, USA).

After an initial evaluation of optoclozapines **7**, **9**, **10**, the structural properties will be adjusted to improve matching the requirements of the biological assays. Further we will prepare tethered switches.

References Chapter 3

(1) Armbruster, B. N.; Li, X.; Pausch, M. H.; Herlitze, S.; Roth, B. L. Evolving the lock to fit the key to create a family of G protein-coupled receptors potently activated by an inert ligand *Proc. Natl. Acad. Sci. USA* **2007**, *104*, 5163–5168.

(2) Urban, D. J.; Roth, B. L. DREADDs (Designer Receptors Exclusively Activated by Designer Druggs): Chemgoenetic Tools with Therapeutic Utility *Annu. Rev. Pharmacol. Toxicol.* **2015**, *55*, 399–417.

(3) Roth, B. L. DREADDs for Neuroscientists *Neuron* **2016**, *89*, 683–694.

(4) Jann, M. W., Lam, Y. W.; Chang, W. H. Rapid formation of clozapine in guinea-pigs and man following clozapine-N-oxide administration *Arch. Int. Pharmacodyn. Ther.* **1994**, *328*, 243–250.

(5) Chang, W.-H.; Lin, S.-K.; Lane, H.-Y.; Wei, F.-C.; Hu, W.-H.; Lam, Y. F., Jann, M. W. Reversible metabolism of clozapine and clozapine N-oxide in schizophrenic patients *Prog. Neurophsychopharmacol. Biol. Psychiatry* **1998**, *22*, 723–739.

(6) Bickel, M. H. The Pharmacology and Biochemistry of *N*-oxides *Pharmacol. Rev.* **1969**, *21*, 325–355.

(7) Rose, J.; Castagnoli, N. The Metabolism of Tertiary Amines *Med. Res. Rev.* **1983**, 3, 73–88.

(8) Gomez, J. L.; Bonaventura, J.; Lesniak, W.; Mathews, W. B.; Sysa-Shah, P.; Rodriguez, L. A.; Ellis, R. J.; Richie, C. T.; Harvey, B. K.; Dannals, R. F.; Pomper, M. G.; Bonci, A.; Michaelides, M. Chemogenetics revealed: DREADD occupancy and activation via converted clozapine *Science* **2017**, *357*, 503–507.

(9) Raper, J.; Morrison, R. D.; Daniels, J. S.; Howell, L.; Bachevalier, J.; Wichmann, T.; Galvan, A. *ACS Chem. Neurosci.* **2017**, *8*, 1570–1576.

(10) Mahler, S. V.; Aston-Jones, G. CNO Evil? Considerations for the Use of DREADDs in Behavioral Neuroscience *Neuropsychopharmacology* **2018**. *43*, 934–936.

(11) Chen, X.; Choo, H.; Huang, X.-P.; Yang, X.; Stone, O.; Roth, B. L.; Jin, J. The First Structure–Activity Relationship Studies for Designer Receptors Exclusively Activated by Designer Drugs *ACS Chem. Neurosci.* **2015**, *6*, 476–484.

(12) Hüll, K.; Morstein, J.; Trauner, D. *In Vivo* Photopharmacology *Chem. Rev.* **2018**, *118*, 10710–10747.

(13) Ricart-Ortega, M.; Font, J.; Llebaria, A. GPCR photopharmacology *Mol. Cell. Endocrin.* **2019**, *488*, 36–51.

(14) Farrants, H.; Gutzeit, V. A.; Acosta-Ruiz, A.; Trauner, D.; Johnsson, K.; Levitz, J., Broichhagen, J. SNAP-tagged nanobodies enable reversible optical control of a G protein-coupled receptor via a remotely tethered photoswitchable ligand. *ACS Chem. Bio.* **2018**, *13*, 2682–2688.

(15) Hunziker F.; Lauener, H.; Schmutz, J. Zur Chemie und Pharmakologie von in 10-Stellung basisch substituierten 5-dibenzo[*b,e*][1,4]-diazepin-derivaten. 1. Über siebengliedrige Heterozyklen *Arzneimittel Forschung/ Drug Research* **1963**, 324–328.

(16) Su, J.; Tang, H.; McKittrick, B. A.; Burnett, D. A.; Zhang, H.; Smith-Torhan, A.; Fawzi, A.; Lachowicz, J. Modification of the clozapine structure by parallel synthesis *Bioorg. Med. Chem. Lett.* **2006**, *16*, 4548–4553.

(17) Capuano, B; Crosby, I. T.; Lloyd, E. J.; Taylor, D. A. Synthesis and Preliminary Pharmacological Evaluation of 4´-Arylmethyl Analogues of Clozapine. I. The Effect of Aromatic Substituents *Aust. J. Chem.* **2002**, *55*, 565–576.

(18) Liao, Y.; DeBoer, P.; Meier, E.; Wikström, H. Synthesis and Pharmacological Evaluation of Triflate-Substituted Analogues of Clozapine: Identification of a Novel Atypical Neuroleptic *J. Med. Chem.* **1997**, *40*, 4146–4153.

(19) Lundgren, R. L.; Stradiotto, M. Palladium-Catalyzed Cross-Coupling of Aryl Chlorides and Tosylates with Hydrazine *Angew. Chem. Int. Ed.* **2010**, *122*, 8868–8872.

(20) Wolter, M.; Klapars, A.; Buchwald, S. L. Synthesis of N-Aryl Hydrazides by Copper-Catalyzed Coupling of Hydrazides with Aryl Iodides *Org. Lett.* **2001**, 3, 3803–3805.

(21) Barber, D. M.; Liu, S.-A.; Gottschling, K.; Sumser, M.; Hollmann, M.; Trauner, D.; Optical control of AMPA receptors using a photoswitchable quinoxaline-2,3-dione antagonist *Chem. Sci.* **2017**, *8*, 611–615.

(22) Lim, Y.-K.; Choi, S.; Park, K. B. Cho, C.-G. Synthesis of Novel 1,3,5-Tris(arylazo)benzenes via Pd-Catalyzed Couplings and Cu(I)-Mediated Direct Oxidations *J. Org. Chem.* **2004**, *69*, 2603–2606.

`

Experimental Details

General Methods Chemistry

All reactions were carried out under magnetic stirring and if air and/or moisture sensitive in flame-dried glass ware using standard *Schlenk* technique. Temperatures for reaction conditions were recorded as external bath temperature of heating blocks or heating baths. Low temperature reactions were carried out in a *Dewar* vessel using acetone/ dry ice (–78 °C), DI water/ NaCl (–10 °C), DI water/ ice (0 °C). When low temperatures were maintained for extended periods of time, a JULABO FT902 – Cryostat 9650892 with an isopropanol cooling bath was used.

High temperature reactions were conducted using metal heating blocks, silicon oil baths or sand baths. When reactions were heated to temperatures near boiling point, reflux condensers or pressure tubes were used.

Dry solvents were purchased as Acros Organics as Extra dry reagents over 4 Å molecular sieves or dried by passing the degassed solvents through activated alumina columns. Reagents were distilled according to standard procedures.

All reagents were purchased from commercial sources (ABCR, Acros Organics, Alfa Aesar, Ark Pharm, Combi-Blocks, Fisher Scientific, Oakwood, OxChem, Sigma Aldrich, Strem, TCI) and used without further purification unless otherwise noted.

Reactions were monitored using analytical thin layer chromatography (TLC) or liquid chromatography- mass spectrometry (LCMS) as specified below.

Analytical Thin Layer Chromatography (TLC) was performed on glass plates precoated with silica gel (0.25 mm, 60-Å pore size, Merck) and visualized under UV light at 254 nm/ 366 nm. Staining was performed with aqueous Ceric Ammonium Molybdate (IV) solution (CAM; 2.0 g $Ce(NH_4)_4(SO_4)_4 \cdot 2\ H_2O$, 48 g $(NH_4)_6Mo_7O_{24} \cdot 4\ H_2O$, 60 ml conc. sulfuric acid, 940 ml H_2O), or aqueous $KMnO_4$ solution (7.5 g $KMnO_4$, 50 g K_2CO_3, 6.25 ml aqueous 10% NaOH, 1000 ml H_2O) and subsequent heating using a heat gun (150–600 °C).

Liquid Chromatography-Mass Spectrometry (LCMS) was performed on an Agilent Technologies 1260 II Infinity system with an LC Kinetex column 2.6 µm C18 (50 x 3 mm) connected to an Agilent Technologies 6120 Quadrupole mass spectrometer with ESI ionization source.

Flash Column Chromatography was performed on Merck Silica Gerudan (60 Å pore size, 40–63 µm, Merck KGaA) and either performed manually with positive nitrogen or air pressure or using a Teledyne Isco Combiflash EZprep flash purification system.

High Pressure Liquid Chromatography (HPLC) was performed on a 260 Infinity Agilent Technologies system with a semipreparative column Phenomenex Gemini 5 µm C18 (150 x 10 mm) flowrate 8 ml/min and preparative column Phenomenex Gemini 5 µm C18 (150 x 30 mm) flowrate 72 ml/min; mobile phase gradients of acetonitrile in H_2O (each containing 0.1% formic acid unless otherwise specified); UV-Vis detection with a 0.3 mm preparative flow cell.

Nuclear Magnetic Resonance Spectra (NMR) were recorded on a Bruker Avance III HD 400 MHz spectrometer equipped with a CryoProbeTM (400 MHz for ^{1}H and 101 MHz for ^{13}C spectra), a Bruker Avance III 400 NMR Spectrometer (377 MHz for ^{19}F and 400 MHz for high temperature ^{1}H spectra) and a Bruker Avance 600 MHz spectrometer equipped with a CPTCI-cryoprobehead (600 MHz ^{1}H and 150 MHz ^{13}C spectra)
Chemical shift signals are reported as parts per million (ppm, δ scale) and referenced to the residual non deuterated solvent signals. NMR spectra were processed and analyzed using MestReNova (Mestrelab Research; Versions 11 and 14)

High-Resolution Mass Spectrometry (HRMS) was performed on an Agilent Technologies 6224 Accurate-Mass TOF/LC/MS spectrometer with electrospray ionization (ESI) or atmospheric pressure chemical ionization (APCI) ionization sources.

Infrared Spectroscopy (IR) was performed in a ThermoScientific Nicolet-6700 Fourier Transform Infrared Spectrometer (FTIR) and the absorption signals are reported in wavenumbers [cm^{-1}].

Optical Rotation was determined on a Jasco P-2000 Polarimeter using the Sodium-D-line (598 nm) at room temperature (T = 20 – 28 °C) and concentration (c in g/mol); path length l = 1 dm; HPLC grade solvents were used. Specific optical rotations were calculated following:

$$[\alpha]_D^T = \frac{\alpha}{c \cdot d} \frac{10^{-1} \cdot \mathrm{deg} \cdot \mathrm{cm}^2}{\mathrm{g}}$$

Optical properties can be influenced by the *cis*:*trans* ratio of azobenzene and diazocine photoswitches and are therefore not reported for photoswitch containing reaction products.

UV-Vis Spectra was performed using a Varian Cary 60 UV-Visible Spectrophotometer using disposable UV-cuvettes (BRAND UV-Cuvette Disposable Spectrophotometer/Photometer Cuvettes, BrandTech; Ultra-Micro Cuvettes Vol. 70 – 850 µl, window height 8.5 mm, pathlength 10 mm; VWR cat# 47743-834)). Sample temperatures were controlled using an Agilent Technologies PCB 1500 Water Peltier system and samples were irradiated orthogonally using a Cairn Research Optoscan Monochromator with Optosource High Intensity Arc Lamp with a 75 W UXL-S50A lamp from USHIO Inc. Japan (15 nm full width at half maximum) or prizmatix (U)HP-LEDs: 365 nm, 415 nm, 460 nm, 520 nm.
Thermal half-lives were determined by first order exponential decay fit using GraphPad Prism 9 for macOS (San Diego, CA, USA).

In-Situ NMR irradiation was achieved with HP and UHP LEDs connected to an optical fiber (with the last 7 cm stripped, last 5 cm sanded) that was inserted into the compound solution in DMSO-d_6 using a coaxial NMR insert.

All yields are isolated yields, unless otherwise specified.

Chemical Procedures for Part 1: 2 Latrunculin

Synthesis of Hex-5-enal:

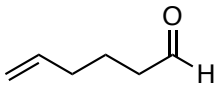

A flame-dried 500 ml *Schlenk* flask was equipped with a stir bar and charged with oxalyl chloride (10.4 ml, 121 mmol, 1.50 eq.) in DCM (90 ml). The solution was cooled to –78 °C and DMSO (17.0 ml, 240 mmol, 3.00 eq.) was added over 10 minutes. The reaction mixture was stirred for 10 min. before a solution of hex-5-enol (8.00 g, 79.9 mmol, 1.00 eq.) in DCM (15 ml) was added over 15 min. After 1.5 h, NEt_3 (33.3 ml, 240 mmol, 3.00 eq.) was added dropwise. Upon addition, the reaction was allowed to warm to 0 °C and water (150 ml) was added. The mixture was stirred for 45 min. at 0 °C, the layers were separated and the aqueous layer was extracted with DCM (2 x 150 ml). The combined organic layers were washed with LiCl (10% aq., 3 x 100 ml), dried over $MgSO_4$, filtered and concentrated (700 mbar, 35 °C water bath). Purification was performed by flash column chromatography (Pent:Et_2O = 10:0 to 9.5:0.5). Upon slow evaporation, residual solvent was removed by fractional distillation. The title compound was obtained as a colorless, volatile liquid (4.00 g, 40.8 mmol, 51%).

R_f (SiO_2, Pent:Et_2O = 9:1; $KMnO_4$) = 0.5

^{1}H-NMR (400 MHz, $CDCl_3$): δ [ppm] = 9.78 (d, J = 1.8 Hz, 1H), 5.77 (ddt, J = 16.9, 9.8, 6.7 Hz, 1H), 5.14 – 4.91 (m, 2H), 2.45 (t, J = 7.3 Hz, 2H), 2.10 (q, J = 7.2 Hz, 2H), 1.74 (p, J = 7.4 Hz, 2H).

^{13}C-NMR (101 MHz, $CDCl_3$): δ [ppm] = 202.7, 137.7, 115.7, 43.3, 33.1, 21.3.

The analytical data matched those previously reported.[1]

[1] Lininger, M.; Neuhaus, C.; Hofmann, T.; Fransioli-Ignazio, L.; Jordi, M.; Drueckes, P.; Trappe, J.; Fabbro, D.; Altmann, K.-H. *ACS Med. Chem. Lett.* **2011**, *2*, 22–27.

Synthesis of (R)-4-isopropylthiazolidine-2-thione:

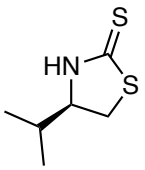

D-Valinol (10.6 g, 0.11 mol, 1.00 eq.) was dissolved in EtOH (30 ml) and CS_2 (15.7 ml, 262 mmol, 2.60 eq.) was added. A solution of KOH (15.3 g, 272 mmol, 2.70 eq.) in EtOH:H_2O (1:1, 120 ml) was added dropwise at room temperature and the reaction was then heated to 105 °C for 3 d. The reaction was cooled to room temperature and N_2 was lead through the solution for 1 h to remove volatile byproducts, which were quenched by passing through a sodium hypochloride solution. All volatiles were removed under reduced pressure and the residues were diluted with DCM (200 ml) and acidified with HCl (120 ml, 1.0 M) under cooling and vigorous stirring. The layers were separated, and the aqueous layer was extracted with dichloromethane (3 x 200 ml). The combined organic layers were washed with brine, dried over $MgSO_4$, filtered and concentrated. (*R*)-4-isopropylthiazolidine-2-thione was obtained as yellow solid (14.0 g, 86.8 mmol, 86%) and used without further purification.

R_f (SiO_2, Hex:EtOAc = 5:1, $KMnO_4$) = 0.3

^{1}H-NMR (400 MHz, $CDCl_3$): δ [ppm] = 8.28 (s, 1H), 4.05 (td, *J* = 8.2, 6.4 Hz, 1H), 3.49 (dd, *J* = 11.1, 8.3 Hz, 1H), 3.30 (dd, *J* = 11.1, 8.2 Hz, 1H), 1.97 (h, *J* = 6.7 Hz, 1H), 1.01 (d, *J* = 6.8 Hz, 3H), 0.98 (d, *J* = 6.8 Hz, 3H).

^{13}C-NMR (101 MHz, $CDCl_3$): δ [ppm] = 201.2, 70.2, 36.1, 32.1, 18.9, 18.4.

The analytical data matched those previously reported.[2]

[2] Kasun, Z. A.; Gao, X.; Lipinski, R. M.; Krische, M. J. *J. Am. Chem. Soc.* 2015, 137, 8900–8903.

Synthesis of Crimmins' Auxiliary (9):

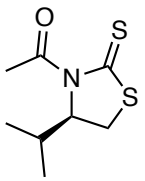

NaH (3.82 g, 95.5 mmol, 1.10 eq.) was dissolved in dry THF (45 ml), degassed and cooled to 0 °C. A solution of (*R*)-4-isopropylthiazolidine-2-thione (14.0 g, 86.8 mmol, 1.00 eq.) in THF (45 ml) was added slowly. After stirring for 20 min. at 0 °C, acetyl chloride (6.80 ml, 95.3 mmol, 1.10 eq.) was added dropwise to the reaction. After stirring at 0 °C for 20 min. the reaction mixture was allowed to warm to room temperature. Full consumption of the starting material was observed by TLC after 1 h. HCl (100 ml, 1 M) and Ethyl acetate (100 ml) were added. The layers were separated, and the aqueous layer was extracted with Ethyl acetate (2 x 100 ml). The combined organic layers were washed with brine, dried over $MgSO_4$ filtered and concentrated. After purification on flash column chromatography (SiO_2; Hex:EtOAc = 20:1 to 10:1) Crimmins' auxiliary was obtained as a yellow oil (14.6 g, 71.8 mmol, 83%).

R_f (SiO_2, Hex:EtOAc = 9:1; $KMnO_4$) = 0.5

^{1}H-NMR (400 MHz, $CDCl_3$): δ [ppm] = 5.15 (dd, *J* = 7.9, 6.3 Hz, 1H), 3.50 (dd, *J* = 11.5, 8.1 Hz, 1H), 3.02 (d, *J* = 11.3 Hz, 1H), 2.77 (s, 3H), 2.37 (h, *J* = 6.9 Hz, 1H), 1.06 (d, *J* = 6.8 Hz, 3H), 0.97 (d, *J* = 6.9 Hz, 3H).

^{13}C-NMR (100 MHz, $CDCl_3$): δ [ppm] = 203.4, 170.9, 71.4, 30.9, 30.5, 27.1, 19.2, 17.9.

HRMS (ESI$^+$, *m/z*): $[M+H]^+$ for $C_8H_{13}NOS_2^+$ calcd.: 203.0439, found: 203.0432.

IR (ATR): $\tilde{\nu}$ [cm^{-1}] = 2962 (w), 2874 (w), 1692 (s), 1467 (w), 1410 (w), 1363 (s), 1305 (m), 1271 (s), 1244 (s), 1201 (s), 1099 (m), 1072 (s), 1030 (s), 1008 (s), 973 (s), 922 (m), 898 (w), 884 (w), 855 (s), 802 (w), 778 (w), 755 (w).

$[\alpha]_D$ = –355 (*c* = 0.01, $CHCl_3$)
The analytical data matched those previously reported.[3]

[3] McNutley, J.; McLeod, D.; Jenkins, H. *A. Eur. J. Org. Chem.* **2016**, 688–692.

Synthesis of (R)-3-hydroxy-1-((R)-4-isopropyl-2-thioxothiazolidin-3-yl)oct-7-en-1-one (10):

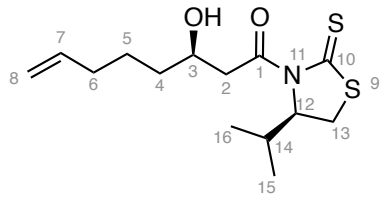

In a flame-dried *Schlenk* flask Crimmins" auxiliary (2.90 g, 14.3 mmol, 1.50 eq.) was dissolved in dry distilled DCM (75 ml), degassed and cooled to –50 °C. After keeping the starting material at –50 °C for 10 min., a solution of $TiCl_4$ in DCM (1.72 ml of a 1.0 M solution, 15.2 mmol, 1.60 eq.) was added dropwise and the reaction was stirred for 20 min. Then a solution of DIPEA (2.63 ml, 15.2 mmol, 1.60 eq.) in DCM (25 ml) was added dropwise and the reaction was warmed to –40 °C and stirred for 1 h. Next, the reaction was cooled to –78 °C and stirred for 10 min. Hex-5-enal (0.93 g, 9.51 mmol, 1.00 eq.) was added dropwise as a solution in DCM (24 ml) whereupon the reaction was warmed to –50 °C and stirred for 16 h. The reaction was quenched with pH = 7.5 phosphate buffer solution and after separation of the two layers, the aqueous layer was extracted with DCM (3 x 100 ml). The combined organic layers were washed with brine, dried over $MgSO_4$, filtered and evaporated. Purification by flash column chromatography (SiO_2, Hex:EtOAc = 20:1 to 5:5) furnished the title compound as a yellow oil (1.90 g, 6.31 mmol, 66%).

R_f (SiO_2, Hex:EtOAc = 7:3, $KMnO_4$) = 0.2

^{1}H-NMR (400 MHz, $CDCl_3$): δ [ppm] = 5.81 (ddt, *J* = 17.0, 10.2, 6.7 Hz, 1H, H-7), 5.16 (ddd, *J* = 7.6, 6.2, 1.1 Hz, 1H, H-12), 5.09 – 4.92 (m, 2H, H-8/8'), 4.13 (dddd, *J* = 9.8, 7.4, 4.6, 2.4 Hz, 1H, H-3), 3.64 (dd, *J* = 17.7, 2.4 Hz, 1H, H-2), 3.52 (dd, *J* = 11.5, 7.9 Hz, 1H, H-13), 3.12 (dd, *J* = 17.7, 9.4 Hz, 1H, H-2'), 3.03 (dd, *J* = 11.5, 1.1 Hz, 1H, H-13'), 2.51 (s_{br}, 1H, OH), 2.36 (dq, *J* = 13.6, 6.8 Hz, 1H, H-14), 2.09 (dt, *J* = 7.9, 6.5, 2H, H-6/6'), 1.66 – 1.39 (m, 4H, H-4/4'/5/5'), 1.07 (d, *J* = 6.9 Hz, 3H, H-15/16), 0.98 (d, *J* = 7.0 Hz, 3H, H-15/16).

^{13}C-NMR (100 MHz, $CDCl_3$): δ [ppm] = 203.2 (C-10), 173.4 (C-1), 138.7 (C-7), 114.9 (C-8), 71.5 (C-12), 68.0 (C-3), 45.7 (C-2), 35.9 (C-4), 33.7 (C-6), 31.0 (C-14), 30.7 (C-13), 25.0 (C-5), 19.2 (C-15/16), 18.0 (C-15/16).

HRMS (ESI$^+$, *m/z*): $[M+H]^+$ for $C_{14}H_{23}NO_2S_2^+$: calcd.: 302.1243, found: 302.1244.

IR (ATR): $\tilde{\nu}$ [cm^{-1}] = 3430 (w), 2963 (w), 1930 (w), 1684 (m), 1640 (w), 1468 (w), 1437 (w), 1391 (w), 1364 (m), 1305 (m), 1279 (m), 1256 (s), 1155 (s), 1122 (m), 1092 (s), 1037 (s), 990 (m), 910 (m), 883 (m), 752 (s), 722 (m).

$[\alpha]_D$ = –326 (*c* = 0.02, $CHCl_3$)

The analytical data matched those previously reported.[4]

Synthesis of (R)-3-((tert-butyldimethylsilyl)oxy)-1-((R)-4-isopropyl-2-thioxothiazolidin-3-yl)oct-7-en-1-one (11):

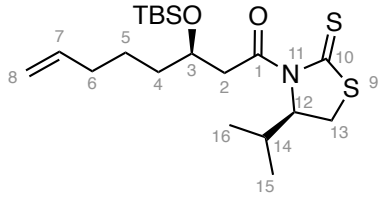

Aldol product 10 (3.07 g, 11.8 mmol, 1.00 eq.) was dissolved in dry DCM (62 ml) and cooled to –78 °C. 2,6-Lutidine (4.10 ml, 35.5 mmol, 3.00 eq.) and TBSOTf (4.10 ml, 17.8 mmol, 1.50 eq.) were added dropwise. The reaction was stirred at –78 °C for 1 h. Upon addition of sat. aq. NH_4Cl solution (60 ml) the reaction was let come to room temperature. The layers were separated and the aqueous layer was extracted with DCM (3 x 80 ml). The combined organic layers were washed with brine, dried over $MgSO_4$, filtered and evaporated. Purification by flash column chromatography (SiO_2; Hex:EtOAc = 30:1 to 10:1) furnished the title compound as yellow oil (4.00 g, 10.7 mmol, 90%).

$\mathbf{R_f}$ (SiO_2, Hex:EtOAc = 10:1) = 0.5

^{1}H-NMR (400 MHz, $CDCl_3$): δ [ppm] = 5.79 (ddt, *J* = 16.9, 10.2, 6.6 Hz, 1H, H-7), 5.08 – 4.92 (m, 2H, H-8/8'), 4.35 – 4.25 (m, 1H, H-3), 3.57 (dd, *J* = 17.0, 7.8 Hz, 1H, H-2), 3.47 (dd, *J* =

[4] Symkenberg, G.; Kalesse, M. *Angew. Chem. Int. Ed.* **2014**, *53*, 1795 –1798.

11.5, 7.8 Hz, 1H, H-13), 3.14 (dd, *J* = 17.0, 4.1 Hz, 1H, H-2'), 3.02 (dd, *J* = 11.5, 1.1 Hz, 1H, H-13'), 2.45 – 2.30 (m, *J* = 6.8 Hz, 1H, H-14), 2.10 – 1.98 (m, 2H, H6/6'), 1.56 – 1.39 (m, 4H, H-4/4'/5/5'), 1.06 (d, *J* = 6.8 Hz, 3H, H-15/16*), 0.97 (d, *J* = 7.0 Hz, 3H, H-15/16*), 0.85 (s, 9H, (H_{tBu}TBS)), 0.07 (s, 3H, (H_{Me}TBS)), 0.03 (s, 3H, (H_{Me}TBS)).

^{13}C-NMR (100 MHz, $CDCl_3$): δ [ppm] = 203.0 (C-10), 172.2 (C-1), 138.8 (C-7), 114.7 (C-8), 71.8 (C-12), 69.2 (C-3), 45.6, 37.2 (C-4), 33.9 (C-6), 31.0 (C-14), 30.9 (C-13), 26.0 (C_{tBu}TBS)0, 24.3 (C-5), 19.3 (C-15/16*), 18.2 ($C_{(q)tBu}$TBS), 18.0 (C-15/16*), –4.3 (C_{Me}TBS), –4.5 (C_{Me}TBS).

HRMS (ESI$^+$, *m/z*): $[M+H]^+$ for $C_{20}H_{38}NO_2S_2Si^+$: calcd.: 416.2108, found: 416.2113.

IR (ATR): $\tilde{\nu}$ [cm^{-1}] = 2928 (m), 2855 (w), 1696 (m), 1641 (w), 1471 (w), 1462 (w), 1391 (w), 1371 (m), 1306 (m), 1279 (m), 1254 (s), 1158 (s), 1123 (m), 1190 (s), 1038 (s), 1005 (m), 990 (m), 939 (m), 910 (m), 869 (m), 834 (s), 809 (s), 774 (s), 733 (m).

Synthesis of methyl (R)-3-((tert-butyldimethylsilyl)oxy)oct-7-enoate (12):

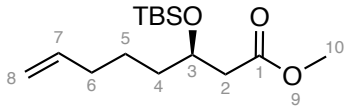

11 (6.49 g, 15.6 mmol, 1.00 eq.) was dissolved in MeOH (213 ml) and imidazole (14.3 g, 210 mmol, 13.5 eq.) was added. The reaction was stirred at room temperature over night and NH_4Cl (sat. aq., 100 ml) and ethyl acetate (100 ml) were added and the layers separated. The aqueous phase was extracted with ethyl acetate (3 x 100 ml) and the combined organic layers were washed with brine, dried over $MgSO_4$, filtered and concentrated. Purification by flash column chromatography (SiO_2, Hex:EtOAc = 40:1 to 10:1) gave methyl ester **12** as a pale-yellow oil (4.02 g, 14.0 mmol, 90%).

R_f (SiO_2, Hex:EtOAc = 20:1; $KMnO_4$) = 0.5

^{1}H-NMR (400 MHz, $CDCl_3$): δ [ppm] = 5.79 (ddt, *J* = 16.9, 10.1, 6.6 Hz, 1H, H-7), 5.04 – 4.92 (m, 2H, H-8/8'), 4.18 – 4.09 (m, 1H, H-3), 3.66 (s, 3H, H-10), 2.44 (dd, *J* = 6.3, 4.7 Hz, 2H, H-

2/2'), 2.05 (q, *J* = 6.5, 5.9 Hz, 2H, H-6/6'), 1.55 – 1.33 (m, 4H, H-4/4'/5/5'), 0.86 (s, 9H, H_{tBu}TBS), 0.06 (s, 3H, H_{Me}TBS), 0.03 (s, 3H, H_{Me}TBS).

^{13}C-NMR (100 MHz, $CDCl_3$): δ [ppm] = 172.4 (C-1), 138.8 (C-7), 114.8 (C-8), 69.4 (C-3), 51.6 (C-10), 42.7 (C-2), 37.1 (C-4), 33.8 (C-2), 25.9 (C_{tBu}TBS), 24.3 (C-5), 18.1 ($C(q)_{tBu}$TBS), -4.4 (C_{Me}TBS, -4.7 (C_{Me}TBS)

HRMS (ESI$^+$, *m/z*): $[M+H]^+$ for $C_{15}H_{31}O_3Si^+$: calcd.: 287.2037, found: 287.2040.

IR (ATR): $\tilde{\nu}$ [cm^{-1}] = 2929 (m), 2857 (w), 1740 (m), 1642 (w), 1473 (w), 1463 (w), 1437 (w), 1361 (w), 1252 (m). 1199 (m), 1168 (m), 1081 (m), 1033 (m), 1005 (m), 939 (w), 910 (m), 834 (s), 810 (m), 774 (s).

$[\alpha]_D$ = –14 (*c* = 0.01, $CHCl_3$)

Synthesis of (R)-3-((tert-butyldimethylsilyl)oxy)oct-7-enal (7):

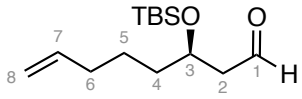

12 (4.01 g, 14.0 mmol, 1.00 eq.) was dissolved in dry DCM (212 ml) and cooled to –78 °C. DIBAL-H (25% in toluene, 18.8 ml, 28.0 mmol, 2.00 eq.) was added dropwise. The reaction as stirred for 2 h at –78 °C, before MeOH (80 ml) was added slowly and the reaction was stirred for another 30 min. Next, aqueous Rochelle's salt solution (200 ml) was added and the reaction was warmed to room temperature. The layers were separated and the aqueous phase was extracted with DCM (3 x 200 ml). The combined organic layers were washed with brine, dried over $MgSO_4$, filtered and concentrated. Purification of the crude product was performed by flash column chromatography (SiO_2, Hex:EtOAc = 30:1) and gave the title compound as a colorless oil (3.23 g, 12.6 mmol, 90%).

$\mathbf{R_f}$ (SiO_2, Hex:EtOAc = 30:1) = 0.26

^{1}H-NMR (400 MHz, $CDCl_3$): δ [ppm] = 9.81 (t, *J* = 2.5 Hz, 1H, H-1), 5.78 (ddt, *J* = 16.9, 10.2, 6.6 Hz, 1H, H-7), 5.05 – 4.93 (m, 2H, H-8/8'), 4.19 (p, *J* = 5.8 Hz, 1H, H-3), 2.52 (dd, *J* = 5.8, 2.5 Hz, 2H, H2/2'), 2.05 (q, *J* = 6.9 Hz, 2H, H-6/6'), 1.62 – 1.36 (m, 4H, H-4/4'/5/5'), 0.87 (s, 9H, H_{tBu}TBS), 0.07 (s, 3H, H_{Me}TBS), 0.05 (s, 1H, H_{Me}TBS).

^{13}C-NMR (101 MHz, $CDCl_3$): δ [ppm] = 202.5 (C-1), 138.6 (C-7), 114.9 (C-8), 68.2 (C-3), 51.0 (C-2), 37.3 (C-4), 33.7 (C-6), 25.9 (C_{tBu}TBS) , 24.5 (C-5), 18.1 ($C_{(q)tBu}$TBS), -4.3 (C_{Me}TBS), -4.6 (C_{Me}TBS).

HRMS (ESI$^+$, *m/z*): $[M+H]^+$ for $C_{14}H_{28}O_2Si^+$: calcd.: 257.1931, found: 257.1934.

IR (ATR): $\tilde{\nu}$ [cm^{-1}] = 2929 (m), 2857 (w), 1710 (m), 1642 (w), 1473 (w), 1463 (w), 1411 (w), 1361 (w), 1298 (w), 1252 (m), 1083 (m), 1005 (m), 939 (m), 910 (m), 834 (s), 809 (m), 773 (s).

$[\alpha]_D$ = +1 (*c* = 0.01, $CHCl_3$)

Synthesis of ethyl (R)-2-oxothiazolidine-4-carboxylate (13):

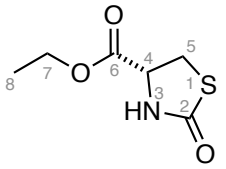

Ethyl L-cysteinate hydrochloride (5.93 g, 31.9 mmol, 1.00 eq.) was dissolved in dry THF (100 ml) and degassed/ backfilled with N_2. CDI (5.70 g, 35.1 mmol, 1.10 eq.) was added in portions at r.t. and the reaction was stirred for 16 h. The reaction mixture was filtered over a plug of celite, rinsed with THF and concentrated under reduced pressure. Purification by flash column chromatography (SiO_2; Hex:acetone = 9:1 to 7:3) gave the title compound as a pale yellow oil (4.48 g, 25.6 mmol, 80%).

R_f (SiO_2, Hex:acetone = 6:2; $KMnO_4$) = 0.2

^{1}H-NMR (400 MHz, $CDCl_3$): δ [ppm] = 6.04 (s, 1H, H-3), 4.42 (ddd, J = 8.0, 5.5, 1.0 Hz, 1H, H-4), 4.28 (q, J = 7.1 Hz, 2H, H-7/7'), 3.74 – 3.59 (m, 2H, H-5/5'), 1.31 (d, J = 7.2 Hz, 3H, H-8).

^{13}C-NMR (100 MHz, $CDCl_3$): δ [ppm] = 174.4 (C-2), 170.0 (C-6), 62.6 (C-7), 56.1 (C-4), 31.9 (C-5), 14.3 (C-8).

HRMS (ESI$^+$, *m/z*): $[M+H]^+$ for $C_6H_{10}NO_3S^+$: calcd.: 176.0376, found: 176.0374.

The analytical data were in agreement with the literature.[5]

Synthesis of ethyl (*R*)-2-oxothiazolidine-4-carboxylate (14):

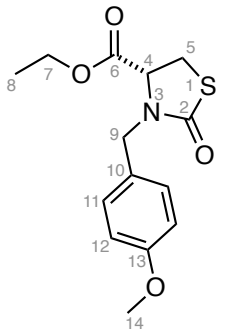

PMBCl (7.40 ml, 52.1 mmol, 120 eq.) was added dropwise to a suspension of **13** (7.60 g, 43.4 mmol, 1.00 eq.), K_2CO_3 (8.99 g, 65.1 mmol, 1.50 eq.) and NaI (1.95 g, 13.0 mmol, 0.30 eq.) in DMF (115 ml) at r.t. After 10 h, more PMBCl (2.17 ml, 15.4 mmol, 0.70 eq.) was added and the reaction stirred for another 12 h. The reaction was diluted with Ethyl acetate (40 ml) and water (60 ml), the layers were separated, and the aqueous layer was extracted with EtOAc (2 x 50 ml). The combined organic layers were washed with LiCl (10% aq., 3 x 100 ml) and brine, dried over $MgSO_4$, filtered and concentrated. The crude mixture was purified by flash column chromatography (SiO_2, Hex:EtOAc = 9:1 to 7:3) and the title compound was obtained as a pale-yellow oil (4.12 g, 13.9 mmol, 61%).

[5] Fürstner, A.; De Souza, D.; Turet, L.; Fenster, M. D. B.; Parra-Rapado, L.; Wirtz, C.; Mynott, R.; Lehmann C.W. *Chem. Eur. J.* **2007**, *13*, 115 – 134.

R_f (SiO_2, Hex:EtOAc = 7:3, $KMnO_4$) = 0.34

^{1}H-NMR (400 MHz, $CDCl_3$): δ [ppm] = 7.15 (d, *J* = 8.3 Hz, 2H, H-11/11'), 6.86 (d, *J* = 8.4 Hz, 2H, H12/12'), 5.08 (d, *J* = 14.8 Hz, 1H, H-9), 4.24 (q, *J* = 7.2 Hz, 1H, H-7/7'), 4.15 – 4.05 (m, 1H, H-4), 3.99 (d, *J* = 14.8 Hz, 1H, H-9'), 3.80 (s, 3H, H-14), 3.47 (dd, *J* = 11.4, 8.5 Hz, 1H, H-5), 3.33 (dd, *J* = 11.4, 3.1 Hz, 1H, H-5'), 1.30 (t, *J* = 7.1 Hz, 3H, H-8).

^{13}C-NMR (100 MHz, $CDCl_3$): δ [ppm] = 171.7 (C-2), 170.1 (C-6), 159.5 (C-13), 129.9 (C-11/11'), 127.7 (C-10), 114.4 (C-12/12'), 62.3 (C-7), 59.4 (C-4), 55.4 (C-14), 47.4 (C-9), 29.2 (C-5), 14.3 (C-8).

HRMS (ESI$^+$, *m/z*): $[M+Na]^+$ for $C_{13}H_{15}NO_3SNa^+$: calcd.: 288.0665, found: 288.0678.

IR (ATR): $\tilde{\nu}$ [cm^{-1}] = 3460 (w), 2936 (w), 2836 (w), 1739 (m), 1739 (m) 1673 (s), 1611 (m), 1585 (w), 1512 (s), 1442 (m), 1390 (m), 1302 (m), 1244 (s), 1210 (s), 1172 (s), 1110 (m), 1027 (s), 814 (m). 760 (m), 724 (m).

Synthesis of (*R*)-N-methoxy-3-(4-methoxybenzyl)-*N*-methyl-2-oxothiazolidine-4-carboxamide (15):

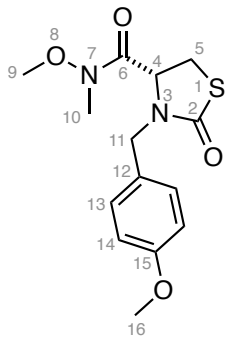

Ethyl (*R*)-2-oxothiazolidine-4-carboxylate (9.69 g, 32.8 mmol, 1.00 eq.) was dissolved in dioxane (54 ml) and a solution of KOH (5.52 g, 98.4 mmol, 3.00 eq.) in H_2O (36 ml) was added. After 1.5 h, the reaction was diluted with diethyl ether (50 ml) and the pH was adjusted to 2 with aq. HCl (aq., 1 M). The layers were separated and the aqueous phase was extracted with Et_2O (3 x 50 ml). The combined organic layers were washed with brine, dried over

$MgSO_4$, filtered and concentrated. The carboxylic acid was used crude and therefore redissolved in dry acetonitrile (129 ml) and degassed. EDCI (9.43 g,49.2 mmol, 1.50 eq.) and MeNH(OMe) · HCl (3.84 g, 39.4 mmol, 1.20 eq.) were added at r.t. and the reaction was stirred for 14 h. Water (100 ml) and ethyl acetate (100 ml) were added. The layers were separated and the aqueous layer was extracted with ethyl acetate (3 x 100 ml). The combined organic layers were washed with brine, dried over $MgSO_4$, filtered and concentrated. The colorless oil was purified by flash column chromatography (SiO_2, Hex:acetone = 8:2 to 7:3) furnishing the title compound (6.90 g, 22.2 mmol, 68% over 2 steps) as a colorless oil.

R_f (SiO_2, Hex:acetone = 7:3; $KMnO_4$) = 0.7

^{1}H-NMR (400 MHz, $CDCl_3$): δ [ppm] = 7.21 – 7.12 (m, 2H, H-13/17), 6.93 – 6.79 (m, 2H, H-14/16), 5.14 (d, *J* = 14.7 Hz, 1H, H-11), 4.40 (dd, *J* = 8.9, 5.2 Hz, 1H, H-4), 3.85 (d, *J* = 14.7 Hz, 1H, H-11), 3.79 (s, 3H, H-18), 3.53 – 3.41 (m, 1H, H-5), 3.38 (s, 3H, H-9), 3.21 (s, 3H, H-10), 3.15 (dd, *J* = 11.2, 5.0 Hz, 1H, H-5').

^{13}C-NMR (100 MHz, $CDCl_3$): δ [ppm] = 172.4 (C-2), 169.4 (C-6), 159.5 (C-15), 130.2 (C-13/13'), 127.8 (C-12), 114.3 (C-14/14'), 61.4 (C-9), 57.6 (C-4), 55.5 (C-18), 47.1 (C-11), 32.7 (C-10), 28.2 (C-5).

HRMS (ESI$^+$, *m/z*): $[M+Na]^+$ for $C_{14}H_{18}N_2O_4SNa^+$: calcd.: 333.0879, found: 333.0878.

IR (ATR): $\tilde{\nu}$ [cm^{-1}] = 2937 (w), 2836 (w), 1669 (s), 1611 (m), 1585 (w), 1512 (s), 1441 (m), 1392 (m), 1326 (w), 1302 (m), 1245 (s), 1173 (s), 1110 (m), 1029 (m), 996 (m), 955 (m), 887 (w), 834 (m), 812 (m), 752 (m).

Synthesis of (*R*)-4-acetyl-3-(4-methoxybenzyl)thiazolidin-2-one (8):

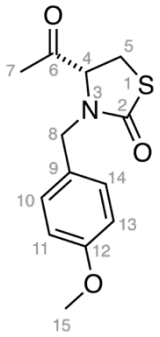

Weinreb amide **15** (6.84 g, 22.0 mmol, 1.00 eq.) was dissolved in dry distilled THF (90 ml) and cooled to 0 °C. A solution of MeMgBr (29.4 ml, 88.2 mmol, 4.00 eq.; 3.0 M in Et_2O) was added dropwise and the reaction was stirred at 0 °C for 2 h. NH_4Cl (sat. aq., 60 ml) at 0 °C. The reaction was warmed to room temperature and diluted with H_2O (60 ml) and EtOAc (100 mL). The layers were separated and the organic layer was extracted with ethyl acetate (3 x 100 ml). The combined organic layers were washed with brine, dried over $MgSO_4$, filtered and concentrated. The title compound was obtained as an off-white solid (5.60 g, 21.1 mmol, 96%) and used without further purification.

R_f (SiO_2, Hex:acetone = 7:3; $KMnO_4$) = 0.6

^{1}H-NMR (400 MHz, $CDCl_3$): δ [ppm] = 7.13 (d, J = 8.2 Hz, 2H, H-10/14), 6.89 – 6.82 (m, 2H, C-11/13), 5.02 (d, J = 14.6 Hz, 1H, H-11), 4.09 (dd, J = 9.4, 3.9 Hz, 1H, H-4), 3.91 (d, J = 14.7 Hz, 1H, H-11'), 3.80 (s, 3H, H-15), 3.50 (dd, J = 11.5, 9.4 Hz, 1H, H-5), 3.11 (dd, J = 11.5, 4.0 Hz, 1H, H-5'), 2.14 (s, 3H, H-7).

^{13}C-NMR (100 MHz, $CDCl_3$): δ [ppm] = 204.9 (C-2), 171.8 (C-6), 159.7 (C-12), 130.1 (C-10/14), 127.3 (C-9), 114.5 (C-11/13), 65.7 (C-4), 55.5 (C-15), 47.7 (C-8), 27.9 (C-5), 26.4 (C-7).

IR (ATR): $\tilde{\nu}$ [cm^{-1}] = 3013 (w), 2911 (w), 2842 (w), 1719 (m), 1658 (s), 1612 (m), 1585 (w), 1512 (s), 1463 (w), 1439 (m), 1393 (m), 1356 (m), 1309 (w), 1285 (m), 1240 (s), 1202 (m), 1185 (s), 1176 (s), 1161 (s), 1151 (s), 1110 (m), 1028 (s). 1012 (m), 997 (s), 942 (m), 902 (m), 839 (m), 825 (m), 812 (s), 799 (m), 763 (m), 707 (m).

$[\alpha]_D$ = –48 (c = 0.01, EtOH)

The analytical data matched those previously reported.[6]

Synthesis of (4R)-4-((5R)-5-((tert-butyldimethylsilyl)oxy)-3-hydroxydec-9-enoyl)-3-(4-methoxybenzyl)thiazolidin-2-one (16):

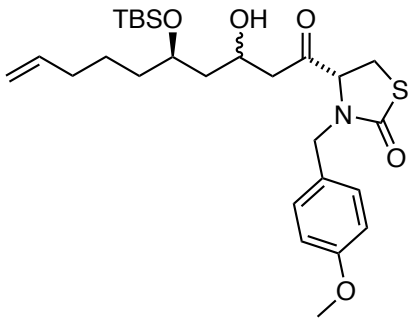

Thoazolidinone **8** (1.00 g, 3.77 mmol, 1.00 eq.) was dissolved in dry DCM (75 ml) and cooled to –78 °C. A solution of $TiCl_4$ (0.44 ml, 3.96 mmol, 1.05 eq.) in dry DCM (4 ml) was added dropwise over 10 minutes and the reaction was stirred for 10 minutes. Next, a solution of dry DIPEA (1.2 mL, 6.78 mmol, 1.80 eq.) in dry DCM (7mL) was added dropwise over 30 minutes. The reaction was stirred at –78 °C for 1 h and then at 0 °C for 2 h, before being cooled to –60 °C. A solution of aldehyde **7** (1.43 g, 5.58 mmol, 1.48 eq.) in dry DCM (7 mL) was added slowly over 1 h. The reaction was stirred at –60 °C for 16 h. NH_4Cl (sat. aq., 100 ml) was added at –60 °C and the reaction was warmed to room temperature. The layers were separated, and the aqueous layer was extracted with DCM (2 x 100 mL). The combined organic layers were washed with brine, dried over $MgSO_4$, filtered and concentrated. Purification by flash column chromatography (SiO_2, Hex:EtOAc, 9.5:0.5 to 7:3) furnished the title compound as a light-brown oil (1.70 g, 3.25 mmol, 86% ,*d.r.* = 1:1.3 (NMR, see appendix))

$\mathbf{R_f}$ (SiO_2, Hex:EtOAc = 7:3; CAM) = 0.3

[6] Fürstner, A.; De Souza, D.; Turet, L.; Fenster, M. D. B.; Parra-Rapado, L.; Wirtz, C.; Mynott, R.; Lehmann C.W. *Chem. Eur. J.* **2007**, *13*, 115 – 134.

Synthesis of (*R*)-4-((2*R*,4*R*,6*R*)-2,4-dihydroxy-6-(pent-4-en-1-yl)tetrahydro-2H-pyran-2-yl)-3-(4-methoxybenzyl)thiazolidin-2-one ((*R*)-17) and (*R*)-4-((2*R*,4*S*,6*R*)-2,4-dihydroxy-6-(pent-4-en-1-yl)tetrahydro-2H-pyran-2-yl)-3-(4-methoxybenzyl)thiazolidin-2-one ((*S*)-17):

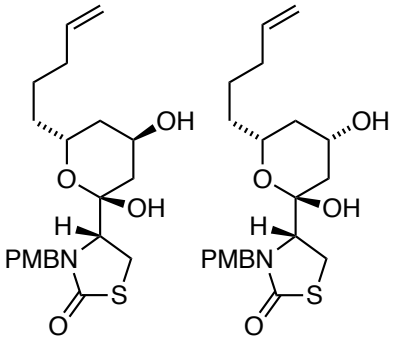

Aldol Product **16** (1.69 g, 3.25 mmol, 1.0 eq.) was dissolved in THF (38.5 ml) and HCl (2 M, 3.86 ml, 7.71 mmol, 2.38 eq.) was added at room temperature. The reaction was stirred for 16 h until full consumption of the starting material was observed by TLC. $NaHCO_3$ (sat. aq., 50 ml) and DCM (50 ml) were added. The layers were separated, and the aqueous phase was extracted with DCM (2 x 50 ml). the combined organic layers were washed with brine, dried over $MgSO_4$, filtered and concentrated. The diastereomeric products were separated by flash column chromatography (SiO_2, Hex:EtOAc = 6:4 to 3:7) and (*R*)-**17** was isolated as a white solid (459 mg, 1.13 mmol, 35%) and (*S*)-**17** was isolated a white foam (632 mg, 1.55 mmol, 48%).

Diastereomer (*R*)-**17:**

R_f (SiO_2, Hex:EtOAc = 5:5) = 0.34

^{1}H-NMR (400 MHz, $CDCl_3$): δ [ppm] = 7.24 – 7.16 (m, 2H), 6.88 – 6.81 (m, 2H), 5.92 – 5.75 (m, 1H), 5.24 (s, 1H), 5.13 – 4.93 (m, 3H), 4.49 – 4.44 (m, 1H), 4.34 (d, J = 14.4 Hz, 1H), 4.29 – 4.16 (m, 1H), 3.80 (s, 3H), 3.64 – 3.56 (m, 1H), 3.42 – 3.28 (m, 2H), 2.34 (s_{br}, 1H), 2.20 – 2.02 (m, 3H), 1.90 – 1.74 (m, 2H), 1.68 – 1.42 (m, 4H).

^{13}C-NMR (101 MHz, $CDCl_3$): δ [ppm] = 173.2, 159.3, 138.7, 130.0, 130.0, 129.1, 115.0, 114.2, 100.6, 66.0, 64.8, 63.3, 55.4, 47.8, 37.9, 35.6, 33.8, 33.2, 27.1, 24.9.

Diastereomer (*S*)-**17:**

R_f (SiO_2, Hex:EtOAc = 5:5) = 0.13

^{1}H-NMR (400 MHz, $CDCl_3$): δ [ppm] = 7.22 – 7.11 (m, 2H), 6.90 – 6.81 (m, 2H), 5.90 – 5.75 (m, 1H), 5.15 (d, *J* = 14.5 Hz, 1H), 5.09 – 4.95 (m, 2H), 4.27 (d, *J* = 14.5 Hz, 1H), 4.21 – 4.07 (m, 1H), 3.98 – 3.84 (m, 1H), 3.80 (s, 3H), 3.56 – 3.48 (m, 1H), 3.42 – 3.22 (m, 2H), 2.31 – 2.22 (m, 1H), 2.17 (s, 1H), 2.16 – 2.07 (m, 2H), 2.06 – 1.99 (m, 1H), 1.91 (s_{br}, 1H), 1.69 – 1.39 (m, 4H), 1.27 – 1.14 (m, 1H).

^{13}C-NMR (101 MHz, $CDCl_3$): δ [ppm] = 173.0, 159.3, 138.5, 129.8, 128.8, 115.1, 114.2, 101.1, 70.1, 64.8, 64.3, 55.4, 47.8, 40.8, 37.2, 35.6, 33.8, 31.1, 26.7, 25.1.

Synthesis of (R)-4-((2R,4R,6R)-4-hydroxy-2-methoxy-6-(pent-4-en-1-yl)tetrahydro-2H-pyran-2-yl)-3-(4-methoxybenzyl)thiazolidin-2-one ((*R*)-20):

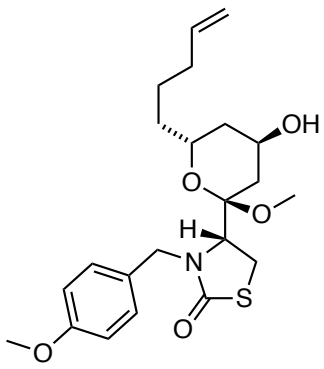

(*R*)-**17** (0.37 g, 0.90 mmol, 1.00 eq.) was dissolved in MeOH (18 ml) and (+)-CSA (53.3 mg, 0.23 mmol, 0.26 eq.) was added. The reaction was stirred at r.t. for 16 h and $NaHCO_3$ (aq. sat., 30 ml) and EtOAc (50 ml) were added. The phases were separated and the aqueous phase was extracted with EtOAc (2 x 30 ml). The combined organic layers were washed with brine, dried over Na_2SO_4, filtered and concentrated. Purification by flash column chromatography (SiO_2, Hex:EtOAc = 9.5:0.5 to 5:5) furnished the title compound as a colorless solid (304 mg, 0.72 mmol, 80%).

R_f (SiO_2, Hex:EtOAc = 4:6; CAM) = 0.33

^{1}H-NMR (400 MHz, $CDCl_3$): δ [ppm] = 7.19 (d, J = 8.6 Hz, 2H), 6.85 (d, J = 8.6 Hz, 2H), 5.92 – 5.78 (m, 1H), 5.12 – 4.98 (m, 3H), 4.21 (d, J = 14.4 Hz, 1H), 4.18 – 4.12 (m, 1H), 3.98 – 3.89 (m, 1H), 3.80 (s, 3H), 3.79 – 3.75 (m, 1H), 3.68 (d, J = 9.4 Hz, 1H), 3.31 – 3.21 (m, 2H), 3.16 (s, 3H), 2.21 – 2.11 (m, 2H), 2.11 – 2.04 (m, 1H), 1.90 – 1.79 (m, 2H), 1.79 – 1.39 (m, 5H).

^{13}C-NMR (101 MHz, $CDCl_3$): δ [ppm] = 172.9, 159.3, 138.4, 129.9, 128.7, 115.1, 114.2, 103.7, 66.3, 64.2, 59.0, 55.4, 47.8, 47.3, 37.9, 35.7, 33.9, 32.4, 25.4, 25.2.

IR (ATR): $\tilde{\nu}$ [cm^{-1}] = 3426 (w), 2938 (w), 1668 (s), 1612 (m), 1586 (w), 1512 (s), 1442 (w), 1403 (m), 1361 (w), 1303 (w), 1286 (w), 1247 (s), 1216 (m), 1199 (m), 1174 (m), 1120 (m), 1109 (m), 1074 (w), 1032 (s), 990 (m), 939 (w), 915 (m), 847 (w), 822 (w), 758 (w), 722 (w).

$[\alpha]_D$ = +34 (c = 0.01, $CHCl_3$)

Synthesis of (R)-4-((2R,4S,6R)-4-hydroxy-2-methoxy-6-(pent-4-en-1-yl)tetrahydro-2H-pyran-2-yl)-3-(4-methoxybenzyl)thiazolidin-2-one ((*S*)-20):

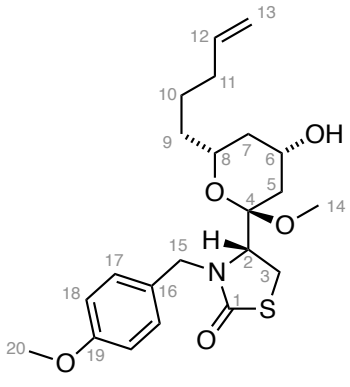

(*S*)-**17** (0.56 g, 1.47 mmol, 1.00 eq.) was dissolved in MeOH (29 mL) and (+)-CSA (87.2 mg, 0.38 mmol, 0.26 eq.) was added. The reaction was stirred at r.t. for 16 h and $NaHCO_3$ (aq. sat., 30 mL) and EtOAc (50 mL) were added. The phases were separated and the aqueous layer was extracted with EtOAc (2 x 30 mL). The combined organic layers were washed with brine, dried over Na_2SO_4, filtered and concentrated. Purification by flash column

chromatography (SiO_2, Hex:EtOAc = 9.5:0.5 to 5:5) furnished the title compound as a colorless foam (0.58 g, 1.37 mmol, 94%).

R_f (SiO_2, Hex:EtOAc = 4:6; CAM) = 0.29

^{1}H-NMR (400 MHz, $CDCl_3$): δ [ppm] = 7.24 – 7.16 (m, 2H, H-17/17'), 6.92 – 6.77 (m, 2H, 18/18'), 5.85 (ddt, *J* = 16.9, 10.2, 6.7 Hz, 1H. H-12), 5.11 (d, J = 14.4 Hz, 1H, H-15), 5.09 – 4.96 (m, 2H, 13/13'), 4.23 (d, *J* = 14.4 Hz, 1H), 4.11 – 4.01 (m, 1H, H-8), 3.84 (dd, *J* = 8.5, 3.5 Hz, 1H, H-2), 3.80 (s, 3H, H-20), 3.63 – 3.55 (m, 1H, H-6), 3.31 – 3.21 (m, 2H, H-3/3'), 3.06 (s, 3H, H-14), 2.22 (ddd, *J* = 12.6, 4.8, 1.8 Hz, 1H, H-5), 2.18 – 2.11 (m, 1H, 11/11'), 2.03 – 1.96 (m, 1H, H-7), 1.75 – 1.44 (m, 5H, H-5'/9/9'/10/10'/), 1.24 – 1.14 (m, 1H, H-7').

^{13}C-NMR (100 MHz, $CDCl_3$): δ [ppm] = 172.9 (C-1), 159.3 (C-19), 138.5 (C-12), 130.0 (C-17/17'), 128.9 (C-16), 115.1 (C-13), 114.1 (C-18/18'), 103.2 (C-4), 70.3 (C-6), 64.8 (C-8), 58.9 (C-2), 55.4 (C-20), 47.6 (C-14), 47.3 (C-15), 40.6 (C-7), 37.2 (C-5), 35.7 (C-9), 33.9 (C-11), 25. 5 (C-3), 25.3 (C-10).

HRMS (ESI$^+$, *m/z*): $[(M+Na)^+]$ for $C_{33}H_{31}NO_5SNa^+$: calcd.: 444.1815, found: 444.1813.

$[(M+H)^+]$ for $C_{33}H_{32}NO_5S^+$: calcd.: 422.1996, found: 422.1994.

IR (ATR): $\tilde{\nu}$ [cm^{-1}] = 3531 (w), 2920 (m), 1850 (w), 1672 (s), 1611 (w), 1586 (w), 1513 (s), 1441 (w), 1403 (w), 1363 (w), 1303 (w), 1288 (w), 1248 (m), 1215 (m), 1197 (m), 1175 (m), 1091 (m), 1030 (m), 938 (w), 907 (w), 847 (w), 821 (w), 760 (w), 728 (w).

$[\alpha]_D$ = +37 (*c* = 0.01, $CHCl_3$)

Synthesis of (R)-4-((2R,4S,6R)-4-hydroxy-2-methoxy-6-(pent-4-en-1-yl)tetrahydro-2H-pyran-2-yl)thiazolidin-2-one (37):

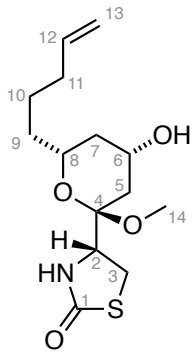

(*S*)-**20** (72.0 mg, 0.17 mmol, 1.00 eq.) was dissolved in MeOH (28 mL) and MeCN (5.5 ml) and CAN (0.49 g, 0.85 mmol, 8.00 eq.) was added in one portion. The reaction was stirred for 16 h under nitrogen. $NaHCO_3$ (sat. aq., 30 ml), H_2O (30 mL) and EtOAc (50 ml) were added, and the layers separated. The aqueous phase was extracted with EtOAc (2 x 50 mL). the combined organic layers were washed with brine, dried over Na_2SO_4, filtered and concentrated. Purification by flash column chromatography (SiO_2, Hex:EtOAc 7:3 to 9:1) furnished the title compound as a colorless solid (32.6 mg, 0.11 mmol, 63%, 85% brsm*.).
**The reaction stalled after 16 h and was therefore stopped, and the residual starting material was reisolated.*

R_f (SiO_2, Hex:EtOAc = 3:7; CAM) = 0.28

^{1}H NMR (400 MHz, CDCl3): δ [ppm] = 6.13 (s, 1H, NH), 5.80 (ddt, *J* = 16.9, 10.1, 6.6 Hz, 1H, H-12), 5.02 (d, *J* = 17.0 Hz, 1H, H-13), 4.98 (d, *J* = 10.5 Hz, 1H , H-13'), 4.17 – 4.09 (m, 1H, H-2), 4.08 – 3.96 (m, 1H, H-8), 3.58 – 3.49 (m, 1H, H-6), 3.44 – 3.27 (m, 2H, H-3/3'), 3.17 (s, 3H, H-14), 2.24 (s, 1H, OH), 2.12 – 2.00 (m, 3H, H-11/11'/5), 1.94 (ddd, *J* = 12.5, 4.3, 2.0 Hz, 1H, H-9), 1.66 – 1.33 (m, 5H, H-5'/9/9'/10/10'), 1.15 (q, *J* = 11.7 Hz, 1H, H-9').

^{13}C-NMR (101 MHz, $CDCl_3$): δ [ppm] = 175.1 (C-1), 138.6 (C-12), 114.9 (C-13), 101.6 (C-2), 70.2 (C-6), 64.8 (C-8), 56.6 (C-4), 47.9 (C-14), 40.5 (C-7), 36.2 (C-5), 35.1 (C-9), 33.8 (C-11), 28.1 (C-3), 25.0 (C-10).

HRMS (ESI$^+$, *m/z*): [(M+Na)$^+$] for $NaC_{14}H_{23}NO_4S^+$: calcd.: 324.1240, found: 324.1237.

IR (ATR): $\tilde{\nu}$ [cm^{-1}] = 3221 (w), 2933 (w), 1674 (s), 1455 (w), 1365 (w), 1227 (w), 1138 (m), 1105 (m), 1029 (s), 955 (w), 909 (w), 852 (w), 720 (w).

$[\alpha]_D$ = +106 (*c* = 0.01, $CHCl_3$)

Synthesis of (2R,4R,6R)-2-methoxy-2-((R)-3-(4-methoxybenzyl)-2-oxothiazolidin-4-yl)-6-(pent-4-en-1-yl)tetrahydro-2H-pyran-4-yl (Z)-3-methylhepta-2,6-dienoate (23):

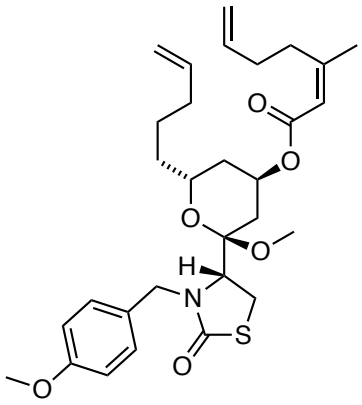

(*S*)-**20** (200 mg, 0.47 mmol, 1.00 eq.) was dissolved in dry DCM (10.0 ml) and pyridine (0.08 ml, 0.95 mmol, 2.00 eq.) was added dropwise. The reaction mixture was cooled to –78 °C and Tf_2O (1.68 ml, 0.57 mmol, 1.20 eq. in dry DCM (8.32 ml; 1.0 M) was added dropwise. The reaction was stirred at –30 to –50 °C for 2 h, until full conversion was observed by TLC, and turned yellow. The cold reaction mixture was poured into ice-cold 10% $KHSO_4$ solution (aq., 100 ml) and extracted with DCM (3 x 100 ml). the combined organic layers were washed with brine, dried over Na_2SO_4, filtered, concentrated (rotavap bath at r.t.) and dried under HV for at least 5 minutes.

In parallel, carboxylic acid **22**[7] (199 mg, 1.42 mmol, 3.00 eq.) was dissolved in dry THF (20 ml) and NaH (55.0 mg, 1.38 mmol, 2.90 eq.) was added as a suspension in THF (5 ml). The reaction mixture was heated to 55 °C for 1 h and cooled to 0 °C. The crude triflate was dissolved in dry THF (12 ml) and added dropwise, followed by the dropwise addition of [15]crown[5] until the reaction appeared clear (ca. 1.4 ml). The reaction was stirred at 0 °C for 1 h, then at r.t. for 18 h. $NaHCO_3$ (sat. aq., 50 ml) and EtOAc (50 ml) were added and phases

[7] Prepared according to She; J., Lampe; J. W., Polianski; A. B., Watson, P. S. *Tet. Lett.* **2009**, *50*, 298-301.

were separated. The aqueous layer was extracted with EtOAc (2 x 50 ml) and the combined organic layers were washed with brine, dried over Na_2SO_4, filtered and concentrated. The crude product was purified by flash column chromatography (SiO_2, Hex:Et_2O = 9:1 to 7:3) and the title compound was obtained as colorless oil (235 mg, 0.43 mmol, 91%).
*Note: yield varied between 30 and 91%.

R_f (triflate **21**) (SiO_2, Hex:EtOAc = 9:1) = 0.18

R_f (product **23**) (SiO_2, Hex:EtOAc = 9:1) = 0.15

LCMS: (MeCN/H_2O, 0.1% FA: gradient 50-100% MeCN): t_{ret} = 4.672 min.

1H-NMR (400 MHz, $CDCl_3$): δ = 7.20 (d, *J* = 8.6 Hz, 1H), 6.85 (d, *J* = 8.5 Hz, 1H), 5.84 (ddtd, *J* = 17.0, 10.9, 6.7, 4.6 Hz, 1H), 5.69 (d, *J* = 1.5 Hz, 1H), 5.19 (dd, *J* = 4.5, 2.5 Hz, 0H), 5.15 – 4.89 (m, 3H), 4.26 (d, *J* = 14.4 Hz, 0H), 3.97 – 3.86 (m, 0H), 3.80 (s, 1H), 3.80 – 3.78 (m, 0H), 3.25 – 3.20 (m, 1H), 3.10 (s, 1H), 2.73 (t, *J* = 7.8 Hz, 1H), 2.28 – 2.19 (m, 1H), 2.19 – 2.12 (m, 1H), 2.09 (dt, *J* = 15.2, 3.8, 2.0 Hz, 1H), 1.92 (dd, *J* = 11.4, 3.9 Hz, 1H), 1.89 (d, *J* = 1.3 Hz, 1H), 1.81 (dq, *J* = 16.5, 2.2 Hz, 1H), 1.77 – 1.44 (m, 2H).

13C-NMR (101 MHz, $CDCl_3$): *δ* [ppm] = 173.1, 165.8, 159.4, 159.1, 138.4, 137.9, 129.8, 129.7, 128.8, 117.1, 115.0, 114.9, 114.0, 114.0, 101.6, 66.1, 65.4, 59.1, 55.3, 47.5, 47.4, 35.5, 34.6, 33.9, 32.6, 32.2, 30.1, 25.4, 25.3, 25.1.

HRMS (ESI$^+$, *m/z*): $[M+Na]^+$ for $C_{30}H_{41}NNaO_6S^+$: calcd.: 566.2547, found: 566.2545.

IR (ATR): ṽ [cm^{-1}] = 3178 (w), 3075 (w), 2935 (w), 2860 (w), 2837 (w), 1704 (m), 1671 (s), 1641 (m), 1612 (m), 1586 (w), 1512 (s), 1442 (m), 1402 (m), 1379 (m), 1359 (m), 1329 (m), 1302 (m), 1284 (m), 1247 (s), 1215 (s), 1194 (s), 1174 (s), 1146 (s), 1127 (s), 1108 (s), 1092 (s), 1032 (s), 993 (s), 940 (m), 910 (s), 846 (m), 820 (m), 757 (m), 724 (m), 703 (m), 683 (m), 663 (m).

$[\alpha]_D$ = +15 (*c* = 0.005, $CHCl_3$)

Synthesis of (R)-4-((1R,4Z,8Z,13R,15R)-15-methoxy-5-methyl-3-oxo-2,14-dioxa-bicyclo[11.3.1]heptadeca-4,8-dien-15-yl)-3-(4-methoxybenzyl)thiazolidin-2-one (24):

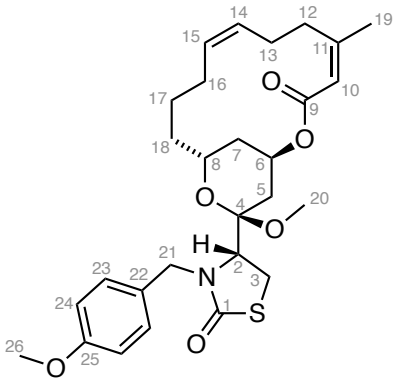

A flame-dried 50 ml *Schlenk* tube was charged with triene **23** (30.0 mg, 55.4 µmol, 1.00 eq.) and dry DCM (degassed, 9.2 ml) were degassed with 3 FPT cycles, backfilled with N_2, and Grubbs *Z*-selective catalyst (12.3 mg, 19.4 µmol, 0.30 eq.) was weighed into a flame-dried vial, evacuated, and backfilled with nitrogen (2x) and added as a solution in dry, degassed DCM (1 ml). The reaction mixture was evacuated and backfilled with nitrogen (3x), and then, under slight vacuum, heated to 50 °C. After 24 h, 0.1 ml DMSO was added and the rection was stirred for 24 h open to air. The title compound was obtained as colorless oil (14.0 mg, 29.0 µmol, 45%, 62% brsm).

**Note: the isolated product yield was variable between 33-48%; use of higher catalyst loading only improved the yield up to 55%.*

Reactions with Grubbs 2nd generation catalyst were performed following the above procedure and yielded up to 64% of an (*Z*)/(*E*) product mixture: (*Z*):(*E*) = 40:60.

R_f (SiO_2, Hex:EtOAc = 7:3; CAM) = 0.24

^{1}H-NMR (400 MHz, $CDCl_3$): δ [ppm] = 7.25 – 7.20 (m, 2H, H-23/23'), 6.88 – 6.84 (m, 2H, H-24/24'), 5.64 (d, *J* = 1.4 Hz, 1H, H-10), 5.43-5.40 (m, 1H, 14/15*), 5.27 – 5.23 (m, 1H, H-6), 5.07 (d, *J* = 14.2 Hz, 1H, H-21), 4.29 (d, *J* = 14.2 Hz, 1H, H-21'), 4.26 – 4.19 (m, 1H, H-8), 3.80 (s, 3H, H-28), 3.80 – 3.74 (m, 1H, H-2), 3.20 – 3.16 (m, 2H, H-3/3'), 3.06 (s, 3H, H-20), 2.91 – 2.81 (m, 1H, H-12), 2.37 – 2.12 (m, 6H, H-12'/13/13'/16/16'/21), 1.91 (d (br), *J* = 1.4 Hz, 3H, H-10), 1.89 – 1.76 (m, 4H, H-5'/7/17/18), 1.67 – 1.53 (m, 2H, H-17'/18), 1.46 (ddd, *J* = 14.0, 11.7, 2.4 Hz, 1H, H-7').

^{13}C-NMR (100 MHz, $CDCl_3$): δ [ppm] = 173.3 (C-1), 166.2 (C-9), 159.3 (C-25), 156.0 (C-4), 130.2 (C-23/23'), 130.1 (C-14/15*), 129.1 (C-14/15*), 129.0 (C-22), 118.8 (C-10), 114.1 (C-24/24'), 102.3 (C-4), 67.2 (C-6), 63.7 (C-8), 59.1 (C-2), 55.4 (C-26), 47.7 (C-20), 47.5 (C-21), 34.4 (C-12), 34.2 (C-7), 31.4 (C-18), 30.1 (C-5), 27.1 (C-13), 25.4 (C-3), 25.1 (C-19), 23.9 (C-16), 21.7 (C-17).

HRMS (ESI$^+$, *m/z*): $[M+NH_4]^+$ for $C_{28}H_{41}O_6N_2S^+$: calcd.: 533.2680, found: 533.2682.

Synthesis of (R)-4-((1R,4Z,8Z,13R,15R)-15-methoxy-5-methyl-3-oxo-2,14-dioxabicyclo [11.3.1]heptadeca-4,8-dien-15-yl)thiazolidin-2-one (25):

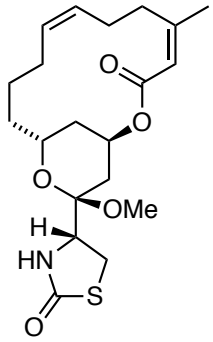

24 (17.3 mg, 33.5 µmol, 1.00 eq.) was dissolved in MeOH (2.0 ml) and MeCN (0.5 ml). CAN (92.0 mg, 0.17 mmol, 5.00 eq.) was added in one portion at room temperature. The reaction was stirred for 14 h. $NaHCO_3$ (sat. aq., 3 ml) and H_2O (3 ml) were added slowly. The reaction was extracted with DCM (3 x 5 ml), dried over Na_2SO_4, filtered and concentrated. Purification by flash column chromatography (SiO_2, Hex:EtOAc = 8:2 to 7:3) furnished the title compound as a colorless solid (8.8 mg, 22.2 µmol, 66%).

R_f (SiO_2, hexanes/Ethyl acetate = 7/3) = 0.17

^{1}H-NMR (400 MHz, $CDCl_3$): δ [ppm] = 5.64 (d, J = 1.7 Hz, 1H), 5.51 – 5.33 (m, 2H), 5.25 (p, J = 3.1 Hz, 1H), 4.20 (dt, J = 11.8, 7.3 Hz, 1H), 4.10 (t, J = 8.1 Hz, 1H), 3.41 – 3.21 (m, 2H), 3.19 (s, 3H), 2.88 – 2.80 (m, 1H), 2.32 – 2.10 (m, 6H), 1.92 (s, 3H), 1.95 – 1.87 (m, 1H), 1.88 – 1.32 (m, 6H).

^{13}C-NMR (100 MHz, $CDCl_3$): δ [ppm] = 174.7, 166.2, 156.3, 130.0, 129.2, 118.7, 100.5, 67.1, 63.5, 56.7, 48.1, 34.5, 34.1, 30.9, 29.5, 28.1, 27.0, 25.2, 23.8, 21.7.

Synthesis of (R)-4-((1R,4Z,8Z,13R,15R)-15-hydroxy-5-methyl-3-oxo-2,14-dioxabicyclo [11.3.1]heptadeca-4,8-dien-15-yl)thiazolidin-2-one (8-*Nor*-Latrunculin B):

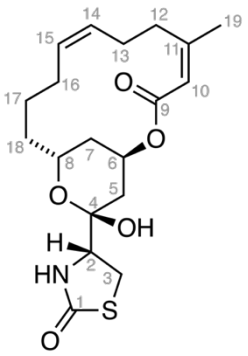

Methylketal **25** (8.80 mg, 22.2 µmol, 1.00 eq.) was dissolved in H_2O (0.6 ml) and AcOH (0.9 ml) and heated to 45 C. After 4 h, the reaction was cooled to room temperature and $NaHCO_3$ (sat. aq., 5 ml) was slowly added. the reaction was extracted with EtOAc (3 x 7 ml), the combined organic layers were washed with brine, dried over Na_2SO_4, filtered and concentrated. Purification by flash column chromatography (SiO_2, Hex:EtOAc = 9:1 to 6:4) furnished **8-*Nor*-Latrunculin B** as a colorless solid (3.00 mg, 7.90 µmol, 35%).

The *E*/*Z* mixture of methyl ketal **24** was hydrolyzed analogously and gave (*E*/*Z*)-8-*Nor*-Latrunculin B (2.00 mg, 5.2 µmol, 41%).

R_f (SiO_2, Hex:EtOAc = 5:5; CAM) = 0.38

^{1}H-NMR (400 MHz, $CDCl_3$): δ [ppm] = 5.68 (d, *J* = 1.5 Hz, 1H, H-10), 5.63 (s, 1H, N-H), 5.46 (p, *J* = 3.2 Hz, 1H, H-6), 5.41 – 5.25 (m, 2H, H-14/15), 4.26 (dddd, *J* = 11.6, 9.8, 3.8, 1.7 Hz, 1H, H-8), 3.85 – 3.76 (m, 1H, H-2), 3.63 (s, 3H, O-H), 3.46 (dd, *J* = 11.6, 8.8 Hz, 1H, H-3), 3.38 (dd, *J* = 11.7, 6.2 Hz, 1H, H-3'), 2.54 (td, *J* = 13.5, 12.6, 3.7 Hz, 1H, H-12), 2.44 – 2.13 (m, 3H, H-12'/13/13'), 2.09 (ddd, *J* = 14.7, 3.1, 1.8 Hz, 1H, H-5), 2.03 – 1.95 (m, 1H, H-16), 1.95-1.90 (m, 1H, H-3'), 1.92 (d (br), *J* = 1.4 Hz, 3H, H-19), 1.82 – 1.72 (m, 2H, H-7/17), 1.55 – 1.33 (m, 4H, H-7'/17'18/18').

^{13}C-NMR (100 MHz, $CDCl_3$): δ [ppm] = 174.7 (C-1), 165.5 (C-9), 155.2 (C-11), 129.8 (C-14 or 15), 129.5 (C-14 or 15), 118.0 (C-10), 98.0 (C-4), 68.6 (C-6) , 62.3 (C-8), 61.6 (C-2), 35.6 (C-12), 35.0 (C-7), 31.3 (C-5), 30.9 (C-18), 28.9 (C-3), 26.9 (C-13), 24.4 (C-19), 23.9 (C-16), 21.9 (C-17).

HRMS (ESI$^+$, *m/z*): [$(M+H)^+$] for $C_{16}H_{27}NO_5SNa^+$ calcd.: 404.1502, found: 404.1517.

IR (ATR): $\tilde{\nu}$ [cm^{-1}] = 3310 (w), 2923 (w), 2853 (w), 1678 (s), 1447 (w), 1378 (w), 1347 (w), 1278 (m), 1186 (w), 1186 (w), 1141 (w), 1076 (w), 1054 (w), 1026 (w), 867 (w), 800 (w).

Synthesis of (R)-4-((1R,4Z,13R,15R)-5-methyl-3-oxo-15-((4-(phenyldiazenyl)benzyl) oxy)-2,14-dioxabicyclo[11.3.1]heptadeca-4,8-dien-15-yl)thiazolidin-2-one (26):

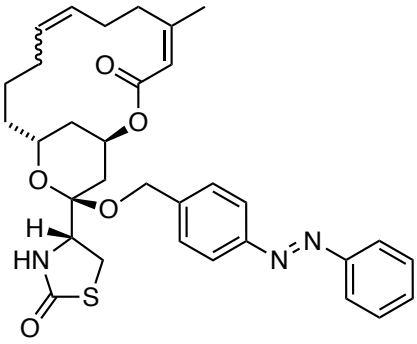

Inspired by a report in the literature[8], a flame-dried 2 ml vial with stir bar was charged with (*E*/*Z*)-**24** (16.0 mg, 40.5 µmol, 1.00 eq.) and azobenzene **S1** (85.9 mg, 0.406 mmol, 10.0 eq.) and evacuated for 10 minutes. The starting materials were dissolved in dry DCM (1.3 ml) and $InCl_3$ (3 spatula tips) was added. The reaction instantly turned dark and was left stirring over night. A spatula tip of solid $NaHCO_3$ was added to the reaction and the mixture was filtered over a pad of silica and eluted with DCM and EtOAc. The crude product was purified by HPLC (semi-prep, 40-100% MeCN in H_2O over 8 min, 3 min MeCN, no FA) and gave the title compound as an orange film (2.50 mg, 4.00 µmol, 10%).

[8] Airken, H. R. M.; Furkert, D. P. F.; Hubert, J. G.; Wood, J. M.; Brimble, M. A. *Org. Biomol. Chem.* **2013**, *11*, 5147–5155.

LCMS (50-100% MeCN in H_2O over 5 min, 0.1% FA): t_{ret} = 2.6 min (*cis*), 4.1 min (*trans*).

HPLC (semi-prep, 40-100% MeCN in H_2O over 8 min, 3 min MeCN, no FA): t_{ret} = 2.6 min.

^{1}H-NMR (400 MHz, $CDCl_3$): δ [ppm] = 7.97 – 7.82 (m, 4H), 7.62 – 7.44 (m, 5H), 5.76 – 5.66 (m, 1H), 5.52 – 5.40 (m, 1H), 5.27 – 5.16 (m, 3H), 4.79 – 4.69 (m, 1H), 4.65 – 4.56 (m, 1H), 4.42 – 4.31 (m, 1H), 4.29 – 4.14 (m, 1H), 3.42 – 3.30 (m, 1H), 3.30 – 3.17 (m, 1H), 2.64 – 2.51 (m, 1H), 2.30 (d, *J* = 15.1 Hz, 1H), 2.14 – 1.85 (m, 4H), 1.82 (m, 3H) 1.81 –1.32 (m, 8H).

^{13}C-NMR (101 MHz, $CDCl_3$): δ [ppm] = 174.6, 166.8, 166.5, 157.1, 155.7, 152.7, 152.2, 152.0, 141.1, 141.0, 131.5, 131.3, 131.3, 130.2, 129.4, 129.3, 128.9, 128.7, 127.5, 127.3, 127.1, 123.1, 120.6, 118.1, 101.0, 67.4, 67.1, 65.8, 63.5, 61.7, 61.5, 57.4, 57.3, 35.7, 35.1, 33.5, 33.0, 32.7, 31.4, 31.2, 29.7, 29.8, 29.6, 28.2, 26.3, 24.9, 24.8, 23.9, 23.4, 22.9, 22.2.

NMRs: mixtures of *E*- and *Z*- olefin and *cis* and *trans* isomers.

HRMS (ESI$^-$, *m/z*): $[M–H]^-$ for $C_{32}H_{36}N_3O_5S^-$: calcd.: 574.2379, found: 574.2381.

Synthesis of (R)-4-((1R,4Z,13R,15R)-5-methyl-3-oxo-15-(4-(phenyldiazenyl)phenethoxy) -2,14-dioxabicyclo[11.3.1]heptadeca-4,8-dien-15-yl)thiazolidin-2-one (27):

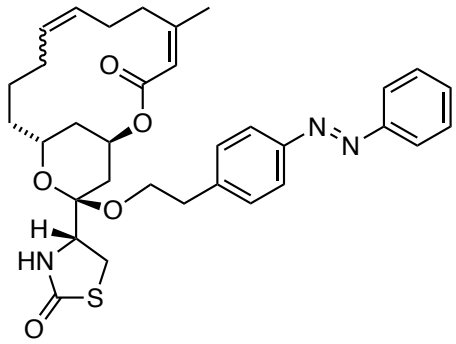

Inspired by a literature report[9], a flame-dried 2 ml vial with stir bar was charged with (*E*/*Z*)-**24** (15.0 mg, 38.0 µmol, 1.00 eq.) and Azobenzene **S2** (86.0 mg, 0.38 mmol, 10.0 eq.) and

[9] Airken, H. R. M.; Furkert, D. P. F.; Hubert, J. G.; Wood, J. M.; Brimble, M. A. *Org. Biomol. Chem.* **2013**, *11*, 5147–5155.

evacuated for 10 minutes. The starting materials were dissolved in dry DCM (1.3 ml) and $InCl_3$ (1 spatula tip) was added. The reaction instantly turned dark and was left stirring for 11 h and another portion of $InCl_3$ (1 spatula tip) was added. A spatula tip of solid $NaHCO_3$ was added to the reaction and the mixture was filtered over a pad of silica (previously rinsed with NEt_3 and Hex) and eluted with Hex:EtOAc:NEt_3 (4:1:3). The crude product was purified by HPLC (semi-prep, 40-100% MeCN in H_2O over 8 min, 3 min, no FA) and gave the title compound as an orange film (3.50 mg, 5.90 µmol, 16%).

LCMS (50-100% MeCN in H_2O over 5 min, 0.1% FA): t_{ret} = 2.9 min (*cis*), 4.3 min (*trans*).

HPLC (semi-prep, 40-100% MeCN in H_2O over 8 min, 3 min, no FA): t_{ret} = 3.0 min.

^{1}H-NMR (600 MHz, $CDCl_3$): δ [ppm] = 7.93 – 7.88 (m, 2H), 7.85 (dd, J = 8.4, 3.1 Hz, 2H), 7.56 – 7.44 (m, 3H), 7.30 (t, J = 8.6 Hz, 2H), 5.69 (dd, J = 17.3, 1.6 Hz, 1H), 5.52 – 5.32 (m, 4H), 5.25 – 5.18 (m, 1H), 4.48 – 4.25 (m, 1H), 4.05 – 3.99 (m, 1H), 3.82 – 3.76 (m, 1H), 3.68 – 3.54 (m, 1H), 3.09 – 2.79 (m, 5H), 2.56 – 2.43 (m, 1H), 2.36 – 1.95 (m, 8H), 1.95 – 1.87 (m, 5H), 1.84 – 1.30 (m, 12H).

^{13}C NMR (151 MHz, $CDCl_3$): δ [ppm] = 174.6, 174.6, 166.6, 166.2, 157.5, 155.9, 152.8, 151.6, 142.2, 142.2, 132.3, 131.1, 130.0, 129.8, 129.8, 129.4, 129.3, 129.2, 128.9, 123.2, 123.2, 123.0, 121.2, 121.1, 120.3, 120.3, 118.7, 118.1, 100.8, 100.6, 67.4, 67.0, 66.0, 63.7, 61.5, 56.8, 56.8, 36.7, 36.6, 36.1, 35.3, 34.7, 33.5, 33.4, 33.1, 32.4, 31.0, 29.9, 29.6, 29.4, 27.9, 27.2, 25.2, 25.1, 24.1, 23.8, 22.0.

NMRs: mixtures of *E*- and *Z*- olefin and *cis* and *trans* isomers. Rotamers observed.

HRMS (ESI$^-$, *m/z*): $[M–H]^-$ for $C_{33}H_{38}N_3O_5S^-$: calcd.: 588.2534, found: 588.2538.

Synthesis of (*R*)-4-((1*R*,4*Z*,8*Z*,13*R*,15*R*)-15-methoxy-5-methyl-3-oxo-2,14-dioxabicyclo[11.3.1]heptadeca-4,8-dien-15-yl)-3-(4-(phenyldiazenyl)benzyl)thiazolidin-2-one (S1):

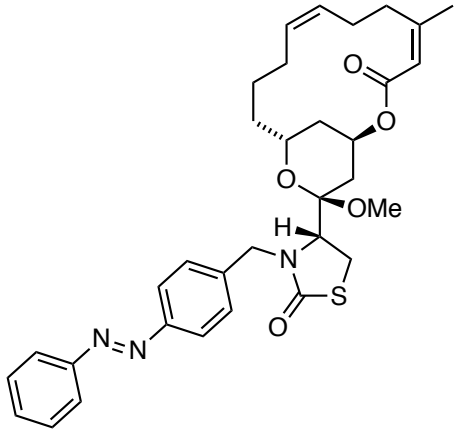

A flame-dried vial with stir bar was charged with **24** (4.50 mg, 11.4 µmol, 1.00 eq.), 1-(4-(bromomethyl)phenyl)-2-phenyldiazene[10] (6.30 mg, 22.8 µmol, 2.00 eq), NaI (0.20 mg, 1.10 µmol, 0.10 eq.) and K_2CO_3 (2.00 mg, 14.8 µmol, 1.30 eq.). The reaction mixture was dissolved in dry DMF (0.10 ml) and stirred at r.t. for 2 d. The reaction mixture was poured into NH_4Cl (sat. aq., 2.0 ml) and extracted with EtOAc (3 x 3 ml). The combined organic layers were washed with brine, dried over Na_2SO_4, filtered and concentrated. The crude product was purified by flash column chromatography (SiO_2, Hex:EtOAc = 8:2 to 5:5) and gave the title compound as an orange film (3.50 mg, 5.90 µmol, 52%).
*For analytical purposes, the product obtained in two runs was combined and repurified by HPLC (*semi-prep, 50 – 90% MeCN in H_2O over 8 min, 3 min MeCN, no FA).

R_f (SiO_2, Hex:EtOAc = 7:3, CAM) = 0.39

LCMS (50 – 100% MeCN in H_2O over 5 min, 0.1% FA): t_{ret} = 3.4 min (*cis*) 4.7 min (*trans*)

HPLC (semi-prep, 50 – 90% MeCN in H_2O over 8 min, 3 min MeCN, no FA) t_{ret} = 9.86 min.

^{1}H NMR (600 MHz, $CDCl_3$): δ [ppm] = 7.94 – 7.87 (m, 4H), 7.57 – 7.45 (m, 3H), 7.44 (d, *J* = 8.0 Hz, 2H), 5.68 – 5.64 (m, 1H), 5.44 – 5.37 (m, 2H), 5.26 (s, 1H), 5.20 (d, *J* = 14.6 Hz, 1H), 4.46 (d, *J* = 14.5 Hz, 1H), 4.29 – 4.20 (m, 1H), 3.83 – 3.76 (m, 1H), 3.32 – 3.17 (m, 2H), 3.06

[10] Obtained from corresponding alcohol using NBS (1.5 eq.), PPh_3 (1.5 eq.), THF (0.2 M), 16 h (83%).

(s, 3H), 2.89 – 2.80 (m, 1H), 2.34 – 2.17 (m, 6H), 1.98 – 1.89 (m, 3H), 1.96 – 1.77 (m, 4H), 1.71 – 1.56 (m, 2H), 1.49 – 1.41 (m, 1H).

^{13}C-NMR (151 MHz, $CDCl_3$): δ [ppm] = 173.5, 166.2, 156.1, 152.7, 152.3, 140.0, 131.3, 130.1, 129.5, 129.3, 129.1, 123.3, 123.0, 118.7, 102.2, 67.1, 63.7, 59.4, 48.0, 47.7, 34.4, 34.3, 31.4, 30.1, 27.1, 25.4, 25.1, 23.9, 21.7.
NMRs reported for major (*trans*) isomer

HRMS (APCI$^+$, *m/z*): $[M+H]^+$ for $C_{33}H_{40}N_3O_5S^+$: calcd.: 590.2683, found: 590.2657.

IR (ATR): $\tilde{\nu}$ [cm^{-1}] = 2936 (w), 1699 (s), 1674 (s), 1447 (w), 1401 (w), 1377 (w), 1352 (w), 1276 (s), 1216 (m), 1196 (s), 1120 (w), 1096 (m), 1060 (w), 1033 (m), 989 (w), 931 (w), 896 (w), 868 (w), 758 (w).

Synthesis of methyl (2Z,6Z)-10-((2R,4S,6R)-4-hydroxy-6-methoxy-6-((R)-3-(4-methoxy benzyl)-2-oxothiazolidin-4-yl)tetrahydro-2H-pyran-2-yl)-3-methyldeca-2,6-dienoate ((*S*)-28):

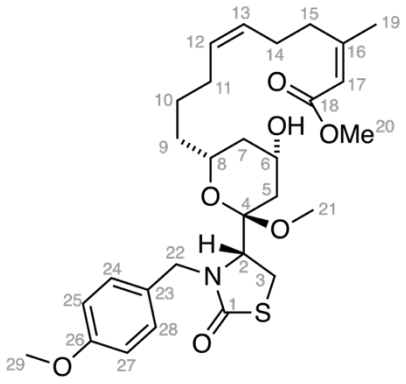

A *Schlenk* tube was charged with (*S*)-**20** (30.0 mg, 71.2 µmol, 1.00 eq.) and (*Z*)-sel Grubbs (450 mg, 7.10 µmol, 0.10 eq.) and evacuated/ backfilled with N_2 three times and methyl (*Z*)-3-methylhepta-2,6-dienoate[11] (146 mg, 0.71 mmol, 10.0 eq.) and dry THF (FPT 3x, 0.10 ml) was added. the reaction was warmed to 40 °C and stirred for 24 h. Et_2O (4.00 ml) and water (4.00 ml) were added, and the layers were separated. The aqueous layer was extracted with diethyl

[11] Prepared according to She; J., Lampe; J. W., Polianski; A. B., Watson, P. S. *Tet. Lett.* **2009**, *50*, 298-301.

ether (2 x 5 ml). The combined organic layers were washed with brine, dried over Na_2SO_4, filtered and concentrated. After flash column chromatography (SiO_2, Hex:EtOAc = 9:1 to 0:10), and HPLC (semi-prep, 50-80% MeCN in H_2O over 8 min, 3 min flush, no FA), the title compound was obtained as a colorless oil (18.2 mg, 33.2 µmol, 47%, 92%brsm).
*The metathesis partner contained about 25% Et_2O, 3 FPT cycles were conducted to ensure no residual oxygen is present.

R_f (SiO_2, Hex:EtOAc = 4:6; CAM) = 0.29 *copolar with starting material

LCMS (semi-prep, 50-100% MeCN in H_2O over 5 min, 0.1% FA): t_{ret} = 2.5 min.

HPLC (semi-prep, 50-80% MeCN in H_2O over 8 min, 3 min MeCN, no FA): t_{ret} = 6.6 min.

^{1}H-NMR (400 MHz, $CDCl_3$): δ [ppm] = 7.21 (d, *J* = 8.6 Hz, 2H, H-24/28), 6.85 (d, *J* = 8.7 Hz, 2H, H-25/27), 5.67 (s, 1H, H-17), 5.51 – 5.37 (m, 2H, H=12/13), 5.11 (d, *J* = 14.4 Hz, 1H, H-22), 4.24 (d, *J* = 14.4 Hz, 1H, H-22'), 4.11 – 4.01 (m, 1H, H-8), 3.84 (dd, *J* = 8.4, 3.5 Hz, 1H, H-2), 3.80 (s, 3H, H-29), 3.66 (s, 3H, H-20), 3.63 – 3.54 (m, br, 1H, H-6), 3.31 – 3.21 (m, 2H, H-3/3'), 3.06 (s, 3H, H-21), 2.73 – 2.62 (m, 2H, H-15/15'), 2.30 – 2.18 (m, 3H, H-14/14'/5), 2.18 – 2.10 (m, 2H, 11/11'), 2.03 – 1.96 (m, z1H, H-7), 1.89 (d, *J* = 1.3 Hz, 3H, H-19), 1.75 – 1.40 (m, 5H, H-5'/9/9'/10/10'), 1.26 – 1.08 (m, 1H, H-7').

^{13}C-NMR (400 MHz, $CDCl_3$): δ [ppm] = 172.9 (C-1), 166.8 (C-18), 160.2 (C-16), 159.3 (C-26), 130.0 (C-12/13*), 130.0 (C-24/28), 129.5 (C-12/13*), 128.9 (C-23), 116.2 (C-17), 114.1 (C-25/27), 103.2 (C-4), 70.4 (C-6), 64.8 (C-8), 58.9 (C-2), 55.4 (C-29), 50.9 (C-20), 47.6 (C-21), 47.3 (C-22), 40.6 (C-7), 37.2 (C-5), 35.8 (9), 33.4 (15), 27.2 (C-11), 26.1 (C-14), 26.0 (C-10), 25.5 (C-3/19*), 25.5 (C-3/19*).
*indistinguishable
The NOESY coupling between H-6 and H-8 was observed.

HRMS (ESI$^+$, *m/z*): [M+Na$^+$] for $NaC_{29}H_{41}NO_7S^+$: calcd.: 570.2496, found: 570.2512.

IR (ATR): $\tilde{\nu}$ [cm^{-1}] = 3408 (w), 2939 (w), 1714 (m), 1668 (s), 1611 (m), 1586 (w), 1512 (m), 1441 (m), 1403 (m), 1362 (w), 1302 (w), 1287 (w), 1246 (s), 1216 (m), 1195 (s), 1172 (s), 1143 (s), 1109 (s), 1069 (m), 1031 (s), 975 (m), 939 (w), 918 (m), 896 (w), 848 (m), 822 (m), 758 (w), 722 (w).

$[\alpha]_D$ = +53 (*c* = 0.01, $CHCl_3$)

Synthesis of (2Z,6Z)-10-((2R,4S,6R)-4-hydroxy-6-methoxy-6-((R)-3-(4-methoxyben zyl)-2-oxothiazolidin-4-yl)tetrahydro-2H-pyran-2-yl)-3-methyldeca-2,6-dienoic acid (29):

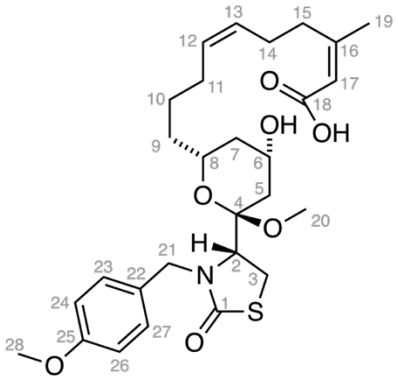

(*S*)-**28** (11.9 mg, 21.7 µmol, 1.00 eq.) was dissolved in MeCN (1.00 ml) and a solution of LiOH (5.20 mg, 0.22 mmol, 10.0 eq.) in H_2O (1.00 ml) was added. After stirring for 6h at r.t., the reaction was warmed to 40 °C and stirred for another 15 h. the reaction was cooled to room temperature, brought to pH = 2 with HCl (aq., 2.0 M) and extracted with EtOAc (3 x 20 ml). the combined organic layers were washed with brine, dried over Na_2SO_4, filtered and concentrated. The crude product was purified by HPLC (semi-prep, 30-70% MeCN in H_2O, no FA) and acid **29** was obtained as a colorless oil (6.00 mg, 11.2 µmol, 52%).

LCMS (5-100% MeCN in H_2O over 5 min, 0.1% FA): t_{ret} = 4.0 min

HPLC (semi-prep, 30-70% MeCN in H_2O over 8 min, 3 min MeCN, no FA): t_{ret} = 7.8 min.

^{1}H-NMR (400 MHz, $CDCl_3$): δ [ppm] = 7.21 (d, *J* = 8.5 Hz, 2H, H-23/27), 6.85 (d, *J* = 8.6 Hz, 2H, H-24/26), 5.69 (s, 1H, H-17), 5.49 – 5.37 (m, 2H, H-12/13*), 5.10 (d, *J* = 14.4 Hz, 1H, H-21), 4.25 (d, *J* = 14.4 Hz, 1H, H-21'), 4.07 (tt, *J* = 11.1, 4.6 Hz, 1H, H-8), 3.84 (dd, *J* = 8.4, 3.5 Hz, 1H, H-2), 3.80 (s, 3H, H-28), 3.64 – 3.54 (m, 1H, H-6), 3.30 – 3.20 (m, 2H, H-3/3'), 3.06 (s, 3H, H-20), 2.74 – 2.62 (m, 1H, H-15/15'), 2.30 – 2.18 (m, 3H, H-14/14'/5), 2.18 – 2.10 (m, 2H, H11/11'), 2.05 – 1.98 (m, 1H, H-7), 1.92 (d, *J* = 1.3 Hz, 3H, H-19), 1.76 – 1.39 (m, 5H, H9/9'/10/10'5'), 1.27 – 1.14 (m, 1H, H-7').

^{13}C-NMR (101 MHz, $CDCl_3$): δ [ppm] = 173.1 (C-1), 169.7 (C-18), 162.9 (C-16), 159.2 (C-25), 130.2 (C-12/13*), 130.0 (C-23/27), 129.4 (C-12/13*), 128.9 (C-22), 115.7 (C-17), 114.2 (C-24/26), (C-4), 103.2 (C-4), 70.4 (C-6), 64.9 (C-8), 59.0 (C-2), 55.4 (C-28), 47.6 (C-20), 47.3 (C-21), 40.4 (C-7), 37.1 (C-5), 35.7 (C-9), 33.6 (C-15), 27.2 (C-11), 26.2 (C-14), 25.9 (C-10), 25.8 (C-19), 25.5 (C-3).

HRMS (ESI$^+$, *m/z*): [(M+Na)$^+$] for $NaC_{28}H_{39}NO_7S$: calcd.: 556.2339, found: 556.2336.

IR (ATR): $\tilde{\nu}$ [cm^{-1}] = 8184 (w), 2981 (m), 2941 (m), 2844 (w), 2360 (w), 2341 (w), 1674 (s), 1613 (m), 1586 (w), 1513 (m), 1442 (w), 1400 (w), 1289 (w) 1249 (s), 1176 (m), 1053 (m), 1033 (s), 943 (w), 896 (w), 855 (w), 762 (w), 734 (w), 709 (w).

$[\alpha]_D$ = –25 (*c* = 0.003, $CHCl_3$)

Synthesis of methyl (2Z,6Z)-10-((2R,4R,6R)-4-hydroxy-6-methoxy-6-((R)-3-(4-methoxy benzyl)-2-oxothiazolidin-4-yl)tetrahydro-2H-pyran-2-yl)-3-methyldeca-2,6-dienoate (*R*)-28:

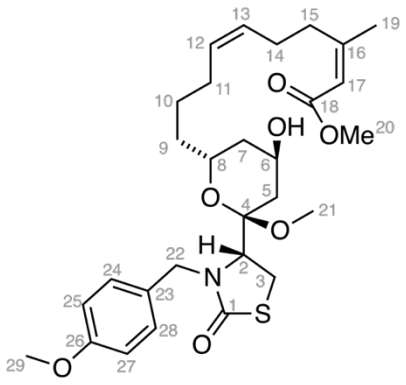

A *Schlenk* tube was charged with (*R*)-**20** (30.0 mg, 71.2 µmol, 1.00 eq.) and (*Z*)-sel. Grubbs (450 mg, 7.10 µmol, 0.10 eq.) and evacuated/ backfilled with N_2 three times and methyl (*Z*)-3-methylhepta-2,6-dienoate[12] (146 mg, 0.71 mmol, 10.0 eq.) and dry THF (FPT 3x, 0.10 ml) was added. the reaction was warmed to 40 °C and stirred for 24 h. Et_2O (4.00 ml) and water (4.00 ml) were added, and the layers separated. The aqueous layer was extracted with Et_2O (2 x 5 ml). The combined organic layers were washed with brine, dried over Na_2SO_4, filtered

[12] Prepared according to She; J., Lampe; J. W., Polianski; A. B., Watson, P. S. *Tet. Lett.* **2009**, *50*, 298-301.

and concentrated. The crude product was purified by flash column chromatography (SiO_2, Hex:EtOAc = 9:1 to 0:10), and HPLC (semi-prep, 50-100% MeCN in H_2O over 8 min, 3 min MeCN, no FA) and the title compound was obtained as a colorless oil (32.9 mg, 60.1 µmol, 84%, 96% brsm).
*The metathesis partner contained about 25% diethyl ether, 3 FPT cycles were conducted to ensure no residual oxygen is present!

R_f (SiO_2, Hex:EtOAc = 4:6, CAM) = 0.29 *copolar with starting material

LCMS (50-100% MeCN in H_2O over 5 min, 0.1% FA): t_{ret} = 2.7 min.

HPLC (semi-prep, 50-100% MeCN in H_2O over 8 min, 3 min MeCN, no FA): t_{ret} =7.2 min.

^{1}H-NMR (400 MHz, $CDCl_3$): δ [ppm] = 7.20 (d, J = 8.6 Hz, 2H, H-24/28), 6.85 (d, J = 8.6 Hz, 2H, 25/27), 5.67 (s, 1H, H-17), 5.52 – 5.37 (m, 2H, H-12/13*), 5.09 (d, J = 14.4 Hz, 1H, H-22), 4.22 (d, J = 14.4 Hz, 1H, H-22'), 4.19 – 4.10 (m, br, 1H, H-6), 3.98 – 3.87 (m, 1H, H-8), 3.80 (s, 3H, H-29), 3.77 (dd, J = 8.5, 3.3 Hz, 1H, H-2), 3.66 (s, 3H, H-20), 3.31 – 3.21 (m, 2H, 3/3'), 3.16 (s, 3H, H-21), 2.71 – 2.64 (m, 2H, H-15/15'), 2.28 – 2.21 (m, 2H, H-14/14'), 2.20 – 2.12 (m, 2H, H-11/11'), 2.12 – 2.03 (m, 1H, H-22), 1.89 (d, J = 1.4 Hz, 3H, H-26), 1.89 – 1.76 (m, 2H, H-5'/7), 1.75 – 1.41 (m, 5H, H-7'/9/9'/10/10').

^{13}C-NMR (101 MHz, $CDCl_3$): δ [ppm] = 172.9 (C-1), 166.8 (C-18), 160.2 (C-16), 159.3 (C-26), 130.0 (C-12/13*), 129.9 (24/28), 129.6 (C-12/13*), 128.8 (C-23), 116.2 (C-17), 114.2 (C-25/27), 103.7 (C-4), 66.3 (C-8), 64.2 (C-6), 59.0 (C-2), 55.4 (C-29), 50.9 (C-20), 47.8 (C-21), 47.4 (C-22), 37.9 (C-7), 35.8 (C-9), 33.4 (C-15), 32.4 (C-5), 27.2 (C-11), 26.1 (C-14), 25.9 (C-10), 25.5 (C-19), 25.5 (C-3).

HRMS (ESI$^+$, *m/z*): $[M+Na]^+$ for $NaC_{29}H_{41}NO_7S^+$: calcd.: 570.2496, found: 570.2513

IR (ATR): $\tilde{\nu}$ [cm^{-1}] = 3532 (w), 2941 (w), 1715 (m), 1671 (s), 1612 (w), 1586 (w), 1513 (m), 1441 (m), 1403 (m), 1364 (w), 1303 (w), 1286 (w), 1247 (s), 1216 (m), 1196 (m), 1174 (m), 1174 (s), 1145 (m), 1107 (m), 1090 (m), 1062 (w), 1032 (s), 939 (w), 921 (w), 848 (w), 725 (w).

$[\alpha]_D$ = +55 (c = 0.01, $CHCl_3$)

Synthesis of 4-((2*R*,4*R*,6*R*)-4-hydroxy-2-methoxy-6-((*Z*)-5-(4-((*E*)-phenyldiazenyl)phenyl)pent-4-en-1-yl)tetrahydro-2*H*-pyran-2-yl)-3-(4-methoxybenzyl)thiazolidin-2-one (33):

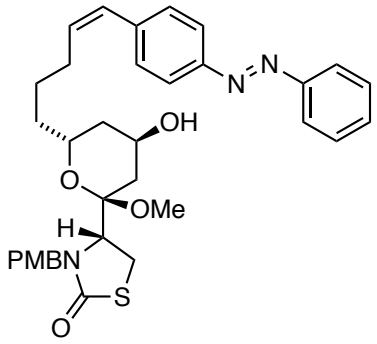

A flame-dried vial with stir bar was charged with (*S*)-**20** (30.0 mg, 71.2 µmol, 1.00 eq.), azobenzene **32** (29.7 mg, 0.14 mmol, 2.00 eq.) and *Z*-sel. Grubbs (4.50 mg, 7.10 µmol, 0.10 eq.), evacuated and backfilled with nitrogen (3 cycles). The reaction mixture was dissolved in DCM (FPT. 3 cycles, 0.2 ml) and heated to 45 °C. After 5 h, another portion of *Z*-selective Grubbs (4.50 mg, 7.10 µmol, 0.10 eq.) was added and the reaction stirred for a total of 16 h. water (4.0 ml) and DCM (4.0 ml) were added and stirred for 30 min. The layers were separated, and the aqueous layer was extracted with DCM (2 x 5 ml). the combined organic layers were dried over Na_2SO_4, filtered and concentrated. The crude product was purified by flash column chromatography (SiO_2, Hex:EtOAc = 8:2 to 5:5) and HPLC (semiprep, 50 – 90% MeCN in H_2O over 8 min, 3 min 100% MeCN, no FA) and the title compound was obtained as an orange film (4.50 mg, 7.50 µmol, 11%).

R_f (SiO_2, Hex:EtOAc = 4:6; UV; CAM) = 0.29. *copolar with starting material

LCMS (50-100% MeCN in H_2O over 5 min, 0.1% FA): 2.8 min (*cis*), 4.2 min (*trans*).

HPLC (semi-prep, 50 – 90% MeCN in H_2O over 8 min, 3 min 100% MeCN, no FA): t_R = 8.89 min.

^{1}H-NMR (400 MHz, $CDCl_3$): δ [ppm] = 7.98 – 7.83 (m, 4H), 7.57 – 7.47 (m, 3H), 7.42 (d, *J* = 8.3 Hz, 2H), 7.18 (d, *J* = 8.6 Hz, 2H), 6.83 (d, *J* = 8.6 Hz, 2H), 6.57 – 6.51 (m, 1H), 5.79 (dt, *J* = 11.7, 7.2 Hz, 1H), 5.09 (d, *J* = 14.4 Hz, 1H), 4.22 (d, *J* = 14.4 Hz, 1H), 4.18 – 4.12 (m, 1H),

4.00 – 3.87 (m, 1H), 3.81 – 3.75 (m, 1H), 3.77 (s, 3H), 3.65 (d, *J* = 9.4 Hz, 1H), 3.31 – 3.20 (m, 2H), 3.10 (s, 3H), 2.54 – 2.44 (m, 2H), 2.12 – 2.01 (m, 1H), 1.91 – 1.59 (m, 6H), 1.50 – 1.41 (m, 1H).

^{13}C-NMR (101 MHz, $CDCl_3$): δ [ppm] = 173.0, 159.3, 152.8, 151.3, 140.5, 133.9, 131.1, 129.8, 129.6, 129.3, 129.1, 128.7, 123.0, 114.2, 103.7, 66.3, 64.2, 59.1, 55.4, 47.8, 47.4, 37.9, 35.8, 32.4, 28.9, 26.3, 25.5.

HRMS (APCI$^+$, *m/z*): $[M+H]^+$ for $C_{34}H_{40}N_3O_5S^+$: calcd.: 602.2683, found: 602.2679.

IR (ATR): $\tilde{\nu}$ [cm^{-1}] = 3529 (w), 2926 (,m), 2855 (w), 2362 (w), 1671 (s), 1611 (w), 1512 (m), 1441 (w), 1403 (w), 1364 (w), 1303 (w), 1248 (m) 1217 (m), 1200 (m), 1175 (m), 1101 (m), 1070 (m), 1030 (s), 939 (w), 904 (w), 857 (w), 819 (w), 770 (w).

$[\alpha]_D$ = +32 (*c* = 0.003, $CHCl_3$)

Synthesis of (2R,4R,6R)-2-methoxy-2-((R)-3-(4-methoxybenzyl)-2-oxothiazolidin-4-yl)-6-(pent-4-en-1-yl)tetrahydro-2H-pyran-4-yl benzoate (34a):

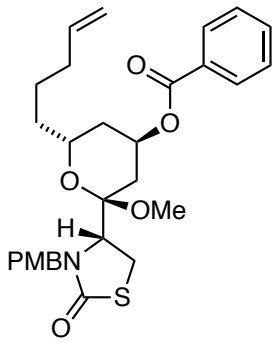

(*S*)-**20** (30.0 mg, 71.2 µmol, 1.00 eq.), benzoic acid (10.4 mg, 85.4 µmol, 1.20 eq.) and PPh_3 (37.3 mg, 0.15 mmol, 2.00 eq.) were dissolved in dry THF (1.40 ml). the reaction mixture was cooled to 0 °C and DEAD (40% in toluene, 68.0 µl, 0.15 mmol, 2.1 eq.) was added. After 10 min., the reaction was allowed to warm to r.t. and stirred over night, concentrated, and purified by flash column chromatography (SiO_2, Hex:EtOAc = 9:1 to 5:5). The title compound was obtained as an orange film (34.2 mg 65.1 µmol, 91%).
The product of this reaction contained H_2DEAD side product that could not be separated by FCC.

R_f (SiO_2, Hex:EtOAc = 8:2; CAM) = 0.24

HRMS (APCI$^+$, *m/z*): [$(M+H)^+$] for $C_{29}H_{36}NO_6S^+$: calc.: 526.2258, found: 526.2278.

Synthesis of (2R,4R,6R)-2-methoxy-2-((R)-2-oxothiazolidin-4-yl)-6-(pent-4-en-1-yl)tetrahydro-2H-pyran-4-yl benzoate (35a):

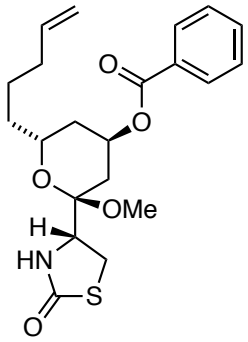

34a (20.3 mg, 38.6 µmol, 1.00 eq.) was dissolved in MeOH (2.00 ml) and MeCN (0.40 ml) and CAN (105.8 mg, 0.19 mmol, 5.00 eq.) was added. the reaction was stirred at room temperature over night. $NaHCO_3$ (sat. aq., 3 ml) and H_2O (3 ml) were added slowly. The reaction was extracted with DCM (3 x 5 ml), dried over Na_2SO_4, filtered and concentrated. The crude product was purified by flash column chromatography (SiO_2, Hex:EtOAc = 9.5:5 to 6:4). The reaction was performed twice and yielded a total of 11.0 mg of the title compound in sufficient yield for the subsequent deprotection. Thus, further purification by HPLC was not performed.

R_f (SiO_2, hexanes: ethyl acetate = 8:2; CAM) = 0.29

LCMS (50-100% MeCN in H_2O over 5 min, 0.1% FA): 2.2 min

LRMS (ESI+, m/z): $[M+Na]^+$ for $C_{21}H_{27}NNaO_5S^+$ calcd.: 428.2, found: 428.1.

Synthesis of (2R,4R,6R)-2-hydroxy-2-((R)-2-oxothiazolidin-4-yl)-6-(pent-4-en-1-yl)tetra hydro-2H-pyran-4-yl benzoate (36a):

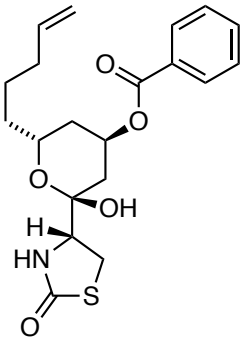

35a (11.0 mg, 27.1 µmol, 1.00 eq.) was dissolved in THF (0.40 ml) and water (0.40 ml) and AcOH (1.20 ml) was added. the reaction was heated to 45 °C for 4 h. After cooling to room temperature, $NaHCO_3$ (sat. aq., 4 ml) was added and the reaction was extracted with Ethyl acetate (3 x 5 ml). the combined organic layers were washed with brine, dried over Na_2SO_4, filtered and concentrated. The crude product was purified by HPLC (semi-prep, 40-70% MeCN in H_2O over 8 min, 3 min MeCN, no FA) and **36a** was obtained as a colorless solid (2.20 mg, 5.60 µmol, 21% over two steps)

R_f (SiO_2, Hex:EtOAc = 5:5; CAM) = 0.58

LCMS (50-100% MeCN in H_2O over 5 min, 0.1% FA): t_{ret} = 1.3 min.

HPLC (semi-prep, 40-70% MeCN in H_2O over 8 min, 3 min MeCN, no FA): t_{ret} = 3.8 min.

^{1}H-NMR (400 MHz, $CDCl_3$): δ [ppm] = 8.03 – 7.96 (m, 2H), 7.67 – 7.55 (m, 1H), 7.53 – 7.43 (m, 2H), 5.79 (ddt, *J* = 16.9, 10.1, 6.7 Hz, 1H), 5.67 – 5.61 (m, 2H), 5.05 – 4.93 (m, 2H), 4.24 – 4.13 (m, 1H), 3.90 (s, 1H), 3.85 (dd, *J* = 8.9, 5.9, 1.1 Hz, 1H), 3.51 (dd, *J* = 11.7, 8.9 Hz, 1H), 3.42 (dd, *J* = 11.7, 5.9 Hz, 1H), 2.15 – 1.98 (m, 5H), 1.63 – 1.39 (m, 5H).

^{13}C-NMR (101 MHz, $CDCl_3$): δ [ppm] = 174.7, 165.2, 138.6, 133.8, 129.8, 129.6, 128.9, 115.0, 97.6, 68.7, 65.4, 61.5, 35.1, 34.5, 33.7, 31.5, 28.9, 24.6.

HRMS (ESI$^+$, *m/z*): $[M+Na]^+$ for $C_{20}H_{25}NO_5SNa^+$: calcd.: 414.1346, found: 414.1359.

IR (ATR): ṽ [cm^{-1}] = 3305 (w), 3071 (w), 2925 (w), 2855 (w), 1680 (s), 1601 (w), 1584 (w), 1451 (w), 1346 (w), 1315 (w), 1278 (s), 1177 (w), 1100 (m), 1069 (m), 1026 (w), 914 (w), 852 (w), 713 (m).

$[\alpha]_D$ = +6 (*c* = 0.001, $CHCl_3$)

Synthesis of (2R,4R,6R)-2-methoxy-2-((R)-3-(4-methoxybenzyl)-2-oxothiazolidin-4-yl)-6-(pent-4-en-1-yl)tetrahydro-2H-pyran-4-yl-11,12-dihydrodibenzo[c,g][1,2]diazocine-3-carboxylate (34a):

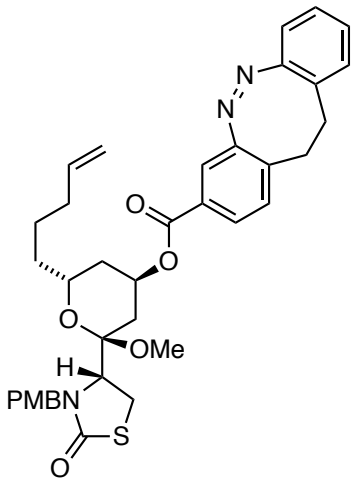

(S)-**20** (30.0 mg, 71.2 µmol, 1.00 eq.), benzoic acid **38**[13] (21.5 mg, 85.4 µmol, 1.20 eq.) and PPh_3 (37.3 mg, 0.15 mmol, 2.00 eq.) were dissolved in dry THF (1.40 ml). the reaction mixture was cooled to 0 °C and DEAD (40% in toluene, 68.0 µl, 0.15 mmol, 2.1 eq.) was added. After 10 min., the reaction was allowed to warm to r.t. and stirred for 3 h, concentrated and purified by flash column chromatography (SiO_2, Hex:EtOAc = 9:1 to 5:5). The title compound was obtained as an orange film (27.2 mg, 41.4 µmol, 58%).

LCMS (50-100% MeCN in H_2O over 5 min, 0.1% FA): t_{ret} = 4.1 min

^{1}H-NMR (400 MHz, $CDCl_3$): δ [ppm] = 7.69 (dd, *J* = 7.9, 1.7 Hz, 1H), 7.50 (d, *J* = 1.7 Hz, 1H), 7.21 (d, *J* = 8.6 Hz, 2H), 7.17 – 7.10 (m, 1H), 7.10 – 6.96 (m, 3H), 6.86 (d, *J* = 8.7 Hz, 2H),

[13] Kindly provided by Martin S. Maier.

6.87 – 6.80 (m, 1H), 5.85 (ddt, *J* = 17.0, 10.2, 6.7 Hz, 1H), 5.34 (s, 1H), 5.13 – 4.98 (m, 3H), 4.27 (d, *J* = 14.4 Hz, 1H), 3.97 (q, *J* = 10.1, 7.9 Hz, 1H), 3.84 – 3.77 (m, 1H), 3.81 (s, 3H), 3.27 – 3.18 (m, 2H), 3.17 – 2.93 (m, 5H), 2.90 – 2.74 (m, 2H), 2.16 (dq, *J* = 13.4, 7.1, 6.2 Hz, 2H), 1.98 – 1.85 (m, 2H), 1.79 – 1.40 (m, 6H).

^{13}C-NMR (101 MHz, $CDCl_3$): δ [ppm] = 173.2, 165.0, 159.3, 155.4, 155.4, 138.4, 133.6, 130.0, 129.9, 129.8, 128.9, 128.3, 127.6, 127.5, 127.1, 120.4, 119.0, 115.2, 114.2, 101.8, 67.1, 66.3**, 66.3**, 59.2, 55.4, 47.7, 47.5, 35.6, 34.6, 34.0, 32.0, 31.6, 30.4*, 30.3*, 29.8, 25.5, 25.2.

* two peaks or split peaks that correspond to the same carbon. shift due to different conformation of *cis*-diazocine with respect to tetrahydropyran core

For NMR spectra, major (*cis*)-isomer reported; NMR Spectra contain traces of H_2DEAD side-product.

HRMS (ESI$^+$, *m/z*): $[M+Na]^+$ for $NaC_{37}H_{41}N_3O_6S^+$: calcd.: 678.2608, found: 678.2634.

IR (ATR): $\tilde{\nu}$ [cm^{-1}] = 2935 (w), 1714 (s), 1670 (s), 1610 (w), 1586 (w), 1512 (s), 1441 (w), 1402 (w), 1353 (w), 1284 (s), 1248 (s), 1216 (m), 1196 (m), 1174 (m), 1121 (m), 1093 (s), 1034 (s), 942 (w), 915 (w), 846 (w), 754 (m).

Synthesis of (2R,4R,6R)-2-methoxy-2-((R)-2-oxothiazolidin-4-yl)-6-(pent-4-en-1-yl)tetrahydro-2H-pyran-4-yl-11,12-dihydrodibenzo[c,g][1,2]diazocine-3-carboxylate (39):

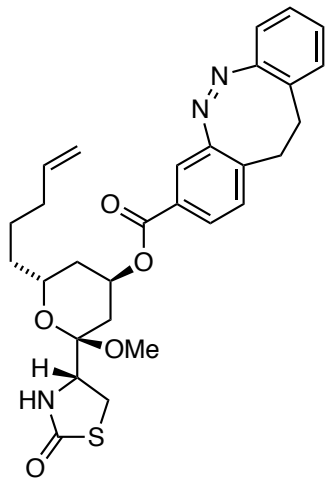

37 (10.0 mg, 33.2 µmol, 1.00 eq.), diazocine *meta*-benzoic acid (**38**) (10.0 mg, 39.8 µmol, 1.20 eq.) and PPh_3 (17.4 mg, 66.4 µmol, 2.00 eq.) were dissolved in dry THF (0.66 ml). the reaction mixture was cooled to 0 °C and DEAD (40% in toluene, 32.0 µl, 69.7 umol, 2.1 eq.) was added. After 10 min., the reaction was allowed to warm to r.t. and stirred for 1 h, concentrated and purified by flash column chromatography (SiO_2, Hex:EtOAc = 9:1 to 5:5). The title compound was separated from the inseparable side-product H_2DEAD by HPLC (semi-prep, 60-80% MeCN in H_2O over 8 min., 3 min MeCN, no FA) and obtained as an orange film (8.9 mg, 16.6 µmol, 50%).

R_f (SiO_2, Hex:EtOAc = 5:5) = 0.5

LCMS (50-100% MeCN in H_2O over 5 min, 0.1% FA): t_{ret} 3.2 min.

HPLC: (semi-prep, 60-80% MeCN in H_2O over 8 min, 3 min MeCN, no FA) t_{ret} = 5.8 min.

^{1}H-NMR (400 MHz, $CDCl_3$): δ [ppm] = 7.69 (d, *J* = 7.9 Hz, 1H), 7.50 (s, 1H), 7.15 (t, *J* = 7.6 Hz, 1H), 7.10 – 6.95 (m, 3H), 6.90 – 6.80 (m, 1H), 5.80 (ddt, *J* = 16.9, 10.1, 6.7 Hz, 1H), 5.47 (s, 1H), 5.35 (s, 1H), 5.08 – 4.93 (m, 2H), 4.15 – 4.07 (m, 1H), 4.00 – 3.90 (m, 1H), 3.37 – 3.18 (m, 6H), 3.10 – 2.95 (m, 2H), 2.91 – 2.70 (m, 2H), 2.16 – 2.01 (m, 3H), 2.01 – 1.91 (m, 1H), 1.87 (d, *J* = 14.4 Hz, 1H), 1.69 – 1.36 (m, 5H).

^{13}C-NMR (101 MHz, $CDCl_3$): δ [ppm] = 174.7, 165.0, 155.4, 155.3, 138.5, 133.7, 130.1, 129.8, 129.7, 128.3*, 127.6* 127.5, 127.1, 120.5, 119.0, 115.1, 100.0, 67.1, 66.2*, 66.1*, 56.6, 48.0*, 35.1, 34.4, 33.9, 32.1, 31.6, 29.7*, 29.5*, 28.1, 24.8.
* two peaks or split peaks that correspond to the same carbon. shift due to different conformation of *cis*-diazocine with respect to tetrahydropyran core

HRMS (ESI$^+$, *m/z*): $[M+Na]^+$ for $C_{29}H_{33}N_3O_5SNa^+$: calcd.: 558.2033, found: 558.2029.

IR (ATR): $\tilde{\nu}$ [cm^{-1}] = 3224 (w), 2937 (w), 1713 (s), 1684 (s), 1457 (w), 1351 (w), 1284 (m), 1256 (m), 1209 (w), 1160 (w), 1120 (s), 1095 (m), 1036 (m), 912 (w), 953 (w).

Synthesis of (2*R*,4*R*,6*R*)-2-hydroxy-2-((*R*)-2-oxothiazolidin-4-yl)-6-(pent-4-en-1-yl)tetra hydro-2*H*-pyran-4-yl-11,12-dihydrodibenzo[*c*,*g*][1,2]diazocine-3-carboxylate (40):

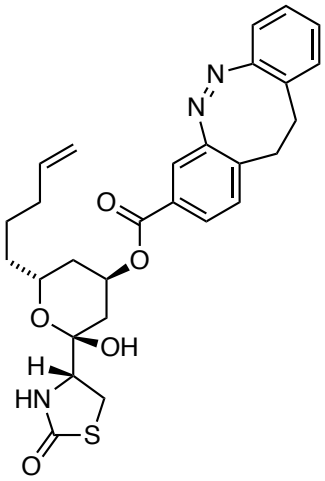

39 (6.90 mg, 12.9 µmol, 1.00 eq.) was dissolved in THF (1.00 ml) and H_2O (0.45 ml) and AcOH (0.45 ml) was added. the reaction was heated to 45 °C and after 3 h, a second amount of AcOH (0.45 ml) was added and the reaction stirred for 3 h at 45 °C. The reaction was cooled to room temperature and $NaHCO_3$ (sat. aq., 5.00 ml) was added. the reaction was extracted with EtOAc (3 x 5 ml). The combined organic layers were washed with brine, dried over Na_2SO_4, filtered and concentrated. The crude product was purified by flash column chromatography (SiO_2, Hex:EtOAc = 6:4 to 0:10) and **40** was obtained as an orange film (1.40 mg, 2.70 µmol, 21%).

R_f (SiO_2, Hex:EtOAc = 5:5; CAM) = 0.27 (minor), 0.45 (major).

^{1}H-NMR (400 MHz, $CDCl_3$): δ [ppm] = 7.62 (dd, J = 8.0, 1.8 Hz, 1H), 7.46 (d, J = 1.8 Hz, 1H), 7.16 (td, J = 7.6, 1.5 Hz, 1H), 7.10 (d, J = 8.0 Hz, 1H), 7.07 – 6.94 (m, 2H), 6.87 (dd, J = 7.8, 1.3 Hz, 1H), 5.77 (ddd, J = 16.9, 10.2, 6.1 Hz, 1H), 5.61 (s, 1H), 5.55 (s, 1H), 5.04 – 4.92 (m, 2H), 4.16 – 4.08 (m, 1H), 3.82 (dd, J = 8.9, 5.8 Hz, 1H), 3.57 (s, 1H), 3.49 (dd, J = 11.3, 9.3 Hz, 1H), 3.42 – 3.34 (m, 1H), 3.09 – 2.97 (m, 2H), 2.92 – 2.74 (m, 2H), 2.09 – 2.00 (m, 4H), 2.00 – 1.90 (m, 1H), 1.61 – 1.36 (m, 5H).

^{13}C-NMR (101 MHz, $CDCl_3$): δ [ppm] = 174.7, 155.6, 155.4, 138.5, 134.6, 130.4, 129.8, 128.6, 128.0, 127.6, 127.5, 127.2, 120.4, 119.1, 115.0, 97.5, 68.8, 65.4, 61.7, 35.0, 34.4, 33.7, 32.1, 31.5, 31.3, 28.9, 24.6.

HRMS (ESI$^+$, *m/z*): $[(M+H)–H_2O]^+$ for $C_{28}H_{31}N_3O_4S^+$: calcd.: 405.1952, found: 405.1972.

IR (ATR): $\tilde{\nu}$ [cm^{-1}] = 3281 (w), 3066 (w), 2926 (m), 2855 (w), 1680 (s), 1402 (w), 1350 (w), 1285 (s), 1256 (s), 1210 (m), 1158 (m), 1098 (s), 948 (s), 910 (w), 792 (w), 754 (m), 718 (w), 706 (w).

Synthesis of (2*R*,4*R*,6*R*)-2-methoxy-2-((*R*)-3-(4-methoxybenzyl)-2-oxothiazolidin-4-yl)-6-(pent-4-en-1-yl)tetrahydro-2*H*-pyran-4-yl 4-(phenyldiazenyl)benzoate (34c):

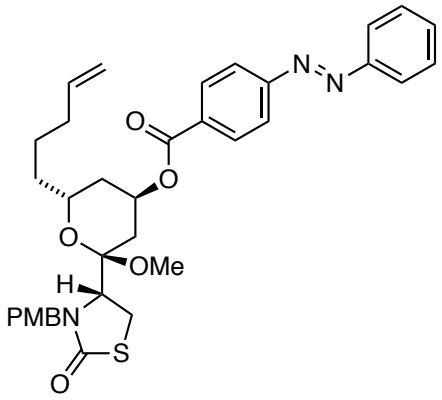

(*S*)-**20** (30.0 mg, 71.2 µmol, 1.00 eq.), *para*-benzoic acid azobenzene (19.3 mg, 85.4 µmol, 1.20 eq.) and PPh_3 (37.3 mg, 0.15 mmol, 2.00 eq.) were dissolved in dry THF (1.40 ml). the reaction mixture was cooled to 0 °C and DEAD (40% in toluene, 68.0 µl, 0.15 mmol, 2.1 eq.) was added. After 10 min., the reaction was allowed to warm to r.t. and stirred for 3 h, concentrated and purified by flash column chromatography (SiO_2, Hex:EtOAc = 9:1 to 5:5). The title compound was obtained as an orange film (33.3 mg, 52.9 µmol, 74%).

^{1}H-NMR (400 MHz, $CDCl_3$): δ [ppm] = 8.24 – 8.18 (m, 2H), 7.99 – 7.92 (m, 4H), 7.58 – 7.50 (m, 3H), 7.25 – 7.21 (m, 2H), 6.91 – 6.84 (m, 2H), 5.93 – 5.81 (m, 1H), 5.45 (s_{br}, 1H), 5.14 (d, J = 14.4 Hz, 1H), 5.11 – 4.99 (m, 2H), 4.31 (d, J = 14.2 Hz, 1H), 4.13 – 4.04 (m, 1H), 3.86 (t, J = 6.0 Hz, 1H), 3.82 (s, 3H), 3.26 (d_{br}, J = 6.2 Hz, 2H), 3.19 (s, 3H), 2.31 – 2.12 (m, 3H), 2.05 – 1.94 (m, 2H), 1.85 – 1.48 (m, 5H).

^{13}C-NMR (100 MHz, $CDCl_3$): δ [ppm] = 173.2, 165.4, 159.3, 155.3, 152.7, 138.4, 132.6, 131.9, 130.8, 129.9, 129.3, 128.9, 123.3, 122.8, 115.2, 114.2, 101.9, 67.3, 66.4, 59.3, 55.4, 47.8, 47.6, 35.7, 34.7, 34.0, 30.4, 25.6, 25.3.

NMR spectra reported for major (*trans*) isomer.

HRMS (ESI$^+$, *m/z*): $[M+Na]^+$ for $NaC_{35}H_{39}N_3O_6S^+$: calc.: 652.2452, found: 652.2452.

IR (ATR): $\tilde{\nu}$ [cm^{-1}] = 2938 (w), 2835 (w), 1715 (s), 1672 (s), 1611 (w), 1513 (m), 1444 (w), 1404 (w), 1353 (w), 1276 (s), 1249 (s), 1217 (m), 1196 (m), 1175 (m), 1143 (m), 1120 (m), 1093 (s), 1035 (m), 1012 (m), 913 (w), 864 (w), 847 (w), 779 (m), 718 (w).

Synthesis of (2*R*,4*R*,6*R*)-2-methoxy-2-((*R*)-2-oxothiazolidin-4-yl)-6-(pent-4-en-1-yl)tetra hydro-2*H*-pyran-4-yl 4-(phenyldiazenyl)benzoate (35c):

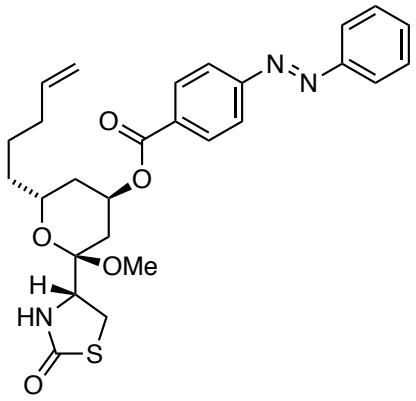

34c (33.3 mg, 52.9 µmol, 1.00 eq.) was dissolved in MeOH (2.70 ml) and MeCN (0.55 ml) and CAN (145 mg, 0.26 mmol, 5.00 eq.) was added. the reaction was stirred at room temperature over night. $NaHCO_3$ (sat. aq. 5 ml), H_2O (5 ml) and EtOAc (5 ml) were added and the layers separated. The aqueous phase was extracted with EtOAc (3 x 10 ml). the combined organic layers were washed with brine, dried over Na_2SO_4, filtered and concentrated. Purification by flash column chromatography (SiO_2, Hex:EtOAc = 8:2 to 2:8) and HPLC (semi-prep, 70-90% MeCN in H_2O over 8 min, 3 min MeCN, no FA) gave the title compound as an orange oil (12.8 mg, 25.1 µmol, 48%).

R_f (SiO_2, Hex:EtOAc = 7:3, CAM) = 0.40

LCMS (50-100% MeCN in H_2O over 5 min, 0.1% FA): 2.5 min (*cis*) 3.9 min (*trans*).

HPLC (semi-prep, 70-90% MeCN in H_2O over 8 min, 3 min MeCN, no FA): t_{ret} = 3.3 min (minor), 6.1 min (major).

^{1}H-NMR (400 MHz, $CDCl_3$): δ = 8.58 (s, 1H), 8.18 – 8.10 (m, 2H), 7.96 – 7.87 (m, 2H), 7.62 (t, J = 7.8 Hz, 1H), 7.57 – 7.48 (m, 3H), 5.88 – 5.72 (m, 1H), 5.57 – 5.45 (m, 2H), 5.07 – 4.93 (m, 2H), 4.16 (t, J = 8.1 Hz, 1H), 4.12 – 4.05 (m, 1H), 3.40 – 3.30 (m, 1H), 3.34 (s. 3H), 2.19 – 1.90 (m, 5H), 1.72 – 1.41 (m, 5H).

^{13}C-NMR (101 MHz, $CDCl_3$): δ = 174.7, 165.4, 152.7, 152.6, 138.5, 132.1, 131.8, 131.6, 129.4, 129.3, 127.6, 123.7, 123.1, 115.1, 100.1, 67.1, 66.2, 56.7, 48.1, 35.2, 34.5, 33.9, 29.8, 28.2, 24.9.

HRMS (ESI$^+$, *m/z*): $[M+H]^+$ for $C_{26}H_{30}N_3O_5S^+$: calc.: 496.1901, found: 496.1896.

IR (ATR): $\tilde{\nu}$ [cm^{-1}] = 3223 (w), 3074 (w), 2939 (w), 1716 (s), 1683 (s), 1437 (w), 1353 (w), 1294 (m), 1272 (m), 1209 (m), 1175 (w), 1153 (m), 1094 (m), 1074 (m), 1035 (m), 911 (w), 819 (w), 769 (m), 723 (w).

Synthesis of (2*R*,4*R*,6*R*)-2-hydroxy-2-((*R*)-2-oxothiazolidin-4-yl)-6-(pent-4-en-1-yl)tetra hydro-2*H*-pyran-4-yl 4-(phenyldiazenyl)benzoate (36c):

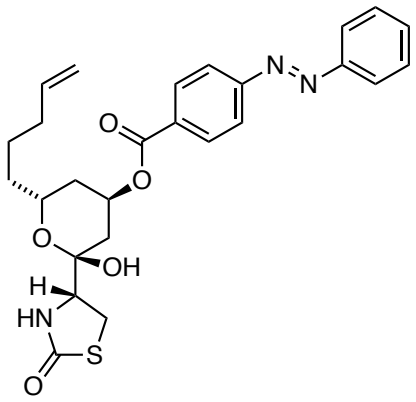

35c (12.8 mg, 25.1 µmol, 1.00 eq.) was dissolved in THF (0.40 ml) and H_2O (0.40 ml) and AcOH (1.20 ml) was added. the reaction was heated to 45 °C and stirred for 4 h. after cooling to room temperature, $NaHCO_3$ (5 ml) was added, and the reaction was extracted with EtOAc (3 x 10 ml). The combined organic layers were washed with brine, filtered, and concentrated. The crude product was purified by flash column chromatography (SiO_2, Hex:EtOAc = 8:2 to 2:8) and HPLC (semi-prep, 50-80% MeCN in H_2O over 8 min, 3 min MeCN, no FA). **36c** was obtained as an orange oil (7.10 mg, 14.3 µmol, 57%).

R_f (SiO_2, Hex:EtOAc = 5:5; CAM) = 0.58

LCMS (50-100% MeCN in H_2O over 5 min, 0.1% FA): 1.8 min (*cis*) 3.1 min (*trans*).

HPLC (semi-prep, 50-80% MeCN in H_2O over 8 min, 3 min MeCN, no FA): 5.5 min (minor), 8.3 min (major).

^{1}H-NMR (400 MHz, $CDCl_3$): δ [ppm] = 8.20 – 8.10 (m, 2H), 8.08 – 7.91 (m, 4H), 7.55 (d, J = 6.3 Hz, 3H), 5.80 (ddt, J = 17.0, 9.5, 6.7 Hz, 1H), 5.70 (s, 1H), 5.69 – 5.61 (m, 1H), 5.08 – 4.93 (m, 2H), 4.29 – 4.17 (m, 1H), 3.86 (dd, J = 8.8, 6.2 Hz, 1H), 3.72 (s, 1H), 3.52 (dd, J = 11.4, 9.2 Hz, 1H), 3.44 (dd, J = 11.8, 6.0 Hz, 1H), 2.24 – 1.96 (m, 5H), 1.70 – 1.34 (m, 5H).

^{13}C-NMR (101 MHz, $CDCl_3$): δ [ppm] = 174.8, 164.8, 155.6, 152.6, 138.6, 132.1, 131.4, 130.7, 129.4, 123.4, 123.1, 115.0z, 97.6, 68.9, 65.4, 61.7, 35.1, 34.5, 33.7, 31.4, 28.9, 24.6.

HRMS (APCI⁺, *m/z*): $[M+H]^+$ for $C_{26}H_{30}N_3O_5S^+$: calcd.: 496.1901, found: 496.1896.

IR (ATR): $\tilde{\nu}$ [cm^{-1}] = 3323 (w), 3067 (w), 2924 (w), 1680 (s), 1604 (w), 1486 (w), 1444 (w), 1408 (w), 1346 (w), 1276 (s), 1221 (w), 1143 (w), 1096 (m), 1012 (w), 912 (w), 866 (w), 778 (m), 762 (w).

Synthesis of (2*R*,4*R*,6*R*)-2-methoxy-2-((*R*)-3-(4-methoxybenzyl)-2-oxothiazolidin-4-yl)-6-(pent-4-en-1-yl)tetrahydro-2*H*-pyran-4-yl 3-(phenyldiazenyl)benzoate (34d):

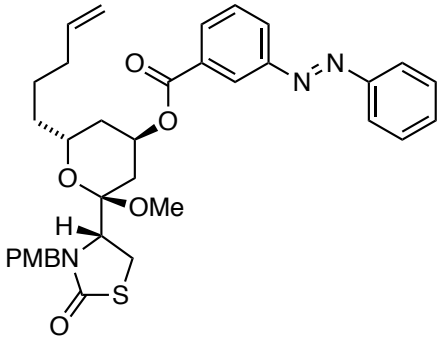

A flame dried vial with stir bar was charged with (*S*)-**20** (30.0 mg, 71.2 µmol, 1.00 eq.), Azobenzene **S5** (193 mg, 85.4 µmol, 1.20 eq.) and PPh_3 (37.3 mg, 0.14 mmol, 2.00 eq.). The reaction was evacuated/ backfilled with nitrogen and dissolved in dry THF (1.42 ml). the reaction was cooled to 0 °C and DEAD (40% in toluene, 68.0 µl, 0.15 mmol, 2.10 eq.) was added dropwise. The reaction was stirred for 10 minutes at 0 °C and warmed to room temperature. After stirring for 4 h at r.t., the reaction mixture was concentrated and subjected to flash column chromatography (SiO_2, Hex:EtOAc = 9:1 to 5:5). The title compound was obtained as orange oil (39.8 mg, 63.2 µmol, 89%).

R_f (SiO_2, Hex:EtOAc = 5:5) = 0.7

^{1}H-NMR (400 MHz, $CDCl_3$): δ [ppm] = 8.59 (d, J = 2.0 Hz, 1H), 8.19 – 8.10 (m, 2H), 7.96 – 7.90 (m, 2H), 7.66 – 7.58 (m, 1H), 7.56 – 7.50 (m, 3H), 7.25 – 7.21 (m, 2H), 6.91 – 6.85 (m, 2H), 5.87 (dtd, J = 17.9, 9.4, 8.5, 6.3 Hz, 1H), 5.48 (s, 1H), 5.14 (d, J = 14.5 Hz, 1H), 5.11 – 4.97 (m, 2H), 4.31 (d, J = 14.5 Hz, 1H), 4.15 – 4.07 (m, 1H), 3.87 (dd, J = 7.1, 4.9 Hz, 1H),

3.82 (s, 3H), 3.28 – 3.25 (m, 2H), 3.23 (s, 3H), 2.33 – 2.12 (m, 3H), 2.07 – 1.94 (m, 2H), 1.83 – 1.49 (m, 5H).

^{13}C-NMR (101 MHz, $CDCl_3$): δ [ppm] = 173.2, 165.4, 159.3, 152.7, 152.6, 138.4, 132.2, 131.8, 131.6, 130.0, 129.3, 128.9, 127.7, 123.7, 123.1, 120.8, 115.2, 114.2 101.9, 67.2, 66.4, 59.3, 55.4, 47.8, 47.6, 35.7, 34.72, 34.0, 30.5, 25.6, 25.2.

HRMS (APCI$^+$, *m*/*z*): $[M+H]^+$ for $C_{35}H_{40}N_3O_6S^+$: calc.: 630.2632, found: 630.2609
$[(M+Na)^+]$ for $NaC_{35}H_{39}N_3O_6S^+$: calc.: 652.2452, found: 652.2493.

IR (ATR): $\tilde{\nu}$ [cm^{-1}] = 2937 (w), 2835 (w), 1715 (m). 1667 (s), 1611 (w), 1586 (w), 1512 (m), 1441 (w), 1401 (w), 1354 (w), 1294 (m) 1269 (s), 1247 (s), 1210 (s), 1174 (s), 1152 (m), 1125 (m), 1091 (s), 1072 (s), 1032 (s), 999 (m), 913 (m), 845 (m), 818 (m), 769 (s), 756 (m), 734 (s).

Synthesis of (2*R*,4*R*,6*R*)-2-methoxy-2-((*R*)-2-oxothiazolidin-4-yl)-6-(pent-4-en-1-yl)tetrahydro-2*H*-pyran-4-yl 3-(phenyldiazenyl)benzoate (35d):

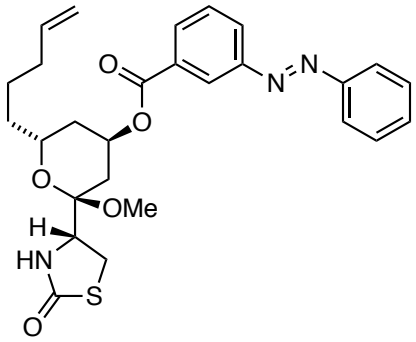

34d (32.4 mg, 51.4 µmol, 1.00 eq.) was dissolved in MeOH (2.6 ml) and MeCN (0.5 ml) and CAN (141 mg, 0.26 mmol, 5.00 eq.) was added at room temperature. The reaction was stirred over night and $NaHCO_3$ (sat. aq., 5 ml), H_2O (5 ml) and EtOAc (5 ml) were added. The layers were separated, and the aqueous layer was extracted with EtOAc (3 x 5 ml). The combined organic layers were washed with brine, dried over Na_2SO_4, filtered and concentrated. The crude product was purified by flash column chromatography (SiO_2, Hex:EtOAc = 8:2 to 5:5)

and HPLC (semi-prep, 70-90% MeCN in H_2O over 8 min, 3 min MeCN, no FA) and furnished **35d** as an orange film (8.90 mg, 17.4 µmol, 34%).

R_f (SiO_2, Hex:EtOAc = 7:3; CAM) = 0.43

LCMS (50-100% MeCN in H_2O over 5 min, 0.1% FA): 2.5 min (*cis*), 3.9 min (*trans*).

HPLC (semi-prep, 70-90% MeCN in H_2O over 8 min, 3 min MeCN, no FA): 3.3 min (minor), 6,1 min (major).

^{1}H-NMR (400 MHz, $CDCl_3$): δ [ppm] = 8.20 (d, J = 8.1 Hz, 2H), 8.00 – 7.91 (m, 4H), 7.58 – 7.49 (m, 3H), 5.81 (ddt, J = 16.9, 9.6, 6.7 Hz, 1H), 5.50 (s, 1H), 5.45 (s_{br}, 1H), 5.08 – 4.94 (m, 2H), 4.15 (t, J = 8.1 Hz, 1H), 4.11 – 4.01 (m, 1H), 3.41 – 3.27 (m, 2H), 3.30 (s, 3H), 2.20 – 1.86 (m, 5H), 1.72 – 1.40 (m, 5H).

^{13}C-NMR (101 MHz, $CDCl_3$): δ [ppm] = 174.7, 165.4, 155.3, 152.7, 138.5, 132.5, 131.9, 130.8, 129.4, 123.3, 122.8, 122.8, 115.1, 100.1, 67.2, 66.2, 56.7, 48.1, 35.2, 34.5, 33.9, 29.7, 28.2, 24.9.

HRMS (APCI$^+$, *m/z*): $[M+H]^+$ for $C_{27}H_{32}N_3O_5S^+$: calc.: 510.2057, found: 510.2036

Synthesis of (2R,4R,6R)-2-hydroxy-2-((R)-2-oxothiazolidin-4-yl)-6-(pent-4-en-1-yl)tetra hydro-2H-pyran-4-yl 3-((E)-phenyldiazenyl)benzoate (36d):

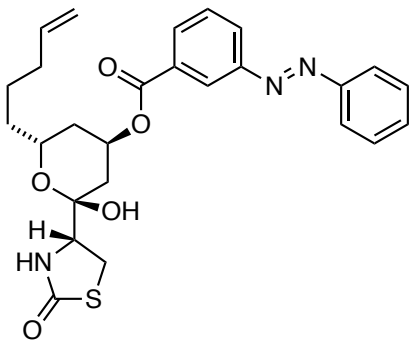

35d (9.00 mg, 17.7 µmol, 1.00 eq.) was dissolved in THF (0.30 ml) and water (0.30 ml). Next, AcOH (0.30 ml) was added and the reaction was heated to 45 °C for 4 h. After cooling to room temperature, $NaHCO_3$ (sat. aq., 5 ml) and EtOAc (5 ml) were added and separated. The aqueous layer was extracted with EtOAc (3 x 5 ml) and the combined organic layers were washed with brine, dried over Na_2SO_4, filtered and concentrated. The crude product was purified by flash column chromatography (SiO_2, Hex:EtOAc = 8:2 to 2:8) and HPLC (semi-prep, 50-80% MeCN in H_2O over 8 min, 3 min MeCN, no FA) and gave **36d** as an orange film (4.70 mg, 9.50 µmol, 54%).

R_f (SiO_2, Hex:EtOAc = 5:5; CAM) = 0.61

LCMS (50-100% MeCN in H_2O over 5 min, 0.1% FA): t_{ret} = 1.8 min (cis), 3.1 min (trans).

HPLC (semi-prep, 50-80% MeCN in H_2O over 8 min, 3 min MeCN, no FA): t_{ret} = 5.4 min (minor), 8.1 min (major).

^{1}H-NMR (400 MHz, $CDCl_3$): δ [ppm] = 8.52 (d, J = 1.9 Hz, 1H), 8.18 – 8.08 (m, 2H), 7.95 (dd, J = 7.4, 2.5 Hz, 2H), 7.67 – 7.60 (m, 1H), 7.60 – 7.49 (m, 3H), 5.80 (ddt, J = 16.9, 8.9, 6.6 Hz, 1H), 5.73 – 5.63 (m, 2H), 4.99 (dd, J = 21.0, 13.7 Hz, 2H), 4.29 – 4.19 (m, 1H), 3.86 (dd, J = 8.8, 6.2 Hz, 1H), 3.72 (s, 1H), 3.56 – 3.39 (m, 2H), 2.25 – 1.96 (m, 5H), 1.71 – 1.41 (m, 5H).

^{13}C-NMR (101 MHz, $CDCl_3$): δ [ppm] = 174.7, 164.8, 152.9, 152.5, 138.6, 131.8, 131.5, 131.0, 129.7, 129.3, 127.1, 124.5, 123.3, 115.0, 97.6, 69.0, 65.4, 61.7, 35.1, 34.5, 33.7, 31.4, 28.9, 24.6.

HRMS (ESI$^+$, *m/z*): $[M+Na]^+$ for $C_{26}H_{29}N_3O_5SNa^+$: calcd.: 518.1720, found: 518.1743.

IR (ATR): $\tilde{\nu}$ [cm^{-1}] = 3317 (w), 2922 (w), 2855 (w), 1716 (m), 1679 (s), 1439 (w), 1349 (w), 1295 (m), 1271 (m), 1210 (m), 1176 (w), 1153 (m), 1100 (m), 1070 (m), 1021 (w), 913 (w), 814 (w), 806 (w), 770 (m), 759 (w), 716 (w).

Synthesis of (2*R*,4*R*,6*R*)-2-methoxy-2-((*R*)-3-(4-methoxybenzyl)-2-oxothiazolidin-4-yl)-6-(pent-4-en-1-yl)tetrahydro-2*H*-pyran-4-yl 2-(phenyldiazenyl)benzoate (34e):

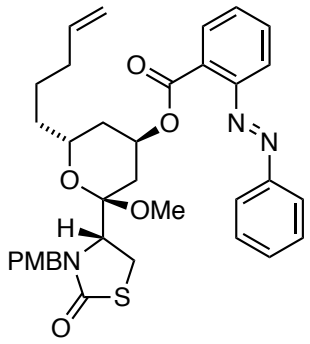

A flame-dried vial was equipped with a stir bar and charged with (*S*)-**20** (30.0 mg, 71.2 µmol, 1.00 eq.), azobenzene **S4** (142 mg, 0.14 mmol, 2.00 eq.) and PPh_3 (93.3 mg, 0.36 mmol, 5.00 eq.). The reaction mixture was evacuated and backfilled with nitrogen, dissolved in dry toluene (1.4 ml) and cooled to 0 °C. DEAD (40% in toluene, 0.20 ml, 0.50 mmol, 7.00 eq.) was added dropwise and the reaction was stirred at 0 °C for 10 minutes, following 14 h at room temperature. The crude reaction mixture was loaded on SiO_2 (3.0 g), dried and subjected to flash column chromatography (SiO_2, Hex:EtOAc = 9.5:0.5 to 6:4). The desired product was inseparable from the H_2DEAD side product and subjected to the subsequent transformation without further purification.

Synthesis of (2R,4R,6R)-2-methoxy-2-((R)-2-oxothiazolidin-4-yl)-6-(pent-4-en-1-yl)tetrahydro-2H-pyran-4-yl 2-(phenyldiazenyl)benzoate (35e):

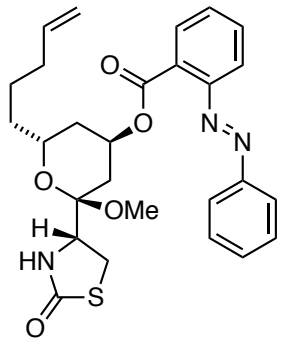

The product mixture of **34e** was dissolved in MeOH (3.6 ml) and MeCN (0.7 ml) and CAN (195 mg, 0.36 mmol, 5.00 eq.) was added. The reaction was stirred over night at room temperature and $NaHCO_3$ (sat. aq., 10 ml) and water (10 ml) were added. The reaction was extracted with DCM (3 x 30 ml). the combined organic layers were washed with brine, dried over Na_2SO_4, filtered and concentrated. The crude product was purified by flash column chromatography (SiO_2, Hex:EtOAc = 8:2 to 5:5) and HPLC (semi-prep, 30 –80% MeCN in H_2O over 8 min, 3 min MeCN, no FA). The title compound was obtained as an orange film (11.3 mg, 22.2 µmol, 31% over two steps).

R_f (SiO_2, Hex:EtOAc = 5/5) = 0.5

LCMS (50-100% MeCN in H_2O over 5 min, 0.1% FA): tRet = 2.5 min. (*cis*), 3.5 min. (*trans*).

HPLC (semi-prep, 40-80% MeCN in H_2O over 8 min, 3 min MeCN, no FA): t_{ret} = 9.19 min (major).

^{1}H-NMR (400 MHz, $CDCl_3$): δ [ppm] = 7.94 – 7.87 (m, 3H), 7.64 – 7.57 (m, 1H), 7.55 – 7.47 (m, 5H), 5.75 (ddt, J = 16.9, 10.1, 6.6 Hz, 1H), 5.45 (s, 1H), 5.44 – 5.40 (m, 1H), 5.03 – 4.92 (m, 2H), 4.08 – 4.00 (m, 1H), 3.85 – 3.74 (m, 1H), 3.28 – 3.07 (m, 2H), 3.11 (s, 3H), 2.15 – 1.79 (m, 5H), 1.56 – 1.10 (m, 5H).

^{13}C-NMR (101 MHz, $CDCl_3$): δ [ppm] = 174.7, 166.5, 152.8, 152.7, 138.5, 132.3, 131.6, 130.2, 129.7, 129.3, 128.9, 123.4, 118.5, 115.0, 99.9, 67.5, 66.0, 56.6, 47.8, 35.1, 34.5, 33.9, 29.5, 28.0, 24.8.

HRMS (ESI$^+$, *m/z*): $[M+Na]^+$ for $NaC_{27}H_{31}N_3O_5S^+$ calcd.: 532.1877, found: 532.1880.

Synthesis of (2R,4R,6R)-2-hydroxy-2-((R)-2-oxothiazolidin-4-yl)-6-(pent-4-en-1-yl)tetrahydro-2H-pyran-4-yl 2-(phenyldiazenyl)benzoate (36e):

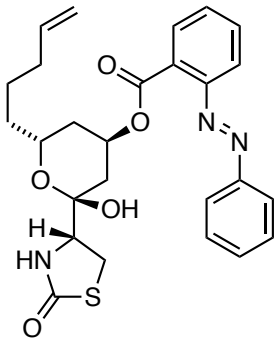

35e (10.0 mg, 19.6 µmol, 1.00 eq.) was dissolved in THF (0.6 ml), H_2O (0.6 ml) and AcOH (0.9 ml) and stirred at 45 °C for 2 h. Then, AcOH (0.9 ml) was again added, and the reaction stopped after 2 h by pouring it into $NaHCO_3$ (sat. aq., 20 ml). the reaction was extracted with EtOAc (3 x 20 ml). The combined organic layers were washed with brine, dried over Na_2SO_4, filtered and concentrated. The crude product was purified twice by HPLC (semi-prep, 40 – 80% MeCN in H_2O over 8 min, 3 min MeCN, no FA) and obtained as an orange film (1.00 mg, 2.00 µmol, 10%).
Note: during the reaction, decomposition was observed. The reaction was thus stopped to obtain a small quantity of the final product for biological evaluation by cell proliferation assay.

R_f (SiO_2, Hex:EtOAc = 5:5; CAM) = 0.54 (major), 0.44 (minor).

LCMS (50-100% MeCN in H_2O over 5 min, 0.1% FA): t_{Ret} = 1.7 min (*cis*), 2.4 min (*trans*).

HPLC (semi-prep, 40 – 80% MeCN in H_2O over 8 min, 3 min MeCN, no FA) t_{ret} = 6.6 min (minor), 7.9 min (major).

^{1}H-NMR (400 MHz, $CDCl_3$): δ [ppm] = 7.96 – 7.83 (m, 3H), 7.74 – 7.45 (m, 6H), 5.77 – 5.59 (m, 3H), 5.51 (s, 1H), 5.08 – 4.80 (m, 3H), 4.39 (s_{br}, 1H), 3.79 – 3.70 (m, 1H), 3.70 – 3.63 (m,

1H), 3.56 – 3.36 (m, 1H), 3.25 (dd, *J* = 11.7, 9.0 Hz, 1H), 2.95 (dd, *J* = 11.7, 5.6 Hz, 1H), 2.18 – 1.05 (m, 7H).

HRMS (ESI$^+$, *m/z*): $[M+Na]^+$ for $C_{26}H_{29}N_3O_5S^+$: calcd.: 518.1720, found: 518.1742.

Synthesis of (R)-4-((2R,4R,6R)-2-methoxy-6-(pent-4-en-1-yl)-4-(4-(phenyldiazenyl) phenoxy)tetrahydro-2H-pyran-2-yl)thiazolidin-2-one (41):

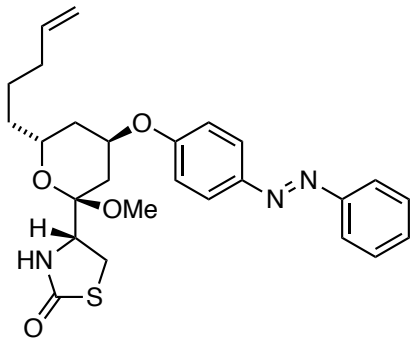

37 (14.8 mg, 49.1 µmol, 1.00 eq.), PPh_3 (32.2 mg, 123 µmol, 2.50 eq.) and 4-hydroxy azobenzene (19.5 mg, 98.2 µmol, 2.00 eq.) were dissolved in dry THF (0.90 ml) and dry toluene (0.30 ml) and cooled to 0 °C using an ice-bath. To the orange reaction mixture, DEAD (40% in toluene, 56.0 µl, 123 µmol, 2.50 eq.) was added and dropwise and the reaction turned dark red. The reaction was stirred at 0 °C for 10 min. before it was warmed to room temperature and stirred over night. The reaction mixture was loaded on isolute, concentrated *in vaccuo* and submitted to purification by flash column chromatography (SiO_2, Hex:EtOAc 9.5:0.5 to 5:5, slow gradient). The title compound was repurified by HPLC (semi-prep, 50 – 90% MeCN in H_2O over 8 min, 3 min MeCN, no FA) yielding the title compound as an orange film (13.0 mg, 27.0 µmol, 55%).

R_f (SiO_2, Hex:EtOAc = 7:3) = 0.44 (major), 0.25 (minor).

LCMS (50-100% MeCN in H2O over 5 min, 0.1% FA): t_{Ret} = 2.4 min (*cis*), 3.8 min. (*trans*)

HPLC (semi-prep, 50 – 90% MeCN in H_2O over 8 min, 3 min MeCN, no FA): 5.8 min (minor), 8.4 min (major).

^{1}H-NMR (600 MHz, $CDCl_3$): δ = 7.91 (d, *J* = 8.9 Hz, 2H), 7.89 – 7.85 (m, 2H), 7.53 – 7.48 (m, 2H), 7.46 – 7.42 (m, 1H), 7.01 (d, *J* = 8.9 Hz, 2H), 5.80 (ddt, *J* = 16.9, 10.1, 6.7 Hz, 1H), 5.52 (s, 1H), 5.05 – 4.94 (m, 2H), 4.87 (s, 1H), 4.15 – 4.11 (m, 1H), 4.10 – 4.04 (m, 1H), 3.38 – 3.25 (m, 2H), 3.27 (s, 3H), 2.14 – 2.06 (m, 3H), 2.03 – 1.97 (m, 2H), 1.65 – 1.41 (m, 5H).

^{13}C-NMR (151 MHz, $CDCl_3$): δ = 174.8, 159.9, 152.9, 147.3, 138.5, 130.6, 129.2, 124.9, 122.7, 116.4, 115.1, 100.0, 69.3, 65.6, 56.7, 48.0, 35.1, 34.2, 33.9, 28.9, 28.2, 24.9.

NMRs are reported for major isomer (*trans*).

HRMS (ESI$^+$, *m/z*): $[M+Na]^+$ for $NaC_{26}H_{31}N_3O_4S^+$: calcd.: 504.1927, found: 504.1935.

IR (ATR): $\tilde{\nu}$ [cm^{-1}] = 3069 (w), 2938 (w), 2361 (w), 2343 (w), 1683 (s), 1599 (m), 1580 (w), 1497 (m), 1442 (w), 1417 (w), 1299 (w), 1248 (m), 1140 (w), 1096 (m), 1036 (w), 913 (w), 839 (w), 769 (w), 721 (w).

Synthesis of (*R*)-4-((2*R*,4*R*,6*R*)-2-hydroxy-6-(pent-4-en-1-yl)-4-(4-(phenyldiazenyl) phenoxy)tetrahydro-2*H*-pyran-2-yl)thiazolidin-2-one (42):

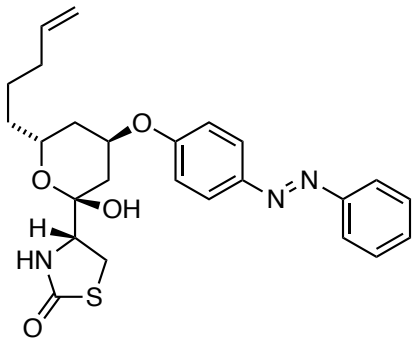

41 (12.8 mg, 26.6 µmol, 1.00 eq.) was dissolved in THF (0.40 ml) and water (0.40 ml) and AcOH (0.40 ml) was added. The reaction mixture was heated to 50 °C for 6.5 h. The reaction was poured into sat. aq. $NaHCO_3$ (30 ml) and Ethyl acetate (30 ml). The layers were separated and the aqueous phase was extracted with Ethyl acetate (2 x 20 ml). The combined organic layers were washed with brine, dried over Na_2SO_4, filtered and concentrated. The crude product was filtered through a plug of silica, eluting with EtOAc and then purified by HPLC

(semi-prep, 40 – 80% MeCN in H_2O over 8 min, 3 min MeCN, no FA). The title compound was obtained in 48% yield (6.0 mg, 12.8 µmol) as an orange film.

R_f (SiO_2, Hex:EtOAc = 4:6; CAM) = 0.59

LCMS (50-100% MeCN in H_2O over 5 min, 0.1% FA): t_{ret} (minor) = 1.7 min, t_{ret} (major) = 3.1 min.

HPLC (semi-prep; 40 – 80% MeCN in H_2O over 8 min., 3 min MeCN, no FA): t_{ret} (minor) = 5.4 min, t_{ret} (major) = 9.2 min.

^{1}H-NMR (400 MHz, $CDCl_3$): δ [ppm] = 7.95 (d, J = 8.9 Hz, 2H), 7.89 (dd, J = 8.4, 1.5 Hz, 2H), 7.56 – 7.43 (m, 3H), 7.05 (d, J = 8.9 Hz, 2H), 5.83 – 5.71 (m, 1H), 5.72 (s, 1H), 5.09 – 4.90 (m, 4H), 4.20 – 4.11 (m, 1H), 3.88 (ddd, J = 9.1, 5.5, 1.1 Hz, 1H), 3.55 (dd, J = 11.7, 9.0 Hz, 1H), 3.44 (dd, J = 11.8, 5.6 Hz, 1H), 2.25 – 2.18 (m, 1H), 2.12 – 1.99 (m, 4H), 1.64 – 1.35 (m, 5H).

^{13}C-NMR (101 MHz, $CDCl_3$): δ [ppm] = 174.9, 158.3, 152.7, 148.1, 138.6, 130.9, 129.2, 125.1, 122.8, 116.2, 115.0, 97.8, 72.5, 64.7, 61.0, 35.0, 33.7, 33.5, 31.7, 29.0, 24.6.

HRMS (ESI$^+$, *m/z*): $[M+H]^+$ for $C_{25}H_{30}N_3O_4S^+$: calcd.: 468.1952, found: 468.1960.

Synthesis of (*R*)-4-((2*R*,4*R*,6*R*)-2-methoxy-6-(pent-4-en-1-yl)-4-(4-((3,4,5-trimethoxy phenyl)diazenyl)phenoxy)tetrahydro-2*H*-pyran-2-yl)thiazolidin-2-one (s43):

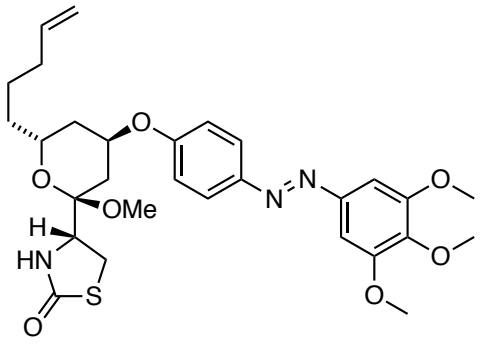

37 (15.0 mg, 49.8 µmol, 1.00 eq.), PPh_3 (32.6 mg, 124 µmol, 2.50 eq.) and **S6** 54.2 mg, 99.6 µmol, 2.00 eq.) were dissolved in dry THF (0.90 ml) and dry toluene (0.30 ml) and cooled to 0 °C using an ice-bath. To the orange reaction micture, DEAD (40% in toluene, 57.0 µl, 124 µmol, 2.50 eq.) was added and dropwise and the reaction turned dark red. The reaction was stirred at 0 °C for 30 min. before it was warmed to room temperature and stirred over night. The reaction mixture was loaded on isolute, concentrated *in vaccuo* and submitted to flash column purification (SiO_2, Hex:EtOAc 9.5:0.5 to 5:5). The purified product contained H_2DEAD, which could be removed by HPLC purification (semi-prep, 50 – 90% MeCN in H_2O over 8 min, 3 min MeCN, no FA). The title compound was obtained in 27% yield (7.60 mg, 13.3 µmol) as an orange film.

R_f (SiO_2, Hex:EtOAc = 7:3) = 0.24

LCMS (50-100% MeCN in H_2O, 0.1% FA) t_{ret} = 2.1 min (*cis*), t_{ret} = 3.3 min (*trans*).

HPLC (semi-prep, 50 – 90% MeCN in H_2O over 8 min, 3 min MeCN, no FA): t_{ret} = 7.4 min (major).

^{1}H-NMR (400 MHz, $CDCl_3$): δ [ppm] = 7.89 (d, J = 8.9 Hz, 2H), 7.21 (s, 2H), 7.01 (d, J = 9.0 Hz, 2H), 5.80 (ddt, J = 17.0, 10.2, 6.7 Hz, 1H), 5.49 (s, 1H), 5.07 – 4.92 (m, 2H), 4.86 (s_{br}, 1H), 4.18 – 4.03 (m, 2H), 3.96 (s, 6H), 3.93 (s, 3H), 3.41 – 3.25 (m, 1H), 3.28 (s, 3H), 2.18 – 1.95 (m, 5H), 1.69 – 1.39 (m, 5H).

^{13}C-NMR (101 MHz, $CDCl_3$): δ [ppm] = 174.7, 159.8, 153.7, 148.8, 147.1, 140.3, 138.5, 124.8, 116.5, 115.1, 100.2, 100.1, 69.3, 65.7, 61.2, 56.7, 56.3, 48.0, 35.2, 34.3, 33.9, 29.0, 28.2, 24.9.

HRMS (APCI$^+$, *m/z*): $[M+H]^+$ for $C_{29}H_{38}N_3O_7S^+$: calcd.: 572.2425, found: 572.2419.

IR (ATR): $\tilde{\nu}$ [cm^{-1}] = 3219 (w), 3077 (w), 2933 (m), 1683 (s), 1597 (m), 1498 (s), 1467 (m), 1409 (w), 1330 (m), 1239 (s), 1146 (m), 1129 (s), 1098 (m), 1036 (m), 1006 (m), 913 (w), 847 (w).

Synthesis of (*R*)-4-((2*R*,4*R*,6*R*)-2-methoxy-6-(pent-4-en-1-yl)-4-(4-((3,4,5-trimethoxy phenyl)diazenyl)phenoxy)tetrahydro-2*H*-pyran-2-yl)thiazolidin-2-one (43):

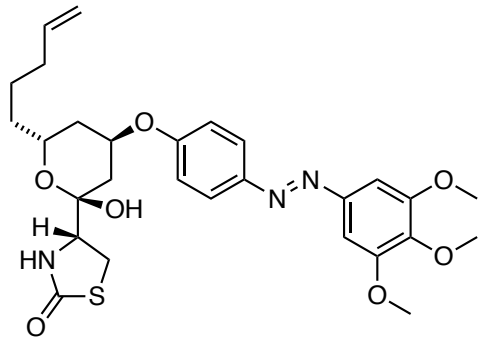

s43 (7.5 mg, 13.1 µmol, 1.00 eq.) was dissolved in THF (0.20 ml) and water (0.20 ml) and AcOH (0.20 ml) was added. The reaction mixture was heated to 50 °C for 4 h. The reaction was poured into sat. aq. $NaHCO_3$ (30 ml) and Ethyl acetate (30 ml). The layers were separated and the aqueous phase was extracted with Ethyl acetate (2 x 20 ml). The combined organic layers were washed with brine, dried over Na_2SO_4, filtered and concentrated. The crude product was purified by HPLC (semi-prep, 45-75% MeCN in H_2O over 8 min, 3 min MeCN, no FA) and the title compound was obtained in 55% yield (4.0 mg, 7.2 µmol) as an orange film.

LCMS (50-100% MeCN in H_2O over 5 min, 0.1% FA) t_{ret} (minor) = 1.4 min and t_{ret} (major) 2.6 min.

HPLC (semi-prep, 45-75% MeCN in H_2O over 8 min, 3 min MeCN, no FA): t_{ret} = 8.3 min (major).

^{1}H-NMR (600 MHz, $CDCl_3$): δ [ppm] = 7.93 (d, *J* = 8.9 Hz, 2H), 7.23 (s, 2H), 7.04 (d, *J* = 8.9 Hz, 2H), 5.77 (ddt, *J* = 16.9, 10.2, 6.7 Hz, 1H), 5.68 (s, 1H), 5.06 (t, *J* = 3.0 Hz, 1H), 5.02 – 4.92 (m, 2H), 4.18 – 4.12 (m, 1H), 3.97 (s, 6H), 3.93 (s, 3H), 3.90 – 3.86 (m, 1H), 3.56 (dd, *J* = 11.8, 9.1 Hz, 1H), 3.44 (dd, *J* = 11.8, 5.4 Hz, 1H), 2.21 (dt, *J* = 14.4, 2.4 Hz, 1H), 2.06 (dtd, *J* = 17.6, 9.3, 8.2, 4.3 Hz, 4H), 1.55 – 1.34 (m, 5H).

^{13}C-NMR (151 MHz, $CDCl_3$): δ [ppm] = 174.9, 158.2, 153.7, 148.6, 147.9, 140.6, 138.6, 125.0, 116.2, 115.0, 100.3, 97.8, 72.5, 64.7, 61.2, 61.0, 56.4, 35.0, 33.7, 33.4, 31.6, 29.1, 24.6.

HRMS (APCI$^+$, *m/z*): $[M+H]^+$ for $C_{28}H_{36}N_3O_7S^+$ calcd.: 558.2268, found: 558.2258.

IR (ATR): $\tilde{\nu}$ [cm^{-1}] = 3524 (w), 3275 (w), 2934 (w), 2360 (w), 2340 (w), 1680 (s), 1597 (s), 1498 (s), 1467 (m), 1410 (m), 1330 (m), 1232 (s), 1147 (m), 1129 (s), 1005 (m), 902 (w), 847 (w), 806 (w), 773 (w), 720 (w).

Synthesis of (*R*)-4-((2*R*,4*R*,6*R*)-4-((11,12-dihydrodibenzo[*c*,*g*][1,2]diazocin-3-yl)oxy)-2-methoxy-6-(pent-4-en-1-yl)tetrahydro-2*H*-pyran-2-yl)thiazolidin-2-one (s44):

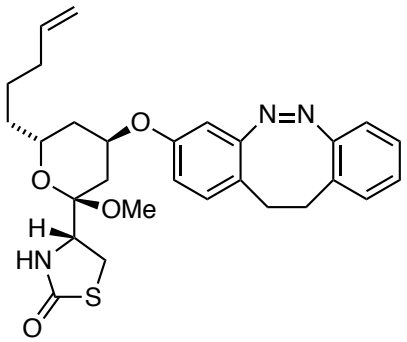

A flame-dried vial with stir bar was charged with **37** (10.0 mg, 33.2 µmol, 1.00 eq.). *meta*-Hydroxy diazocine[14] (14.9 mg, 66.4 mg, 2.00 eq.) and PPh_3 (21.8 mg, 82.3 umol, 2.50 eq.).

[14] Diazocine was provided by Martin S. Maier

The reaction mixture was evacuated,backfilled with nitrogen and dissolved in dry toluene (0.6 ml) and dry THF (0.2 ml). The reaction was cooled to 0 °C and DEAD (40 wt% in toluene, 38.0 ul, 83.4 umol, 2.51 eq.) was added dropwise. The reaction was stirred at 0 °C for 10 minutes and then at room temperature for 20 h. The reaction mixture was loaded onto celite, concentrated to dryness and submitted to flash column chromatography (SiO_2, Hex:EtOAc = 9/1 to 5/5) and HPLC (semi-prep, 50-90% MeCN in H_2O over 8 min, 3 min MeCN, no FA). The title compound was obtained as a yellow film (2.72 mg, 5.40 µmol, 16%).

R_f (SiO_2, Hex:EtOAc = 5/5) = 0.38

LCMS (Azo; 5-100% MeCN in H_2O over 5 min.): t_{ret} = 4.85 min.

HPLC (semi-prep, 50-90% MeCN in H_2O over 8 min, 3 min MeCN, no FA): t_{ret} = 6.5 min.

^{1}H-NMR (600 MHz, $CDCl_3$): δ [ppm] = 7.11 (d, J = 7.8 Hz, 1H), 7.04 – 6.95 (m, 2H), 6.87 (d, J = 8.4 Hz, 1H), 6.80 (t, J = 9.3 Hz, 1H), 6.55 (dd, J = 8.5, 2.5 Hz, 1H), 6.39 (d, J = 2.5 Hz, 1H), 5.83 – 5.73 (m, 1H), 5.41 (s, 1H), 5.04 – 4.94 (m, 2H), 4.62 – 4.59 (m, 1H), 4.12 – 4.05 (m, 1H), 4.02 – 3.91 (m, 1H), 3.33 (t, J = 10.7 Hz, 1H), 3.23 (s, 3H), 3.25 – 3.16 (m, 1H), 2.98 – 2.89 (m, 2H), 2.78 – 2.67 (m, 2H), 2.09 – 2.03 (m, 2H), 2.01 – 1.81 (m, 3H), 1.60 – 1.53 (m, 1H), 1.47 – 1.36 (m, 4H).

^{13}C-NMR (151 MHz, $CDCl_3$): δ [ppm] = 174.7, 156.4, 156.0*, 155.9*, 155.6, 138.5, 130.8, 129.8, 128.4, 127.3, 126.7, 121.2, 121.2, 118.8, 115.5*, 115.5*, 115.0, 107.5*, 107.4*, 100.0, 69.8*, 69.7*, 65.6, 56.6, 48.0, 35.1, 34.2, 33.9, 31.8, 31.1*, 31.1*, 29.1*, 28.7*, 28.1, 24.8.
* split signals due to orientation of diazocine with respect to latrunculin core.

HRMS (APCI$^+$, m/z): $[M+H]^+$ for $C_{28}H_{35}N_3O_4S^+$ calcd.: 508.2265, found: 508.2258.

IR (ATR): v (tilde) = 3206 (w), 3068 (w), 2925 (m), 2855 (w), 2361 (w), 1683 (s), 1607 (w), 1568 (w), 1492 (w), 1458 (w), 1354 (w), 1263 (w), 1241 (m), 1135 (w), 1100 (m), 1035 (m), 909 (w), 814 (w), 755 (w), 726 (w).

Synthesis of (R)-4-((2R,4R,6R)-4-(((Z)-11,12-dihydrodibenzo[c,g][1,2]diazocin-3-yl)oxy)-2-hydroxy-6-(pent-4-en-1-yl)tetrahydro-2H-pyran-2-yl)thiazolidin-2-one (44):

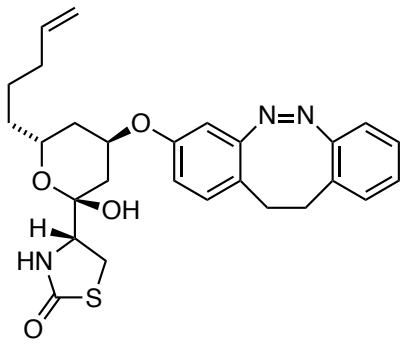

s44 (2.72 mg, 5.30 µmol, 1.00 eq.) was dissolved in THF (0.1 ml), H_2O (0.1 ml) and AcOH (0.1 ml) was added. the reaction was stirred for 3 h at 50 °C. The reaction was cooled to room temperature, pured into $NaHCO_3$ (sat. aq., 30 ml) and EtOAc (30 ml). The layers were separated and the aqueous layer was extracted with EtOAc (2 x 20 ml). The combined organic layers were washed with brine, dried over Na_2SO_4, filtered and concentrated. The crude product was purified by HPLC (semi-prep, 45-75% MeCN in H_2O over 8 min, 3 min MeCN, no FA) and gave **44** as a pale yellow film (1.40 mg, 2.80 µmol, 53%).

LCMS (50-100% MeCN in H2O over 5 min, 0.1% FA): 2.2 (major) and 2.7 (minor)

HPLC (semi-prep, 45-75% MeCN in H_2O over 8 min, 3 min MeCN, no FA): t_{ret} = 7.3 min.

^{1}H-NMR (600 MHz, $CDCl_3$): δ [ppm] = 7.17 – 7.13 (m, 1H), 7.04 (td, J = 7.5, 1.2 Hz, 1H), 7.00 – 6.97 (m, 1H), 6.92 (d, J = 8.4 Hz, 1H), 6.85 – 6.81 (m, 1H), 6.57 (d, J = 8.5 Hz, 1H), 6.38 (s, 1H), 5.83 – 5.70 (m, 1H), 5.60 (s, 1H), 5.03 – 4.93 (m, 3H), 4.81 (s, 1H), 4.07 – 4.00 (m, 1H), 3.83 (dd, J = 9.1, 5.4 Hz, 1H), 3.52 (dd, J = 11.8, 9.1 Hz, 1H), 3.41 – 3.31 (m, 1H), 2.98 – 2.90 (m, 2H), 2.79 – 2.71 (m, 2H), 2.11 – 1.83 (m, 5H), 1.50 – 1.28 (m, 5H).

^{13}C-NMR (151 MHz, $CDCl_3$): δ [ppm] = 174.8, 156.5*, 156.5*, 155.5*, 155.4*, 154.7, 138.6, 131.4*, 131.3*, 129.9, 128.2, 127.4, 126.8, 122.4*, 118.8, 118.8, 115.4*, 115.0, 114.7*, 106.8*, 106.2*, 97.8, 72.7, 64.6, 60.9, 35.0, 33.7, 33.2*, 31.8*, 31.7*, 31.5, 31.1, 29.9, 29.0, 24.5.
* split peak or two peaks that correspond to the same carbon. Splitting pattern due to conformation of diazocine relative to latrunculin core.

HRMS (APCI$^+$, *m*/*z*): [M+H]$^+$ = calcd. for $C_{27}H_{32}N_3O_4S^+$: 494.2108; found: 494.2106.

IR (ATR): $\tilde{\nu}$ [cm^{-1}] = 3507 (w), 3227 (w), 3069 (w), 2923 (s), 2853 (m), 2361 (w), 2341 (w), 1678 (w), 1607 (m), 1571 (w), 1491 (m), 1458 (m), 1409 (m), 1349 (m), 1261 (s), 1237 (s), 1100 (s), 912 (m), 806 (s), 754 (m), 722 (m).

Synthesis of (*R*)-4-((2*R*,4*R*,6*R*)-4-(4-((2,3-dihydrobenzo[*b*][1,4]dioxin-6-yl)diazenyl) phenoxy)-2-methoxy-6-(pent-4-en-1-yl)tetrahydro-2*H*-pyran-2-yl)thiazolidin-2-one (s45):

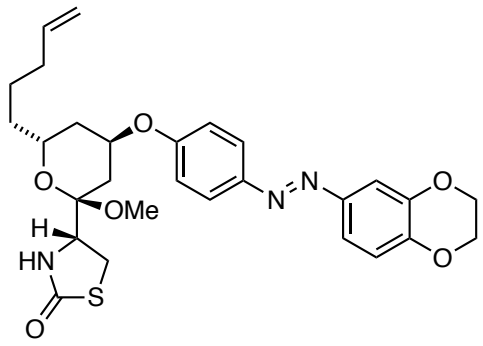

37 (17.1 mg, 56.7 µmol, 1.00 eq.), PPh_3 (37.2 mg, 124 µmol, 2.50 eq.) and **S7** (29.1 mg, 0.114 mmol, 2.00 eq.) were dissolved in dry THF (0.34 ml) and dry toluene (1.00 ml) and cooled to 0 °C using an ice-bath. To the orange reaction mixture, DEAD (40% in toluene, 65.0 µl, 142 µmol, 2.50 eq.) was added and dropwise and the reaction turned dark red. The reaction was stirred at 0 °C for 30 min. before it was warmed to room temperature and stirred over night. The reaction mixture was loaded on isolute, concentrated *in vaccuo* and submitted to flash column chromatography (SiO_2, Hex:EtOAc 10:0 to 5:5 to 0:10, slow gradient). The purified product contained H_2DEAD and was submitted ketal cleavage without further purification.

R$_f$ (SiO_2, Hex:EtOAc = 5:5, CAM) = 0.57.

LCMS (5-100% MeCN in H_2O over 5 min, 0.1% FA) t_{ret} = 3.6 min (major).

Synthesis of (R)-4-((2R,4R,6R)-4-(4-((E)-(2,3-dihydrobenzo[b][1,4]dioxin-6-yl)diazenyl) phenoxy)-2-hydroxy-6-(pent-4-en-1-yl)tetrahydro-2H-pyran-2-yl)thiazolidin-2-one (45):

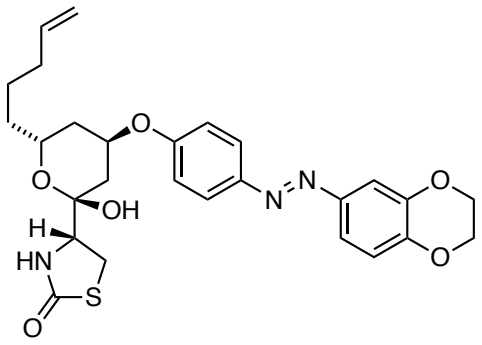

s45 was dissolved in THF (0.90 ml) and water (0.90 ml) and AcOH (0.90 ml) was added. The reaction mixture was heated to 50 °C for 6 h. The reaction was poured into sat. aq. $NaHCO_3$ (30 ml) and EtOAc (30 ml). The layers were separated and the aqueous phase was extracted with EtOAc (2x 20 ml). The combined organic layers were washed with brine, dried over Na_2SO_4, filtered and concentrated. The crude product was purified by HPLC (semi-prep, 50-95% MeCN in H_2O over 8 min, 3 min MeCN, no FA) and the title compound was obtained as an orange film (1.29 mg, 2.5 µmol, 4% over 2 steps).

R_f (SiO_2, Hex:EtOAc = 5:5, CAM) = 0.29.

LCMS (AZO, 50-100% MeCN in H_2O, 0.1% FA) t_{ret} = 2.9 (major).

HPLC (semi-prep, 50-95% MeCN in H_2O over 8 min, 3 min MeCN, no FA): t_{ret} = 6.4 min.

^{1}H-NMR (600 MHz, $CDCl_3$): δ [ppm] = 7.89 (d, J = 9.0 Hz, 2H), 7.49 (dd, J = 8.6, 2.1 Hz, 1H), 7.46 (d, J = 2.4 Hz, 1H), 7.02 (d, J = 9.0 Hz, 2H), 6.98 (dd, J = 8.6, 1.6 Hz, 1H), 5.77 (ddt, J = 16.8, 9.7, 6.6 Hz, 1H), 5.67 – 5.59 (m, 1H), 5.05 (s, 1H), 5.03 (s, 1H), 5.02 – 4.92 (m, 2H), 4.36 – 4.29 (m, 4H), 4.18 – 4.11 (m, 1H), 3.88 (dd, J = 9.2, 5.5 Hz, 1H), 3.55 (td, J = 10.0, 9.0, 1.6 Hz, 1H), 3.43 (dd, J = 11.8, 5.4 Hz, 1H), 2.23 – 2.18 (m, 1H), 2.09 – 2.02 (m, 4H), 1.52 – 1.37 (m, 5H).

^{13}C-NMR (151 MHz, $CDCl_3$): δ [ppm] = 174.8, 157.9, 148.1, 147.5, 146.4, 144.0, 138.6, 124.8, 118.2, 117.6, 116.2, 115.0, 110.8, 97.9, 72.6, 64.8, 64.7, 64.4, 61.0, 35.1, 33.7, 33.5, 31.6, 29.1, 24.6.

HRMS (APCI$^+$, *m/z*): [(M+H)$^+$] for $C_{27}H_{32}N_4O_6S^+$ calcd.: 526.2006, found: 526.1983.

IR (ATR): $\tilde{\nu}$ [cm^{-1}] = 3521 (w), 3229 (w), 3073 (w), 2924 (m), 2853 (m), 2363 (w), 1676 (s), 1596 (m), 1581 (m), 1494 (s), 1456 (m), 1320 (m), 1286 (s), 1257 (s), 1231 (s), 1137 (m), 1095 (s), 1063 (s), 883 (m), 838 (m), 803 (s), 724 (m).

Synthesis of (R)-4-((2R,4R,6R)-4-(4-((4-benzyl-3,4-dihydro-2H-benzo[b][1,4]oxazin-7-yl)diazenyl)phenoxy)-2-methoxy-6-(pent-4-en-1-yl)tetrahydro-2H-pyran-2-yl)thiazolidin-2-one (s48):

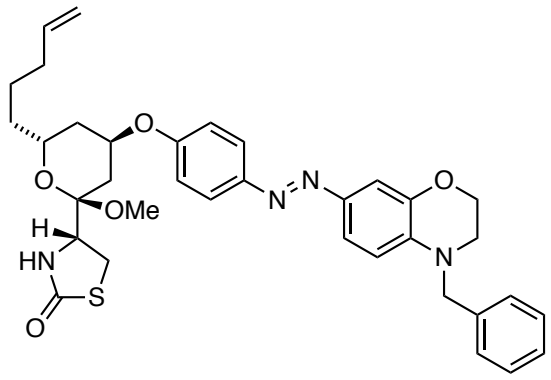

37 (16.8 mg, 55.7 µmol, 1.00 eq.), PPh_3 (36.5 mg, 138 µmol, 2.50 eq.) and **47** (38.5 mg, 112 µmol, 2.00 eq.) were dissolved in dry THF (0.34 ml) and dry toluene (1.00 ml) and cooled to 0 °C using an ice-bath. To the orange reaction mixture, DEAD (40% in toluene, 63.0 µl, 139 µmol, 2.50 eq.) was added and dropwise and the reaction turned dark red. The reaction was stirred at 0 °C for 30 min. before it was warmed to room temperature and stirred over night. The reaction mixture was loaded on isolute, concentrated *in vaccuo* and submitted to flash column chromatography (SiO_2, Hex:EtOAc = 10:0 to 5:5 to 0:10, slow gradient). The purified product contained H_2DEAD and was submitted ketal cleavage without further purification.

$\mathbf{R_f}$(SiO_2, Hex:EtOAc = 5:5, CAM) = 0.59

LCMS (50-100% MeCN in H_2O over 5 min, 0.1% FA): t_R (major) = 4.3 min (trans).

Synthesis of (R)-4-((2R,4R,6R)-4-(4-((4-benzyl-3,4-dihydro-2H-benzo[b][1,4]oxazin-7-yl)diazenyl)phenoxy)-2-hydroxy-6-(pent-4-en-1-yl)tetrahydro-2H-pyran-2-yl)thiazolidin-2-one (48):

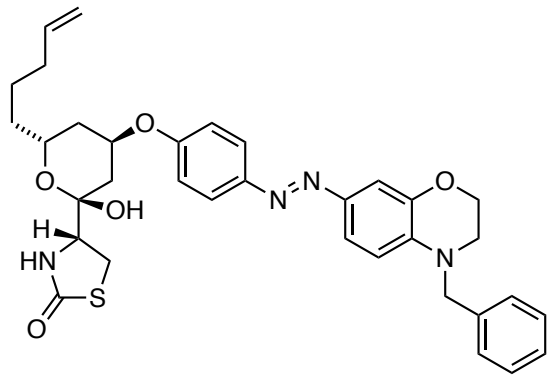

s48 was dissolved in THF (0.90 ml) and water (0.90 ml) and AcOH (0.90 ml) was added. The reaction mixture was heated to 50 °C for 6 h. The reaction was poured into sat. aq. $NaHCO_3$ (30 ml) and EtOAc (30 ml). The layers were separated and the aqueous phase was extracted with EtOAc (2x 20 ml). The combined organic layers were washed with brine, dried over Na_2SO_4, filtered and concentrated. The crude product was purified by HPLC (semi-prep, 50-96% MeCN in H_2O over 8 min, 3 min MeCN, no FA) and the title compound was obtained as an orange film (2.54 mg, 4.1 µmol, 7% over 2 steps).

R_f (SiO_2, Hex:EtOAc = 5:5, CAM) = 0.31.

LCMS (5-100% MeCN in H_2O over 5 min, 0.1% FA) t_{ret} = 5.3 min.

HPLC (semi-prep, 50-96% MeCN in H_2O over 8 min, 3 min MeCN, no FA): t_{ret} = 7.7 min.

^{1}H-NMR (600 MHz, $CDCl_3$): δ [ppm] = 7.84 (d, J = 8.5 Hz, 2H), 7.46 (d, J = 2.0 Hz, 1H), 7.45 (s, 1H), 7.36 (t, J = 7.5 Hz, 2H), 7.28 (d, J = 7.8 Hz, 3H), 7.00 (d, J = 8.6 Hz, 2H), 6.74 (d, J = 8.4 Hz, 1H), 5.77 (ddt, J = 16.9, 10.2, 6.7 Hz, 1H), 5.64 (s, 1H), 5.09 (s, 1H), 5.02 (s, 1H), 5.01 – 4.92 (m, 2H), 4.59 (s, 2H), 4.30 (t, J = 4.5 Hz, 2H), 4.14 (td, J = 7.7, 7.1, 4.1 Hz, 1H), 3.88 (dd, J = 9.1, 5.6 Hz, 1H), 3.55 (dd, J = 11.7, 9.2 Hz, 1H), 3.50 (t, J = 4.5 Hz, 2H), 3.43 (dd, J = 11.8, 5.5 Hz, 1H), 2.19 (d, J = 14.3 Hz, 1H), 2.08 – 2.01 (m, 4H), 1.53 – 1.37 (m, 5H).

^{13}C-NMR (151 MHz, $CDCl_3$): δ [ppm] = 174.8, 157.2, 148.5, 144.7, 144.0, 138.6, 137.2, 129.0, 127.6, 127.0, 124.4, 121.0, 116.3, 115.0, 111.2, 108.6, 97.9, 72.6, 64.7, 64.4, 61.0, 54.7, 47.5, 35.1, 33.7, 33.5, 31.6, 29.1, 24.6.

HRMS (ESI$^+$, *m/z*): [$(M+H)^+$] for $C_{34}H_{39}N_4O_5S^+$ calcd.: 615.2636, found: 615.2645.

IR (ATR): $\tilde{\nu}$ [cm^{-1}] = 3528 (w), 3227 (w), 3070 (w), 2924 (m), 2854 (w), 1678 (s), 1596 (s), 1515 (s), 1496 (s), 1452 (m), 1396 (m), 1350 (m), 1319 (s), 1232 (s), 1201 (s), 1152 (m), 1093 (s), 1051 (s), 884 (m), 838 (m), 802 (m), 727 (m).

Synthesis of (4-(phenyldiazenyl)phenyl)methanol (S1)

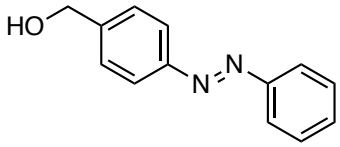

The title compound was synthesized following a reported procedure[15]. Yield: 54%; The analytical data matched those reported.

R_f (SiO_2, Hex:EtOAc = 8:2; UV) = 0.18

^{1}H-NMR (400 MHz, $CDCl_3$): δ [ppm] 7.97 – 7.88 (m, 4H), 7.57 – 7.43 (m, 5H), 4.80 (d, J = 5.6 Hz, 2H), 1.75 (t, J = 5.9 Hz, 1H).

^{13}C-NMR (101 MHz, $CDCl_3$): δ [ppm] = 152.8, 152.3, 144.0, 131.2, 129.2, 127.6, 123.2, 123.0, 65.1.

[15] Rao, J.; Hottinger, C.; Khan, A. *J. Am. Chem. Soc.* **2014**, *136*, 5872–5875.

Synthesis of 2-(4-(phenyldiazenyl)phenyl)ethan-1-ol (S2):

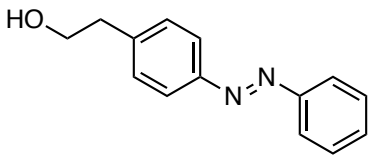

The title compound was synthesized following a reported procedure[16]. Yield: 59%; The analytical data matched those reported.

R_f (SiO_2, Hex:EtOAc = 8:2; UV) = 0.15

^{1}H-NMR (400 MHz, $CDCl_3$): δ [ppm] = 7.95 – 7.82 (m, 4H), 7.59 – 7.43 (m, 3H), 7.43 – 7.32 (m, 2H), 3.98 – 3.87 (m, 2H), 2.96 (t, J = 6.5 Hz, 2H), 1.45 – 1.39 (m, 1H).

^{13}C-NMR (101 MHz, $CDCl_3$): δ [ppm] = 152.8, 151.6, 142.1, 131.0, 129.9, 129.2, 123.3, 122.9, 63.6, 39.2.

Synthesis of 4-(phenyldiazenyl)benzaldehyde (S3):

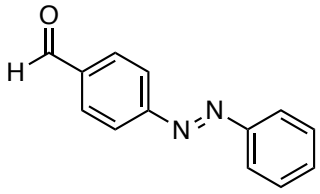

(4-(phenyldiazenyl)phenyl)methanol (300 mg, 1.41 mmol, 1.00 eq.) was dissolved in wet DCM (14 ml) and DMP (778 mg, 1.84 mmol, 1.30 eq.) was added. The suspension was stirred at r.t. for 2 h . A mixture of aq. sat. $Na_2S_2O_3$ and $NaHCO_3$ (1:1; 20 ml) was added and stirred for 1 h. The phases were separated and the aqueous layer was extracted with DCM (2 x 20 ml). The combined organic layers were dried over Na_2SO_4, filtered and concentrated. The crude product was purified by flash column chromatography (SiO_2, Hex:EtOAc = 10:0 to 9:1) and gave the title compound as red solid (255 mg, 1.21 mmol, 86%).

[16] Schönberger, M; Trauner, D. *Angew. Chem. Int. Ed.* **2014**, *53*, 3264–4367.

R_f (SiO_2, Hex:EtOAc = 95:5; UV) = 0.31

^{1}H-NMR (400 MHz, $CDCl_3$): δ [ppm] = 10.11 (s, 1H), 8.05 (s, 4H), 8.01 – 7.94 (m, 2H), 7.60 – 7.50 (m, 3H).

^{13}C-NMR (101 MHz, $CDCl_3$): δ [ppm] = 191.8, 156.1, 152.7, 137.6, 132.1, 130.9, 129.4, 123.5, 123.4.

HRMS (ESI$^+$, m/z): for $[(M–H_2O)+H]^+$ $C_{13}H_9N_2^+$ calcd.: 215.0580, found: 215.0588.

IR (ATR): $\tilde{\nu}$ [cm^{-1}] = 2844 (w), 1695 (s), 1596 (m), 1580 (w), 1487 (w), 1464 (w), 1442 (w), 1382 (w), 1316 (w), 1306 (w), 1290 (w), 1196 (s), 1147 (w), 1129 (w), 1102 (w), 1070 (w), 1018 (w), 1000 (w), 919 (w), 844 (s), 830 (s), 795 (s), 764 (s), 714 (m).

Synthesis of 1-phenyl-2-(4-vinylphenyl)diazene (32):

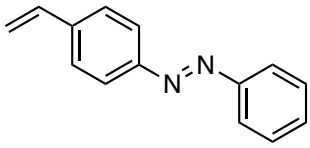

Methyltriphenylphosphonium bromide (589 mg, 1.65 mmol, 1.20 eq.) was dissolved in dry THF (19.3 ml) and cooled to 0 °C. NaH (60% in paraffin oil; 220 mg, 5.50 mmol, 4.00 eq.) was added in one portion and the suspension was stirred for 15 minutes. Aldehyde **S3** (289 mg, 1.37 mmol, 1.00 eq.) in THF (4 ml) was added dropwise (rinses with THF, 2 mL) and the reaction was stirred for 12 h and let come to room temperature. EtOAc (10 mL) was added, followed by the slow addition of aq. sat. NH_4Cl (10 ml) and water (10 ml). The phases were separated and the aqueous layer was extracted with EtOAc (2 x 20 mL), the combined organic layers were washed with brine, dried over Na_2SO_4, filtered and concentrated. The crude product was purified by flash column chromatography (SiO_2, Hex:EtOAc 10:0 to 9:1) and gave the title compound as a red solid (278 mg, 1.34 mmol, 97%).

R_f (SiO_2, Hex:EtOAc = 9.5:0.5; UV) = 0.73.

^{1}H-NMR (400 MHz, CDCl3): δ [ppm] = 7.95 – 7.85 (m, 4H), 7.59 – 7.42 (m, 5H), 6.79 (dd, J = 17.6, 10.9 Hz, 1H), 5.87 (d, J = 17.5 Hz, 1H), 5.37 (d, J = 10.9 Hz, 1H).

^{13}C-NMR (101 MHz, CDCl3): δ [ppm] = 152.9, 152.2, 140.3, 136.3, 131.1, 129.2, 127.1, 123.4, 123.0, 115.8.

HRMS (ESI$^+$, *m/z*): $[M+H]^+$ for $C_{14}H_{13}N_2^+$ calcd.: 209.1073, found: 209.1071.

IR (ATR): $\tilde{\nu}$ [cm^{-1}] = 3056 (w), 2998 (w), 1815 (w), 1624 (w), 1596 (w), 1584 (w), 1499 (w), 1483 (w), 1465 (w), 1443 (w), 1422 (w), 1403 (w), 1315 (w), 1301 (w), 1225 (w), 1201 (w), 1187 (w), 1154 (w), 1111 (w), 1071 (w), 1033 (w), 1017 (w), 1009 (w), 993 (m), 956 (w), 926 (w), 902 (s), 851 (s), 768 (s), 748 (m).

Synthesis of 2-(phenyldiazenyl)benzoic acid (S4):

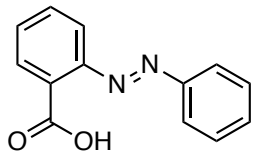

2-Aminobenzoic acid (461 mg, 3.36 mmol, 1.20 eq.) was dissoved in glacial acetic acid (4 ml) at room temperature and a solution of nitrosobenzene (300 mg, 2.80 mmol, 1.00 eq.) in acetic acid (4 ml) was added dropwise over 5 min. The brown reaction mixture was stirred at room temperature for 48 h and then concentrated under reduced pressure. The crude product was purified by flash column chromatography (SiO_2, DCM:MeOH 10:0 to 9:1) and gave the title compound as an orange-brown solid.

R_f (DCM; UV) = 0.54 (major)

^{1}H-NMR (400 MHz, $CDCl_3$): δ [ppm] = 12.83 (s_{br}, 1H), 8.51 – 8.44 (m, 1H), 8.09 – 8.02 (m, 1H), 7.92 – 7.86 (m, 2H), 7.75 – 7.67 (m, 2H), 7.64 – 7.58 (m, 3H).

^{13}C-NMR (101 MHz, $CDCl_3$): δ [ppm] = 166.2, 151.7, 149.5, 134.0, 133.7, 133.4, 132.9, 130.0, 127.3, 123.8, 115.9.

HRMS (ESI$^+$, *m/z*): $[M+H]^+$ for $C_{13}H_{11}N_2O_2^+$ calcd.: 227.0815, found: 227.0816.

Synthesis of 3-(phenyldiazenyl)benzoic acid (S5):

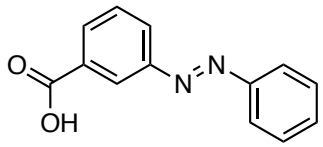

3-Aminobenzoic acid (400 mg, 3.70 mmol, 1.00 eq.) was dissolved in glacial acetic acid (3 ml) at room temperature and a solution of nitrosobenzene (615 mg, 4.50 mmol, 1.20 eq.) in acetic acid (4.5 ml) was added dropwise over 5 min. The brown reaction mixture was stirred at room temperature for 48 h and then concentrated under reduced pressure. The crude product was purified by flash column chromatography (SiO_2, DCM:MeOH 10:0 to 9:1) and gave the title compound as an orange solid (559 mg, 2.48 mmol, 55%).

R_f (SiO_2, DCM:MeOH = 95:5; UV) = 0.4

^{1}H-NMR (400 MHz, $CDCl_3$): δ [ppm] = 8.66 (d, J = 2.1 Hz, 1H), 8.28 – 8.20 (m, 1H), 8.18 (dd, J = 7.9, 1.7 Hz, 1H), 8.02 – 7.92 (m, 2H), 7.65 (t, J = 7.8 Hz, 1H), 7.60 – 7.44 (m, 4H).

^{13}C-NMR (101 MHz, $CDCl_3$): δ [ppm] = 170.6, 152.7, 152.4, 132.2, 131.5, 130.3, 129.4, 129.2, 127.7, 124.8, 123.1.

HRMS (ESI$^+$, *m/z*): for $C_{13}H_{11}N_2O_2^+$ calcd.: 227.0815, found: 227.0823.

IR (ATR): $\tilde{\nu}$ [cm^{-1}] = 2817 (w), 2565 (w), 1674 (s), 1598 (w), 1585 (m), 1473 (w), 1448 (w), 1423 (m), 1326 (m), 1307 (m), 1277 (m), 1211 (m), 1159 (m), 1093 (w), 1077 (m), 1019 (w), 998 (m), 937 (m), 917 (m), 820 (m), 785 (m), 762 (s)

Synthesis of 4-((3,4,5-trimethoxyphenyl)diazenyl)phenol (S6):

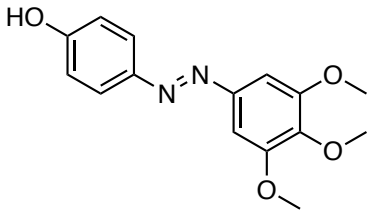

Following a reported procedure[17] for a related compound, 3,4,5-trimethoxyaniline (366 mg, 2.00 mmol, 1.00 eq.) was dissolved in THF (5.0 ml) and HCl (1M, 6.0 ml) and cooled to 0 °C. H_2O (4.0 ml) was added and an aqueous solution of $NaNO_2$ (2.0 M in H_2O, 1.2 ml, 2.40 mmol, 1.20 eq.) was added dropwise and the resulting dark-red suspension was stirred for 30 min. at 0 °C. A solution of phenol (226 mg, 2.40 mmol, 1.20 eq.) was added dropwise and the reaction mixture was stirred for 1 h at 0 °C. The volatiles were removed under reduced pressure and the residue was redissolved in EtOAc (20 ml) and H_2O (20 ml) and the phases separated. The aqueous layer was extracted with EtOAc (3 x 30 ml) and the combined organic layers were washed with water and brine, dried over $MgSO_4$, filtered and concentrated. The crude product was purified by flash column chromatography (SiO_2, Hex:EtOAc = 8:2 to 5:5) and gave the title compound as a brown solid (526 mg, 1.82 mmol, 91%).

R_f (SiO_2, Hex:EtOAc = 6:4; UV) = 0.33 (major), 0.47 (minor).

^{1}H-NMR (400 MHz, $CDCl_3$): δ [ppm] = 7.86 (d, J = 8.8 Hz, 2H), 7.22 (s, 2H), 6.95 (d, J = 8.8 Hz, 2H), 5.17 (s_{br}, 1H), 3.96* (s, 6H), 3.93* (s, 3H). *main peaks reported

^{13}C-NMR (101 MHz, $CDCl_3$): δ [ppm] = 158.3, 153.7, 148.7, 147.2, 140.3, 125.0, 116.0, 100.3, 61.2, 56.4.

HRMS (ESI$^+$, *m/z*): $[M+H]^+$ for $C_{16}H_{16}N_2O_4^+$ calcd.: 289.1183, found: 289.1180.

IR (ATR): $\tilde{\nu}$ [cm^{-1}] = 3277 (w), 2950 (w), 2839 (w), 1599 (m), 1585 (m), 1496 (m), 1472 (m), 1461 (m), 1430 (w), 1411 (m), 1332 (m), 1316 (w), 1302 (w), 1278 (m), 1225 (m), 1208 (m), 1180 (m), 1145 (m), 1128 (s), 1100 (m), 991 (s), 922 (w), 866 (m), 847 (s), 781 (m).

[17] Eisel, B.; Hartrampf, F. W. W.; Meier, T.; Trauner, D. *FEBS lett.* **2018**, *592*, 343–355.

Synthesis of 4-((2,3-dihydrobenzo[b][1,4]dioxin-6-yl)diazenyl)phenol (S7):

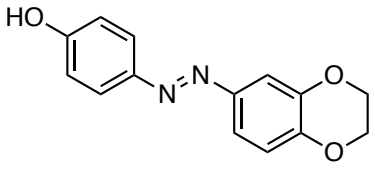

2,3-dihydrobenzo[*b*][1,4]dioxin-6-amine (500 mg, 3.31 mmol, 1.00 eq.) was dissolved in THF (8.3 ml), water (6.3 ml) and 1 M HCl (9.9 ml) and cooled to 0 °C. An aqueous solution of $NaNO_2$ (2 M, 2.0 ml, 3.97 mmol, 1.20 eq.) was added dropwise and the reaction was stirred for 30 minutes at 0 °C. Phenol (374 mg, 3.97 umol, 1.20 eq.) was dissolved in aqueous NaOH (1 M, 9.9 ml, 9.92 mmol, 3.00 eq.) and added dropwise. The reaction was stirred for 2 h at 0 °C and upon completion, the volatiles were removed under reduced pressure. The residue was taken up in EtOAc (100 ml) and H_2O (50 ml), the layers were separated and the organic layer was extracted with EtOAc (2 x 100 ml). The combined organic layers were washed with brine, dried over $MgSO_4$, filtered and concentrated. The crude product was purified by flash column chromatography (SiO_2, Hex:DCM:EtOAc = 6:3:1 to 0:6:2) and the title compound was obtained as an orange solid (531 mg, 2.07 mmol, 63%).

R_f (SiO_2, Hex:DCM:EtOAc = 6:3:1; UV) = 0.22

^{1}H-NMR (400 MHz, $CDCl_3$): δ = 7.86 – 7.79 (m, 2H), 7.49 – 7.43 (m, 2H), 6.97 (d, J = 8.4 Hz, 1H), 6.95 – 6.89 (m, 2H), 5.17 (s, 1H), 4.34 – 4.27 (m, 4H).

^{13}C-NMR (101 MHz, $CDCl_3$): δ 157.9, 147.6, 147.3, 146.1, 144.0, 124.8, 117.9, 117.5, 115.9, 110.7, 64.7, 64.4.

HRMS (ESI$^+$, *m*/*z*): [(M+H)$^+$] for $C_{14}H_{13}N_2O_3^+$ calcd.: 257.0921, found: 257.0920.

IR (ATR): $\tilde{\nu}$ [cm^{-1}] = 3378 (w), 1592 (m), 1491 (s), 1434 (w), 1318 (w), 1284 (s), 1268 (m), 1255 (s), 1239 (m), 1212 (m), 1190 (m), 1138 (m), 1115 (m), 1099 (w), 1059 (s), 1037 (m), 923 (m), 896 (m), 884 (m), 867 (m), 835 (s), 809 (m), 762 (m), 741 (m), 724 (w).

Synthesis of 7-nitro-3,4-dihydro-2*H*-benzo[*b*][1,4]oxazine (s46):

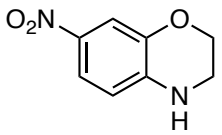

2-Amino-5-nitrophenol (10.0 g, 64.9 mmol, 1.00 eq.) and K_2CO_3 (35.7 g, 260 mmol, 4.00 eq.) were dissolved in dry DMF (130 ml) and 1,2-dibromoethane (22.4 ml, 260 mmol, 4.00 eq.) was added. The reaction was heated to 120 °C over night. Upon cooling to room temperature, DMF was removed under reduced pressure and by trituation with hexanes. The resulting crude product was partitioned between H_2O (400 ml) and DCM (400 ml) and the layers were separated. The organic layer was dried over $MgSO_4$ and concentrated. Excess DMF was removed by coevaporation with hexanes. The title compound was obtained as a yellow solid (9.43 g, 52.3 mmol, 81%).

^{1}H-NMR (400 MHz, $CDCl_3$): δ [ppm] = 7.78 – 7.66 (m, 2H), 6.52 (d, J = 8.7 Hz, 1H), 4.29 – 4.21 (m, 2H), 3.61 – 3.49 (m, 2H), 2.96 (s, 1H), 2.88 (s, 1H).

Synthesis of 4-benzyl-7-nitro-3,4-dihydro-2H-benzo[b][1,4]oxazine (46):

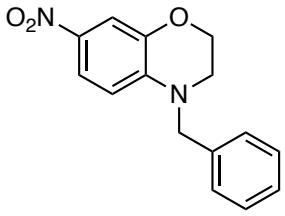

Following a known procedure[18], 7-nitro-3,4-dihydro-2*H*-benzo[*b*][1,4]oxazine **s46** (400 mg, 2.22 mmol, 1.00 eq.) and K_2CO_3 (1.04 g, 7.55 mmol, 3.40 eq.) were dissolved in dry DMF (3.2 ml) and benzyl bromide (0.53 ml, 4.44 mmol, 2.00 eq.) was added. The reaction mixture was heated to 80 °C for 22 h. After cooling to room temperature the reaction mixture was

[18] Beijing University of Technology; Hu, L.; Rong, J.; Mao, Z.; Wang, Y.; Zeng C. CN104693216, 2017, B; Location in patent: Paragraph 0062-0066

partitioned between H_2O (100 ml) and EtOAc (100 ml). The phases were separated and the aqueous layer was extracted with EtOAc (2 x 100 ml). The combined organic layers were washed with brine, dried over Na_2SO_4, filtered and concentrated. The crude product was purified by flash column chromatography (SiO_2, Hex:EtOAc = 8:2 to 0:10) and gave the title compound as a yellow solid (348 mg, 1.29 mmol, 58%).

R_f (SiO_2, Hex:EtOAc = 8:2; UV) = 0.32

^{1}H-NMR (400 MHz, $CDCl_3$): δ [ppm] = 7.58 (s, 1H), 7.60 – 7.55 (m, 1H), 7.42 – 7.33 (m, 2H), 7.33 – 7.26 (m, 3H), 6.84 (dt, *J* = 8.9, 1.3 Hz, 1H), 4.51 (s, 2H), 4.36 – 4.32 (m, 2H), 3.42 – 3.37 (m, 2H).

^{13}C-NMR (101 MHz, $CDCl_3$): δ [ppm] = 149.5, 142.6, 136.5, 135.6, 129.1, 127.9, 127.4, 116.2, 114.4, 107.3, 65.2, 54.8, 46.2.

HRMS (ESI$^+$, *m/z*): $[M+H]^+$ for $C_{15}H_{15}N_2O_3^+$: calcd.: 271.1077, found: 271.1075.

IR (ATR): $\tilde{\nu}$ [cm^{-1}] = 2850 (w), 1722 (w), 1617 (w), 1575 (w), 1512 (s), 1452 (m), 1321 (s), 1235 (s), 1215 (s), 1161 (m), 1105 (s), 1076 (w), 1039 (m), 985 (w), 935 (w), 913 (m), 855 (m), 803 (m), 741 (s), 714 (m).

Synthesis of 4-benzyl-3,4-dihydro-2H-benzo[b][1,4]oxazin-7-amine (S8):

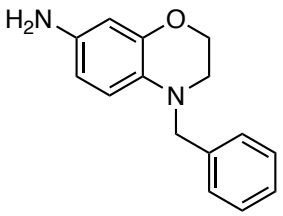

4-Benzyl-7-nitro-3,4-dihydro-2*H*-benzo[*b*][1,4]oxazine (348 mg, 1.29 mmol, 1.00 eq.) and $SnCl_2 \cdot 2\ H_2O$ (1.16 g, 5.15 mmol, 4.00 eq.) were dissolved in ethanol (5.1 ml) and conc. HCl (1.0 ml) and heated to 80 °C for 16 h. The reaction was cooled to room temperature and poured slowly into sat. aq. $NaHCO_3$ (80 ml). The mixture was basified with NaOH (2.0 M) and H_2O (30 ml) was added. The aqueous layer was extracted with EtOAc (3 x 100 ml), washed

with brine, dried over Na_2SO_4, filtered and concentrated. The crude product was purified by flash column chromatography (SiO_2, Hex:DCM:EtOAc 7:2:1 to 0:8:2) and furnished the title compound as a light beige solid (285 mg, 1.19 mmol, 92%). The product was unstable and darkened when kept under air for prolonged times and was thus kept under high vacuum for 24 h and used immediately.

R_f (SiO_2, Hex:DCM:EtOAc = 4:4:2) = 0.30.

^{1}H-NMR (400 MHz, $CDCl_3$): δ [ppm] = 7.35 – 7.31 (m, 4H), 7.29 – 7.23 (m, 1H), 6.56 (d, J = 8.4 Hz, 1H), 6.26 (d, J = 2.4 Hz, 1H), 6.20 (dd, J = 8.5, 2.6 Hz, 1H), 4.31 (s, 2H), 4.26 – 4.21 (m, 2H), 3.32 (s_{br}, 2H), 3.22 – 3.17 (m, 2H). *contains residual EtOAc.

Synthesis of 4-((4-benzyl-3,4-dihydro-2H-benzo[b][1,4]oxazin-7-yl)diazenyl)phenol (47):

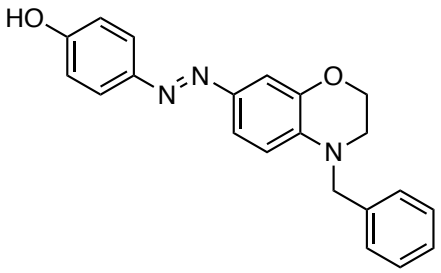

Aniline **S8** (150 mg, 0.62 mmol, 1.00 eq.) was dissolved in THF (1.6 ml), water (1.2 ml) and 1.0 M HCl (1.9 ml) and cooled to 0 °C. An aqueous solution of $NaNO_2$ (2.0 M, 0.38 ml, 0.75 umol, 1.20 eq.) was added dropwise and the reaction was stirred for 30 minutes at 0 °C. Phenol (70.5 mg, 0.75 umol, 1.20 eq.) was dissolved in aqueous NaOH (1.0 M, 1.9 ml, 1.87 mmol, 3.00 eq.) and added dropwise. The reaction was stirred for 2 h at 0 °C and upon completion poured into water (80 ml) and extracted with Ethyl acetate (3 x 80 ml, 1 x 30 ml). The combined organic layers were washed with brine, dried over $MgSO_4$, filtered and concentrated. The crude product was purified by flash column chromatography (SiO_2, Hex:EtOAc 10:0 to 5:5) and the title compound was obtained as a dark red solid (190 mg, 0.55 mmol, 88%).

R_f (SiO_2, Hex:EtOAc = 7:3; UV/ CAM) = 0.24.

LCMS (5-100% MeCN in H_2O over 5 min, 0.1% FA): t_{ret} = 4.5 min.

^{1}H-NMR (400 MHz, $CDCl_3$): δ [ppm] = 7.77 (d, J = 8.6 Hz, 24H), 7.47 – 7.43 (m, 2H), 7.38 – 7.32 (m, 2H), 7.28 (d, J = 8.2 Hz, 3H), 6.90 – 6.86 (m, 2H), 6.73 (d, J = 9.2 Hz, 1H), 5.61 (s_{br}, 1H), 4.57 (s, 2H), 4.29 (t, J = 4.5 Hz, 2H), 3.48 (t, J = 4.5 Hz, 2H).

^{13}C-NMR (101 MHz, $CDCl_3$): δ [ppm] = 157.4, 147.5, 144.7, 143.9, 138.3, 137.2, 129.0, 127.5, 127.0, 124.3, 120.5, 115.8, 111.3, 108.7, 64.4, 54.7, 47.5.

HRMS (ESI$^+$, m/z): [(M+H)$^+$] for $C_{21}H_{20}N_3O_2^+$ calcd.: 346.1550, found: 346.1554.

IR (ATR): $\tilde{\nu}$ [cm^{-1}] = 1586 (m), 1515 (m), 1451 (w), 1396 (w0, 1348 (w), 1317 (s), 1274 (m), 1248 (s), 1216 (s), 1150 (s), 1123 (s), 1091 (m), 1048 (m), 973 (w), 911 (w), 877 (m), 836 (s), 802 (m), 754 (w), 712 (m).

Selected UV-Vis Spectra for Latrunculin Compounds

UV-Vis spectrum for 45:

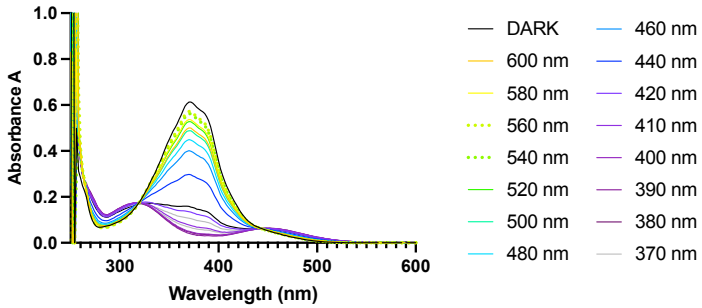

UV-Vis-Spectrum for 43:

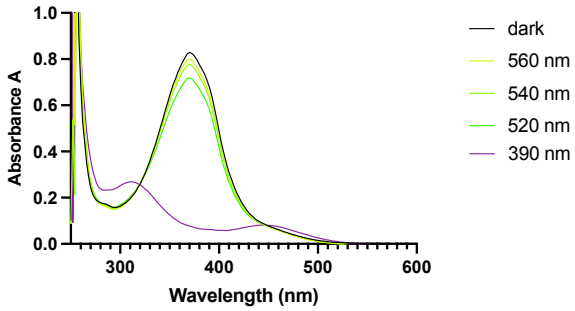

UV-Vis-Spectrum for 44:

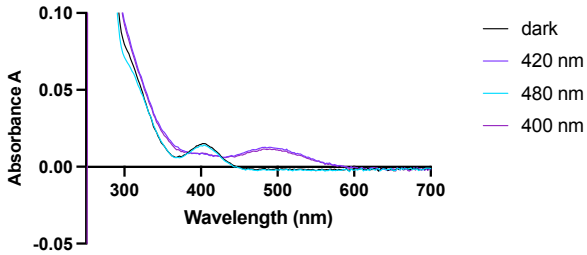

UV-Vis Spectrum for 42

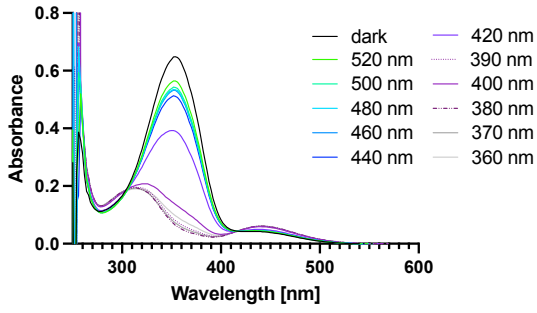

UV-Vis-Spectrum for 36e:

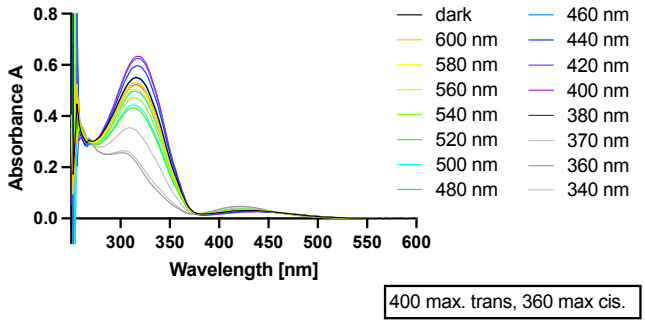

400 max. trans, 360 max cis.

`

Chemical Procedures for Part 1: 4 Arp2/3 Complex

Synthesis of methyl 3-amino-2-fluorobenzoate (117):

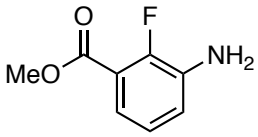

Methyl 2-fluoro-3-nitrobenzoate (500 mg, 2.51 mmol, 1.00 eq.) and 10% Pd/C (80.2 mg, 0.75 mmol, 0.30 eq.) were suspended in EtOAc (10 ml) and degassed with nitrogen. Using a double-walled balloon filled with hydrogen, the reaction mixture was sparged with H_2 for 10 seconds and subsequently stirred under hydrogen atmosphere for 2.5 h until full consumption of the starting material was detected by LCMS. The reaction mixture was filtered over celite using positive nitrogen pressure and rinsing with ethyl acetate. The crude reaction product, a brown oil, was concentrated and used without further purification.

LCMS (5-100% MeCN in H_2O over 5 min, 0.1% FA) t_{ret} = 2.4 min.

^{1}H-NMR (400 MHz, $CDCl_3$): δ [ppm] = 7.29 – 7.22 (m, 1H), 7.00 – 6.91 (m, 2H), 4.39 – 3.34 (s_{br}, 2H), 3.92 (s, 3H).

^{13}C-NMR (100 MHz, $CDCl_3$): δ [ppm] = 165.3, 165.3, 152.0, 149.5, 135.8, 135.7, 124.0, 124.0, 120.9, 120.8, 120.7, 118.9, 118.8, 52.4.

Synthesis of *N*-(2-(2-methyl-1*H*-indol-3-yl)ethyl)-11,12-dihydrodibenzo[*c*,*g*][1,2]diazocine-3-carboxamide (121):

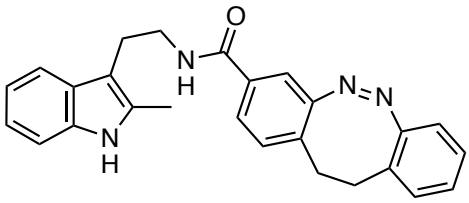

2-Methyltryptamine (10.0 mg, 57.4 µmol, 1.00 eq.), diazocine-3-carboxylic acid[19] (7.2 mg, 28.7 µmol, 1.00 eq.) and HATU (16.4 mg, 43.0 µmol, 1.50 eq.) were dissolved in dry DMF (2.0 ml). Dry DIPEA (15 µl, 86.1 µmol, 3.00 eq.) was added and the reaction was stirred at room temperature for 16 h. The reaction was diluted with EtOAc (20 ml), washed with 10% aq. LiCl solution (3 x 20 ml) and brine, dried over Na_2SO_4, filtered and concentrated. The crude product was purified by flash column chromatography (SiO_2, hexanes/ ethyl acetate 5/5 to 2/8), followed by HPLC (semi-prep, 50-65% MeCN in H_2O over 8 min, 3 min MeCN, 0.1% FA). The title compound was obtained as yellow film (8.3 mg, 20.2 µmol, 71%).

R_f (SiO_2, Hex:EtOAc= 5:5; UV) = 0.41

LCMS (5-100% MeCN in H_2O over 5 min, 0.1% FA): t_{ret} = 4.1 min.

HPLC: (semi-prep, 50-65% MeCN in H_2O over 8 min, 3 min MeCN, 0.1% FA): t_{ret} = 5.4 min.

^{1}H-NMR (400 MHz, $CDCl_3$): δ [ppm] = 7.88 (s, 1H), 7.49 (d, J = 7.8 Hz, 1H), 7.32 – 7.27 (m, 2H), 7.19 – 7.09 (m, 2H), 7.09 – 7.04 (m, 2H), 7.04 – 6.92 (m, 3H), 6.80 (d, J = 7.8 Hz, 1H), 6.07 (t, J = 5.9 Hz, 1H), 3.64 (q, J = 6.4 Hz, 2H), 2.99 (t, J = 6.6 Hz, 2H), 3.02 – 2.92 (m, 2H), 2.89 – 2.68 (m, 2H), 2.32 (s, 3H).

^{13}C-NMR (101 MHz, $CDCl_3$): δ [ppm] = 166.4, 155.4, 135.4, 133.4, 132.1, 131.9, 130.2, 129.7, 128.7, 127.4, 127.1, 125.6, 121.5, 119.7, 119.0, 117.9, 117.5, 110.6, 108.5, 40.6, 31.8, 31.5, 24.0, 11.8.

[19] Diazocine from Martin Maier

HRMS (ESI+, *m/z*): [(M+H)+] for $C_{26}H_{26}N_4O^+$: calcd.: 409.2023, found: 409.2034.

Synthesis of methyl 2-fluoro-3-((3,4,5-trimethoxyphenyl)diazenyl)benzoate (118b):

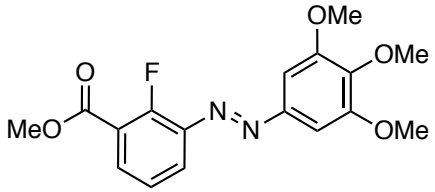

Aniline **117** (50.0 mg, 0.30 mmol, 1.00 eq.) was dissolved in DCM (1.0 ml) and a suspension of oxone® (363 mg, 0.59 mmol, 2.00 eq.) in water (1 ml) was added slowly. The reaction as stirred at room temperature for 17 h. EtOAc (5 ml) was added to the reaction mixture and the phases were separated. The organic layer was washed with sat. aq. NH_4Cl, sat. aq. $NaHCO_3$, water and brine dried over Na_2SO_4, filtered and concentrated. The crude nitrosobenzene was dried under high-vacuum for 10 minutes. 3,4,5-Trimethoxyaniline (54.2 mg, 0.30 mmol, 1.00 eq.) was added and the mixture was dissolved in DCM (1.0 ml) and c. AcOH (1.0 ml) was added. the reaction was stirred at 40 °C for 20 h. The volatiles were removed under reduced pressure and the residue was purified by flash column chromatography (SiO_2, Hex: EtOAc = 5:5 to 0:10). The title compound was obtained as an orange solid (44.4 mg, 0.13 umol, 43%).

R_f (SiO_2, Hex:EtOAc = 7:3; UV) = 0.47 (major), 0.58 (minor).

LCMS (5-100% MeCN in H_2O) t_{ret} = 3.7 min (minor), 4.3 min (major).

^{1}H-NMR (400 MHz, $CDCl_3$): δ [ppm] = 8.04 (ddd, *J* = 8.0, 6.4, 1.8 Hz, 1H), 7.90 (ddd, *J* = 8.4, 6.7, 1.8 Hz, 1H), 7.32 – 7.24 (m, 3H), 4.01 – 3.94 (m, 9H), 1.55 (s, 3H).

^{13}C-NMR (101 MHz, $CDCl_3$): *δ* [ppm] = 164.3, 153.7, 148.7, 141.6, 134.2, 129.7, 123.9 (d), 122.1, 121.2, 120.8, 101.1, 61.2, 56.4, 52.7. (*not all signals observed, too low #scans).

HRMS (ESI+, m/z): $[M+Na]^+$ for $C_{17}H_{17}FN_2O_5Na^+$ calcd.: 371.1014, found: 371.1030.

Synthesis of 2-fluoro-*N*-(2-(2-methyl-1*H*-indol-3-yl)ethyl)-3-((3,4,5-trimethoxyphenyl) diazenyl)benzamide (119b):

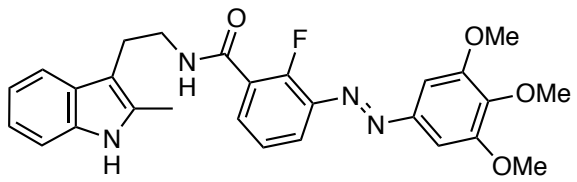

118b (10.0 mg, 28.7 mmol, 1.00 eq.) was dissolved in acetonitrile (1.0 ml) and a solution of LiOH (13.8 mg, 0.57 mmol, 20.0 eq.) in water (1.0 ml) was added at room temperature. The reaction was stirred over night and then slowly poured into aq. HCl (2 M, 10 ml) and extracted with ethyl acetate (3 x 10 ml). The combined organic layers were washed with brine, dried over Na_2SO_4, filtered, concentrated and dried under high vacuum.
The crude carboxylic acid, 2-methyltryptamine (10.1 mg, 58.0 umol, 2.00 eq.) and HATU (16.5 mg, 43.5 umol, 1.50 eq.) were dissolved in dry DMF (2.0 ml) and dry DIPEA (15 ul, 87.0 umol, 3.00 eq.) was added and the reaction was stirred for 16 h at room temperature. The reaction mixture was diluted with ethyl acetate (20 ml) and washed with 10% aq. LiCl (3 x 20 ml) and brine, dried over Na_2SO_4, filtered and concentrated. The crude product was purified by flash column chromatography (SiO_2, hexanes/ ethyl acetate 5/5 to 8/2), followed by HP-LC (semiprep, 60 – 75% acetonitrile in water (0.1 % formic acid) over 8 min. The title compound was obtained as an orange film (5.3 mg, 10.8 umol, 37%).

R_f (SiO_2, hexanes: ethyl acetate = 5:5; UV) = 0.54.

LCMS (5-100% MeCN in H_2O) t_R = 4.0 min (minor), 4.5 min (major).

HPLC (semiprep, 60 – 75% acetonitrile in water (0.1 % formic acid) over 8 min.) t_{ret} = 4.6 min.

^{1}H-NMR (400 MHz, $CDCl_3$): δ [ppm] = 8.19 (td, J = 7.4, 1.8 Hz, 1H), 7.88 – 7.78 (m, 2H), 7.57 (d, J = 7.2, 1.6 Hz, 1H), 7.35 – 7.27 (m, 3H), 7.18 – 7.04 (m, 2H), 6.95 – 6.83 (m, 1H), 3.97 (s, 6H), 3.95 (s, 4H), 3.79 (q, J = 7.1, 6.7 Hz, 2H), 3.09 (t, J = 6.9 Hz, 2H), 2.41 (s, 3H).

^{13}C-NMR (101 MHz, $CDCl_3$): δ [ppm] = 163.0 (d, $^3J_{CF}$ = 2.6 Hz), 157.8 (d, $^1J_{CF}$ = 258.2 Hz), 153.7, 148.7, 141.6, 140.9 (d, $^2J_{CF}$ = 9.2 Hz), 135.5, 134.2 (d, $^4J_{CF}$ = 2.5 Hz), 132.3, 128.6,

124.7 (d, $^3J_{CF}$ = 4.1 Hz), 123.1 (d, $^2J_{CF}$ = 10.7 Hz), 121.4, 120.9, 119.6, 118.0, 110.4, 108.5, 101.1, 61.25, 56.4, 40.8, 24.3, 11.8.

HRMS (ESI$^+$, *m/z*): [(M+H)$^+$] for $C_{27}H_{29}FN_4O_4^+$: calcd.: 491.2089, found: 491.2077.

Synthesis of methyl 2-fluoro-3-((4-methoxyphenyl)diazenyl)benzoate (118a):

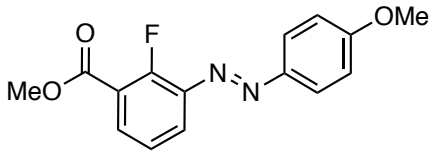

Anilline **117** (50.0 mg, 0.30 mmol, 1.00 eq.) was dissolved in dichloromethane (1.0 ml) and a suspension of oxone® (363 mg, 0.59 mmol, 2.00 eq.) in water (1 ml) was added slowly. The reaction as stirred at room temperature for 17 h. Ethyl acetate (5 ml) was added to the reaction mixture and the phases were separated. The organic layer was washed with sat. aq. NH_4Cl, sat. aq. $NaHCO_3$, water and brine dried over Na_2SO_4, filtered and concentrated. The crude nitrosobenzene was dried under high-vacuum for 10 minutes. 4-Methoxyaniline (36.4 mg, 0.30 mmol, 1.00 eq.) was added and the mixture was dissolved in dichloromethane (1.0 ml) and glacial acetic acid (1.0 ml) was added. the reaction was stirred at 40 °C for 20 h. The reaction mixture was diluted with dichloromethane (30 ml) and the mixture was basified withaq. sat. $NaHCO_3$ and sat. aq. Na_2CO_3. The layers were separated and the aqueous layer was extracted with dichloromethane (2 x 30 ml). The combined organic layers were washed with brine, died over Na_2SO_4, filtered and concentrated. The crude reaction product was purified by flash column chromatography (SiO_2, Hex:EtOAc = 8:2 to 5:5) and the title compound was obtained as orange film (54.5 mg, 0.19 mmol, 64%).

R_f (SiO_2, Hex:EtOAc = 8:2; UV): 0.36, 0.20.

LCMS (5-100% MeCN in H_2O over 5 min, 0.1% FA) t_{ret} = 3.9 min (minor), 4.7 min (major).

^{1}H-NMR (400 MHz, $CDCl_3$): δ [ppm] = 8.03 – 7.93 (m, 3H), 7.91 (ddd, *J* = 8.4, 6.9, 1.9 Hz, 1H), 7.29 – 7.23 (m, 1H), 7.02 (d, *J* = 9.0 Hz, 2H), 3.99 (s, 3H), 3.91 (s, 3H).

^{13}C-NMR (101 MHz, $CDCl_3$): δ [ppm] = 164.8 (d, $^3J_{CF}$ = 3.2 Hz), 162.9, 159.1 (d, $^1J_{CF}$ = 270.7 Hz), 147.3, 141.9 (d, $^2J_{CF}$ = 7.4 Hz), 133.6, 125.5, 123.8 (d, $^4J_{CF}$ = 4.9 Hz), 122.1, 120.4 (d, $^2J_{CF}$ = 9.2 Hz)., 114.5, 55.8, 52.7.

LRMS (ESI$^+$, *m*/*z*): [(M+H)$^+$] for $C_{15}H_{14}FN_2O_3^+$: calcd.: 289.1, found: 289.1.

Synthesis of 2-fluoro-3-((4-methoxyphenyl)diazenyl)-*N*-(2-(2-methyl-1*H*-indol-3-yl)ethyl) benzamide (119a):

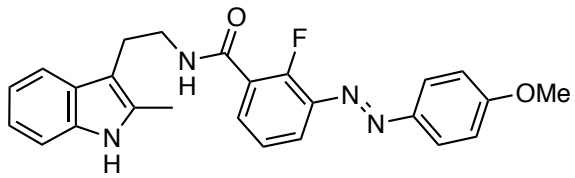

118a (27.0 mg, 93.7 umol, 1.00 eq.) was dissolved in acetonitrile (3.0 ml) and a solution of LiOH (40.0 mg, 1.67 mmol, 17.8 eq.) in water (3.0 ml) was added at room temperature. The reaction was stirred over night and then slowly poured into aq. HCl (2 M, 20 ml) and extracted with ethyl acetate (3 x 20 ml). The combined organic layers were washed with brine, dried over Na_2SO_4, filtered, concentrated and dried under high vacuum.
The crude carboxylic acid, 2-methyltryptamine (32.8 mg, 0.19 mmol, 2.00 eq.) and HATU (53.6 mg, 0.14 mmol, 1.50 eq.) were dissolved in dry DMF (6.5 ml) and dry DIPEA (49 ul, 0.28 mmol, 3.00 eq.) was added and the reaction was stirred for 13 h at room temperature. The reaction mixture was diluted with ethyl acetate (20 ml) and extracted against 10% aq. LiCl (20 ml). The layers were separated and the aqueous phase was extracted with ethyl acetate (2 x 10 ml). the combined organic layers were washed with brine, dried over Na_2SO_4, filtered and concentrated. The crude product was purified by flash column chromatography (SiO_2, hexanes/ ethyl acetate 8/2 to 5/5), followed by HPLC (semiprep, 60 – 80% acetonitrile in water (0.1 % formic acid) over 8 min). The title compound was obtained as an orange film (40.0 mg , 92.9 umol, 99%).

R_f (SiO_2, hexanes: ethyl acetate = 5:5; UV) = 0.60.

LCMS (5-100% MeCN in H_2O) t_R = 4.1 min (minor), 4.6 min (major).

HPLC (semiprep, 60 – 80% acetonitrile in water (0.1 % formic acid) over 8 min): t_{ret} (minor) = 3.1 min, = t_{ret} (major) = 5.1 min.

^{1}H-NMR (400 MHz, $CDCl_3$): δ [ppm] = 8.15 (td, J = 7.5, 1.8 Hz, 1H), 7.93 (d, J = 8.9 Hz, 2H), 7.82 (td, J = 7.7, 1.8 Hz, 1H), 7.59 – 7.54 (m, 1H), 7.31 – 7.26 (m, 2H), 7.17 – 7.06 (m, 2H), 7.02 (d, J = 9.0 Hz, 2H), 6.89 (dt, J = 11.8, 5.7 Hz, 1H), 3.90 (s, 3H), 3.79 (q, J = 6.7 Hz, 2H), 3.08 (t, J = 6.9 Hz, 2H), 2.41 (s, 3H).

^{13}C-NMR (101 MHz, $CDCl_3$): δ [ppm] = 163.1 (d, $^3J_{CF}$ = 2.7 Hz), 162.9, 157.7 (d, $^1J_{CF}$ = 257.6 Hz), 147.3, 141.1 (d, $^2J_{CF}$ = 9.1 Hz), 135.5, 133.7 (d, $^4J_{CF}$ = 2.6 Hz), 132.3, 128.5, 128.5, 125.5, 124.6 (d, $^3J_{CF}$ = 4.3 Hz), 122.9 (d, $^2J_{CF}$ = 10.8 Hz), 121.4, 120.9, 119.6, 118.0, 114.5, 110.4, 108.5, 55.8, 40.7, 24.3, 11.8.

HRMS (ESI$^+$, *m/z*): [(M+H)$^+$] for $C_{25}H_{24}FN_4O_2^+$: calcd.: 431.1878, found: 431.1870.

Synthesis of 118c:

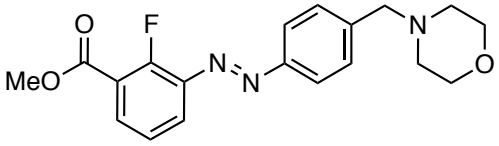

Anilline **117** (50.0 mg, 0.30 mmol, 1.00 eq.) was dissolved in dichloromethane (1.0 ml) and a suspension of oxone® (363 mg, 0.59 mmol, 2.00 eq.) in water (1 ml) was added slowly. The reaction as stirred at room temperature for 6 h. Ethyl acetate (5 ml) was added to the reaction mixture and the phases were separated. The organic layer was washed with sat. aq. NH_4Cl, sat. aq. $NaHCO_3$, water and brine dried over Na_2SO_4, filtered and concentrated. The crude beige nitrosobenzene was dried under high-vacuum for 10 minutes. ANILINE (56.8 mg, 0.30 mmol, 1.00 eq.) was added and the mixture was dissolved in dichloromethane (1.0 ml) and glacial acetic acid (1.0 ml) was added. the reaction was stirred at 40 °C for 20 h. The reaction mixture was diluted with dichloromethane (30 ml) and the mixture was basified withaq. sat. $NaHCO_3$ and sat. aq. Na_2CO_3. The layers were separated and the aqueous layer was extracted with dichloromethane (2 x 30 ml). The combined organic layers were washed

with brine, died over Na_2SO_4, filtered and concentrated. The crude reaction product was repeatedly purified by flash column chromatography (SiO_2, dichloromethane/ ethyl acetate/ hexanes/ methanol 2/3/5/0.5) and the title compound was obtained as orange film (81.4 mg, 0.23 mmol, 77%). The product contained residual impurities and was used for the subsequent step without further purification.

LCMS (5-100% MeCN in H_2O) t_R = 3.7 min (minor), 4.3 min (major).

^{1}H-NMR (400 MHz, $CDCl_3$): δ [ppm] = 8.04 (ddd, J = 7.9, 6.5, 1.8 Hz, 1H), 7.92 (dq, J = 5.6, 2.3, 1.8 Hz, 3H), 7.52 (d, J = 7.9 Hz, 2H), 7.31 – 7.26 (m, 1H), 3.99 (s, 3H), 3.83 – 3.67 (m, 4H), 3.59 (s_{br}, 2H), 2.49 (s, 4H).

^{13}C-NMR (101 MHz, $CDCl_3$): δ [ppm] = 164.7 (d, $^3J_{CF}$ = 3.2 Hz), 159.3 (d, $^1J_{CF}$ = 271.5 Hz), 152.1, 142.4, 141.7 (d, $^2J_{CF}$ = 7.3 Hz), 134.3, 129.9, 123.9 (d, $^4J_{CF}$ = 4.9 Hz), 123.4, 122.1, 120.5 (d, $^2J_{CF}$ = 9.1 Hz), 67.1, 63.2, 53.8, 52.7.

HRMS (ESI$^+$, *m/z*): [(M+H)$^+$] for $C_{19}H_{21}FN_3O_3^+$: calcd.: 358.1561, found: 358.1566.

Synthesis of (*E*)-4-(4-((2-fluoro-3-((2-(2-methyl-1*H*-indol-3-yl)ethyl)carbamoyl)phenyl) diazenyl)benzyl)morpholin-4-ium (119c):

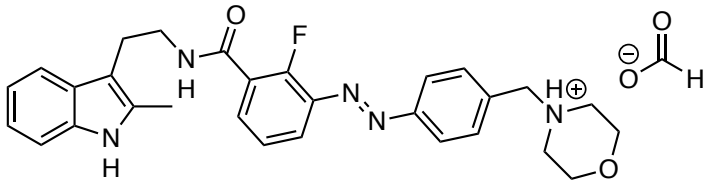

118c (34.0 mg, 95.2 umol, 1.00 eq.) was dissolved in acetonitrile (3.0 ml) and a solution of LiOH (42.0 mg, 1.75 mmol, 18.4 eq.) in water (3.0 ml) was added. The reaction was stirred at room temperature and upon completion the reaction mixture was acidified to pH = 1 using aq. HCl (2 M) and concentrated under reduced pressure. Remaining water was removed azeotropically using toluene and sonication. The lithium salt was dried under high vacuum and used without further purification.

The crude HCl salt, 2-methyltryptamine (33.1 mg, 0.19 mmol, 2.00 eq.) and HATU (54.2 mg, 0.14 mmol, 1.50 eq.) were dissolved in dry DMF (6.6 ml) and dry DIPEA (0.5 ml, 2.87 mmol, 30.2 eq.) was added at room temperature. The reaction was stirred for 10 h and poured into 10% aq. LiCl (30 ml) and extracted with EtOAc (50 ml). The organic layer was washed with

10% aq. LiCl (3 x 10 ml) and brine, dried over Na_2SO_4, filtered and concentrated. The crude product was purified by flash column chromatography (SiO_2, Hex:EtOAc 8/2 to 0/10) and HPLC (semi-prep, 10 – 40% MeCN in H_2O over 8 min, 3 min MeCN, 0.1% FA) and furnished the title compound as the formate salt (30 mg, 60.0 umol, 63%).

R_f (SiO_2, Hex:EtOAc = 8:2; UV) = 0.30.

LCMS (5-100% MeCN in H_2O) t_R = 2.9 min (minor), 3.1 min (major).

HPLC (semiprep, 10 – 40% acetonitrile in water (0.1 % formic acid) over 8 min): t_{ret} (minor) = 6.4 min, = t_{ret} (major) = 7.6 min.

^{1}H-NMR (400 MHz, $CDCl_3$): δ [ppm] = 8.20 (td, *J* = 7.4, 1.9 Hz, 1H), 7.93 – 7.88 (m, 3H), 7.84 (td, *J* = 7.7, 1.8 Hz, 1H), 7.60 – 7.55 (m, 1H), 7.55 – 7.49 (m, 2H), 7.35 – 7.06 (m, 8H), 6.94 – 6.82 (m, 1H), 3.83 – 3.74 (m, 6H), 3.64 (s, 2H), 3.09 (t, *J* = 6.8 Hz, 2H), 2.58 – 2.50 (m, 4H), 2.42 (s, 3H).

^{13}C-NMR (101 MHz, $CDCl_3$): δ [ppm] = 164.76, 163.0 (d, *J* = 2.5 Hz), 163.0, 156.0 (d, *J* = 258.5 Hz), 152.22, 141.0 (d, *J* = 9.1 Hz), 138.01, 135.52, 134.4 (d, *J* = 2.7 Hz), 132.3, 130.2, 129.2, 128.5, 128.4, 125.4, 124.6 (d, *J* = 4.2 Hz), 123.4, 123.1 (d, *J* = 10.8 Hz), 121.4, 119.5, 118.0, 110.5, 108.4, 66.8, 62.9, 53.6, 40.7, 24.3, 11.8.
NMR: rotamers, *cis:trans* isomers observed. Major signals reported.

HRMS (ESI$^+$, *m/z*): [$(M+H)^+$] for $C_{29}H_{31}FN_5O_2^+$: calcd.: 500.2456, found: 500.2451.

Formate salt **119c** (6.2 mg) was dissolved in dioxane (2.0 ml) and 0.07 ml HCl in dioxane (4.0 M) was added under agitation. The reaction became cloudy and was concentrated and subsequently coevaporated with dioxane (3x) and dried under high vacuum yielding the HCl salt.

Synthesis of 118d

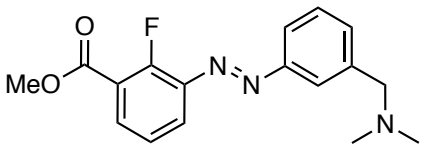

Anilline **117** (50.0 mg, 0.30 mmol, 1.00 eq.) was dissolved in dichloromethane (1.0 ml) and a suspension of oxone® (363 mg, 0.59 mmol, 2.00 eq.) in water (1 ml) was added slowly. The reaction as stirred at room temperature for 6 h. Ethyl acetate (5 ml) was added to the reaction mixture and the phases were separated. The organic layer was washed with sat. aq. NH_4Cl, sat. aq. $NaHCO_3$, water and brine dried over Na_2SO_4, filtered and concentrated. The crude beige nitrosobenzene was dried under high-vacuum for 10 minutes. ANILINE (44.4 mg, 0.30 mmol, 1.00 eq.) was added and the mixture was dissolved in dichloromethane (1.0 ml) and glacial acetic acid (1.0 ml) was added. the reaction was stirred at 40 °C for 20 h. The reaction mixture was diluted with dichloromethane (30 ml) and the mixture was basified with aq. sat. $NaHCO_3$ and sat. aq. Na_2CO_3. The layers were separated and the aqueous layer was extracted with dichloromethane (2 x 30 ml). The combined organic layers were washed with brine, died over Na_2SO_4, filtered and concentrated. The crude reaction product was purified by flash column chromatography (SiO_2, ethyl acetate/ methanol/ triethylamine 10/0/0 to 9/1/0.5) and the title compound was obtained as orange film (50.0 mg, 0.16 mmol, 54%).

R_f (SiO_2, EtOAc:MeOH:NEt_3 = 9:1:0.5; UV): 0.25

LCMS (5-100% MeCN in H_2O over 5 min, 0.1% FA): t_{ret} = 3.7 min (minor), 4.3 min (major).

^{1}H-NMR (400 MHz, $CDCl_3$): δ [ppm] = 8.05 (ddd, J = 8.0, 6.5, 1.8 Hz, 1H), 7.97 – 7.84 (m, 3H), 7.59 – 7.47 (m, 2H), 7.32 – 7.27 (m, 1H), 4.00 (s, 3H), 3.61 (s, 2H), 2.34 (s, 6H).

^{13}C-NMR (101 MHz, $CDCl_3$): δ [ppm] = 164.7 (d, $^3J_{CF}$ = 3.2 Hz), 159.4 (d, $^1J_{CF}$ = 271.7 Hz), 152.9, 141.7 (d, $^2J_{CF}$ = 7.3 Hz), 134.4, 132.8, 130.7, 129.4, 129.1, 124.2, 123.9 (d, $^4J_{CF}$ = 5.0 Hz), 122.5, 122.1, 120.5 (d, $^2J_{CF}$ = 9.1 Hz)., 63.8, 52.7, 45.3.
NMR: cis/ trans isomers observed, main reported.

HRMS (ESI$^+$, *m/z*): [$(M+H)^+$] for $C_{17}H_{19}FN_3O_2^+$: calcd.: 316.1456, found: 316.1454.

Synthesis of 1-(3-((2-fluoro-3-((2-(2-methyl-1*H*-indol-3-yl)ethyl)carbamoyl)phenyl)diazenyl) phenyl)-*N*,*N*-dimethylmethanaminium (119d):

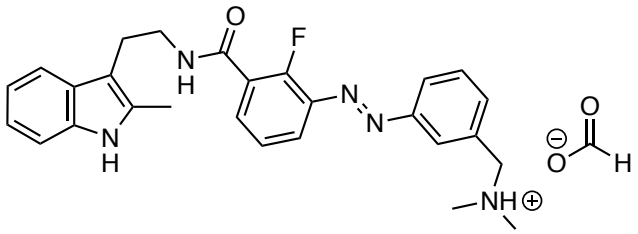

118d (34.0 mg, 0.11 mmol, 1.00 eq.) was dissolved in MeCN (3.9 ml) and a solution of LiOH (40.0 mg, 1.67 mmol, 15.5 eq.) in water (3.9 ml) was added. The reaction was stirred at room temperature and upon completion, the reaction mixture was acidified to pH = 1 using aq. HCl (2.0 M) and concentrated under reduced pressure. Remaining water was removed azeotropically using toluene and sonication. The lithium salt was dried under high vacuum and used without further purification.

The crude HCl salt, 2-methyltrypatmine (37.6 mg, 0.22 mmol, 2.00 eq.) and HATU (61.6 mg, 0.16 mmol, 1.50 eq.) were dissolved in dry DMF (7.4 ml) and dry DIPEA (0.57 ml, 3.27 mmol, 30.3 eq.) was added. The reaction was stirred at room temperature for 12 h and then poured into 10% aq. LiCl (50 ml). The aqueous layer was extracted with ethyl acetate (3 x 50 ml). The combined organic layers were washed with 10% aq. LiCl (3 x 20 ml) and brine, dried over Na_2SO_4, filtered and concentrated. The crude product was purified by flash column chromatography (SiO_2, ethyl acetate/ methanol/ triethylamine = 10/0/0 to 9/1/0.5) and HP-LC (prep, 20-40% acetonitrile in water (0.1% formic acid) over 8 minutes) giving the title compound as the formate salt as an orange film (26.6 mg, 52.8 mmol, 49%).

R_f (SiO_2, DCM:EtOAc:MeOH:NEt_3 = 5:5:0.1:0.1; UV) = 0.21

LCMS (5-100% MeCN in H_2O) t_R = 2.9 min (minor), 3.1 min (major).

HPLC (prep, 20-40% acetonitrile in water (0.1% formic acid) over 8 minutes): t_{Ret} (prep) = 5.2 min.

^{1}H-NMR (400 MHz, $CDCl_3$): δ [ppm] = 8.44 (s, 1H), 8.36 (s, 1H), 8.21 (td, *J* = 7.4, 1.9 Hz, 0.5H), 8.19 – 8.14 (m, 1H), 7.96 – 7.88 (m, 1H), 7.88 – 7.78 (m, 1H), 7.59 – 7.49 (m, 2H), 7.36 – 7.29 (m, 2H), 7.24 – 7.17 (m, 1H), 7.16 – 7.05 (m, 3H), 6.93 – 6.84 (m, 1H), 6.84 – 6.78 (m,

1H), 6.67 (s, 0.5H), 3.88 – 3.76 (m, 2H), 3.68 (dd, *J* = 6.4 Hz, 1H), 3.54 (s, 1H), 3.09 (t, *J* = 6.8 Hz, 1H), 3.00 (t, *J* = 6.6 Hz, 1H), 2.47 (s, 3H), 2.45 – 2.28 (m, 3H), 2.17 (s, 3H).

^{13}C-NMR (101 MHz, CDCl3): signal to noise not sufficient to report reliably.

HRMS (ESI$^+$, *m/z*): [(M+H)$^+$] for $C_{27}H_{29}FN_5O^+$: calcd.: 458.2351, found: 458.2348.

Synthesis of 1-(2-methoxy-4-nitrophenyl)-*N,N*-dimethylmethanamine (S9):

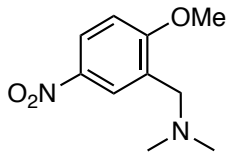

Following a known procedure[20], 2-(chloromethyl)-1-methoxy-4-nitrobenzene (100 mg, 0.50 mmol, 1.00 eq.) was dissolved in THF (0.8 ml) and water (0.3 ml) and a solution of dimethylamine in THF (2 M, 1.2 ml, 2.48 mmol, 5.00 eq.) was added. The reaction heated to reflux over night and then concentrated under reduced pressure. The aqueous residue was taken up in water (10.0 ml) and basified with aq. NaOH (2 M). The aqueous layer was extracted with DCM (2 x 10 ml), dried over Na_2SO_4, filtered and concentrated. The title compound was obtained as a yellow oil (105 mg, 0.50 mmol, quant.).

LCMS (5-100% MeCN in H_2O over 5 min., 0.1% FA): 1.2 t_{ret} = 1.2 min.

^{1}H-NMR (400 MHz, $CDCl_3$): δ = 8.21 (d, *J* = 2.9 Hz, 1H), 8.13 (dd, *J* = 9.0, 2.9 Hz, 1H), 6.90 (d, *J* = 9.0 Hz, 1H), 3.92 (s, 3H), 3.44 (s, 2H), 2.27 (s, 6H).

^{13}C-NMR (101 MHz, $CDCl_3$): δ = 162.8, 141.3, 128.5, 126.1, 124.7, 110.1, 110.0, 57.4, 56.3, 45.7.

LRMS (ESI$^+$, m/z): [M+H]$^+$ for $C_{10}H_{15}N_2O_3^+$ calcd.: 211.1, found: 211.1.

[20] Angelo, M.; Ortwine, D.; Worth, D.; Werbel, L. M.; McCall, J. W. *J. Med. Chem.*, **1983**, *26*, 1258–1267.

Synthesis of 3-((dimethylamino)methyl)-4-methoxyaniline (S10):

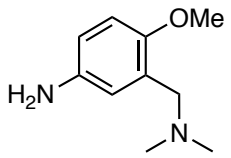

S9 (90 mg, 0.43 mmol, 1.00 eq.) was dissolved in ethyl acetate (10 ml) and sparged with nitrogen. Then Pd/C (6.0 mg, 0.06 mmol, 0.13 eq.) was added. The reaction mixture was again sparged with nitrogen before the reaction mixture was sparged with hydrogen for 10 seconds and subsequently kept under hydrogen atmosphere and stirred for 2.5 h. The reaction was sparged with nitrogen and then filtered over celite using positive nitrogen pressure and rinsing with ethyl acetate followed by concentration under reduced pressure. The crude product, a brown oil, was dried under high vacuum and used without further purification.

^{1}H-NMR (400 MHz, $CDCl_3$): δ = 6.72 – 6.67 (m, 2H), 6.57 (dd, J = 8.5, 2.9 Hz, 1H), 3.74 (s, 3H), 3.43 (s_{br}, 2H), 3.39 (s, 2H), 2.26 (s, 6H).

Synthesis of 3-((3-((dimethylamino)methyl)-4-methoxyphenyl)diazenyl)-2-fluorobenzoic acid (118e):

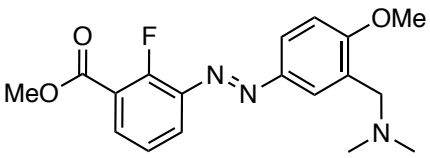

Anilline **117** (107 mg, 0.63 mmol, 1.00 eq.) was dissolved in dichloromethane (2.1 ml) and a suspension of oxone® (778 mg, 1.27 mmol, 2.00 eq.) in water (2.1 ml) was added slowly. The reaction as stirred at room temperature for 6 h. Ethyl acetate (10 ml) was added to the reaction mixture and the phases were separated. The organic layer was washed with sat. aq. NH_4Cl, sat. aq. $NaHCO_3$, water and brine dried over Na_2SO_4, filtered and concentrated. The crude beige nitrosobenzene was dried under high-vacuum for 10 minutes. **S10** (ca. 0.67 eq.) was added and the mixture was dissolved in dichloromethane (2.1 ml) and glacial acetic acid

(2.1 ml) was added. the reaction was stirred at 40 °C for 20 h. The reaction mixture was diluted with ethyl acetate (15 ml) and water (6 ml) and the mixture was basified with aq. sat. $NaHCO_3$ (6 ml) and sat. aq. Na_2CO_3 (6 ml). The layers were separated and the aqueous layer was extracted with ethyl acetate (2 x 20 ml). The combined organic layers were washed with brine, died over Na_2SO_4, filtered and concentrated. The crude reaction product was purified by flash column chromatography (SiO_2, EtOAc:MeOH:NEt_3 = 10:0:0 to 9:1:0.5) and the title compound was obtained as orange film (126 mg, 0.37 mmol, 58%). The reaction product showed traces of impurity and was used without further purification.

LCMS (5-100% MeCN in H_2O): t_{ret} = 2.4 min (minor), 2.8 min (major).

^{1}H-NMR (400 MHz, $CDCl_3$): δ = 8.05 – 7.99 (m, 1H), 7.99 – 7.96 (m, 1H), 7.96 – 7.88 (m, 2H), 7.31 – 7.27 (m, 1H), 7.02 (d, J = 8.7 Hz, 1H), 4.01 (s, 3H), 3.96 (s, 3H), 3.57 (s, 2H), 2.35 (s, 6H).

HRMS (ESI$^+$, m/z): $[M+H]^+$ for $C_{18}H_{21}FN_3O_3^+$ calcd.: 346.1561, found: 346.1559.

Synthesis of 1-(5-((2-fluoro-3-((2-(2-methyl-1*H*-indol-3-yl)ethyl)carbamoyl)phenyl) diazenyl)-2-methoxyphenyl)-*N*,*N*-dimethylmethanaminium (119e):

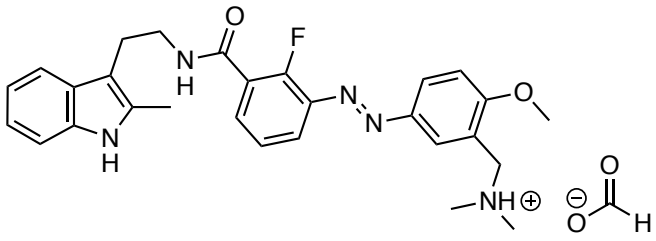

118e (63.0 mg, 0.18 mmol, 1.00 eq.) was dissolved in MeCN (6.6 ml) and a solution of LiOH (67.7 mg, 2.83 mmol, 15.5 eq.) in H_2O (6.6 ml) was added. The reaction was stirred at room temperature and upon completion, the reaction mixture was acidified to pH = 1 using aq. HCl (2 M) and concentrated under reduced pressure. Remaining water was removed azeotropically using toluene and sonication. The lithium salt was dried under high vacuum and used without further purification.

The crude HCl salt, 2-methyltrypatmine (62.7 mg, 0.36 mmol, 2.00 eq.) and HATU (103 mg, 0.27 mmol, 1.50 eq.) were dissolved in dry DMF (12.4 ml) and dry DIPEA (0.95 ml, 5.44 mmol, 30.2 eq.) was added. The reaction was stirred at room temperature over night and then poured into 10% aq. LiCl (50 ml). The aqueous layer was extracted with EtOAc (3 x 50 ml). The combined organic layers were washed with 10% aq. LiCl (3 x 20 ml) and brine, dried over Na_2SO_4, filtered and concentrated. The crude product was purified by flash column chromatography (SiO_2, EtOAc:MeOH:NEt_3 = 10:0:0 to 9:1:0.5) and HPLC (semiprep, 10-40% over 8 min, 3 min MeCN, 0.1% FA) giving the title compound as the formate salt as an orange film (32.0 mg, 60 µmol, 33% over 2 steps).

R_f (SiO_2, DCM:EtOAc:MeOH:NEt_3 = 5:5:0.1:0.1) = 0.17.

LCMS (25-75% MeCN in H_2O over 5 min., 0.1% FA): t_{ret} = 2.2 min (minor), 2.8 min (major).

HPLC (semi-prep, 10-40% MeCN in H_2O over 8 min, 3 min. MeCN, 0.1% FA): t_{ret} = 7.65 min (major).

^{1}H-NMR (400 MHz, MeOD): δ [ppm] = 8.48 (s_{br}, 2H), 8.20 – 8.11 (m, 1H), 8.11 – 8.05 (m, 1H), 7.88 – 7.79 (m, 1H), 7.73 – 7.62 (m, 1H), 7.53 (d, *J* = 7.6 Hz, 1H), 7.38 – 7.28 (m, 2H), 7.28 – 7.13 (m, 2H), 7.10 – 6.90 (m, 3H), 4.37 (s, 2H), 4.05 (s, 3H), 3.72 – 3.48 (m, 2H), 3.12 – 2.92 (m, 2H), 2.86 (s, 6H), 2.48 – 2.29 (m, 3H).

^{13}C-NMR (101 MHz, MeOD): δ [ppm] = 166.5, 162.5, 159.6, 158.3 (d, *J* = 256.8 Hz), 148.1, 142.1 (d, *J* = 7.6 Hz), 137.2, 133.4, 133.3 (d, *J* = 2.9 Hz), 130.0, 129.6, 127.5, 125.5 (d, *J* = 4.6 Hz), 121.4, 120.9, 120.8, 119.5, 118.5, 113.0, 111.3, 108.7, 57.6, 57.1, 43.6, 42.0, 25.1, 11.4.
NMRs: mixtures of rotamers and *cis*:*trans* isomers observed

HRMS (APCI$^+$, *m/z*): $[M+H]^+$ for $C_{28}H_{31}FN_5O_2^+$: calcd.: 488.2456, found: 488.2457.

The formate salt was then dissolved in MeOH and trituated with HCl in MeOH (3 M), followed by concentration and coevaporation with methanol (3 x 5 ml).The HCl-salt was dried under high vacuum and obtained as an orange film.

Selected UV-Vis information for Chapter 1-4:

119d

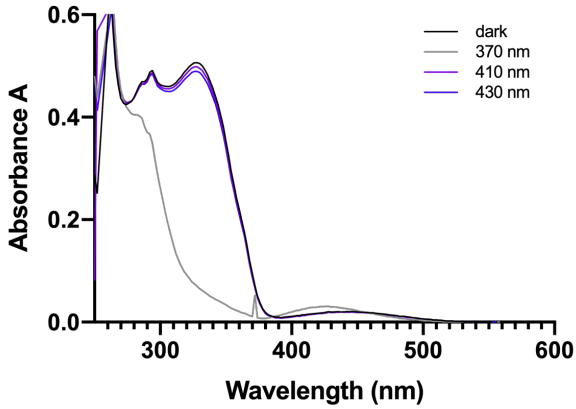

119d

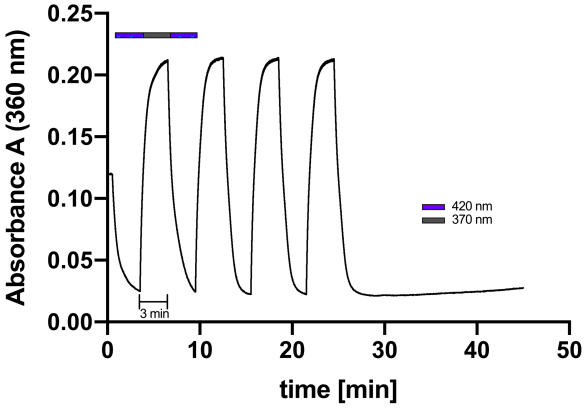

119c

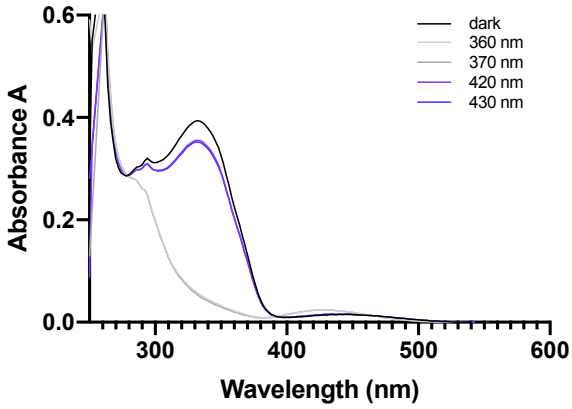

119c

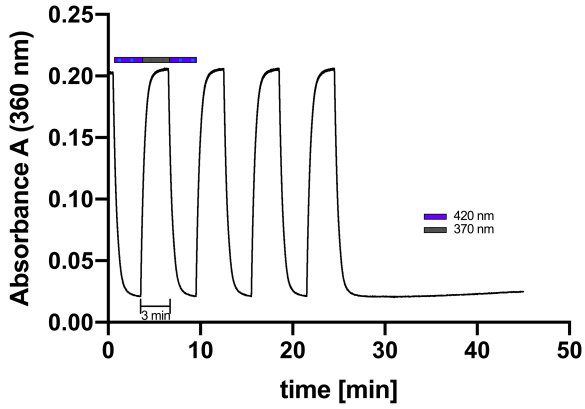

121

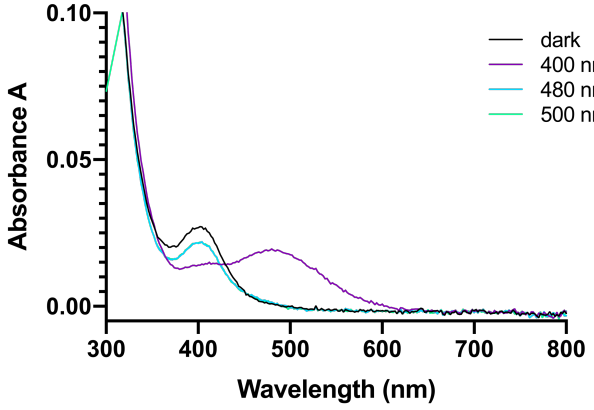

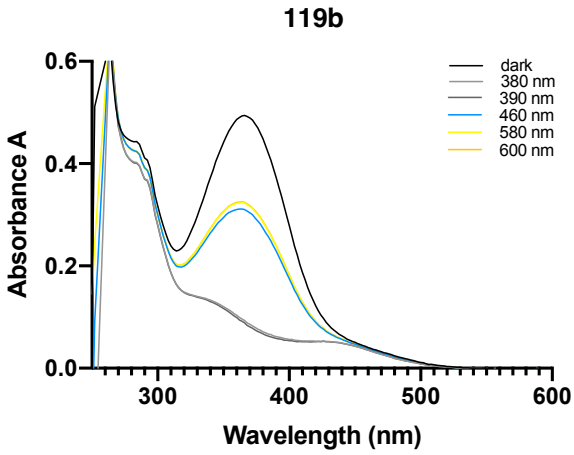
119b
Absorbance A
Wavelength (nm)
dark
380 nm
390 nm
460 nm
580 nm
600 nm
0.0
0.2
0.4
0.6
300
400
500
600

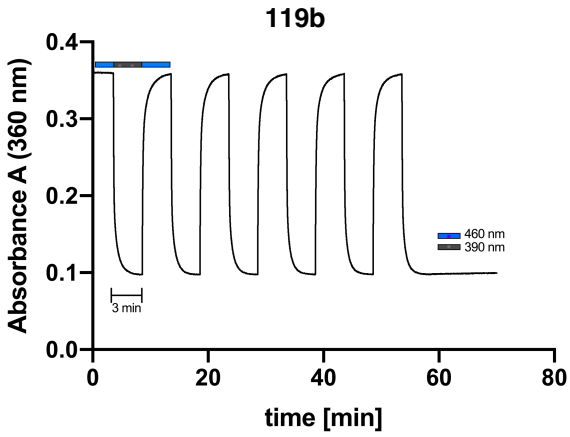
119b
Absorbance A (360 nm)
time [min]
460 nm
390 nm
3 min
0.0
0.1
0.2
0.3
0.4
0
20
40
60
80

`

General Methods Biology

Cell Culture: HeLa (ATCC), MDA-MB-231 (ATCC) and mCherry-LifeAct MDA-MB-231 cells (gift from A. Akhmanova, Utrecht University) were cultured in antibiotic free Dulbecco's Modified Eagle Medium (DMEM) (Gibco, Thermo Fisher cat# 10566024) supplemented with 10% fetal bovine serum (FBS) (Gibco, Thermo Fischer cat# 10437036) for the first 2 passages after thawing. Thereafter they were conditioned to phenol-red free DMEM (Thermo Fisher cat# 31053036), supplemented with 10% FBS (Gibco, Thermo Fischer cat# 10437036), 1% penicillin-streptomycin-glutamine (Gibco, Thermo Fischer cat# 10378016) and a final concentration of 4 mM L-glutamine (Gibco, Thermo Fischer cat# 25030081) for 2 passages before use in assays. Cells were grown in a cell culture incubator at 37 °C in a 5% CO_2 atmosphere and passaged at 70-90% confluency every 2-4 days. Cells were used for up to 25 passages for cell proliferation assays and up to 15 passages for imaging studies.

Handling of Photoswitchable Compounds: Test compounds were dissolved in DMSO (sterile filtered) to the desired stock-concentration (e.g. 10 mM) and stored at –20 °C. In case of long half-lives, the compound stock was left in the dark at room temperature for an appropriate time to ensure full thermal relaxation of the photoswitch. Compounds were protected from light and only handled in the dark or under red-light to avoid isomerization.

MTT Cell Proliferation Assays: Cells (HeLa: 5000, MDA-MB-231: 4000 cells) were seeded in 96 well-plates using 90 µl phenolred-free DMEM (Thermo Fisher cat# 31053036), supplemented with 10% FBS (Gibco, Thermo Fischer cat# 10437036), 1% penicillin-streptomycin-glutamine (Gibco, Thermo Fischer cat# 10378016) and a final concentration of 4 mM L-glutamine (Gibco, Thermo Fischer cat# 25030081). After 24 h, cells were treated with compound stocks (1% DMSO, 2% MeCN as cosolvents for better solubility), which were applied as 10x concentrations in 10 µl medium. Light-dependent assays were performed as duplicates where one plate was kept in light-proof boxes, shielded from light (dark) and the second one was exposed to a specific irradiation protocol (slow: 75 ms per 15s; fast: 25 ms per 0.5 s) using a cell DISCO as described previously[21]. After 48 h of treatment, 3-(4,5-dimethylthiazol-2-yl)-2,5-diphenyl tetrazolium bromide (MTT; Invitrogen, Thermo Fischer Cat# M6494; 10 µl, 5 mg/ml in PBS) was added to each well and incubated for 3 h (37 °C, 5% CO_2). The wells were emptied and the purple formazan crystals at the bottom of the wells were

[21] Borowiak, M.; Nahaboo, W.; Reynders, M.; Nekolla, K.; Jalinot, P.; Hasserodt, J.; Rehberg, M.; Delattre, M.; Zahler, S.; Vollmaer, A.; Trauner, D.; Thorn-Seshold, O. *Cell* **2015**, *162*, 403–411.

dissolved in 100 µl DMSO (incubated 10 minutes, 37 °C), followed by colorimetric read-out using a FLUOstar Omega microplate reader (BMG LABTECH) (120 sec. shaking, readout at 570 nm, blank corrected).
Viability was reported as mean percentage of viable cells relative to control. ± standard deviation (SD) was reported from N independent experiments, performed in triplicates. EC_{50}-values were determined by four-parameter curve fitting for sigmoidal dose-response with a variable slope.

Fixed Cell Fluorescent Staining:

Glass coverslips (ø12 mm, thickness #1; VWR cat# 89167-106) were cleaned with HCl (1 M, aq.) at 60 °C with frequent, gentle agitation for 10 h, rinsed dd H_2O (10 x), 70% EtOH (aq., 3 x) and stored under EtOH (absolut). The coverslips were flamed and upon cooling, treated with 40 µl of poly-L lysine (Sigma Aldrich cat# P4707-50ML) for 1 h at 37 °C. the coverslips were washed with dd H_2O (3 x) and dried at 37 °C for at least 4 h or over night. The coverslips were stored at +4 °C for up to 3 months.

In a 24 well plate, HeLa cells were seeded on poly-L-lysine coated coverslips at a density of 40 000 cells/ 450 µl phenol red free full growth medium. The next morning, the test compound was added as a 10 x concentration (50 µl, 1% DMSO, 2% MeCN, DMEM) in the dark. Two well-plates were subjected to the respective irradiation conditions for 5 h, while one was kept in the dark. After the irradiation period, one of the irradiated plates was kept in the dark for an additional 16 h, and the two remining plates (one light and one dark) were fixed and blocked immediately under exclusion of ambient light.
Fixing/ Blocking:
Under red light, medium was removed and MTSB Buffer (190 µl, 37 °C) was added. After 30 seconds, glutaraldehyde (10% aq., 10 µl) was added and the cells were incubated for 10 minutes. The buffer was removed and $NaBH_4$ (0.1% in PBS, 200 µl) was added and incubated for 7 minutes. $NaBH_4$/PBS was removed and the fixed cells were washed with PBS (3 x 500 ul, 37 °C) and blocked with FBS (10% in PBS, 500 ul, 37 °C) over night at +4 °C or for 3 h at room temperature.
Staining:
Coverslips were placed on a drop (40 µl) of a mixture of Phallodin AF 594 (abcam cat# ab176757), anti alpha Tubulin AF 488 (abcam cat# ab195887) and Hoechst 33342 (Thermo

Fischer cat# 62249) and incubated in the dark (ensure humidity to avoid drying) for 1 h. the coverslips were washed three times with PBS, excess PBS was removed and the coverslip was mounted using fluoroshield aqueous mounting medium (abcam cat# ab104135). The mounted samples were dried at room temperature in the dark and imaged by confocal microscopy on an upright Leica SP8 laser scanning confocal within the next days. Samples were thereafter stored at +4 °C.

Image analysis and processing was performed using ImageJ and Fiji – ImageJ (National Institutes of Health, USA)[22].

For statistical analysis and graphical representation, GraphPad Prism 9 for macOS (San Diego, CA, USA) was used. The absorbance values for untreated controls (cosolvent only) were normalized to 100%.

[22] Schindelin, J.; Arganda-Carreras, I.; Frise, E.; Kaynig, V.; Longair, M.; Pietzsch, T.; Preibisch, S.; Rueden, C.; Saalfeld, S.; Schmid, B.; Tinevez, J.-Y.; White, D. J.; Hartenstein, V.; Eliceiri, K.; Tomancak, P.; Cardona, A. *Nat Methods* **2012**, *9* (7), 676–682.

Biological Data for Part 1: 2 Latrunculin

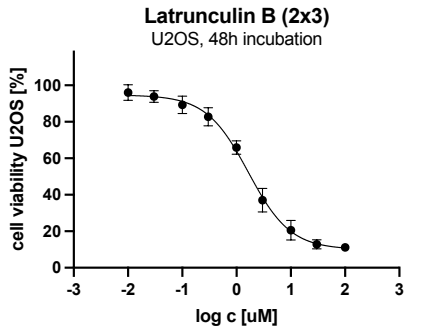

IC50	1.648

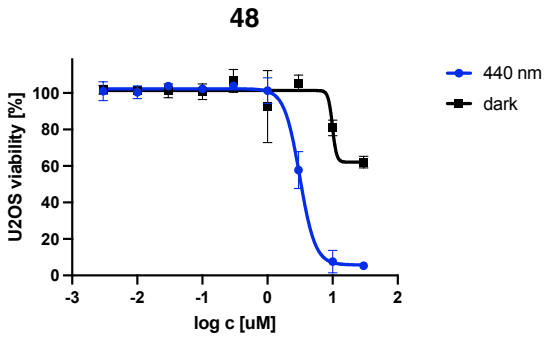

	440 nm	dark
IC50	3.132	9.934

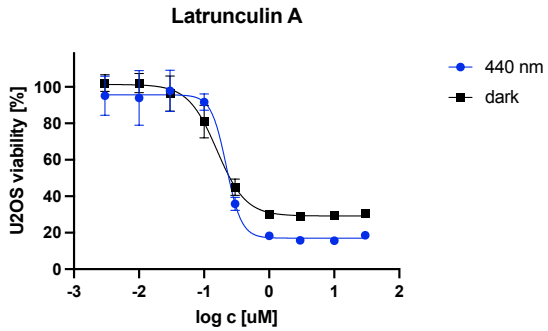

	440 nm	dark
IC50	0.2200	0.1576

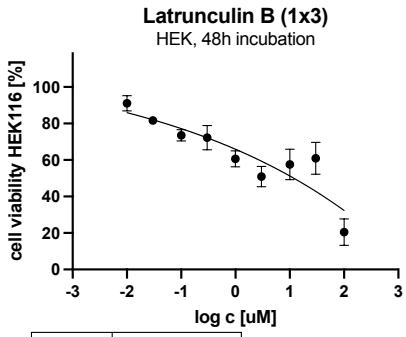

IC50	~ 2.402e+024

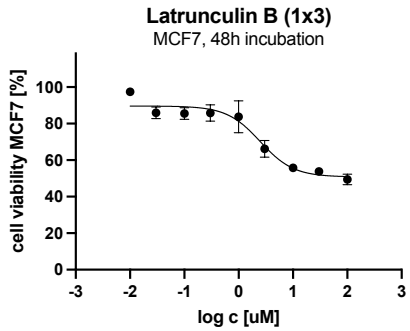

IC50	2.484

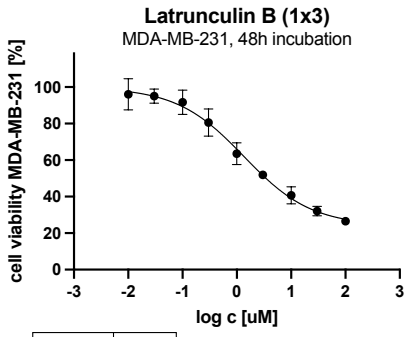

IC50	1.354

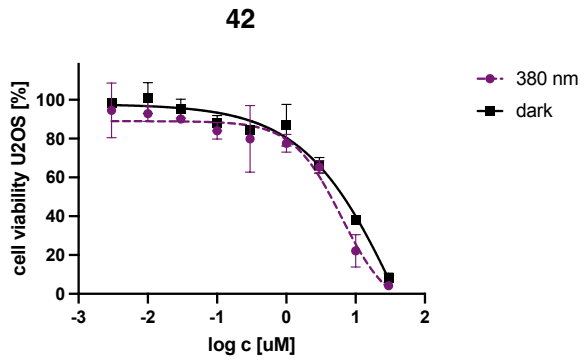

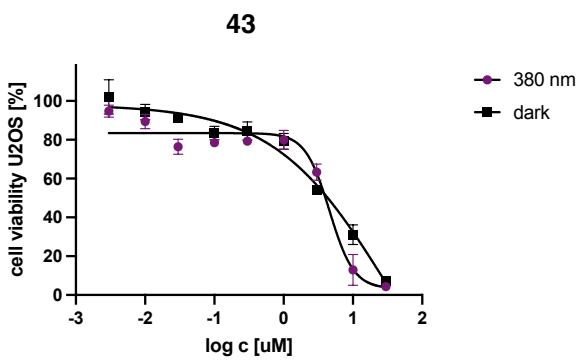

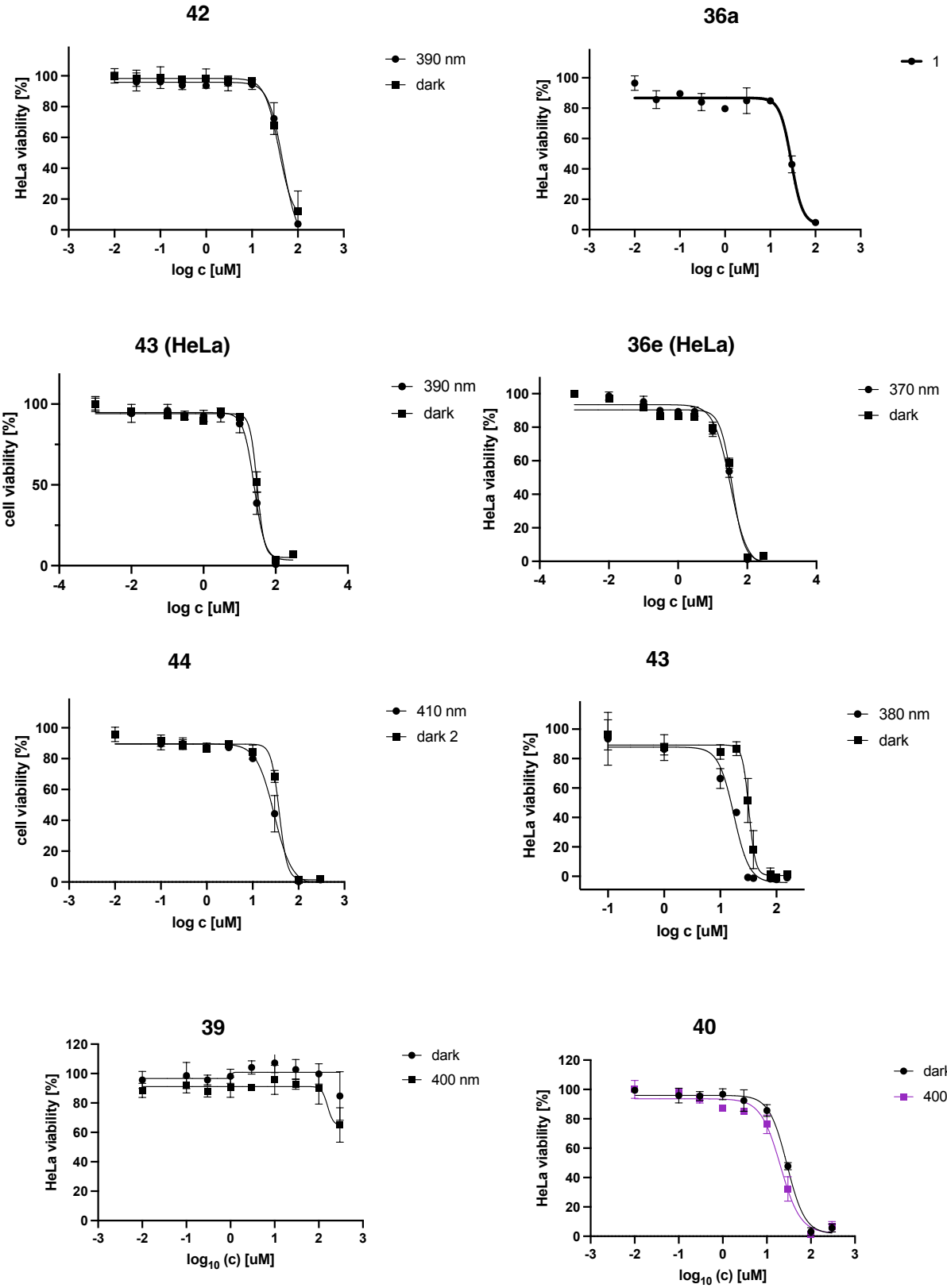
42
HeLa viability [%]
log c [uM]
390 nm
dark
36a
HeLa viability [%]
log c [uM]
1
43 (HeLa)
cell viability [%]
log c [uM]
390 nm
dark
36e (HeLa)
HeLa viability [%]
log c [uM]
370 nm
dark
44
cell viability [%]
log c [uM]
410 nm
dark 2
43
HeLa viability [%]
log c [uM]
380 nm
dark
39
HeLa viability [%]
log10 (c) [uM]
dark
400 nm
40
HeLa viability [%]
log10 (c) [uM]
dark
400 nm

`

Biological Data for Part 1: 3 Jasplakinolide

Wavelength Dependent Cell Proliferation Assays:

The wavelength dependent cell proliferation assay was performed as sixplikett. EC_{50}-values for Wavelength dependent cell proliferation assay.

Wavelength dependent cell proliferation assay: EC50 values for different wavelengths or dark.

conditions (25 ms/0.5s)	**dark**	**410 nm**	**440 nm**	**477 nm**	**505 nm**	**525 nm**	**565 nm**
EC_{50} [µM]	N/A	0.66	0.37	0.91	N/A	N/A	N/A

Dose-Response Curves for Cell Proliferation Assays:

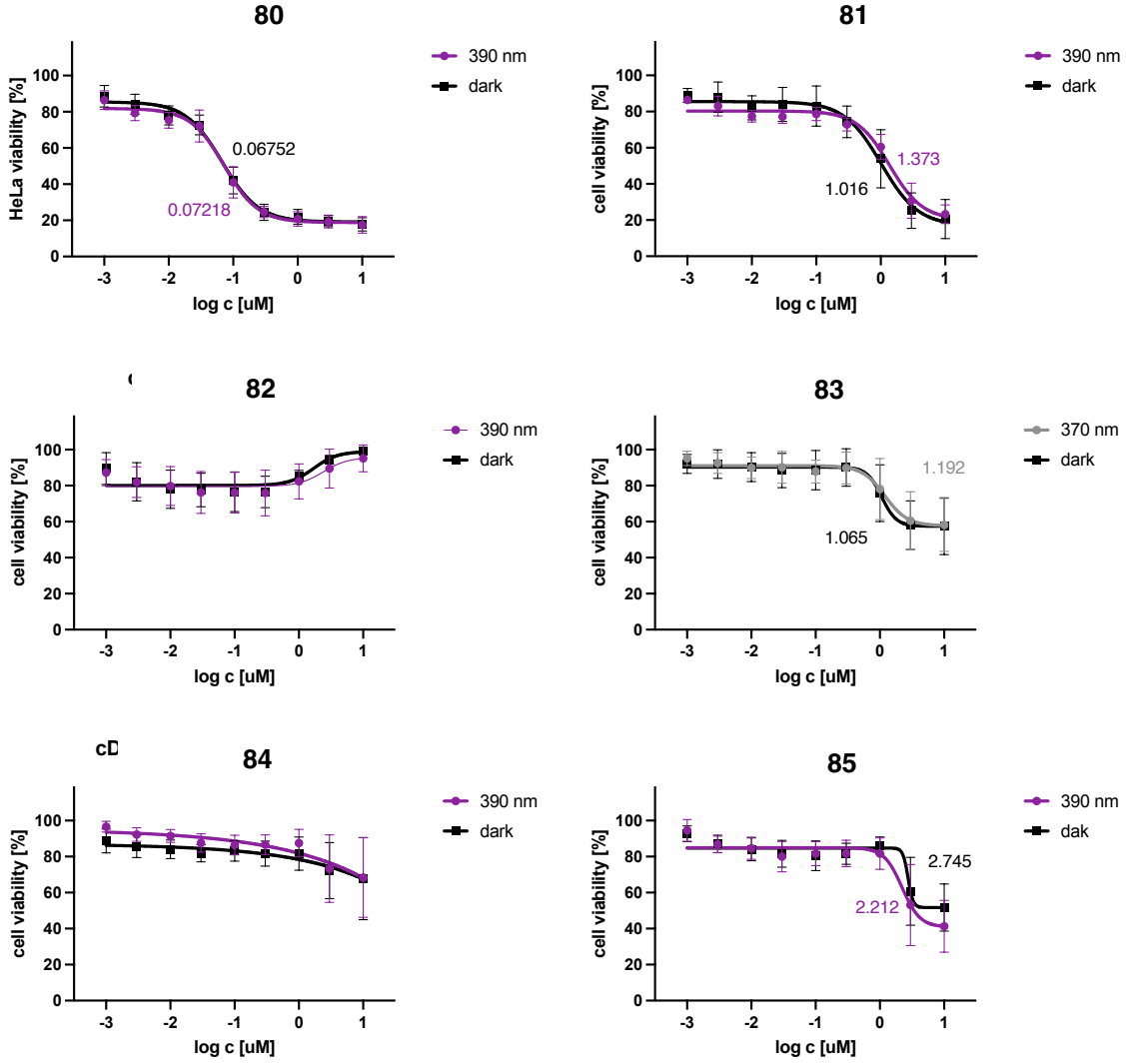

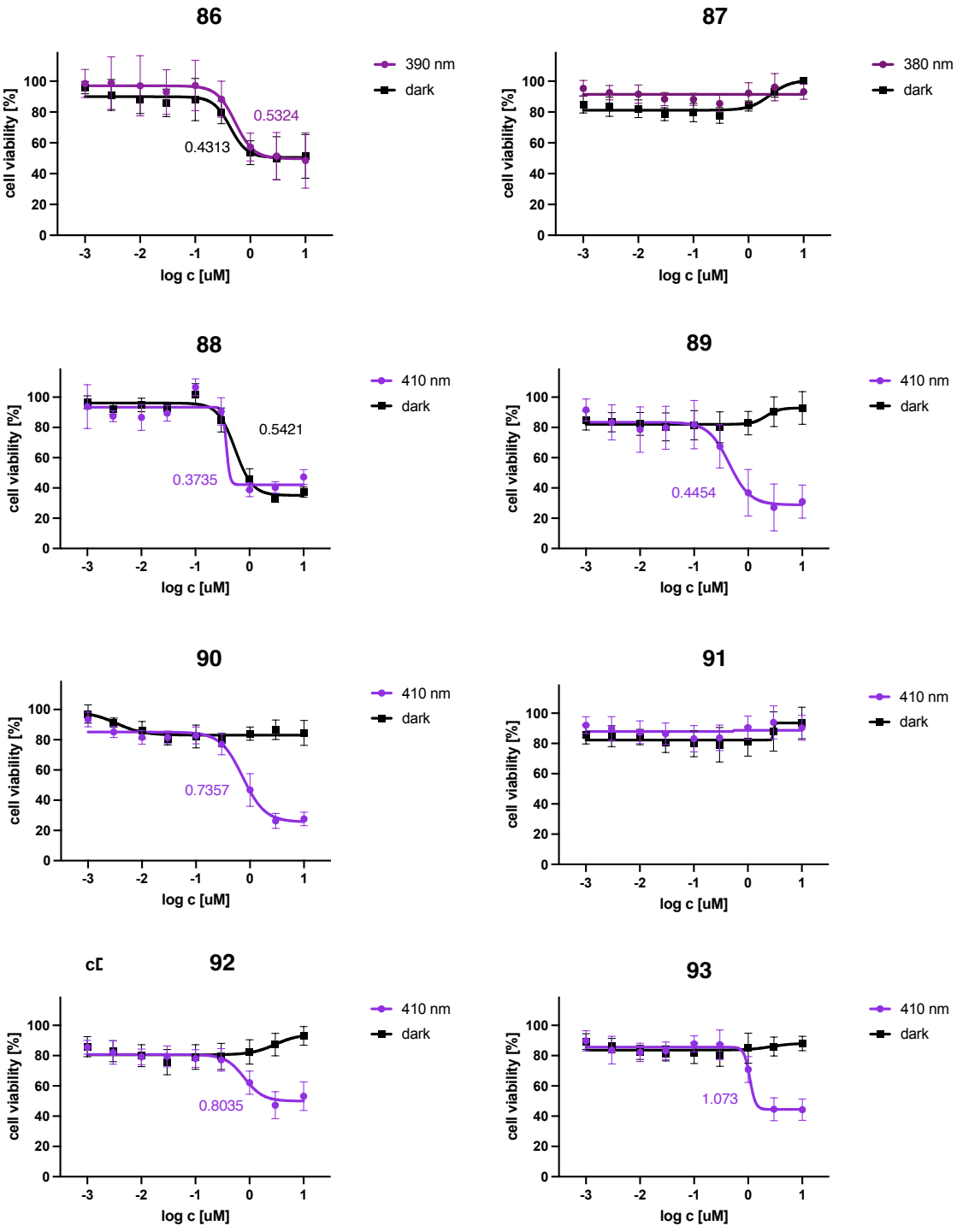
86
cell viability [%]
log c [uM]
390 nm
dark
0.5324
0.4313
87
380 nm
dark
88
410 nm
dark
0.5421
0.3735
89
410 nm
dark
0.4454
90
410 nm
dark
0.7357
91
410 nm
dark
92
410 nm
dark
0.8035
93
410 nm
dark
1.073

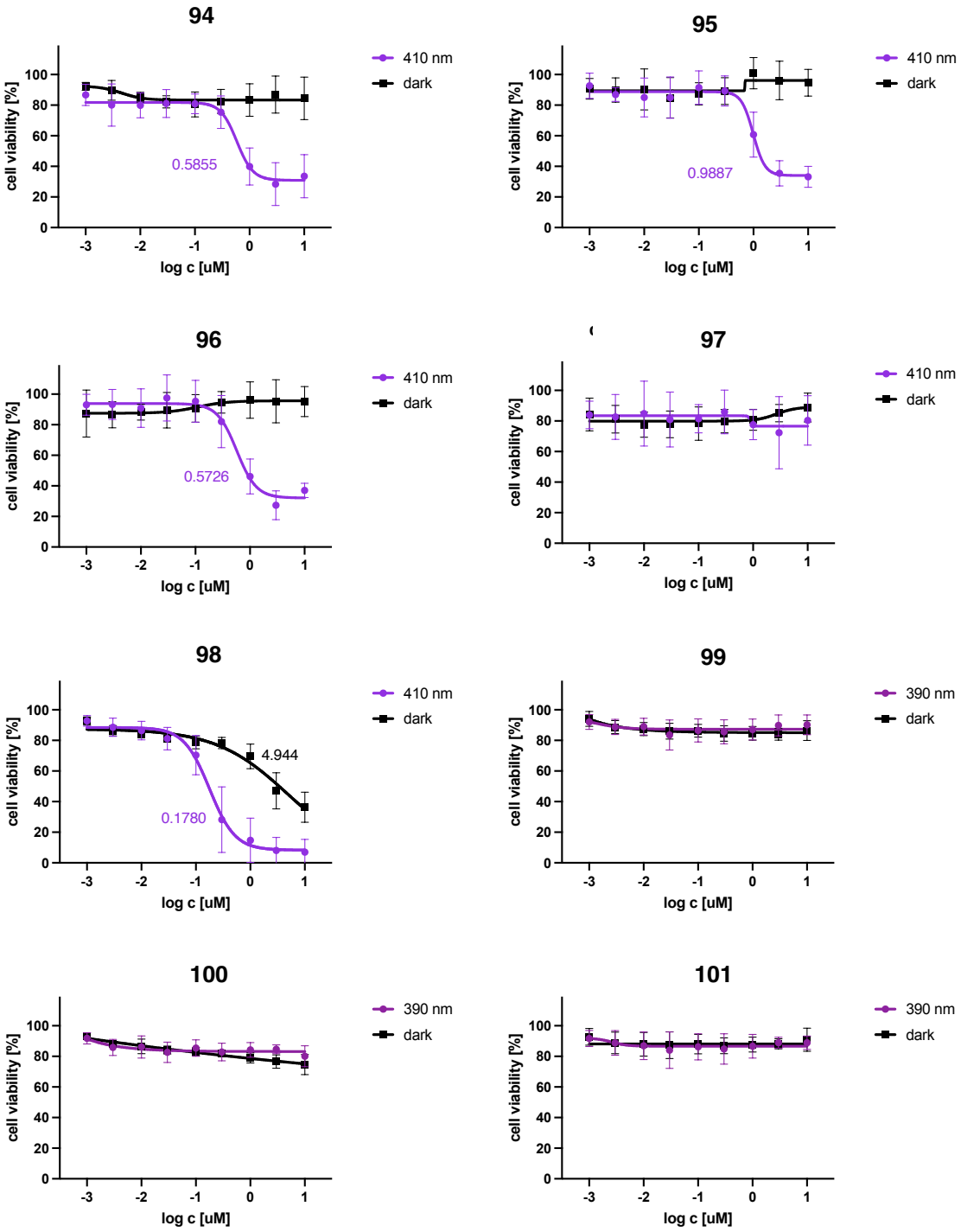
94
cell viability [%]
log c [uM]
0.5855
410 nm
dark
95
0.9887
410 nm
dark
96
0.5726
410 nm
dark
97
410 nm
dark
98
4.944
0.1780
410 nm
dark
99
390 nm
dark
100
390 nm
dark
101
390 nm
dark

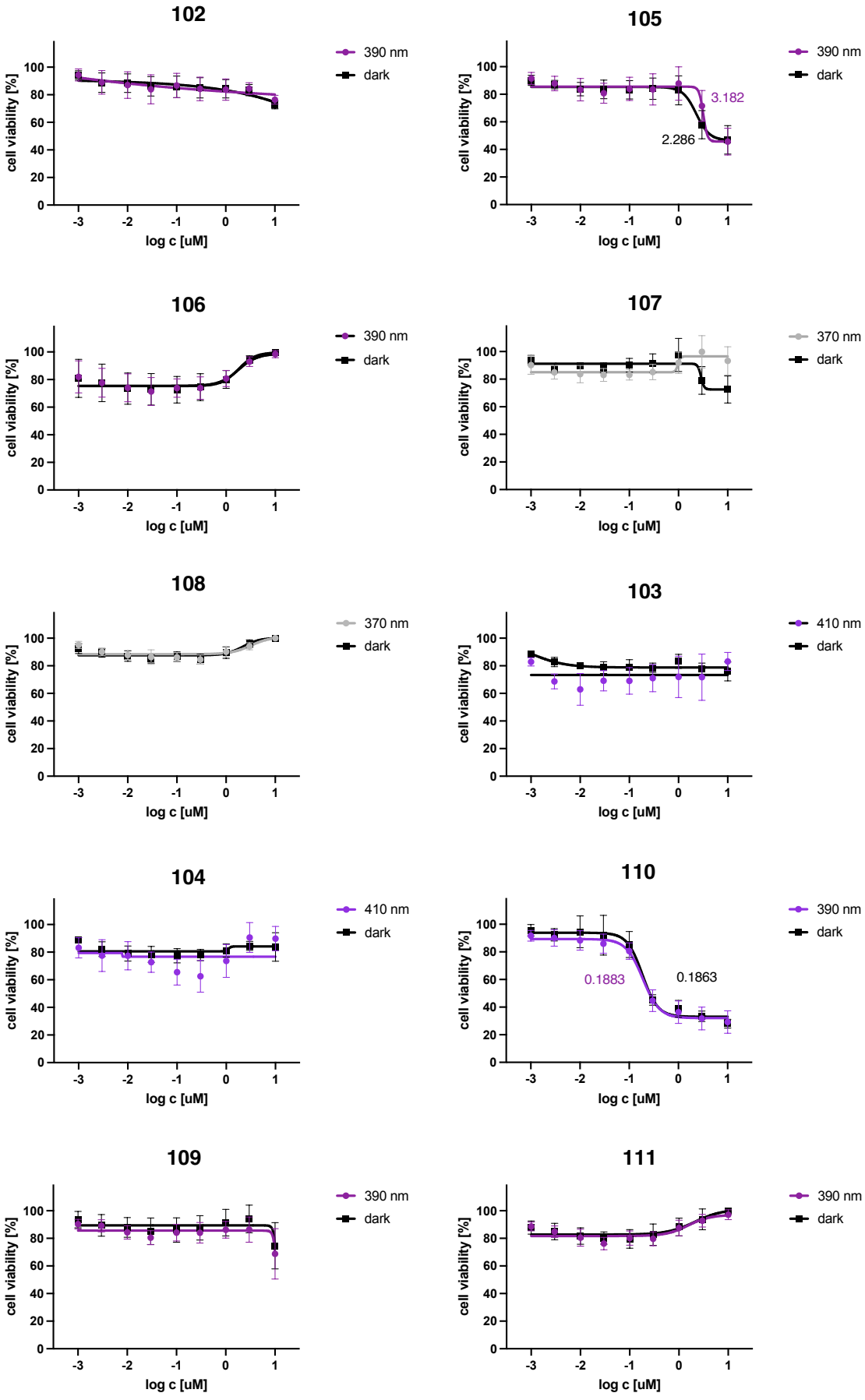
102
105
106
107
108
103
104
110
109
111
cell viability [%]
log c [uM]
390 nm
dark
370 nm
410 nm
3.182
2.286
0.1883
0.1863

Wound Healing Assays:

MDA-MB-231 cells were plated in 96 well-plates at a concentration of 40.000 cells/well in 100 ul phenolred-free DMEM (Thermo Fisher cat# 31053036), supplemented with 10% FBS (Gibco, Thermo Fischer Cat# 10437036), 1% penicillin-streptomycin-glutamine (Gibco, Thermo Fischer Cat# 10378016) and a final concentration of 4 mM L-glutamine (Gibco, Thermo Fischer cat# 25030081). The next day, cells were starved over night by exchanging the medium for phenolred-free DMEM (Thermo Fisher cat# 31053036), supplemented with 1% FBS (Gibco, Thermo Fischer Cat# 10437036), 1% penicillin-streptomycin-glutamine (Gibco, Thermo Fischer cat# 10378016) and a final concentration of 4 mM L-glutamine (Gibco, Thermo Fischer cat# 25030081). After a fully confluent monolayer was obtained, the monolayer was scratched using a sterilized wooden toothpick, the medium was removed, the cells washed with PBS (pH 7.4, Gibco, Thermo Fischer cat# 10010023; 3 x 100 µl, 37 °C) and 90 µl full growth medium was added. The obtained scratches were imaged using a Leica DMI6000B inverted fluorescent microscope with a Tokai Hit stage-top incubator at 37 °C at 2.5 x magnification, DIC filter (timepoint t=0), before the compounds were added (10 x concentration, 10 µl). Experiments were run in sets of two (or three) duplicates (dark/ light (/ rescue) protocol) using the cell DISCO system with a 24-LED array as previously reported. Quantification of scratch area was performed using a custom macro script for ImageJ (National Institutes of Health, USA). The final selection area was adjusted to fit the wound in every image of the image-stack. Relative wound closure per well was referenced to timepoint t_0 and further analyzed using GraphPad Prism 9 for macOS (San Diego, CA, USA). Three independent experiments were combined by internal normalization to the wound closure (dark) after 24 h. Statistical analysis was performed using GraphPad Prism 9 for macOS (San Diego, CA, USA). Error bars are reported as ± standard deviation (SD) from 3 independent experiments, performed in (5/)6-plicates.

The wound closure was monitored over 48 h in total. After this time period, cell viability was assessed using PrestoBlue viability assay (Thermo Fischer cat# A13261; 10 µl/ well), incubated for 30 minutes and analyzed by fluorescence readout λ_{Ex} 544 nm/ λ_{Em} 590 nm using a FLUOstar Omega microplate reader (BMG LABTECH, Ortenberg, Germany).

Macro:

```
run("Images to Stack", "name=Stack title=[] use");
run("Find Edges", "stack");
setOption("BlackBackground", true);
```

```
run("Make Binary", "method=Default background=Default calculate black");
run("Dilate", "stack");
run("Fill Holes", "stack");
run("Dilate", "stack");
run("Fill Holes", "stack");
run("Invert", "stack");
makeRectangle(657, 753, 768, 576);
```

Live Cell Imaging General Considerations:

MDA-MB-231 cells that stably express mCherry LifeAct were seeded using phenol-red free DMEM, supplemented with 10% FBS, 1% penicillin-streptomycin-glutamine and a final concentration of 4 mM l-glutamine (Gibco, Thermo Fischer cat# 25030081) at a density of 40K cells/ 2 ml in a ø35 mm imaging dish (previously coated with poly-L-lysine; see procedure for cover slips) and left to adhere for 16-24 h. Next, the medium was removed and new medium containing optojasp (2.5 µM) was added. The cells were left to incubate for 16-24 h in the dark. When transporting cells, it was ensured that cells were kept in a warm environment and in the dark.

Image analysis and processing was performed using ImageJ and Fiji – ImageJ[23] (National Institutes of Health, USA).

Live-Cell Imaging with Global Illumination:

The stage-top incubator (spec info) was preheated to 37 °C and equilibrated to 5% CO_2 using a dummy imaging dish for 60 minutes prior to imaging. The cell containing imaging dish was mounted under minimal ambient light using red head lamps and focused using minimal light intensity. Cells were imaged using a Leica DMI6000B inverted fluorescent microscope with a TexasRed filter set and a 40x oil immersion objective. Cells were first imaged for 3 h in the dark. Next, 395 nm light pulses were applied orthogonally using a single LED (see setup picture Figure S1) that was connected to the DISCO system (25 ms pulse per 0.5 s) and images acquired every 10 minutes and then every 30 minutes. After light treatment, cells were monitored for an additional 24 h.

[23] Schindelin, J.; Arganda-Carreras, I.; Frise, E.; Kaynig, V.; Longair, M.; Pietzsch, T.; Preibisch, S.; Rueden, C.; Saalfeld, S.; Schmid, B.; Tinevez, J.-Y.; White, D. J.; Hartenstein, V.; Eliceiri, K.; Tomancak, P.; Cardona, A. *Nat Methods* **2012**, *9* (7), 676–682.

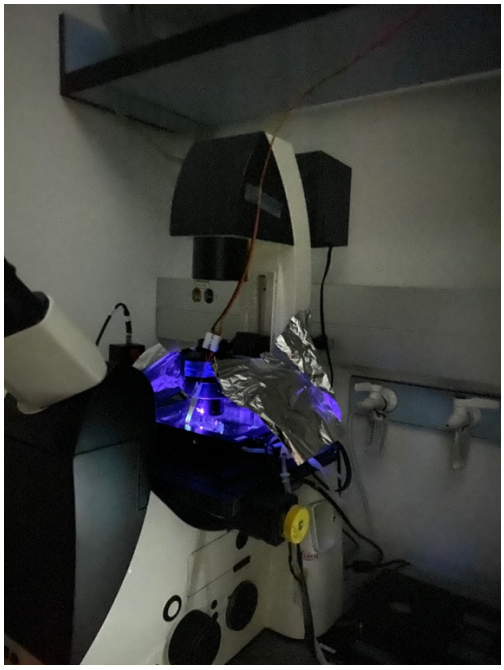

Figure S1: Setup for orthogonal light delivery.

Live-Cell Imaging with Local Illumination:

The environmental chamber of a Zeiss LSM880 Airyscan microscope system (ZEISS, Oberkochen, Germany) was preheated to 37 °C for at least 2 h prior to imaging. Cells were transported as quickly as possible in a tightly sealed styrofoam box with 2 x 500 ml water bottles that had been equilibrated to 37 °C and cells immediately transferred to the environmental chamber of the microscope. The imaging dish was mounted on the stage under minimal ambient light and using red head lamps and manually focused using a red filter foil in the light path to avoid blue light from reaching the sample during prolonged light exposure that was required to focus.

Images were acquired using a 63x objective (N/A 1.4). 440 nm light pulses and ROI were specified using the FRAP tool and different acquisition blocks were programmed in row using the experiment designer in ZEN (ZEISS, Oberkochen, Germany).

Biological Data for Part 1: 5 Kinesin Eg-5

Cell-Cycle Synchronization of HeLa cells:

A cell cycle analysis was performed to determine the timing of the cell cycle after release from double thymidine block[24]. HeLa cells were seeded in phenol red-free DMEM supplemented with 10% FBS, 1% penicillin-streptomycin-glutamine and a final concentration of 4 mM L-glutamine at a density of 100K cells/ 2 ml in 6 well plates. The next day, cells were subjected to a double-thymidine block as described below and wells were harvested at different time-points after release and analyzed by Flow Cytometry[25]. We determined that the optimal treatment window for Azo-EMD would lie between 6 and 12 h after release in early S-phase.

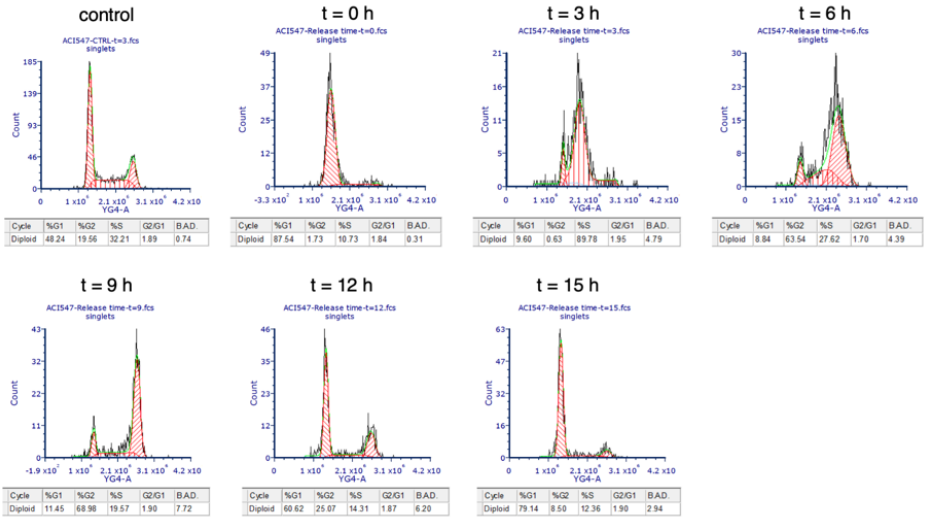

Figure S2: Cell Cycle Analysis of HeLa cells that were synchronized by double thymidine block at different time points after release.

Fluorescent Imaging of the Light-Dependent Monoastral Spindle Phenotype Formation:

In a 24 well plate, HeLa cells were seeded on poly-L-lysine coated coverslips at a density of 30 000 cells/ 450 µl phenol red free full growth medium. The next day, thymidine (100 mM in PBS) solution was added to a final concentration of 2 mM. After 18-20 h, the medium was aspirated and cells were washed three times with warm phenolred-free DMEM (Thermo Fisher cat# 31053036), supplemented with 10% FBS (Gibco, Thermo Fischer cat# 10437036), 1% penicillin-streptomycin-glutamine (Gibco, Thermo Fischer cat# 10378016) and a final concentration of 4 mM L-glutamine (Gibco, Thermo Fischer cat# 25030081). The cells were incubated in DMEM for 10 h and thymidine solution was again added to a final concentration

[24] Ma, H. T.;Poon, R. Y. C. *Synchronization of HeLa Cells* in Cell Cycle Synchronization, Springer Nature Experiments, New York, 2017, *Vol. 1524*, p. 189-201.
https://flowcytometry-embl.de/wp-content/uploads/2016/09/Synchronization-of-human-cells.pdf (Nov 10, 2020); https://celldivisionlab.com/2014/08/12/how-to-synchronise-mammalian-cells-in-culture/ (Jan 8, 2021).
[25] Flow Cytometry analysis was performed by A. C. Impastato.

of 2 mM. The cells were incubated for 14 h and released again by aspiration of the medium, washing with DMEM (3 x). The cells were kept in 450 ul DMEM (10% FBS, 1% pen-strep, 4 mM L-glutamine) at 37 °C. After 5.5 h, the test compound was added as a 10x concentration stock (50 µl, final 1% DMSO, DMEM) in the dark. Cells were incubated for 6.5 h: during this time, one plate was kept in the dark while the second was incubated under irradiation with pulsed 370 nm (75 ms/ 0.5 s). Next, direct addition of cell extraction buffer and fixative was performed without prior aspiration of the medium to ensure mitotic cells were not lost in the process.

Cells were fixed, stained and mounted according to the general procedure above. The biggest light dependent difference was observed at 1 µM Azo-EMD (figure S3).

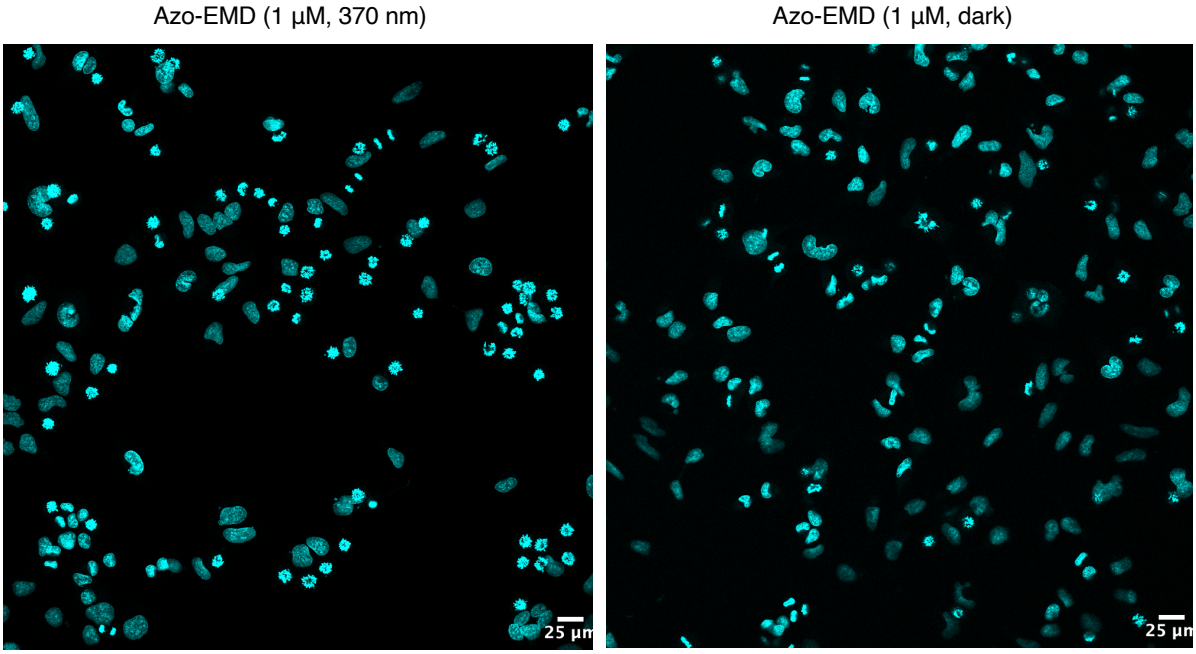

Figure S3: Images of fixed HeLa cells treated with Azo-EMD in the light or dark. cyan: nuclei stained with Hoechst 33342, confocal microscopy, 20x, tile scan; scale bar = 25 µm.

`

Chemical Procedures for Part 2 De novo Design of SARS-Cov-2 Main Protease Inhibitors

The project was highly collaborative, therefore certain intermediates were prepared by various authors at different stages of the project. Only the procedures towards structures, that were made by the author of this thesis are reported below. Numberings and labelling were kept the same as in the submitted manuscript and SI.

General Procedure B:

To a mixture of a pyridone derivative (1.00 equiv.), K_2CO_3 (3.00 equiv.) in acetone (0.10 M based on pyridone derivative) was added an alkyl halide (1.00 or 1.40 equiv., specified individually) at room temperature and the mixture was stirred at 50 °C for an individually specified time. Worked-up by one of two methods:

Method 1: The mixture as concentrated in vacuo, treated with water (70 mL per mmol pyridone) and extracted with CH_2Cl_2 (3 x 70 mL per mmol pyridone). The combined organic layers were dried over Na_2SO_4, filtered and concentrated in vacuo.

Method 2: The mixture was suspended by addition of hexanes (20 mL per mmol pyridone), filtered and washed with portionwise addition of hexanes (15 mL per mmol pyridone) and water (40 mL per mmol pyridone). The remaining solid was dried in vacuo.

In some cases, further purification either column chromatography or recrystallization were required to give clean *N*-alkylated compounds (individually specified).

General Procedure C:

Prepared according to a modified literature procedure.[26] To a solution of pyridone derivative (1.00 equiv.) in glacial acetic acid (4.0 mL per mmol pyridone) was added dropwise bromine (2.00 equiv.) at room temperature. The orange mixture was stirred at 60 °C for 4 hours. When cooled to room temperature the mixture was treated with aqueous saturated sodium thiosulfate (0.600 mL per mmol pyridone) and adjusted to pH 7 with aqueous saturated $NaHCO_3$ (6 mL per mmol pyridone). The suspension was filtered and washed extensively with water. The filter cake was dried in vacuo to give the desired brominated pyridone derivative.

[26] Bist, S.; Dangel, B.; Sherer, B. *WO2009/106885*, **2009**.

General Procedure D:

Prepared according to a modified literature procedure.[27] A mixture of bromopyridone (1.00 equiv.), arylboronic acid or arylboronic acid pinacol ester (2.50 equiv.), Na_2CO_3 (4.00 equiv.) and $Pd(PPh_3)_4$ (5.00-10.0 mol%) was evacuated for 5-10 minutes under high vacuum and backfilled with N_2. The mixture was treated with PhMe, EtOH and H_2O (8:3:1; 0.10 M) or for some reactions DMF (0.090 M) and the mixture was heated to 75 °C for an individually specified time in a pre-heated sand bath. The mixture was poured into water and rinsed with CH_2Cl_2 (both 30 mL per 0.10 mmol pyridone). The layers were separated, and the aqueous layer was extracted with fresh CH_2Cl_2 (2 x 30 mL per 0.10 mmol pyridone). The combined organic layers were dried over Na_2SO_4, filtered and concentrated in vacuo. The residue was purified by column chromatography over silica gel with an individually specified eluent to give the desired products. Some of the products were additionally purified by recrystallization

General Procedure E:

Prepared according to a modified literature procedure.[28] A deaerated mixture of bromo-pyridone (0.100 mmol), amine (0.150 mmol), Cs_2CO_3 (0.400 mmol), RuPhos (17.0 mol%), and $Pd_2(dba)_3$ (10 mol%) was treated with 1,4-dioxane (1.0 mL) and stirred for an individually specified time (18-20h) in a sand bath preheated to 110 °C. The mixture was filtrated through a plug of Celite, washed with CH_2Cl_2 and the filtrate was concentrated in vacuo. The residue was purified by column chromatography over silica gel with an individually specified eluent to give the desired products. Some of the products were additionally purified by recrystallization.

General Procedure H:

Prepared according to a modified literature procedure.[29] To a suspension of 4-nitrobenzene-1,2-diamine *or* 4-bromobenzene-1,2-diamine (1.00 equiv.) and $Co(OH)_2$ (10.0 mol%) in EtOH (3.0 mL/mmol diamine) vigorously stirred in a container open to air atmosphere was added an aryl aldehyde (1.10 *or* 1.20 equiv.) at r.t. over an individually specified time period. The mixture was filtered over a plug of Celite using solvent EtOH or CH_2Cl_2 and the filtrate was concentrated in vacuo and purified with individually specified technics to give 6-nitro-2-aryl-1*H*-benzo[*d*]imidazoles *or* 6-bromo-2-aryl-1*H*-benzo[*d*]imidazoles *or* 6-bromo-2-aryl-2,3-dihydro-1*H*-benzo[*d*]imidazoles *or* 2-(3,5-difluorophenyl)-6-nitro-1*H*-benzo[*d*]imidazoles.

---

[27] Wysocki, J.; Schlepphorst, C.; Glorius, F. *Synlett* **2015**, *26*, 1557–1562.
[28] Do, S.; Hu, H.; Kolesnikov, A.; Tsui, V.; Wang, X. *WO2014/1377*, **2014**.
[29] Chari, M. A.; Shobha, D.; Sasaki, T. *Tet. Lett.* **2011**, *52*, 5575–5580.

General Procedure I:

Prepared according to a modified literature procedure.[30] To a solution of the ester (1.00 equiv.) in THF and water at room temperature was added sodium hydroxide (4.0-10 equiv.). The reaction mixture was stirred at an individually specified temperature and for an individually specified time. The mixture was diluted with water, adjusted to pH 2-3 with aqueous 1 M HCl and extracted with ethyl acetate. The combined organic layers were dried over Na_2SO_4, filtered and concentrated in vacuo to give the corresponding carboxylic acid, which was used without further purification in the next step.

General Procedure J:

To a mixture of carboxylic acid (1.00 equiv), HATU (1.50 equiv), *N,N*-diisopropylethylamine (5.00 equiv) in dry DMF (10-14 mL per mmol carboxylic acid) at room temperature was added a secondary *or* primary amine (1.20 equiv). The mixture was stirred at room temperature for an individually specified time, poured into aqueous 10% LiCl (50 mL per mmol acid) and extracted with EtOAc (80 mL per mmol acid). The organic layer was washed with brine, dried over Na_2SO_4, filtered, and concentrated in vacuo. The residue was purified by column chromatography over silica gel with an individually specified eluent to give the desired amide.

[30] Tzvetkov, N. T.; Hinz, S.; Küppers, P.; Gastreich, M.; Müller, C. E. *J. Med. Chem.* **2014**, *57*, 6679–6703.

Methyl 1-(2-(cyclohexylamino)-2-oxoethyl)-6-oxo-1,6-dihydropyridine-3-carboxylate (4'):

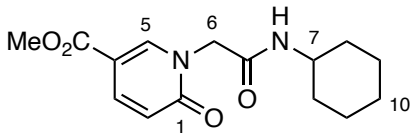

Prepared according to general procedure **B** and *Work-up Method 1* using methyl 6-hydroxynicotinate **(4)** (2.22 g, 14.5 mmol) and 2-chloro-*N*-cyclohexylacetamide (2.55 g, 14.5 mmol), acetone (145 mL), K_2CO_3 (6.00 g, 43.5 mmol). Stirred at 50 °C for 3 hours. Methyl 1-(2-(cyclohexylamino)-2-oxoethyl)-6-oxo-1,6-dihydropyridine-3- carboxylate was obtained as a white solid without further purification (3.90 g, 92%).

R_f 0.45 (EtOAc, 100%, UV/$KMnO_4$);

IR: $\tilde{\nu}$ = 3302m, 3036w, 2930m, 2853w, 1721m, 1663s, 1647s, 1609m, 1548m, 1449w, 1415w, 1346m, 1303s, 1261w, 1248m, 1202w, 1117m, 1105w, 982w, 993w, 930w, 892w, 840w, 799w, 774m;

^{1}H-NMR (400 MHz, $CDCl_3$): δ = 8.29 (1H, d, ^4J 2.4, C5*H*), 7.91 (1H, dd, ^3J 9.5, ^4J 2.5, C3*H*), 6.58 (1H, d, ^3J 9.5,C2*H*), 6.40 (1H, d, ^3J 7.9, N*H*), 4.53 (2H, s, C6H_2), 3.86 (3H, *s*, OCH_3), 3.66–3.77 (1H, m, C7*H*), 1.82–1.91 (2H, m, 2 x C8*H*), 1.64–1.72 (2H, m, 2 x C9*H*), 1.54–1.63 (1H, m, C10*H*), 1.25–1.40 (2H, m, 2 x C9*H*), 1.11–1.23 (3H, m, 2 x C8*H,* C10*H*);

^{13}C-NMR (101 MHz, $CDCl_3$): δ = 165.2 (*C*=O), 164.5 (*C*=O), 162.8 (*C1*), 143.5 (*C5*), 139.7 (*C3*), 119.6 (*C2*), 110.7 (C*4*), 54.1 (*C6*), 52.3 (O*C*H_3), 48.8 (*C7*), 32.8 (*C8*), 25.5 (*C10*), 24.7 (C*9*);

APCI-HRMS: m/z calcd. for $[C_{15}H_{21}N_2O_4]^+$ 293.1496 found 293.150 $[M+H]^+$.

Methyl 5-bromo-1-(2-(cyclohexylamino)-2-oxoethyl)-6-oxo-1,6-dihydropyridine-3-carboxylate:

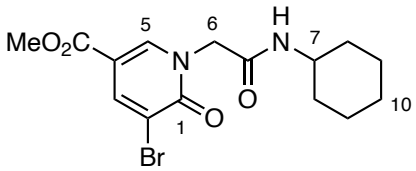

Prepared according to general procedure **C** using methyl 1-(2-(cyclohexylamino)-2-oxoethyl)-6-oxo-1,6-dihydropyridine-3-carboxylate **(4')** (1.57 g, 5.37 mmol), bromine (0.550 mL, 10.7 mmol), acetic acid (21.5 mL). Methyl 5-bromo-1-(2-(cyclohexylamino)-2-oxoethyl)-6-oxo-1,6-dihydropyridine-3-carboxylate was obtained as a white solid (1.79 g, 90%).

R_f 0.65 (EtOAc, 100%, UV/$KMnO_4$);

IR: $\tilde{\nu}$ = 3282w, 3077w, 2931w, 2855w, 2359w, 1715m, 1653s, 1560w, 1438w, 1331w, 1281m, 1227w, 1201w, 1145m, 1006w, 923w, 856w, 769w, 708w;

^{1}H-NMR (400 MHz, $CDCl_3$): δ = 8.31 (1H, d, ^4J 2.3, C3*H*), 8.28 (1H, d, ^4J 2.3, C5*H*), 6.23 (1H, d, ^3J 8.1, N*H*), 4.57 (2H, s, C6H_2), 3.87 (3H, s, OCH_3), 3.66–3.77 (1H, m, C7*H*), 1.84–1.92 (2H, m, 2 x C8H), 1.64–1.74 (2H, m, 2 x C9*H*), 1.56–1.63 (m, 1H, C10*H*), 1.24–1.39 (m, 2H, 2 x C9*H*), 1.12–1.23 (3H, m, 2 x C8*H,* C10*H*);

^{13}C NMR (101 MHz, $CDCl_3$): δ = 164.6 (*C*=O), 163.6 (*C*=O), 159.3 (C*1*), 142.6 (*C5*), 141.4 (*C3*), 115.3 (*C2*), 110.7 (*C4*), 54.8 (*C6*), 52.6 (O*C*H_3), 49.1 (*C7*), 32.9 (*C8*), 25.5 (*C10*), 24.8 (*C9*);

APCI-HRMS: m/z calcd. for $[C_{15}H_{20}BrN_2O_4]^+$ 371.0601 found 371.0603 $[M+H]^+$.

Methyl 1-(2-(cyclohexylamino)-2-oxoethyl)-5-(4-(dimethylamino)phenyl)-6-oxo-1,6-dihydropyridine-3-carboxylate (6a):

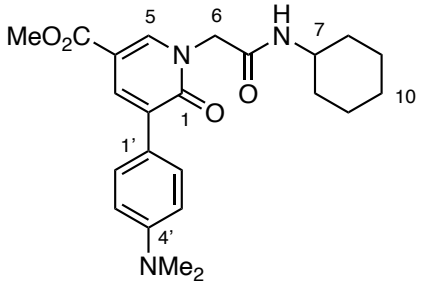

Prepared according to general procedure **D** using methyl 5-bromo-1-(2-(cyclohexylamino)-2-oxoethyl)-6-oxo-1,6-dihydropyridine-3-carboxylate (50.0 mg, 0.140 mmol), *N,N*-dimethyl-4-(4,4,5,5-tetramethyl-1,3,2-dioxaborolan-2-yl)aniline (83.2 mg, 0.340 mmol), Na_2CO_3, (57.1 mg, 0.540 mmol), $Pd(PPh_3)_4$ (15.6 mg, 0.0135 mmol) in PhMe:EtOH:H_2O (0.80:0.30:0.10 mL). Stirred at 75 °C for 1 hour. Column chromatography over silica gel with eluent 1:1 hexanes:(EtOAc:CH_2Cl_2, 6:4) to 100% (EtOAc:CH_2Cl_2, 6:4) gives product as a yellow solid (50.9 mg, 91%).

R_f 0.34 (hexanes:(EtOAc: CH_2Cl_2 6:4), 2:8; UV);

IR: $\tilde{\nu}$ = 3279w, 3077w, 2923w, 2853w, 1708m, 1652w, 1608s, 1553m, 1522m, 1432m, 1357m, 1333m, 1307m, 1268m, 1250m, 1225s, 1204m, 1152m, 1113m, 1103m, 1011m, 967w, 946m, 918m, 882w, 867w, 816m, 789m, 764m, 707m;

^{1}H-NMR (400 MHz, $CDCl_3$): δ = 8.21 (1H, d, ^4J 2.5, C5*H*), 8.01 (1H, d, ^4J 2.5, C3*H*), 7.60–7.64 (2H, m, 2 x C2'*H*), 6.74–6.79 (2H, m, 2 x C3'*H*), 6.52 (1H, d, *J* 8.2, CON*H*), 4.59 (2H, s, C6*H*$_2$), 3.87 (3H, s, CO_2CH_3), 3.64–3.77 (1H, m, C7*H*), 2.99 (6H, s, 2 x NC*H*$_3$), 1.79–1.91 (2H, m, 2 x C8*H*), 1.61– 1.73 (2H, m, 2 x C9*H*), 1.52–1.61 (1H, m, C10*H*), 1.23–1.40 (2H, m, 2 x C9*H*), 1.08–1.22 (3H, m, 2 x C8*H*, C10*H*);

^{13}C-NMR (101 MHz, $CDCl_3$): δ = 165.7 (*C*ONH), 165.0 (*C*OCH_3), 162.3 (*C1*), 150.6 (*C4'*), 140.6 (*C5*), 135.1 (*C3*), 131.0 (*C2*), 129.5 (*C2'*), 123.5 (*C1'*), 112.1 (C3'), 110.8 (*C4*), 54.9 (*C6*), 52.3 (CO_2CH_3), 48.8 (*C7*), 40.6 ($N(CH_3)_2$), 32.8 (*C8*), 25.6 (*C10*), 24.8 (*C9*);

APCI-HRMS: m/z calcd. for $[C_{23}H_{30}N_3O_4]^+$ 412.2231 found 412.2230 $[M+H]^+$.

Methyl 1-(2-(cyclohexylamino)-2-oxoethyl)-6-oxo-5-phenyl-1,6-dihydropyridine-3-carboxylate (6b):

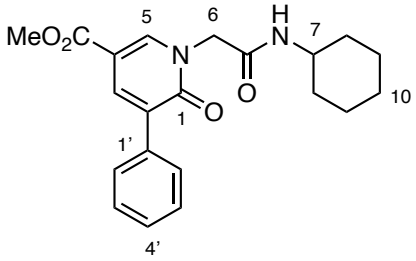

Prepared according to general procedure **D** using methyl 5-bromo-1-(2-(cyclohexylamino)-2-oxoethyl)-6-oxo-1,6-dihydropyridine-3-carboxylate (10.0 mg, 0.0269 mmol), phenylboronic acid (3.90 mg, 0.0323 mmol), $PdCl_2(PPh_3)_2$ (1.40 mg, 0.00188 mmol), Na_2CO_3 (10.7 mg, 0.10 mmol) in PhMe:EtOH:H_2O (0.36:0.14:0.050 mL). Stirred at 75 °C for 5 hours. Column chromatography over silica gel with eluent 100% hexanes to 1:1 hexanes:(EtOAc:CH_2Cl_2, 6:4) gives product as an off-white solid (7.90 mg, 80%).

R_f 0.40 (hexanes:(EtOAc: CH_2Cl_2 6:4), 2:8; UV);

LC-MS t_R=3.80 min. (5% to 100% MeCN in H_2O with 1% formic acid over 5 min.);

IR: $\tilde{\nu}$ = 3295w, 3085w, 2929w, 2856w, 1704m, 1655s, 1557m, 1496w, 1451w, 1434w, 1424m, 1379w, 1333m, 1322m, 1305m, 1255m, 1222s, 1179w, 1151w, 1119m, 1006w, 969w, 952w, 920w, 884w, 871w, 843w, 825w, 794m, 771w, 759m;

^{1}H-NMR (400 MHz, $CDCl_3$): δ = 8.30 (1H, d, ^4J 2.5, C5*H*), 8.07 (1H, d, ^4J 2.4, C3*H*), 7.65 (2H, d, J 7.4, 2 x C2'*H*), 7.33–7.45 (2H, m, 2 x C3'*H*), 6.50 (1H, d, J 8.1, C4'*H*), 4.61 (2H, s, C6H_2), 3.88 (3H, s, CO_2CH_3), 3.62–3.78 (1H, m, C7*H*), 1.77–1.93 (2H, m, 2 x C8*H*), 1.61– 1.74 (2H, m, 2 x C9*H*), 1.51–1.62 (1H, m, C10*H*), 1.24–1.37 (2H, m, 2 x C9*H*), 1.05–1.18 (3H, m, 2 x C8*H*, C10*H*).

^{13}C-NMR (101 MHz, $CDCl_3$): δ = 165.4 (*C*ONH), 164.7 (*C*O_2CH_3), 162.0 (*C1*), 142.4 (*C5*), 137.5 (*C3*), 135.8 (*C1'*), 130.8 (*C2*), 128.7 (C2'), 128.5 (**C4'*), 128.4 (**C3'*), 110.5 (*C4*), 54.5 (*C6*), 52.3 ($CO_2C$$H_3$), 48.9 (*C7*), 32.8 (*C8*), 25.5 (*C10*), 24.8 (*C*9); * indistinguishable signals.

APCI-HRMS: m/z calcd. for $[C_{21}H_{25}N_2O_4]^+$ 369.1809 found 369.1809 $[M+H]^+$.

Methyl 1-(2-(cyclohexylamino)-2-oxoethyl)-5-(4-fluorophenyl)-6-oxo-1,6-dihydropyridine-3-carboxylate (6c):

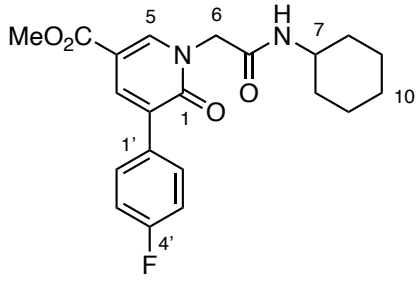

Prepared according to general procedure **D** using methyl 5-bromo-1-(2-(cyclohexylamino)-2-oxoethyl)-6-oxo-1,6-dihydropyridine-3-carboxylate (519 mg, 1.40 mmol), 4-fluorophenylboronic acid (490 mg, 3.50 mmol), Na_2CO_3, (594 mg, 5.60 mmol), $Pd(PPh_3)_4$ (80.9 mg, 0.0700 mmol), PhMe:H_2O:EtOH (8.7:1.2:3.4 mL). Stirred at 75 °C for 4 hours. Column chromatography over silica gel with eluent 9:1 hexanes:(EtOAc:CH_2Cl_2, 6:4) to 100% (EtOAc:CH_2Cl_2, 6:4) and additional recrystallization from toluene gives product as an off-white solid (412 mg, 1.07 mmol, 76%).

R_f = 0.39 (hexanes:(EtOAc:CH_2Cl_2 6:4), 2:8; UV);

IR: $\tilde{\nu}$ = 3276w, 3078w, 2934w, 2854w, 1717m, 1649s, 1559m, 1509m, 1433m, 1363w, 1329m, 1299m, 1271m, 1250m, 1232s, 1222s, 1162m, 1126w, 1102m, 1026w, 1008m, 970w, 953w, 925w, 883w, 871w, 848m, 809m, 786w, 763m;

^{1}H-NMR (400 MHz, $CDCl_3$): δ = 8.32 (1H, d, *J* 2.5, C5*H*), 8.06 (1H, d, *J* 2.4, C3*H*), 7.62–7.70 (2H, m, 2 x C2'*H*), 7.06–7.19 (2H, m, 2 x C3'*H*), 6.33 (1H, d, *J* 8.1, N*H*), 4.61 (2H, s, C6*H*), 3.91 (3H, s, CO_2CH_3), 3.67–3.82 (1H, m, C7*H*), 1.83–1.95 (2H, m, 2 x C8*H*), 1.66–1.77 (2H, m, 2 x C9*H*), 1.54–1.64 (2H, m, C10*H*), 1.30–1.43 (2H, m, 2 x C9*H*), 1.09–1.25 (3H, m, 2 x C8*H,* C10*H*);

^{13}C-NMR (101 MHz, $CDCl_3$): δ = 165.2 (*C*ONH), 164.6 (CO_2CH_3), 162.9 (d, $^1J_{CF}$ = 248, *C4'*), 161.9 (*C2*), 142.4 (*C5*), 137.2 (*C3*), 131.8 (d, $^4J_{CF}$ = 3.3, *C1'*), 130.5 (d, $^3J_{CF}$ = 8.1, *C2'*), 129.8 (*C1*), 115.5 (d. $^2J_{CF}$ = 22, *C3'*), 110.5 (*C4*), 54.5 (*C6*), 52.4 (CO_2CH_3), 49.0 (*C7*), 32.9 (*C8*), 25.5 (*C10*), 24.8 (*C9*).

^{19}F-NMR (377 MHz, $CDCl_3$): δ = –113.28.

APCI-HRMS: m/z calcd. for $[C_{21}H_{24}FN_2O_4]^+$ 387.1715 found: 387.1717 $[M+H]^+$.

Methyl 1-(2-(cyclohexylamino)-2-oxoethyl)-5-(3,5-difluorophenyl)-6-oxo-1,6-dihydropyridine-3-carboxylate (6d):

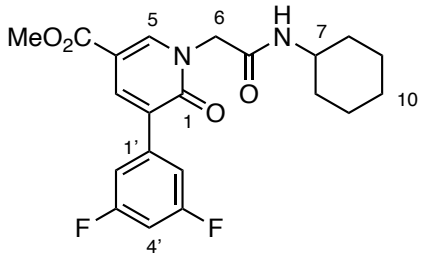

Prepared according to general procedure **E** using methyl 5-bromo-1-(2-(cyclohexylamino)-2-oxoethyl)-6-oxo-1,6-dihydropyridine-3-carboxylate (30.0 mg, 0.0808 mmol), 3,5-difluorophenylboronic acid (31.9 mg, 0.202 mmol), Cs_2CO_3, (34.3 mg, 0.323 mmol) $Pd(PPh_3)_4$ (9.30 mg, 0.00810 mmol), DMF (0.90 mL). Reaction was heated stepwise at 75 °C for 2 hours, 100 °C for 2 hours and at 115 °C for 18 hours. Column chromatography over silica gel with eluent 100% hexanes to 1:1 hexanes:(EtOAc:CH_2Cl_2, 6:4) to 100% (EtOAc:CH_2Cl_2, 6:4) and additional recrystallization from toluene gives product as an off-white solid (5.70 mg, 17%).

R_f 0.46 (hexanes:(EtOAc:CH_2Cl_2 6:4), 2:8; UV);

IR: $\tilde{\nu}$ = 3283w, 3081w, 2923w, 2850w, 1708m, 1652s, 1625m, 1590m, 1548m, 1477w, 1448m, 1438m, 1426w, 1409w, 1371w, 1338m, 1324m, 1306m, 1281m, 1252m, 1232s, 1207m, 1152w, 1120m, 1109m, 1093m, 1013m, 988m, 950m, 934w, 890m, 852m, 826m, 790m, 779w, 764m;

^{1}H-NMR (400 MHz, $CDCl_3$): δ = 8.33 (1H, d, *J* 2.4, C5*H*), 8.09 (1H, d, *J* 2.4, C3*H*), 7.22–7.28 (2H, m, C2'*H*), 6.81 (1H, tt, $^3J_{HF}$ 8.8, $^4J_{HH}$ 2.4, C4'*H*), 6.25 (1H, d, *J* 7.9, N*H*), 4.60 (2H, s, C6H_2), 3.89 (3H, s, CO_2CH_3), 3.65–3.79 (1H, m, C7*H*), 1.82–1.96 (2H, m, 2 x C8*H*), 1.64–1.74

(2H, m, 2 x C9*H*), 1.53–1.62 (1H, m, C10*H*), 1.25–1.42 (2H, m, 2 x C9*H*), 1.07–1.21 (3H, m, 2 x C8*H*, C10*H*);

^{13}C-NMR (101 MHz, $CDCl_3$): δ = 164.8 (*C*ONH), 164.3 (*C*O_2CH_3), 162.8 (dd, $^1J_{CF}$ = 248, $^3J_{CF}$ 13.2, C3'), 161.5 (*C1*), 143.1 (*C5*), 138.5 (t, $^3J_{CF}$ 10.3, *C1'*), , 137.9 (*C3*), 128.1 (t, $^4J_{CF}$ 2.7 Hz, *C2*), 111.2–111.7 (m, *C2'*), 110.2 (*C4*), 103.7 (t, $^2J_{CF}$ 25.3, *C4'*), 54.2 (*C6*), 52.3 (CO_2CH_3), 48.9 (*C7*), 32.7 (*C8*), 25.4 (*C10*), 24.7 (*C9*);

^{19}F-NMR (377 MHz, $CDCl_3$): δ = –109.9;

ESI-HRMS: m/z calcd. for $[C_{42}H_{45}F_4N_4O_8]^+$ 809.3168 found 809.3200 $[2M+H]^+$.

Methyl 1-(2-(cyclohexylamino)-2-oxoethyl)-6'-fluoro-2-oxo-1,2-dihydro-[3,3'-bipyridine]-5-carboxylate (6e):

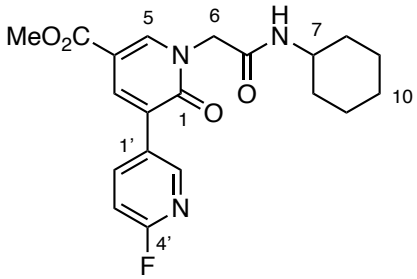

Prepared according to general procedure **D** using methyl 5-bromo-1-(2-(cyclohexylamino)-2-oxoethyl)-6-oxo-1,6-dihydropyridine-3-carboxylate (30.0 mg, 0.0808 mmol), (6-fluoropyridin-3-yl)boronic acid (28.5 mg, 0.200 mmol), Na_2CO_3, (34.3 mg, 0.320 mmol), $Pd(PPh_3)_4$ (4.70 mg, 0.00400 mmol), PhMe:H_2O:EtOH (0.50:0.70:0.20 mL). Stirred at 75 °C for 30 hours. Column chromatography over silica gel with eluent 100% hexanes to 2:8 hexanes:(EtOAc:CH_2Cl_2, 6:4) and additional recrystallization from toluene gives product as an off-white solid (20.0 mg, 64%).

R_f 0.18 (hexanes:(EtOAc:CH_2Cl_2 6:4), 2:8; UV);

IR: $\tilde{\nu}$ = 3271w, 3088w, 2939w, 2855w, 1717m, 1650s, 1616m, 1590m, 1564m, 1484m, 1438m, 1428m, 1376w, 1363w, 1337w, 1315s, 1298m, 1263m, 1247s, 1224s, 1153w, 1122m, 1104m, 1021m, 1009m, 970w, 953w, 929m, 877w, 843m, 822m, 787m, 763s, 746m, 730m, 718m;

^{1}H-NMR (400 MHz, $CDCl_3$): δ = 8.48 (1H, m, C5'*H*), 8.33 (1H, d, ^{4}J 2.5, C5*H*), 8.12–8.20 (1H, m, C2'*H*), 8.09 (1H, d, *J* 2.4, C3*H*), 6.99 (1H, dd, *J* 8.5, 3.0, C3'*H*), 6.22 (d, *J* 8.1, N*H*), 4.60 (2H, s, C6H_2), 3.89 (3H, s, CO_2CH_3), 3.67–3.80 (1H, m, C7*H*), 1.83–1.96 (2H, m, 2 x C8*H*), 1.63–1.74 (2H, m, 2 x C9*H*), 1.54–1.63 (1H, m, C10*H*), 1.27–1.41 (2H, m, 2 x C9*H*), 1.10–1.23 (3H, m, 2 x C8*H*, C10*H*);

^{13}C-NMR (101 MHz, $CDCl_3$): δ = 164.9 (*C*ONH), 164.4 (CO_2CH_3), 163.4 (d, $^{1}J_{CF}$ 241, *C4'*), 161.5 (*C1*), 147.4 (d, $^{3}J_{CF}$ 15.1, *C5'*), 143.3 (*C5*), 141.5 (d, $^{3}J_{CF}$ 8.0, *C2'*), 137.6 (C3), 129.7 (d, $^{4}J_{CF}$ 4.7, *C1'*), 129.6, 126.4, 110.5 (*C4*), 109.1 ($^{2}J_{CF}$ 37.4, *C3'*), 54.3 (*C6*), 52.5 (CO_2CH_3), 49.1 (*C7*), 32.9 (*C8*), 25.5 (*C10*), 24.8 (*C9*);

^{19}F-NMR (377 MHz, $CDCl_3$): δ = –68.3;

APCI-HRMS: m/z calcd. for $C_{20}H_{23}FN_3O_4^+$ 388.1667 found 388.1673 $[M+H]^+$.

Methyl 1-(2-(cyclohexylamino)-2-oxoethyl)-6-oxo-5-(4-(trifluoromethyl)phenyl)-1,6-dihydropyridine-3-carboxylate (6f):

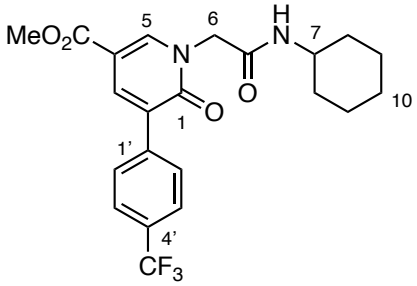

Prepared according to general procedure **D** using methyl 5-bromo-1-(2-(cyclohexylamino)-2-oxoethyl)-6-oxo-1,6-dihydropyridine-3-carboxylate (30.0 mg, 0.0808 mmol), 4-trifluoromethylboronic acid (38.4 mg, 0.200 mmol), Cs_2CO_3, (105 mg, 0.320 mmol),

$Pd(PPh_3)_4$ (9.30 mg, 0.00810 mmol), DMF (0.80 mL). Stirred at 75 °C for 24 hours. Column chromatography over silica gel with eluent 100% hexanes to 2:8 hexanes:(EtOAc:CH_2Cl_2, 6:4) and additional recrystallization from toluene gives product as an off-white solid (6.10 mg, 17%).

R_f 0.44 (hexanes:(EtOAc: CH_2Cl_2 6:4), 2:8; UV);

IR: $\tilde{\nu}$ = 3293w, 3081w, 2930w, 2855w, 1709s, 1651s, 1626m, 1553s, 1433m, 1327s, 1308s, 1254s, 1230s, 1163s, 1110s, 1068s, 1013m, 968w, 954m, 940m, 923w, 892w, 870m, 846s, 820m, 789m, 766m, 730m;

^{1}H-NMR (400 MHz, $CDCl_3$): δ = 8.34 (1H, d, *J* 2.4, C5*H*), 8.11 (1H, d, *J* 2.4, C3*H*), 7.79 (2H, d, *J* 8.2, C3'*H*), 7.68 (2H, d, *J* 8.2, C2'*H*), 6.25 (1H, d, *J* 8.0, N*H*), 4.60 (2H, s, C6H_2), 3.89 (3H, s, CO_2CH_3), 3.67–3.79 (1H, m, C7*H*), 1.88 (2H, dt, *J* 13, 4.0, 2 x C8*H*), 1.63–1.77 (2H, m, 2 x C9*H*), 1.54–1.63 (1H, m, C10*H*), 1.26–1.42 (2H, m, 2 x C9*H*), 1.12–1.21 (3H, m, 2 x C8*H*, C10*H*);

^{13}C-NMR (101 MHz, $CDCl_3$): δ = 164.9 (*C*ONH), 164.3 (CO_2CH_3), 161.5 (*C1*), 143.0 (*C5*), 139.2 (*C1'*), 138.0 (*C3*), 130.2 ($^2J_{CF}$ 32.4, *C4'*), 129.2 (*C2*), 128.9 (2 x *C2'*), 125.3 (q, $^3J_{CF}$ 3.8, *C3'*), 124.2 ($^1J_{CF}$ 272, CF_3), 110.3 (*C4*), 54.3 (*C6*), 52.3 (CO_2CH_3), 48.9 (*C7*), 32.8 (*C8*), 25.4 (*C10*), 24.7 (*C9*);

^{19}F-NMR (377 MHz, $CDCl_3$): δ = –62.7;

ESI-HRMS: m/z calcd. $[C_{44}H_{46}F_6KN_4O_8]^+$ 911.2851 found 911.2866 $[2M+K]^+$.

Methyl 5-(4-acetamidophenyl)-1-(2-(cyclohexylamino)-2-oxoethyl)-6-oxo-1,6-dihydropyridine-3-carboxylate (6g):

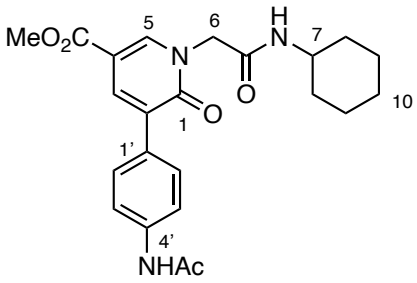

Prepared according to general procedure **D** using methyl 5-bromo-1-(2-(cyclohexylamino)-2-oxoethyl)-6-oxo-1,6-dihydropyridine-3-carboxylate (30.0 mg, 0.0808 mmol), (4-acetamidophenyl)pinacol borane (52.8 mg, 0.200 mmol), Na_2CO_3, (34.3 mg, 0.320 mmol), $Pd(PPh_3)_4$ (9.30 mg, 0.00810 mmol), PhMe:H_2O:EtOH (0.50:0.070:0.20 mL). Stirred at 75 °C for 4.5 hours. Column chromatography over silica gel with eluent 1:1 hexanes:(EtOAc:CH_2Cl_2, 6:4) to 100% (EtOAc:CH_2Cl_2, 6:4) gives product as an off-white solid (24.4 mg, 71%).

R_f 0.21 (CH_2Cl_2:MeOH, 95:5; UV);

IR: $\tilde{\nu}$ = 3289w, 3081w, 2923w, 2851w, 2414w, 1711m, 1645s, 1606m, 1590m, 1553m, 1518m, 1436m, 1397m, 1371m, 1331m, 1307m, 1251m, 1227s, 1189m, 1116m, 1101m, 1009m, 965m, 930w, 874w, 840m, 818m, 788m, 765m, 724m;

^{1}H-NMR (400 MHz, CD_3OD): δ = 8.42 (1H, d, ^4J 2.4, C5*H*), 8.07 (1H, d, ^4J 2.5, C3*H*), 7.63 (4H, s, 2 x C2'*H*, 2 x C3'*H*), 4.76 (2H, s, C6H_2), 3.90 (3H, s, CO_2CH_3), 3.64–3.74 (1H, m, C7*H*), 2.15 (3H, s, NHCH_3), 1.87–1.96 (2H, m, 2 x C8*H*), 1.74–1.82 (2H, m, 2 x C9*H*), 1.61–1.69 (1H, m, C10*H*), 1.18–1.45 (5H, m, 2 x C8*H*, 2 x C9*H*, C10*H*);

^{13}C-NMR (101 MHz, CD_3OD): δ = 171.7 (NH*C*OCH_3), 167.9 (NH*C*O), 166.3 (*C*O_2CH_3), 163.4 (*C1*), 144.8 (*C5*), 140.0 (*C4'*), 137.9 (*C3*), 132.8 (*C1'*), 131.0 (*C2*), 130.1 (C2'), 120.6 (C3'), 111.2 (*C4*), 53.9 (*C6*), 52.6 (CO_2*C*H_3), 50.2 (*C7*), 33.7 (*C8*), 26.6 (*C10*), 26.1 (*C9*), 23.9 (NH*C*H_3).

APCI-HRMS: m/z calcd. for $[C_{23}H_{28}N_3O_5]^+$ 426.2023 found 426.2025 $[M+H]^+$;

UV/Vis & Fluorescence Spectroscopy: (in aqueous PBS, 1% DMSO): λ_{abs} 318 nm, λ_{abs} $1.1 \cdot 10^4$ M^{-1} cm; λ_{em}(exc 320) 420 nm.

Methyl 1-(2-(cyclohexylamino)-2-oxoethyl)-2-oxo-1,2-dihydro-[3,4'-bipyridine]-5-carboxylate (6h):

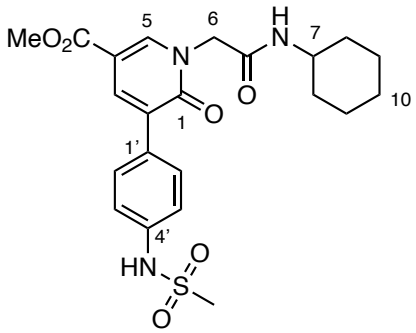

Prepared according to general procedure **D** using methyl 5-bromo-1-(2-(cyclohexylamino)-2-oxoethyl)-6-oxo-1,6-dihydropyridine-3-carboxylate (30.0 mg, 0.0808 mmol), (4-(methylsulfonamido)phenyl)boronic acid (43.4 mg, 0.202 mmol), Na_2CO_3, (34.3 mg, 0.320 mmol), $Pd(PPh_3)_4$ (9.30 mg, 0.00810 mmol), PhMe:H_2O:EtOH (0.50:0.070:0.20 mL). Stirred at 75 °C for 5 hours. Column chromatography over silica gel with eluent 100% (EtOAc:CH_2Cl_2, 6:4) to 97:3 (EtOAc:CH_2Cl_2, 6:4):MeOH and additional recrystallization from toluene gives product as a white solid (9.90 mg, 27%).

R_f 0.50 ((CH_2Cl_2:EtOAc 6:4):MeOH, 95/5; UV);

IR: $\tilde{\nu}$ = 3222w, 3076w, 2928w, 2851w, 2426w, 1713m, 1652s, 1607m, 1556w, 1512w, 1448m, 1432m, 1407w, 1332m, 1307m, 1251m, 1227s, 1196w. 1147s, 1117m, 1071w, 1014w, 990w, 980m, 968w, 931w, 842m, 806w, 789w, 764m, 734w, 725w;

^{1}H-NMR (400 MHz, $(CD_3)_2SO$): δ = 9.85 (1H, s, N*H*SO_2CH_3), 8.48 (1H, d, ^4J 2.5, C5*H*), 7.91 (1H, d, ^4J 2.5, C3*H*), 7.65 (2H, d, *J* 8.56, 2 x C2'*H*), 7.23 (2H, d, *J* 8.56, 2 x C3'*H*), 4.71 (2H, s, 2 x C6*H*), 3.82 (3H, s, COC*H*$_3$), 3.53 (1H, td, *J* 10.3, 5.0, C7*H*), 3.01 (3H, s, SO_2C*H*$_3$), 1.63–1.79 (4H, m, 2 x C8*H*, 2 x C9*H*), 1.54 (1H, d, *J* 12.4, C10*H*), 1.09–1.37 (5H, m, 2 x C8*H*, 2 x C9*H*, C10*H*).

^{13}C-NMR (101 MHz, $(CD_3)_2SO$): δ = 165.1 (*C*ONH), 164.5 (*C*O_2CH_3), 160.5 (*C1*), 144.5 (*C5*), 138.1 (*C4'*), 135.4 (*C3*), 131.1 (*C1'*), 129.3 (*C2'*), 127.9 (*C2*), 119.0 (*C3'*), 107.7 (*C4*), 51.9 (*C6,* CO_2CH_3), 47.7 (*C7*), 39.3 (SO_2CH_3) 32.4 (*C8*), 25.2 (*C10*), 24.4 (*C9*);

APCI-HRMS: m/z calcd. for $[C_{22}H_{28}N_3O_6S]^+$ 462.1693 found 462.1698 $[M+H]^+$.

Methyl 1-(2-(cyclohexylamino)-2-oxoethyl)-2-oxo-1,2-dihydro-[3,4'-bipyridine]-5-carboxylate (6i):

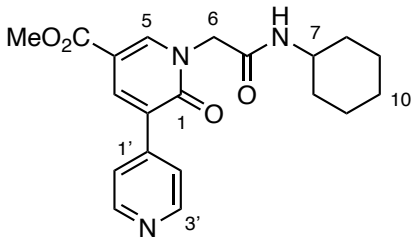

Prepared according to general procedure **D** using methyl 5-bromo-1-(2-(cyclohexylamino)-2-oxoethyl)-6-oxo-1,6-dihydropyridine-3-carboxylate (120 mg, 0.323 mmol), pyridine-4-boronic acid hydrate (114 mg, 0.808 mmol), Na_2CO_3, (137 mg, 1.29 mmol), $Pd(PPh_3)_4$ (18.7 mg, 0.0162 mmol), PhMe:H_2O:EtOH (2.0:0.30:0.80 mL). Stirred at 75 °C for 40 hours. Column chromatography over silica gel with eluent 1:1 hexanes:(EtOAc:CH_2Cl_2, 6:4) to 100% (EtOAc:CH_2Cl_2, 6:4) and additional recrystallization from toluene gives product as an off-white solid (45.9 mg, 38%).

R_f 0.27 ((CH_2Cl_2:EtOAc 6:4):MeOH, 95:5; UV);

IR: $\tilde{\nu}$ = 3281w, 2933w, 2855w, 1716s, 1652s, 1596w, 1557m, 1440m, 1397w, 1332m, 1305w, 1255m, 1224w, 1193w, 1119w, 1104w, 1004w, 997w, 937w, 891w, 833w, 816w, 787w, 768w, 729w;

^{1}H-NMR (400 MHz, $CDCl_3$): δ = 8.63–8.70 (2H, m, 2 x C3'*H*), 8.36 (1H, d, ^4J 2.4, C5*H*), 8.18 (1H, d, ^4J 2.4, C3*H*), 7.61–7.65 (2H, m, 2 x C2'*H*), 6.23 (1H, d, *J* 8.1, N*H*), 4.60 (2H, s, C6H_2), 3.90 (3H, s, CO_2CH_3), 3.68–3.81 (1H, m, C7*H*), 1.84–1.94 (2H, m, 2 x C8*H*), 1.64–1.74 (2H,

m, 2 x C9*H*), 1.55–1.64 (1H, m, C10*H*), 1.28–1.41 (2H, m, 2 x C9*H*), 1.10–1.23 (3H, m, 2 x C8*H*, C10*H*);

^{13}C-NMR (101 MHz, $CDCl_3$): δ = 164.9 (*C*ONH), 164.4 (*C*O_2CH_3), 161.2 (C1), 150.1 (2 x *C3'*), 143.8 (*C5*), 143.3 (*C1'*), 138.5 (*C3*), 127.7 (*C2*), 123.0 (*C2'*), 110.4 (C4), 54.3 (*C6*), 52.5 (CO_2*C*H_3), 49.1 (*C7*), 32.9 (*C8*), 25.5 (C10), 24.8 (*C9*);

APCI-HRMS: m/z calcd. for $[C_{20}H_{24}N_3O_4]^+$ 370.1761 found 370.1762 $[M+H]^+$;

UV/Vis & Fluorescence Spectroscopy: (in aqueous PBS, 1% DMSO): λ_{abs} 318 nm, λ_{abs} 0.86 $\cdot 10^4$ M^{-1} cm; λ_{em}(exc 320) 401 nm.

Ethyl 1-(2-(cyclohexylamino)-2-oxoethyl)-2-oxo-1,2-dihydro-[3,4'-bipyridine]-5-carboxylate (6j):

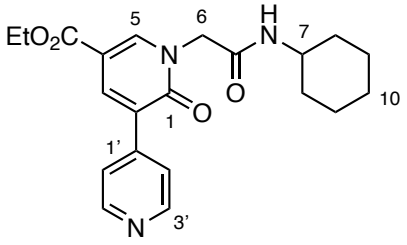

To a solution of methyl 1-(2-(cyclohexylamino)-2-oxoethyl)-2-oxo-1,2-dihydro-[3,4'-bipyridine]-5-carboxylate (13.5 mg, 0.0380 mmol), in THF:H_2O (1:1, 1.5 mL) was added NaOH (15.2 mg, 0.380 mmol) at room temperature. The mixture was stirred at the same temperature for 1.5 hours. The mixture was filtered through a plug of Celite and the filtrate was concentrated in vacuo. The residue was dissolved in EtOH (0.38 mL) and treated with concentrated H_2SO_4 (20.0 μL, 0.380 mmol) at room temperature. The mixture was stirred at reflux for 20 hours, cooled to room temperature and adjusted to pH 10 using aqueous saturated $NaHCO_3$ followed by extraction with EtOAc. The combined organic layers were dried over Na_2SO_4, filtered and concentrated in vacuo to give product as an off-white solid (7.00 mg, 48%).

R_f 0.19 (EtOAc, 100%, UV/$KMnO_4$):

IR: $\tilde{\nu}$ = 3398w, 2930m, 2854w, 2359w, 1715m, 1658s, 1596w, 1554m, 1432w, 1366w, 1325m, 1302m, 1253m, 1220m, 1107m, 1026w, 951w, 889w, 786w, 764w;

^{1}H-NMR (400 MHz, $CDCl_3$): δ = 8.68 (2H, br s, C3'*H*), 8.36 (1H, d, ^4J 2.4, C5*H*), 8.19 (1H, d, ^4J 2.4, C3*H*), 7.66 (2H, d, ^3J 5.1, C2'*H*), 6.33 (1H, d, ^3J 8.0, N*H*), 4.62 (2H, s, C6H_2), 4.36 (2H, q, ^3J 7.1, OCH_2Me), 3.69–3.78 (1H, m, C7*H*), 1.85–1.93 (2H, m, 2 x C8*H*), 1.64–1.73 (2H, m, 2 x C9*H*), 1.55–1.63 (1H, m, C10*H*), 1.38 (3H, t, ^3J 7.2, OCH_2CH_3), 1.27–1.33 (2H, m, 2 x C9*H*), 1.11–1.22 (3H, m, 2 x C8*H,* C10*H*);

^{13}C-NMR (101 MHz, $CDCl_3$): δ = 164.9 (*C*ONR), 163.9 (*C*O_2Et), 161.2 (*C1*), 149.8 (*C3'*), 143.80 (*C5)*, 143.6 (*C1'*), 138.7(*C3)*, 127.5 (*C2*), 123.1 (*C2'*), 110.7 (*C4*), 61.6 (O*Et*), 54.3 (*C6*), 49.1 (*C7*), 32.9 (*C8*), 25.5 (*C10*), 24.8 (*C9*), 14.5(O*Et*);

APCI-HRMS: m/z calcd. for $[C_{21}H_{26}N_3O_4]^+$ 384.1918 found 384.1920 $[M+H]^+$.

Methyl 1-(2-(cyclohexylamino)-2-oxoethyl)-5-(4-methoxyphenyl)-6-oxo-1,6-dihydropyridine-3-carboxylate (6k):

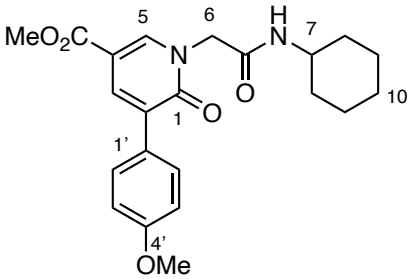

Prepared according to general procedure **D** using methyl 5-bromo-1-(2-(cyclohexylamino)-2-oxoethyl)-6-oxo-1,6-dihydropyridine-3-carboxylate (30.0 mg, 0.0808 mmol), 4-methoxyphenylboronic acid (30.7 mg, 0.200 mmol), Na_2CO_3, (34.3 mg, 0.320 mmol), $Pd(PPh_3)_4$ (9.30 mg, 0.00810 mmol), PhMe:H_2O:EtOH (0.50:0.70:0.20 mL). Stirred at 75 °C for 2 hours. Column chromatography over silica gel with eluent 100% hexanes to 3:7

hexanes:(EtOAc:CH_2Cl_2, 6:4) and additional recrystallization from toluene gives product as a colorless solid (27.3 mg, 85%).

R_f 0.36 (hexanes:(EtOAc:CH_2Cl_2 6:4), 2:8; UV);

IR: $\tilde{\nu}$ = 3281w, 3080w, 2924w, 2853w, 1709m, 1652s, 1607m, 1556m, 1513m, 1431m, 1376w, 1334m, 1318m, 1305m, 1249s, 1224s, 1180m, 1153w, 1114m, 1026m, 1009m, 968w, 955w, 923w, 891w, 870w, 834m, 819m, 795w, 786w, 765m;

^{1}H-NMR (400 MHz, $CDCl_3$): δ = 8.26 (1H, d, *J* 2.4, C5*H*), 8.02 (1H, d, *J* 2.5, C3*H*), 7.63 (2H, d, *J* 8.8, 2 x C3'*H*), 6.95 (2H, d, *J* 8.8, 2 x C2'*H*), 6.43 (1H, d, *J* 8.1, N*H*), 4.59 (2H, s, C6H_2), 3.88 (3H, s, CO_2CH_3), 3.84 (3H, s, OCH_3), 3.65–3.77 (1H, m, C7*H*), 1.86 (2H, dt, *J* 12, 4.0, 2 x C8*H*), 1.62–1.72 (2H, m, 2 x C9*H*), 1.53–1.58 (1H, m, C10*H*), 1.20–1.41 (2H, m, 2 x C9*H*), 0.95–1.22 (3H, m, 2 x C9*H*, C10*H*);

^{13}C-NMR (101 MHz, $CDCl_3$): δ = 165.5 (*C*ONH), 164.8 (*C*O_2CH_3), 162.1 (*C1*), 159.9 (*C4'*), 141.6 (C5), 136.4 (C3), 130.5 (*C1'*), 129.9 (C3'), 128.2 (*C2*), 113.9 (C2'), 110.6 (*C4*), 55.5 (OCH_3), 54.7 (*C6*), 52.3 (CO_2CH_3), 48.9 (*C7*), 32.9 (*C*8), 25.5 (*C*10), 24.8 (*C*9);

ESI-HRMS: m/z calcd. for $[C_{22}H_{27}N_2O_5]^+$ 399.1914 found 399.1933 $[M+H]^+$.

Methyl 1-(2-(cyclohexylamino)-2-oxoethyl)-5-(2-methoxypyrimidin-5-yl)-6-oxo-1,6-dihydropyridine-3-carboxylate (6l):

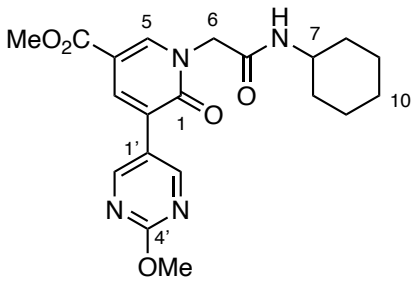

Prepared according to general procedure **D** using methyl 5-bromo-1-(2-(cyclohexylamino)-2-oxoethyl)-6-oxo-1,6-dihydropyridine-3-carboxylate (30.0 mg, 0.0808 mmol), 2-

methoxypyrimidine-5-boronic acid (31.1 mg, 0.200 mmol), Na_2CO_3, (34.3 mg, 0.320 mmol), $Pd(PPh_3)_4$ (9.30 mg, 0.00810 mmol), PhMe:H_2O:EtOH (0.50:0.70:0.20 mL). Stirred at 75 °C for 4 hours. Column chromatography over silica gel with eluent 100% CH_2Cl_2 to CH_2Cl_2:MeOH 9:1 and additional recrystallization from toluene gives product as an off-white solid (19.8 mg, 61%).

R_f 0.37 (CH_2Cl_2:MeOH, 95:5; UV);

IR: $\tilde{\nu}$ = 3230w, 3086w, 2995w, 2934w, 2853w, 1724m, 1672m, 1647s, 1617m, 1590m, 1574m, 1551m, 1478s, 1453m, 1433m, 1417m, 1408m, 1365w, 1328s, 1305s, 1293s, 1262m, 1220s, 1151w, 1123m, 1046m, 1028m, 1014m, 969w, 954w, 933m, 890m, 882m, 846w, 832w, 817w, 801m, 788s, 762s, 721m;

^{1}H-NMR (400 MHz, $CDCl_3$): δ = 8.86 (1H, s, 2 x C2'*H*), 8.32 (1H, d, *J* 2.4, C5*H*), 8.08 (1H, d, *J* 2.4, C3*H*), 6.22 (1H, br, N*H*), 4.60 (1H, s, C6*H_2*), 4.06 (3H, s, C4'OC*H_3*), 3.90 (3H, s, CO_2C*H_3*), 3.67–3.80 (1H, m, C7*H*), 1.89 (2H, dt, *J* 12, 3.9, 2 x C8*H*), 1.64–1.72 (2H, m, 2 x C9*H*), 1.54–1.64 (1H, m, C10*H*), 1.26–1.42 (2H, m, 2 x C9*H*), 1.09–1.23 (3H, m, 2 x C8*H*, C10*H*);

^{13}C-NMR (101 MHz, $CDCl_3$): δ = 165.3 (*C4'*), 164.9 (*C*ONH), 164.4 (*C*O_2CH_3), 161.5 (*C1*), 158.8 (*C2'*), 143.2 (*C5*), 136.7 (*C3*), 124.7 (*C2*), 123.4 (*C1'*), 110.5 (*C4*), 55.3 (C4'O*C*H_3), 54.4 (*C6*), 52.5 (CO_2C*H_3*), 49.1 (*C7*), 32.9 (*C8*), 25.5 (*C10*), 24.8 (*C9*);

APCI-HRMS: m/z calcd. for $[C_{20}H_{25}N_4O_5]^+$ 401.1819 found 401.1823 $[M+H]^+$.

Methyl 1-(2-(cyclohexylamino)-2-oxoethyl)-5-(4-morpholinophenyl)-6-oxo-1,6-dihydropyridine-3-carboxylate (6o):

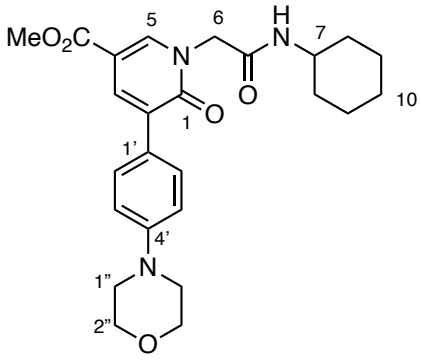

Prepared according to general procedure **D** using methyl 5-bromo-1-(2-(cyclohexylamino)-2-oxoethyl)-6-oxo-1,6-dihydropyridine-3-carboxylate (30.0 mg, 0.0808 mmol), 4-morpholinophenylboronic acid (41.8 mg, 0.200 mmol), Na_2CO_3, (34.3 mg, 0.320 mmol), $Pd(PPh_3)_4$ (9.30 mg, 0.00810 mmol), PhMe:H_2O:EtOH (0.50:0.70:0.20 mL). Stirred at 75 °C for 2 hours. Column chromatography over silica gel with eluent 1:1 hexanes:(EtOAc:CH_2Cl_2, 6:4) to 100% EtOAc:CH_2Cl_2, 6:4 and additional recrystallization from EtOAc gives product as an off-white solid (30.9 mg, 84%).

R_f 0.11 (Hexanes:(EtOAc:CH_2Cl_2, 6:4), 2:8; UV);

IR: $\tilde{\nu}$ = 3285w, 3079w, 2928w, 2852w, 1709m, 1655s, 1608m, 1556m, 1516m, 1434m, 1375w, 1332m, 1306m, 1254m, 1225s, 1119m, 1070w, 1052w, 1030w, 1007w, 955w, 928m, 891w, 869w, 816m, 788w, 764m, 713w;

^{1}H-NMR (400 MHz, $CDCl_3$): δ = 8.24 (1H, d, ^3J 2.5, C5*H*), 8.03 (1H, d, ^3J 2.4, C3*H*), 7.64 (2H, d, ^2J 8.8, 2 x C2'*H*), 6.95 (2H, d, ^2J 8.8, 2 x C3'*H*), 6.43 (1H, d, ^2J 8.1, N*H*), 4.59 (2H, s, C6H_2), 3.85–3.92 (7H, m, CO_2CH_3, 2 x C2"H_2), 3.65–3.80 (1H, m, C7*H*), 3.15–3.27 (4H, m, 2 x C1"H_2), 1.86 (2H, dt, *J* 12, 4.0, 2 x C8*H*), 1.60–1.74 (2H, m, 2 x C9*H*), 1.56–1.62 (1H, m, C10*H*), 1.27–1.41 (2H, m, 2 x C9*H*), 1.09–1.22 (3H, m, 2 x C8*H*, C10*H*);

^{13}C-NMR (101 MHz, $CDCl_3$): δ = 165.5 (*C*ONH), 164.9 (CO_2CH_3), 162.2 (*C1*), 151.3(*C4'*), 141.3 (*C5*), 135.9 (*C3*), 130.5 (C2), 129.6 (*C2'*), 126.9 (C1'), 115.1 (*C3'*), 110.7 (*C4*), 67.0 (*C2"*), 54.8 (*C6*), 52.3 (CO_2CH_3), 49.0 (*C1"*), 48.9 (*C7*), 32.9 (*C8*), 25.6 (*C10*), 24.8 (*C9*);

APCI-HRMS: m/z calcd. for $[C_{25}H_{32}N_3O_5]^+$ 454.2336 found 454.2346 $[M+H]^+$.

2-(3,5-Difluorophenyl)-6-nitro-1H-benzo[d]imidazole:

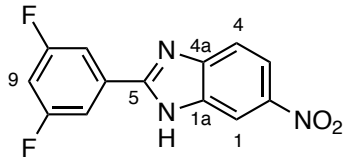

Prepared according to general procedure **H** using 4-nitrobenzene-1,2-diamine (500 mg, 3.27 mmol), $Co(OH)_2$ (30.3 mg, 0.330 mmol) in EtOH (10 mL) and 3.5-difluorobenzaldehyde (557 mg, 3.92 mmol, 1.20 equiv.) was added in one portion. The mixture was stirred vigorously at room temperature for 5 hours. Column chromatography over silica gel with eluent hexanes:EtOAc 9:1 to 1:1 gives product as a yellow solid (851 mg, 95%).

R_f 0.18 (hexanes:EtOAc, 9:1, UV);

IR: $\tilde{\nu}$ = 3487w, 3374w, 3090w, 2361w, 1629m, 1616m, 1591s, 1484m, 1450w, 1329s, 1314s, 1272m, 1219w, 1196w, 1156w, 1116m, 1097w, 1002w, 984w, 900w, 859w, 832w, 815w, 747w, 735w, 711w;

^{1}H-NMR (400 MHz, $(CD_3)_2CO$): δ = 8.94 (1H, s, N*H*), 8.12 (1H, d, ^4J 2.4, C1*H*), 7.99 (1H, dd, ^3J 9.0, ^4J 2.5, C3*H*), 7.77 (2H, dt, $^3J_{HF}$ 6.7, ^4J 2.1, 2 x C7*H*), 7.21 (1H, tt, $^3J_{HF}$ 9.0, ^4J 2.4, C9*H*), 6.90 (1H, d, ^3J 9.0, C4*H*);
^{13}C-NMR (101 MHz, $(CD_3)_2CO$) δ = 163.2 (dd, $^1J_{CF}$ 147, $^3J_{CF}$ 12.5, *C8*), 157.0 (t, J_{CF} 3.4)*, 150.8, 140.1 (m)*, 137.4, 133.4 (m)*, 124.6 (*C3*), 113.2 (*C4*)*, 113.1 (*C1*), 111.9, 111.6 (m, 2 x *C7*)*, 106.3 (t, $^2J_{CF}$ 26.3, *C9*);

^{19}F-NMR (377 MHz, $CDCl_3$): δ = –110.9.

** spectrum shows a mixture of tautomers and long-range C–F-couplings are observed.*

2-(3,5-Difluorophenyl)-1*H*-benzo[*d*]imidazolamine (7):

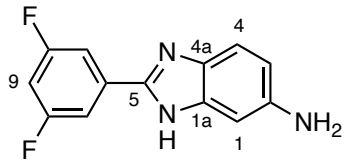

Prepared according to a modified literature procedure.[31] To a suspension of 2-(3,5-difluorophenyl)-6-nitro-1*H*-benzo[*d*]imidazole (82.6 mg, 0.300 mmol), and NH_4Cl (192.6 mg, 12.00 mmol) in MeOH/H_2O (1:1, 5.0 mL) was added iron powder (100.5 mg, 1.80 mmol) and the mixture was stirred at 90 °C for 1 hour. The mixture was cooled to room temperature, filtered over Celite using EtOAc. The filtrate was concentrated in vacuo and purified by column chromatography over silica gel with eluent hexanes 100% to hexanes:acetone 40:60 to give the desired 2-(3,5-difluorophenyl)-1*H*-benzo[*d*]imidazolamine **(7)** as a beige-brown solid (34.5 mg, 47%).

R_f 0.58 (CH_2Cl_2:MeOH, 9:1, UV/$KMnO_4$);

^{1}H-NMR (400 MHz, $(CD_3)_2CO$): δ = 7.73 (2H, dq, ^3J 6.7, ^3J 4.6, ^4J 3.4), 7.37 (1H, d, ^3J 8.3), 7.03–7.09 (1H, m), 6.80 (1H, s), 6.69 (1H, dd, ^3J 8.6, ^4J 2.1), 4.65 (1H, br).

[31] Fischer, C.; Sparr, C. *Tetrahedron* **2018**, *74*, 5486–5493.

1-(2-(Cyclohexylamino)-2-oxoethyl)-*N*-(2-(3,5-difluorophenyl)-1*H*-benzo[*d*]imidazol-6-yl)-5-(4-(dimethylamino)phenyl)-6-oxo-1,6-dihydropyridine-3-carboxamide (1):

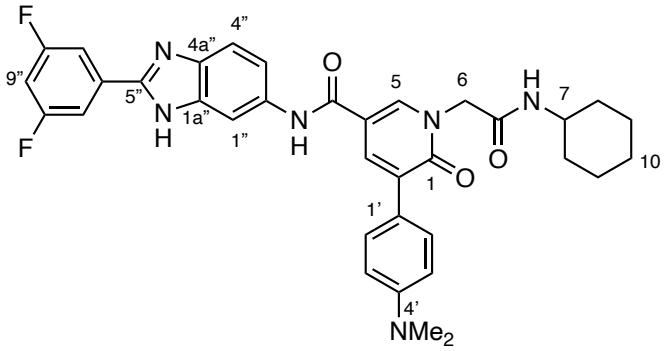

Prepared according to general procedure **I** using methyl 1-(2-(cyclohexylamino)-2-oxoethyl)-5-(4-(dimethylamino)phenyl)-6-oxo-1,6-dihydropyridine-3-carboxylate (10.3 mg, 0.0250 umol, 1.00 equiv.), THF (0.50 mL), water (0.50 mL) and NaOH (3.00 mg, 0.0750 mmol, 3.00 equiv.). Stirred at 40 °C for 2 hours. 1-(2-(Cyclohexylamino)-2-oxoethyl)-5-(4-(dimethylamino)phenyl)-6-oxo-1,6-dihydropyridine-3-carboxylic acid.

LC-MS: (5-100% MeCN in H_2O over 5 min, 0.1% formic acid): t_{ret} = 2.6 min.

Prepared according to general procedure **J** using 1-(2-(cyclohexylamino)-2-oxoethyl)-5-(4-(dimethylamino)phenyl)-6-oxo-1,6-dihydropyridine-3-carboxylic acid (16.0 mg, 0.0403 mmol), HATU (23.0 mg, 0.0604 mmol) *N,N*-diisopropylethylamine (0.0320 mL, 0.180 mmol, 4.56 equiv.), DMF (2.8 mL), and 2-(3,5-difluorophenyl)-1*H*-benzo[*d*]imidazolamine (14.8 mg, 0.0604 mmol, 1.50 equiv.). Stirred at room temperature for 16 hours. The crude product was filtered over a plug of silica gel and chromatographed over a semi-preparative column using eluent 30% to 45% MeCN in H_2O (with constant 0.1% formic acid) in 8 minutes and 100% MeCN (with 0.1% formic acid) for 3 min, ($t_{R,Prod}$: 9.26, 9.58 min) to yield product as a brown solid (9.6 mg, 38% over two steps).

^{1}H-NMR (400 MHz, $(CD_3)_2CO$): δ = 9.58 (1H, s, N*H*), 8.24–8.36 (2H, m, C5*H*, N*H*), 8.08 (1H, d, *J* 2.4, C3*H*), 7.76–7.87 (2H, m, 2 x C7"*H*), 7.69 (2H, d, ^2J 8.4, 2 x C2'*H*), 7.55–7.61 (1H, m, C1"*H*), 7.41–7.51 (2H, m, C3"*H*, C4"*H*), 7.09–7.19 (1H, m, C9"*H*), 6.75 (2H, d, ^2J 8.4, 2 x C3'*H*), 4.75 (2H, s, C6H_2), 3.67–3.80 (1H, m, C7*H*), 2.97 (6H, s, 2 x NCH_3), 1.82–1.96 (2H, m, 2 x C8*H*), 1.67–1.78 (2H, m, 2 x C9*H*), 1.54–1.62 (1H, m, C10*H*), 1.15–1.40 (5H, m, 2 x C8*H*, 2 x C9*H*, C10*H*);

ESI-HRMS: m/z calcd. for $[C_{35}H_{35}F_2N_6O_3]^+$ calcd. 625.2733 found 625.2718 $[M+H]^+$.

1-(2-(Cyclohexylamino)-2-oxoethyl)-5-(4-methoxyphenyl)-6-oxo-1,6-dihydropyridine-3-carboxylic acid (22a):

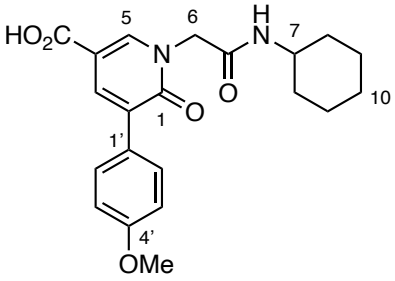

Prepared according to general procedure **I** using methyl 1-(2-(cyclohexylamino)-2-oxoethyl)-5-(4-methoxyphenyl)-6-oxo-1,6-dihydropyridine-3-carboxylate (100 mg, 0.250 mmol), THF (4.8 ml), water (4.8 ml) and NaOH (102 mg, 2.55 mmol, 10 equiv). Stirred at room temperature for 19 hours. The product was obtained as a light beige solid (98.0 mg, quant.).
IR: $\tilde{\nu}$ =2933w, 2853w, 2412w, 1691m, 1643s, 1606s, 1573w, 1554m, 1513m, 1441s, 1416m, 1347w, 1317m, 1305m, 1256s, 1223m, 1180s, 1156m, 1117m, 1097m, 1022m, 946m, 894w, 868m, 834m, 809m, 785w, 766m, 749w;

^{1}H-NMR (400 MHz, CD_3OD): δ = 8.36 (1H, d, *J* 2.4, C5*H*), 8.04 (1H, d, *J* 2.4, C3*H*), 7.57–7.64 (2H, m, 2 x *C2'*H), 6.94–7.01 (2H, m, 2 x *C3'*H), 4.75 (2H, s, C6H_2), 3.84 (3H, s, OCH_3), 3.64–3.67 (1H, m, C7*H*), 1.86–1.96 (2H, m, 2 x C8*H*), 1.73–1.82 (2H, m, 2 x C9*H*), 1.61–1.70 (1H, m, C10*H*), 1.16–1.44 (5H, m, 2 x C9*H*, 2 x C8*H*, C10*H*);

^{13}C-NMR (101 MHz, CD_3OD): δ = 168.0 (*C*ONH), 167.8 (*C*O_2H), 163.6 (*C1*), 161.1 (*C4'*), 144.4 (*C5*), 138.0 (*C3*), 131.1 (*C2*), 130.9 (*C2'*), 129.7 (C1'), 114.6 (*C3'*), 112.2 (*C4*), 55.7 (O*C*H_3), 54.0 (*C6*), 50.2 (*C7*), 33.7 (*C8*), 26.6 (*C10*), 26.1 (*C9*);

APCI-HRMS: m/z calcd. for $[C_{21}H_{25}N_2O_5]^+$ calcd. 385.1758 found 385.1763 $[M+H]^+$.

***N*-Cyclohexyl-2-(3-(4-methoxyphenyl)-5-(morpholine-4-carbonyl)-2-oxopyridin-1(2*H*)-yl)acetamide (23a):**

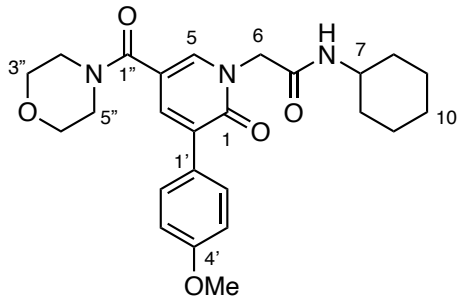

Prepared according to general procedure **J** using 1-(2-(cyclohexylamino)-2-oxoethyl)-5-(4-methoxyphenyl)-6-oxo-1,6-dihydropy-ridine-3-carboxylic acid **(22a)** (23.1 mg, 0.0600 mmol), HATU (34.2 mg, 0.0900 mmol), *N,N*-diisopropylethylamine (0.052 mL, 0.300 mmol), DMF (0.86 mL) and morpholine (6.30 mg, 0.0720 mmol). Stirred at room temperature for 18 hours. Column chromatography over silica gel with eluent 100% CH_2Cl_2 to 98:2 CH_2Cl_2:MeOH gives product as an off-white solid (6.60 mg, 24%).

R_f 0.34 (CH_2Cl_2:MeOH, 95:5, UV);

IR: $\tilde{\nu}$ = 3552w, 3297w, 2923m, 2852m, 2418w, 1647s, 1602s, 1572m, 1551m, 1509m, 1452s, 1429s, 1366m, 1339m, 1308m, 1300m, 1288m, 1276m, 1251s, 1232s, 1195m, 1177m, 1149m, 1103s, 1064m, 1028s, 979m, 961m, 943m, 932m, 894m, 860m, 835s, 816m, 796m, 744m;

^{1}H-NMR (400 MHz, CD_3OD): δ = 7.86 (1H, d, *J* 2.5, C5*H*), 7.68 (1H, d, *J* 2.4, C3*H*), 7.59–7.64 (2H, m, 2 x C2'*H*), 6.93–7.00 (2H, m, C3'*H*), 4.74 (2H, s, C6H_2), 3.84 (3H, s, OCH_3), 3.73 (8H, s, C2"H_2, C3"H_2, C4"H_2, C5"H_2), 3.64–3.73 (1H, m, C7*H*), 1.86–1.96 (2H, m, 2 x C8*H*), 1.74–1.85 (2H, m, 2 x C9*H*), 1.65 (1H, dp, *J* 12, 3.5, C10*H*), 1.16–1.47 (5H, m, 2 x C8*H,* 2 x C9*H*, C10*H*);

^{13}C-NMR (101 MHz, CD_3OD): δ = 168.9 (*C1"*), 168.1 (*C*ONH), 163.0 (*C1*), 161.2 (*C4'*), 140.7 (*C5*), 138.0 (*C3*), 131.8 (*C2*), 131.0 (*C2'*), 129.6 (*C1'*), 115.1 (*C4*), 114.7 (*C3'*), 67.8 (*C2"*, *C3"*, *C4"*, *C5"*), 55.7 (O*C*H$_3$), 53.4 (*C6*), 50.2 (*C7*), 33.7 (*C8*), 26.6 (*C10*), 26.1 (*C9*);

APCI-HRMS: m/z calcd. for $[C_{25}H_{32}N_3O_5]^+$ calcd. 454.2336 found 454.2342 $[M+H]^+$.

1-(2-(Cyclohexylamino)-2-oxoethyl)-5-(4-methoxyphenyl)-*N,N*-dimethyl-6-oxo-1,6-dihydropyridine-3-carboxamide (23b):

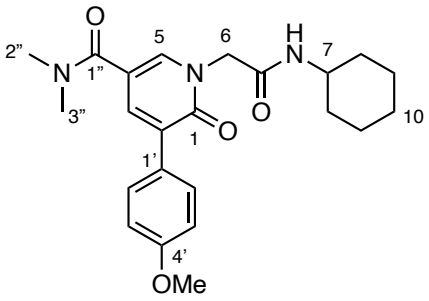

Prepared according to general procedure **J** using 1-(2-(cyclohexylamino)-2-oxoethyl)-5-(4-methoxyphenyl)-6-oxo-1,6-dihydropy-ridine-3-carboxylic acid **(22a)** (23.1 mg, 0.0600 mmol), HATU (34.2 mg, 0.0900 mmol), *N,N*-diisopropylethylamine (0.052 mL, 0.300 mmol), DMF (0.86 mL), dimethylamine (0.036 mL, 0.0720 mmol). Stirred at room temperature for 3 hours. Column chromatography over silica gel with eluent 100% CH_2Cl_2 to 98:2 CH_2Cl_2:MeOH and additional recrystallization from EtOH gives product as an off-white solid (16.9 mg, 68%).

R_f 0.33 (95:5 CH_2Cl_2:MeOH, UV);

IR: $\tilde{\nu}$ = 2928w, 2852w, 2401w, 1676m, 1652m, 1616s, 1605s, 1551m, 1497m, 1450s, 1413m, 1400m, 1380m, 1341w, 1302m, 1249s, 1235m, 1207m, 1176s, 1108m, 1036m, 981w, 944w, 924w, 903w, 891m, 865w, 849s, 826m, 793m, 767w, 754w;

^{1}H-NMR (400 MHz, CD_3OD): δ = 7.82 (1H, d, *J* 2.5, C5*H*), 7.70–7.76 (2H, m, 2 x C2'*H*), 7.67 (1H, d, *J* 2.5, C3*H*), 7.32 (1H, d, *J* 7.8, N*H*), 6.91–6.97 (2H, m, 2 x C3'*H*), 4.70 (2H, s, C6*H*), 3.82 (3H, s, OC*H*$_3$), 3.63–3.74 (1H, m, C7*H*), 3.09 (6H, s, C2"*H*$_3$, C3"*H*$_3$), 1.82–1.91 (2H, m, 2 x C8*H*), 1.66–1.76 (2H, m, 2 x C9*H*), 1.55–1.63 (1H, m, C10*H*), 1.12–1.39 (5H, m, 2 x C8*H*, 2 x C9*H*, C10*H*);

^{13}C-NMR (101 MHz, CD_3OD): δ = 168.2 (*C1"*), 166.5 (*C*ONH), 161.4 (*C1*), 160.4 (*C4'*), 140.5 (*C5*), 136.9 (*C3*), 130.6 (2 x *C3'*), 129.9 (*C1'*), 129.8 (*C2*), 114.5 (*C4*), 114.1 (*C2'*), 55.5 (O*C*H$_3$), 52.6 (C6), 49.3 (*C7*), 33.5 (*C8*), 26.3 (*C10*), 25.6 (*C9*), *signals for C2" and C3" were not found*;

APCI-HRMS: m/z calcd. for $[C_{23}H_{30}N_3O_4]^+$ $[M+H]^+$ calcd. 412.2231 found 412.2235.

1-(2-(Cyclohexylamino)-2-oxoethyl)-5-(4-methoxyphenyl)-6-oxo-*N*-phenyl-1,6-dihydropyridine-3-carboxamide (23c):

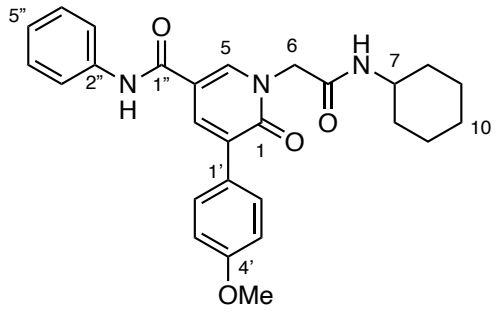

Prepared according to general procedure **J** using 1-(2-(cyclohexylamino)-2-oxoethyl)-5-(4-methoxyphenyl)-6-oxo-1,6-dihydropy-ridine-3-carboxylic acid **(22a)** (23.1 mg, 0.0600 mmol), HATU (34.2 mg, 0.0900 mmol), *N,N*-diisopropylethylamine (0.052 mL, 0.300 mmol), DMF (0.86 ml), and aniline (6.70 mg, 0.0720 mmol). Stirred at room temperature for 3 hours. Column chromatography over silica gel with eluent 100% CH_2Cl_2 to 98:2 CH_2Cl_2:MeOH and additional recrystallization from toluene gives product as an off-white solid (16.1 mg, 58%).

R_f 0.25 (Hexanes:(EtOAc:CH_2Cl_2, 6:4), 2:8; UV);

IR: $\tilde{\nu}$ = 2928w, 2852w, 2384w, 1669w, 1635s, 1601s, 1554m, 1499s, 1465s, 1423m, 1403s, 1376s, 1330m, 1302m, 1287m, 1248s, 1213m, 1192m, 1151m, 1105m, 1015m, 976w, 949m, 914m, 885m, 835s, 796m, 786m, 755s, 731m, 715m;

^{1}H-NMR (400 MHz, CD_3OD): δ = 8.34 (1H, d, *J* 2.6, C5*H*), 8.15 (1H, d, *J* 2.6, C3*H*), 7.63–7.70 (4H, m, 2 x C2'*H*, 2 x C3"*H*), 7.34–7.41 (2H, m, 2 x C4"*H*), 7.13–7.19 (1H, m, C5"*H*), 6.96–7.02 (2H, m, 2 x C3'*H*), 4.77 (2H, s, C6*H_2*), 3.84 (3H, s, OC*H_3*), 3.63–3.81 (1H, m, C7*H*), 1.89–1.97 (2H, m, 2 x C8*H*), 1.74–1.83 (2H, m, 2 x C9*H*), 1.61–1.71 (1H, m, C10*H*), 1.18–1.49 (5H, m, 2 x C8*H*, 2 x C9*H*, C10*H*);

^{13}C-NMR (101 MHz, CD_3OD): δ = 168.0 (*C*ONH), 165.3 (*C1"*), 163.4 (*C1*), 161.2 (*C4'*), 141.9 (*C5*), 139.7 (*C2"*), 136.9 (*C3*), 131.2 (*C2*), 131.0 (*C2'*), 129.8 (*C4"*), 129.8 (*C1'*), 125.6 (*C5"*), 122.2 (*C3"*), 115.6 (*C4*), 114.6 (*C3'*), 55.7 (*C*H_3), 54.1 (*C6*), 50.2 (*C7*), 33.7 (*C8*), 26.6 (*C10*), 26.1 (*C9*);

APCI-HRMS: m/z calcd. for $[C_{27}H_{30}N_3O_4]^+$ calcd. 460.2231 found 460.2231 $[M+H]^+$.

`

Chemical Procedures for Part 3 Photoswitchable Clozapine Derivatives

The procedures consulted until clozapine were in addition to the references cited based on corresponding reports in the literature.[32]

Synthesis of 2-((4-chloro-2-nitrophenyl)amino)benzoic acid (2):

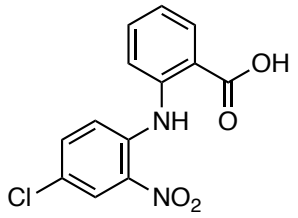

Following a known procedure[33], 2-bromo-5-chloronitrobenzene (25.0 g, 106 mmol, 1.05 eq.) and anthranilic acid (13.8 g, 101 mmol, 1.00 eq.) were slowly added into stirring 3-methyl-1-butanol (200 ml), that no clotting occurred. Once the starting materials were fully dissolved, K_2CO_3 (13.9 g, 101 mmol, 1.00 eq.) and copper (0.57 g, 8.99 mmol, 0.09 eq.) were added and the reaction mixture was heated to reflux. After 1.5 h the formation of a red precipitate/ cake could be observed. After 4 h, the crude reaction product was transferred into a 2-neck round bottom flask using DCM. Upon removal of DCM, residual organic starting materials were removed by steam distillation[34]. The aqueous residue was acidified with aq. HCl (2.0 M) and the formed precipitate was collected by filtration. The crude reaction product was recrystallized from aqueous ethanol and gave the title compound as deep red-brown crystals (24.2 g, 82.7 mmol, 82%).

^{1}H-NMR (600 MHz, DMSO): δ [ppm] = 12.10 (s_{br}, 1H), 8.13 (s, 1H), 7.85 (s_{br}, 1H), 7.63 – 7.52 (m, 3H), 7.35 (s, 1H), 7.06 (s, 1H).

^{13}C-NMR (151 MHz, DMSO): δ [ppm] = 138.6, 137.3, 135.5, 132.2, 125.8, 122.7, 122.5, 121.1.

---

[32] Hunziker F.; Lauener, H. Schmutz, J. *Arzneimittel Forschung/ Drug Research* **1963**, 324–328.

[33] a) Su, J.; Tang, H.; McKittrick, B. A.; Burnett, D. A.; Zhang, H.; Smith-Torhan, A.; Fawzi, A.; Lachowicz, J. *Bioorg. & Med. Chem. Lett.* **2006**, *16*, 4548–4553. b) Capuano, B; Crosby, I. T.; Lloyd, E. J.; Taylor, D. A. *Aust. J. Chem.* **2002**, *55*, 565–576.

[34] Note: a traditional steam distillation apparatus was not available. Therefore, a glass apparatus following the same principle was built from conventional glassware.

Synthesis of 2-((2-carboxyphenyl)amino)-5-chlorobenzenaminium (3):

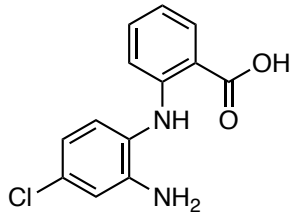

Nitrobenzene **2** (5.38 g, 18.4 mmol, 1.00 eq)was dissolved in wet methanol (540 ml) and sparged with nitrogen. 10% Pd/C (196 mg, 0.18 mmol, 0.01 eq.) was added and the reaction mixture further sparged with nitrogen. Then, the reaction was sparged with hydrogen for 20 seconds and subsequently left under a hydrogen atmosphere using a double-walled balloon. The reaction was monitored by LCMS and full conversion of the starting material was observed after 5 h. The reaction mixture was sparged with nitrogen for 10 minutes and then filtered over a short column of celite applying positive nitrogen pressure and rinsing with methanol. The volatiles were removed under reduced pressure and dried under high vacuum. The crude product was obtained as a deep purple solid (4.86 g, 18.5 mmol, quant.)

LCMS (5-100% MeCN in H_2O over 5 min, 0.1% FA): t_{Ret} = 3.9 min.

LRMS (ESI$^+$, m/z): $[M+H]^+$ for $C_{13}H_{12}ClN_2O_2^+$ calcd.: 263.1, found: 263.1.

^{1}H-NMR (400 MHz, DMSO-d_6) δ = 9.77 (s_{br}, 1H), 7.85 (d, J = 7.7 Hz, 1H), 7.20 (t, J = 7.7 Hz, 1H), 7.02 (d, J = 8.3 Hz, 1H), 6.79 (d, J = 2.3 Hz, 1H), 6.69 – 6.57 (m, 2H), 6.55 (dd, J = 8.3, 2.3 Hz, 1H), 5.12 (s, 2H).

Synthesis of 8-chloro-5,10-dihydro-11*H*-dibenzo[*b*,*e*][1,4]diazepin-11-one (4):

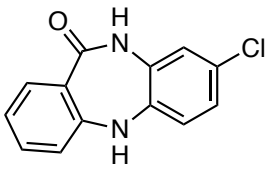

Following a reported procedure[35], aniline **3** was dissolved in xylenes (135 ml) and heated to reflux using a *Dean-Stark* apparatus. After 3 d, LCMS showed the presence of starting material and cyclization product. The solvent was removed under reduced pressure and the solid residue was washed with 10% aq. NH_3 (3 x 25 ml) and recrystallized from acetone/water. The title compound was obtained as dark brown solid (1.54 g, 6.00 mmol, 29%).

R_f (SiO_2, Hex:EtOAc = 5:5, UV) = 0.22

LCMS (5-100% MeCN in H_2O over 5 min, 0.1% FA): t_{ret} = 3.4 min.

^{1}H-NMR (400 MHz, Acetone-d$_6$): δ [ppm] = 7.83 (dt, J = 7.9, 1.3 Hz, 1H), 7.40 – 7.28 (m, 2H), 7.15 (d, J = 1.0 Hz, 1H), 7.11 – 6.91 (m, 5H).

Synthesis of 8,11-dichloro-5*H*-dibenzo[*b*,*e*][1,4]diazepine (5):

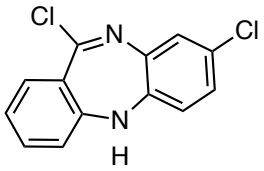

Following a known procedure[36], **4** (1.80 g, 7.36 mmol, 1.00 eq.) was dissolved in dry toluene (105 ml) and $POCl_3$ (40.9 ml, 0.45 mol, 60.7 eq.) and *N*,*N*-dimethylaniline (5.1 ml, 40.3 mmol,

[35] a) Su, J.; Tang, H.; McKittrick, B. A.; Burnett, D. A.; Zhang, H.; Smith-Torhan, A.; Fawzi, A.; Lachowicz, J. *Bioorg. & Med. Chem. Lett.* **2006**, *16*, 4548–4553. b) Capuano, B; Crosby, I. T.; Lloyd, E. J.; Taylor, D. A. *Aust. J. Chem.* **2002**, *55*, 565–576.

[36] Liao, Y.; DeBoer, P.; Meier, E.; Wikström, H. *J. Med. Chem.* **1997**, *40*, 4146–4153.

5.48 eq.) were added. The reaction was heated to reflux for 3 h. The volatiles were removed under reduced pressure and the product was used without further purification.

Synthesis of 8-chloro-11-(4-methylpiperazin-1-yl)-5*H*-dibenzo[*b*,*e*][1,4]diazepine (clozapine):

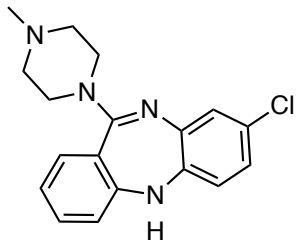

Following a known procedure[28], imine chloride **5** was dissolved in dry toluene (98.0 ml) and *N*-methyl pipererazine (28.6 ml, 0.26 mol, 35 eq.) was added. The reaction was heated to reflux for 3 h. The volatiles were removed under reduced pressure and the crude residue was purified by flash-column chromatography (SiO_2, DCM:EtOAc:MeOH:NEt_3 = 5:5:0.1:0.1 to 5:5:0.5:1). Clozapine was obtained as an off-white solid (2.24 g, 6.85 mmol, 93%).

R_f (SiO_2, DCM:EtOAc:MeOH:NEt_3 = 5:5:0.1:0.1, UV) = 0.19

LCMS (5-100% MeCN in H_2O over 5 min, 0.1% FA): t_{ret} = 2.3 min.

^{1}H-NMR (400 MHz, $CDCl_3$): δ [ppm] = 7.32 – 7.25 (m, 2H), 7.07 (d, J = 2.4 Hz, 1H), 7.01 (td, J = 7.6, 1.1 Hz, 1H), 6.82 (dd, J = 8.2, 1.8 Hz, 2H), 6.61 (d, J = 8.3 Hz, 1H), 4.88 (s, 1H), 3.47 (s_{br}, 4H), 2.50 (s_{br}, 4H), 2.35 (s, 3H).

^{13}C-NMR (101 MHz, $CDCl_3$): δ [ppm] = 163.0, 152.9, 141.9, 140.5, 132.0, 130.4, 129.2, 126.9, 123.6, 123.2, 123.2, 120.2, 120.1, 55.2, 47.4, 46.3.

LRMS (ESI$^+$, m/z): $[M+H]^+$ for $C_{18}H_{20}ClN_4^+$ calcd.: 327.1, found: 327.2.

Synthesis of *tert*-butyl 8-chloro-11-(4-methylpiperazin-1-yl)-5*H*-dibenzo[*b*,*e*][1,4]diazepine-5-carboxylate (7):

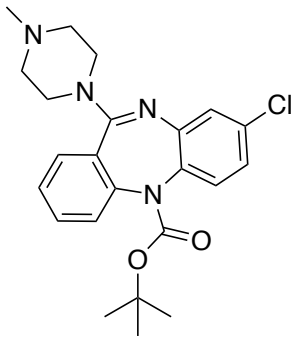

Clozapine (200 mg, 0.61 mmol, 1.00 eq.) was dissolved in dry tetrahydrofuran (10 ml) and dry triethylamine (0.17 ml, 1.22 mmol, 2.00 eq.), DMAP (74.8 mg, 0.61 mmol, 1.00 eq.) and Boc_2O (668 mg, 3.06 mmol, 5.00 eq.) were subsequently added. The reaction mixture was stirred at room temperature for 30 minutes and then heated to reflux for 17 h. The reaction was cooled to room temperature and sat. aq. NaHCO3 (5 ml) was added. The aqueous phase was extracted with ethyl acetate (3 x 10 ml), washed with brine, dried over Na2SO4, filtered and concentrated. The crude product was purified by flash column chromatography (SiO2, ethyl acetate/ dichloromethane/ methanol/ triethylamine = 5/5/0.1/0.1 to 5/5/0.5/1) and furnished the title compound as off-white solid (222 mg, 0.52 mmol, 85%).

R_f (SiO_2, dichloromethane: ethyl acetate: methanol: triethylamine = 5:5:0.1:0.1, UV) = 0.28

LCMS (5-100% MeCN in H_2O over 5 min, 0.1% FA): t_{ret} = 3.2 min 5-100%

1H-NMR (400 MHz, MeOD): δ [ppm] = 7.61 – 7.54 (m, 1H), 7.50 – 7.38 (m, 3H), 7.24 (d, J = 8.5 Hz, 1H), 7.09 (d, J = 2.4 Hz, 1H), 7.00 (dd, J = 8.5, 2.5 Hz, 1H), 3.83 – 3.41 (m, 4H), 2.64 – 2.37 (m, 4H), 2.31 (s, 3H), 1.41 (s, 9H).

^{13}C-NMR (101 MHz, MeOD): δ [ppm] = 161.8, 155.7, 154.7, 146.6, 145.7, 135.4, 135.0, 134.1, 133.4, 130.4, 129.7, 129.3, 129.0, 127.7, 126.4, 124.3, 82.8, 55.6, 49.9, 46.1, 28.5.

LRMS (ESI$^+$, m/z): $[M+H]^+$ for $C_{23}H_{28}ClN_4O_2^+$ calcd.: 427.2, found: 427.3.

Synthesis of 11-(4-methylpiperazin-1-yl)-8-(phenyldiazenyl)-5*H*-dibenzo[*b*,*e*][1,4]diazepine (6):

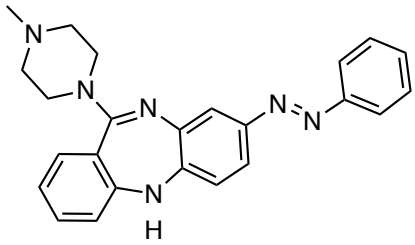

Based on a literature procedure[37], a flame-dried vial was charged with clozapine (50.0 mg, 0.15 mmol, 1.00 eq.), *t*-BuONa (29.4 mg, 0.31 mmol, 2.00 eq.) palladium (II) (π-cinnamyl) chloride dimer (4.10 mg, 8.00 µmol, 0.05 eq.), Mor-Dalphos (10.7 mg, 23.0 µmol, 0.15 eq.) and evacuated for 10 minutes. The vial was pback filled with nitrogen and the olids were dissolved in dry toluene (1.5 ml) and Phenyl hydrazine (18.0 µl, 0.18 mmol, 1.20 eq.) was added. the reaction was heated to 50 °C and stirred for 5 h. The reaction mixture was cooled to room temperature, filtered over a pad of celite, rinsed with DCM and concentrated. Purification by flash column chromatography (SiO_2, DCM:EtOAc:MeOH:Net_3 = 5:5:0.1:0.1 to 5:5:1:0.1) and HPLC (prep, 5-61% MeCN over 7 min, 3 min MeCN, 0.1% FA) gave the title compound as an orange film (7.5 mg, 19.0 µmol, 12%).

R_f (SiO_2, DCM:MeOH = 9.5:5, UV) = 0.13

LCMS (5-100% MeCN in H_2O over 5 min, 0.1% FA): t_{ret} = 3.1 min

^{1}H-NMR (400 MHz, MeOD): δ [ppm] = 7.85 (dt, J = 6.2, 1.3 Hz, 2H), 7.61 – 7.43 (m, 5H), 7.42 – 7.33 (m, 2H), 7.11 – 7.02 (m, 2H), 7.00 (d, J = 8.3 Hz, 1H), 3.63 – 3.47 (m, 4H), 2.89 – 2.77 (m, 4H), 2.67 (s, 1H), 2.55 (s, 3H).

^{13}C-NMR (101 MHz, MeOD): δ [ppm] = 164.4, 155.0, 154.1, 150.9, 148.2, 141.4, 133.9, 131.7, 131.3, 130.2, 124.2, 123.9, 123.5, 121.8, 121.6, 121.4, 120.9, 54.7, 46.8, 44.5.

HRMS (ESI$^+$, *m/z*): [(M+H)$^+$] for $C_{24}H_{25}N_6^+$: calcd.: 397.2135, found: 397.2139.

[37] Lundgren, R. L.; Stradiotto, M. *Angew. Chem.* **2010**, *122*, 8868–8872.

Synthesis of *tert*-butyl 1-phenylhydrazine-1-carboxylate:

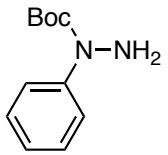

The title compound was prepared following a known procedure and the analytical data matched those reported.[38] 89% yield.

R_f (SiO_2, Hex:EtOAc = 8:2; UV) = 0.41

^{1}H-NMR (400 MHz, $CDCl_3$): δ [ppm] = 7.49 – 7.42 (m, 2H), 7.31 (dd, J = 8.6, 7.3 Hz, 2H), 7.11 (td, J = 7.3, 1.2 Hz, 1H), 4.44 (s, 2H), 1.50 (s, 9H).

^{13}C-NMR (101 MHz, $CDCl_3$): δ [ppm] = 155.4, 143.2, 128.3, 124.8, 123.6, 81.9, 28.5.

Synthesis of *tert*-butyl 1-(4-methoxyphenyl)hydrazine-1-carboxylate:

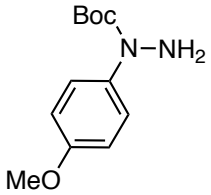

The title compound was prepared following a known procedure and the analytical data matched those reported.[39] 84% yield.

R_f (SiO_2, Hex:EtOAc = 8:2, UV) = 0.22

^{1}H-NMR (400 MHz, $CDCl_3$): δ [ppm] = 7.30 (d, J = 8.7 Hz, 2H), 6.88 – 6.81 (m, 2H), 4.44 (s, 2H), 3.80 (s, 3H), 1.48 (s, 9H).

[38] Wolter, M.; Klapars, A.; Buchwald, S. L. *Org. Lett.* **2001**, 3, 3803–3805.

[39] Wolter, M.; Klapars, A.; Buchwald, S. L. *Org. Lett.* **2001**, 3, 3803–3805.

13C-NMR (100 MHz, CDCl3): δ [ppm] = 157.0, 155.7, 136.5, 125.4, 113.6, 81.6, 55.6, 28.5.

HRMS (ESI$^+$, *m/z*): [(M+K)$^+$] for $C_{12}H_{18}KN_2O_3^+$: calcd.: 277.0949, found: 277.0940.

Synthesis of *N*-(4-iodophenyl)acetamide:

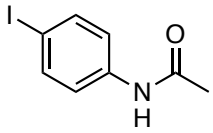

Following a known procedure[40], 4-iodo aniline (500 mg, 2.28 mmol, 1.00 eq.) was dissolved in dry dichloromethane (5.7 ml) and acetic anhydride (0.26 ml, 2.74 mmol, 1.20 eq.) was added dropwise at room temperature. After 30 minutes, the reaction mixture was neutralized with sat. ac. $NaHCO_3$ (25 ml) and extracted with dichloromethane (2 x 40 ml). The combined organic layers were washed with brine, dried over $MgSO_4$, filtered and concentrated. The title compound was used without further purification (588 mg, 2.25 mmol, 99%).

R_f (SiO_2, Hex:EtOAc = 8:2, UV) = 0.08

1H-NMR (400 MHz, $CDCl_3$): δ [ppm] = 7.64 – 7.59 (m, 2H), 7.29 (d, *J* = 8.5 Hz, 2H), 7.16 (s, 1H), 2.17 (s, 3H).

HRMS (ESI$^+$, *m/z*): [(M+Na)$^+$] for $C_8H_8INNaO^+$: calcd.: 283.9543, found: 283.9556.

[40] Astra Pharma Inc.US6187792, 2001, B1.

Synthesis of tert-butyl 1-(4-acetamidophenyl)hydrazine-1-carboxylate:

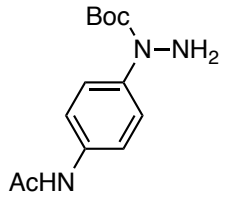

Following a related literature procedure[41], *N*-(4-iodophenyl)acetamide (588 mg, 2.25 mmol, 1.0 eq.), N-Boc-hydrazine (298 mg, 2.25 mmol, 1.00 eq.), copper (I) iodide (21.4 mg, 0.11 mmol, 0.05 eq.), 1,10-phenantroline (81.2 mg, 0.45 mmol, 0.20 eq.) and caesium carbonate (1.03 g, 3.15 mmol, 1.40 eq.) were combined in a flame-dried glass vial with stir bar and evacuated for 10 minutes. The vial was backfilled with argon and dry DMF (2.3 ml) was added. The reaction was heated to 80 °C over night. The suspension was cooled to room temperature and filtered over a pad of celite, eluted with EtOAc and concentrated. The crude reaction product was purified by flash column chromatography (SiO_2, Hex:EtOAc = 9:1 to 0:10) and gave the title compound as orange solid (339 mg, 1.28 mmol, 57%).

R_f (SiO_2, Hex:EtOAc = 8:2; UV) = 0.35

^{1}H-NMR (400 MHz, $CDCl_3$): δ [ppm] = 7.48 – 7.34 (m, 4H), 7.25 – 7.14 (m, 2H), 4.42 (s, 2H), 2.16 (s, 3H), 1.49 (s, 9H).

^{13}C-NMR (101 MHz, $CDCl_3$): δ [ppm] = 168.3, 155.3, 139.5, 134.7, 124.2, 119.7, 82.0, 28.5, 24.7.

HRMS (ESI$^-$, *m/z*): $[M–H]^-$ for $C_{13}H_{18}N_3O_3^-$: calcd.: 264.1354, found: 263.1345.

[41] Wolter, M.; Klapars, A.; Buchwald, S. L. *Org. Lett.* **2001**, 3, 3803–3805.

Synthesis of *tert*-butyl 8-(2-(4-acetamidophenyl)-2-(*tert*-butoxycarbonyl)hydrazineyl)-11-(4-methylpiperazin-1-yl)-5*H*-dibenzo[*b*,*e*][1,4]diazepine-5-carboxylate (8a):

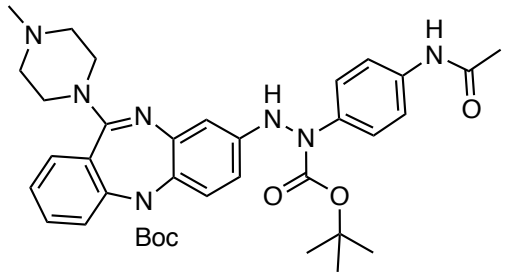

Inspired by a known procedure[42], a flame-dried vial was charged with **7** (50.0 mg, 0.12 mmol, 1.00 eq.), *N*-Boc-*N*-(4-acetylamido)phenyl hydrazine (62.1 mg, 0.23 mmol, 2.00 eq.), Cs_2CO_3 (53.4 mg, 0.16 mmol, 1.40 eq.) and bis(tri-tert-butylphosphine)palladium(0) (9.00 mg, 17.6 umol, 0.15 eq.) and evacuated for 10 minutes, then backfilled with nitrogen. Dry toluene (1.9 ml) was added and the suspension was stirred for 15 minutes at room temperature and subsequently heated to 120 °C. The reaction was monitored by LCMS and after 6 h concentrated and subjected to purification by flash column chromatography (SiO_2, ethyl acetate/ dichloromethane/ methanol/ triethylamine 5/5/0.1/0.1 to 5/5/1/0.1). The product fraction was isolated as a mixture of product that were copolar with clozapine and therefore subjected to the subsequent step without further purification.

LCMS (5-100% MeCN in H_2O over 5 min, 0.1% FA): t_{ret} = 3.2 min.

LRMS (ESI$^+$, m/z): $[M+H]^+$ for $C_{36}H_{46}N_7O_5^+$ calcd.: 656.4, found: 656.4.

[42] Barber, D. M.; Liu, S.-A.; Gottschling, K.; Sumser, M.; Hollmann, M.; Trauner, D.; *Chem. Sci.* **2017**, *8*, 611–615.

Synthesis of *tert*-butyl 8-((4-acetamidophenyl)diazenyl)-11-(4-methylpiperazin-1-yl)-5*H*-dibenzo[*b*,*e*][1,4]diazepine-5-carboxylate (s9):

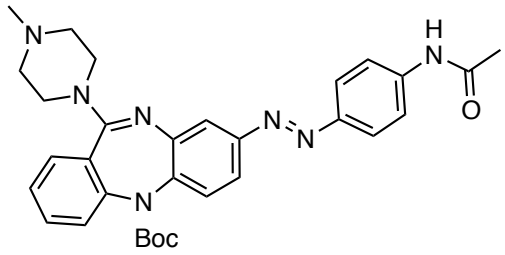

Inspired by a reported procedure[43], the product mixture that was obtained from the previous Buchwald-Hartwig amination, copper iodide (22.3 mg, 0.12 mmol, 1.00 eq.) and Cs_2CO_3 (35.7 mg, 0.11 umol, 0.94 eq.) were added and the combined solids were evacuated for 10 minutes and backfilled with nitrogen. Dry dimethylformamide (6.5 ml) was added and the reaction was heated to 110 °C and monitored by LCMS. After two days, the reaction mixture was diluted with ethyl acetate (20 ml) and sat. aq. $NaHCO_3$ (20 ml) was added. The phases were separated, and the aqueous layer was extracted with ethyl acetate (3 x 20 ml). The combined organic layers were washed with 10% aq. LiCl (4 x 20 ml) and brine and subsequently dried over Na_2SO_4, filtered and concentrated. The residue was subjected to a quick flash column (SiO_2, ethyl acetate/ dichloromethane/ methanol/ triethylamine 5/5/0.1/0.01 to 5/5/1/0.01) and a mixed fraction of reaction products that looked promising by LCMS but was hard to analyze by NMR was obtained and used without further purification.

LCMS (5-100% MeCN in H_2O over 5 min, 0.1% FA): t_{ret} = 3.2 min.

LRMS (ESI$^+$, m/z): $[M+H]^+$ for $C_{31}H_{36}N_7O_3^+$ calcd.: 554.3, found: 554.3.

[43] Lim, Y.-K.; Choi, S.; Park, K. B. Cho, C.-G. *J. Org. Chem.* **2004**, *69*, 2603–2606.

***N*-(4-((11-(4-methylpiperazin-1-yl)-5*H*-dibenzo[*b*,*e*][1,4]diazepin-8-yl)diazenyl)phenyl) acetamide (9):**

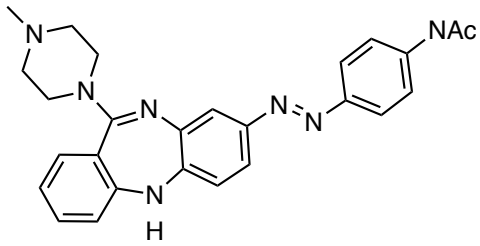

The azobenzene product mixture from the previous step was heated to 100 °C under high vacuum over night. Full consumption of the starting material was observed by LCMS and the reaction product was purified by HP-LC (big-prep, 10-60% MeCN over 15 min, no FA). The title compound was isolated as orange film (7.1 mg, 15.7 umol, 13%). Additionally, an impure fraction consisting of deacetylated product and the desired reaction product was obtained (9.6 mg).

R_f (SiO_2, DCM:MeOH 9.5:0.5, UV) = 0.12

LCMS (5-100% MeCN in H_2O over 5 min, 0.1% FA): t_{ret} = 2.5 min.

^{1}H-NMR (400 MHz, MeOD): δ = 7.83 (d, J = 8.8 Hz, 2H), 7.73 (d, J = 9.0 Hz, 2H), 7.56 (d, J = 2.1 Hz, 1H), 7.53 (dd, J = 8.3, 2.3 Hz, 1H), 7.43 – 7.34 (m, 2H), 7.11 – 7.03 (m, 2H), 6.99 (d, J = 8.3 Hz, 3H), 3.60 (s_{br}, 4H), 3.01 (s_{br}, 4H), 2.67 (s, 3H), 2.17 (s, 3H).

^{13}C-NMR (100 MHz, MeOD): δ = 171.8, 164.6, 155.0, 150.9, 150.2, 147.9, 142.4, 141.4, 133.8, 131.3, 124.4, 124.1, 123.9, 121.7, 121.5, 121.1, 121.0, 120.9, 54.9, 47.1, 44.9, 24.0.

HRMS (APCI$^+$, *m/z*): [(M+H)$^+$] for $C_{26}H_{28}N_7O^+$: calcd.: 454.2350, found: 454.2342.

Synthesis of *tert*-butyl 8-(2-(*tert*-butoxycarbonyl)-2-(4-methoxyphenyl)hydrazineyl)-11-(4-methylpiperazin-1-yl)-5*H*-dibenzo[*b*,*e*][1,4]diazepine-5-carboxylate (8b):

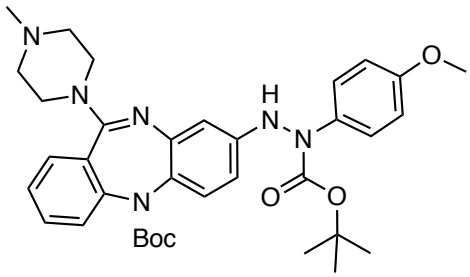

Inspired by a known procedure[44], a flame-dried vial was charged with **7** (50.0 mg, 0.12 mmol, 1.00 eq.), *N*-Boc-*N*-(4-methoxy)phenyl hydrazine (55.8 mg, 0.23 mmol, 2.00 eq.), caesium carbonate (53.4 mg, 0.16 mmol, 1.40 eq.) and bis(tri-tert-butylphosphine)palladium(0) (9.00 mg, 17.6 umol, 0.15 eq.) and evacuated for 10 minutes, then backfilled with nitrogen. Dry toluene (1.9 ml) was added and the suspension was stirred for 30 minutes at room temperature and subsequently heated to 120 °C. The reaction was monitored by LCMS and after 3 h concentrated and subjected to purification by flash column chromatography (SiO_2, ethyl acetate/ dichloromethane/ methanol/ triethylamine 5/5/0.1/0.1 to 5/5/1/0.1 to 5/5/1/1). The product fraction was isolated as a mixture of products that were copolar with clozapine and therefore subjected to the subsequent step without further purification.

LCMS (5-100% MeCN in H_2O over 5 min, 0.1% FA): t_{ret} = 3.6 min.

LRMS (ESI$^+$, m/z): $[M+H]^+$ for $C_{35}H_{45}N_6O_5^+$ calcd.: 629.3, found: 629.4.

[44] Barber, D. M.; Liu, S.-A.; Gottschling, K.; Sumser, M.; Hollmann, M.; Trauner, D.; *Chem. Sci.* **2017**, *8*, 611–615.

Synthesis of *tert*-butyl 8-((4-methoxyphenyl)diazenyl)-11-(4-methylpiperazin-1-yl)-5*H*-dibenzo[*b*,*e*][1,4]diazepine-5-carboxylate (s10):

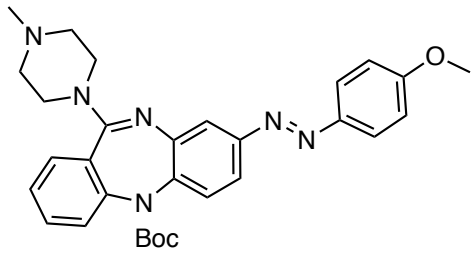

Inspired by a reported procedure[45], the product mixture that was obtained from the previous Buchwald-Hartwig amination, copper iodide (22.3 mg, 0.12 mmol, 1.00 eq.) and caesium carbonate (35.8 mg, 0.11 umol, 0.94 eq.) were added and the combined solids were evacuated for 10 minutes and backfilled with nitrogen. Dry dimethylformamide (6.5 ml) was added and the reaction was heated to 110 °C and monitored by LCMS. After 18 h, the reaction mixture was diluted with ethyl acetate (20 ml) and sat. aq. $NaHCO_3$ (20 ml) was added. The phases were separated and the aqueous layer was extracted with ethyl acetate (3 x 20 ml). The combined organic layers were washed with 10% aq. LiCl (4 x 20 ml) and brine and subsequently dried over Na_2SO_4, filtered and concentrated. The residue was subjected to a quick flash column (SiO_2, ethyl acetate/ dichloromethane/ methanol/ triethylamine 5/5/0.1/0.01 to 5/5/1/0.01) and a mixed fraction of reaction products that looked promising by LCMS but was hard to analyze by NMR was obtained and used without further purification.

LCMS (5-100% MeCN in H_2O over 5 min, 0.1% FA): t_{Ret} = 3.7 min.

LRMS (ESI$^+$, m/z): $[M+H]^+$ for $C_{30}H_{35}N_6O_3^+$ calcd.: 527.3, found: 527.3.

[45] Lim, Y.-K.; Choi, S.; Park, K. B. Cho, C.-G. *J. Org. Chem.* **2004**, *69*, 2603–2606.

Synthesis of 8-((4-methoxyphenyl)diazenyl)-11-(4-methylpiperazin-1-yl)-5H-dibenzo[b,e] [1,4]diazepine (10):

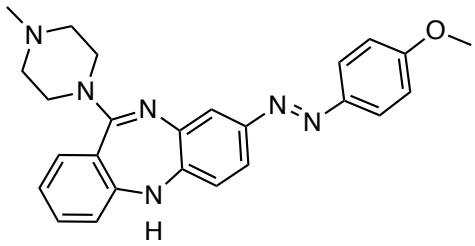

The azobenzene product mixture from the previous step was heated to 110 °C under high vacuum over night. Full consumption of the starting material was observed by LCMS and the reaction product was purified by HPLC (big-prep, 10-70% MeCN over 15 min, no FA). The title compound was isolated as orange film (19.4 mg, 45.5 umol, 39%). Additionally, an impure fraction containing the desired reaction product was obtained (8.2 mg).

R_f (SiO_2, DCM:MeOH 9.5:5, UV) = 0.47

LCMS (5-100% MeCN in H_2O over 5 min, 0.1% FA): t_{ret} = 3.0 min.

^{1}H-NMR (400 MHz, MeOD): δ [ppm] = 7.86 – 7.80 (m, 2H), 7.53 (d, J = 2.2 Hz, 1H), 7.48 (dd, J = 8.3, 2.3 Hz, 1H), 7.42 – 7.30 (m, 3H), 7.09 – 7.01 (m, 4H), 6.97 (d, J = 8.4 Hz, 1H), 3.87 (s, 3H), 3.57 – 3.45 (m, 4H), 2.81 – 2.72 (m, 4H), 2.49 (s, 3H).

^{13}C-NMR (101 MHz, MeOD): δ [ppm] = 164.8, 163.4, 155.0, 150.9, 148.3, 147.6, 141.6, 133.6, 131.4, 125.4, 124.2, 124.0, 121.5, 121.4, 120.8, 120.6, 115.3, 56.1, 55.3, 47.7, 45.5.

HRMS (APCI$^+$, *m/z*): $[M+H]^+$ for $C_{25}H_{27}N_6O^+$: calcd.: 427.2241, found: 427.2238.

Photophysical Properties for Chapter 3

UV-Vis Characterization was performed at a concentration of 30 µM in DMSO.

UV-Vis for 6:

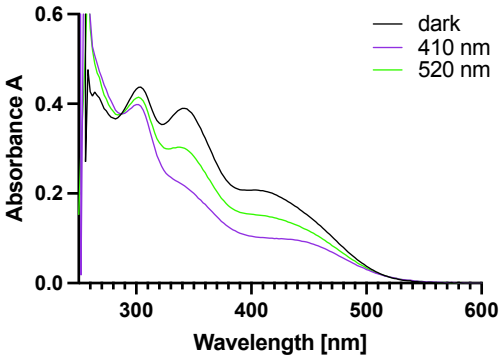

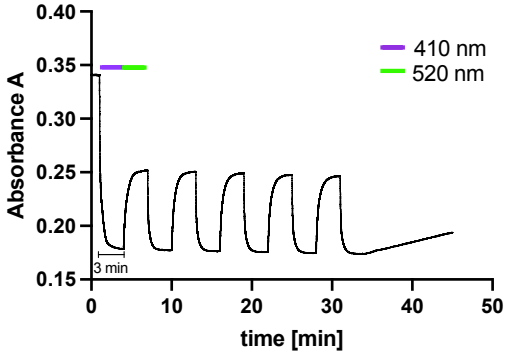

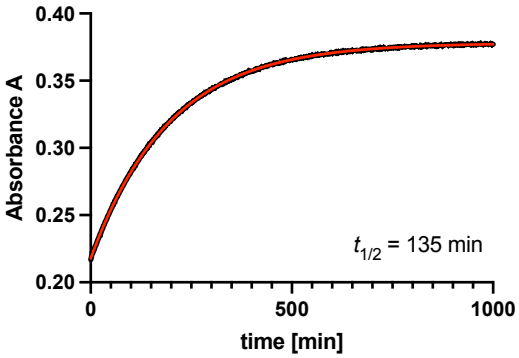

UV-Vis for 9:

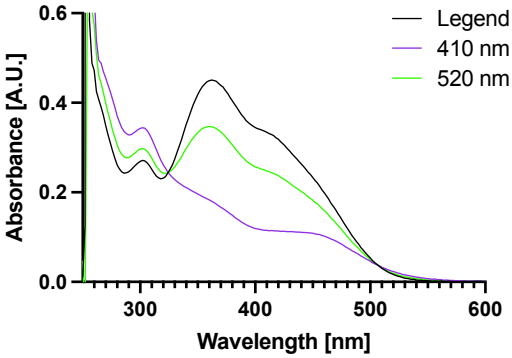

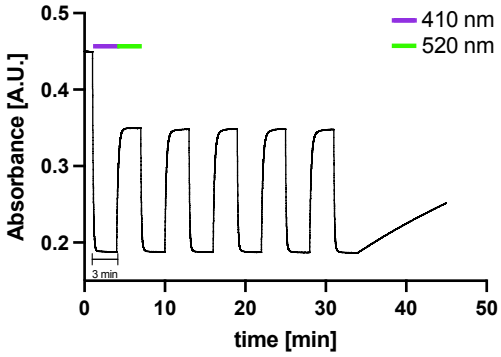

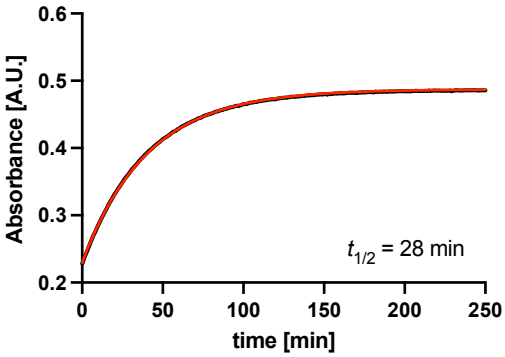
Absorbance [A.U.]
time [min]
$t_{1/2}$ = 28 min

UV-Vis for 10:

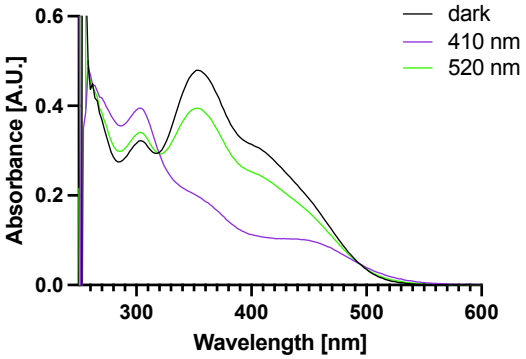
dark
410 nm
520 nm
Absorbance [A.U.]
Wavelength [nm]

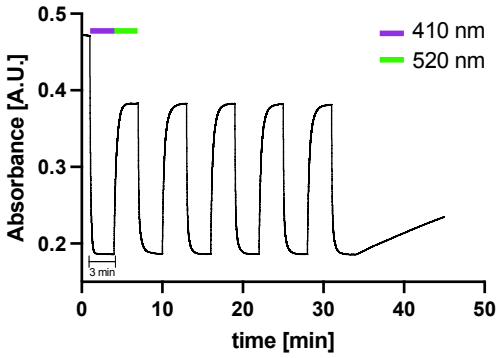
410 nm
520 nm
Absorbance [A.U.]
3 min
time [min]

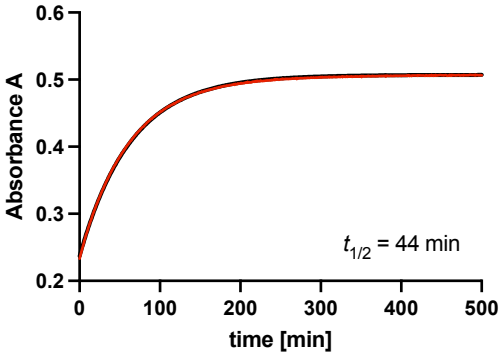
Absorbance A
$t_{1/2}$ = 44 min
time [min]

Selected NMR-Spectra

NMR-Spectra for 1.2 Latrunculin

NMR for hex-5-enal

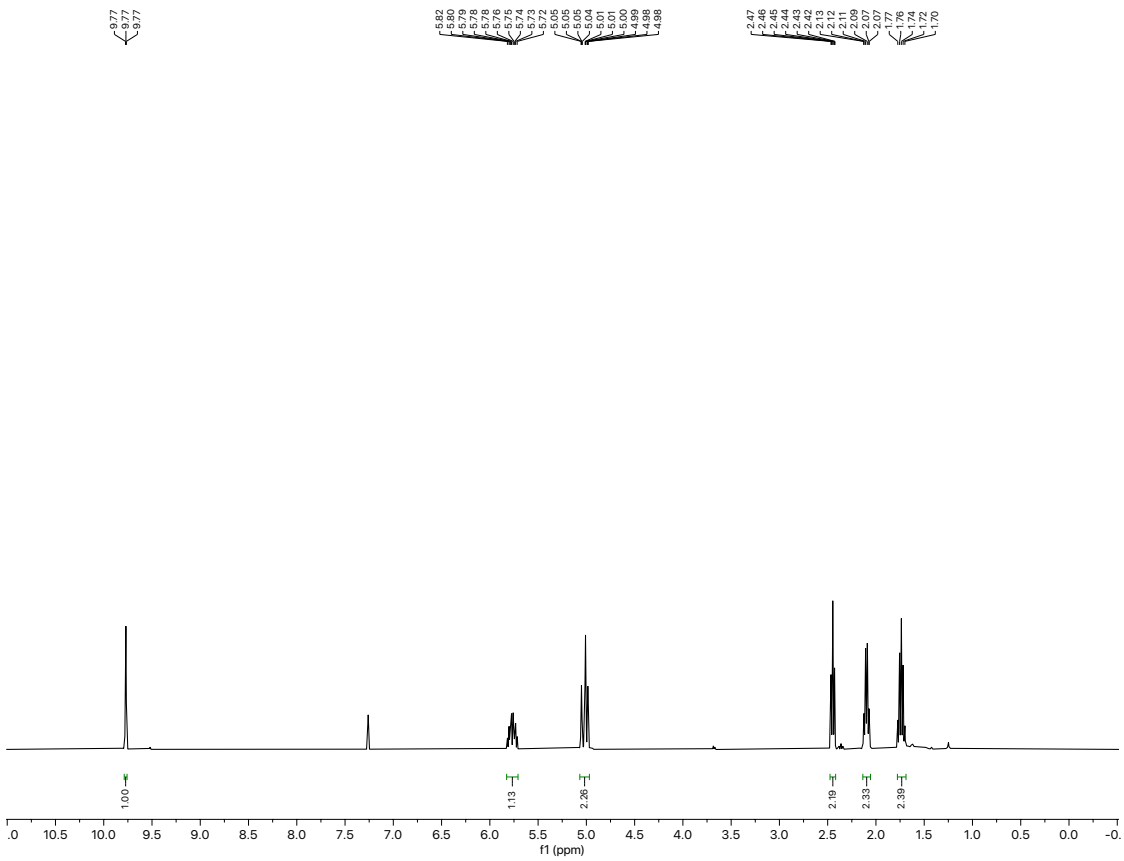

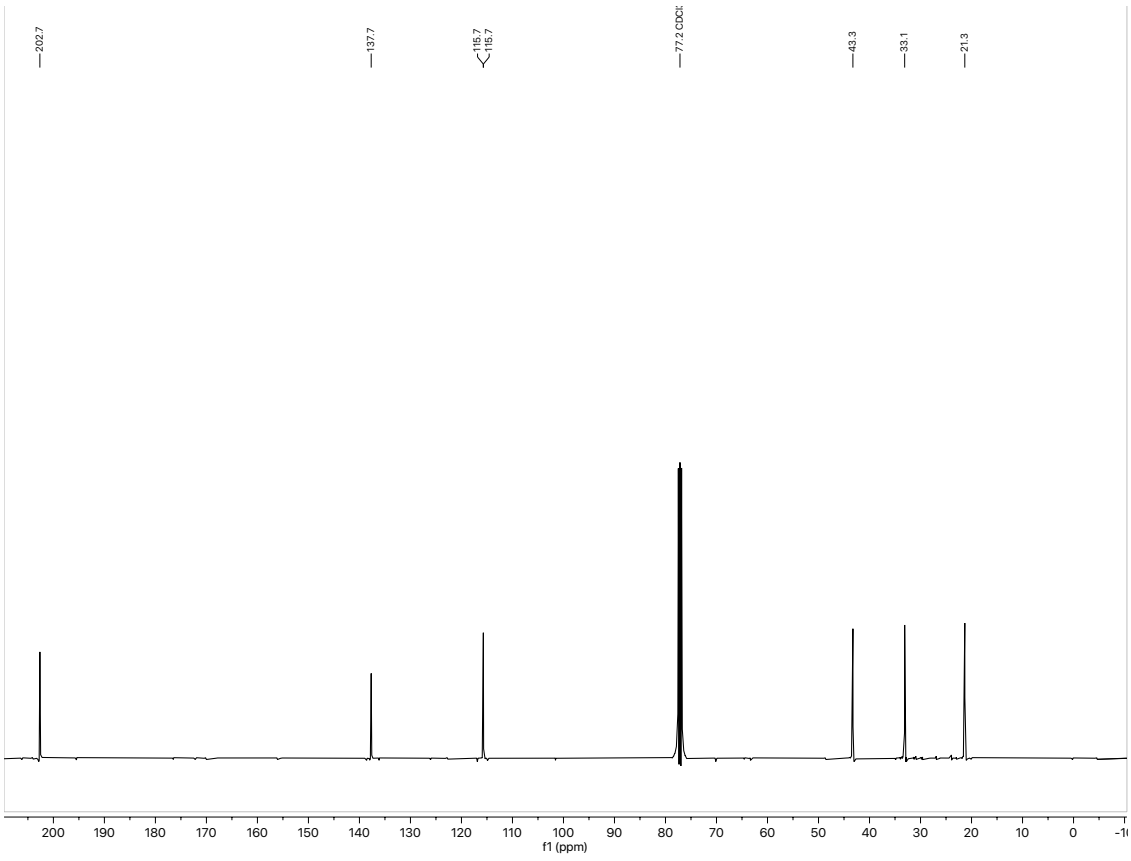

NMR for Crimmin's Auxiliary:

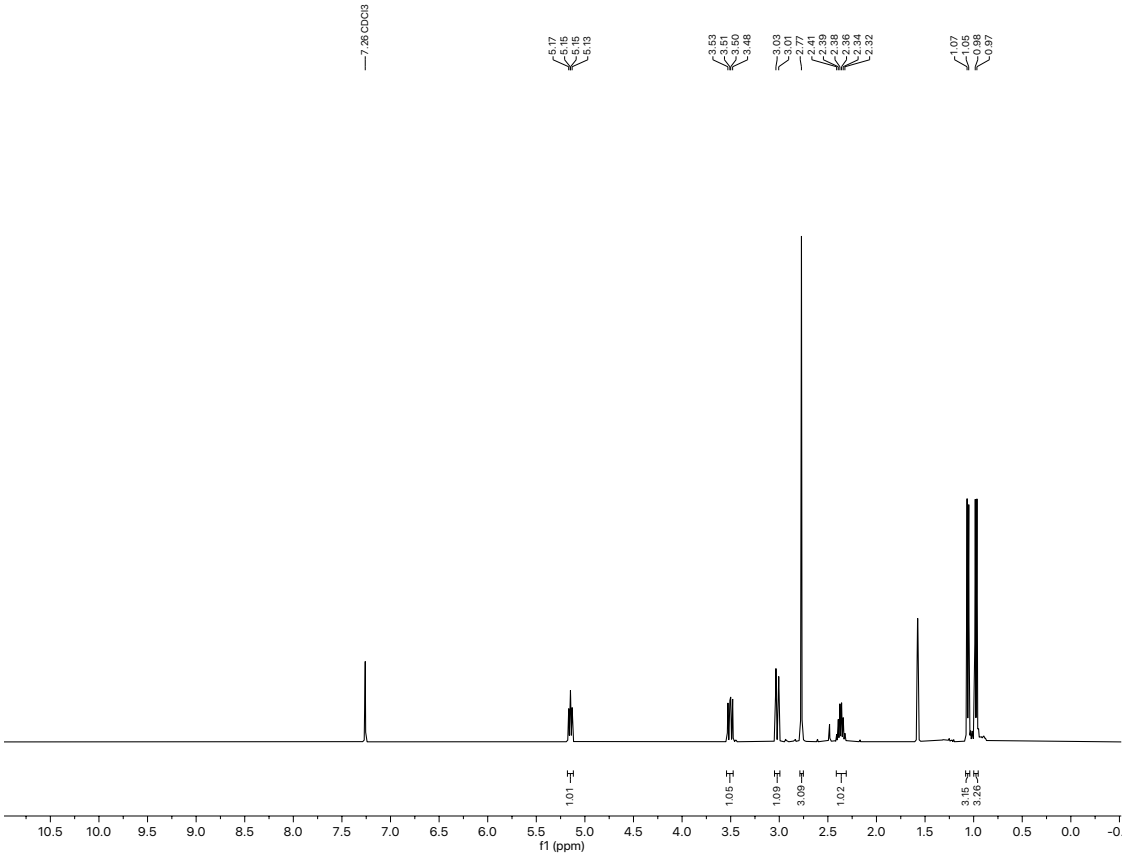

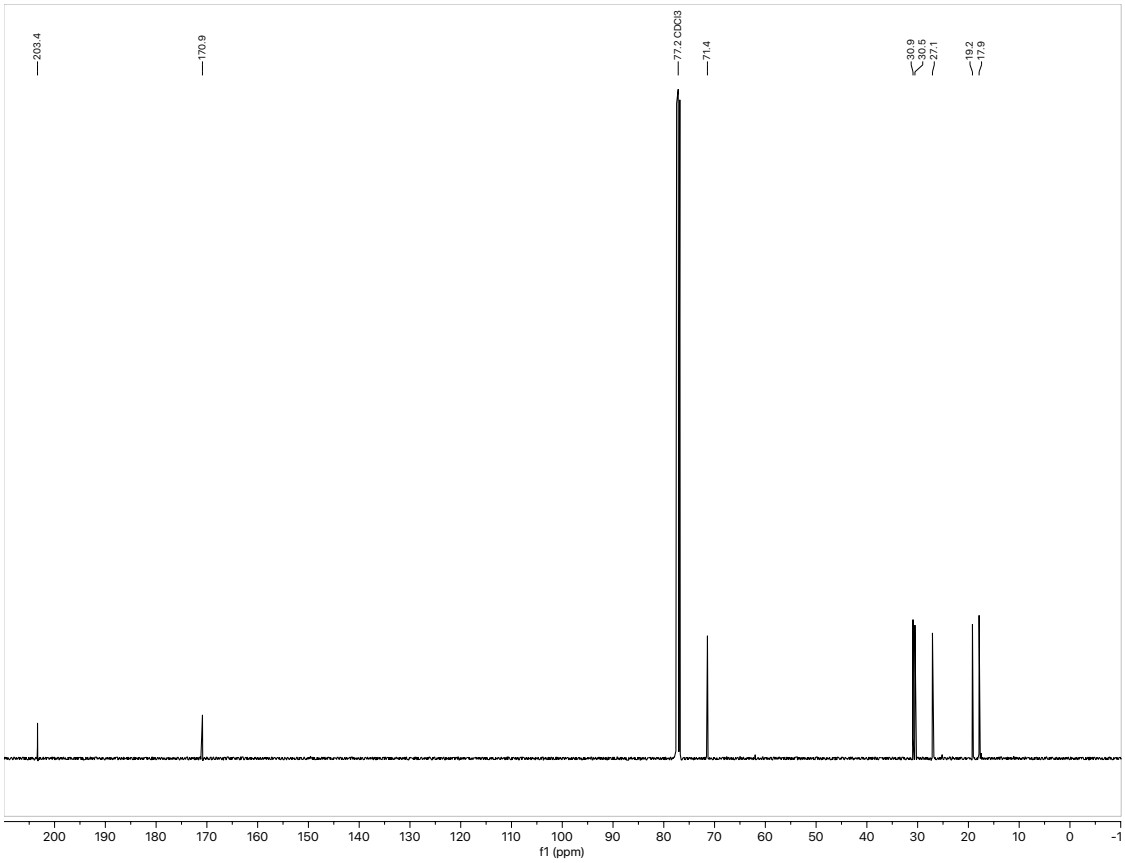

NMR for 10


OH
O
S
N
S
f1 (ppm)

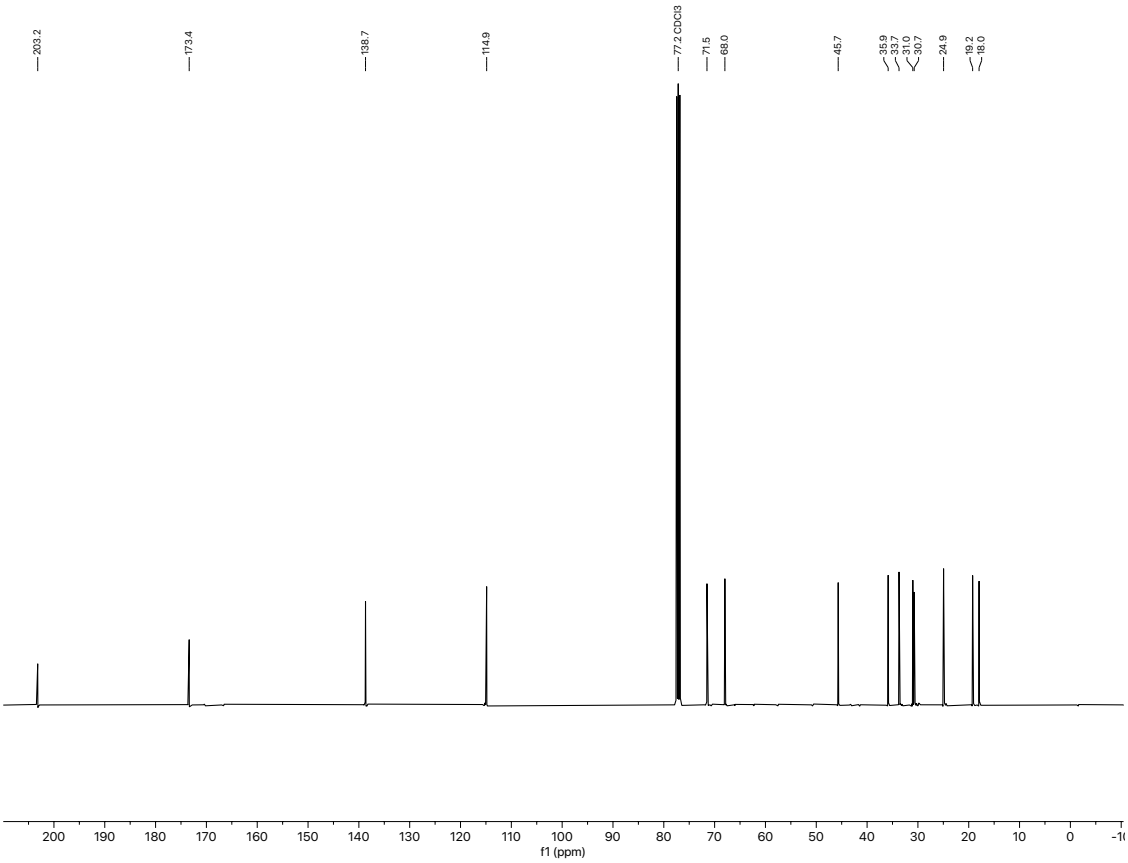
203.2
173.4
138.7
114.9
77.2 CDCl3
71.5
68.0
45.7
35.9
33.7
31.0
30.7
24.9
19.2
18.0
f1 (ppm)

NMR for 11:

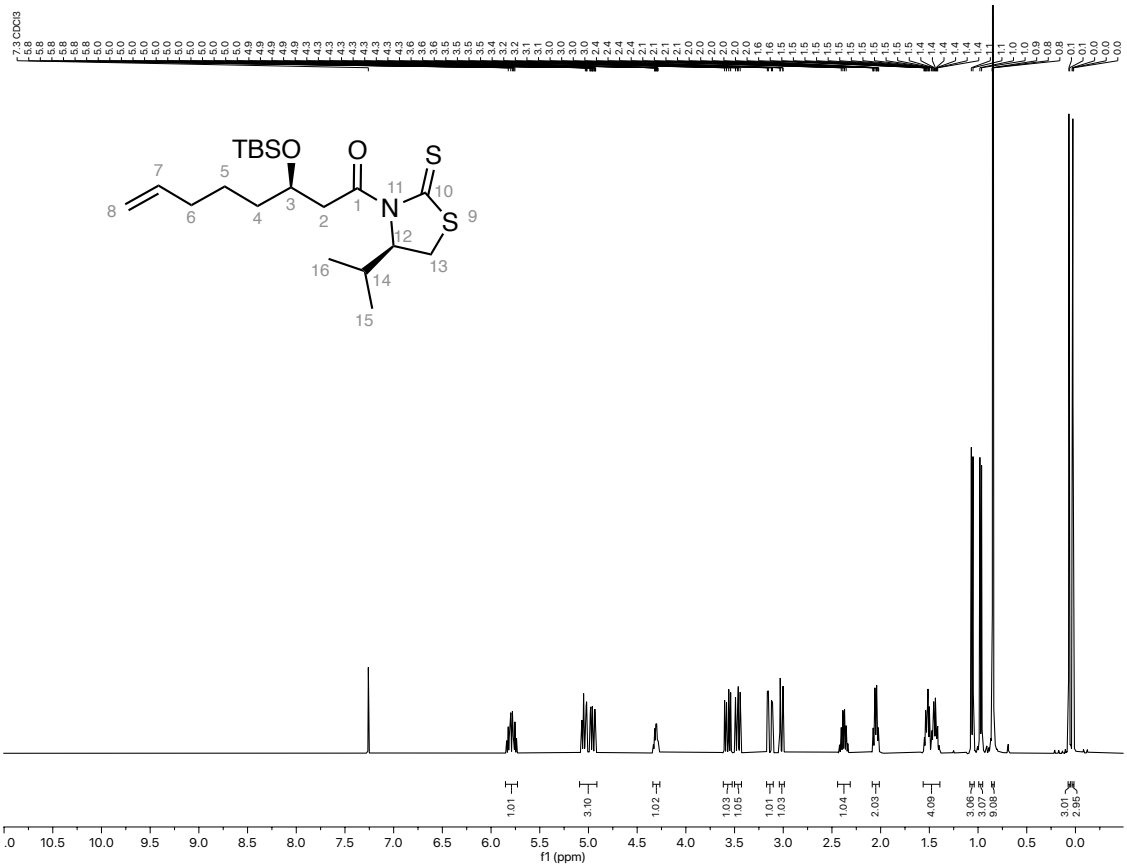
TBSO
O
S
N
S
1
2
3
4
5
6
7
8
9
10
11
12
13
14
15
16
f1 (ppm)

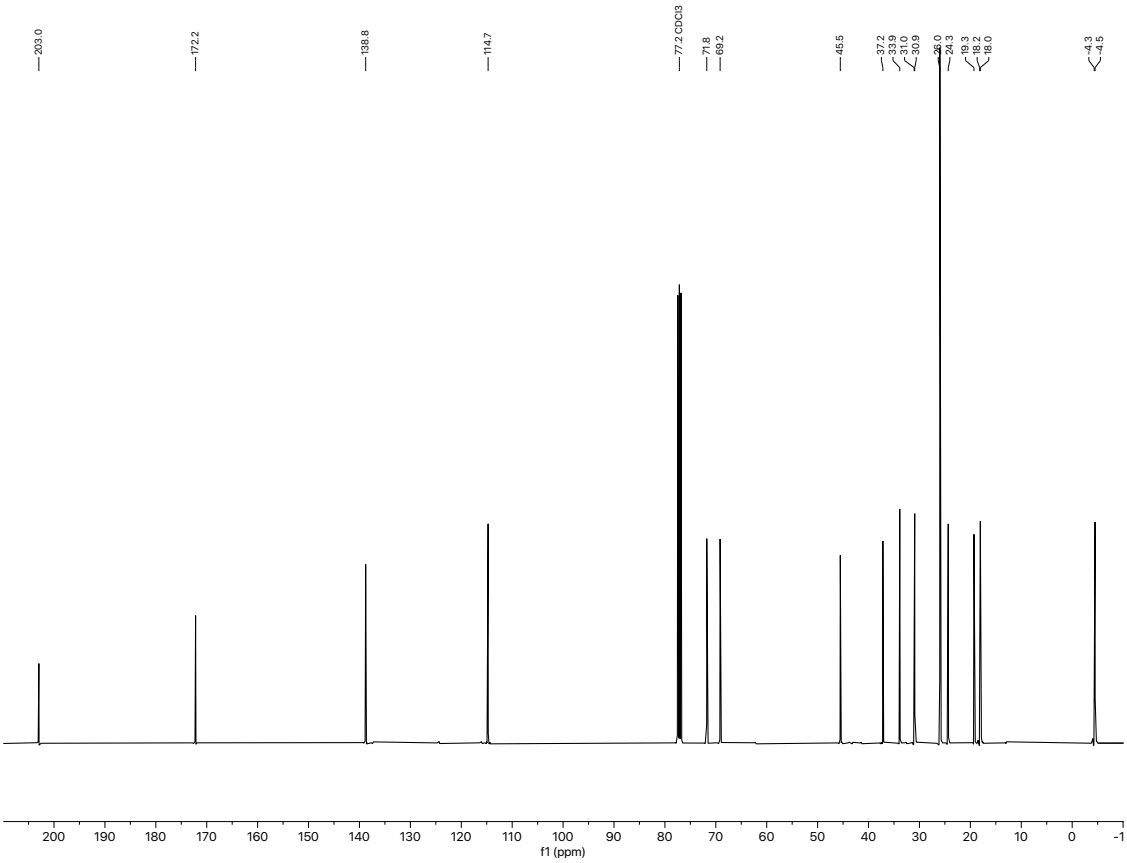
203.0
172.2
138.8
114.7
77.2 CDCl3
71.8
69.2
45.5
37.2
33.9
31.0
30.9
26.0
24.3
19.3
18.2
18.0
-4.3
-4.5
f1 (ppm)

NMR for 12:

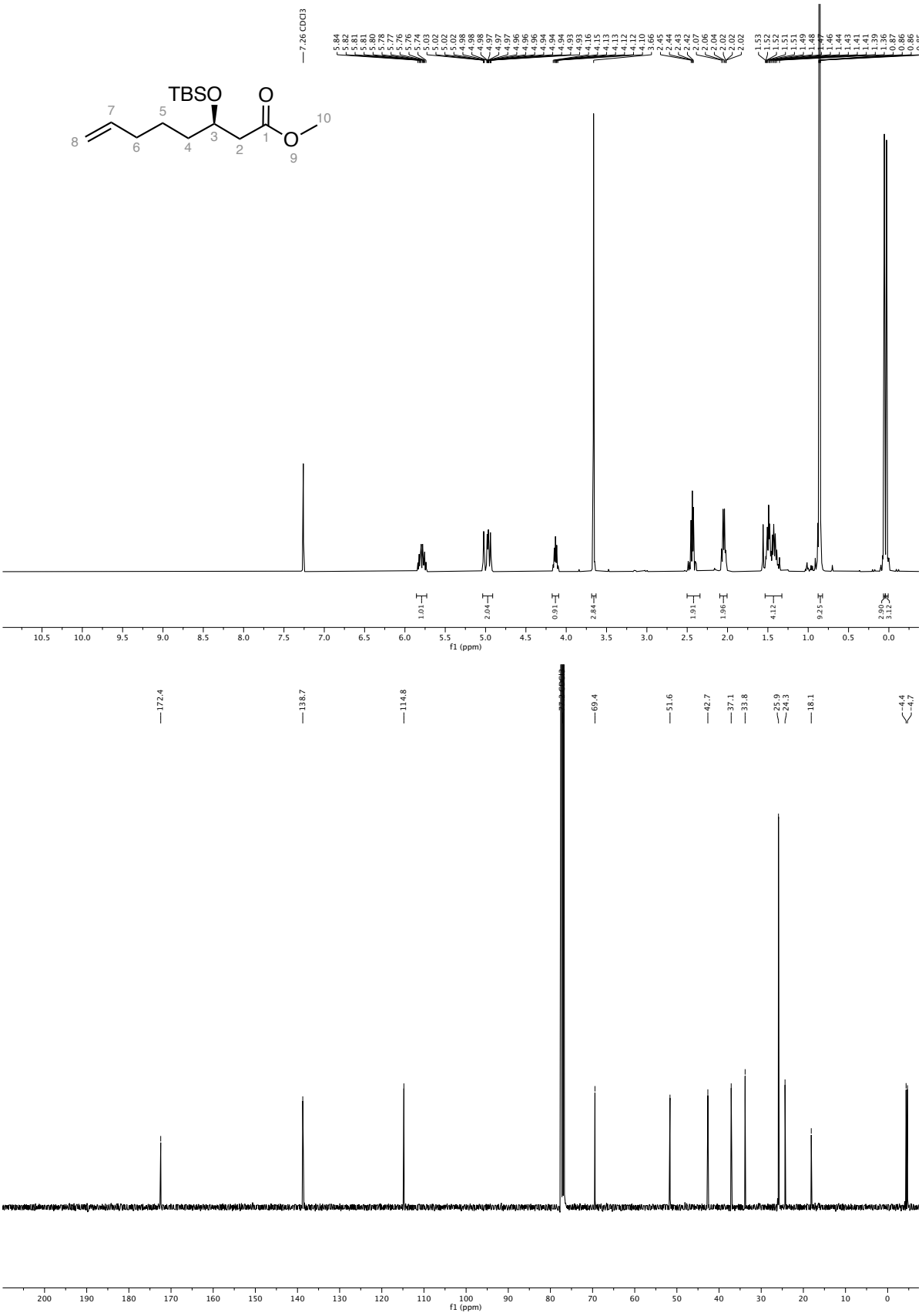

NMR for 7:


9.81
9.81
9.80
7.26 CDCl3
5.83
5.82
5.81
5.80
5.79
5.77
5.77
5.76
5.75
5.73
5.03
5.02
5.02
4.98
4.98
4.97
4.97
4.95
4.95
4.94
4.21
4.20
4.19
4.17
4.16
2.53
2.52
2.51
2.51
2.08
2.08
2.06
2.04
2.03
2.03
2.02
2.02
1.59
1.57
1.56
1.54
1.54
1.53
1.52
1.51
1.49
1.49
1.48
1.47
1.46
1.45
1.44
1.43
1.42
1.41
1.41
1.39
1.37
0.87
0.07
TBSO
O
H
1
2
3
4
5
6
7
8
0.89
1.01
2.07
0.90
1.81
2.07
4.45
9.93
2.88
3.07
f1 (ppm)

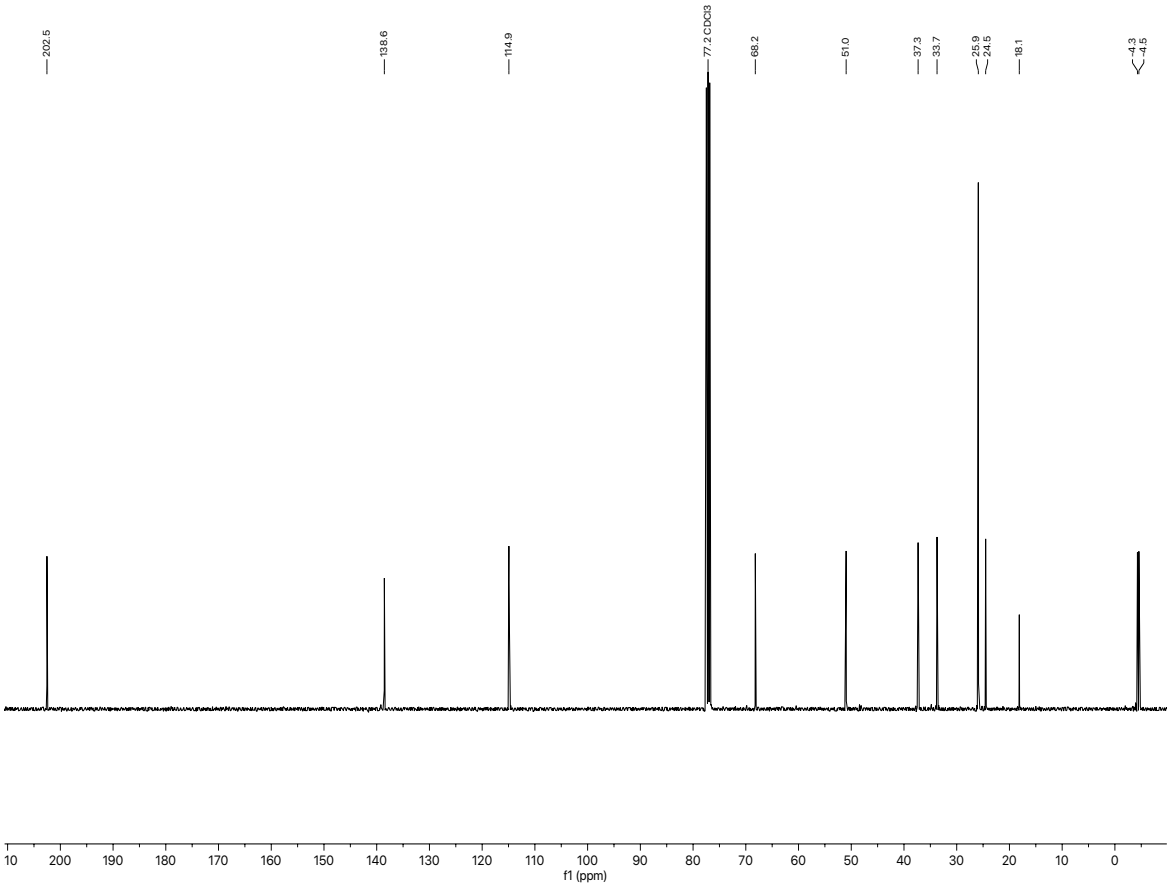
202.5
138.6
114.9
77.2 CDCl3
68.2
51.0
37.3
33.7
25.9
24.5
18.1
-4.3
-4.5
f1 (ppm)

NMR for 13:

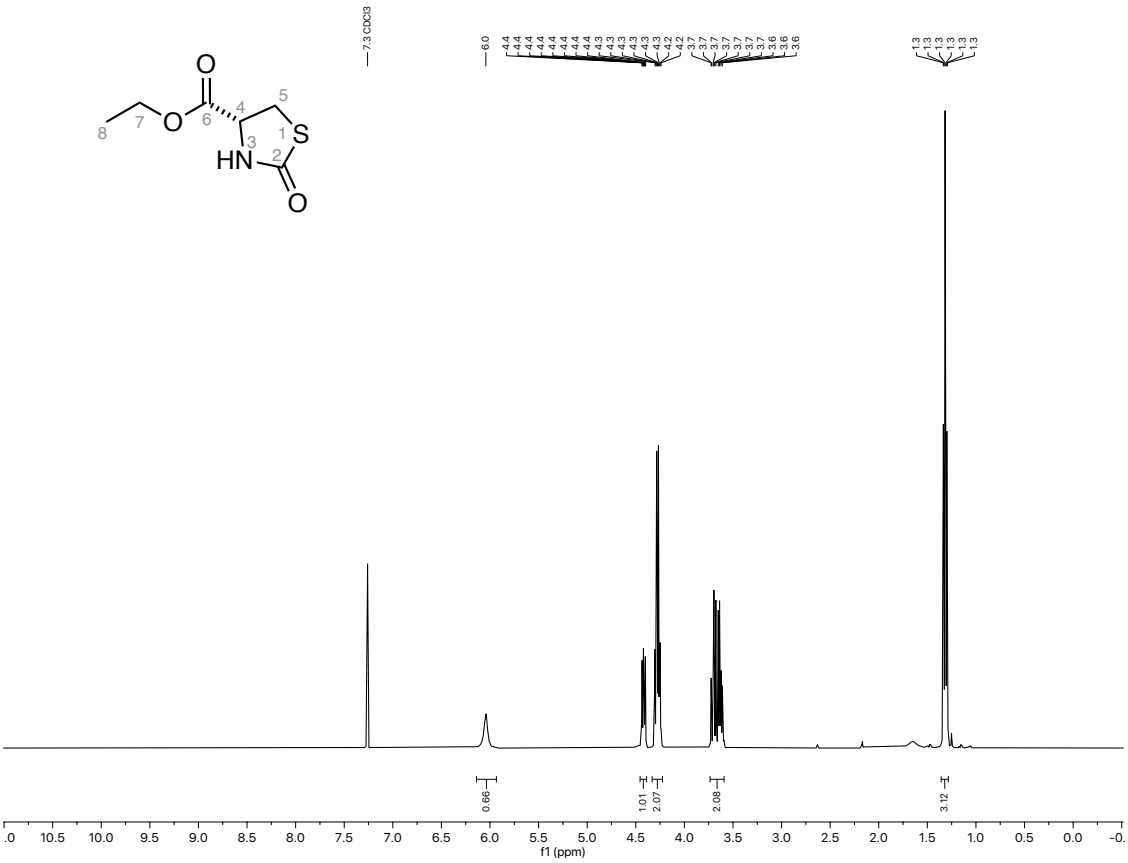
7.3 CDCl3
6.0
4.4
4.3
4.2
3.7
3.6
1.3
0.66
1.01
2.07
2.08
3.12
f1 (ppm)

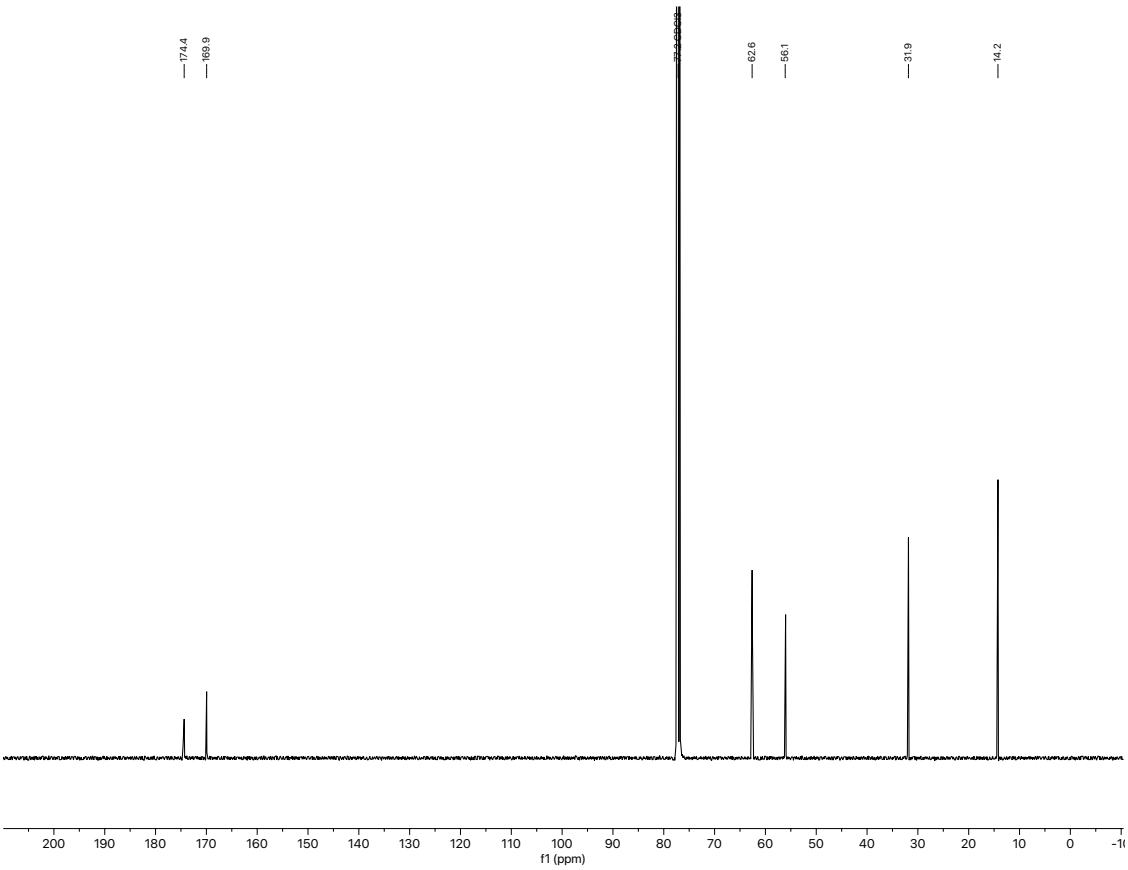
174.4
169.9
77.3 CDCl3
62.6
56.1
31.9
14.2
f1 (ppm)

NMR for 14:

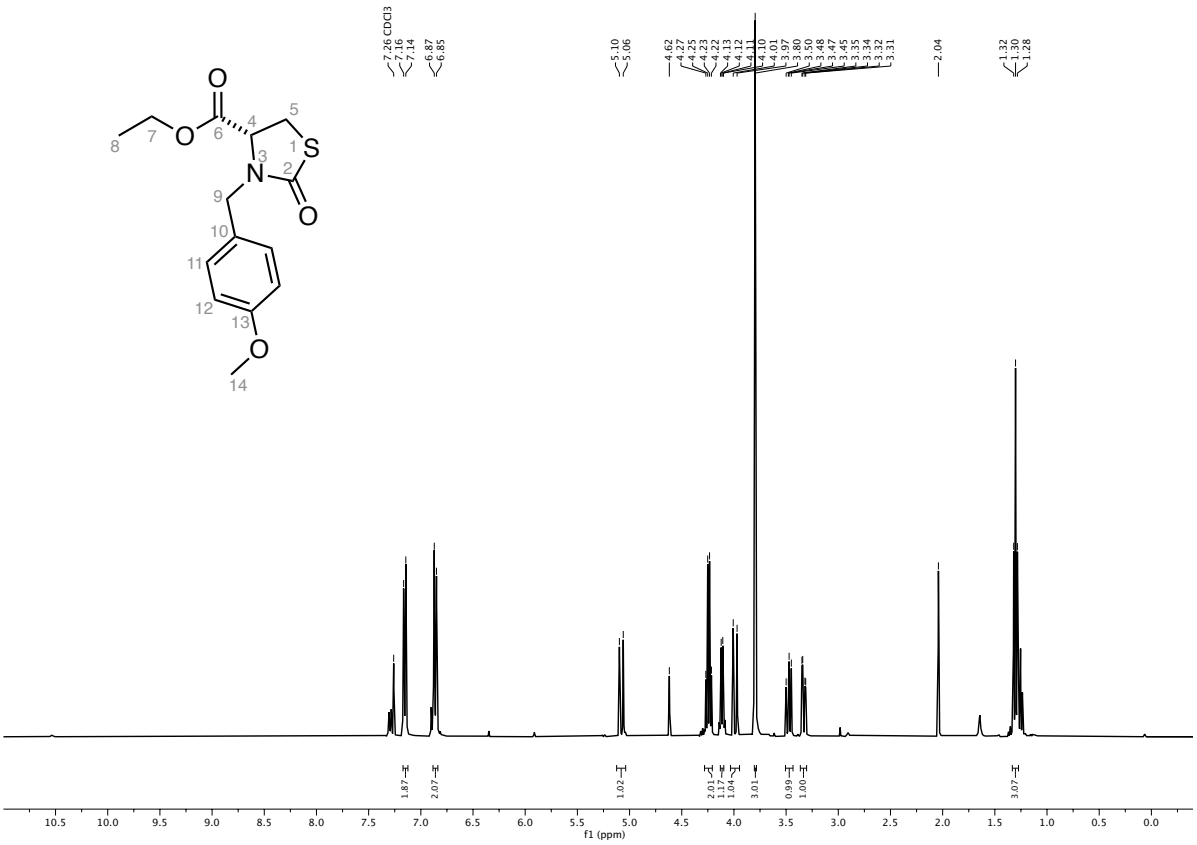
7.26 CDCl3
7.16
7.14
6.87
6.85
5.10
5.06
4.62
4.27
4.25
4.23
4.22
4.13
4.12
4.10
4.01
3.97
3.80
3.50
3.48
3.47
3.45
3.35
3.34
3.32
3.31
2.04
1.32
1.30
1.28
1.87
2.07
1.02
2.01
1.17
1.04
3.01
0.99
1.00
3.07
f1 (ppm)

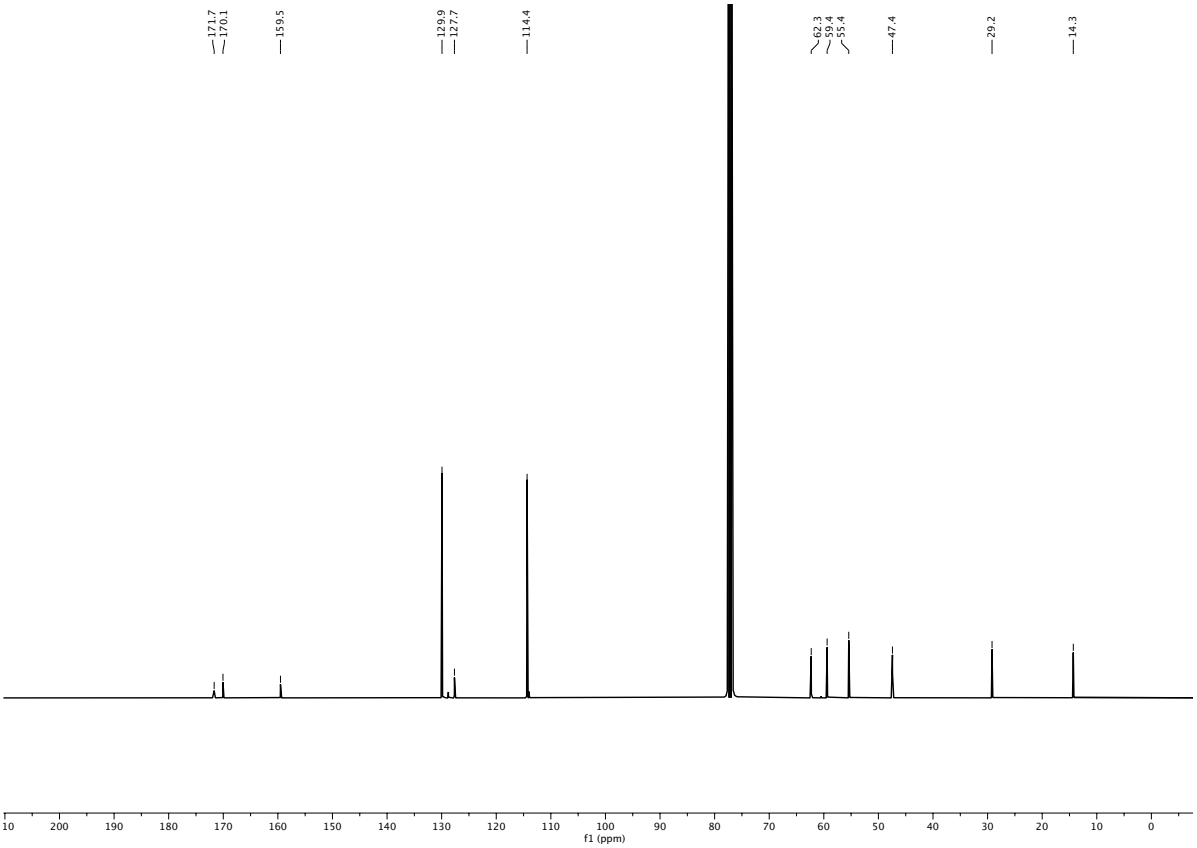
171.7
170.1
159.5
129.9
127.7
114.4
62.3
59.4
55.4
47.4
29.2
14.3
f1 (ppm)

NMR for 15:

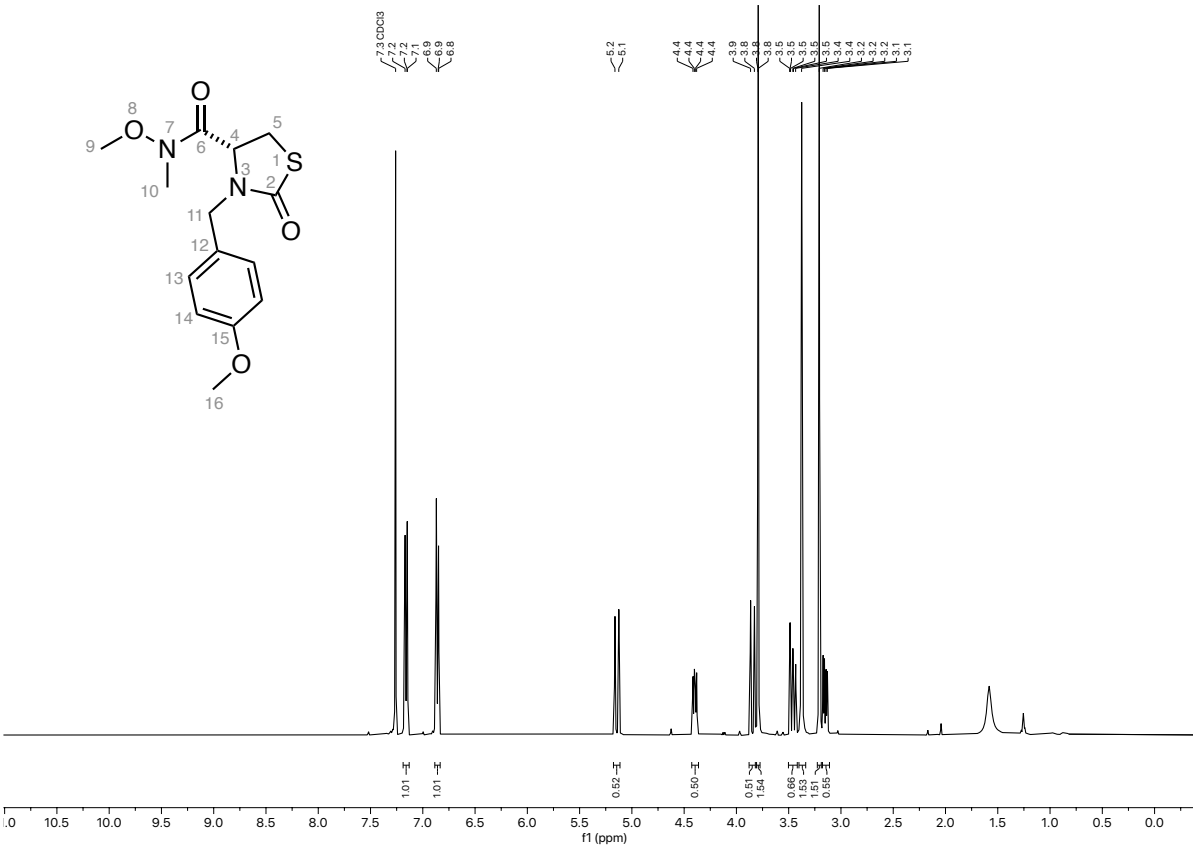
7.3 CDCl3
7.2
7.2
7.1
6.9
6.9
6.8
5.2
5.1
4.4
4.4
4.4
4.4
3.9
3.8
3.8
3.8
3.5
3.5
3.5
3.5
3.5
3.4
3.4
3.2
3.2
3.2
3.1
3.1
1.01
1.01
0.52
0.50
0.51
1.54
0.66
1.53
1.51
0.55
f1 (ppm)

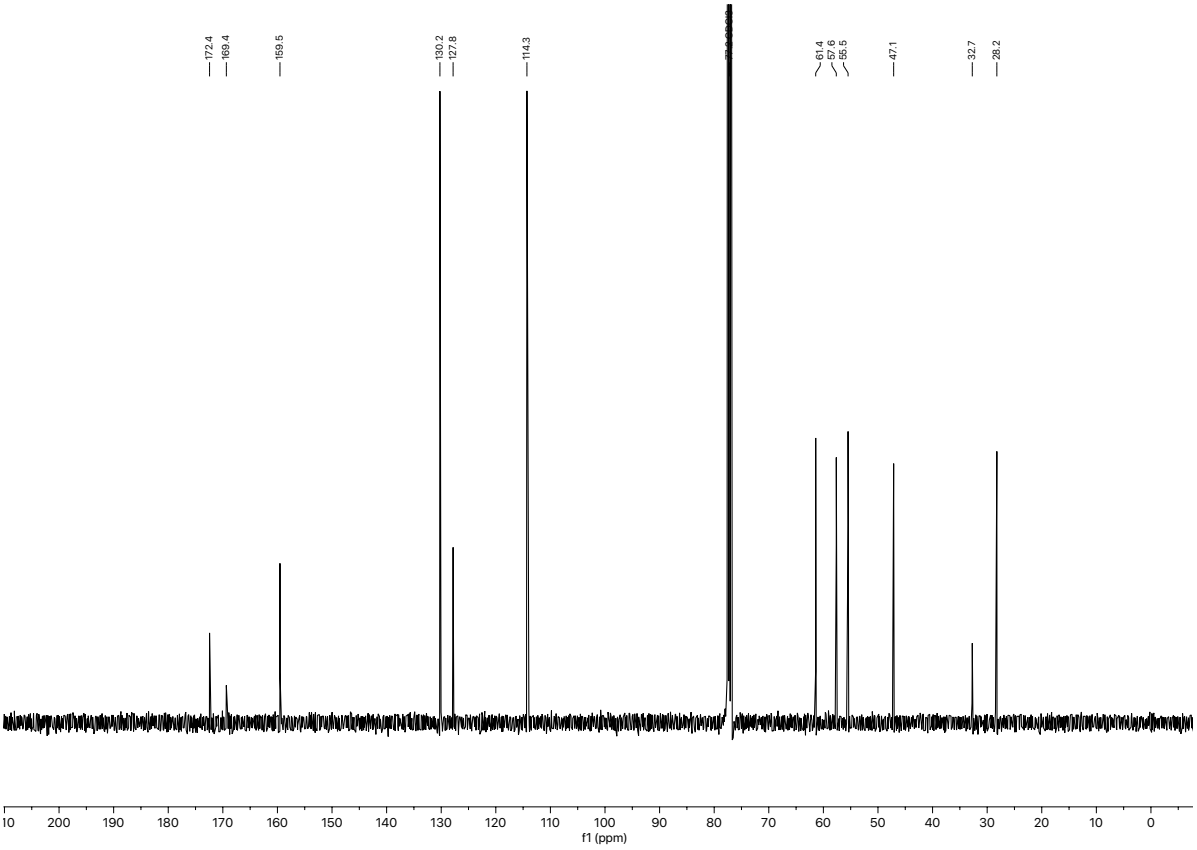
172.4
169.4
159.5
130.2
127.8
114.3
61.4
57.6
55.5
47.1
32.7
28.2
f1 (ppm)

NMR for 8:

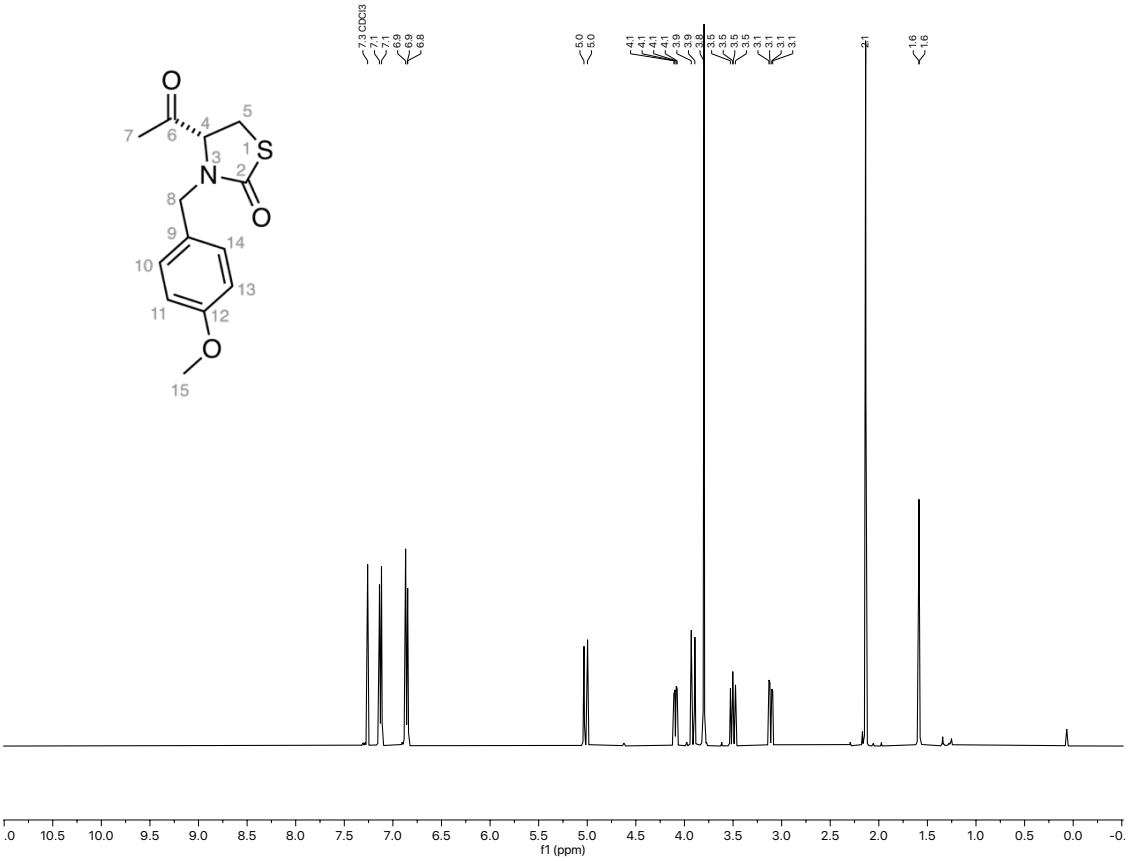
7.3 CDCl3
7.1
7.1
6.9
6.9
6.8
5.0
5.0
4.1
4.1
4.1
4.1
3.9
3.9
3.8
3.5
3.5
3.5
3.5
3.1
3.1
3.1
2.1
1.6
1.6
f1 (ppm)

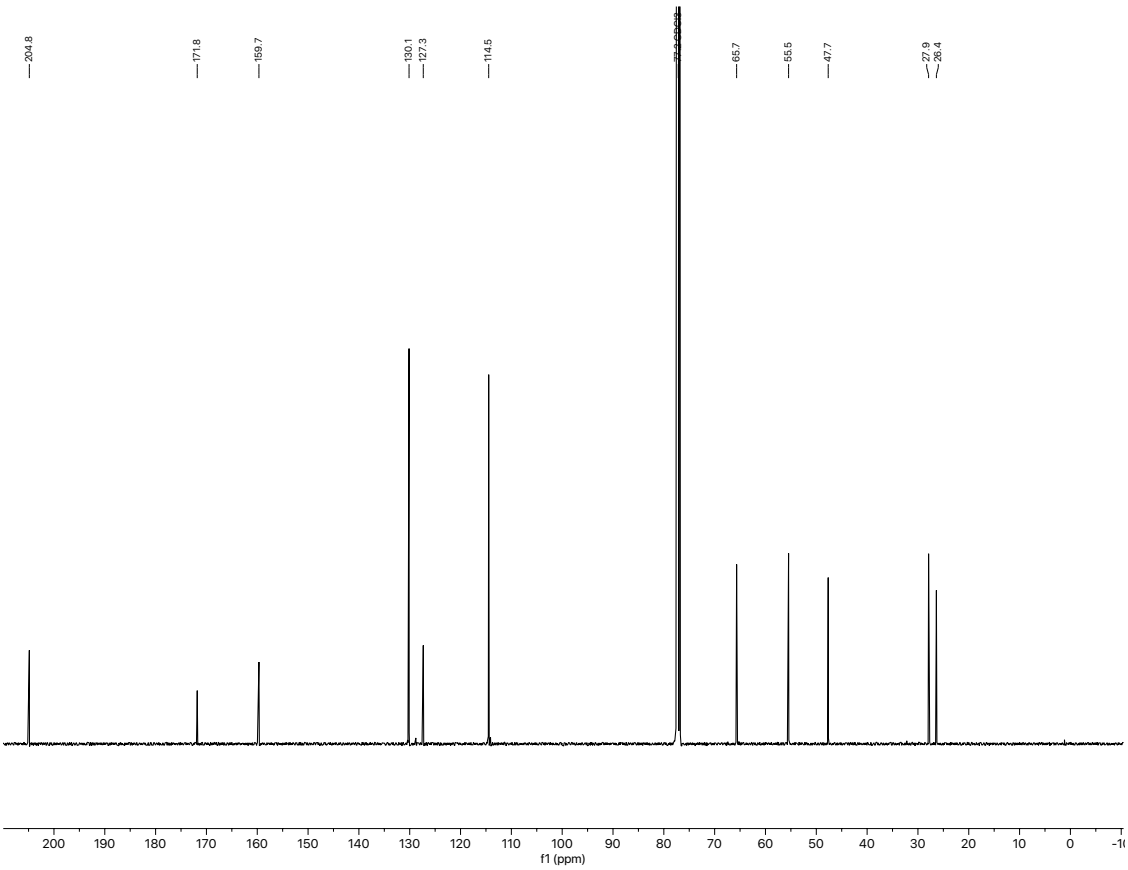
204.8
171.8
159.7
130.1
127.3
114.5
77.3 CDCl3
65.7
55.5
47.7
27.9
26.4
f1 (ppm)

NMR for 16:

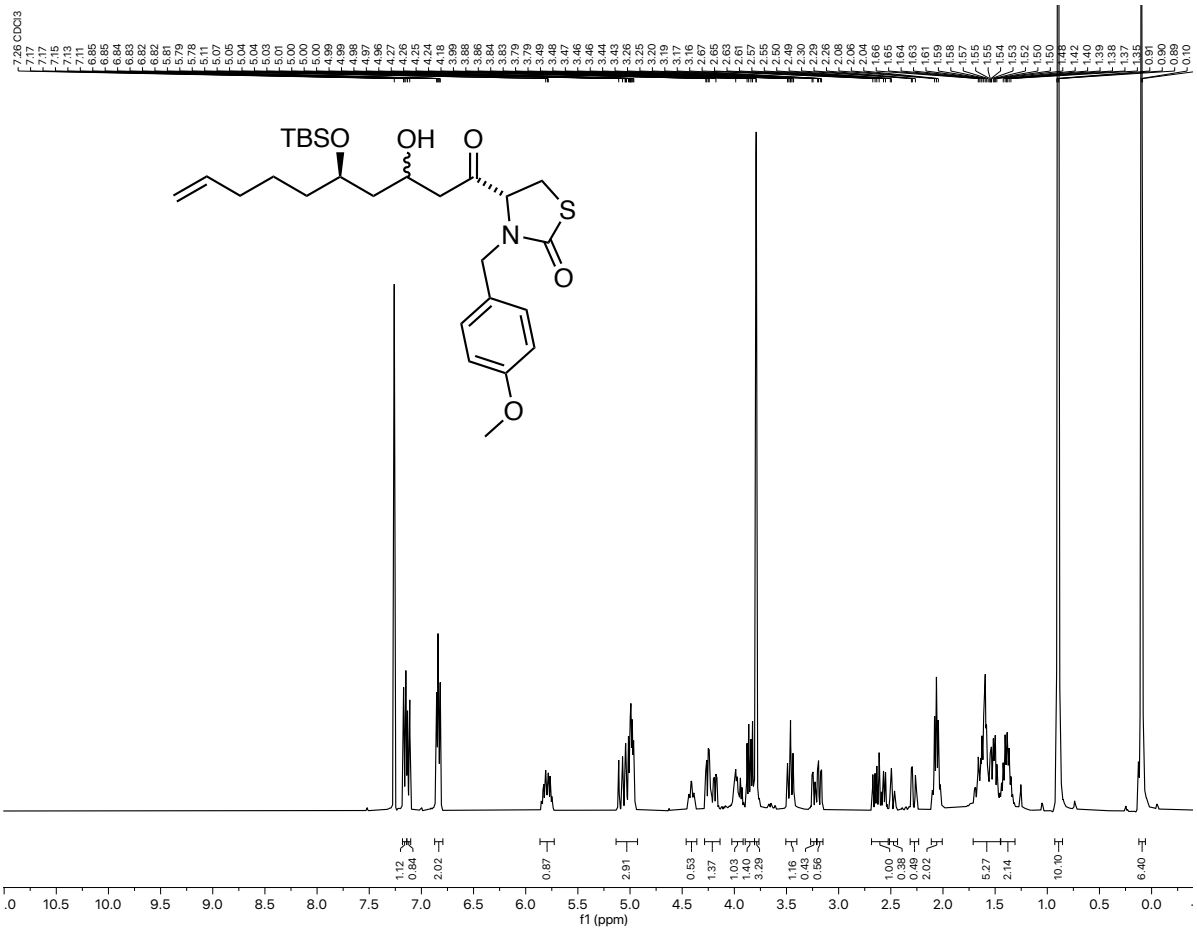

NMR for (*R*)-17:

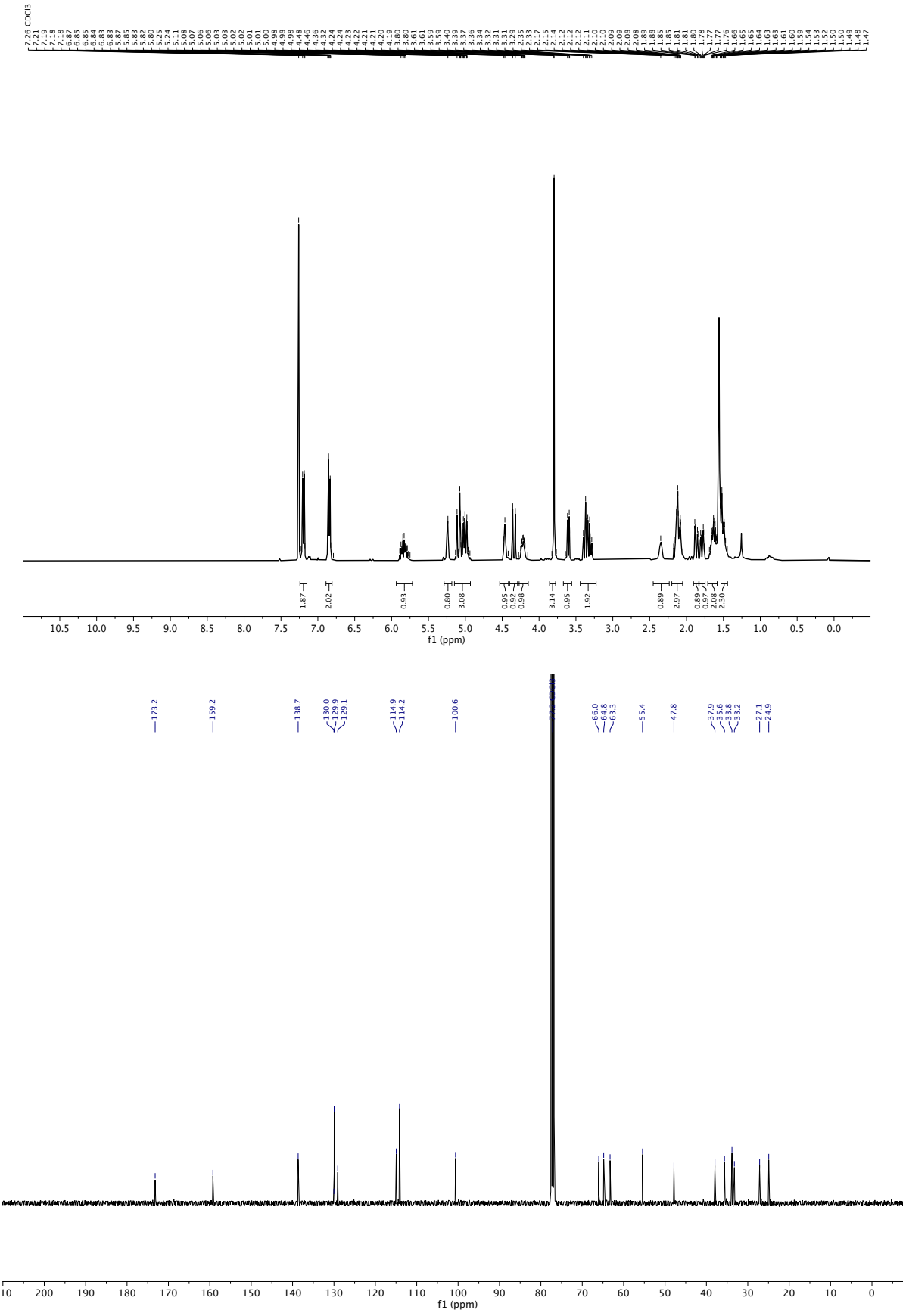
7.26 CDCl3
1.87
2.02
0.93
0.80
3.08
0.95
0.92
0.98
3.14
0.95
1.92
0.89
2.97
0.89
0.97
2.04
2.30
f1 (ppm)
173.2
159.2
138.7
130.0
129.9
129.1
114.9
114.2
100.6
66.0
64.8
63.3
55.4
47.8
37.9
35.6
33.8
33.2
27.1
24.9
f1 (ppm)

NMR for (*S*)-17

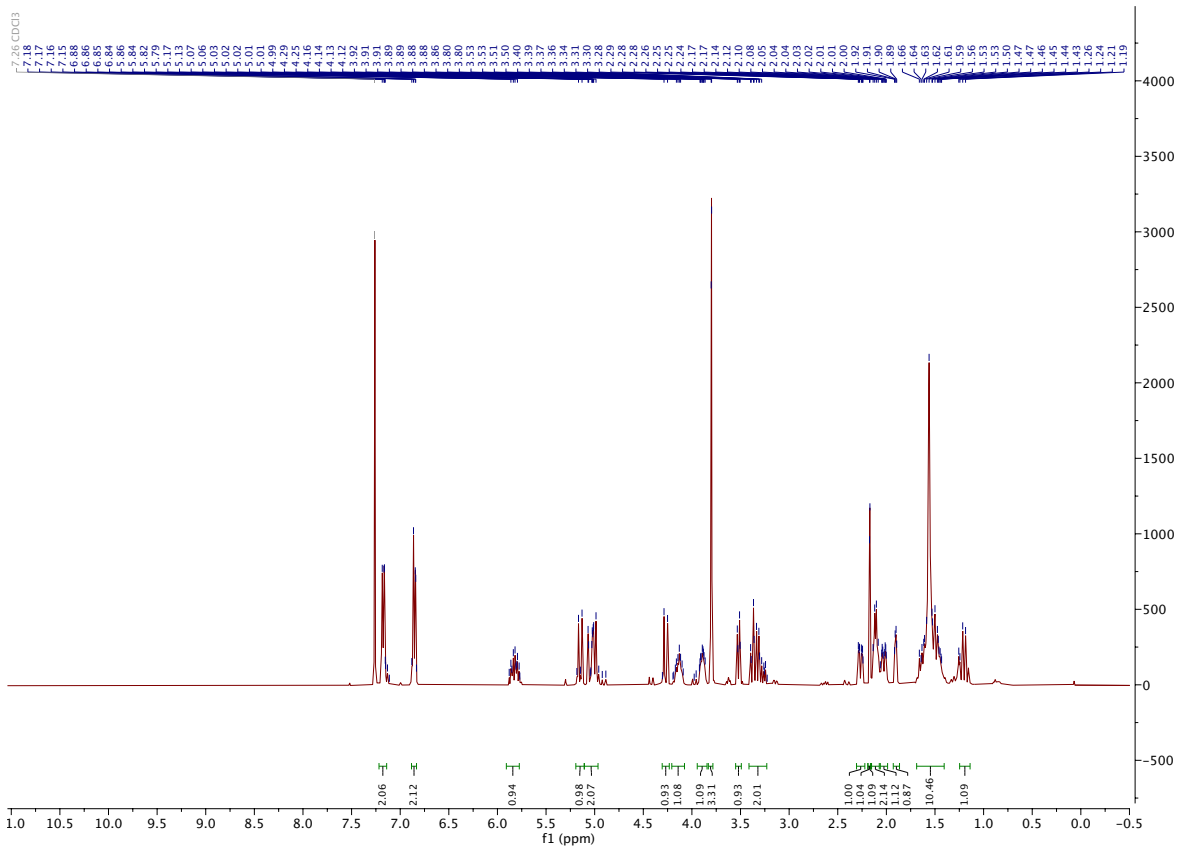

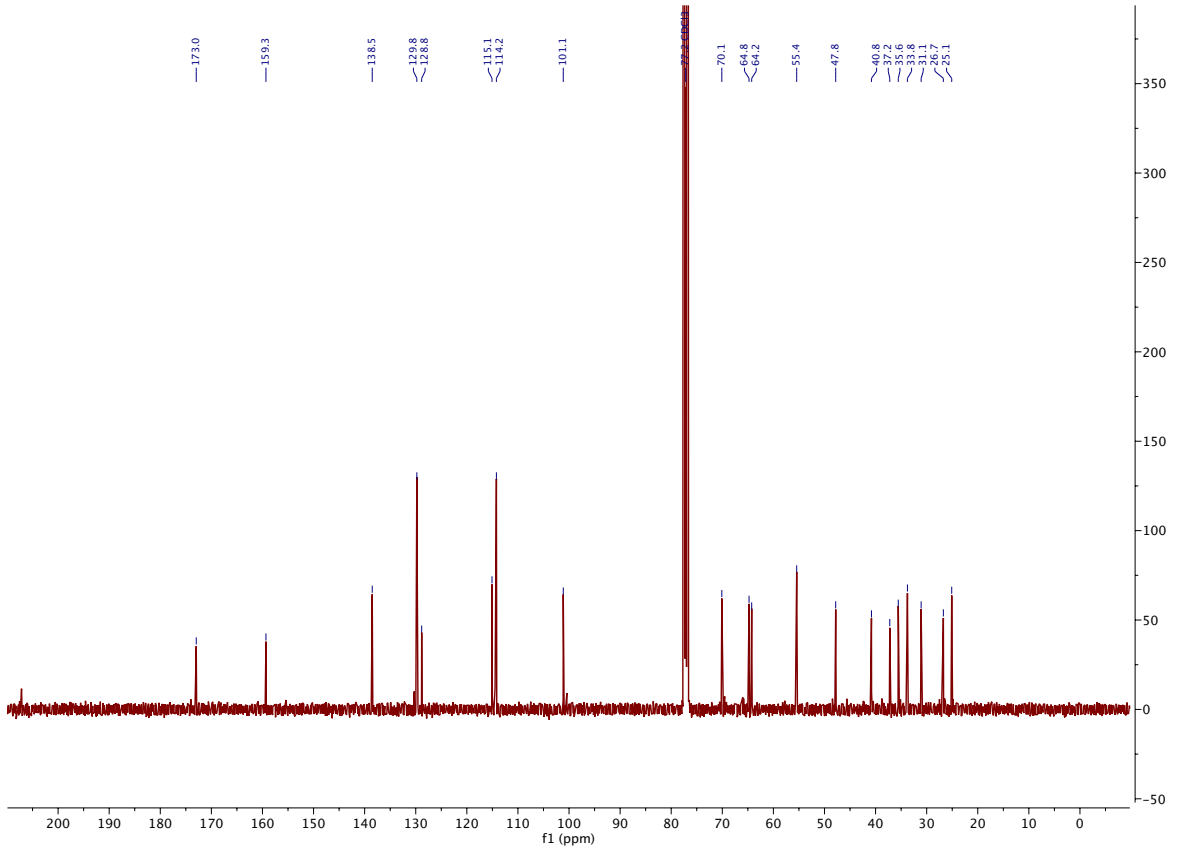

NMR for (*R*)-20:

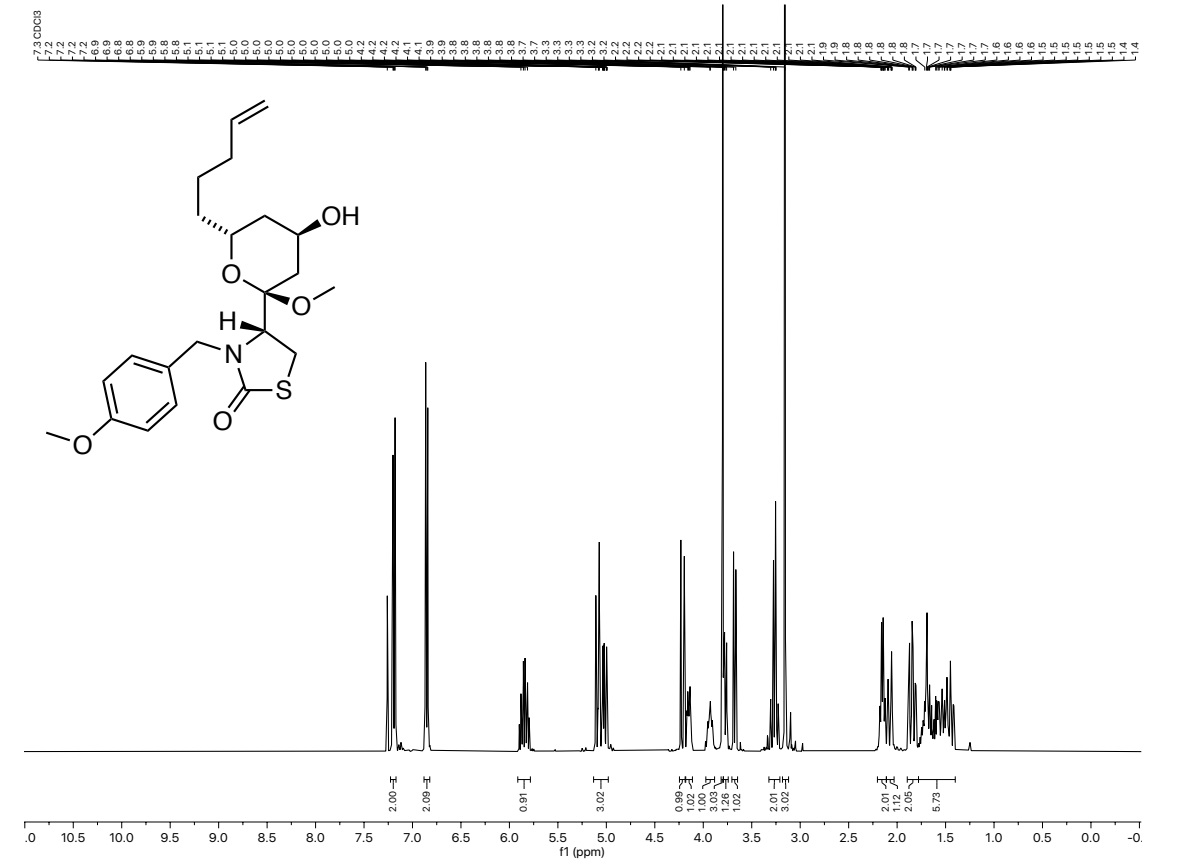
OH
O
O
H
N
S
O
O
f1 (ppm)

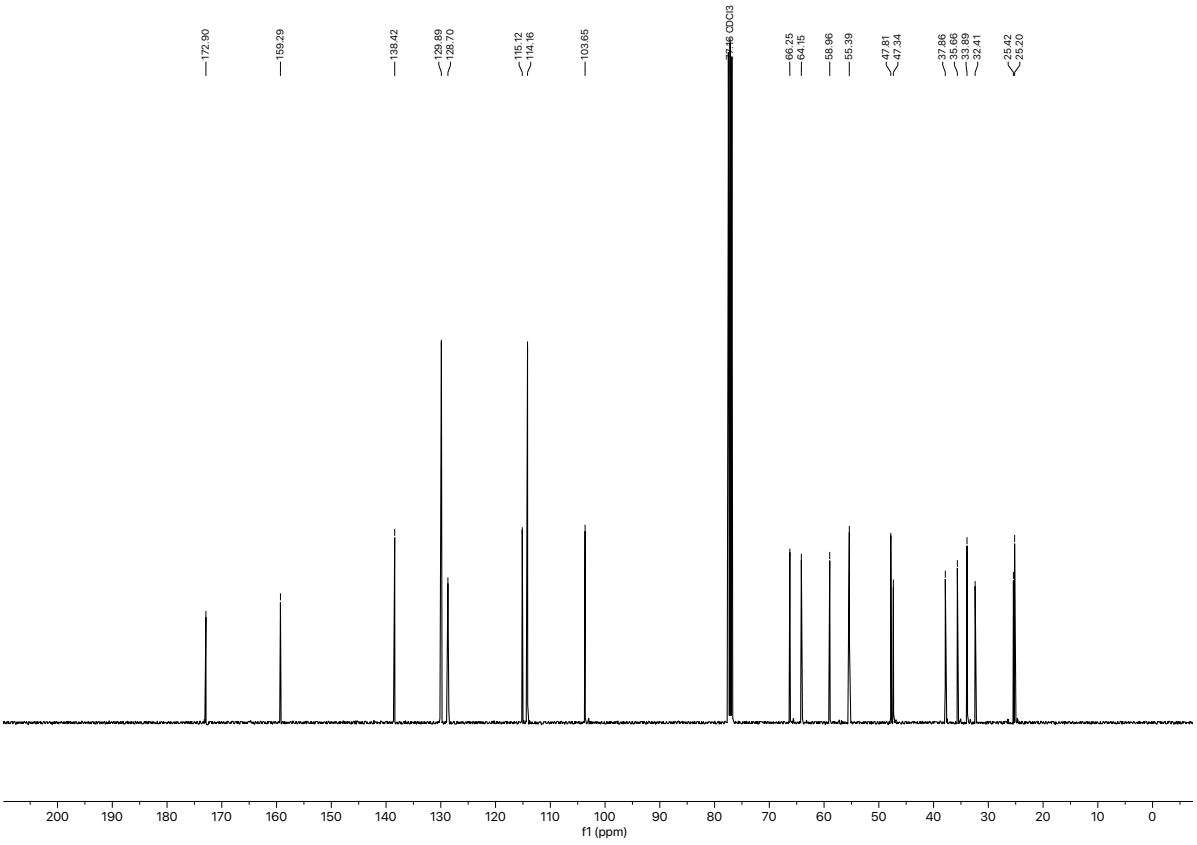
172.90
159.29
138.42
129.89
128.70
115.12
114.16
103.65
CDCl3
66.25
64.15
58.96
55.39
47.81
47.34
37.86
35.66
33.89
32.41
25.42
25.20
f1 (ppm)

NMR for (*S*)-20:

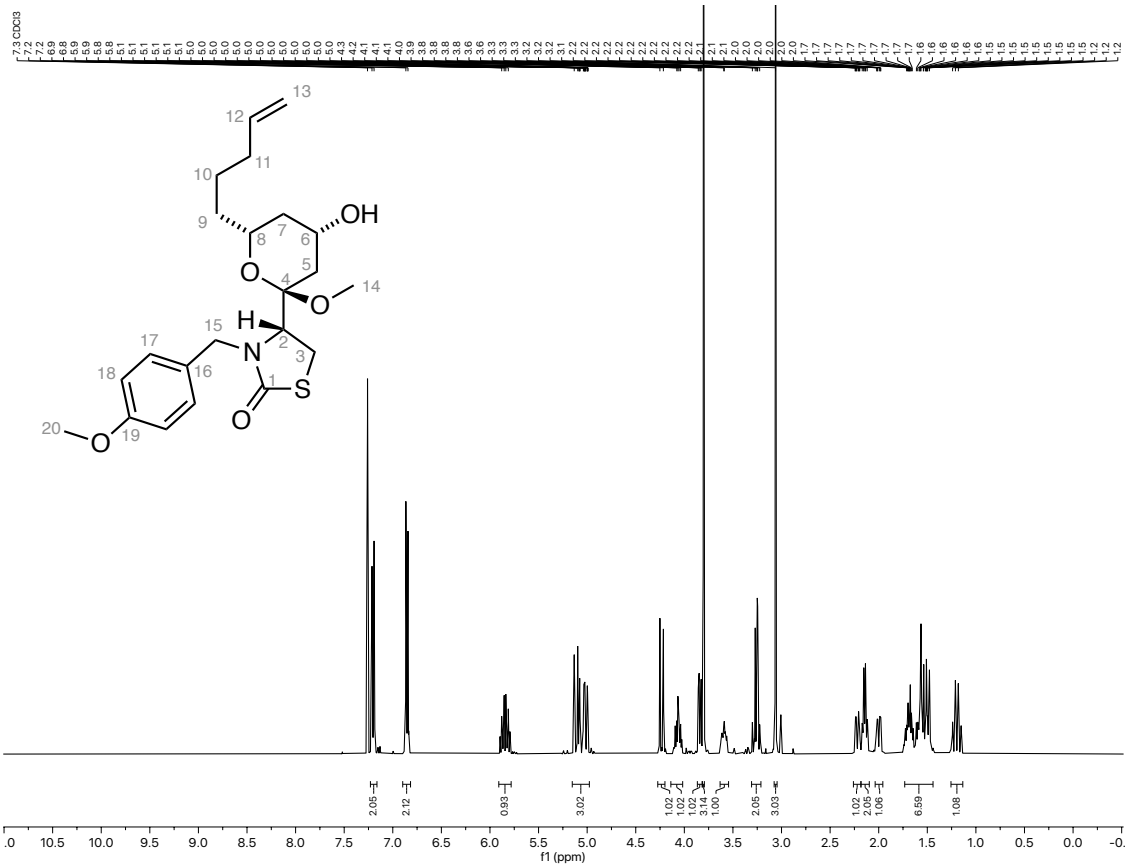
7.3 CDCl3
OH
O
O
H
N
S
O
O
f1 (ppm)

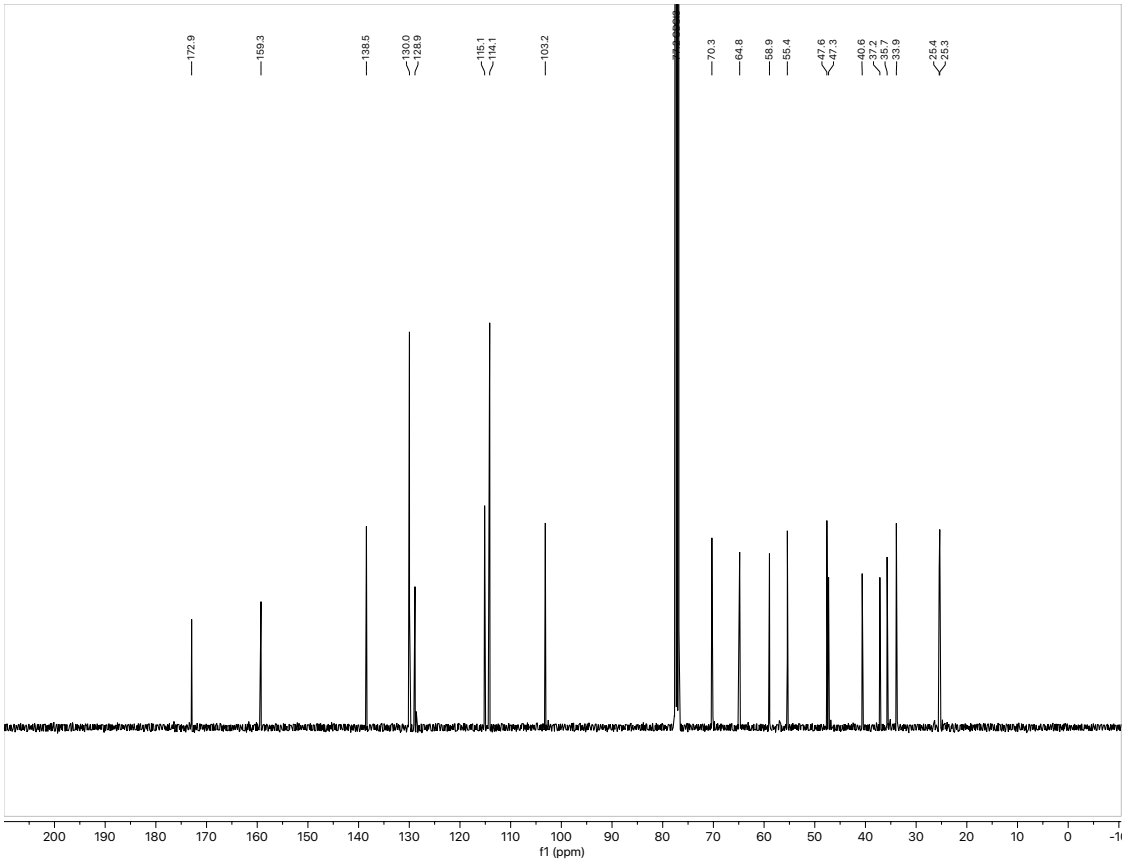
172.9
159.3
138.5
130.0
128.9
115.1
114.1
103.2
77.4 CDCl3
70.3
64.8
58.9
55.4
47.6
47.3
40.6
37.2
35.7
33.9
25.4
25.3
f1 (ppm)

NMR for 37:

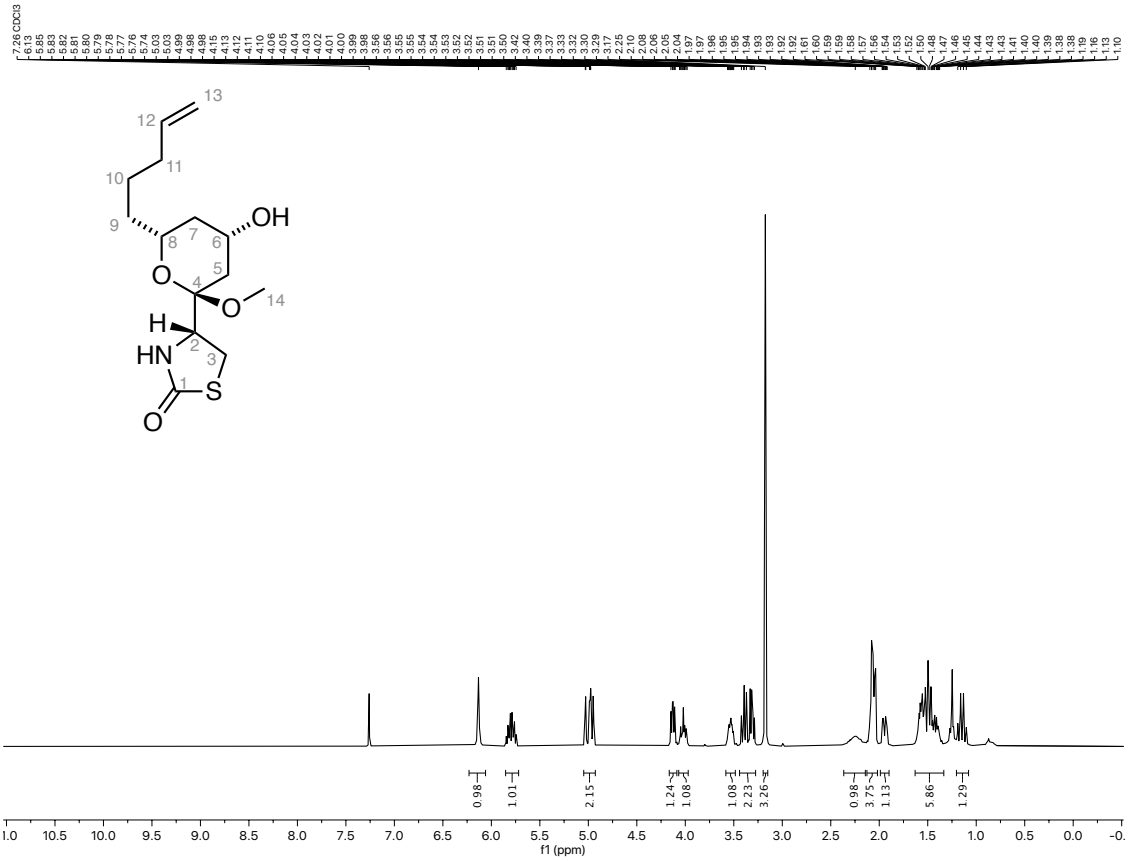
7.26 CDCl3
13
12
11
10
9
8
7
6
5
4
OH
O
O
14
H
HN
2
3
1
S
O
0.98
1.01
2.15
1.24
1.08
1.08
2.23
3.26
0.98
3.75
1.13
5.86
1.29
f1 (ppm)

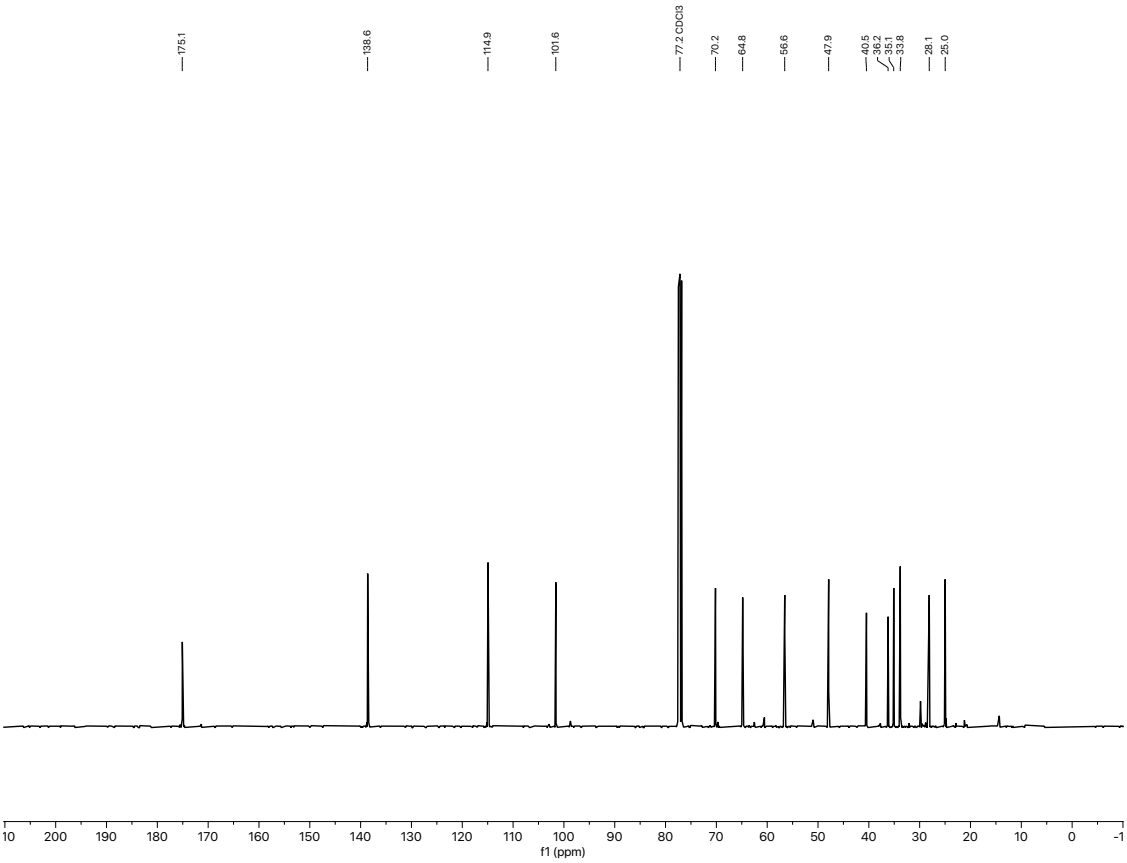
175.1
138.6
114.9
101.6
77.2 CDCl3
70.2
64.8
56.6
47.9
40.5
36.2
35.1
33.8
28.1
25.0
f1 (ppm)

NMR for 23:

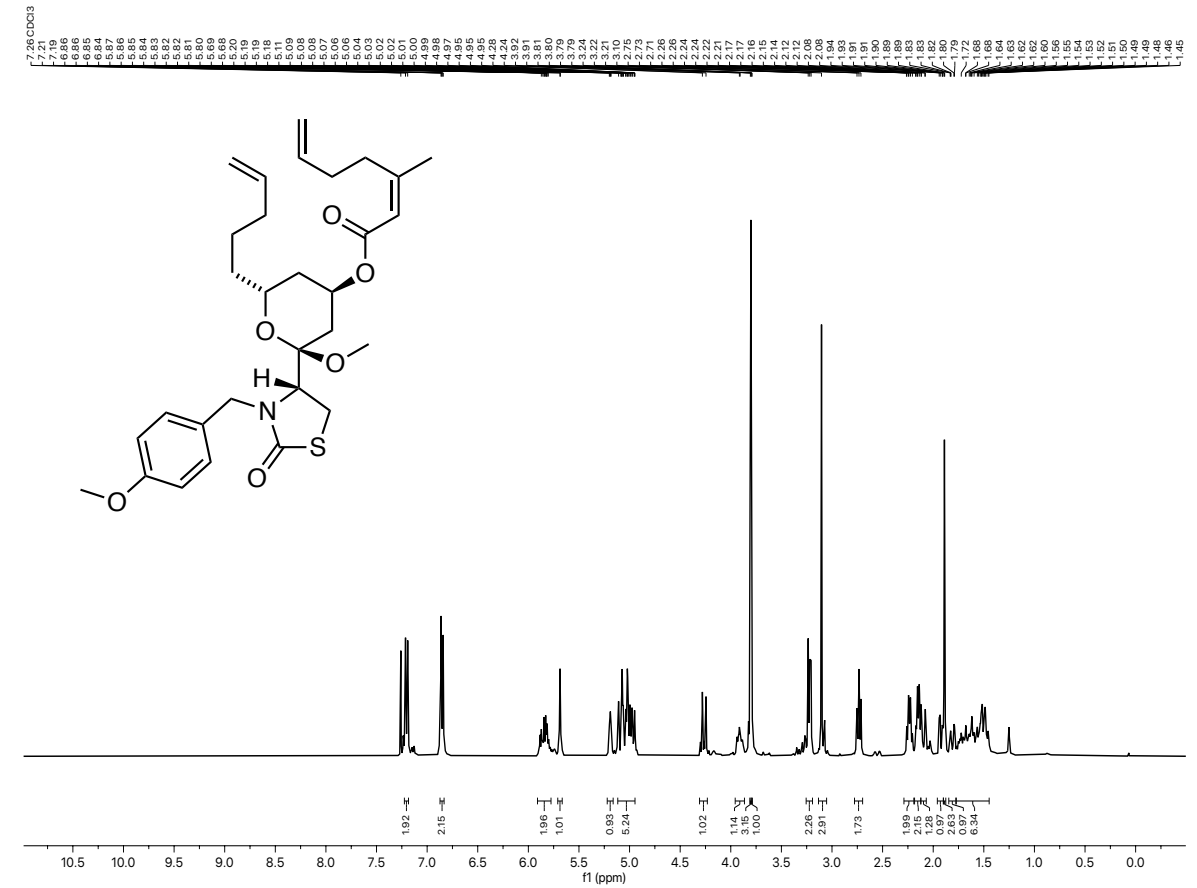

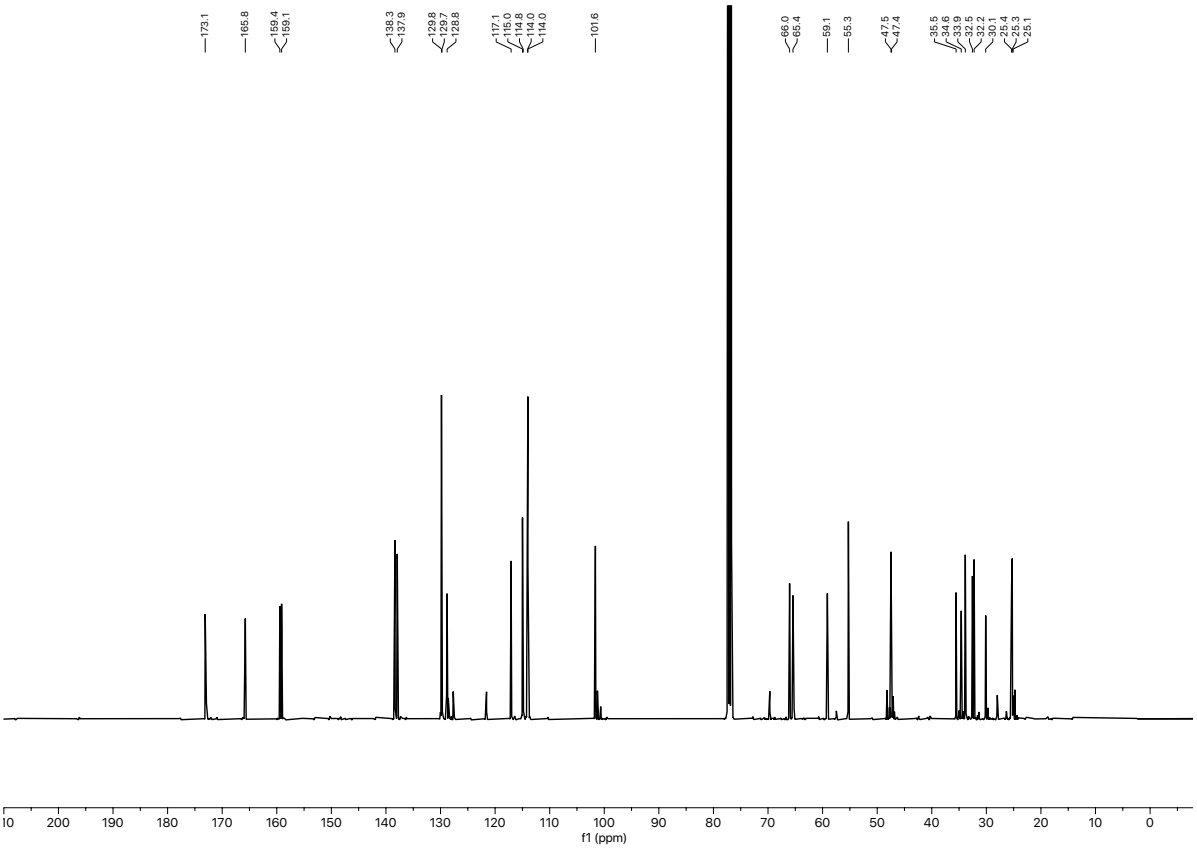

NMR for 24:

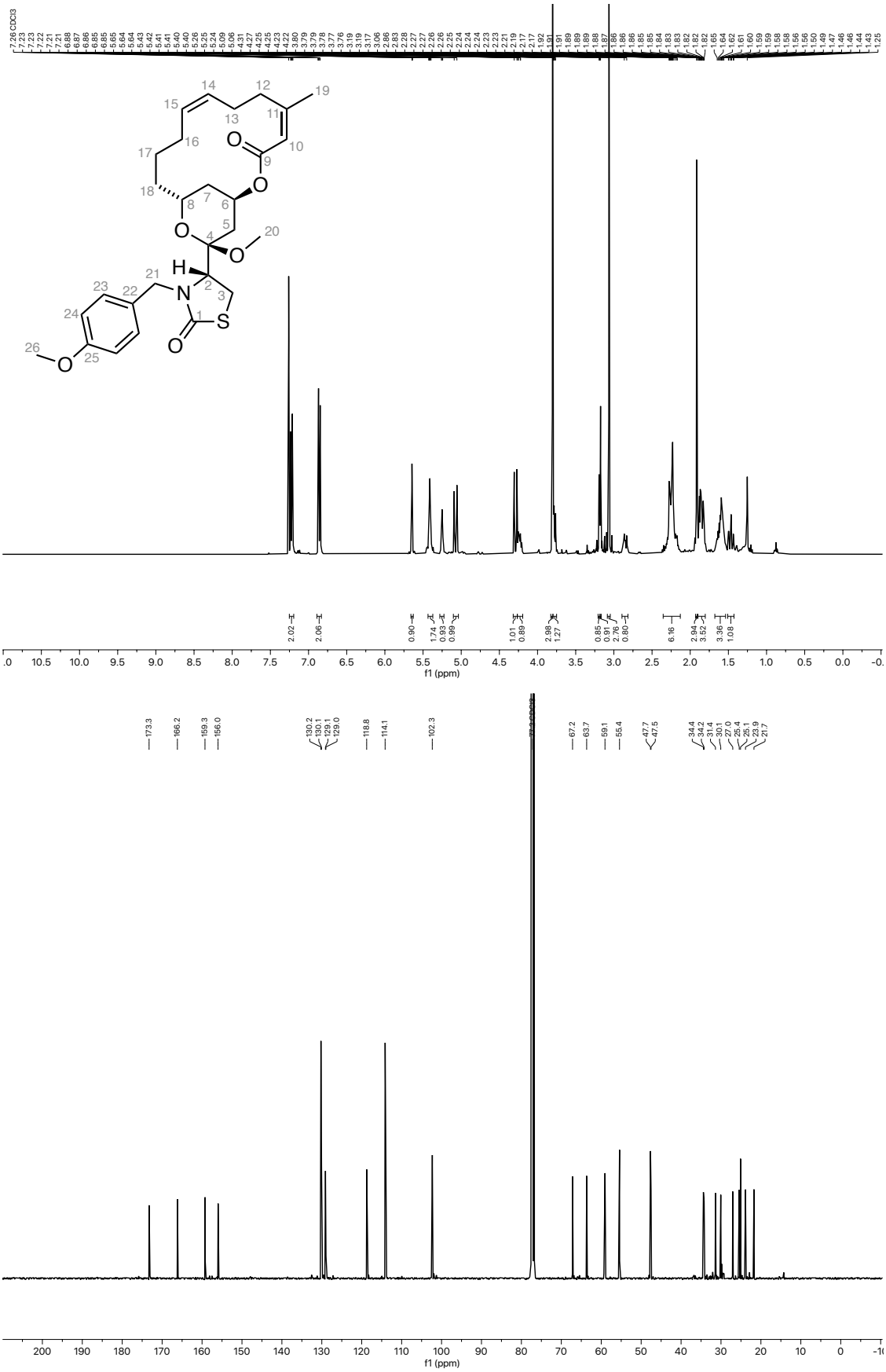

NMR for (*E*/*Z*)-24:

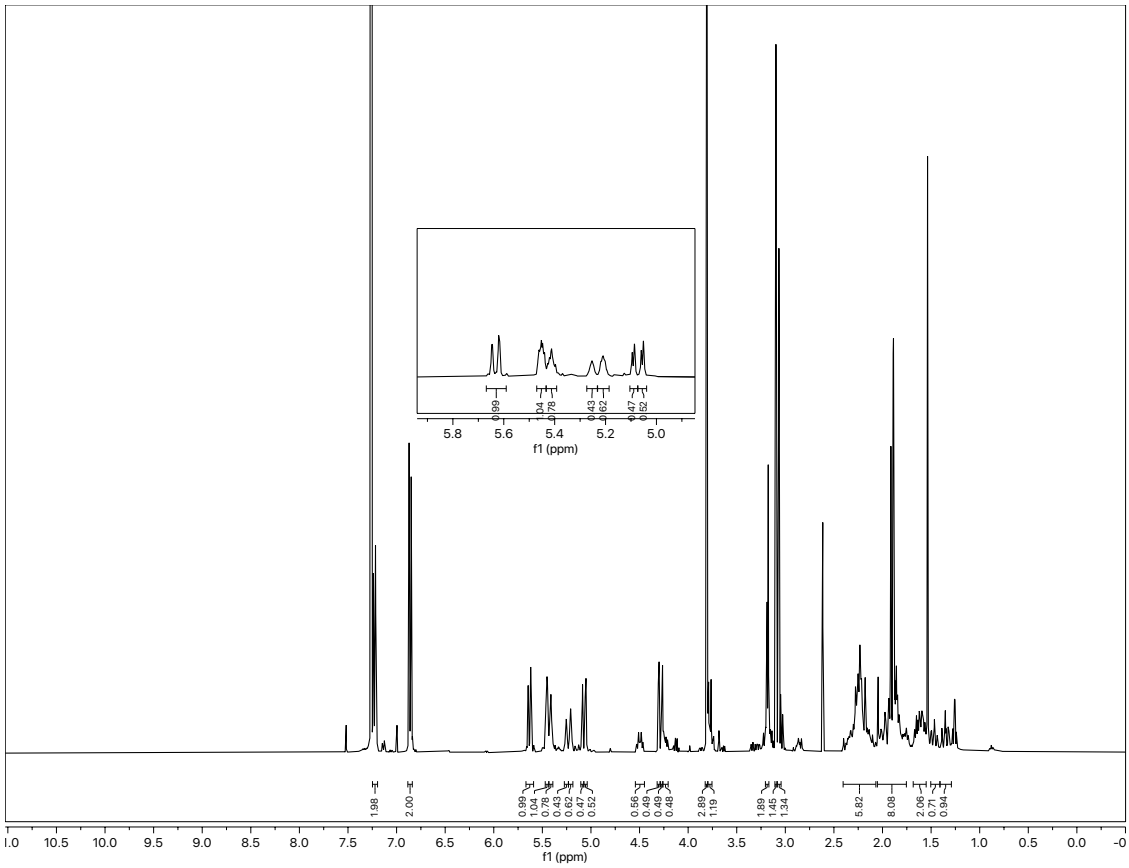
0.99
1.04
0.78
0.43
0.62
0.47
0.52
5.8
5.6
5.4
5.2
5.0
f1 (ppm)
1.98
2.00
0.99
1.04
0.78
0.43
0.62
0.47
0.52
0.56
0.49
0.49
0.48
2.89
1.19
1.89
1.45
1.34
5.82
8.08
2.06
2.01
0.94
10.5
10.0
9.5
9.0
8.5
8.0
7.5
7.0
6.5
6.0
5.5
5.0
4.5
4.0
3.5
3.0
2.5
2.0
1.5
1.0
0.5
0.0
f1 (ppm)

NMR for 25:

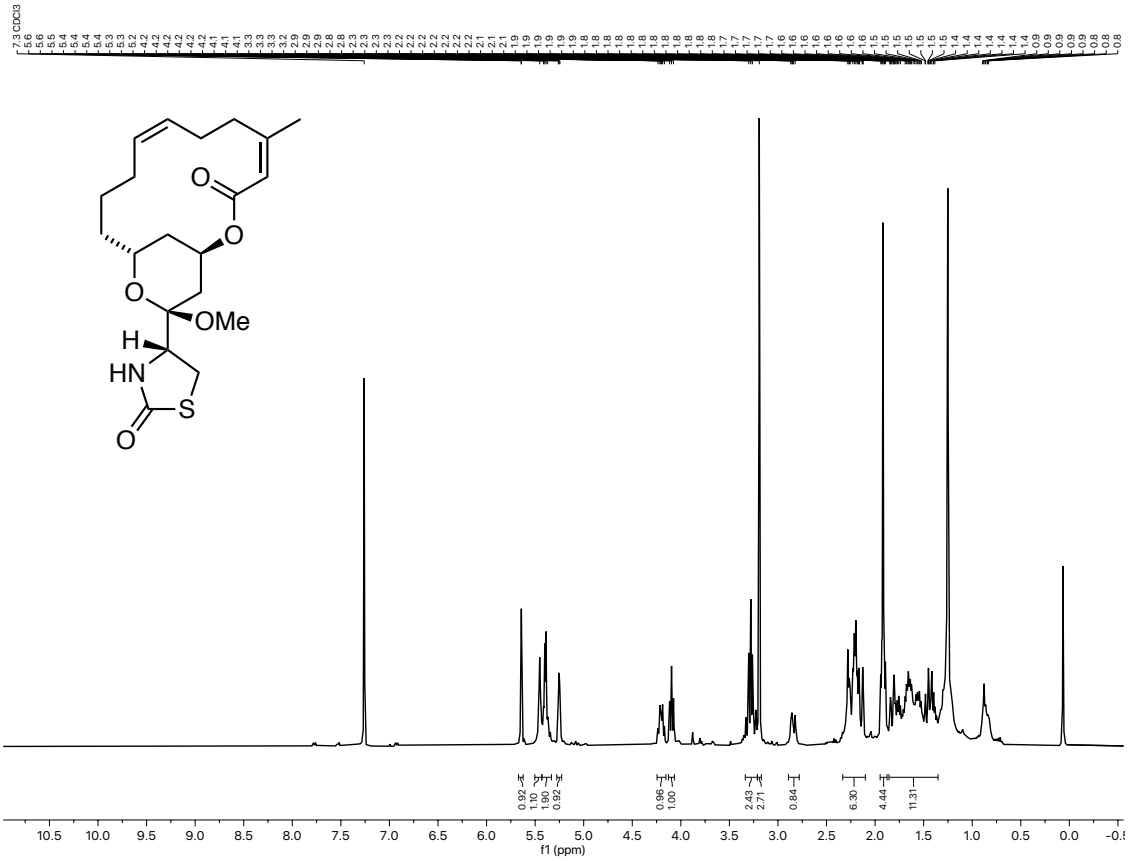
7.3 CDCl3
O
O
O
OMe
H
HN
S
O
0.92
1.10
1.90
0.92
0.96
1.00
2.43
2.71
0.84
6.30
4.44
11.31
f1 (ppm)

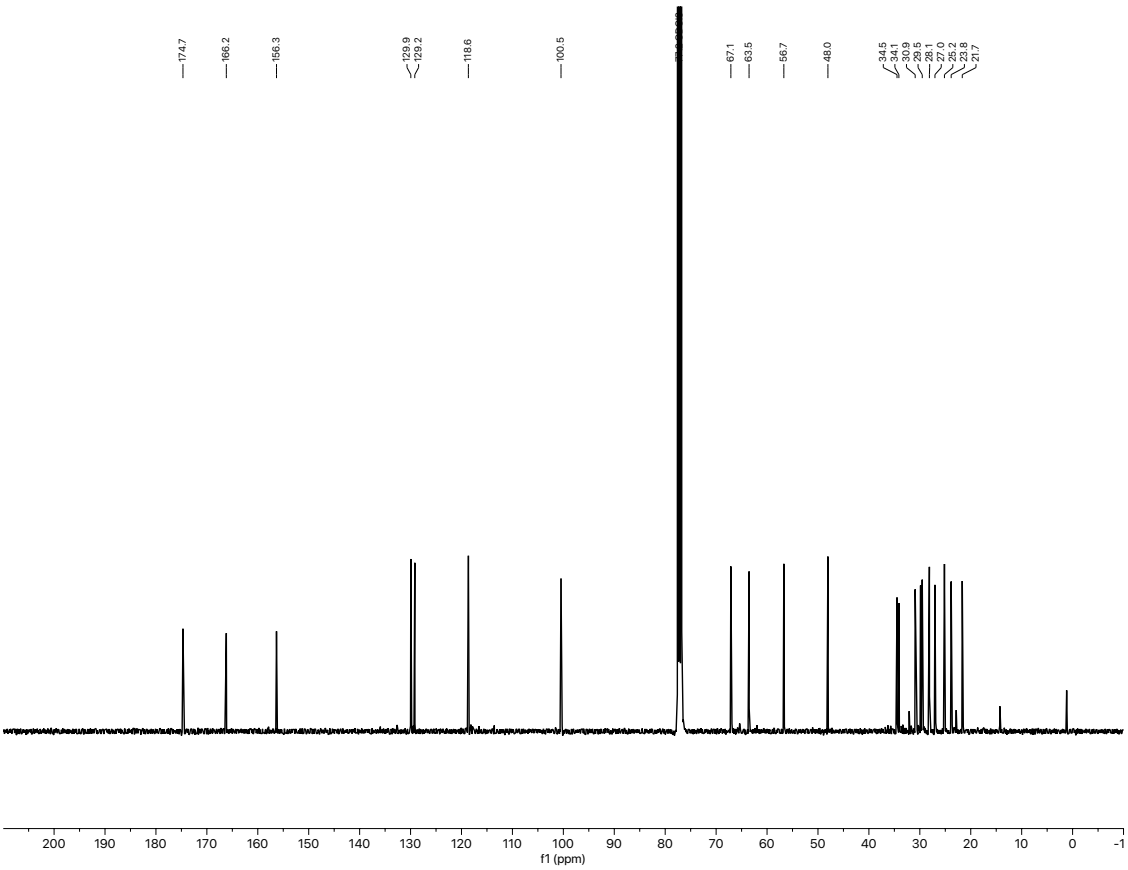
174.7
166.2
156.3
129.9
129.2
118.6
100.5
67.1
63.5
56.7
48.0
34.5
34.1
30.9
29.5
28.1
27.0
25.2
23.8
21.7
f1 (ppm)

NMR for 8-*Nor*-Latrunculin B:

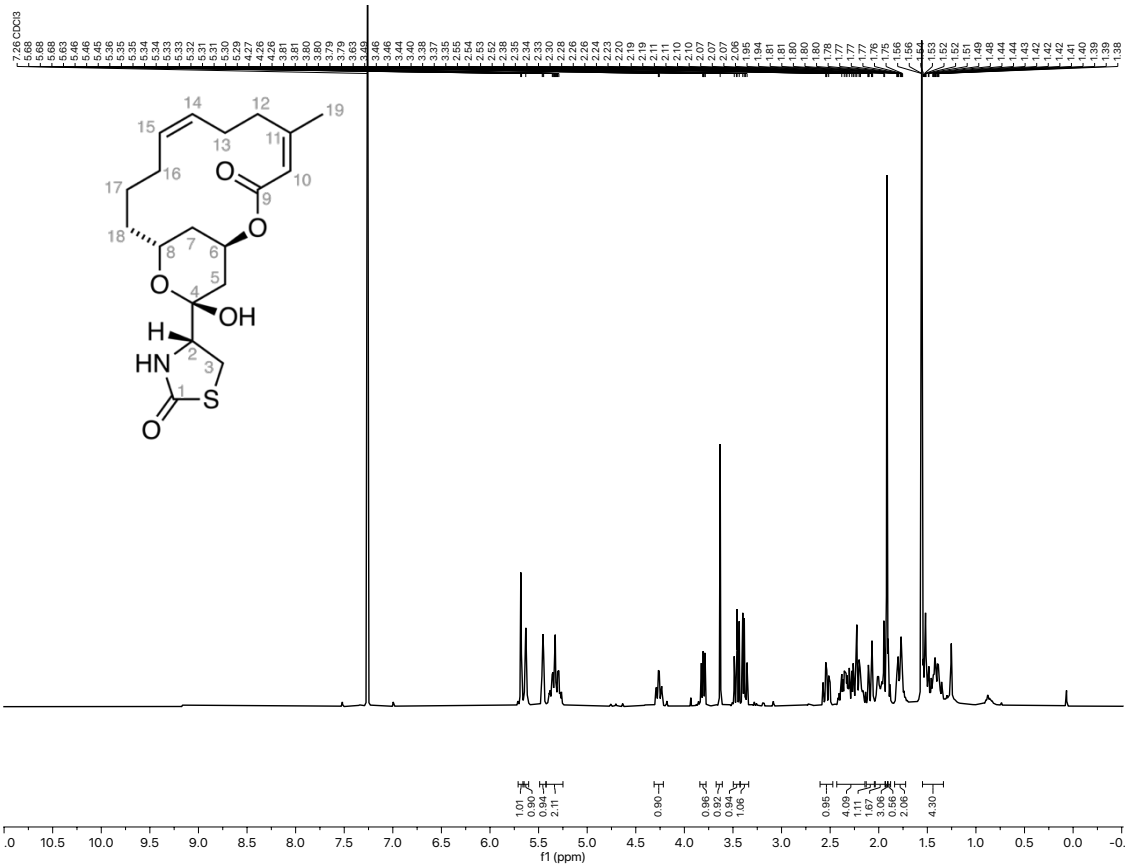

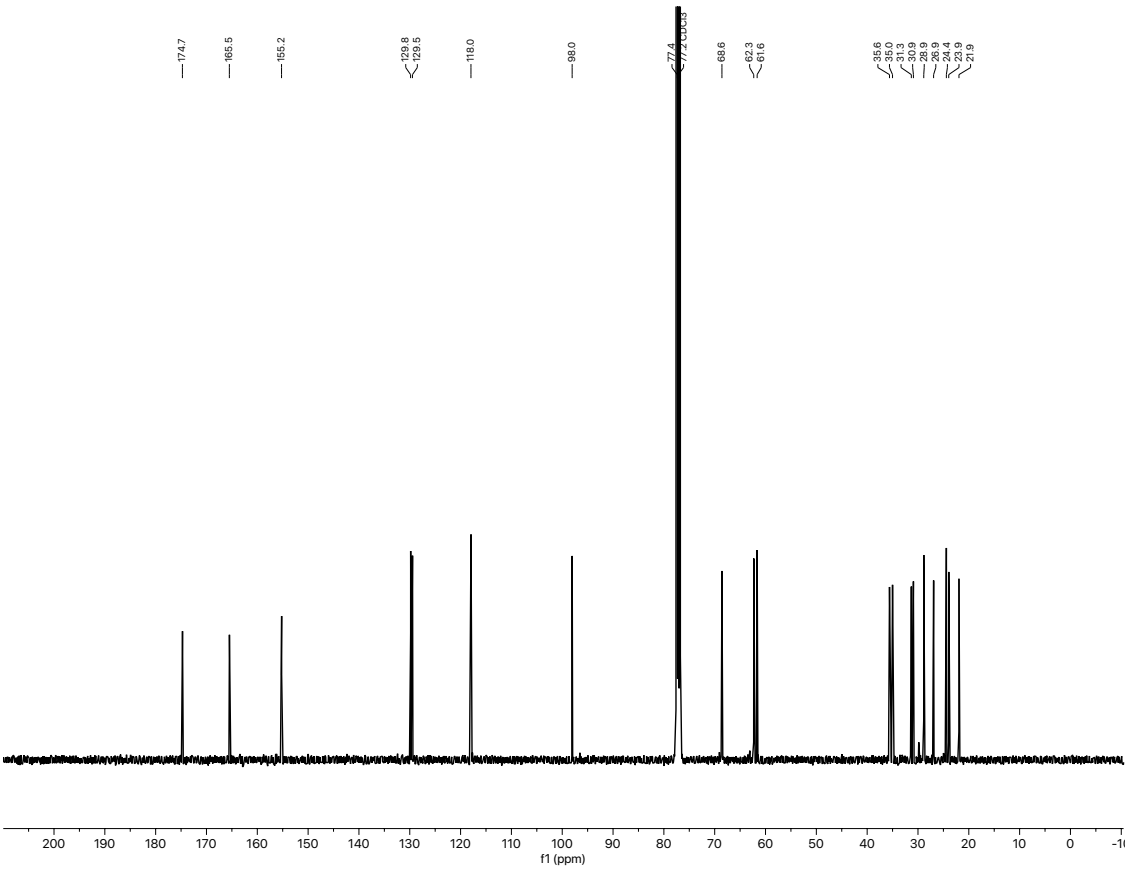

NMR for 26:

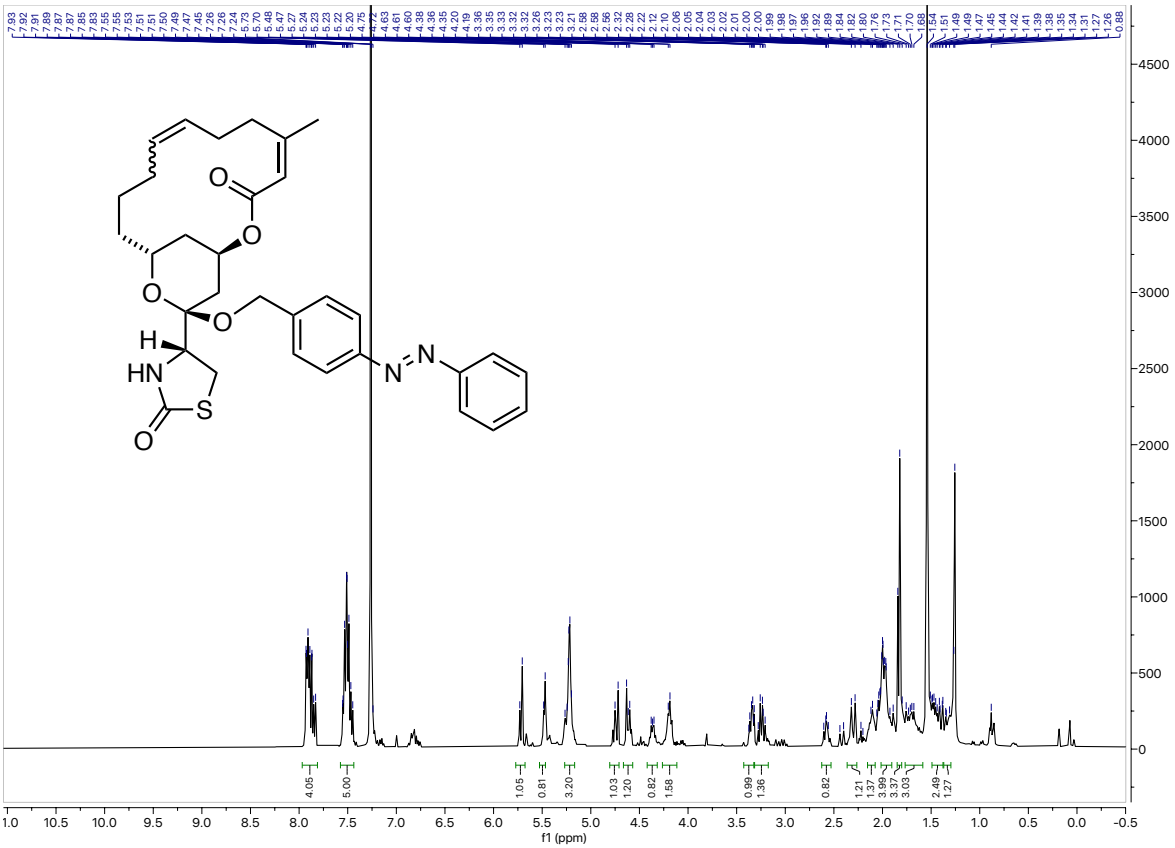

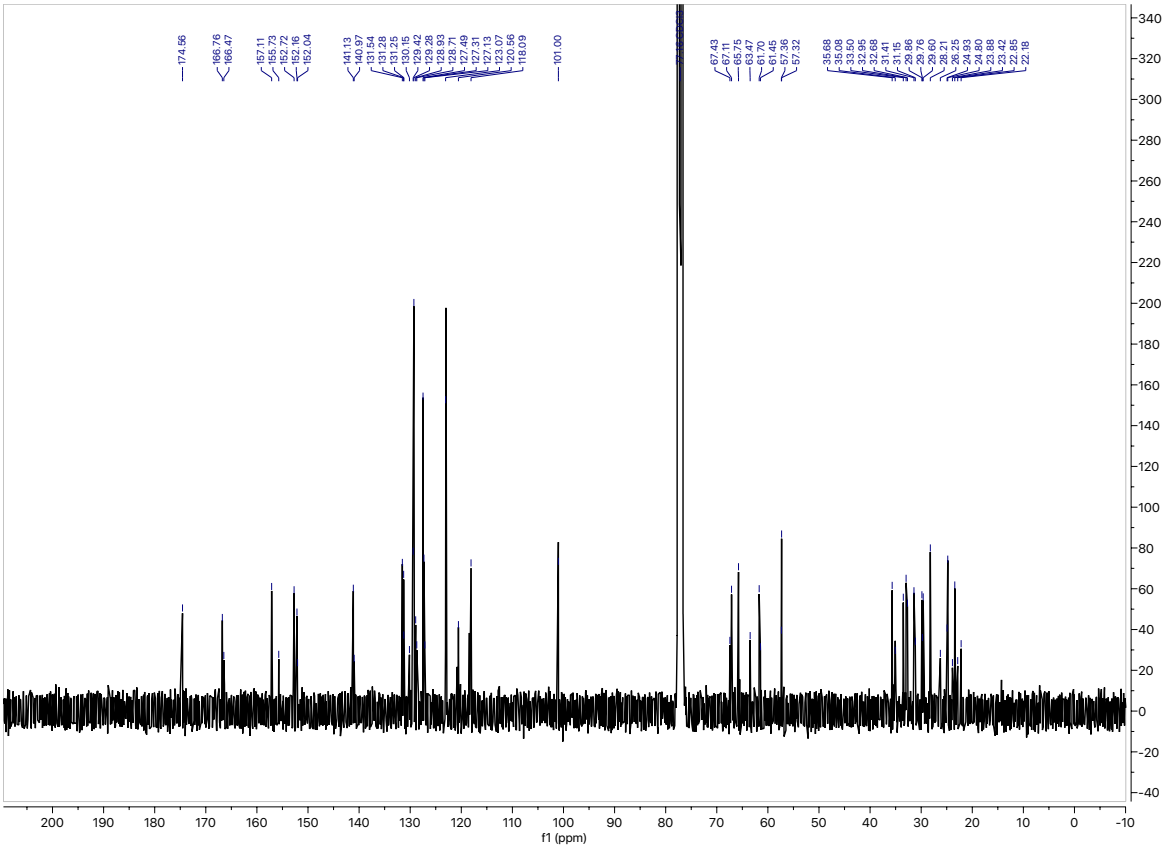

NMR for 27:

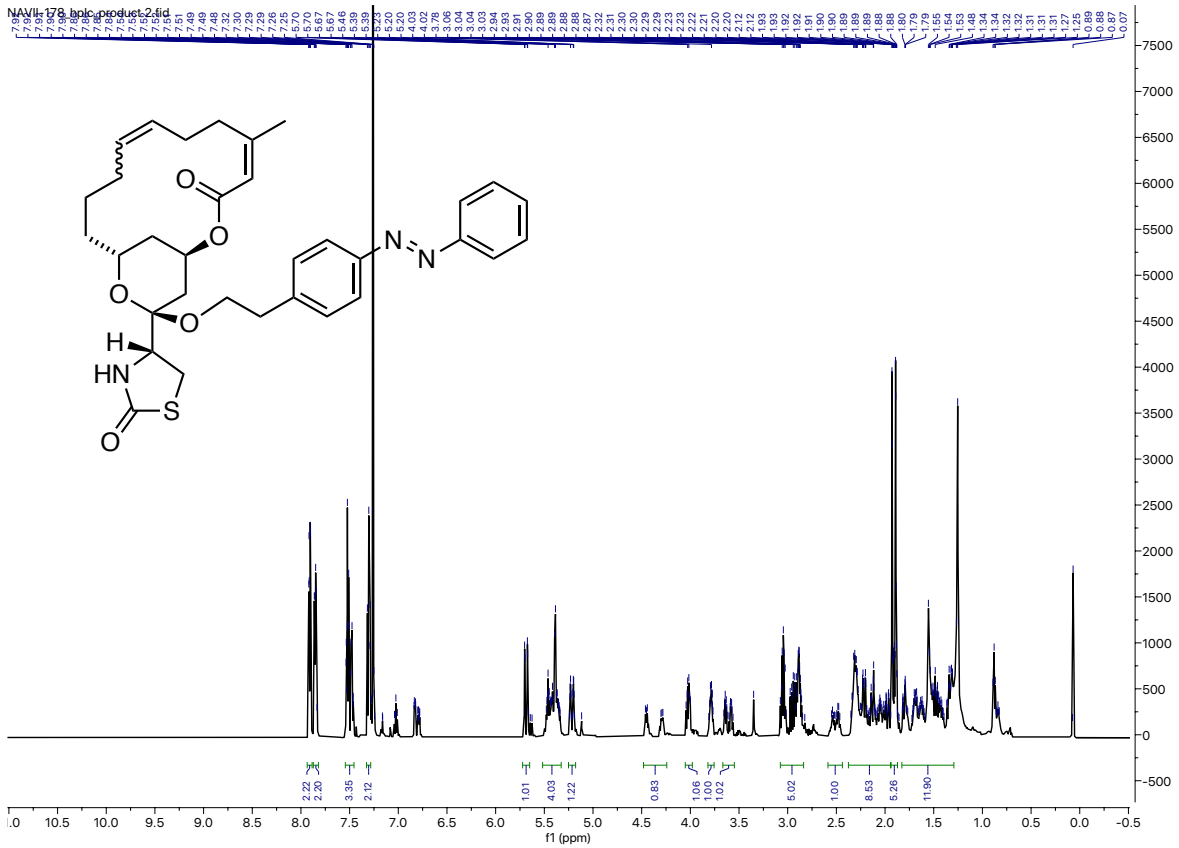

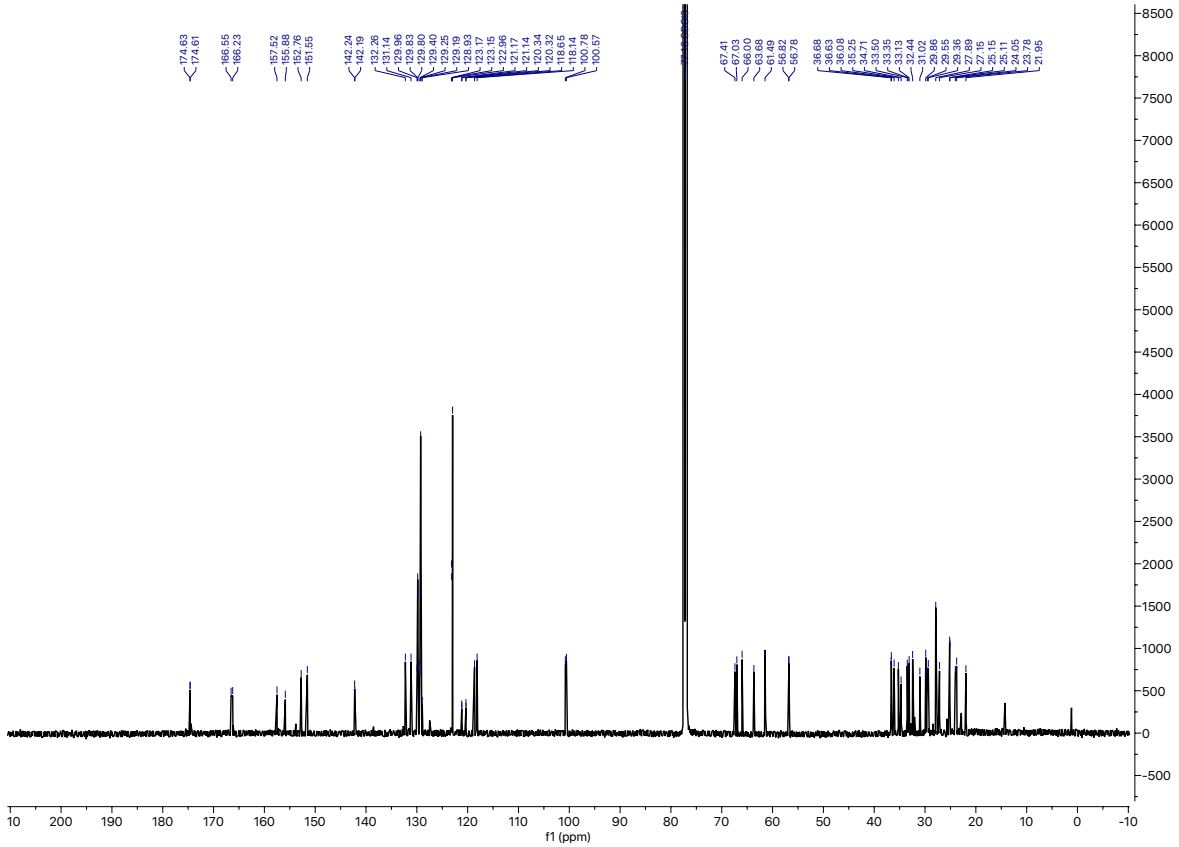

NMR for (*S*)-28:

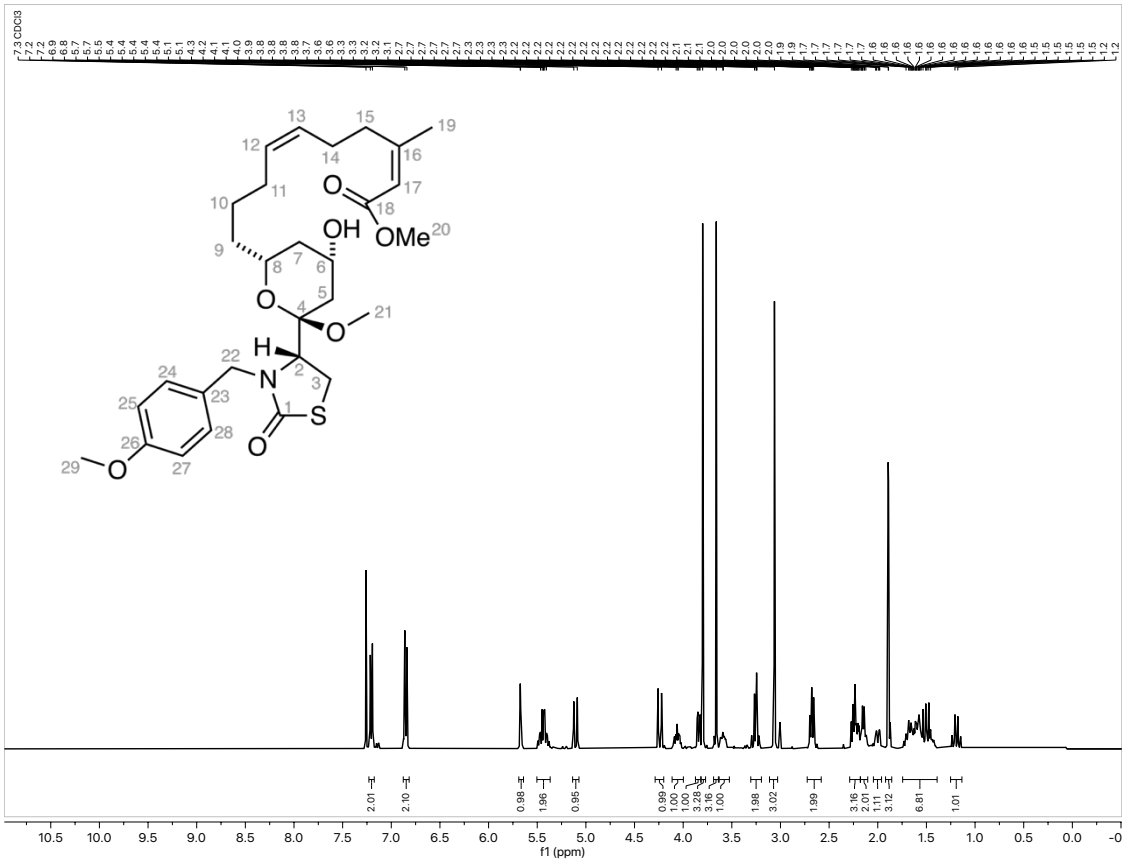
7.3 CDCl3
OH
OMe
f1 (ppm)

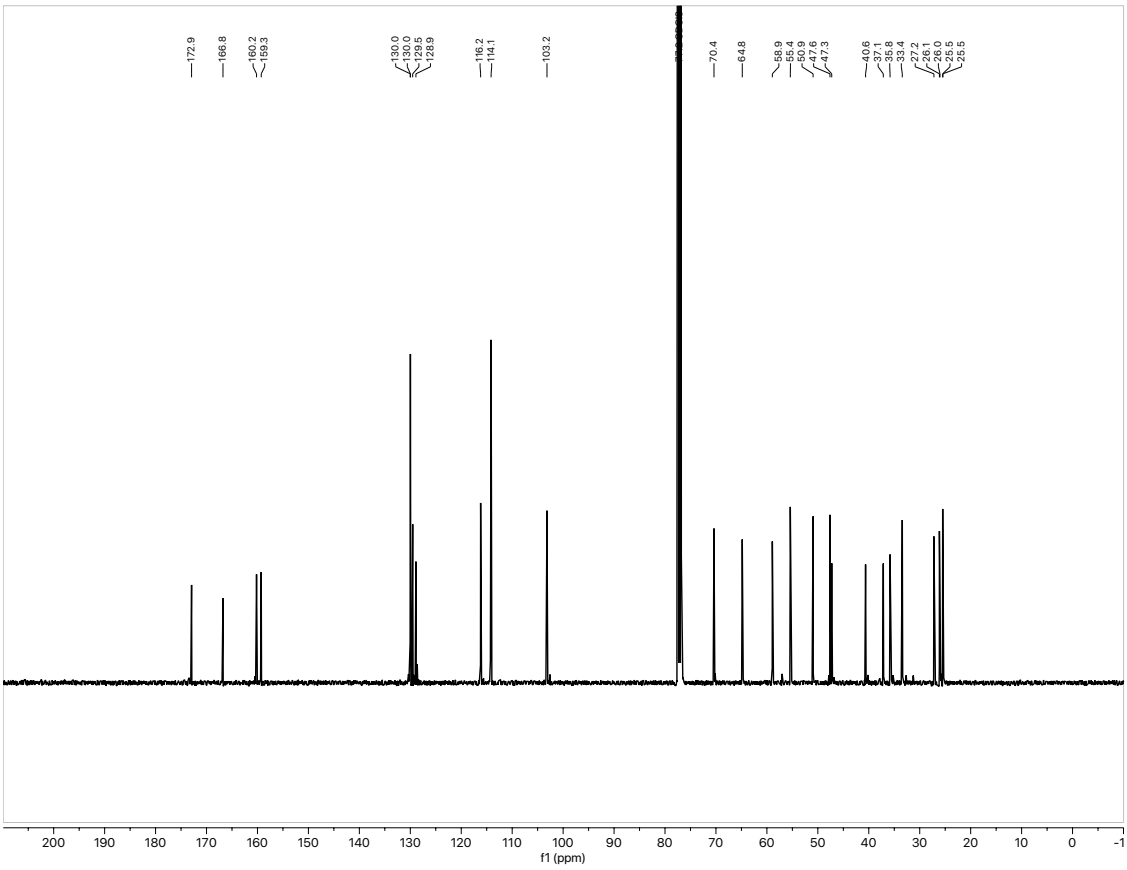
172.9
166.8
160.2
159.3
130.0
130.0
129.5
128.9
116.2
114.1
103.2
77.0
70.4
64.8
58.9
55.4
50.9
47.6
47.3
40.6
37.1
35.8
33.4
27.2
26.1
26.0
25.5
25.5
f1 (ppm)

NMR for 29:

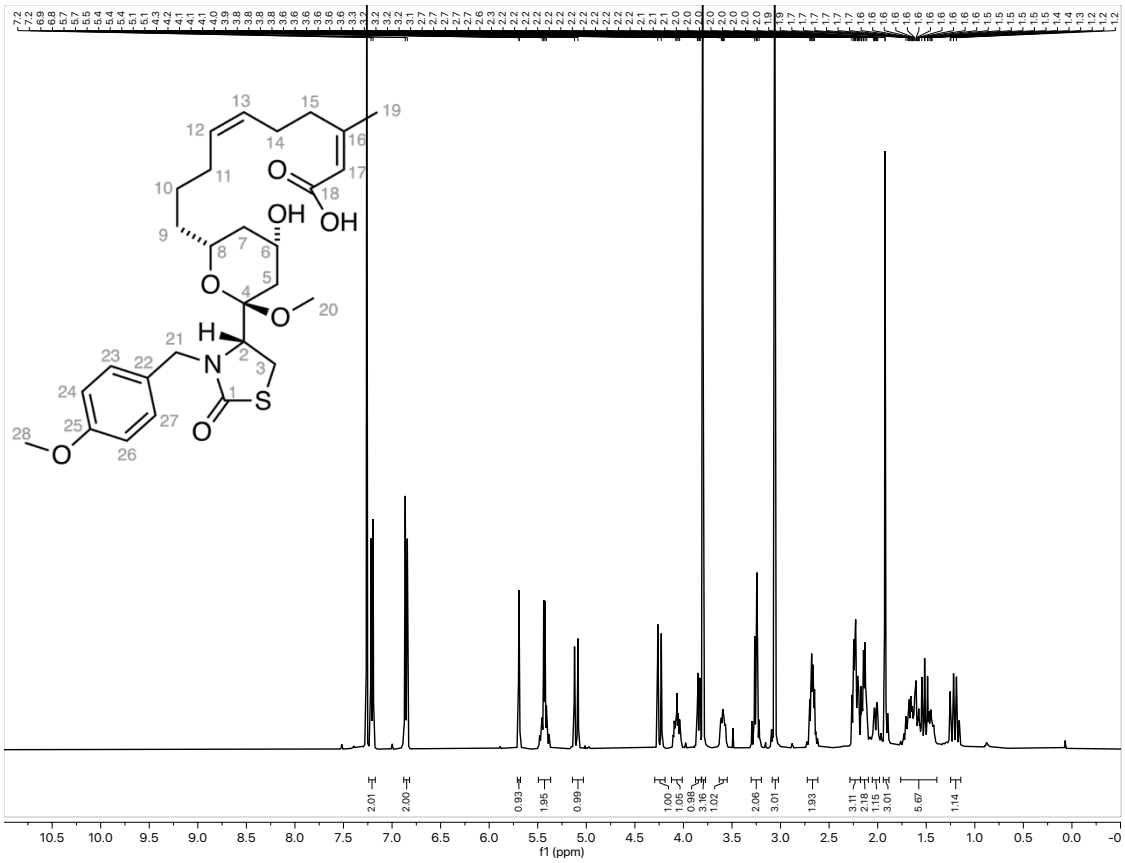

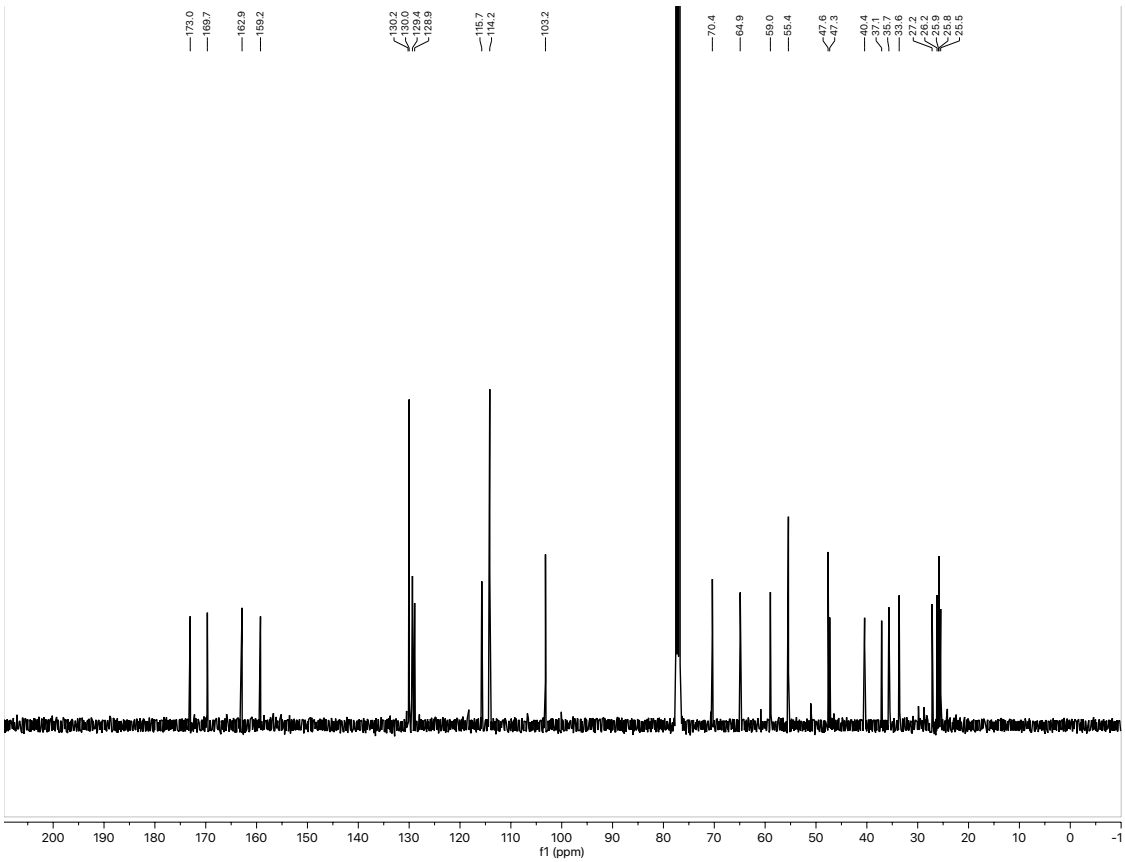

NMR for (*R*)-28:

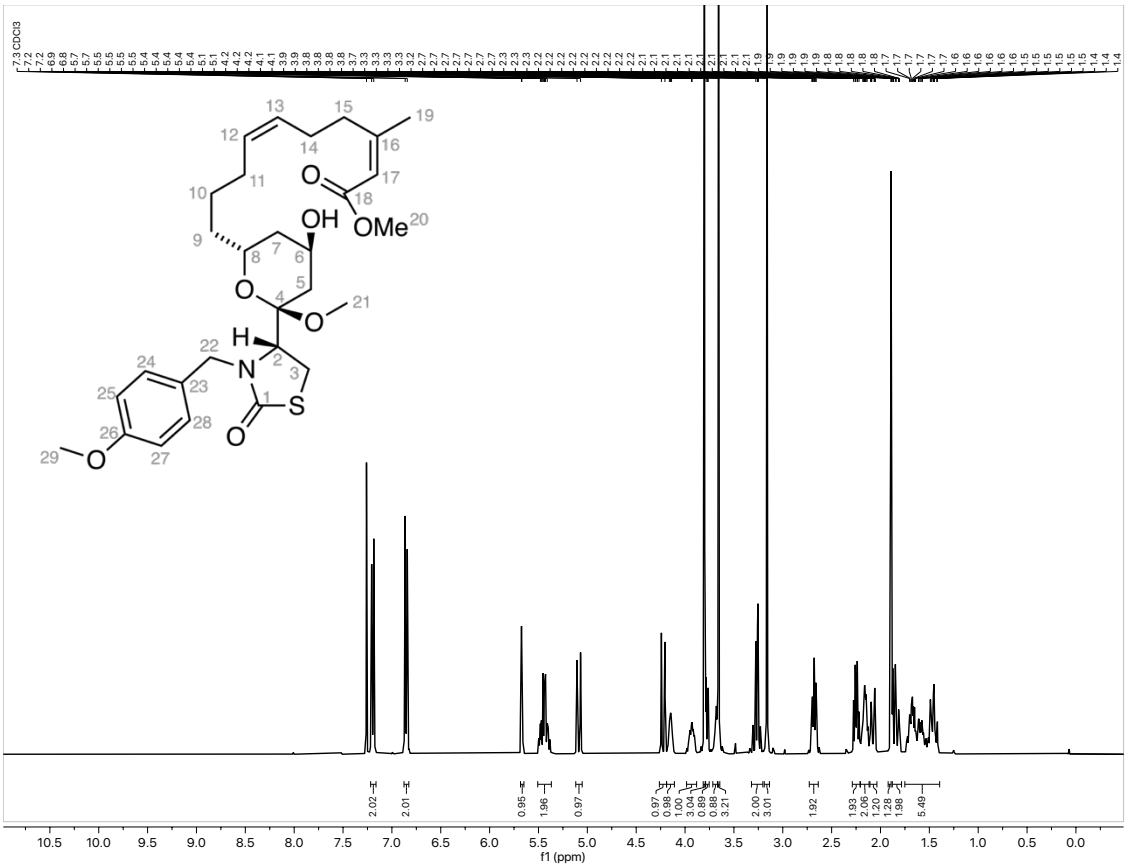

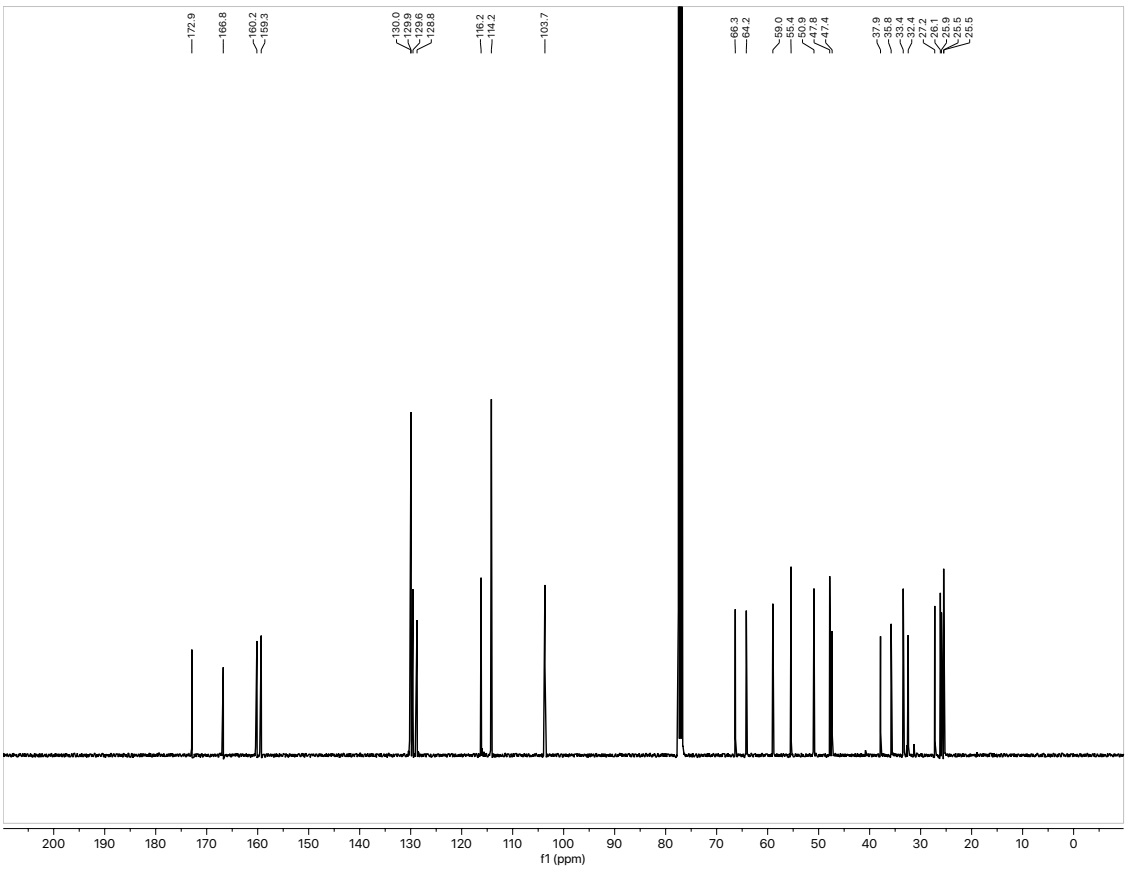

NMR for 33:

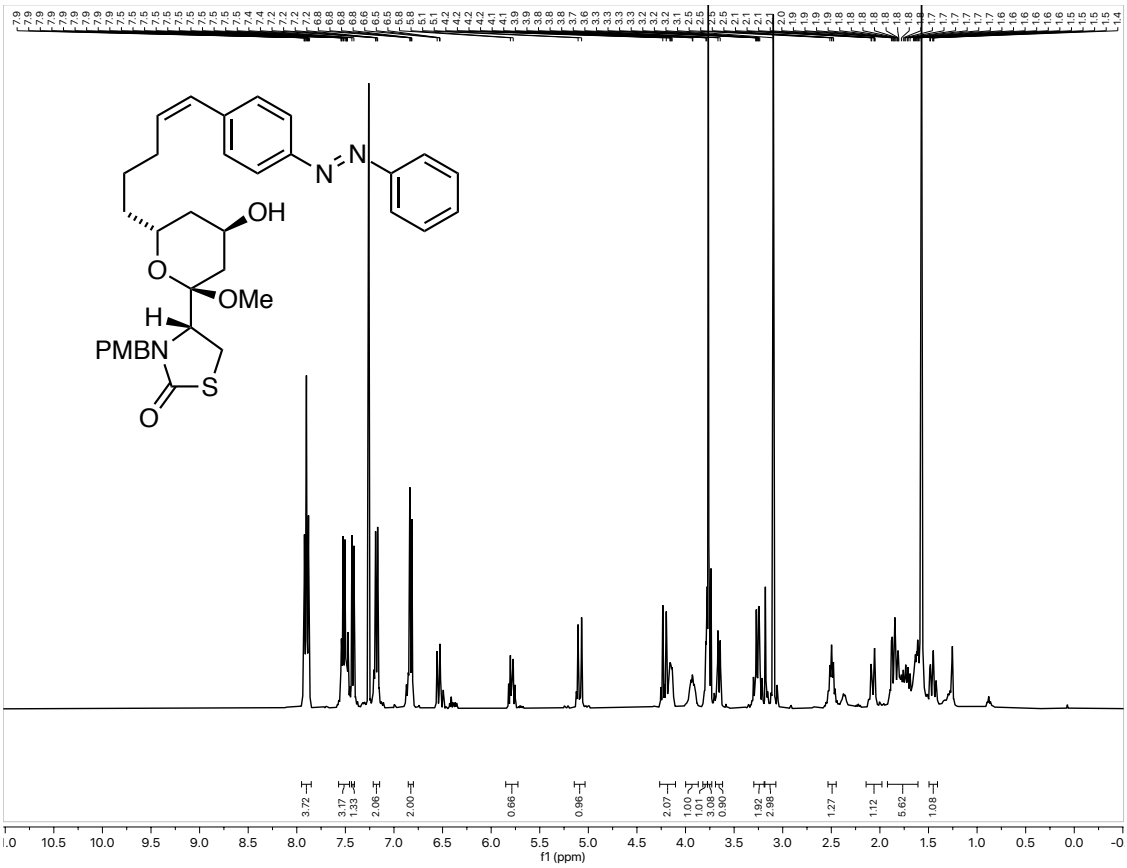
N
N
OH
O
OMe
H
PMBN
S
O
f1 (ppm)

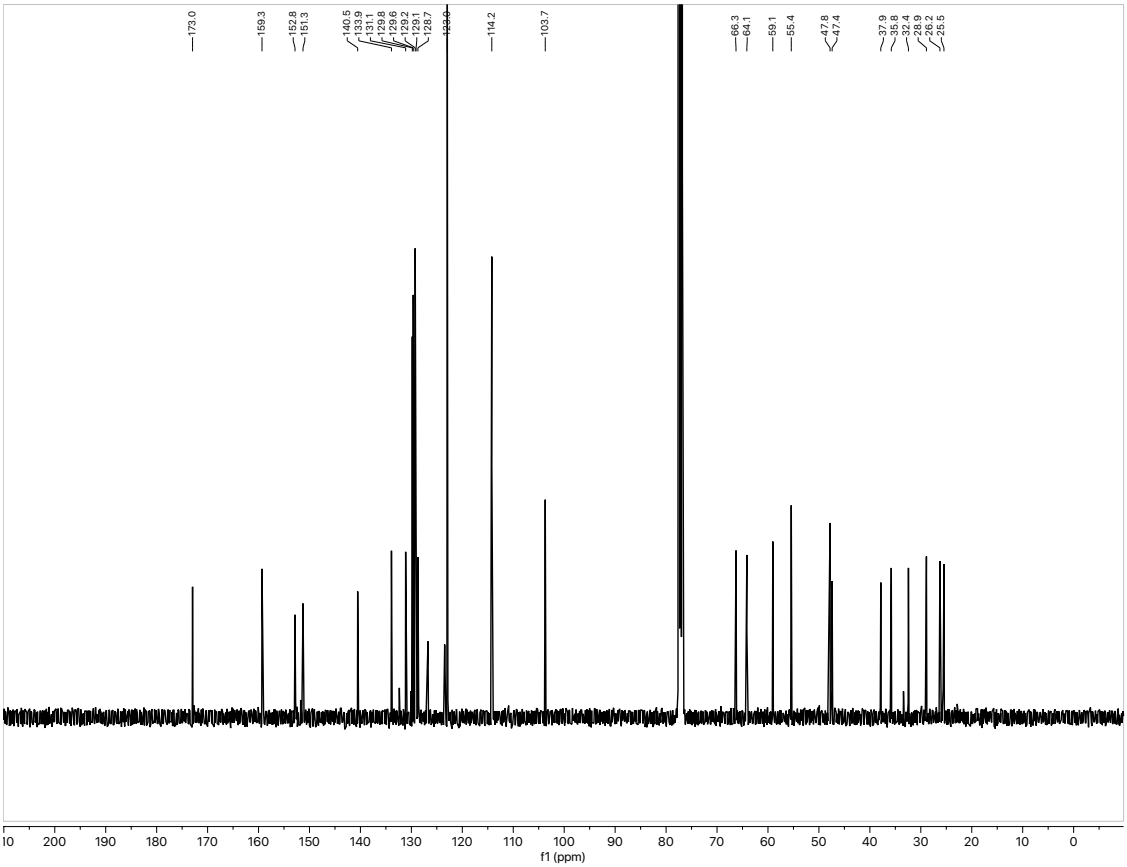
173.0
159.3
152.8
151.3
140.5
133.9
131.1
129.8
129.6
129.2
129.1
126.7
123.0
114.2
103.7
66.3
64.1
59.1
55.4
47.8
47.4
37.9
35.8
32.4
28.9
28.2
25.5
f1 (ppm)

NMR for 36a

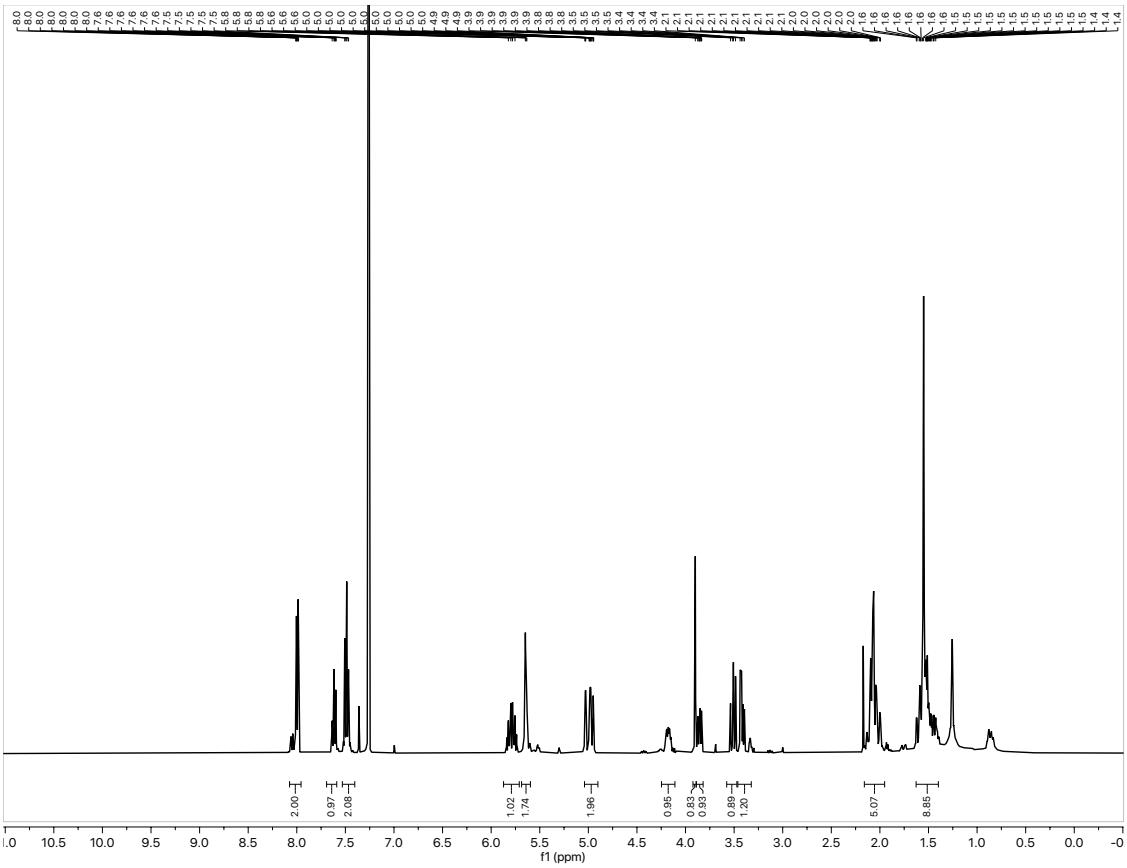
2.00
0.97
2.08
1.02
1.74
1.96
0.95
0.83
0.93
0.89
1.20
5.07
8.85
f1 (ppm)

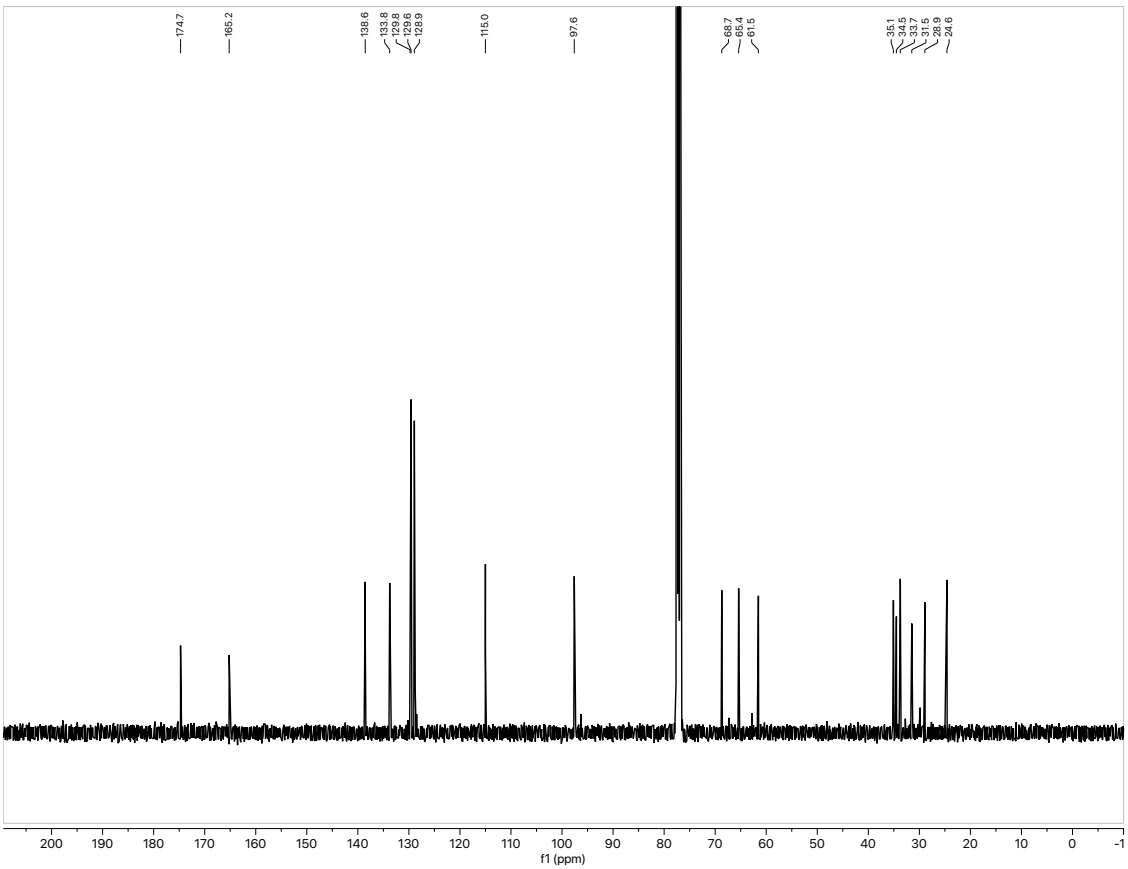
174.7
165.2
138.6
133.8
129.8
129.6
128.9
115.0
97.6
68.7
65.4
61.5
35.1
34.5
33.7
31.5
28.9
24.6
f1 (ppm)

NMR for 34a:

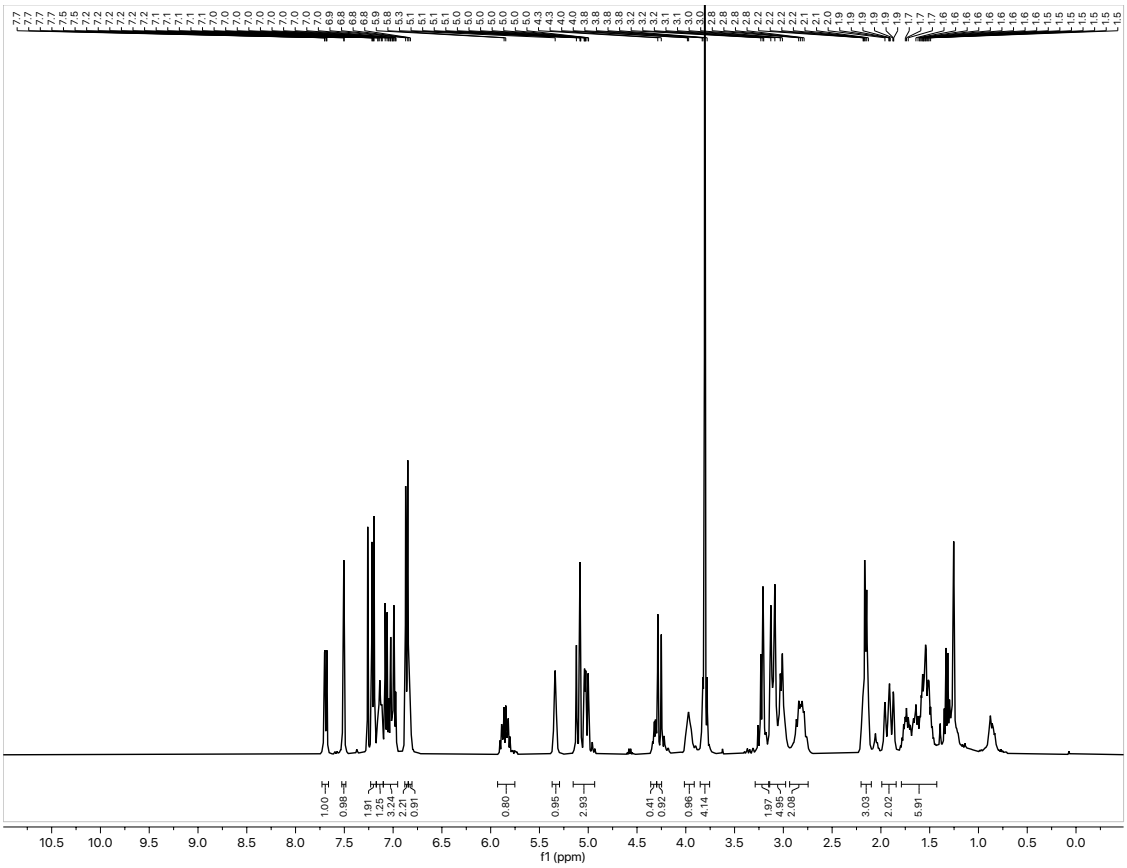

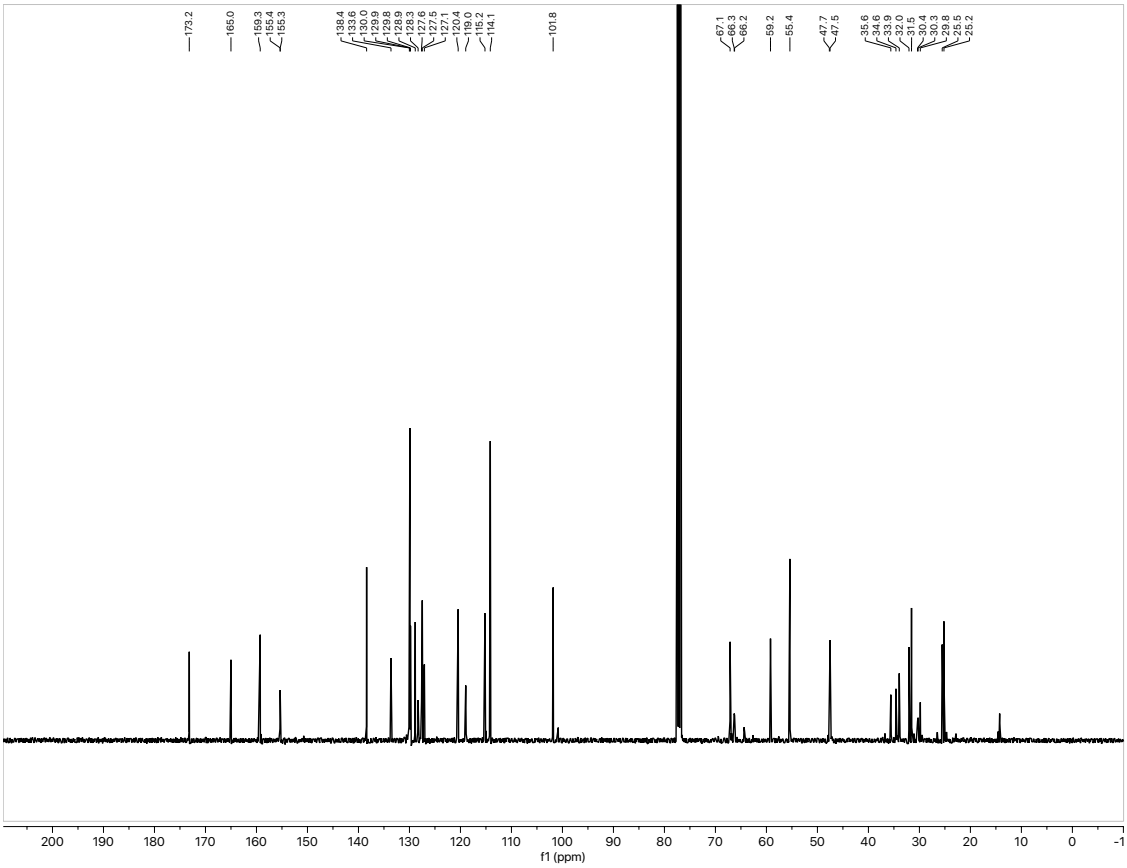

NMR for 39:

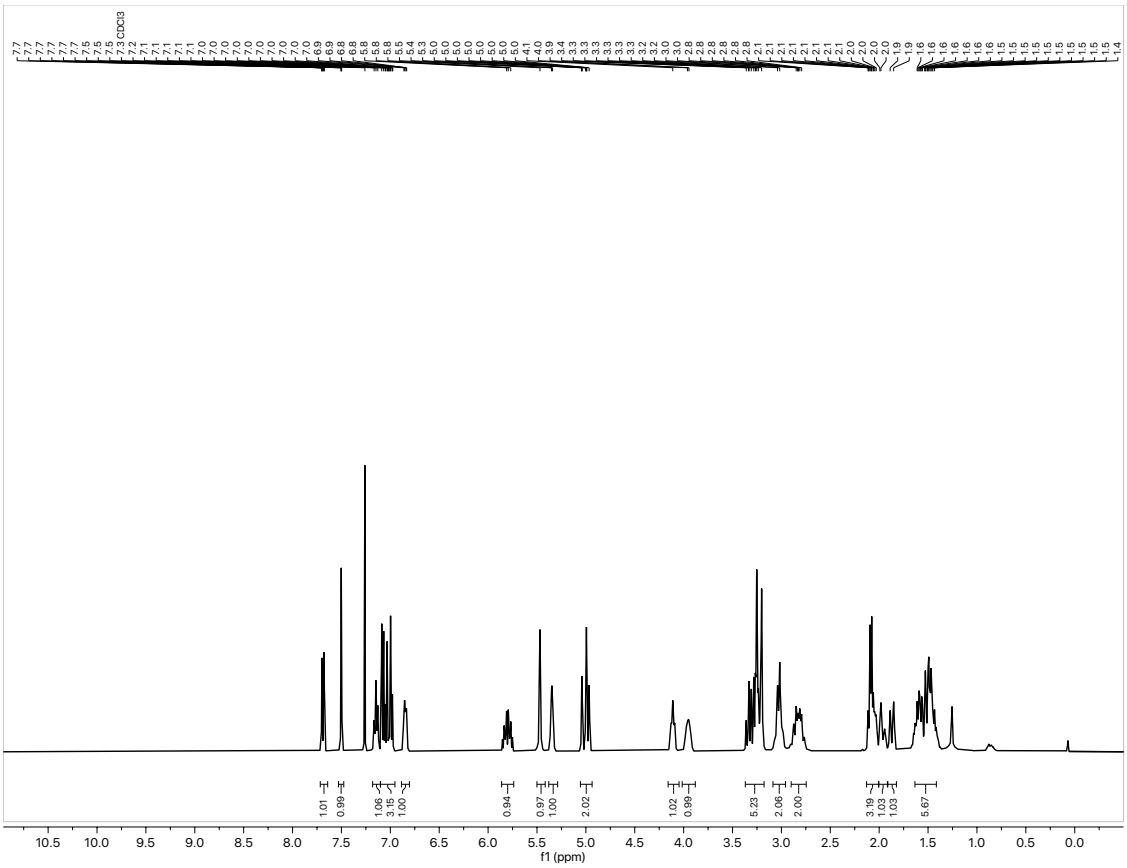
CDCl3
1.01
0.99
1.06
3.15
1.00
0.94
0.97
1.00
2.02
1.02
0.99
5.23
2.06
2.00
3.19
1.03
1.03
5.67
f1 (ppm)

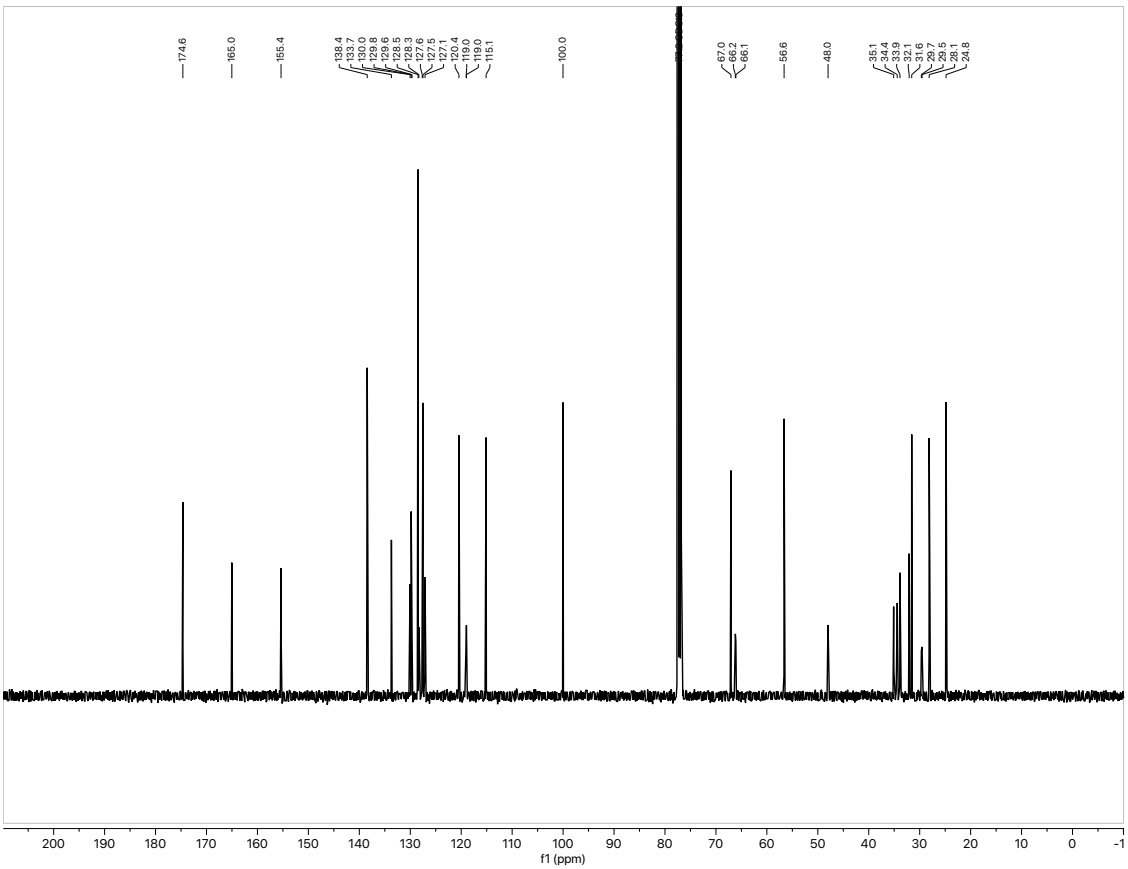
174.6
165.0
155.4
138.4
133.7
130.0
129.8
129.6
128.5
128.3
127.6
127.5
127.1
120.4
119.0
119.0
115.1
100.0
67.0
66.2
66.1
56.6
48.0
35.1
34.4
33.9
32.1
31.6
29.7
29.5
28.1
24.8
f1 (ppm)

NMR for 40:

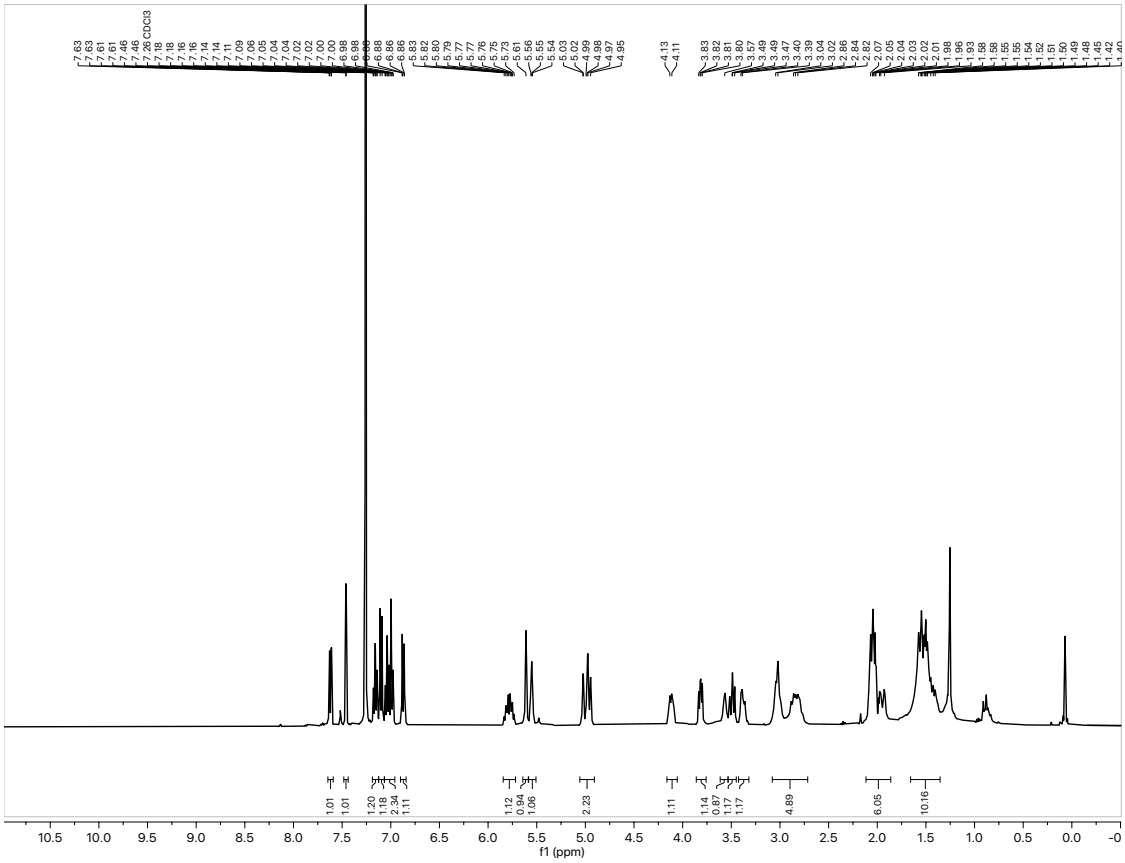
7.63
7.63
7.61
7.61
7.46
7.46
7.26 CDCl3
7.18
7.18
7.16
7.16
7.14
7.14
7.11
7.09
7.06
7.05
7.04
7.04
7.02
7.02
7.00
7.00
6.98
6.98
6.88
6.88
6.86
6.86
5.83
5.82
5.80
5.79
5.77
5.77
5.76
5.75
5.73
5.61
5.56
5.55
5.54
5.03
5.02
4.99
4.98
4.97
4.95
4.13
4.11
3.83
3.82
3.81
3.80
3.57
3.49
3.49
3.47
3.40
3.39
3.04
3.02
2.86
2.84
2.82
2.07
2.05
2.04
2.03
2.02
2.01
1.98
1.96
1.93
1.88
1.88
1.55
1.55
1.54
1.52
1.51
1.50
1.49
1.48
1.45
1.42
1.40
1.01
1.01
1.20
1.18
2.34
1.11
1.12
0.94
1.06
2.23
1.11
1.14
0.67
1.17
1.17
4.89
6.05
10.16
f1 (ppm)

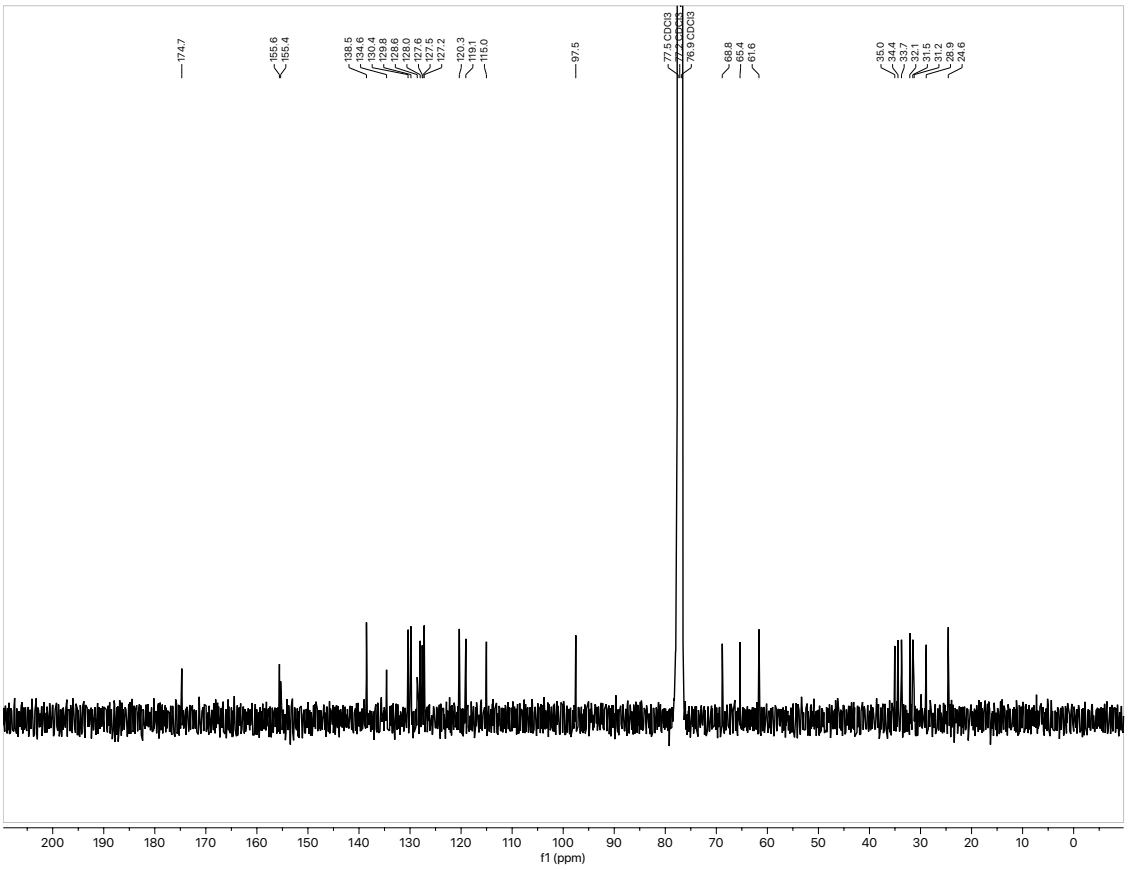
174.7
155.6
155.4
138.5
134.6
130.4
129.8
128.6
128.0
127.6
127.5
127.2
120.3
119.1
115.0
97.5
77.5 CDCl3
77.2 CDCl3
76.9 CDCl3
68.8
65.4
61.6
35.0
34.4
33.7
33.1
31.5
31.2
28.9
24.6
f1 (ppm)

NMR for 34c:

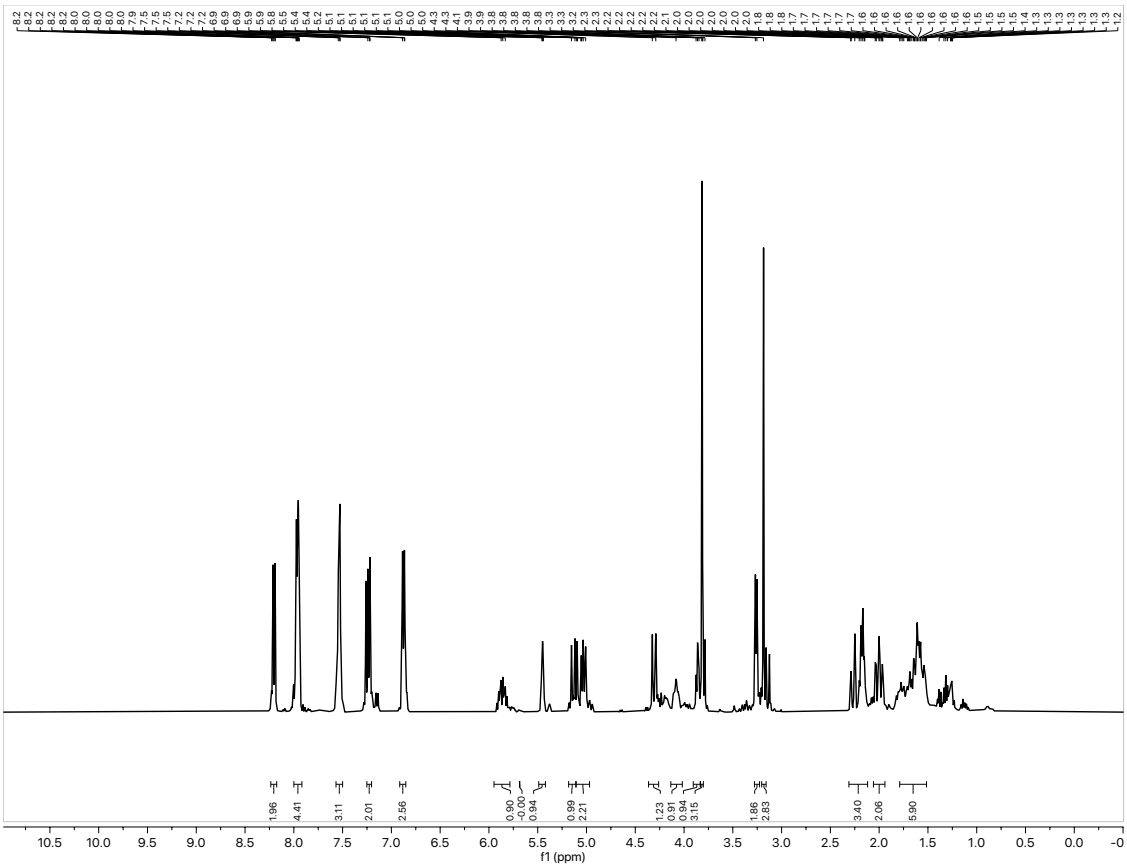

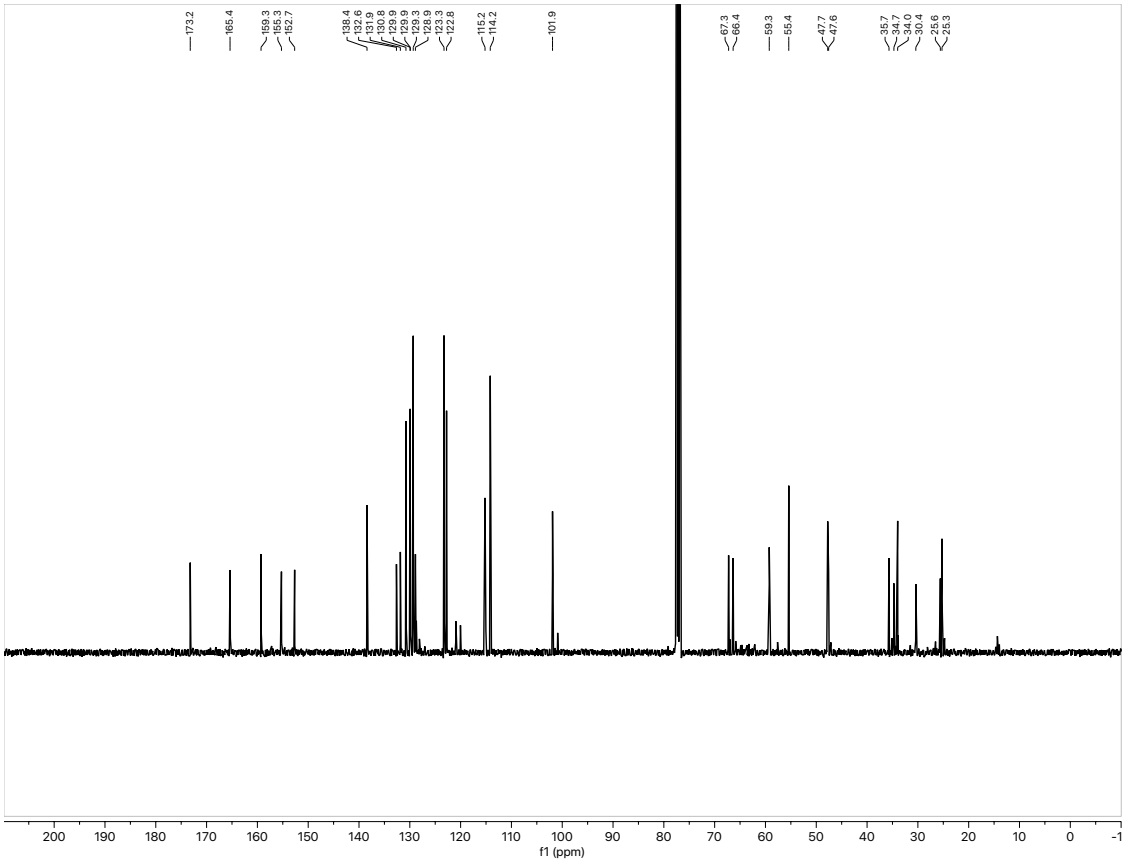

NMR for 35c:

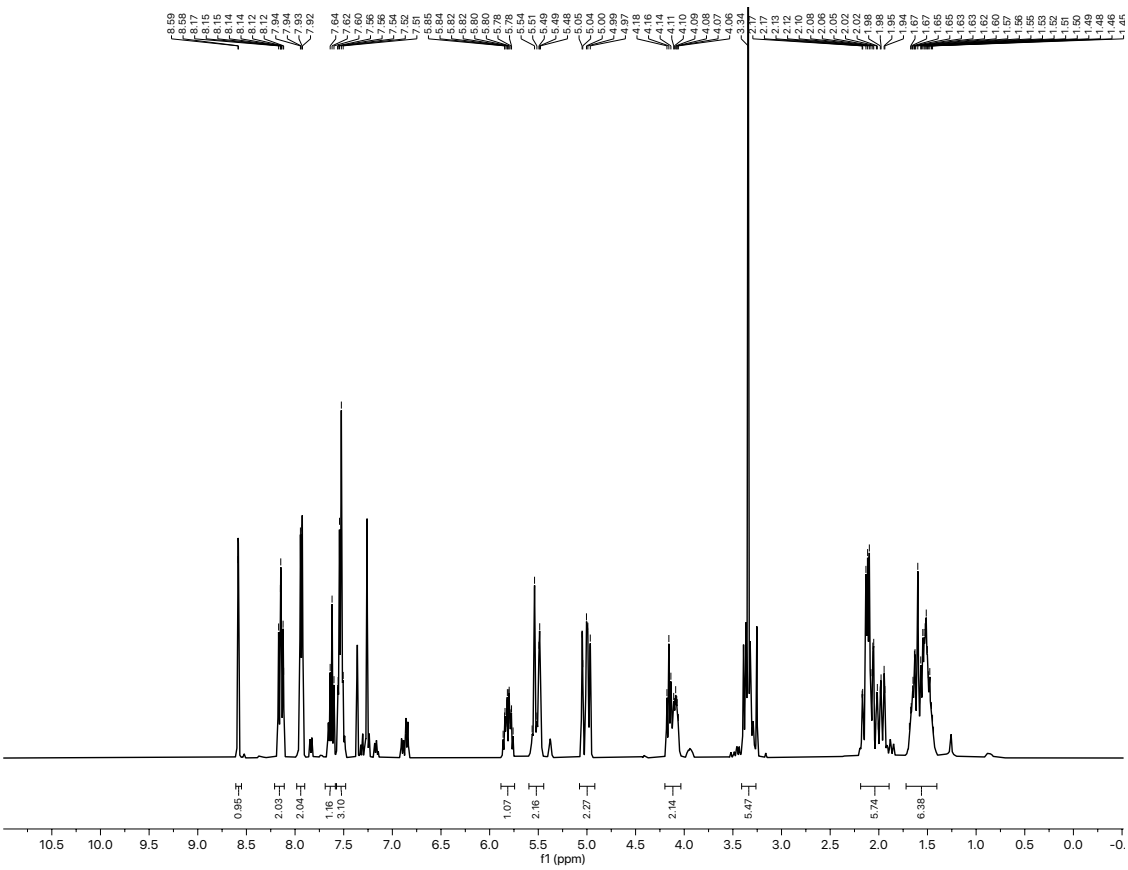
8.59
8.58
8.17
8.15
8.15
8.14
8.14
8.12
8.12
7.94
7.94
7.93
7.92
7.64
7.62
7.60
7.58
7.56
7.54
7.52
7.51
5.85
5.84
5.82
5.82
5.80
5.80
5.78
5.78
5.54
5.51
5.49
5.49
5.48
5.48
5.05
5.04
5.00
4.99
4.97
4.18
4.16
4.14
4.11
4.10
4.09
4.09
4.07
4.06
3.34
2.17
2.17
2.13
2.12
2.10
2.08
2.06
2.05
2.02
2.02
1.98
1.98
1.95
1.94
1.67
1.67
1.65
1.65
1.63
1.63
1.62
1.62
1.60
1.57
1.56
1.55
1.53
1.53
1.51
1.50
1.49
1.48
1.46
1.45
0.95
2.03
2.04
1.16
3.10
1.07
2.16
2.27
2.14
5.47
5.74
6.38
10.5
10.0
9.5
9.0
8.5
8.0
7.5
7.0
6.5
6.0
5.5
5.0
4.5
4.0
3.5
3.0
2.5
2.0
1.5
1.0
0.5
0.0
f1 (ppm)

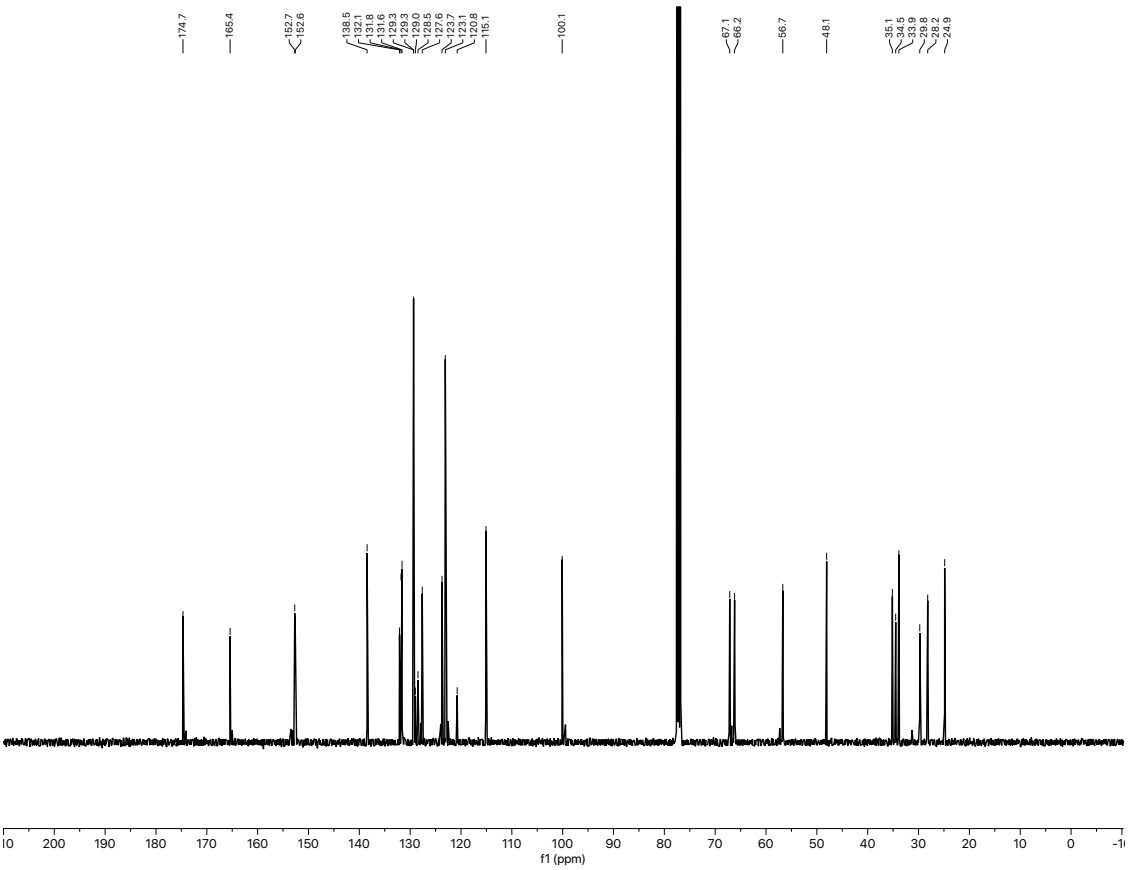
174.7
165.4
152.7
152.6
138.5
132.1
131.8
131.6
129.3
129.3
129.0
128.5
127.6
123.7
123.1
120.8
115.1
100.1
67.1
66.2
56.7
48.1
35.1
34.5
33.9
29.8
28.2
24.9
200
190
180
170
160
150
140
130
120
110
100
90
80
70
60
50
40
30
20
10
0
f1 (ppm)

NMR for 36c:

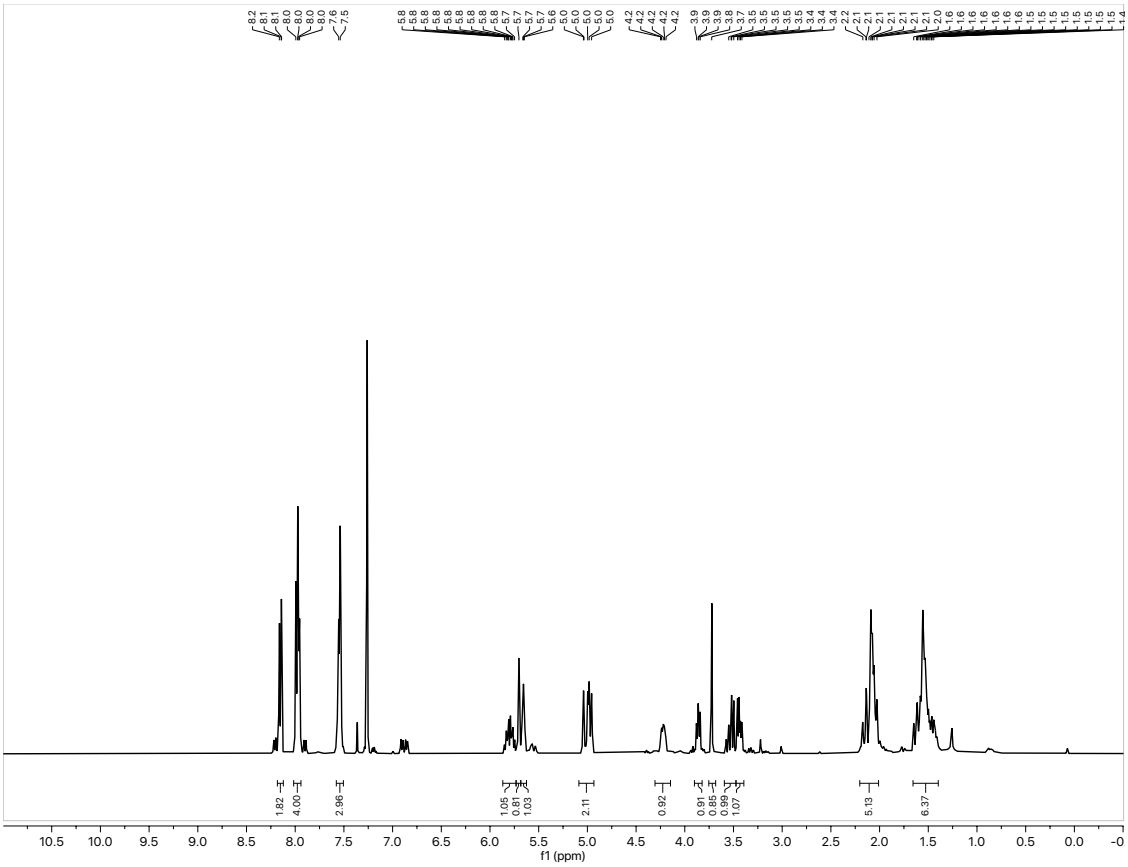

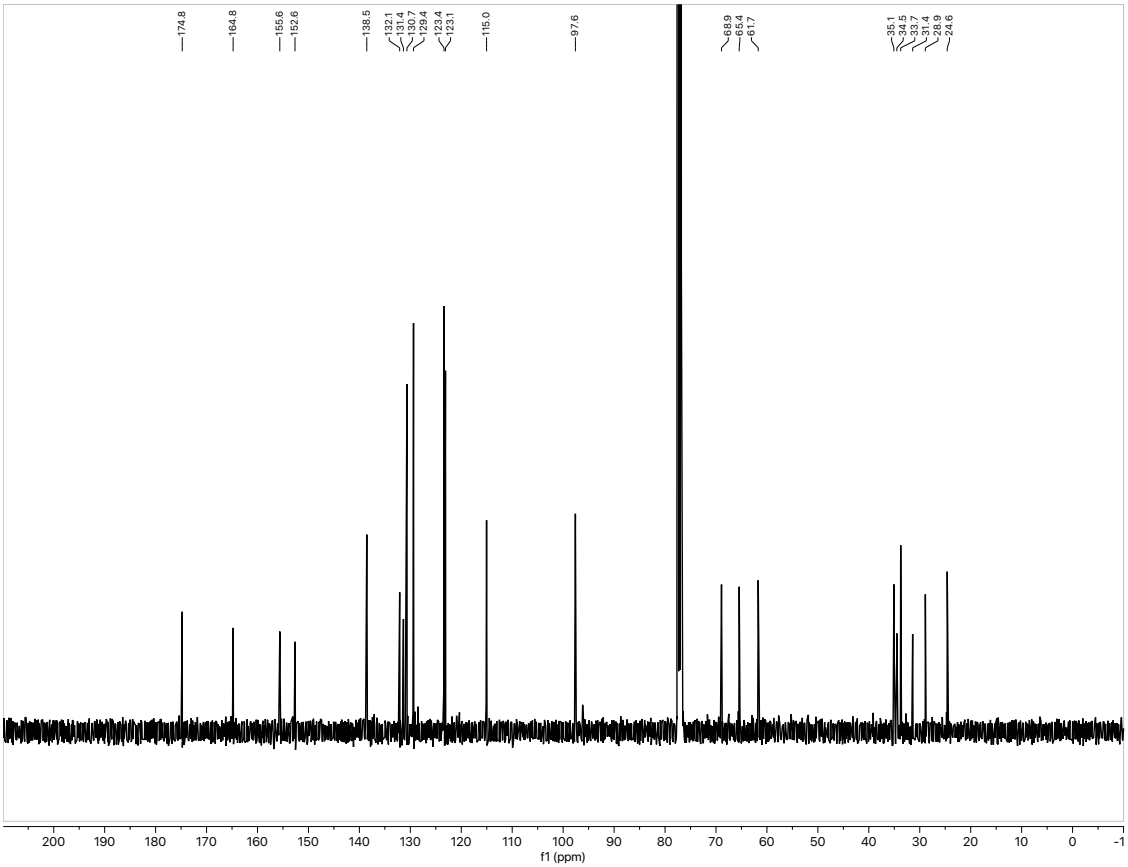

NMR for 34d:

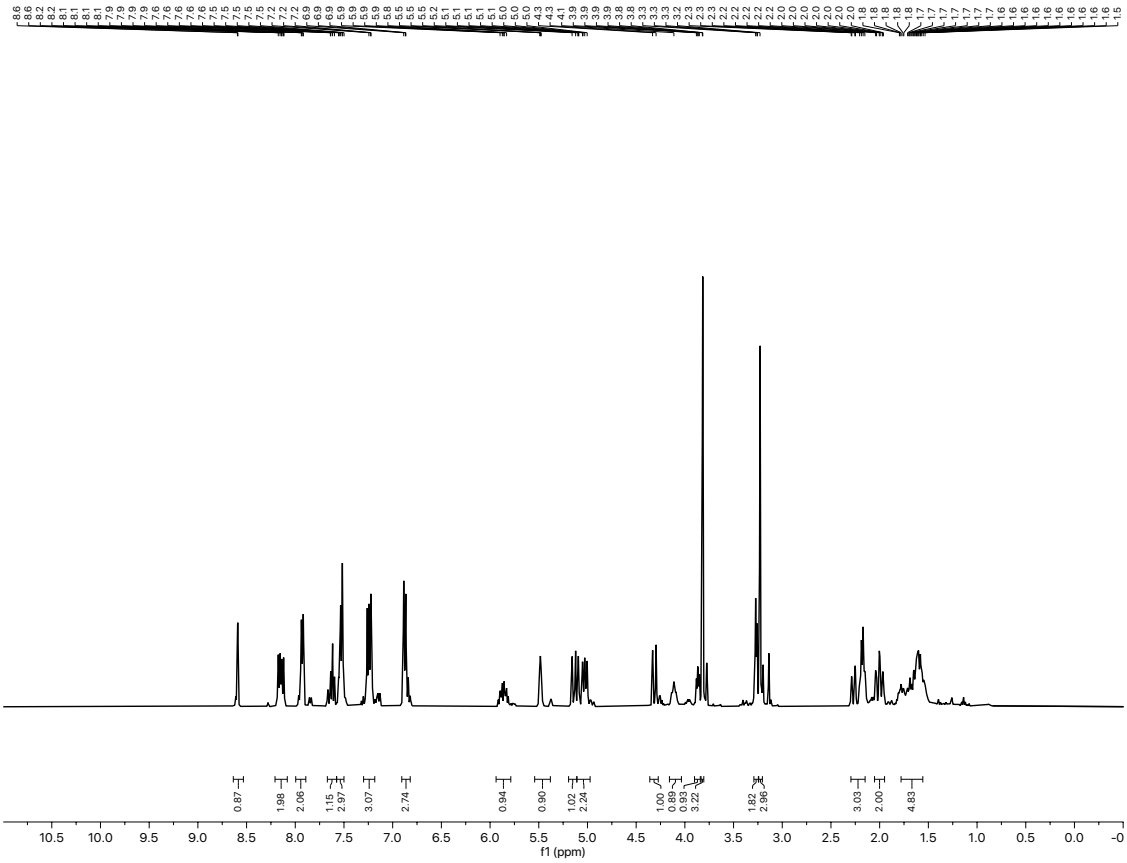

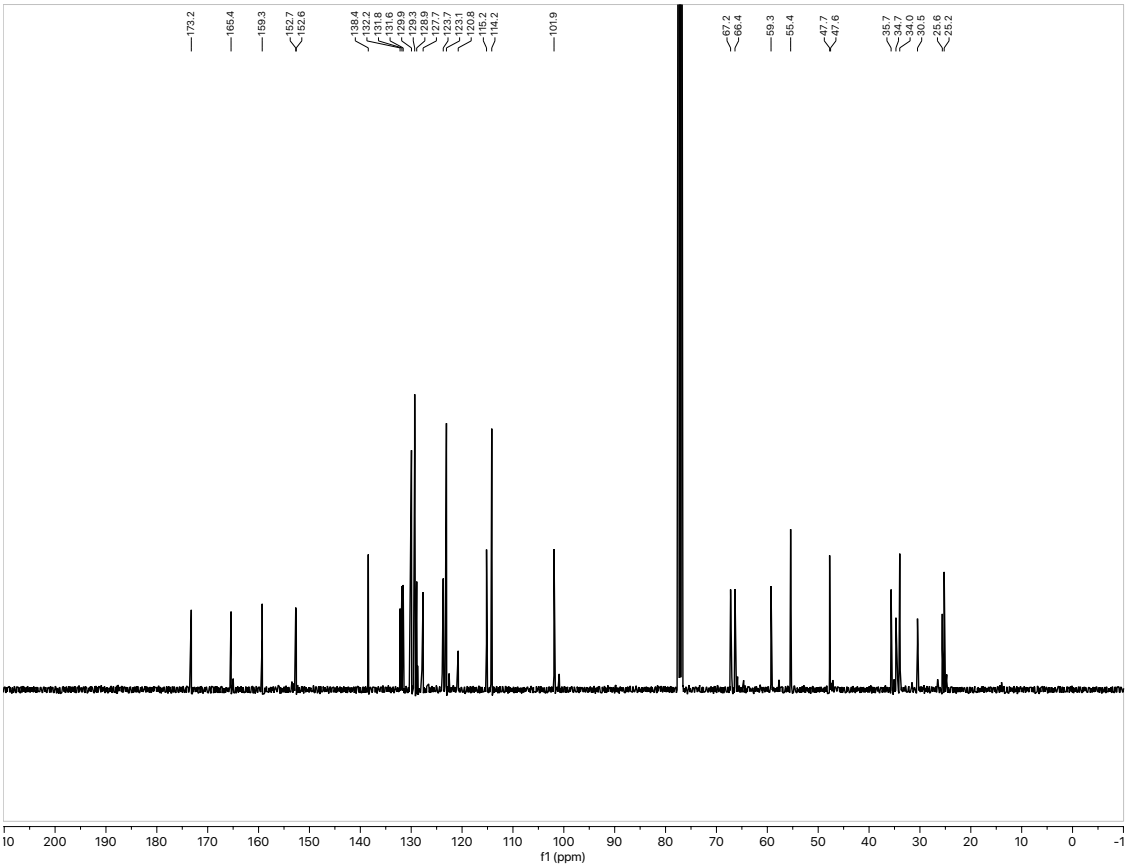

NMR for 35d:

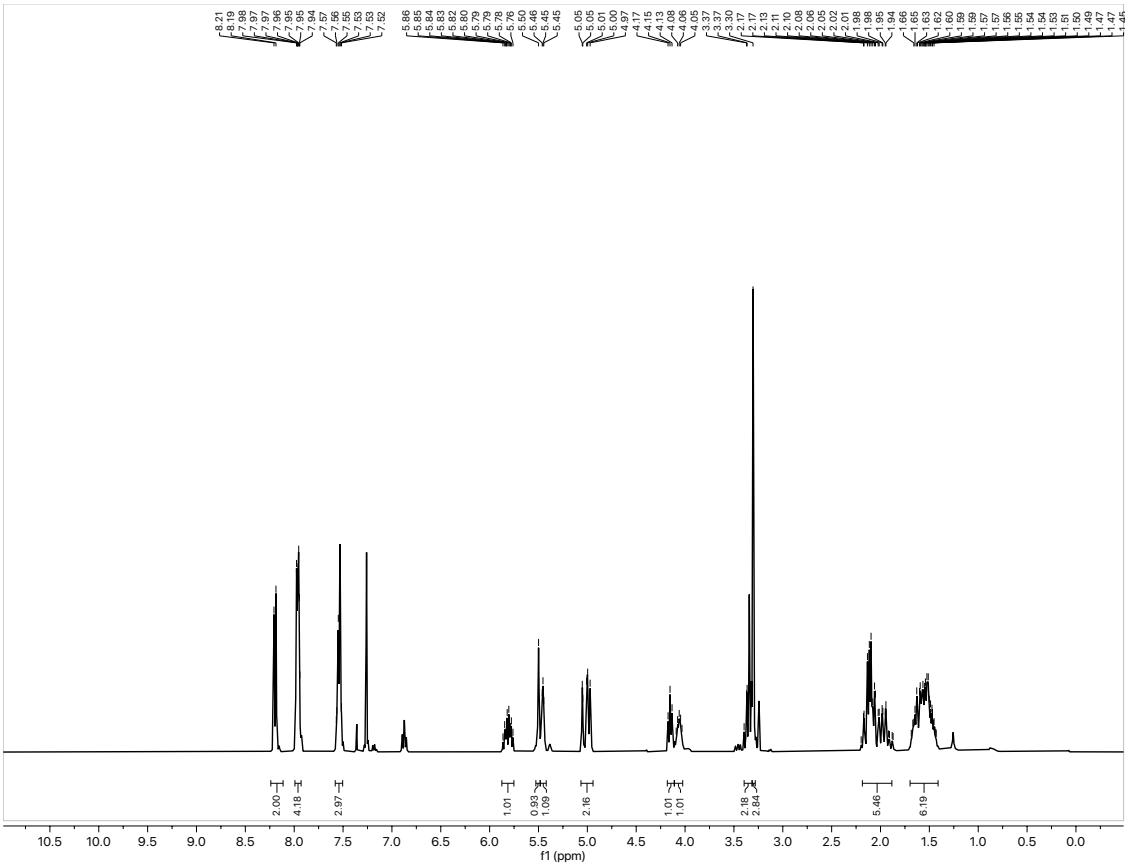
8.21
8.19
7.98
7.97
7.97
7.96
7.95
7.95
7.94
7.57
7.56
7.55
7.53
7.53
7.52
5.86
5.85
5.84
5.83
5.82
5.80
5.79
5.79
5.78
5.76
5.50
5.46
5.45
5.45
5.05
5.05
5.01
5.00
4.97
4.17
4.15
4.13
4.08
4.06
4.05
4.03
3.37
3.30
2.17
2.17
2.13
2.11
2.10
2.08
2.06
2.05
2.02
2.01
1.98
1.98
1.95
1.94
1.66
1.65
1.63
1.62
1.60
1.59
1.59
1.57
1.57
1.56
1.55
1.54
1.54
1.53
1.51
1.50
1.49
1.47
1.47
2.00
4.18
2.97
1.01
0.93
1.09
2.16
1.01
1.01
2.18
2.84
5.46
6.19
10.5
10.0
9.5
9.0
8.5
8.0
7.5
7.0
6.5
6.0
5.5
5.0
4.5
4.0
3.5
3.0
2.5
2.0
1.5
1.0
0.5
0.0
f1 (ppm)

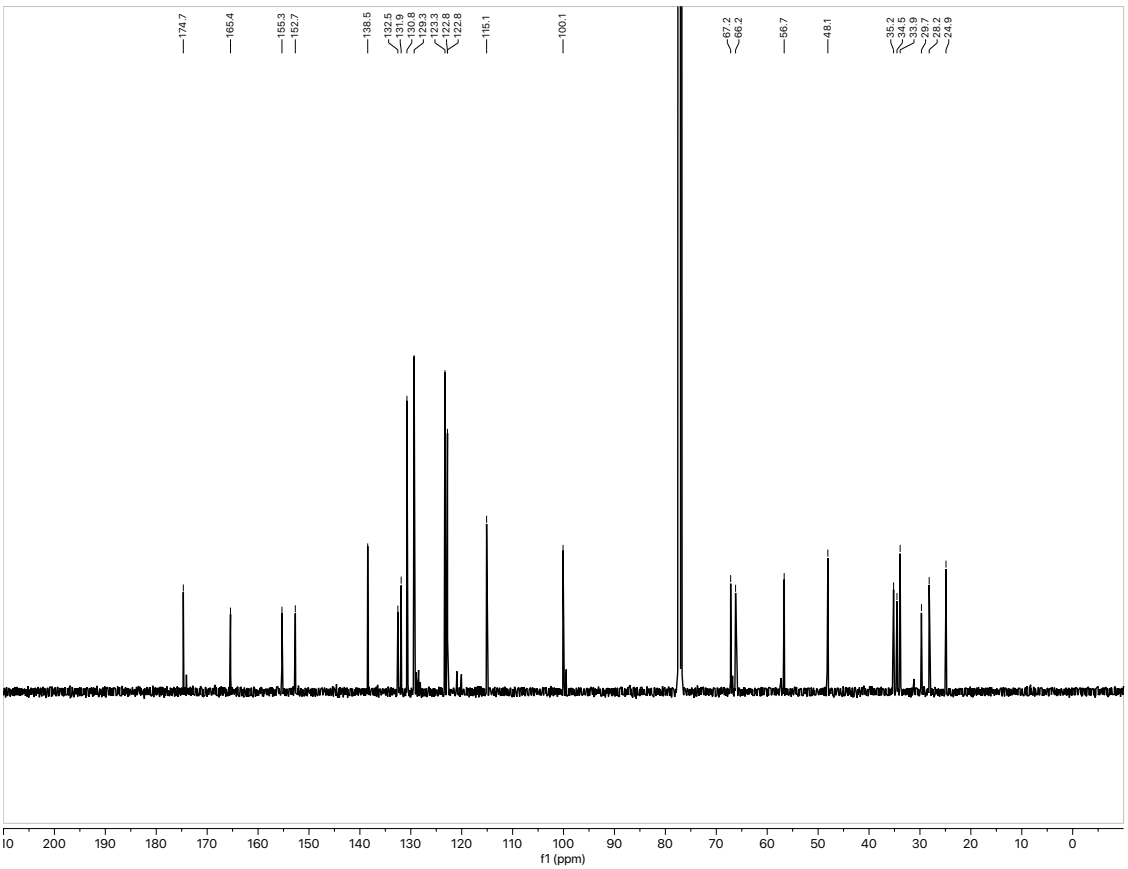
174.7
165.4
155.3
152.7
138.5
132.5
131.9
130.8
129.3
123.3
122.8
122.8
115.1
100.1
67.2
66.2
56.7
48.1
35.2
34.5
33.9
29.7
28.2
24.9
200
190
180
170
160
150
140
130
120
110
100
90
80
70
60
50
40
30
20
10
0
f1 (ppm)

NMR for 36d:

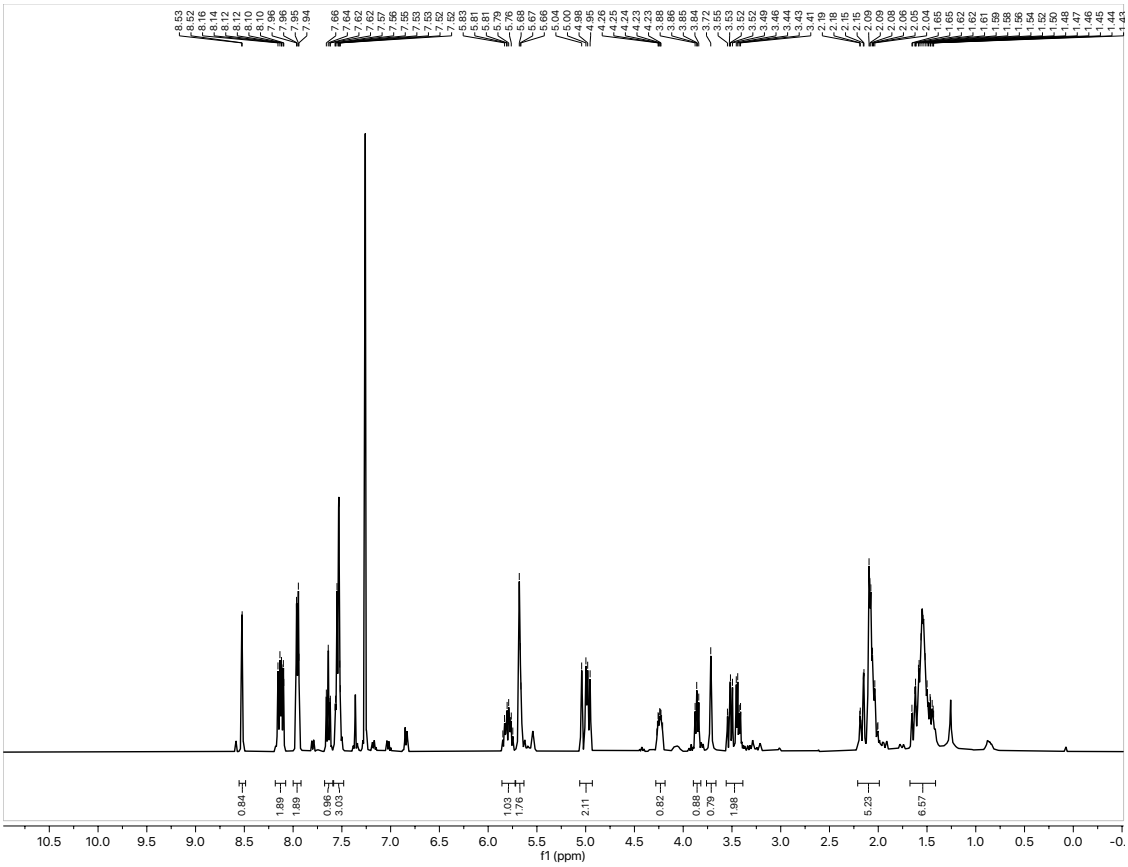
8.53
8.52
8.15
8.14
8.12
8.12
8.10
7.96
7.96
7.95
7.94
7.66
7.64
7.62
7.60
7.57
7.56
7.55
7.53
7.53
7.52
5.83
5.81
5.81
5.79
5.78
5.68
5.67
5.66
5.04
5.00
4.98
4.95
4.26
4.25
4.24
4.23
4.23
3.88
3.86
3.85
3.84
3.77
3.55
3.53
3.52
3.49
3.46
3.44
3.43
3.41
2.19
2.18
2.15
2.15
2.09
2.09
2.08
2.06
2.05
2.04
1.65
1.65
1.62
1.62
1.61
1.59
1.58
1.56
1.54
1.52
1.50
1.48
1.47
1.46
1.45
1.44
1.43
0.84
1.89
1.89
0.96
3.03
1.03
1.76
2.11
0.82
0.88
0.79
1.98
5.23
6.57
10.5 10.0 9.5 9.0 8.5 8.0 7.5 7.0 6.5 6.0 5.5 5.0 4.5 4.0 3.5 3.0 2.5 2.0 1.5 1.0 0.5 0.0
f1 (ppm)

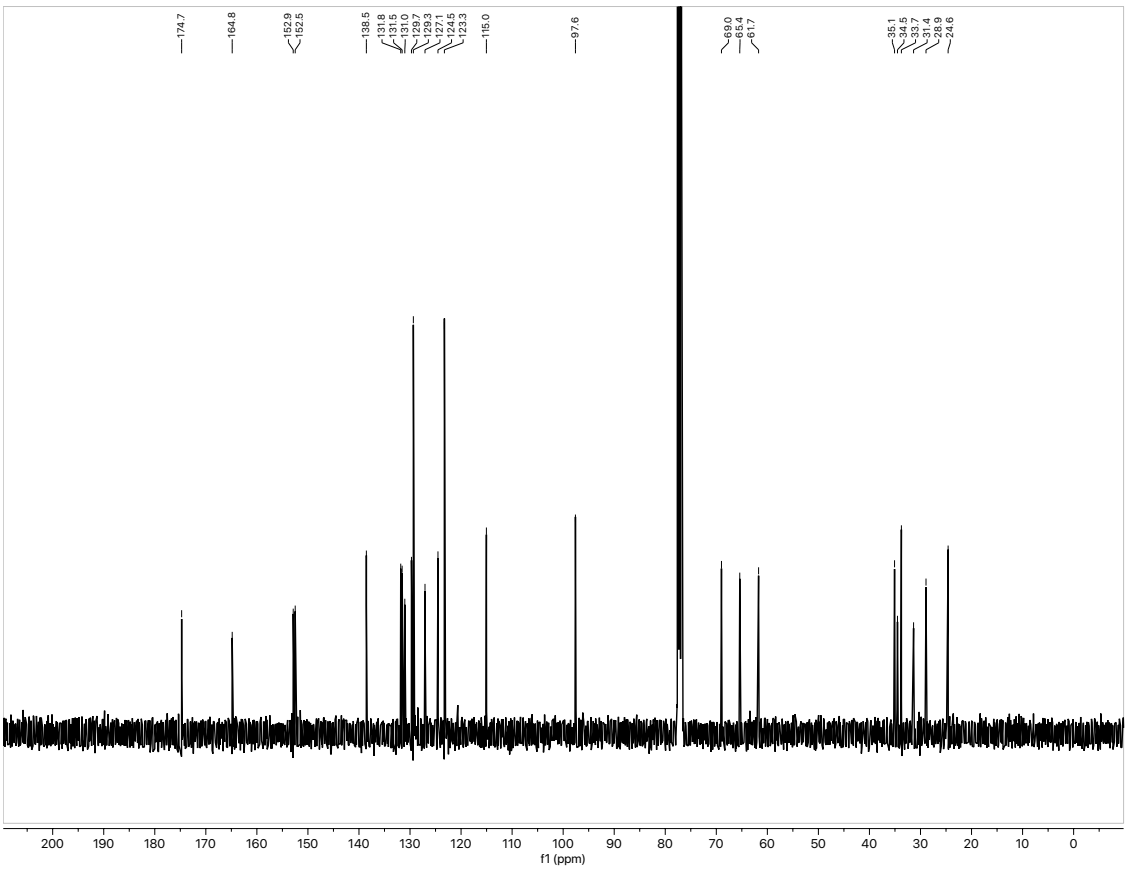
174.7
164.8
152.9
152.5
138.5
131.8
131.5
131.0
129.7
129.3
127.1
124.5
123.3
115.0
97.6
69.0
65.4
61.7
35.1
34.5
33.7
31.4
28.9
24.6
200 190 180 170 160 150 140 130 120 110 100 90 80 70 60 50 40 30 20 10 0
f1 (ppm)

NMR for 35e:

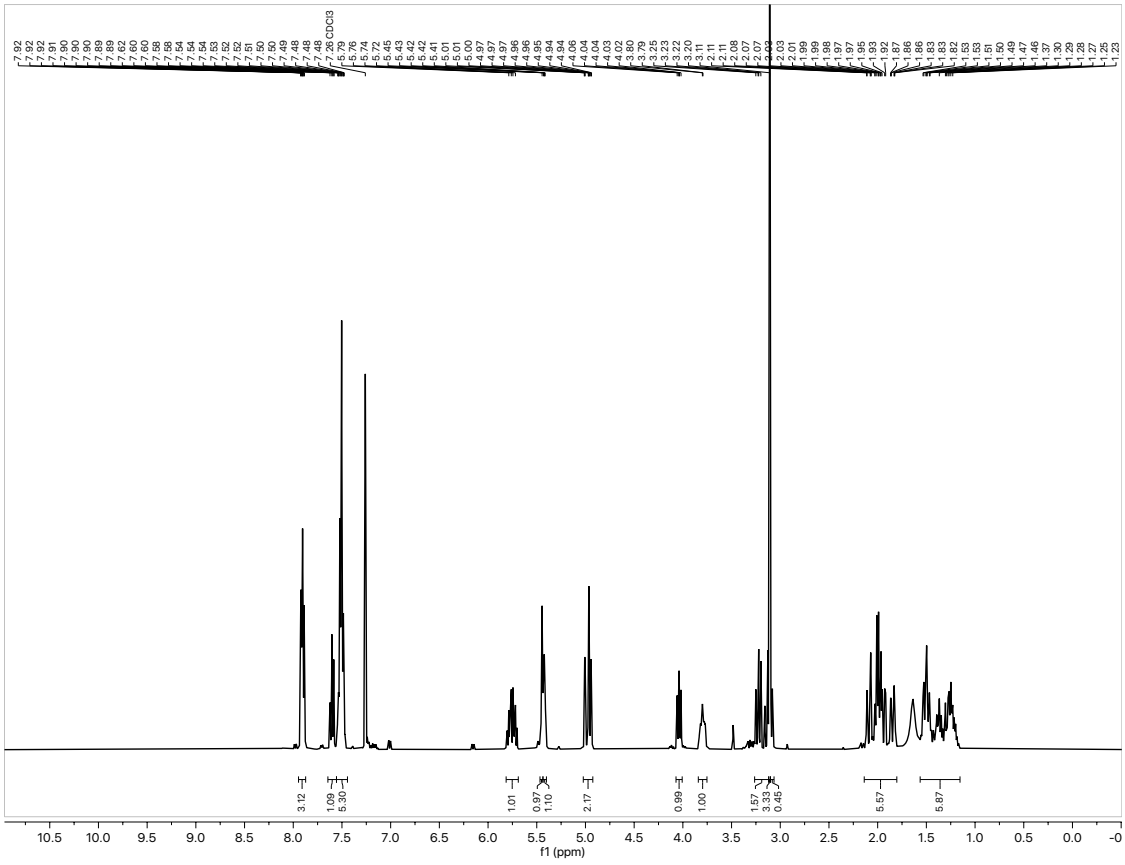
7.92
7.92
7.92
7.91
7.90
7.90
7.90
7.89
7.89
7.62
7.60
7.60
7.58
7.58
7.54
7.54
7.54
7.53
7.52
7.52
7.51
7.50
7.50
7.49
7.48
7.48
7.48
CDCl3
5.79
5.76
5.74
5.72
5.46
5.45
5.43
5.42
5.42
5.41
5.01
5.01
5.00
4.97
4.97
4.97
4.96
4.96
4.95
4.94
4.94
4.06
4.04
4.04
4.03
4.02
3.80
3.79
3.25
3.23
3.22
3.20
3.11
2.11
2.08
2.07
2.07
3.03
2.03
2.01
2.00
1.99
1.98
1.97
1.97
1.95
1.93
1.92
1.87
1.86
1.86
1.83
1.83
1.82
1.53
1.53
1.51
1.50
1.50
1.49
1.47
1.46
1.37
1.30
1.29
1.28
1.27
1.25
1.23
3.12
1.09
5.30
1.01
0.97
1.10
2.17
0.99
1.00
1.57
3.33
0.45
5.57
5.87
f1 (ppm)

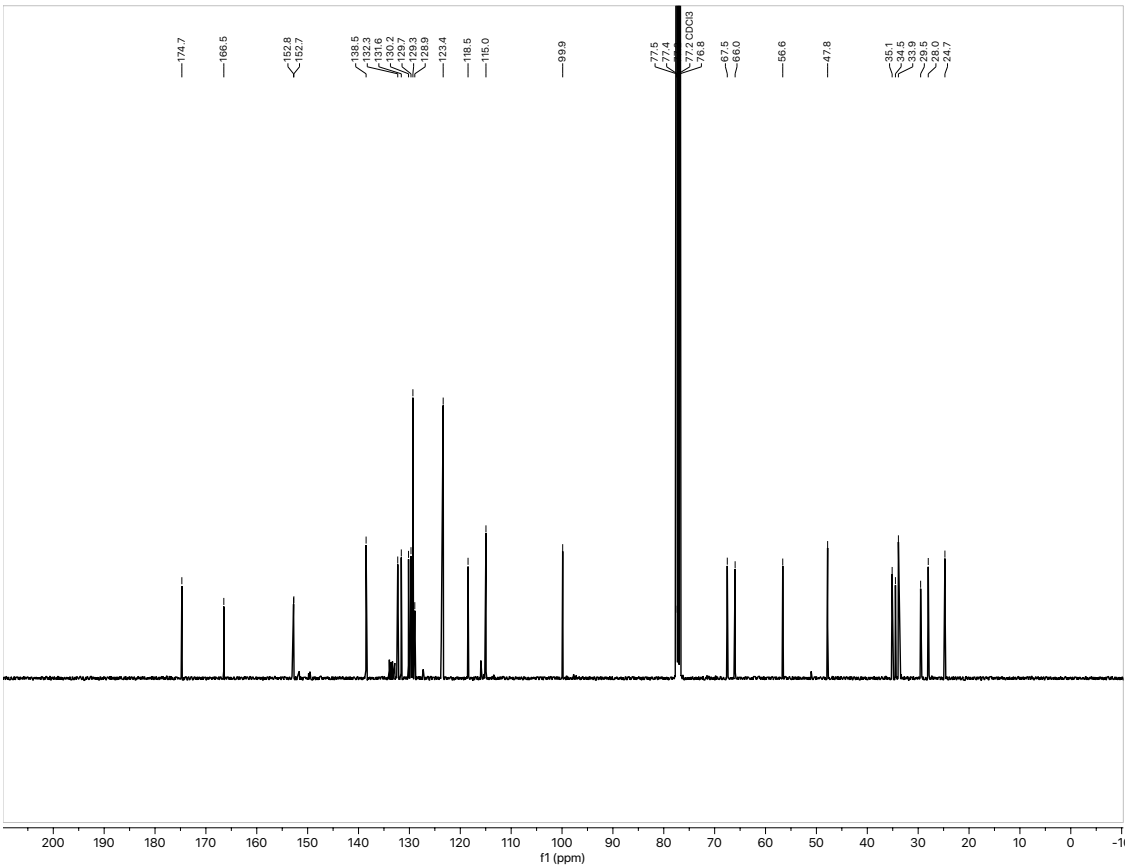
174.7
166.5
152.8
152.7
138.5
132.3
131.6
130.2
129.7
129.3
128.9
123.4
118.5
115.0
99.9
77.5
77.4
77.2 CDCl3
76.8
67.5
66.0
56.6
47.8
35.1
34.5
33.9
29.5
28.0
24.7
f1 (ppm)

NMR for 36e:

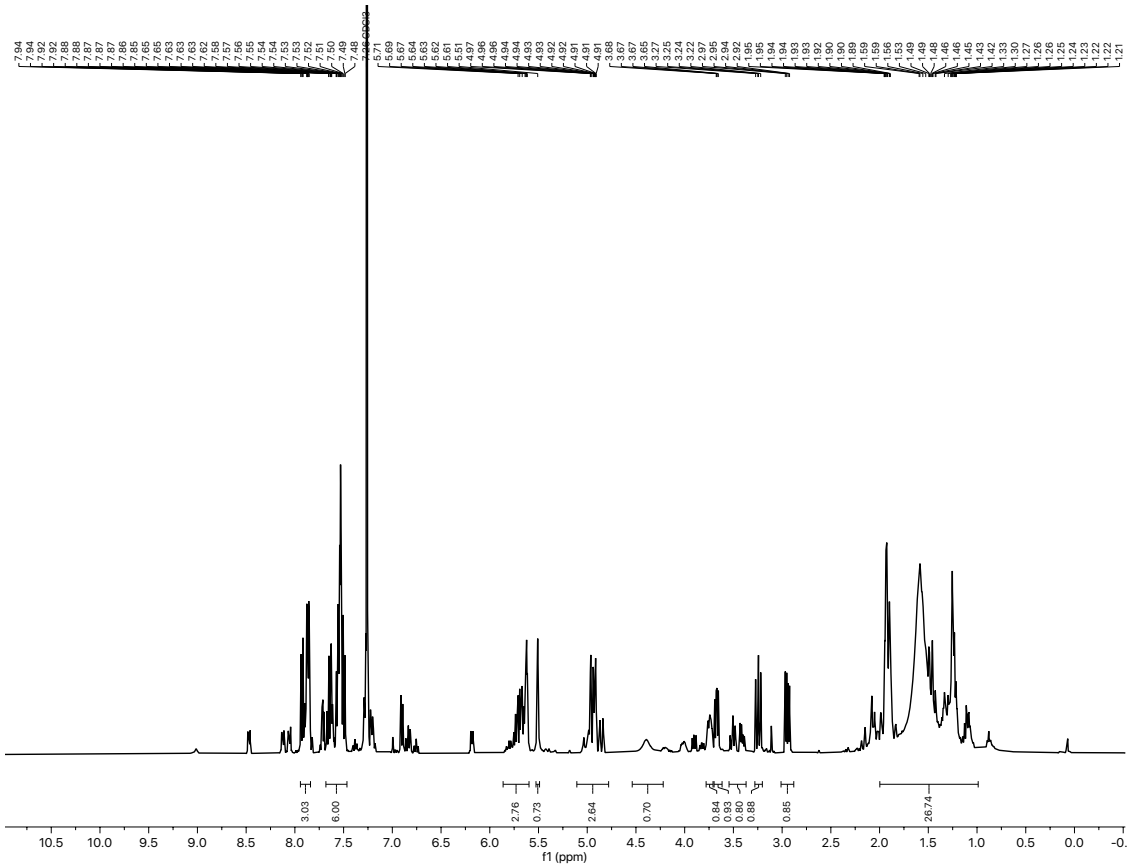

NMR for 41:

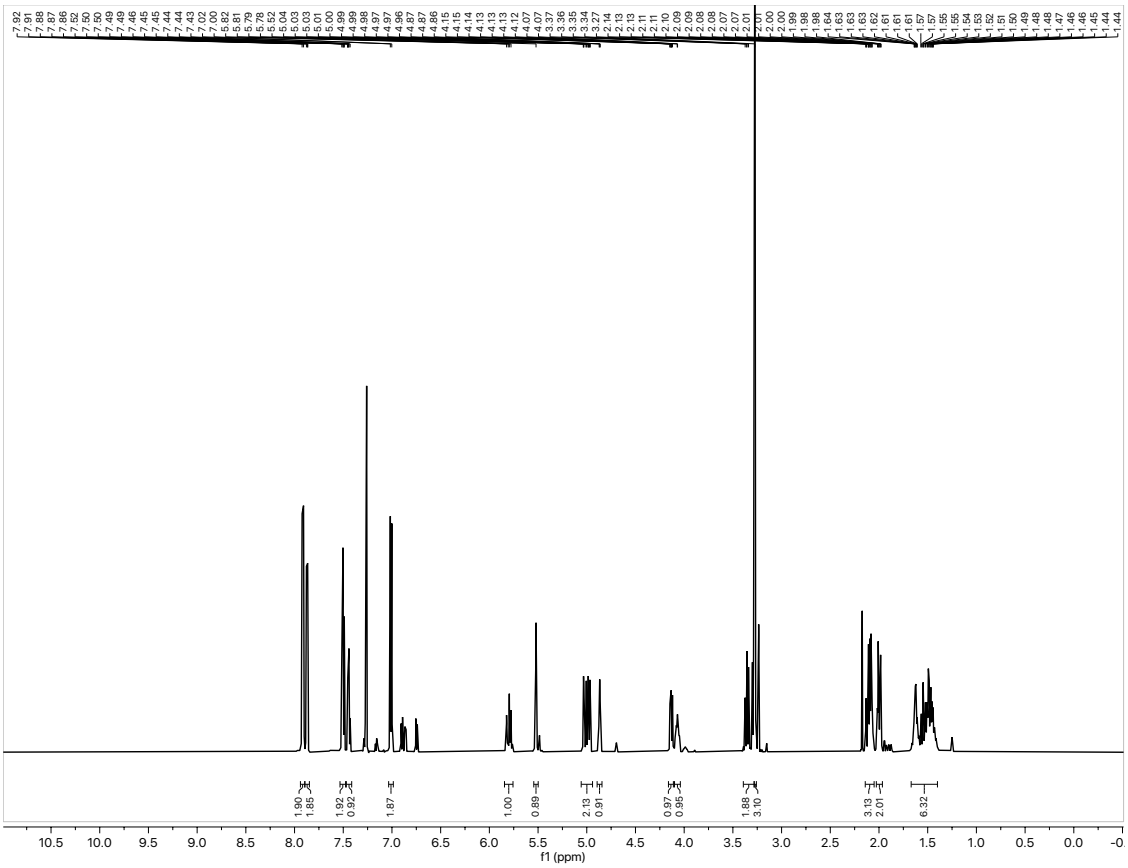

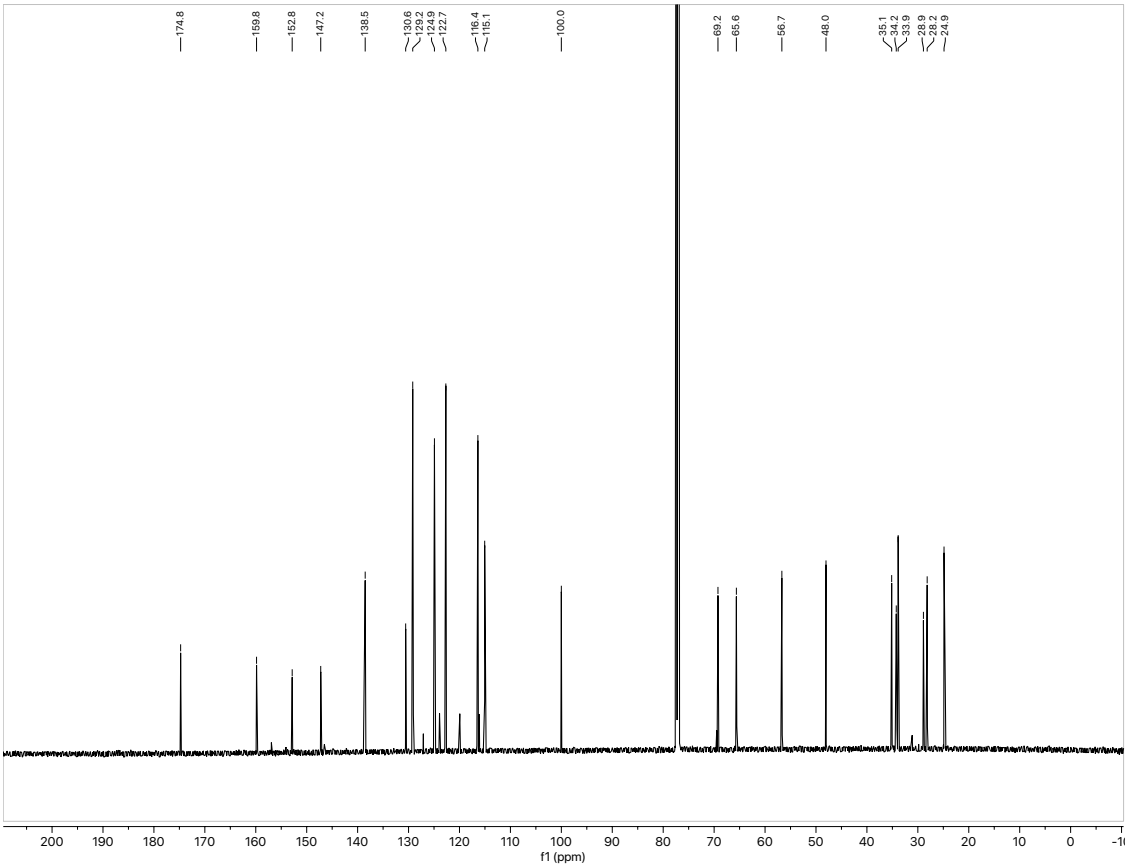

NMR for 42:

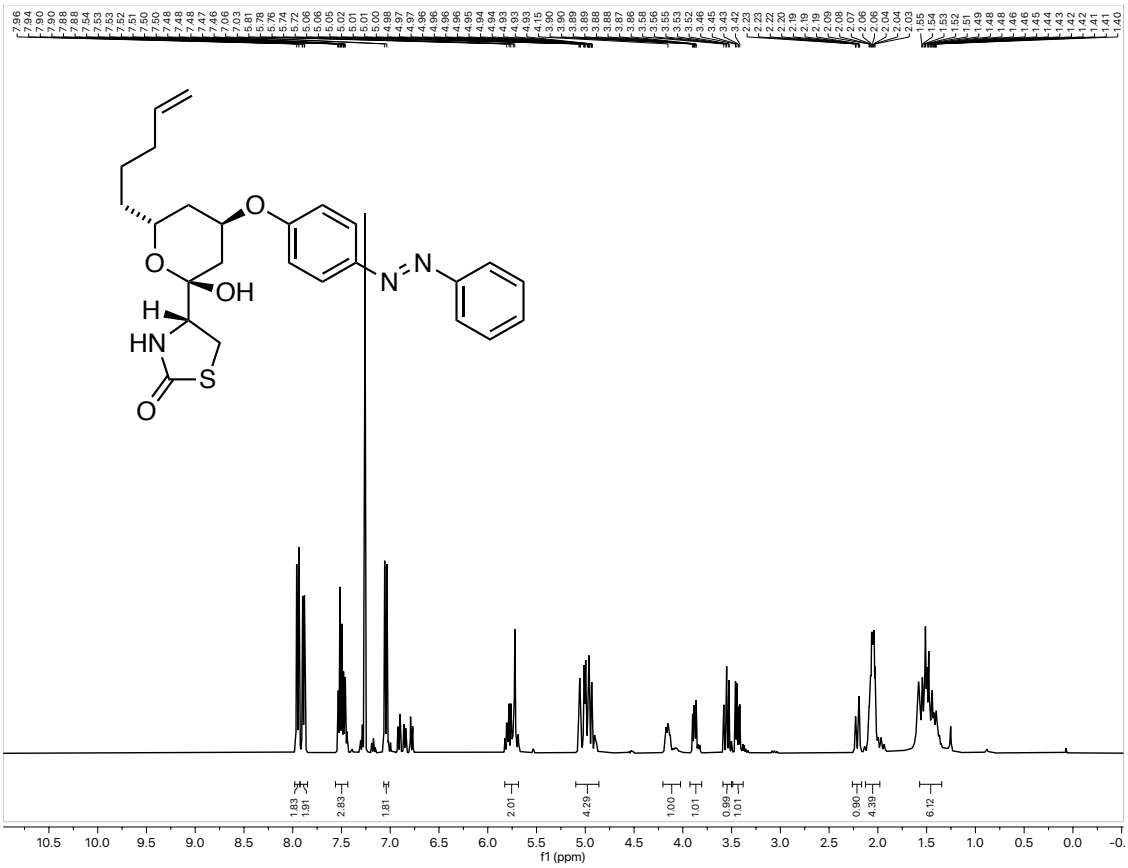
O
O
OH
H
HN
S
O
N
N
f1 (ppm)

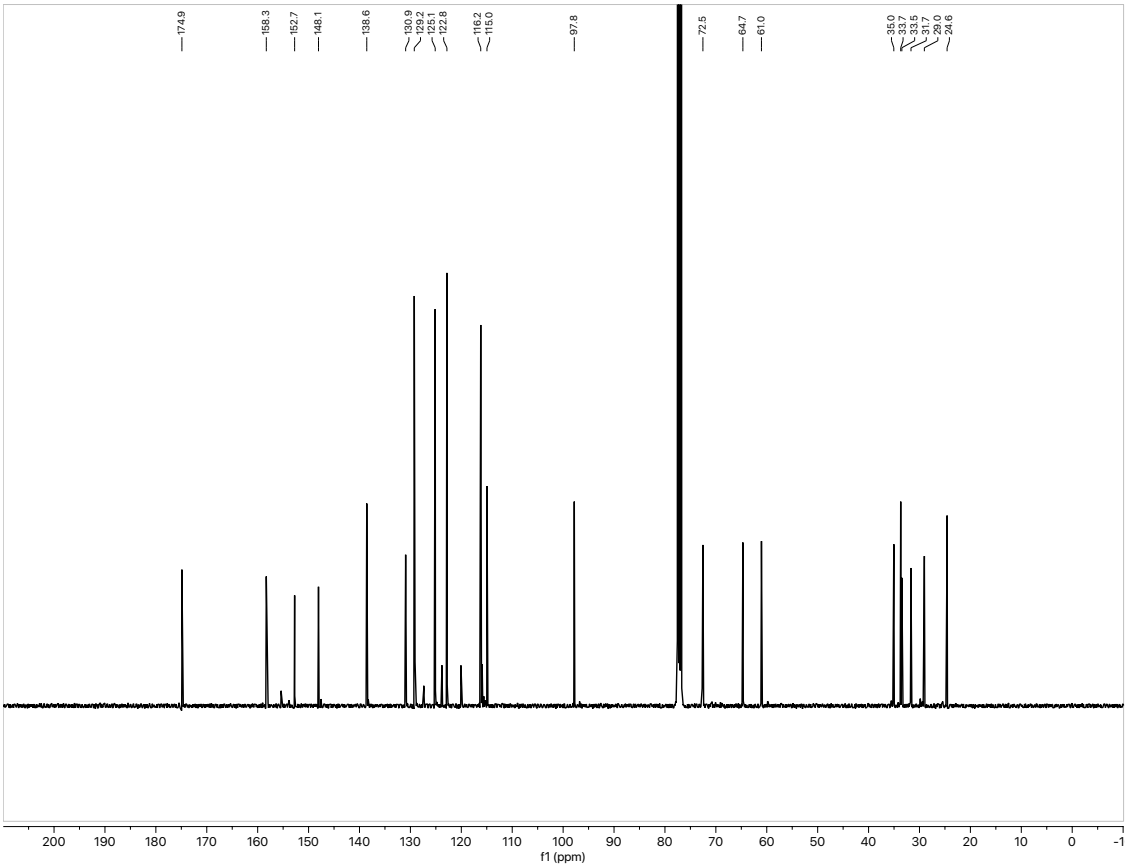
174.9
168.3
162.7
148.1
138.6
130.9
129.2
125.1
122.8
116.2
115.0
97.8
72.5
64.7
61.0
35.0
33.7
33.5
31.7
29.0
24.6
f1 (ppm)

NMR for s43:

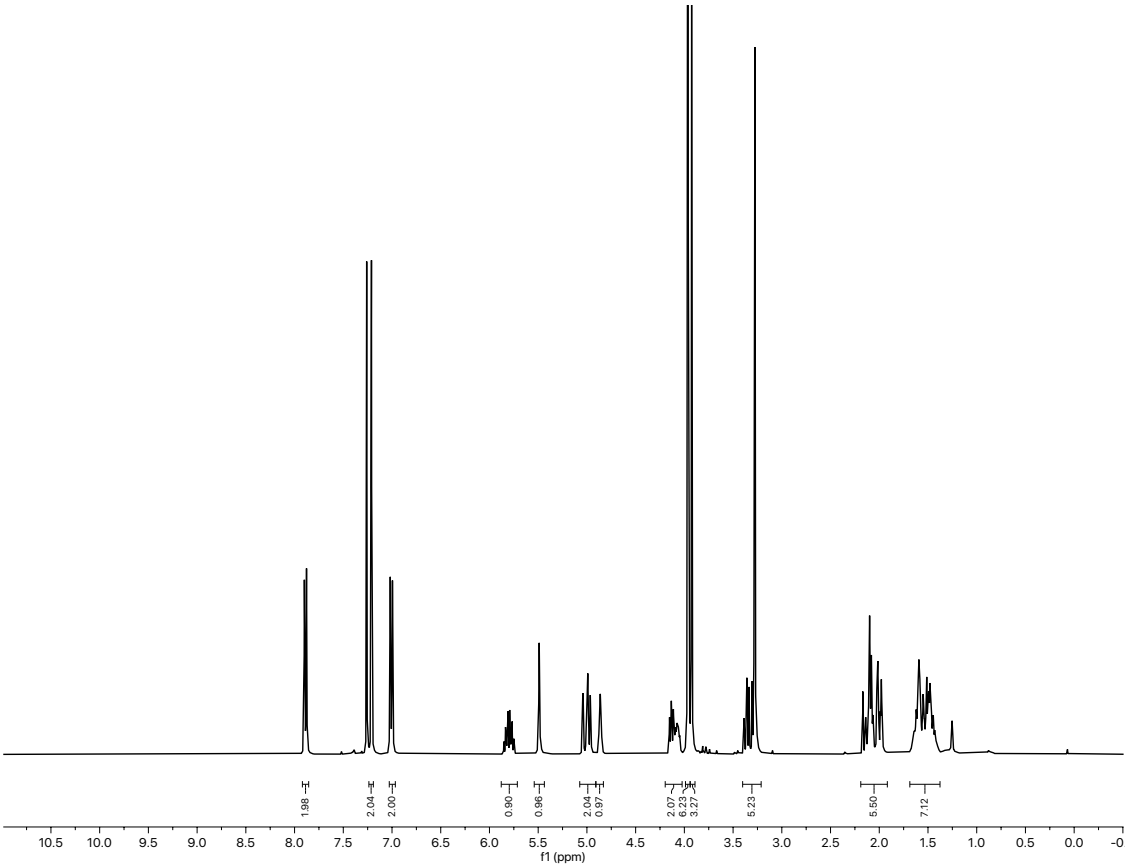
1.98
2.04
2.00
0.90
0.96
2.04
0.97
2.07
6.23
3.27
5.23
5.50
7.12
f1 (ppm)

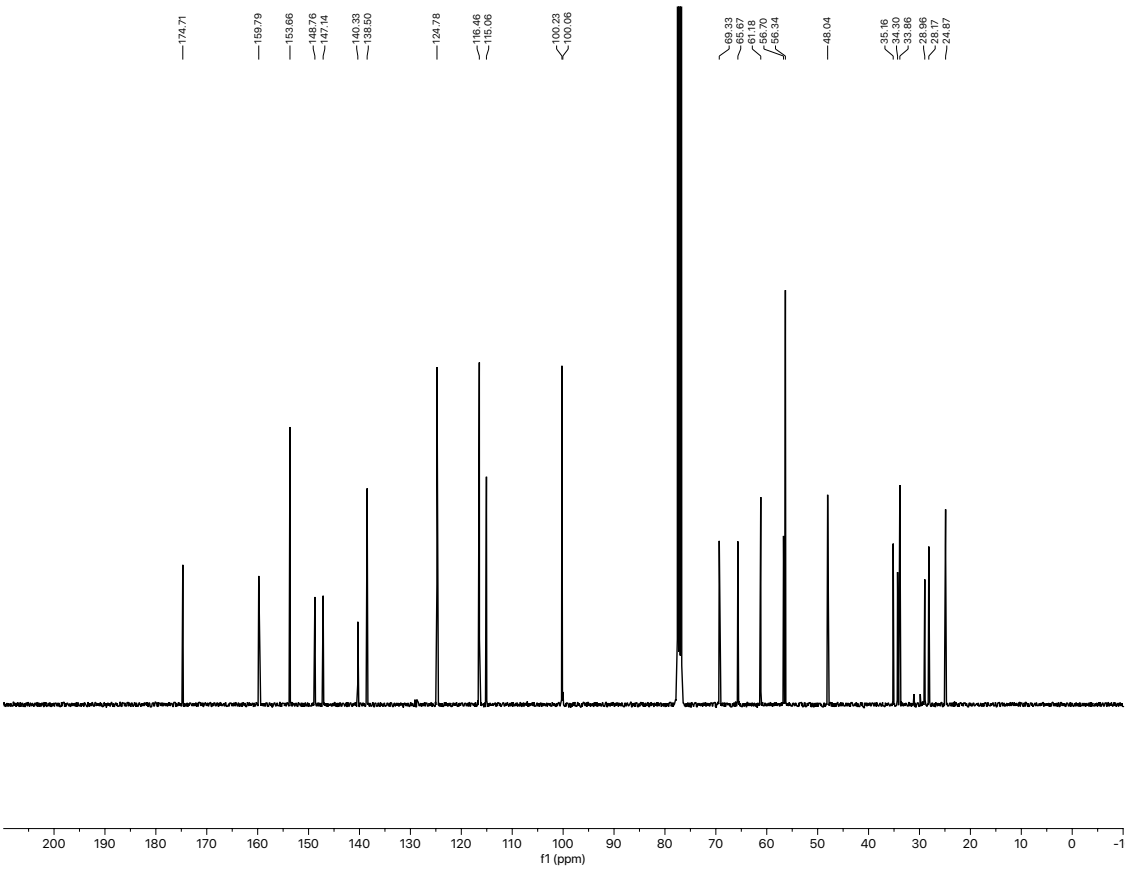
174.71
159.79
153.66
148.76
147.14
140.33
138.50
124.78
116.46
115.06
100.23
100.06
69.33
65.67
61.18
58.70
56.34
48.04
35.16
34.30
33.86
28.96
28.17
24.87
f1 (ppm)

NMR for 43:

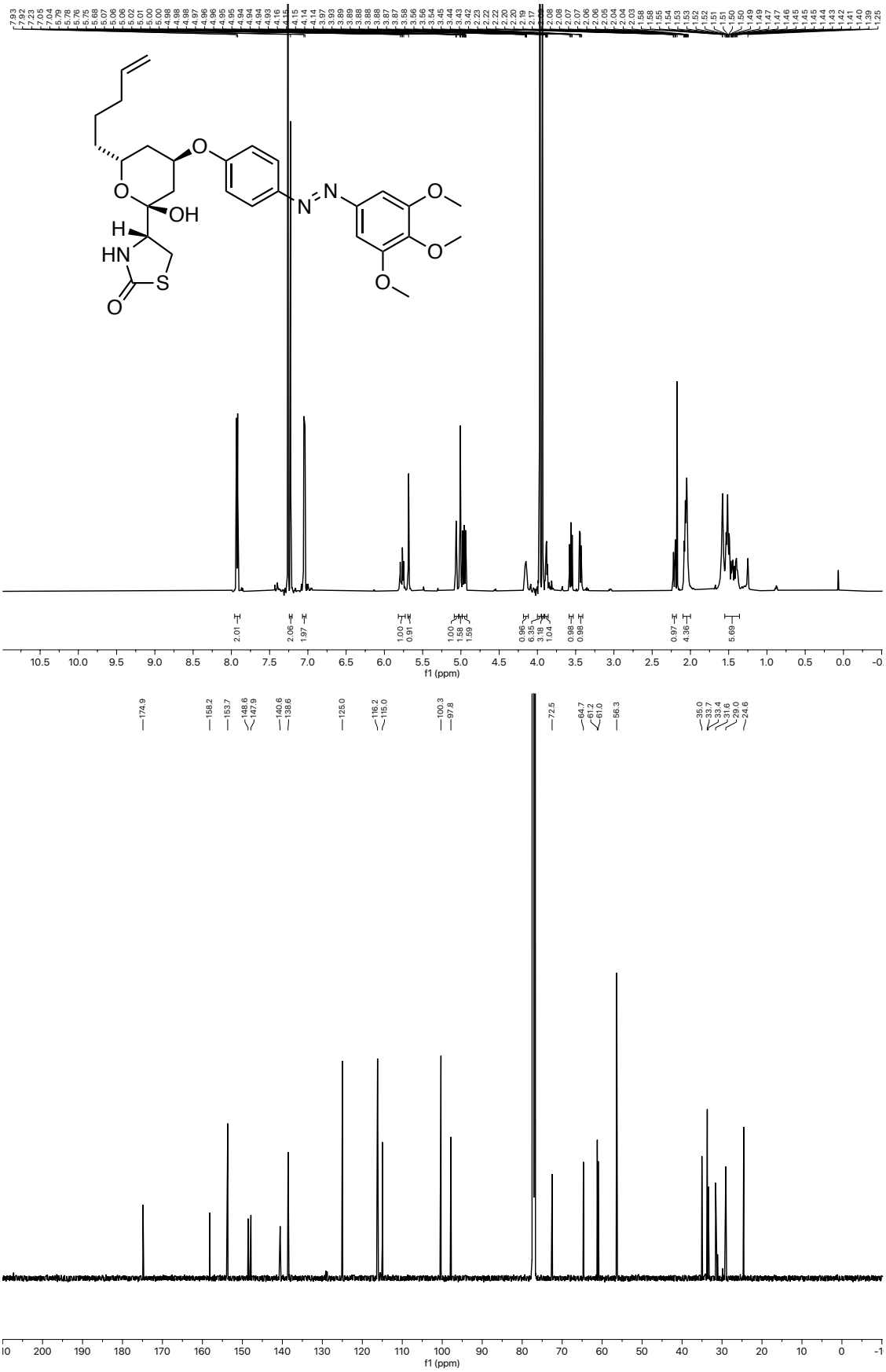

NMR for s44:

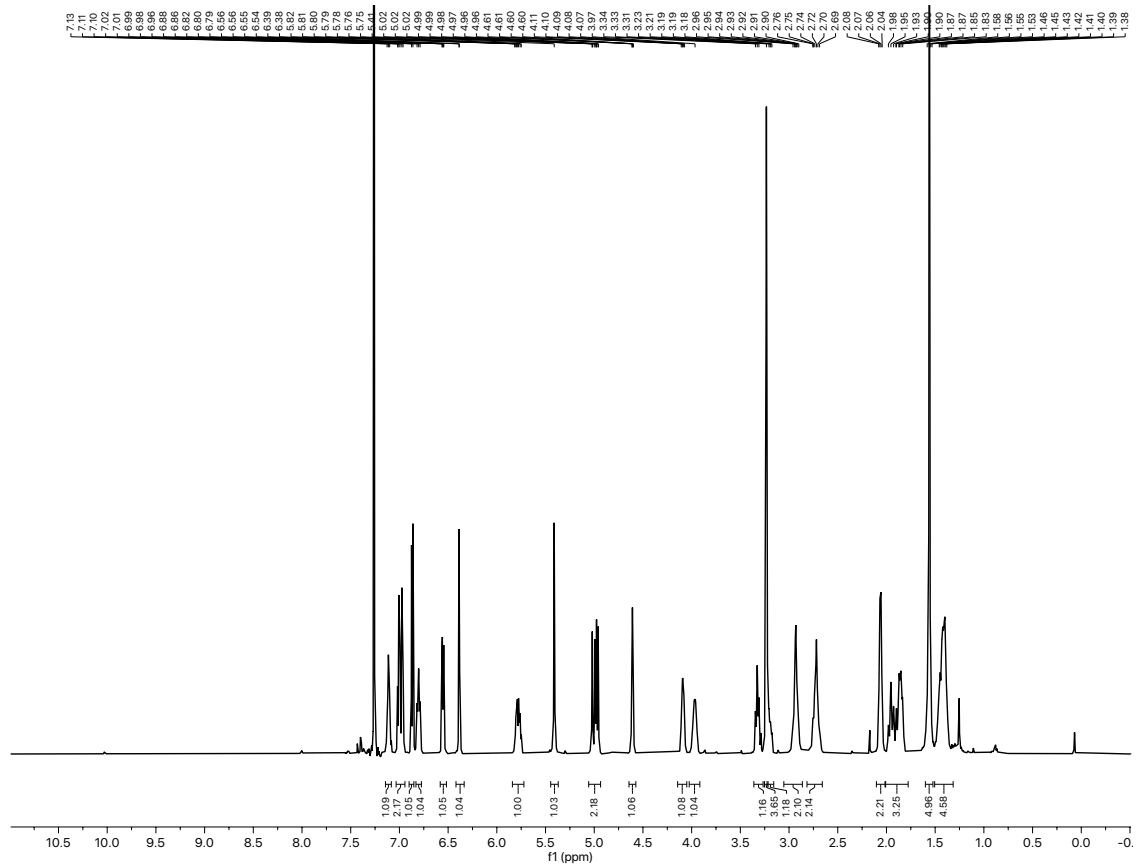

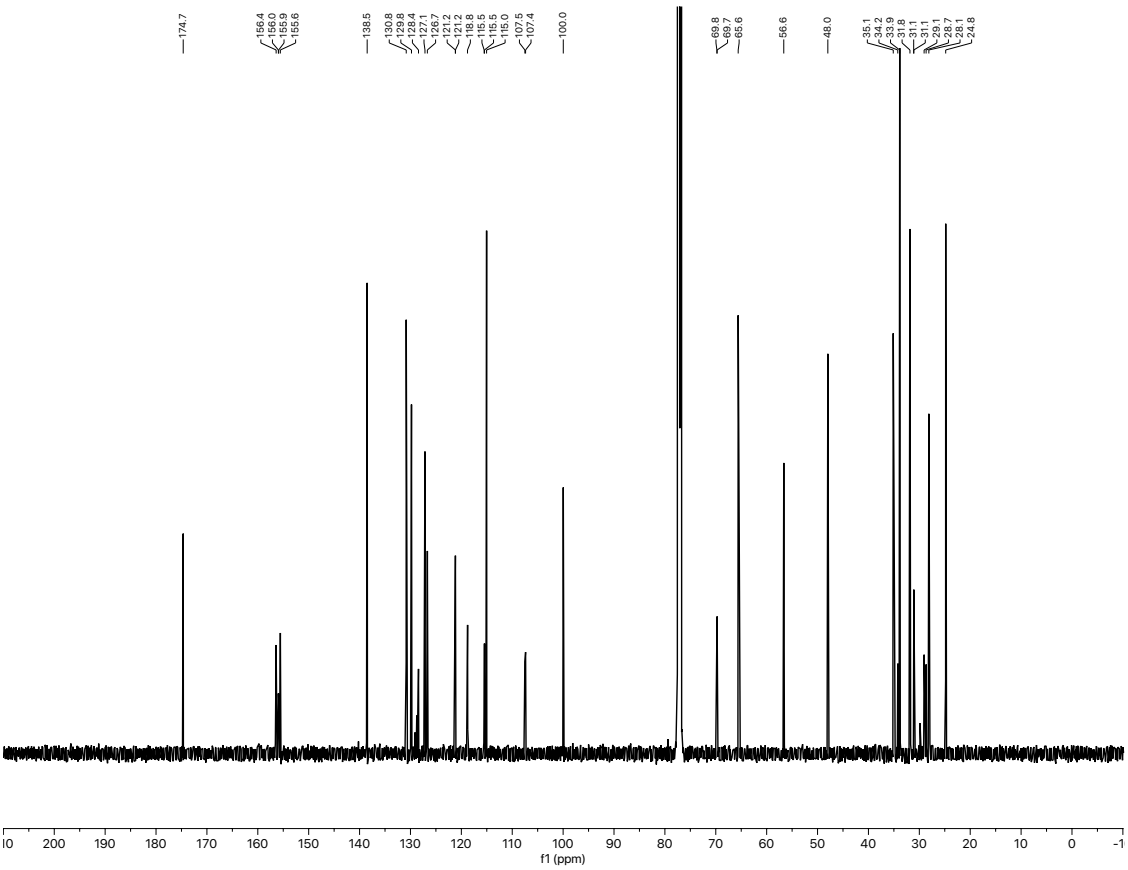

NMR for 44:

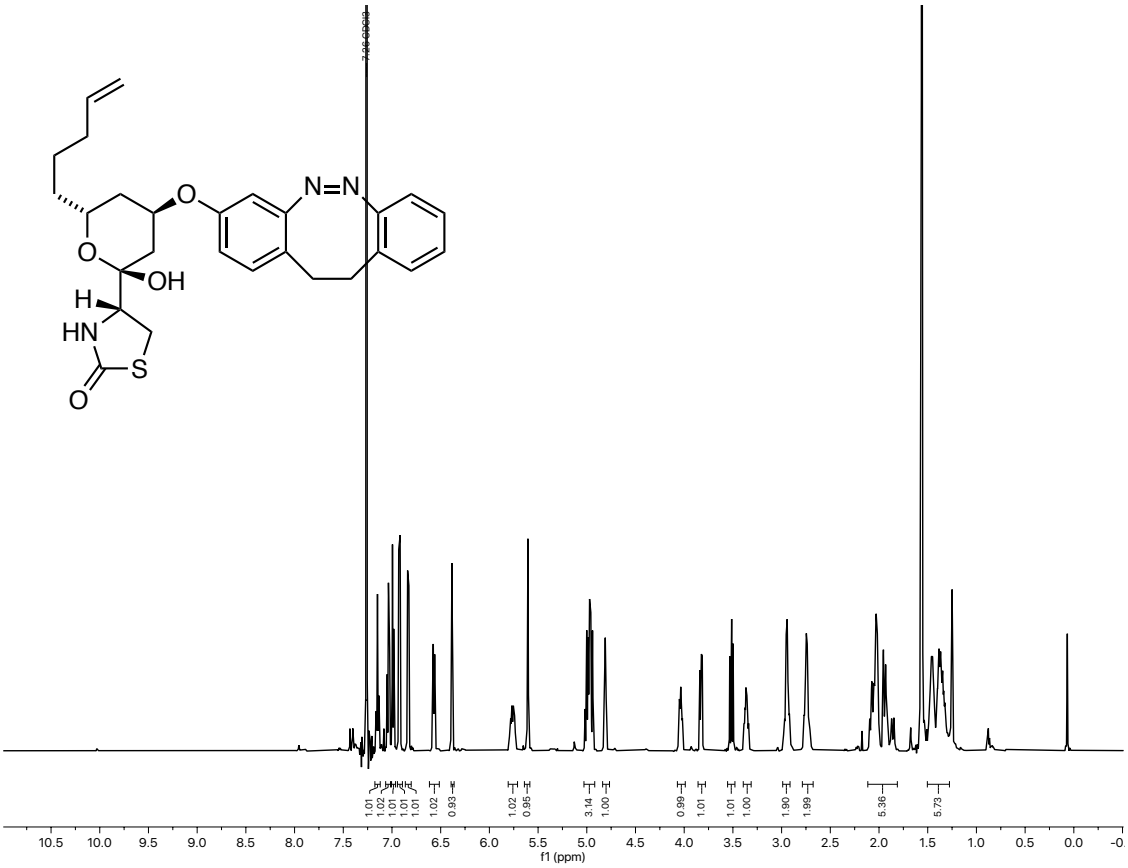
7.26 CDCl3
N=N
O
OH
H
HN
S
O
1.01
1.02
1.01
1.01
1.01
1.02
0.93
1.02
0.95
3.14
1.00
0.99
1.01
1.01
1.00
1.90
1.99
5.36
5.73
f1 (ppm)

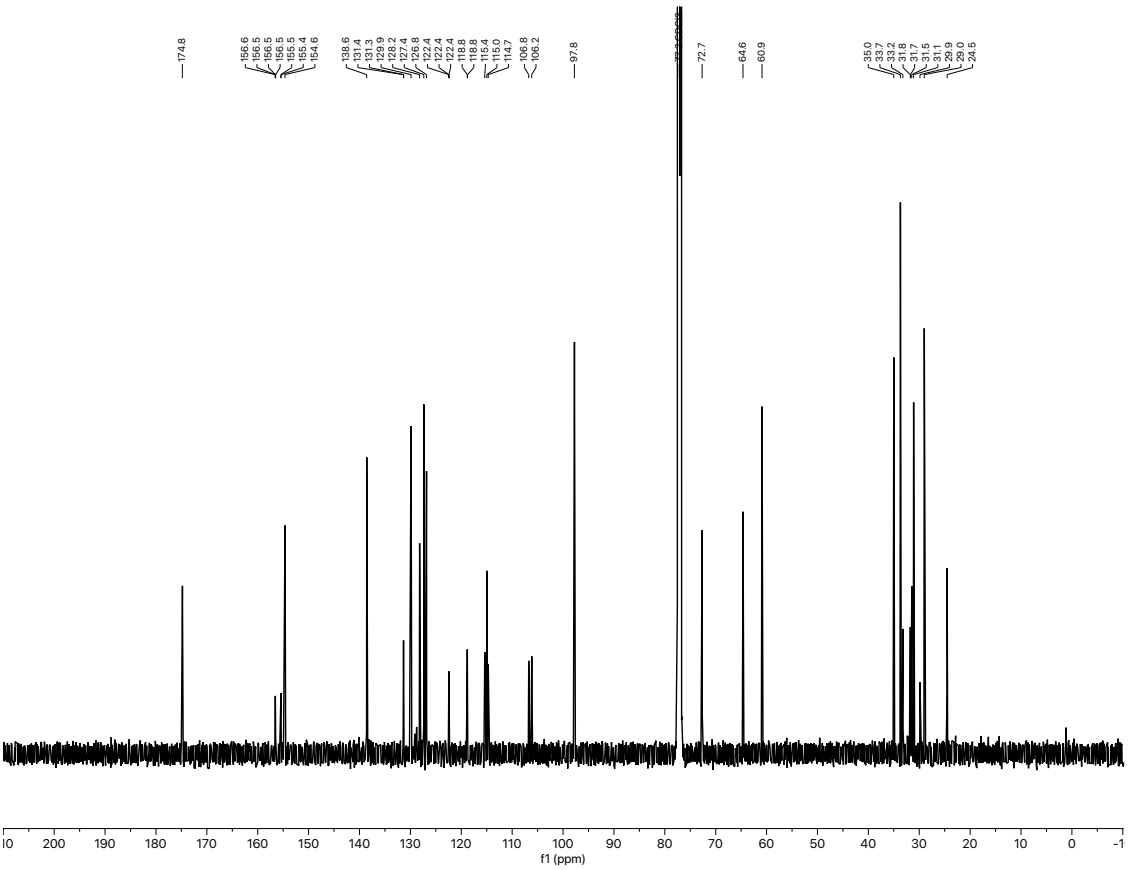
174.8
156.6
156.5
156.5
156.5
155.5
155.4
154.6
138.6
137.4
131.3
129.9
128.2
127.4
126.8
122.4
122.4
118.8
118.8
115.4
115.0
114.7
106.8
106.2
97.8
77.2 CDCl3
72.7
64.6
60.9
35.0
33.7
33.2
31.8
31.7
31.5
31.1
29.9
29.0
24.5
f1 (ppm)

NMR for 45:

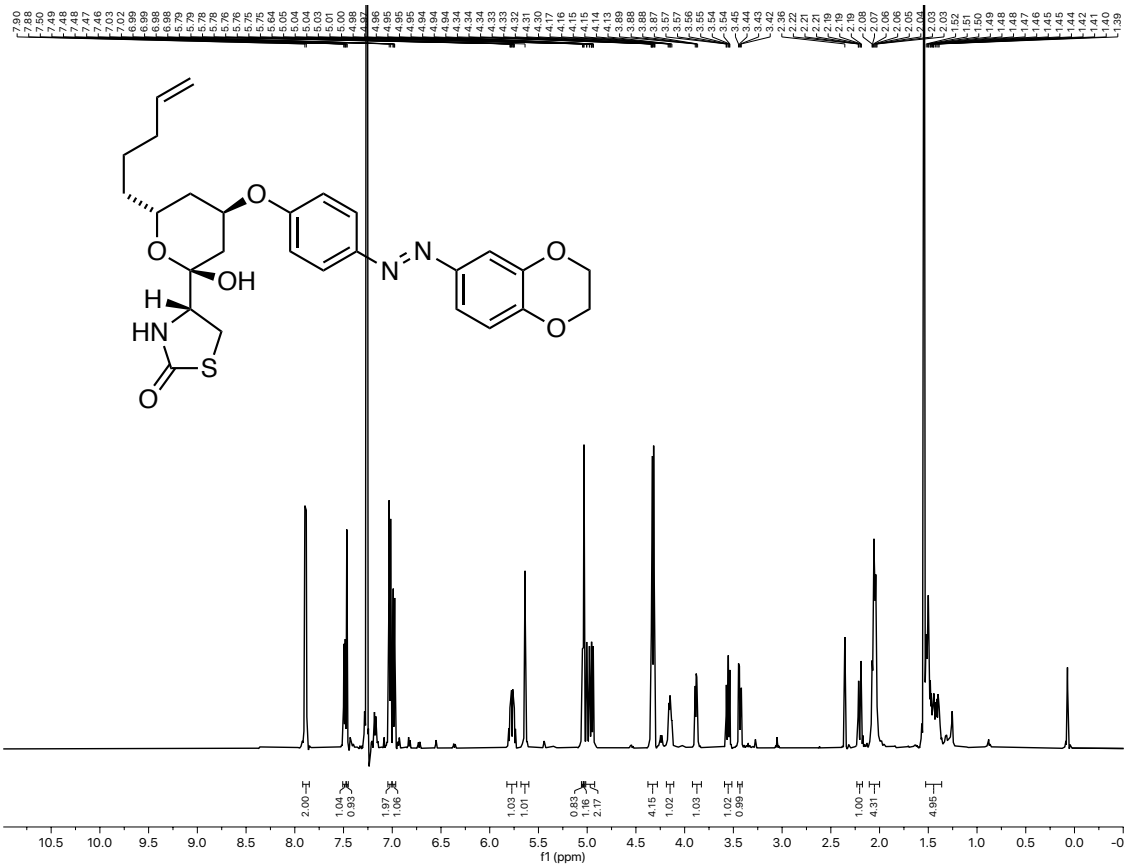

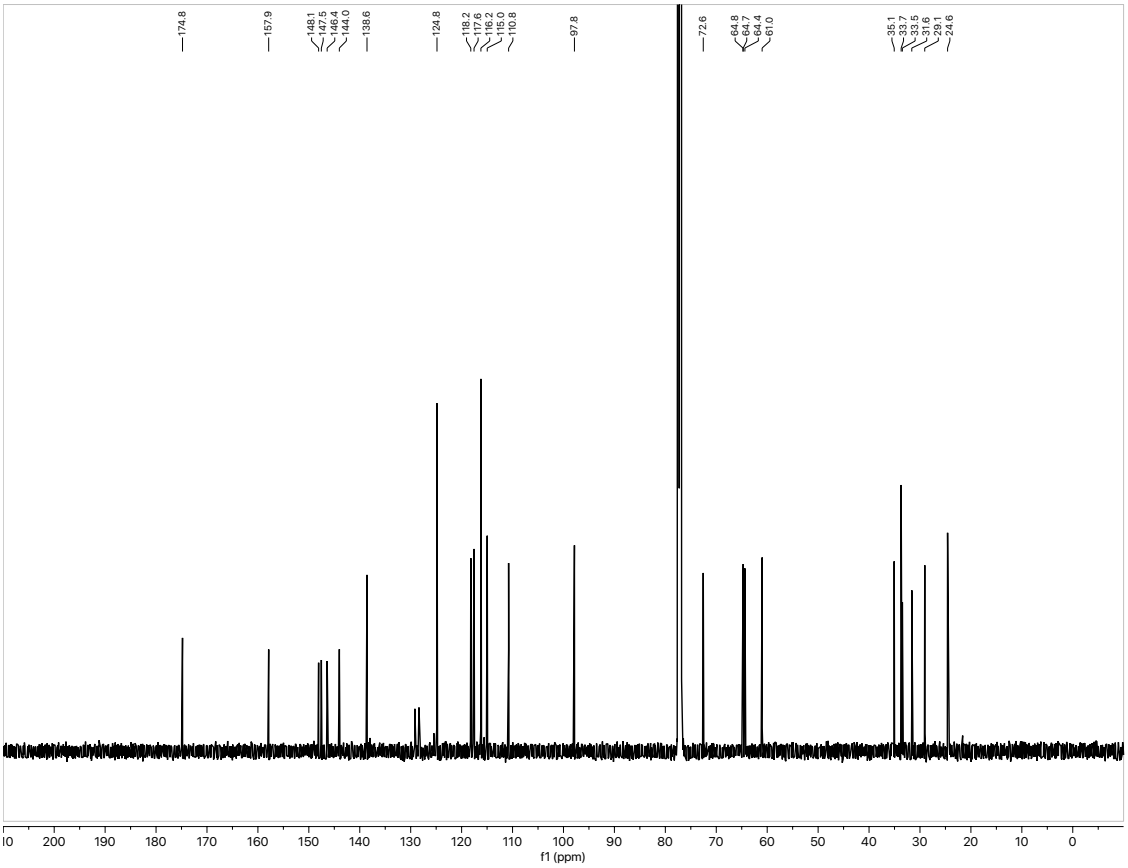

NMR for 48:

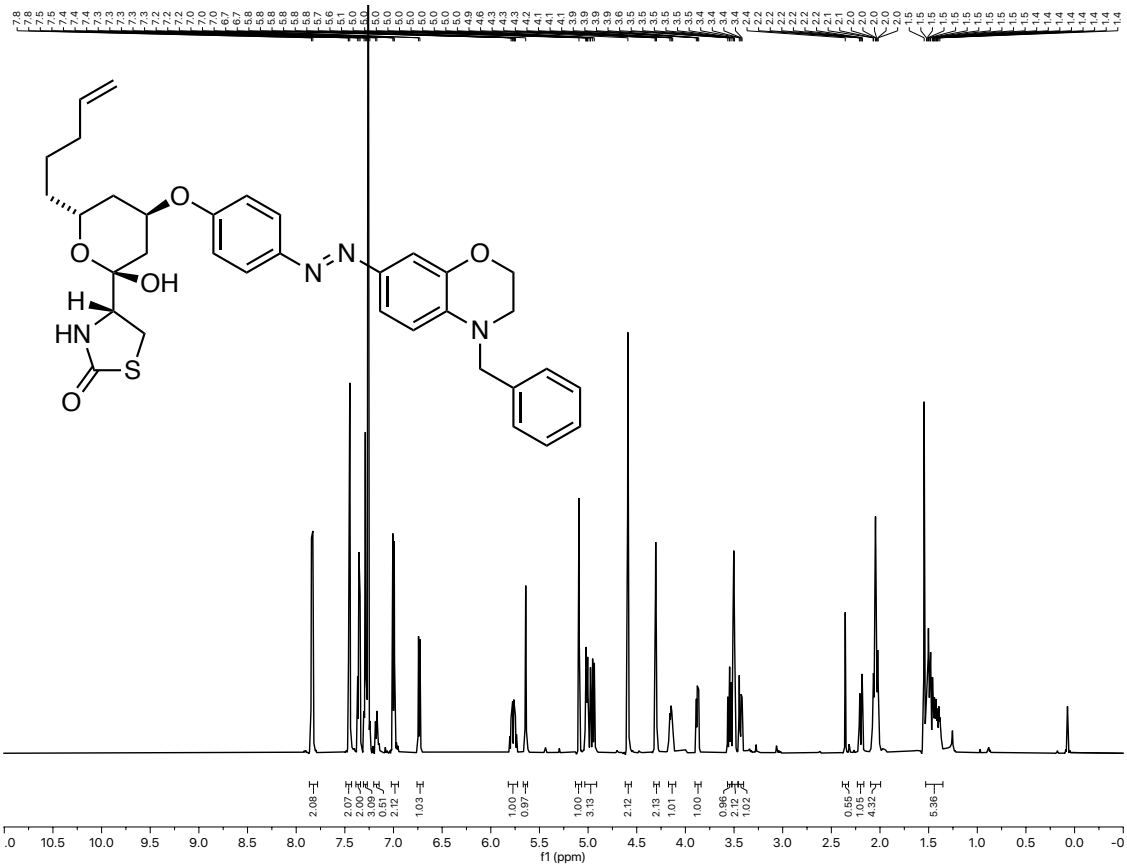
O
O
OH
H
HN
S
O
N
N
O
N
f1 (ppm)

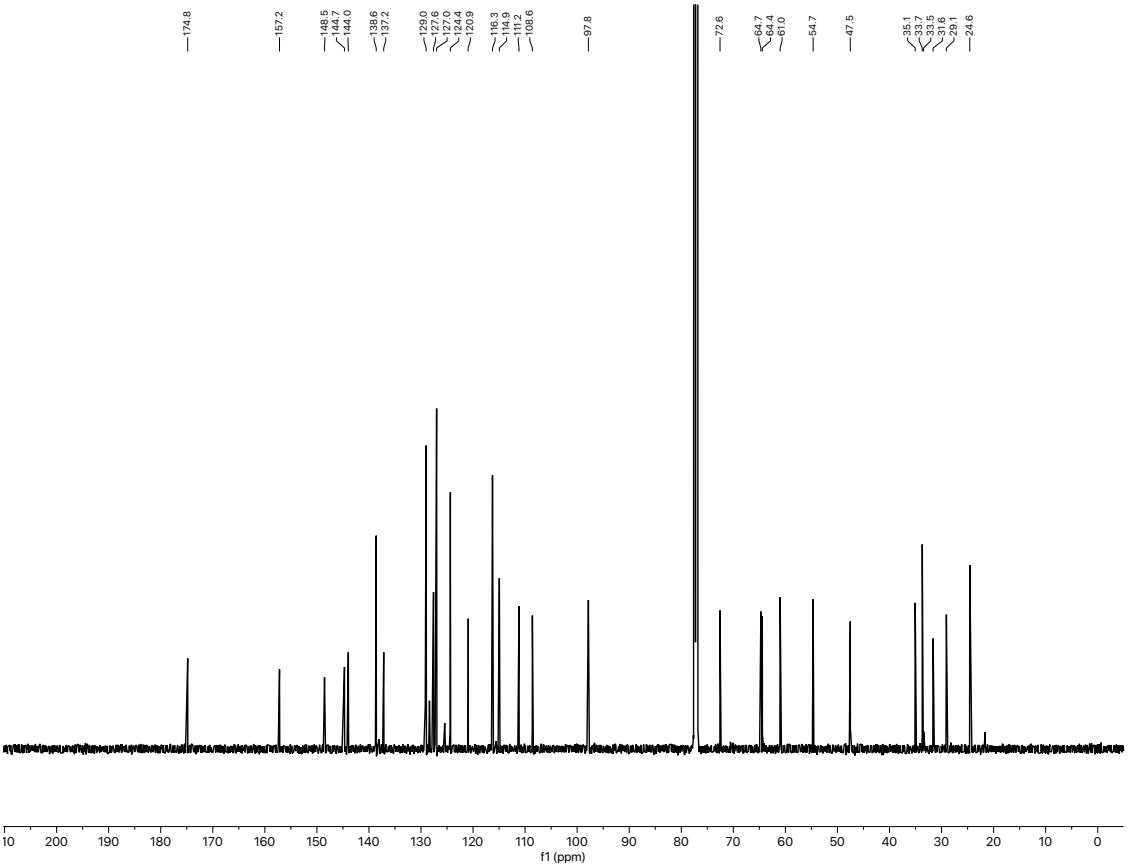
174.8
157.2
148.5
144.7
144.0
139.6
137.2
129.0
127.6
127.0
124.4
120.9
116.3
114.9
111.2
108.6
97.8
72.6
64.7
64.4
61.0
54.7
47.5
35.1
33.7
33.5
31.6
29.1
24.6
f1 (ppm)

NMR for S3:

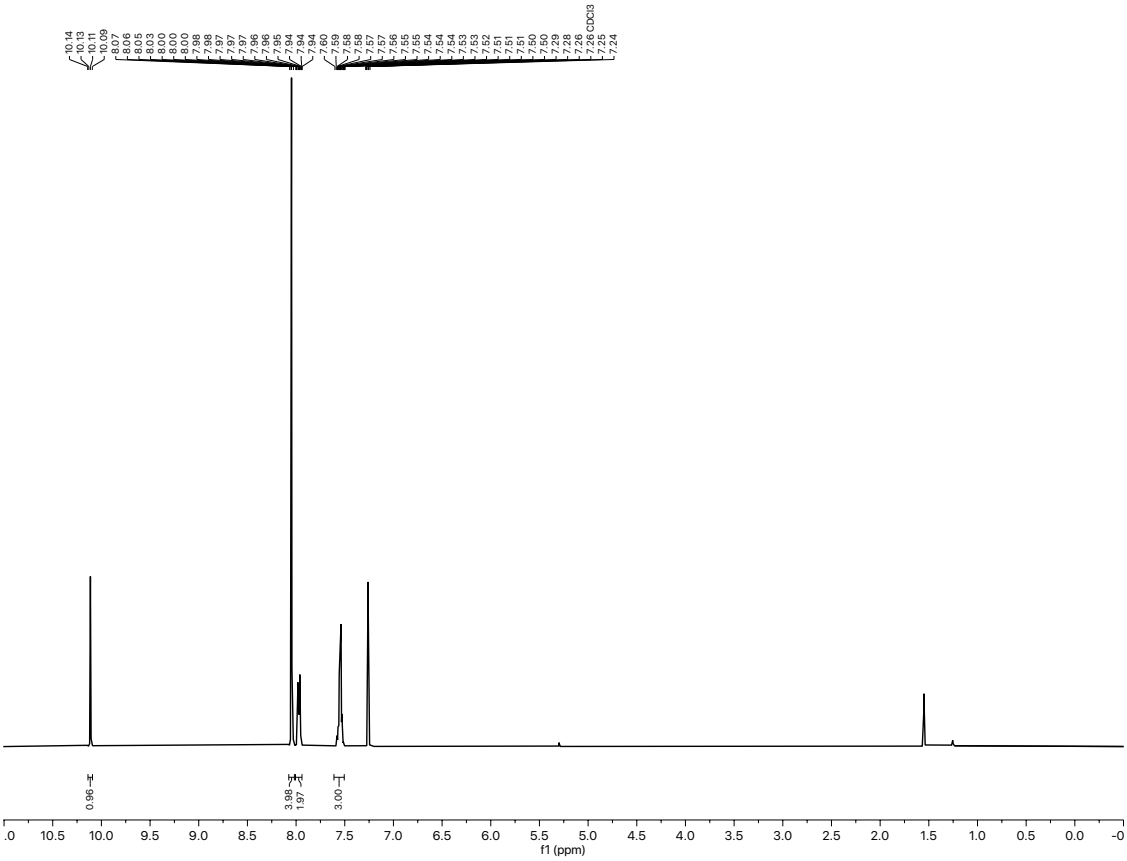
10.14
10.13
10.11
10.09
8.07
8.06
8.05
8.03
8.00
8.00
8.00
7.98
7.98
7.97
7.97
7.97
7.96
7.96
7.95
7.94
7.94
7.94
7.60
7.59
7.58
7.58
7.57
7.57
7.56
7.55
7.55
7.54
7.54
7.54
7.53
7.53
7.52
7.51
7.51
7.51
7.50
7.50
7.29
7.28
7.26 CDCl3
7.25
7.24
0.96
3.98
1.97
3.00
f1 (ppm)

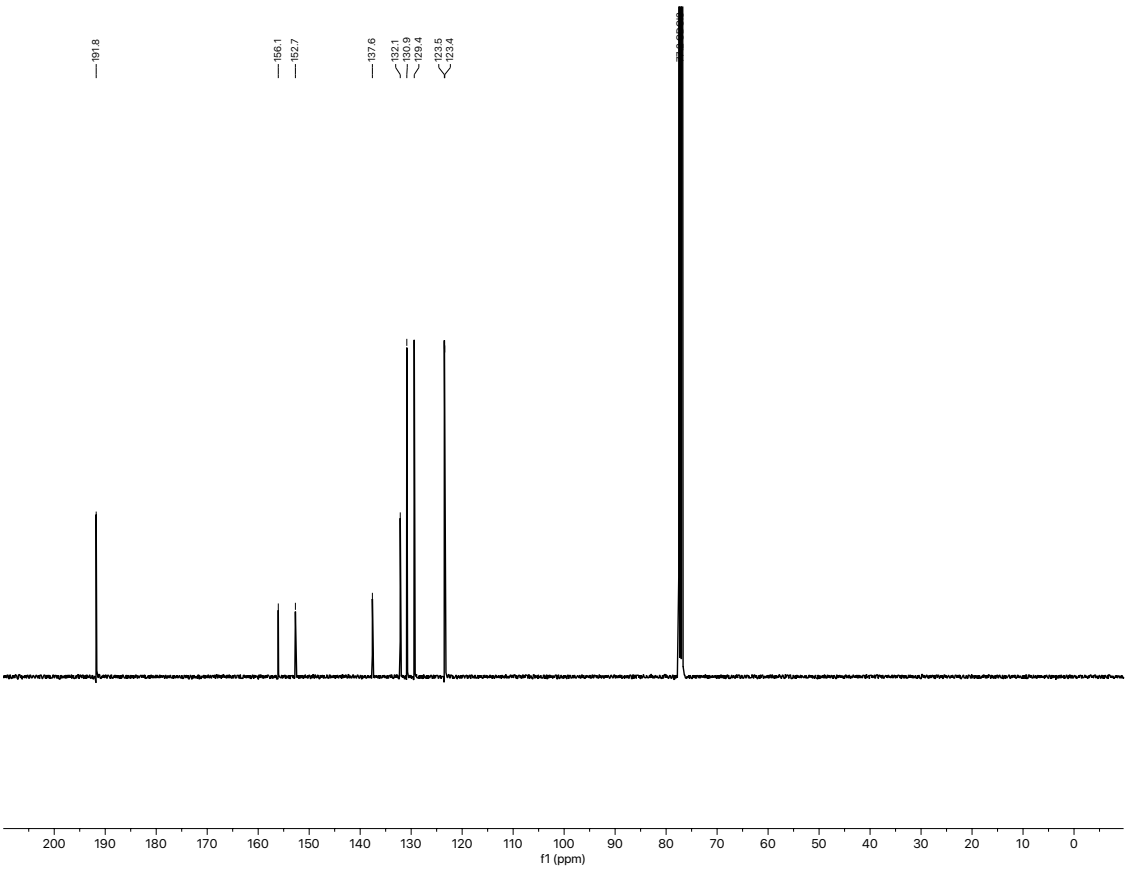
191.8
156.1
152.7
137.6
132.1
130.9
129.4
123.5
123.4
f1 (ppm)

NMR for 32:

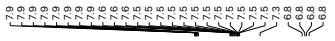
7.9
7.9
7.9
7.9
7.9
7.9
7.9
7.9
7.6
7.6
7.5
7.5
7.5
7.5
7.5
7.5
7.5
7.5
7.5
7.3
6.8
6.8
6.8
6.8
5.9
5.8
5.4
5.4
5.3

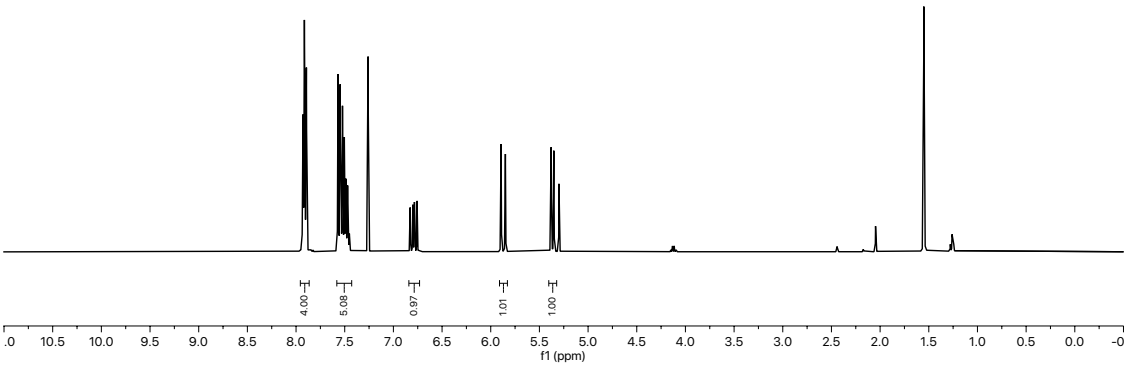
4.00
5.08
0.97
1.01
1.00
f1 (ppm)

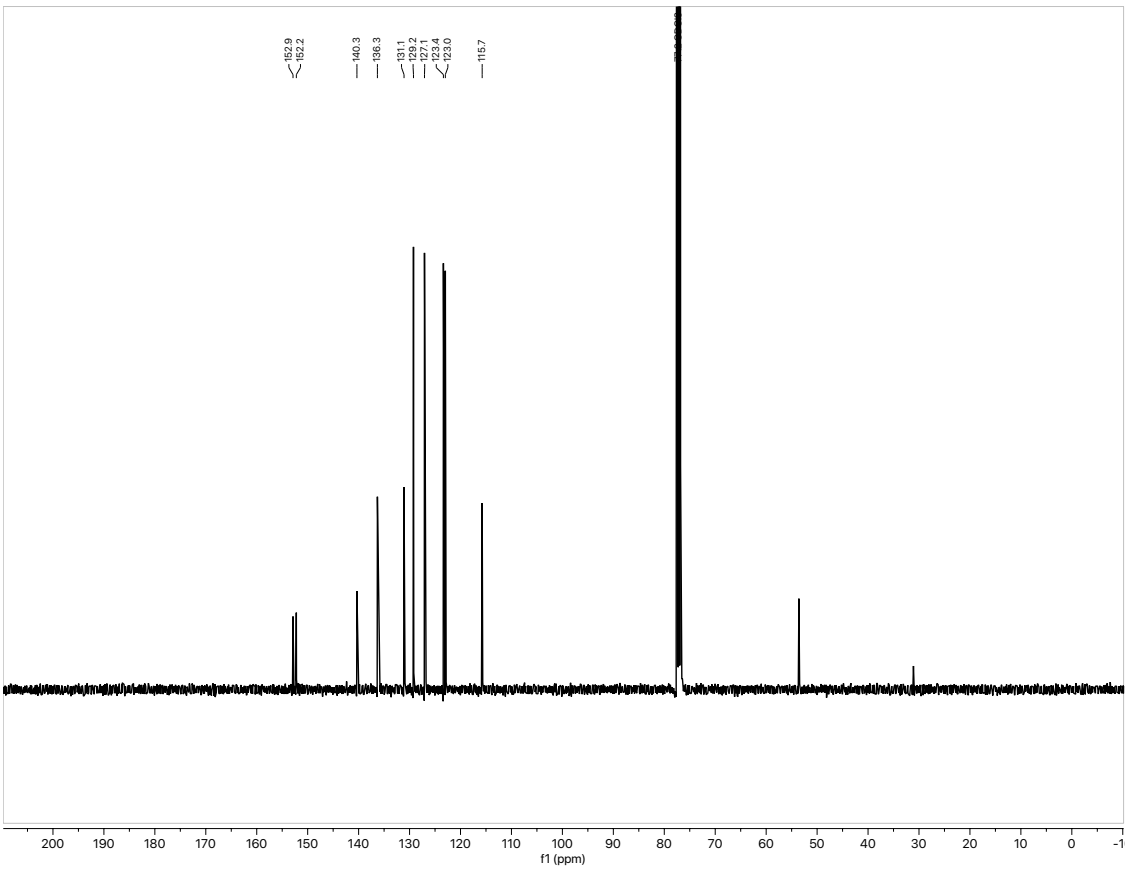
152.9
152.2
140.3
136.3
131.1
129.2
127.1
123.4
123.0
115.7
f1 (ppm)

NMR for S4:

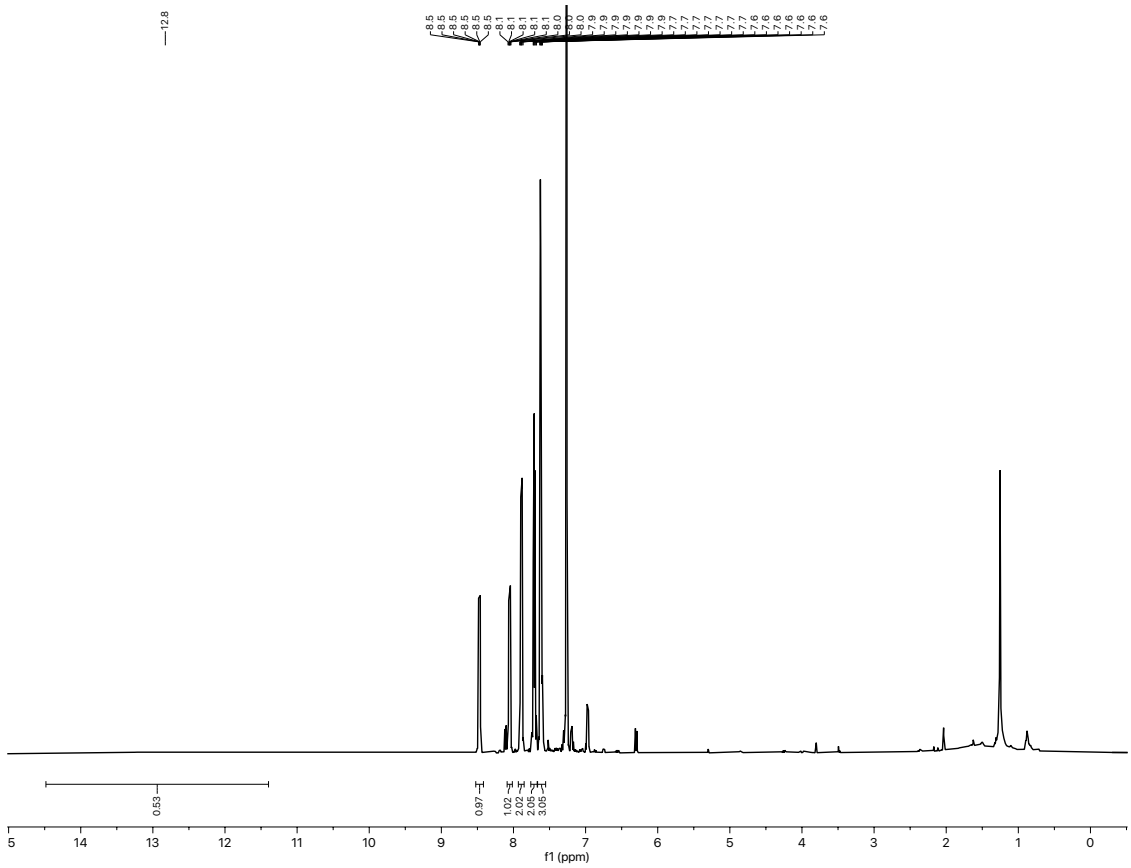
12.8
0.53
0.97
1.02
2.02
2.05
3.03
f1 (ppm)

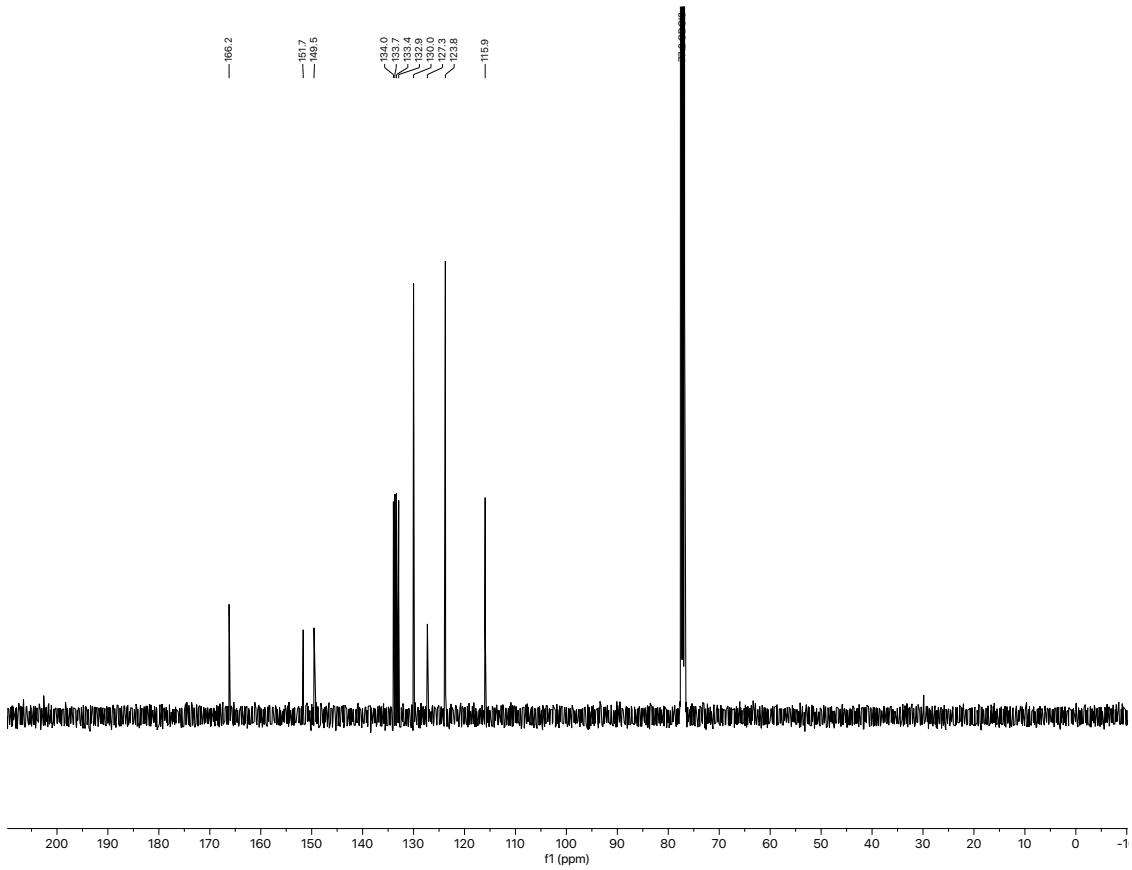
166.2
151.7
149.5
134.0
133.7
133.4
132.9
130.0
127.3
123.8
115.9
f1 (ppm)

NMR for S5:

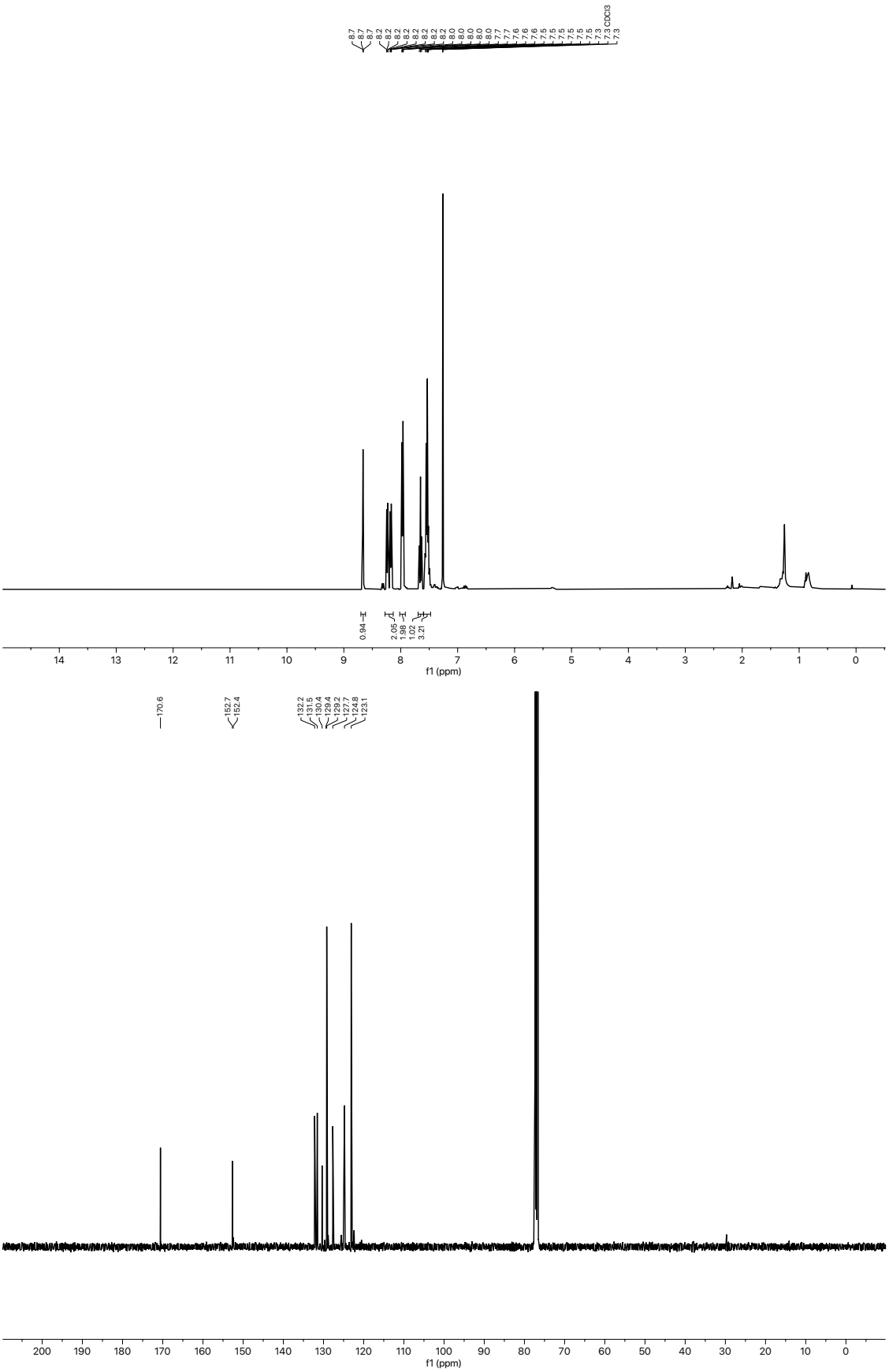
8.7
8.7
8.7
8.2
8.2
8.2
8.2
8.2
8.2
8.2
8.0
8.0
8.0
8.0
7.7
7.7
7.6
7.6
7.5
7.5
7.5
7.5
7.3
7.3 CDCl3
7.3
0.94
2.08
1.98
1.00
3.21
f1 (ppm)
170.6
152.7
152.4
132.2
131.5
130.4
129.4
129.2
127.7
124.8
123.1
f1 (ppm)

NMR for S6:

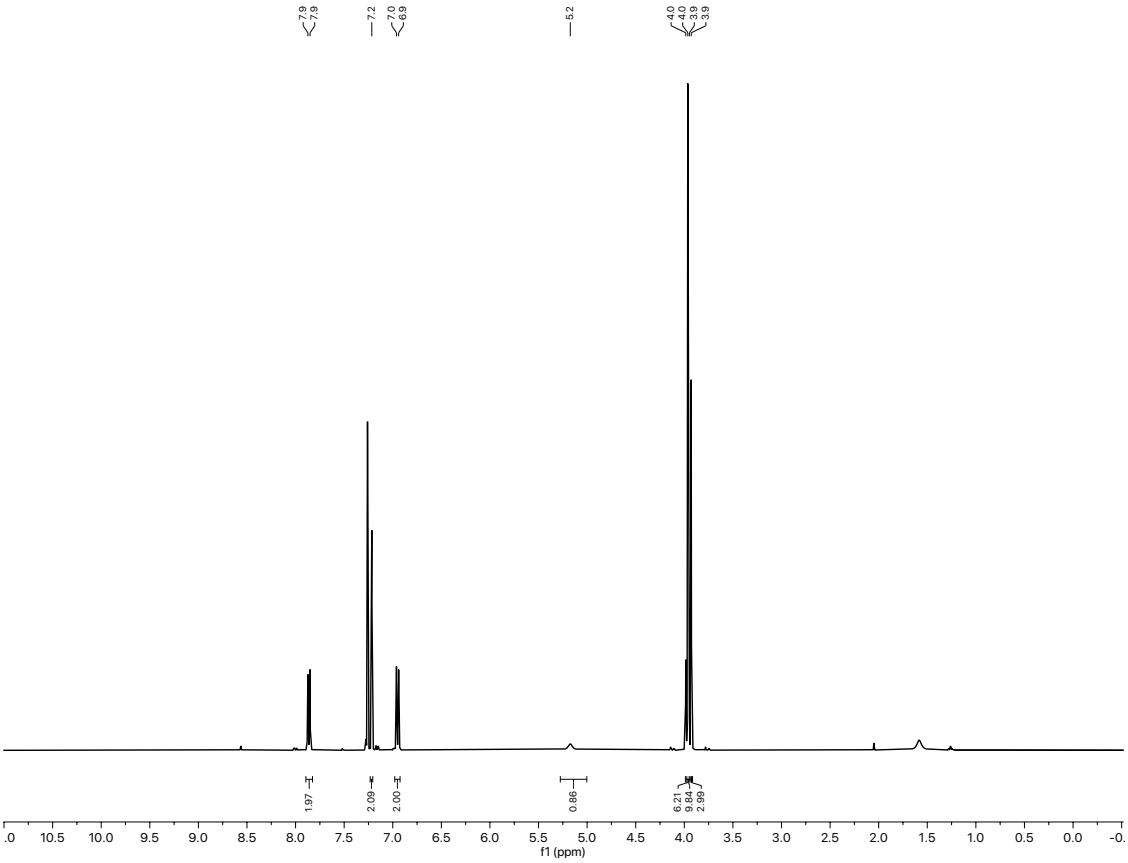
7.9
7.9
7.2
7.0
6.9
5.2
4.0
4.0
3.9
3.9
1.97
2.09
2.00
0.86
6.21
9.84
2.99
f1 (ppm)

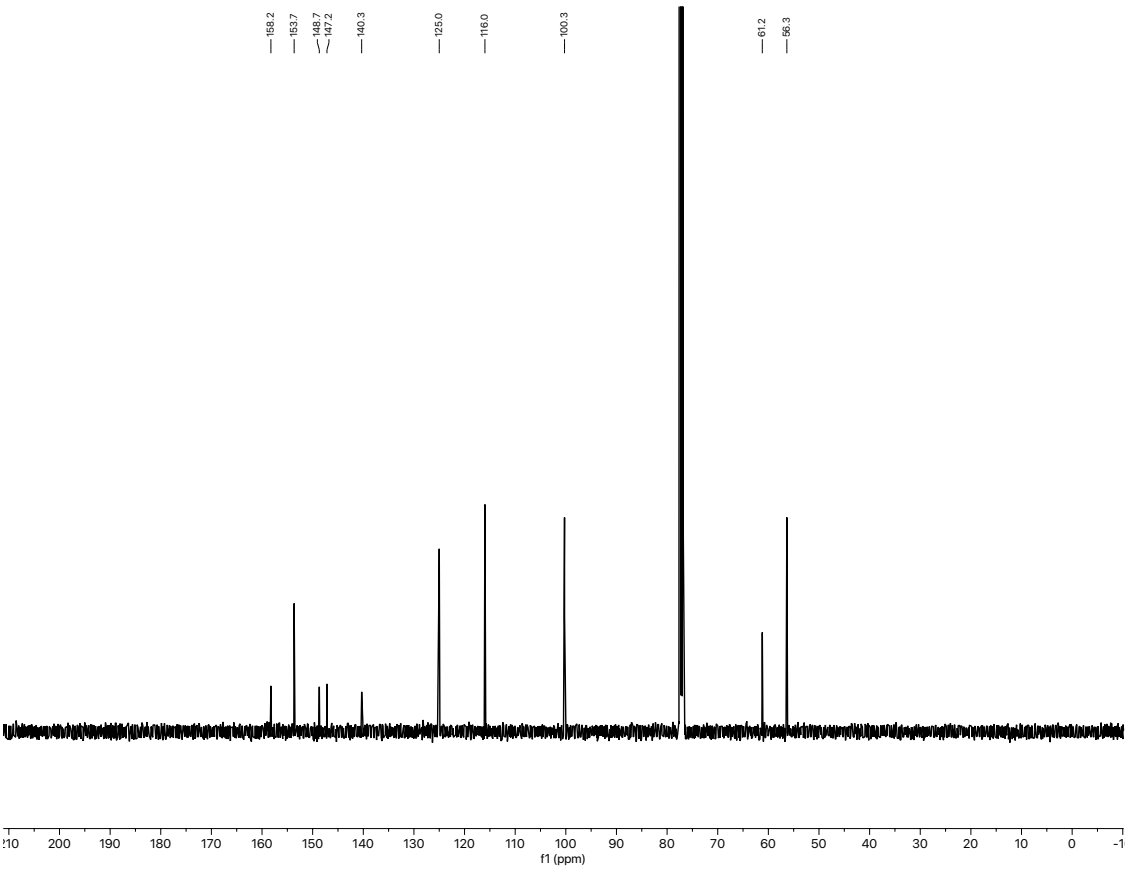
158.2
153.7
148.7
147.2
140.3
125.0
116.0
100.3
61.2
56.3
f1 (ppm)

NMR for S7:

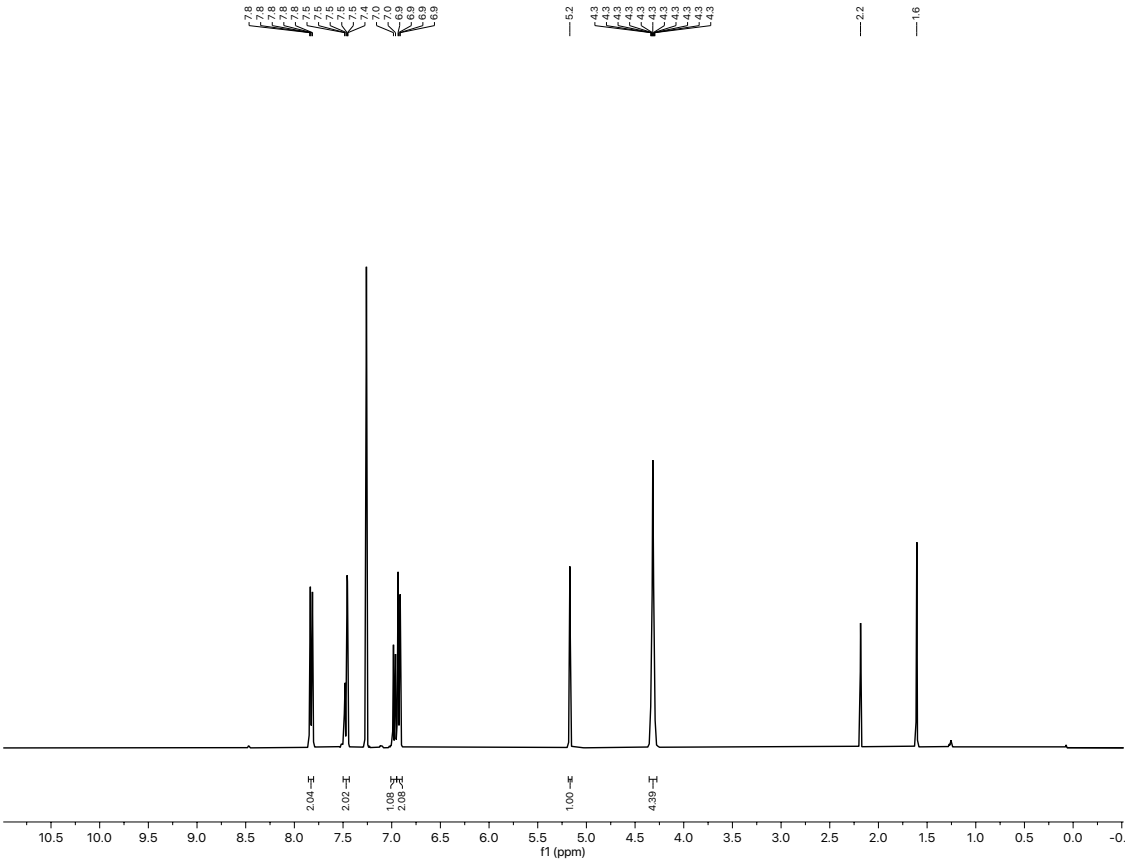
7.8
7.8
7.8
7.8
7.5
7.5
7.5
7.5
7.4
7.0
7.0
6.9
6.9
6.9
5.2
4.3
4.3
4.3
4.3
4.3
4.3
4.3
4.3
4.3
2.2
1.6
2.04
2.02
1.08
2.08
1.00
4.39
f1 (ppm)

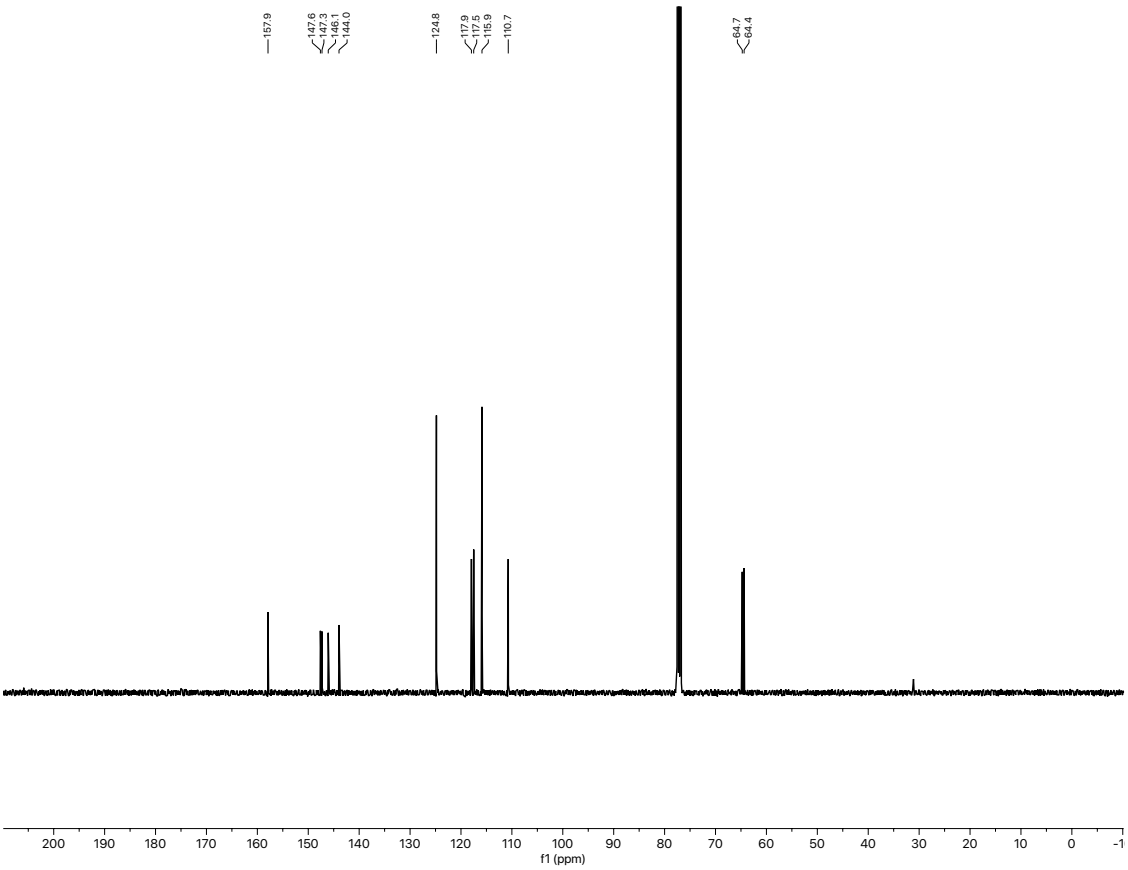
157.9
147.6
147.3
146.1
144.0
124.8
117.9
117.5
115.9
110.7
64.7
64.4
f1 (ppm)

NMR for 46:

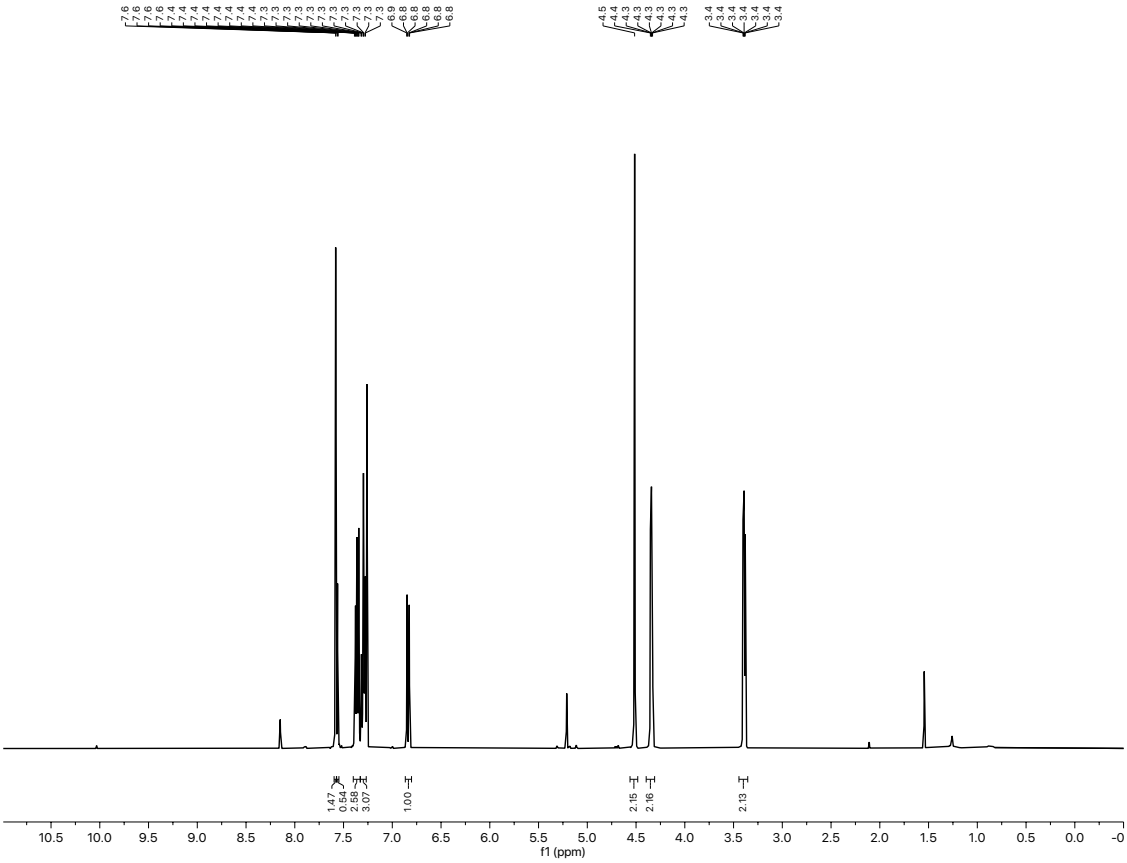
1.47
5.41
2.58
3.07
1.00
2.15
2.16
2.13
f1 (ppm)

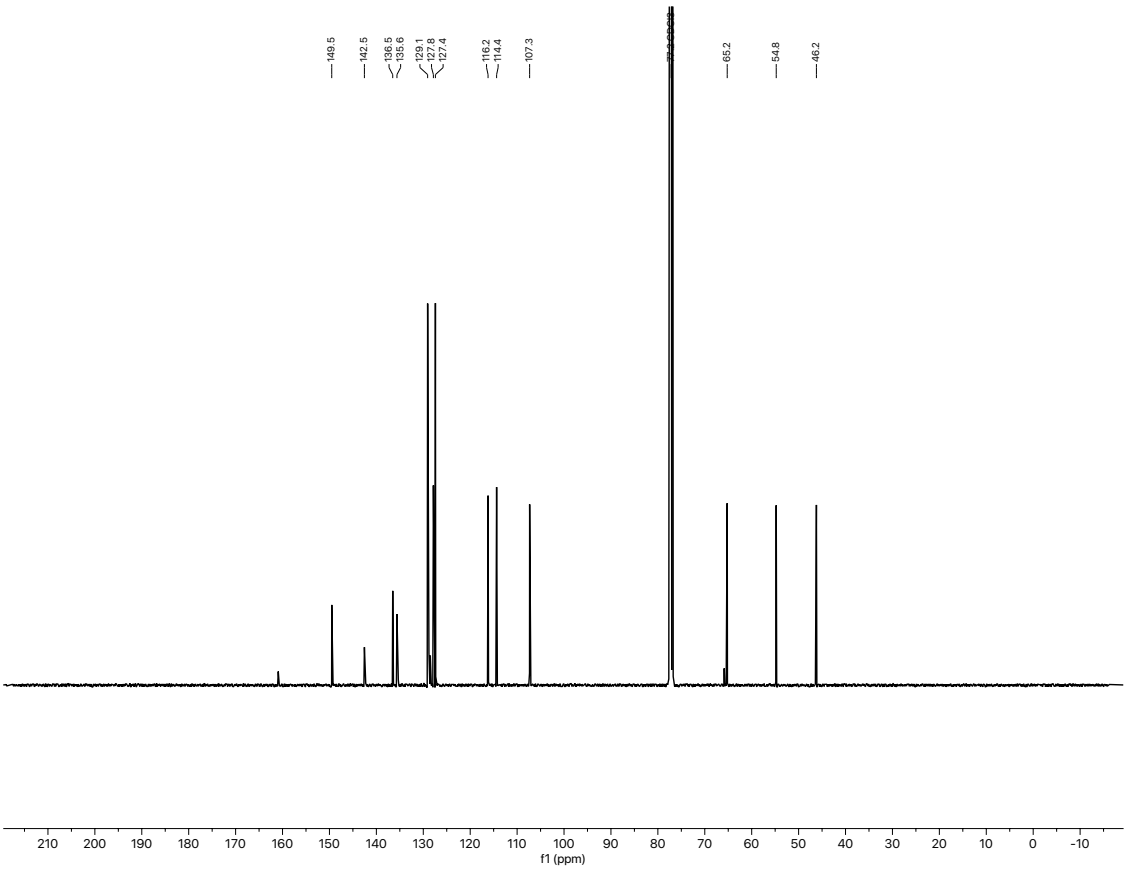
149.5
142.5
136.5
135.6
129.1
127.8
127.4
116.2
114.4
107.3
65.2
54.8
46.2
f1 (ppm)

NMR for 47:

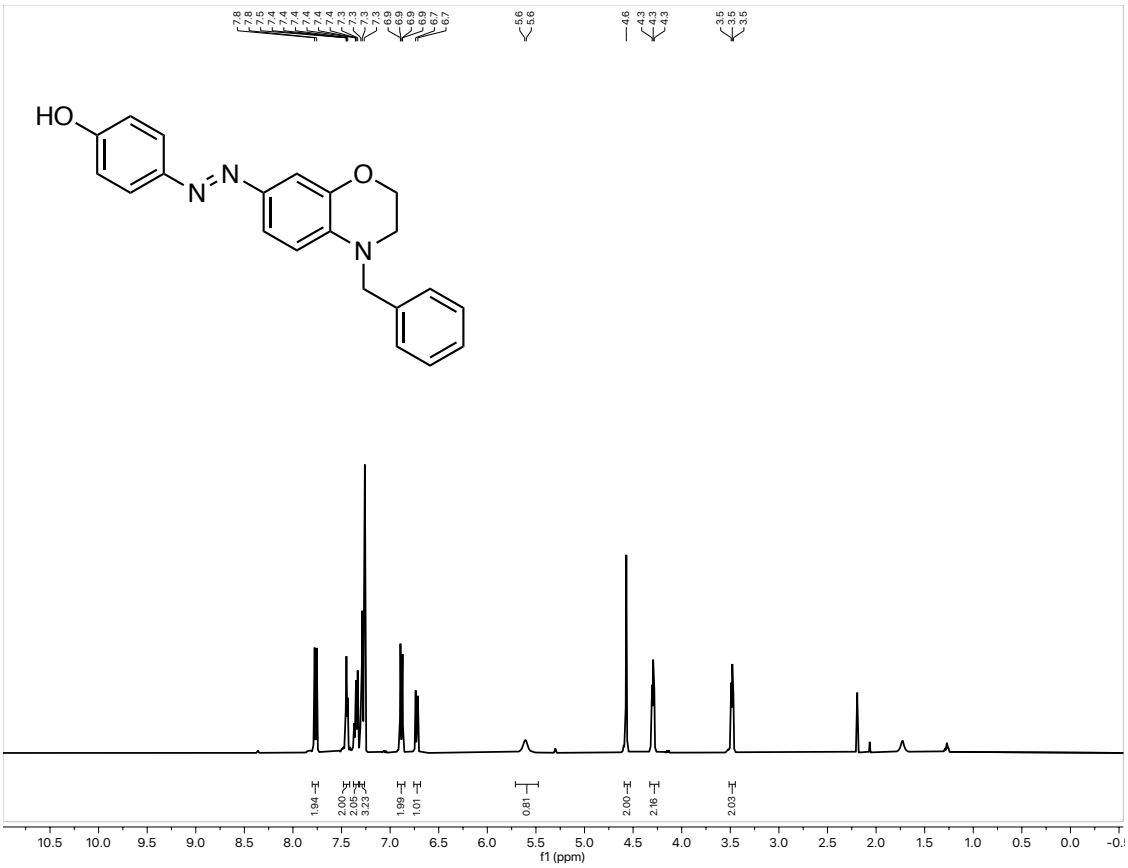

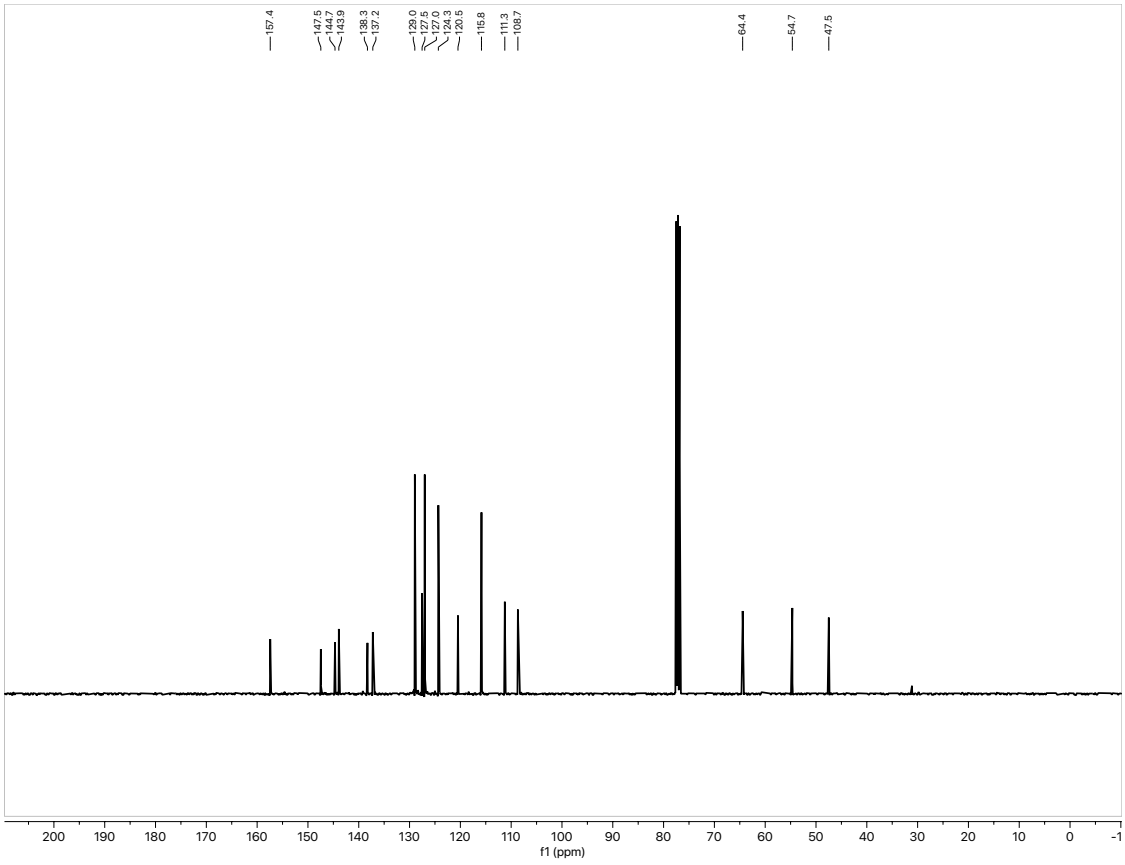

NMR-Spectra for 1.3 Arp2/3

NMR for 121:

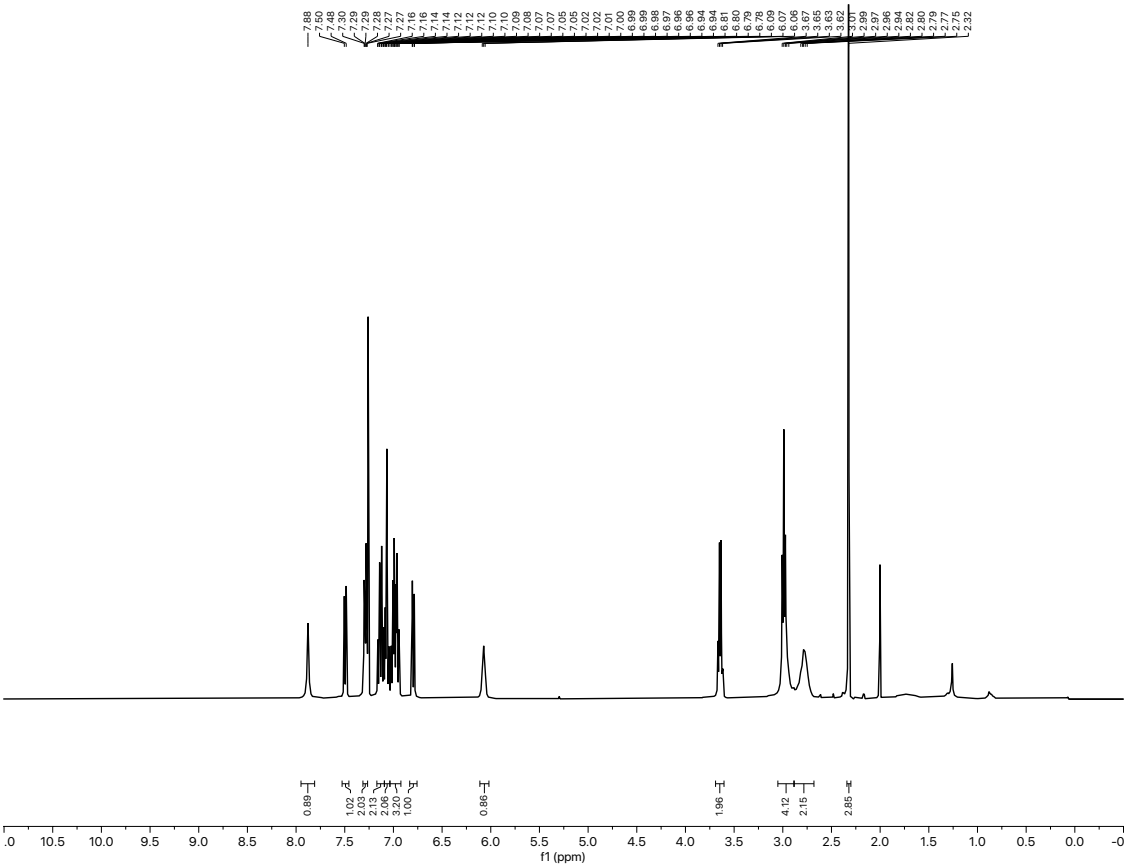

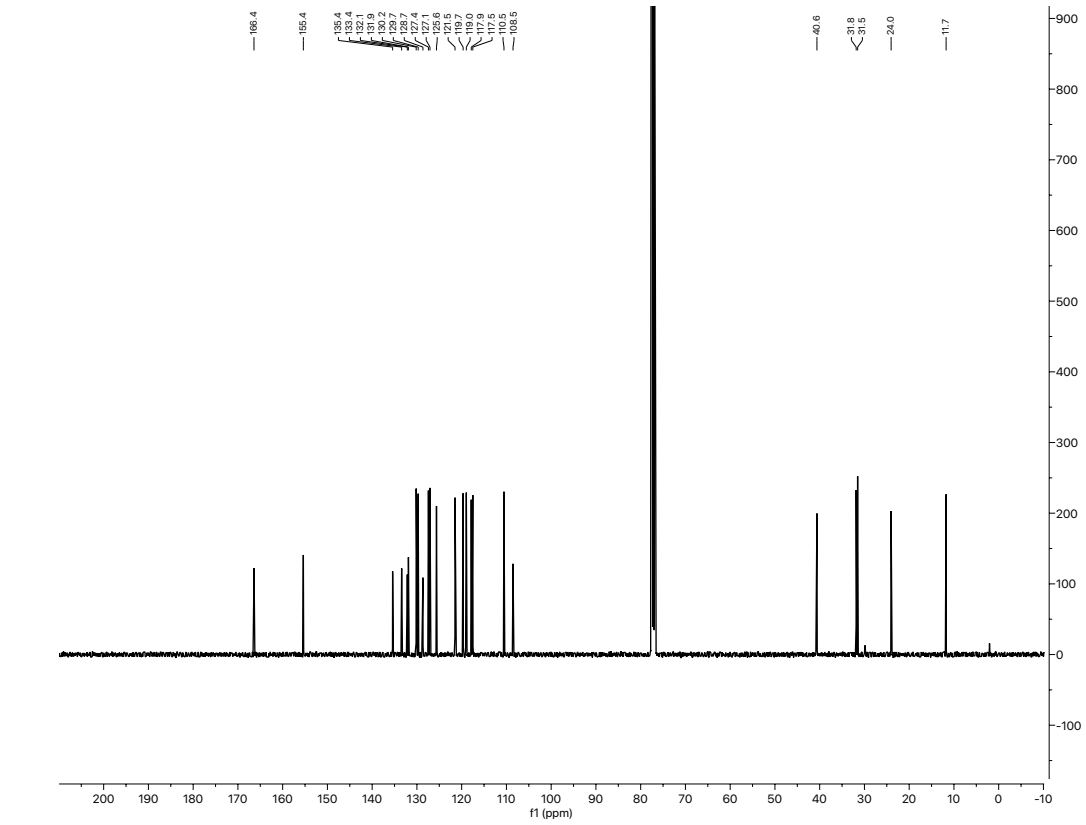

NMR for 119b:

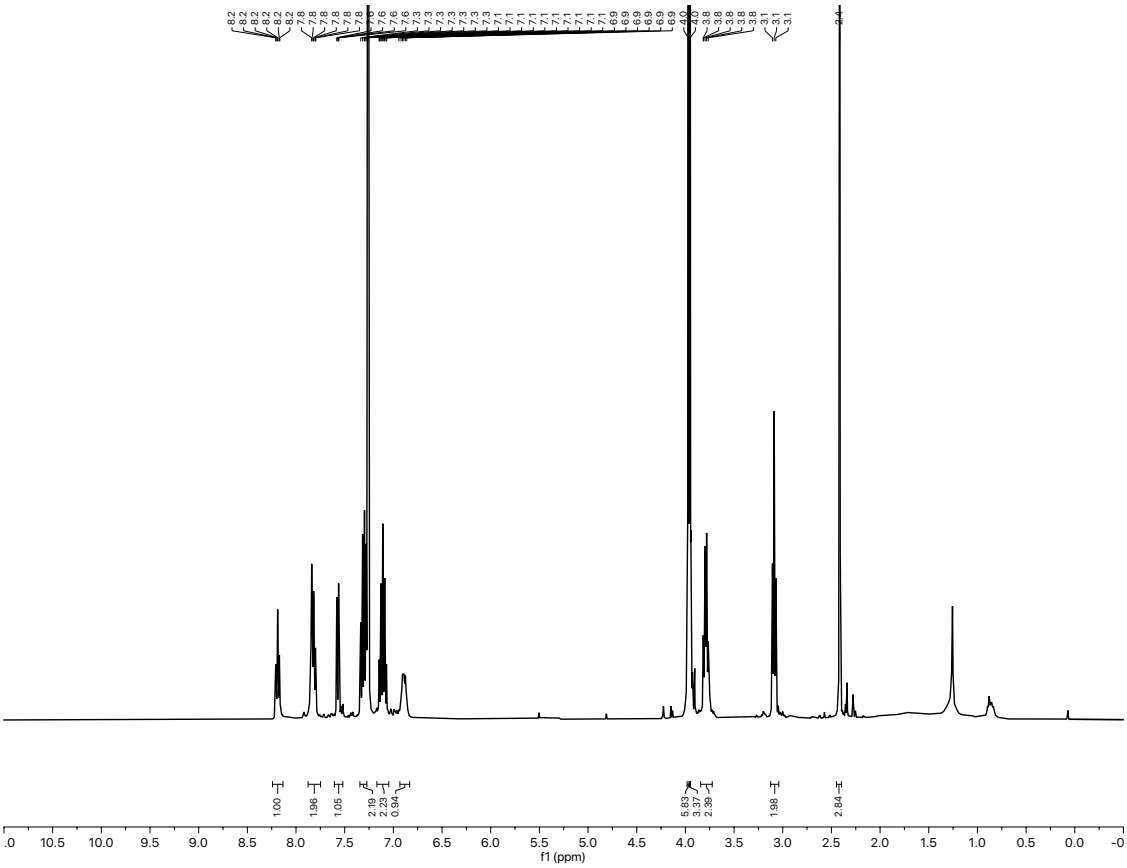

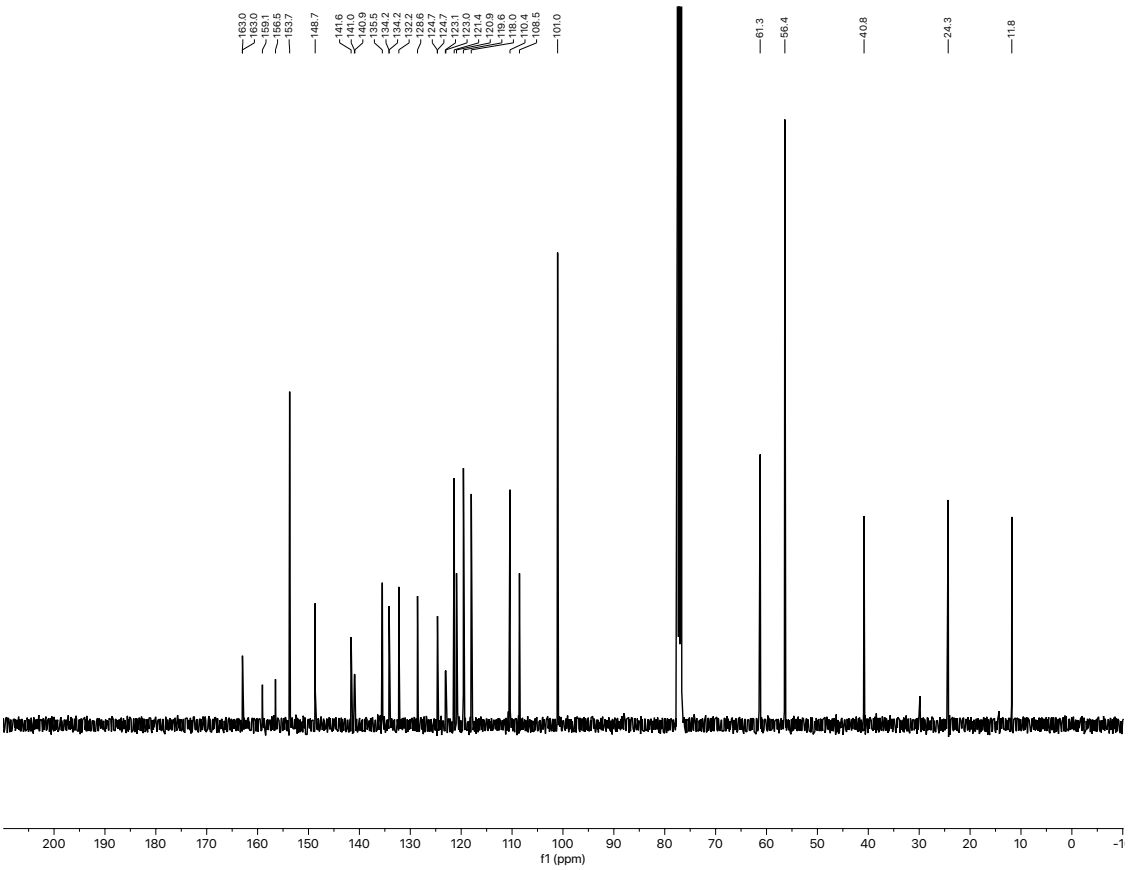

NMR for 119a:

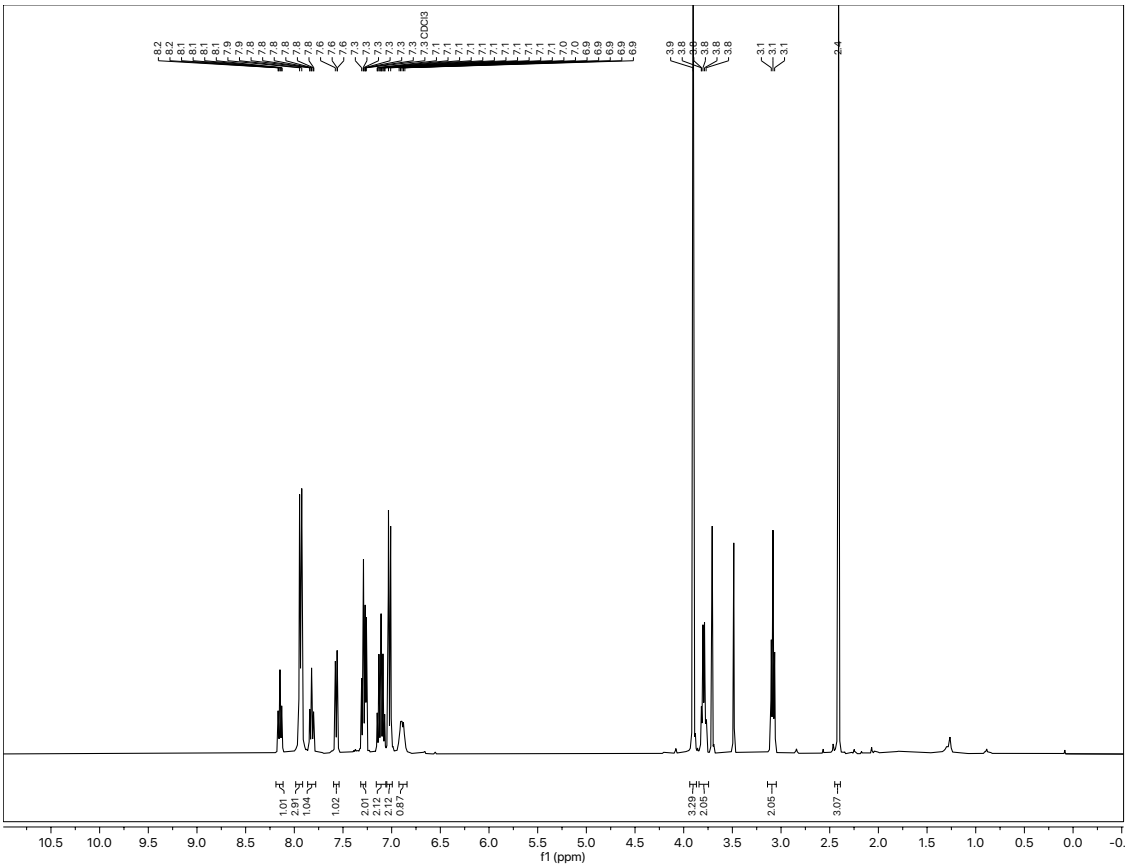
8.2
8.2
8.1
8.1
8.1
8.1
7.9
7.9
7.8
7.8
7.8
7.8
7.8
7.8
7.6
7.6
7.6
7.6
7.3
7.3
7.3
7.3
7.3 CDCl3
7.1
7.1
7.1
7.1
7.1
7.1
7.1
7.1
7.1
7.1
7.1
7.0
7.0
6.9
6.9
6.9
6.9
6.9
6.9
3.9
3.8
3.8
3.8
3.8
3.8
3.1
3.1
3.1
2.4
1.01
2.91
1.04
1.02
2.01
2.12
2.12
0.87
3.29
2.05
2.05
3.07
10.5 10.0 9.5 9.0 8.5 8.0 7.5 7.0 6.5 6.0 5.5 5.0 4.5 4.0 3.5 3.0 2.5 2.0 1.5 1.0 0.5 0.0
f1 (ppm)

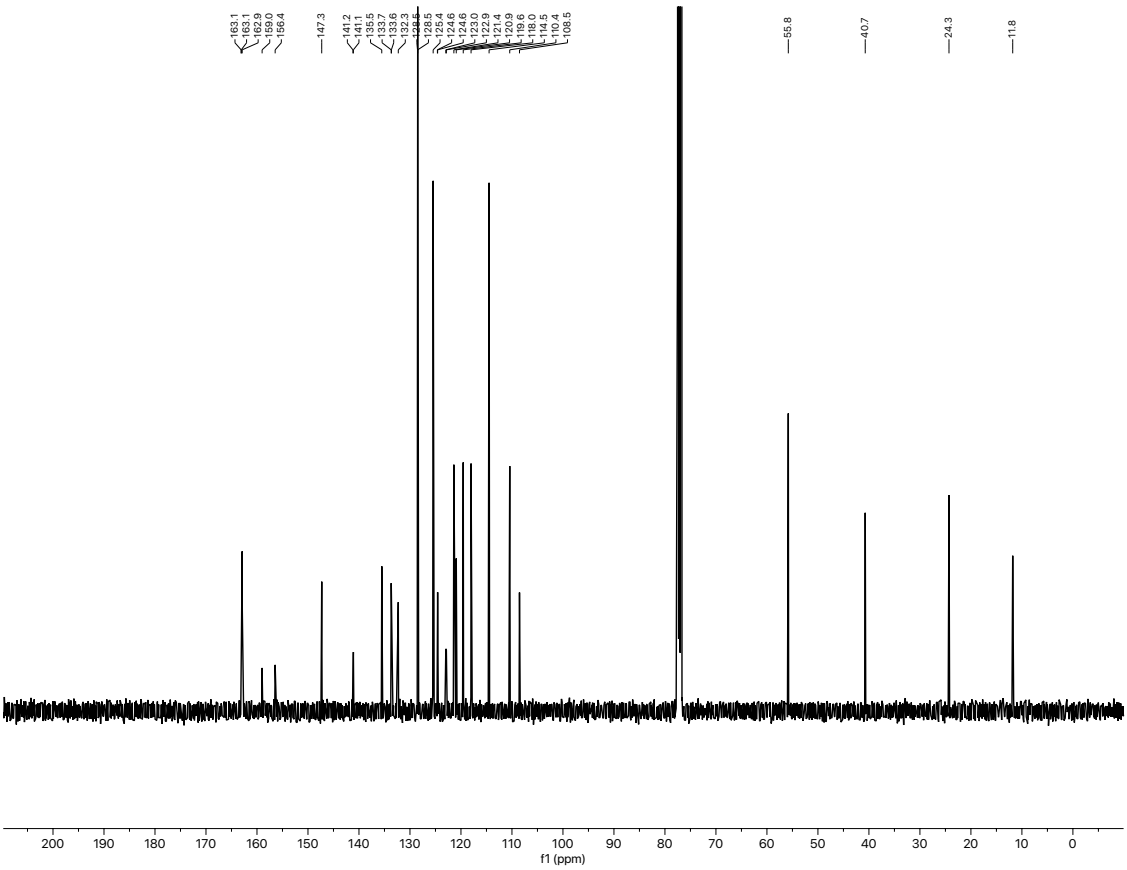
163.1
163.1
162.9
159.0
156.4
147.3
141.2
141.1
135.5
133.7
133.6
132.3
128.5
128.5
125.4
124.6
124.6
123.0
122.9
121.4
120.9
119.6
118.0
114.5
110.4
108.5
55.8
40.7
24.3
11.8
200 190 180 170 160 150 140 130 120 110 100 90 80 70 60 50 40 30 20 10 0
f1 (ppm)

NMR for 119c:

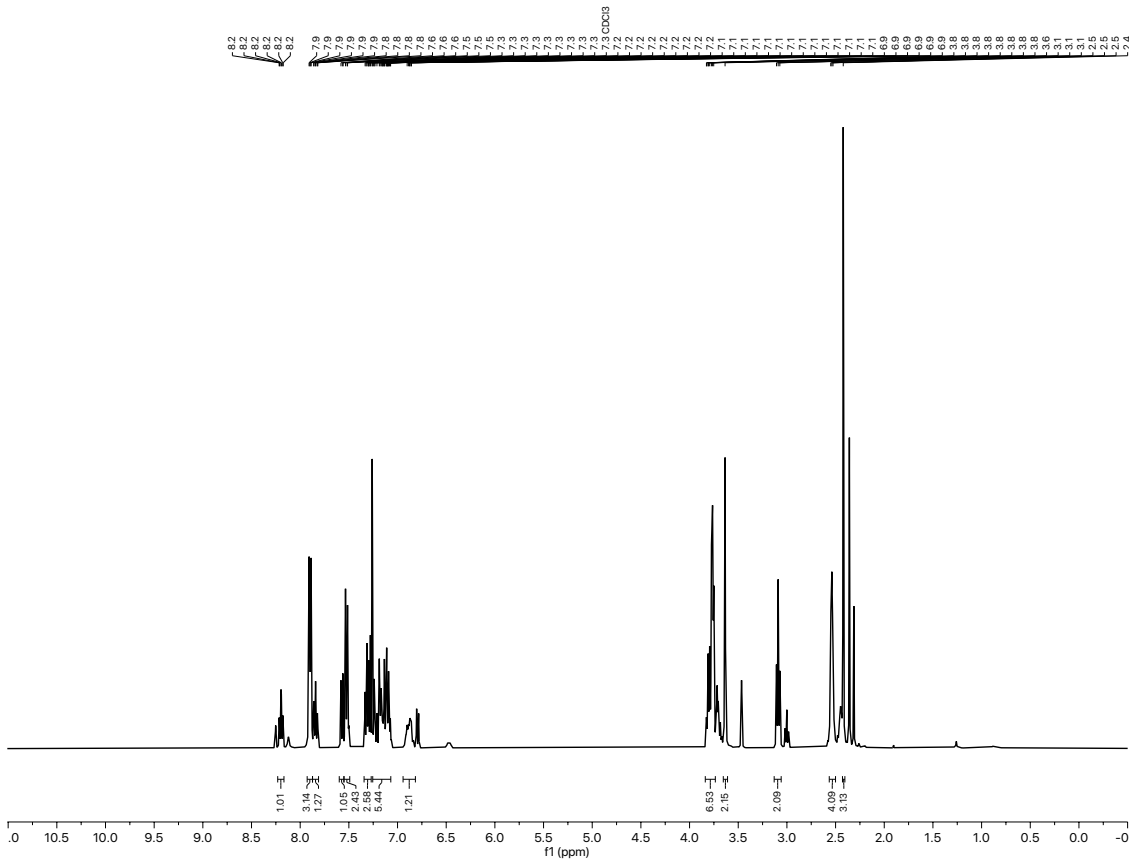

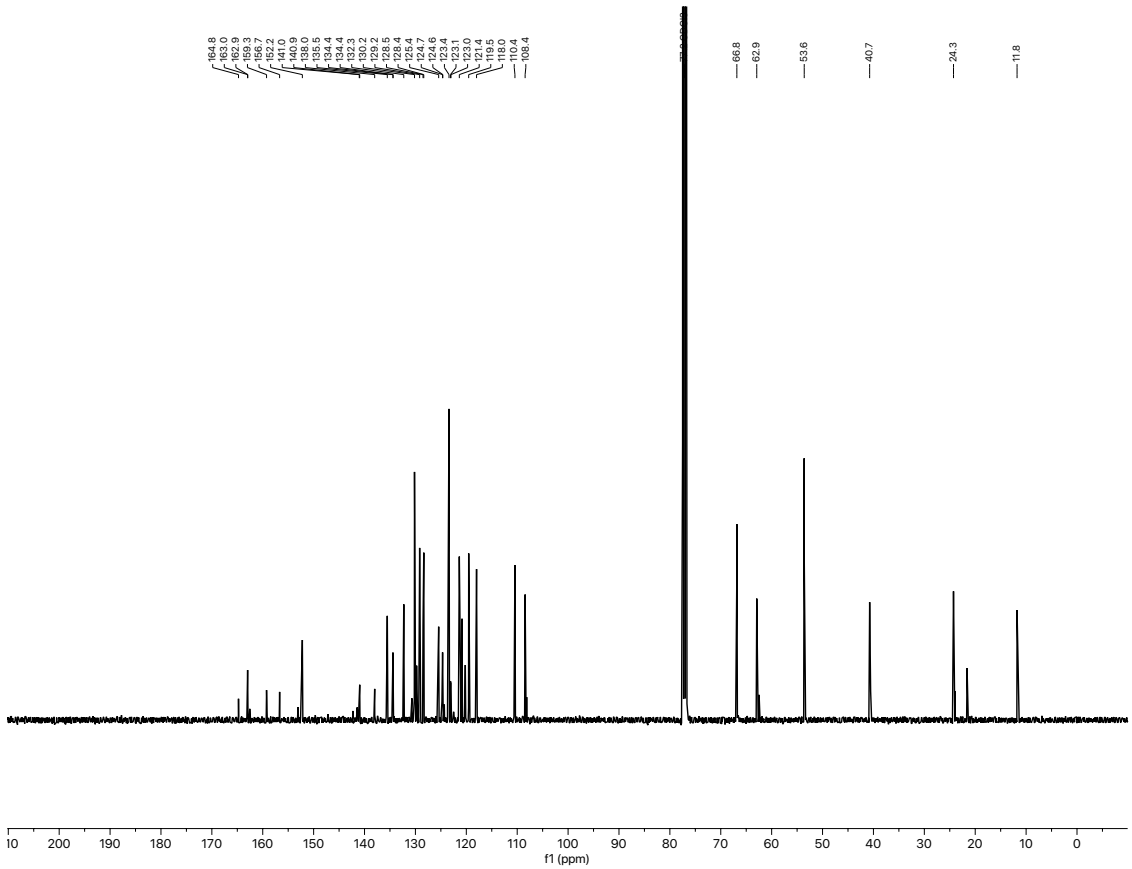

NMR for 119d:

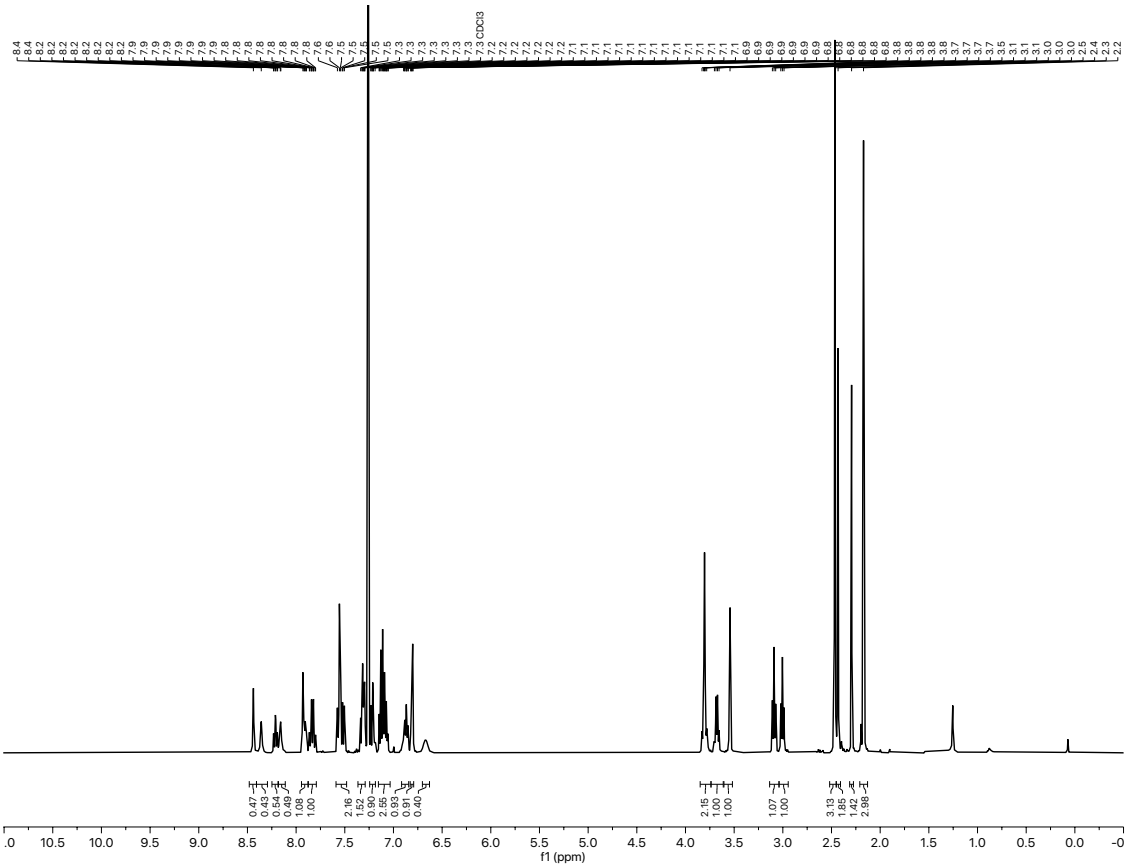

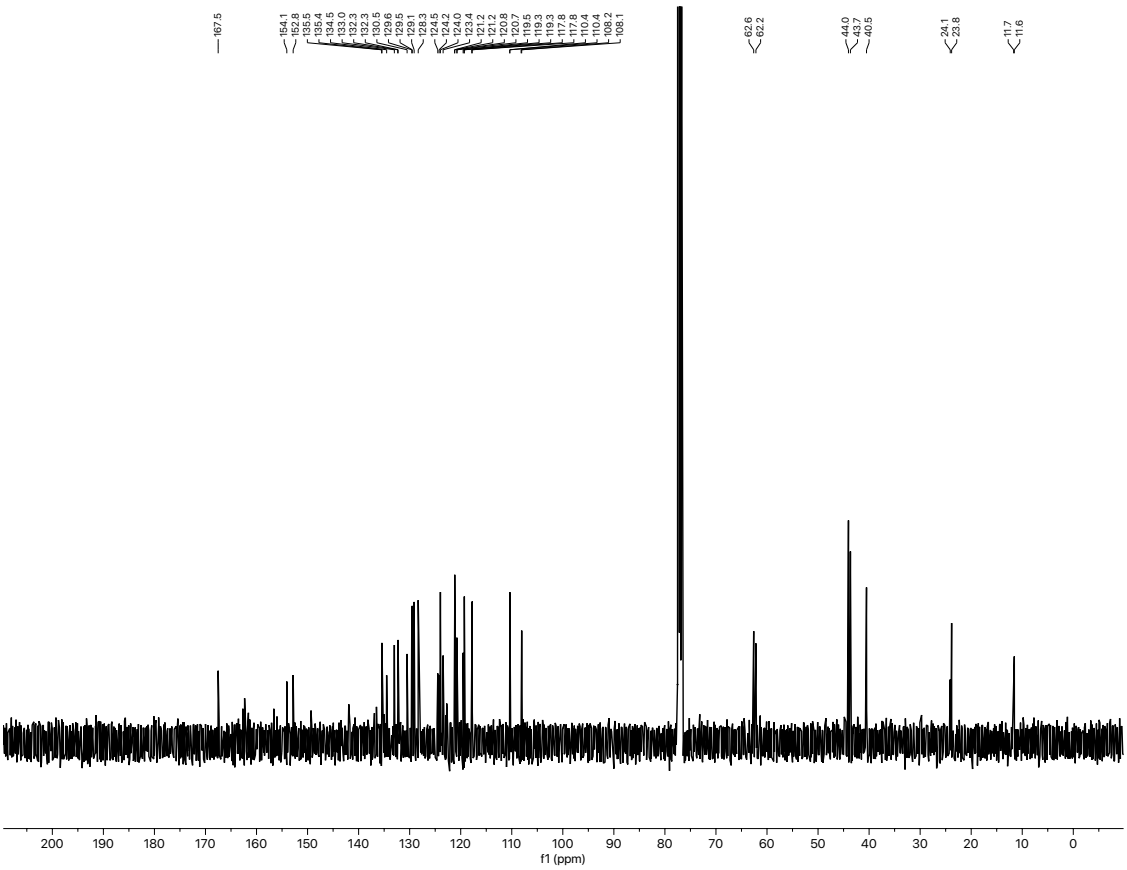

NMR for 119e:

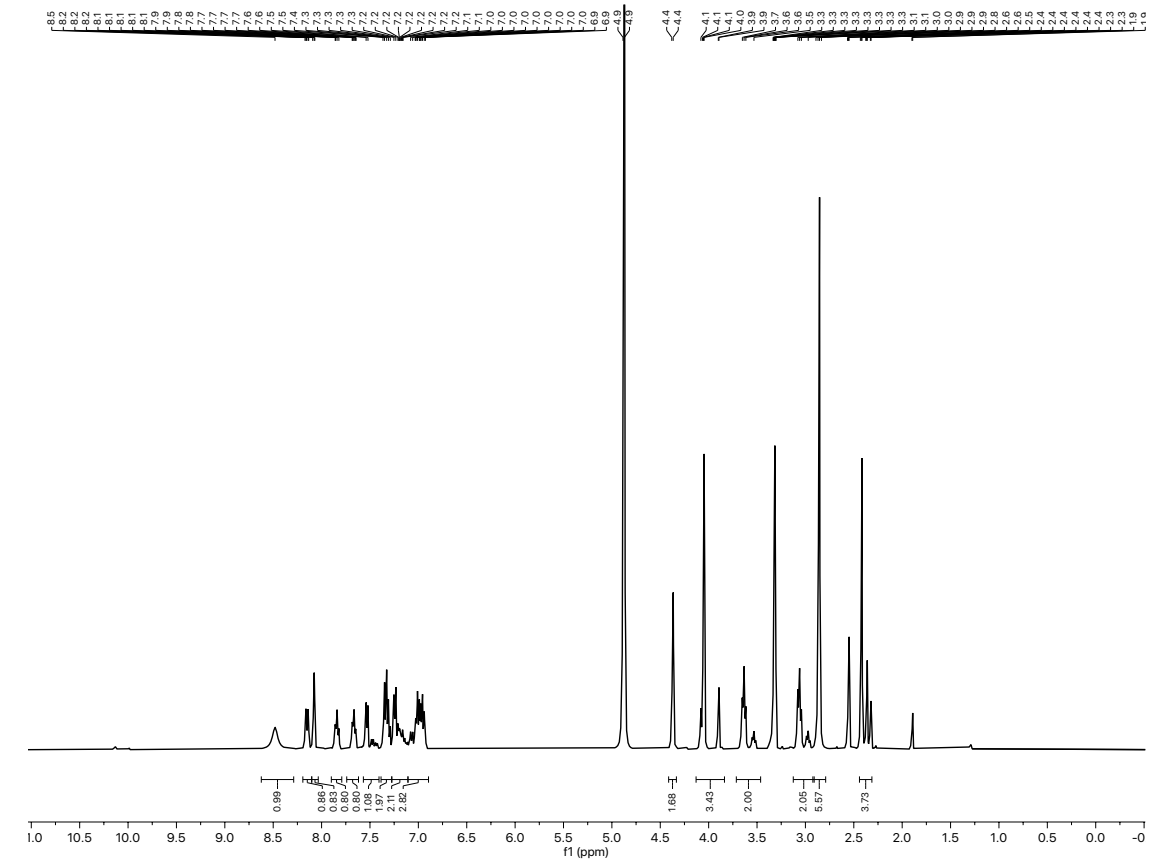

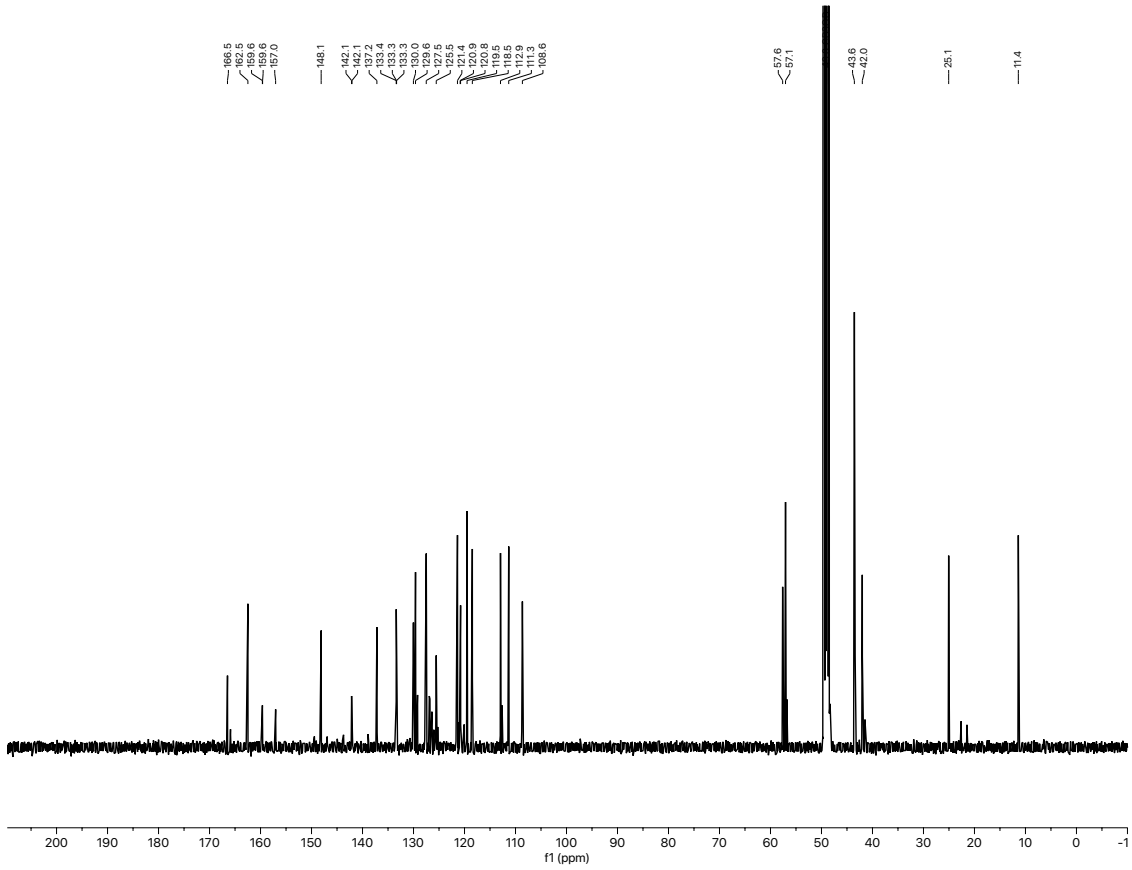

NMR-Spectra for Part 3: Photoswitchable Control of DREADD

NMR for clozapine:

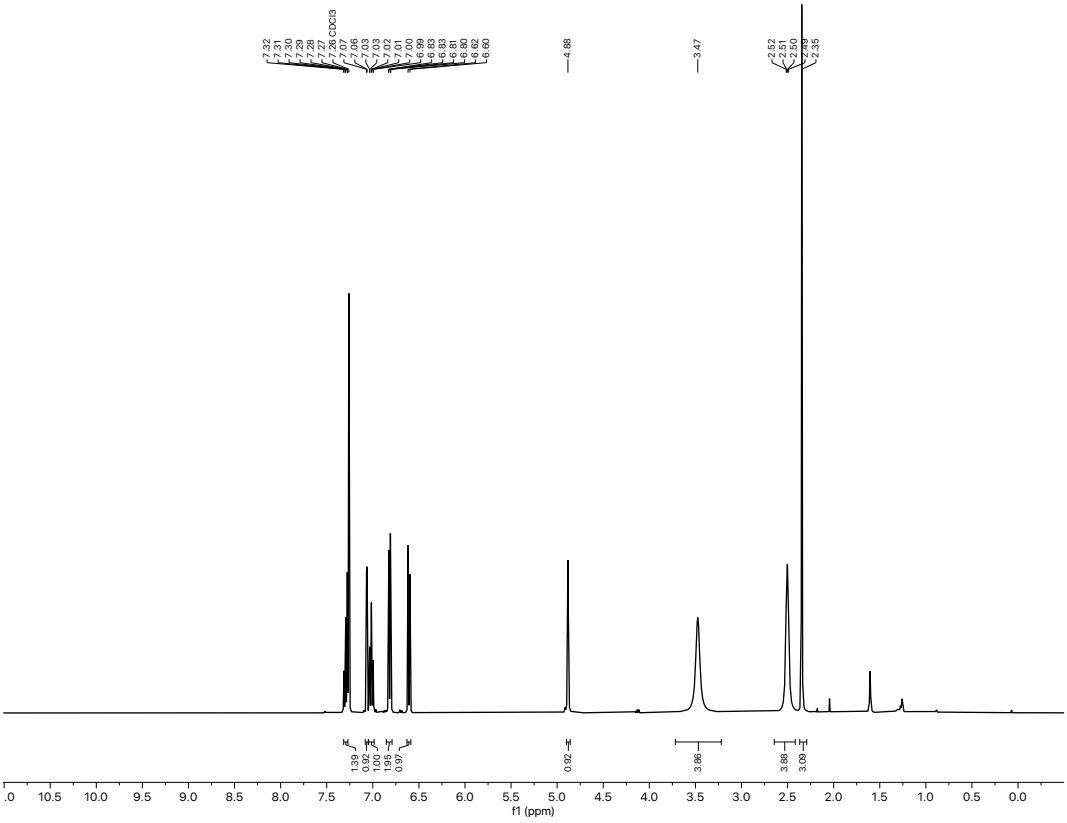

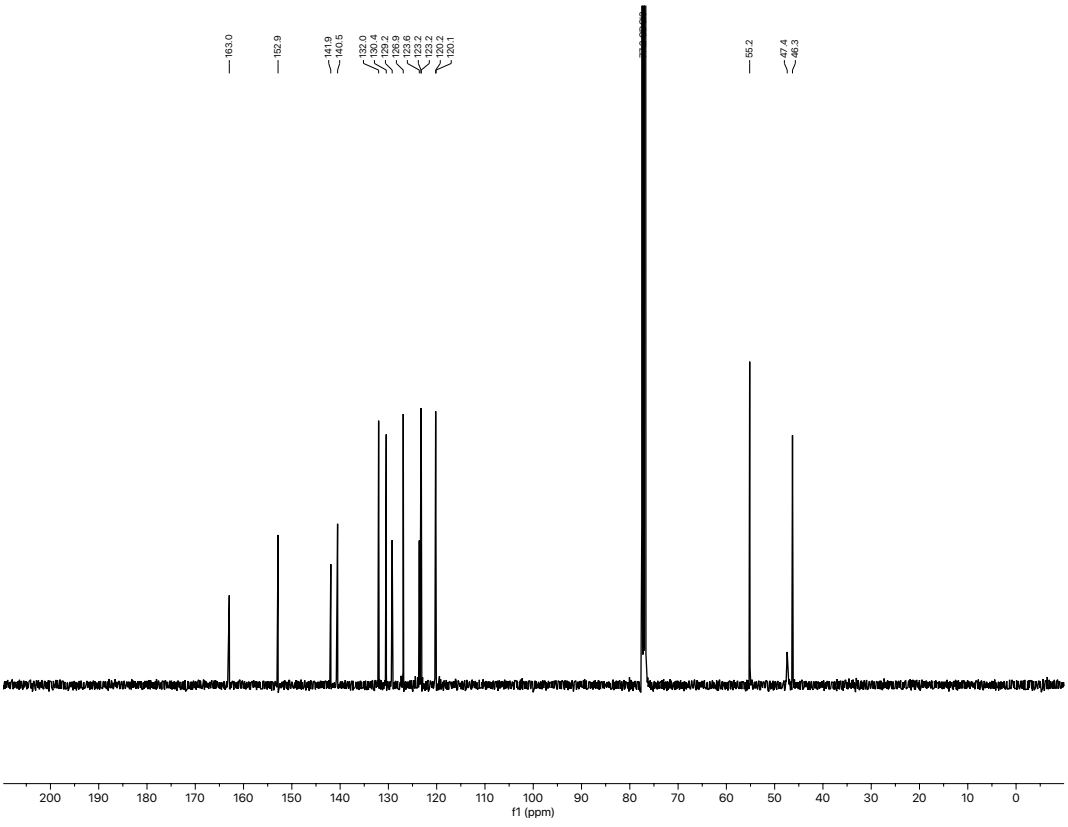

NMR for Boc-clozapine:

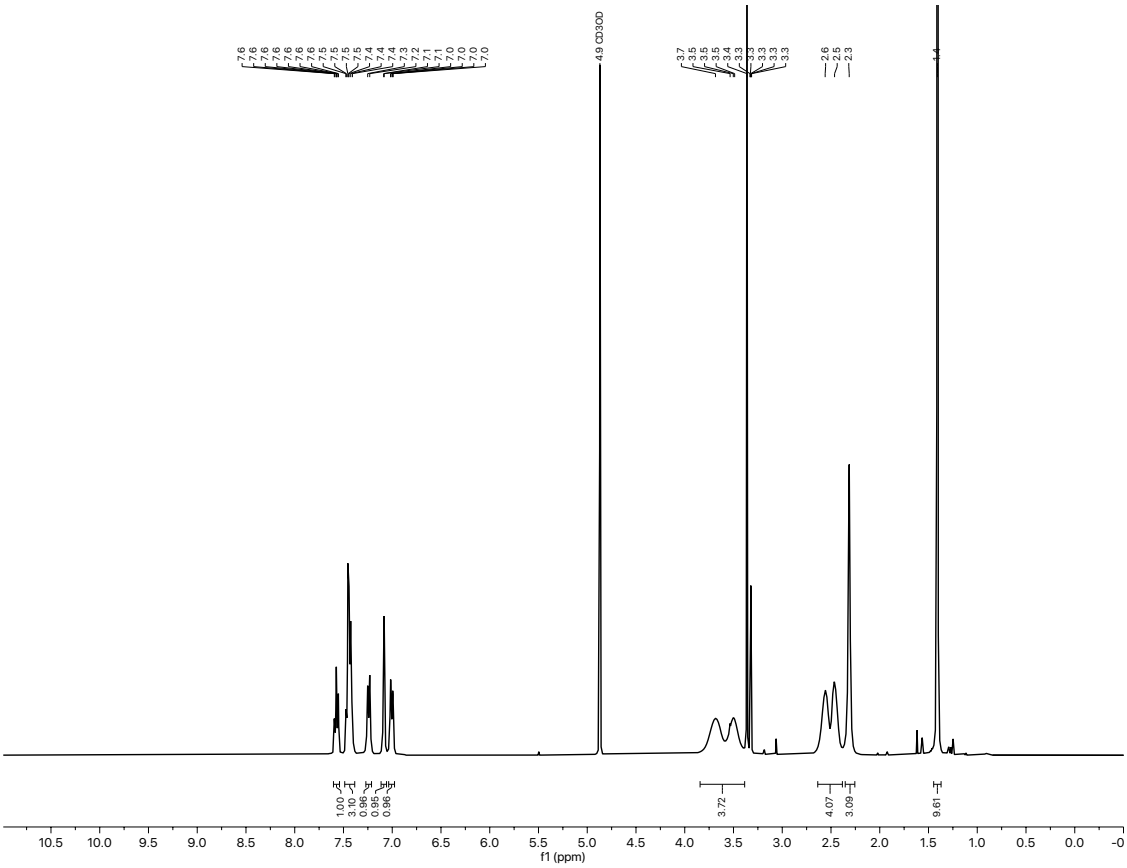

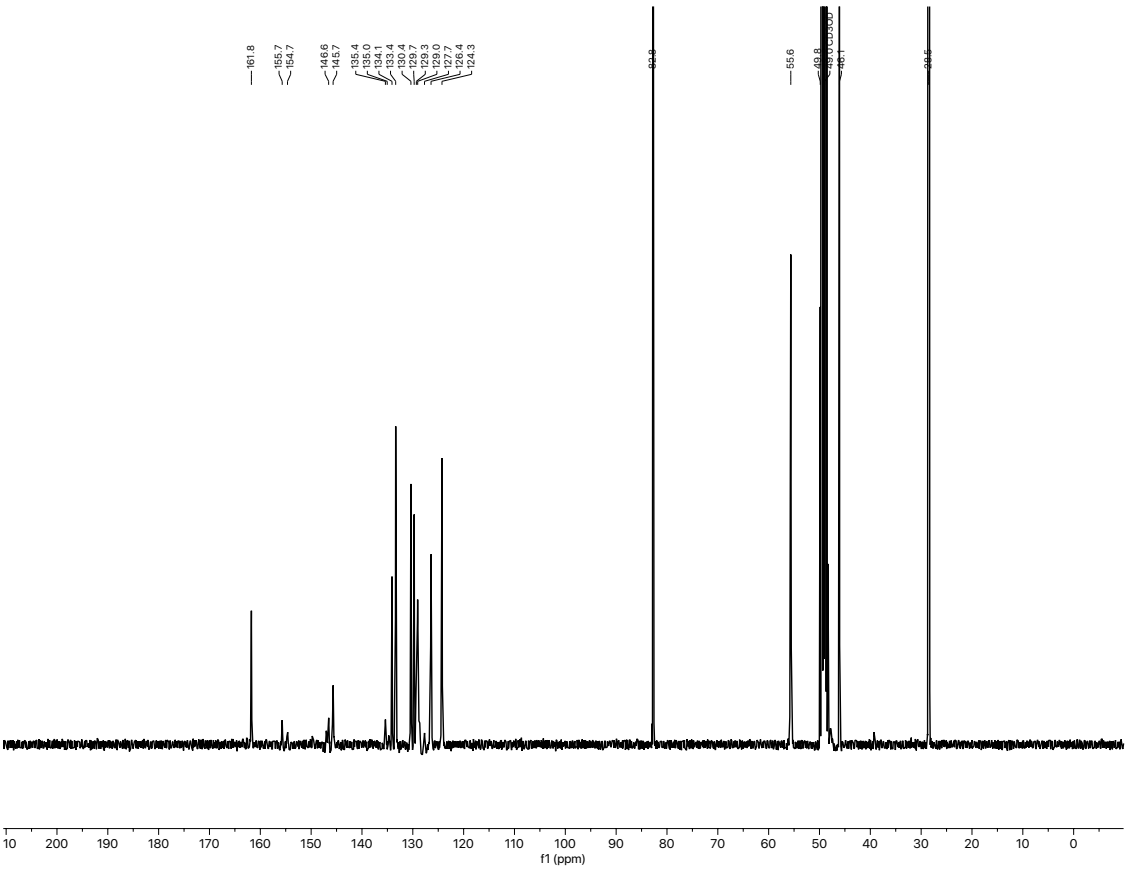

NMR for 3-6:

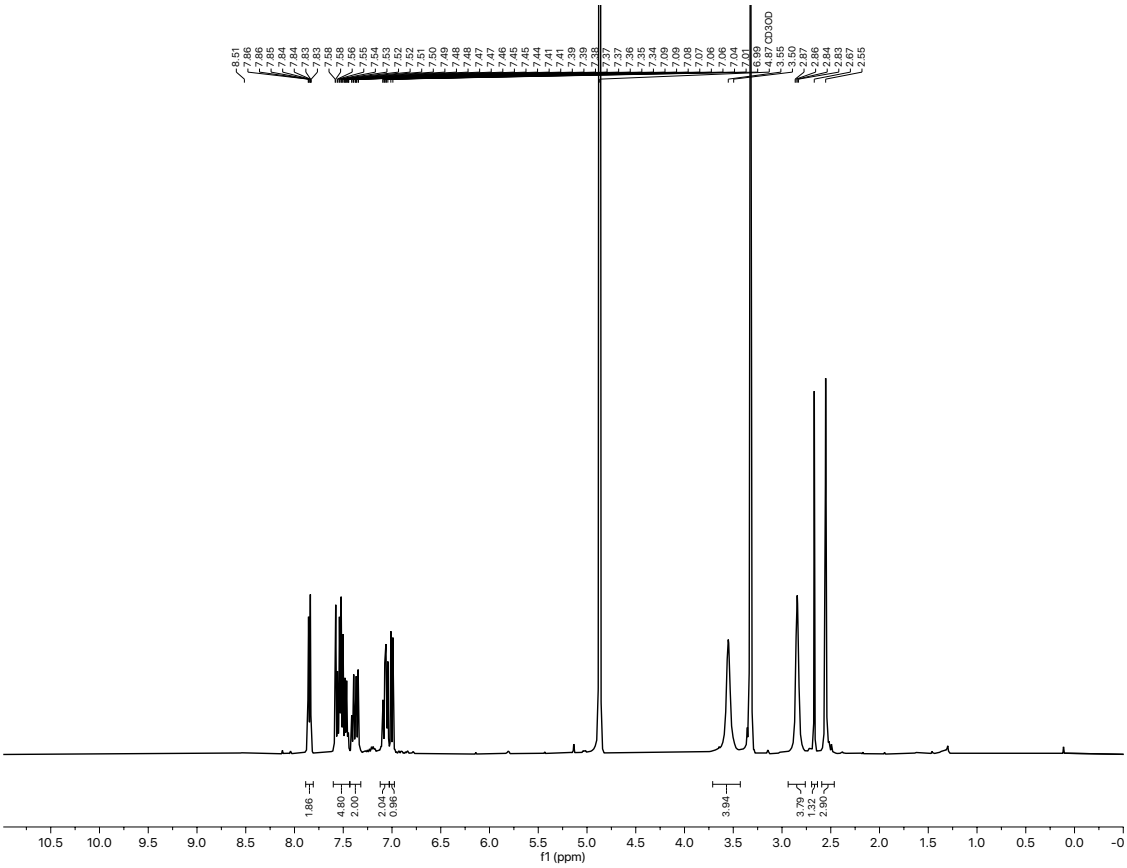
8.51
7.86
7.86
7.85
7.84
7.84
7.83
7.83
7.58
7.58
7.56
7.55
7.54
7.53
7.52
7.52
7.51
7.50
7.49
7.48
7.48
7.47
7.47
7.46
7.45
7.45
7.44
7.41
7.41
7.39
7.39
7.38
7.37
7.37
7.36
7.35
7.34
7.09
7.09
7.08
7.07
7.06
7.06
7.05
7.04
7.01
6.99
4.87 CD3OD
3.55
3.50
3.37
2.86
2.84
2.83
2.67
2.55
1.86
4.80
2.00
2.04
0.96
3.94
3.79
1.32
2.90
f1 (ppm)

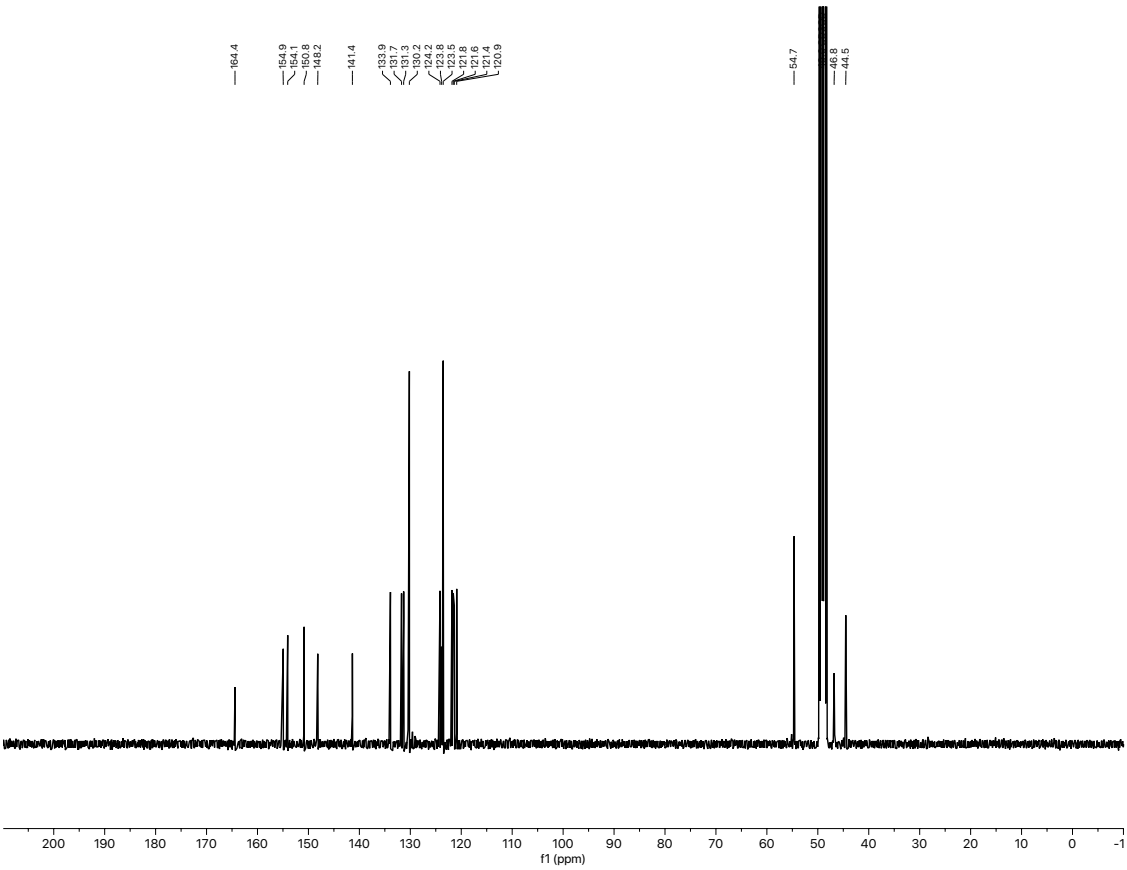
164.4
154.9
154.1
150.8
148.2
141.4
133.9
131.7
131.3
130.2
124.2
123.8
123.5
121.8
121.6
121.4
120.9
54.7
46.8
46.6
44.5
f1 (ppm)

NMR for 3-9:

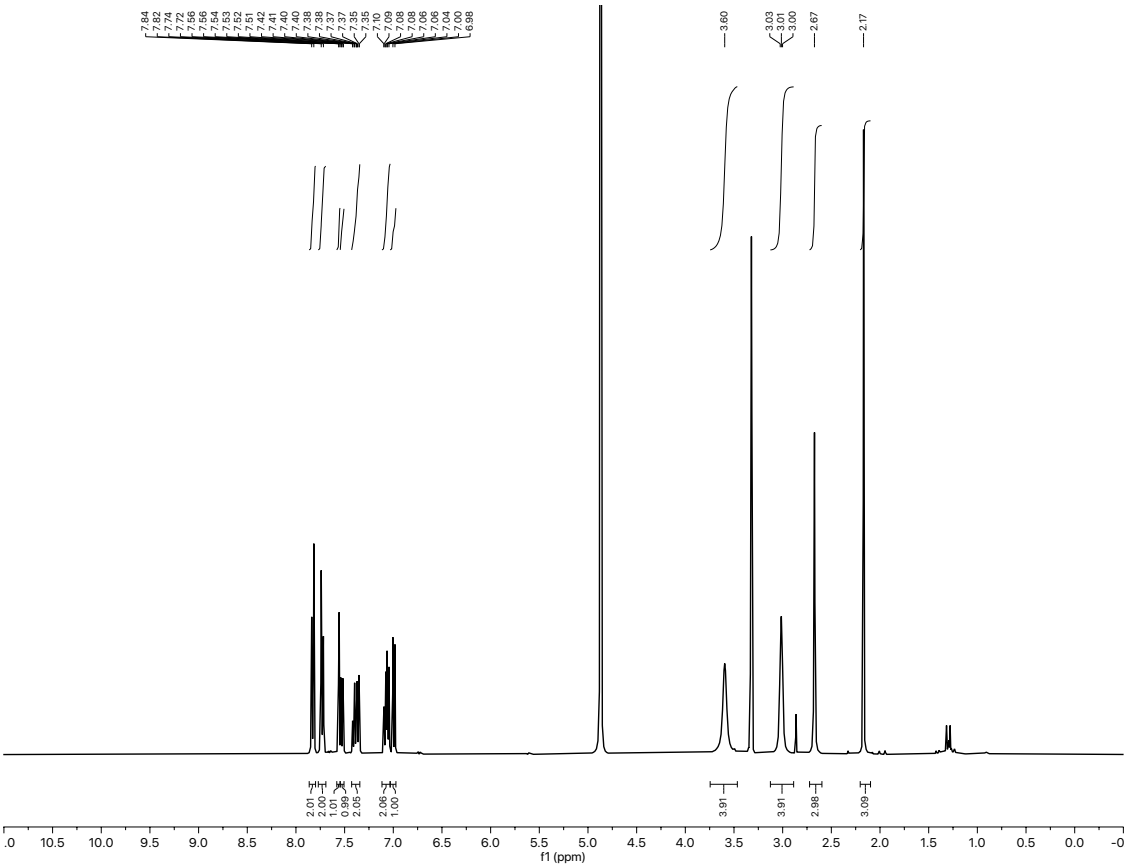
7.84
7.82
7.74
7.72
7.56
7.55
7.54
7.53
7.52
7.51
7.42
7.41
7.40
7.40
7.38
7.38
7.37
7.37
7.35
7.35
7.10
7.09
7.08
7.08
7.06
7.06
7.04
7.00
6.98
3.60
3.03
3.01
3.00
2.67
2.17
2.01
2.00
1.01
0.99
2.05
2.06
1.00
3.91
3.91
2.98
3.09
f1 (ppm)

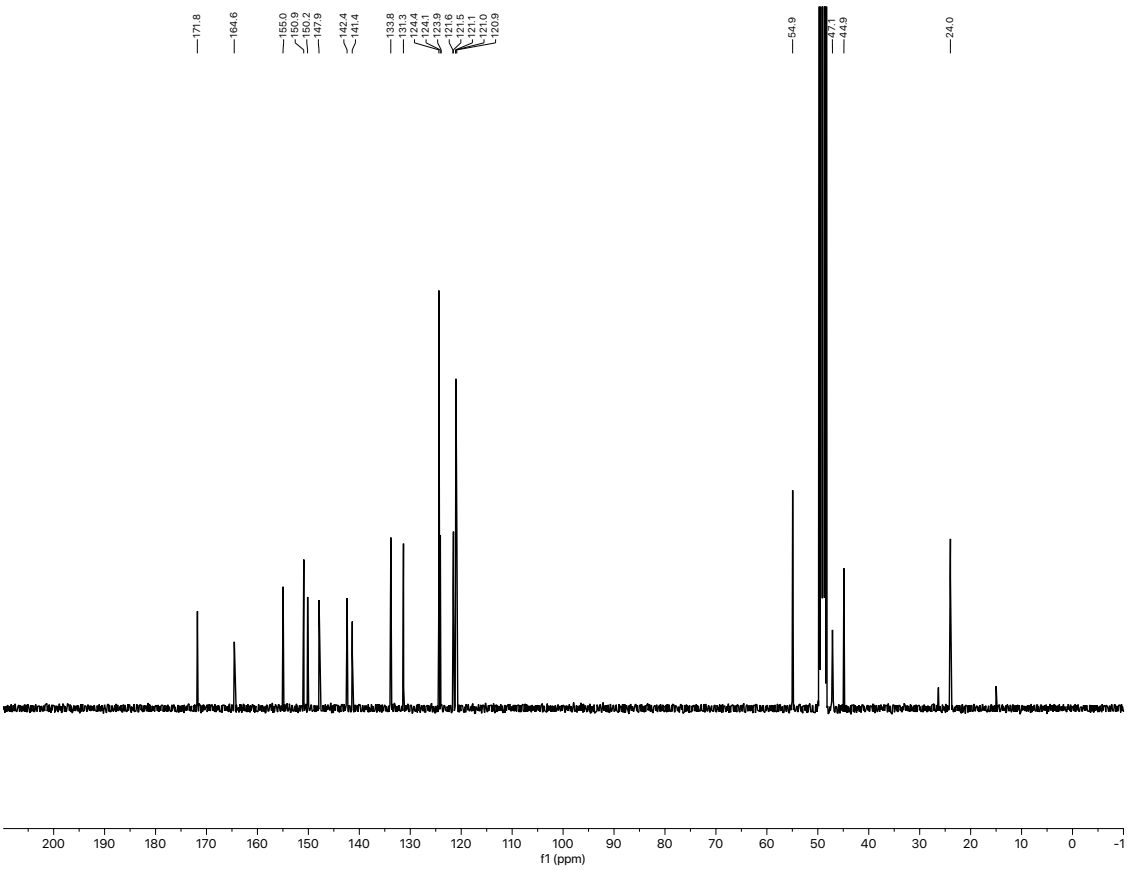
171.8
164.6
155.0
150.9
150.2
147.9
142.4
141.4
133.8
131.3
124.4
124.1
123.9
121.6
121.5
121.1
121.0
120.9
54.9
47.1
44.9
24.0
f1 (ppm)

NMR for 3-10:

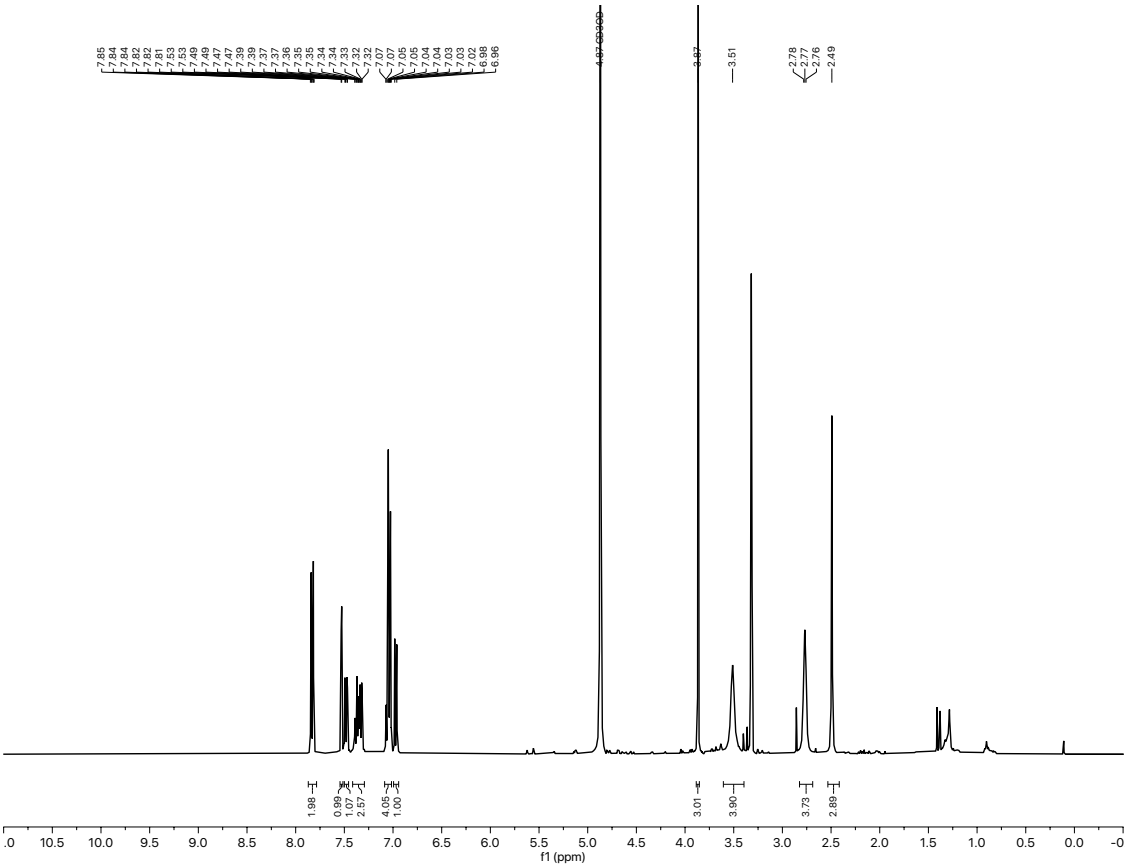
7.85
7.84
7.84
7.82
7.82
7.81
7.81
7.53
7.53
7.49
7.49
7.47
7.47
7.39
7.39
7.37
7.37
7.36
7.35
7.35
7.34
7.34
7.33
7.32
7.32
7.07
7.07
7.06
7.05
7.04
7.04
7.03
7.03
7.02
6.98
6.98
4.87
3.87
3.51
2.78
2.77
2.76
2.49
1.98
0.99
1.07
2.57
4.05
1.00
3.01
3.90
3.73
2.89
f1 (ppm)

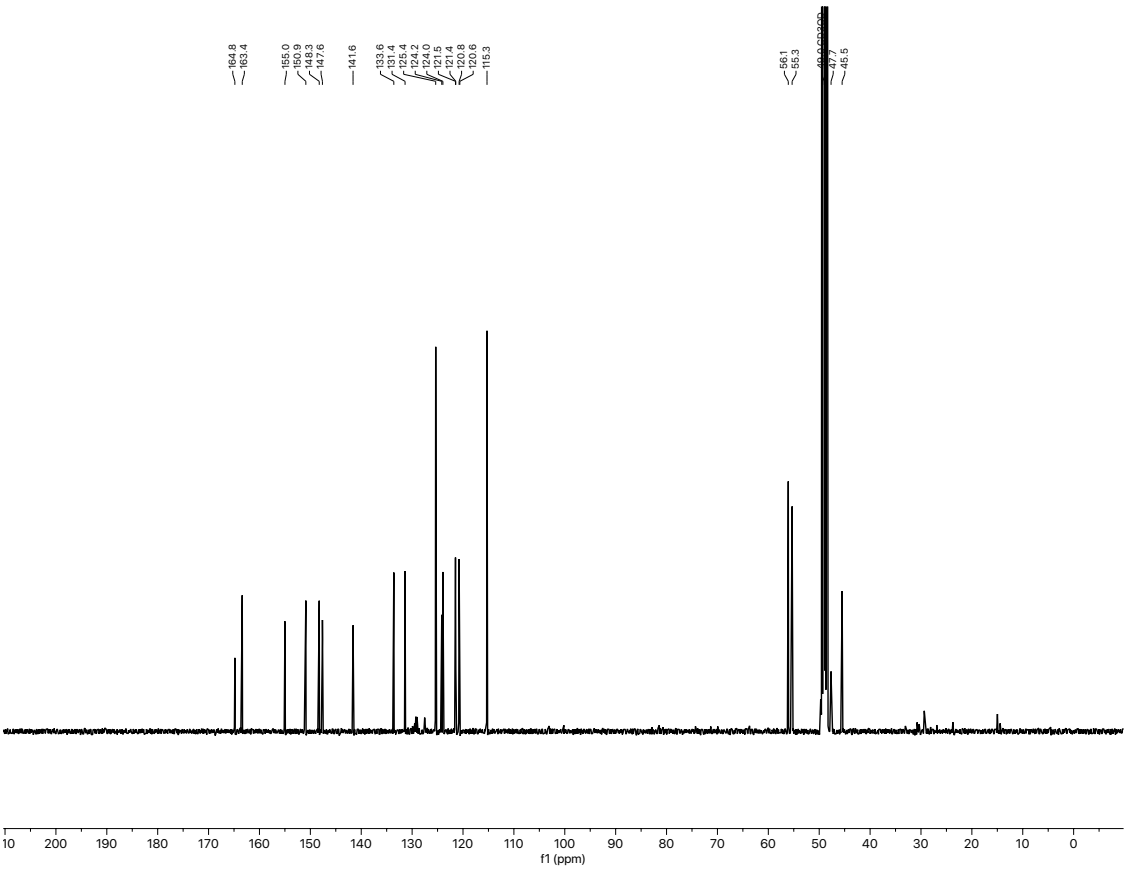
164.8
163.4
155.0
150.9
148.3
147.6
141.6
133.6
131.4
125.4
124.2
124.0
121.5
121.4
120.8
120.6
115.3
56.1
55.3
45.5
f1 (ppm)